THE DURABILITY OF HIGHLY LOADED, LUBRICATED, CASE HARDENED STEEL GEARS

by

CHRISTIAN MARCO RAYMOND WILKINSON

A thesis submitted to the University of London for the degree of Doctor of Philosophy and to the Imperial College of Science, Technology and Medicine for the Diploma of Imperial College.

JULY 1998

Tribology Section,
Department of Mechanical Engineering,
Imperial College of Science, Technology and Medicine,
London SW7 2BX

BIBL
LONDON
UNIV.

Dedicated to Raymond, Maria-Luisa, Samantha and Stefania Wilkinson

There is a problem with doing something right the first time: nobody appreciates how difficult it was.

The Fatigue Life of a PhD Student.



Increasing Number of Cycles

Abstract

Gears can sometimes fail by pitting, micropitting, or scuffing. This can limit the service life of a gearbox or lead to catastrophic failure.

One potential solution to pitting and micropitting failures is reinforcement of the extreme surface by using a suitable steel-treatment combination. Several promising temper resistant carburising steels have been developed in which hardness is maintained at elevated temperatures, hence allowing them to operate at higher temperatures. In addition, some of these carburised steels have the potential to be duplex hardened by nitrogen surface treatment, further enhancing their surface hardness. These steels have been developed primarily for the aerospace industry because of the requirement for smaller, lighter, more reliable, and higher temperature operating transmissions.

This thesis reports an investigation of the behaviour of these new materials and treatments under conditions of high load. Particular attention is given to the determination of surface endurance limits under a range of operating conditions using both gear and disc specimens.

Four materials have been tested: a standard carburised steel; two temper resistant steels (one carburised and one nitrided); and a duplex hardened steel.

An analysis of the relationship between the gear and disc tests, used to simulate gears, is also presented based on tooth load sharing analysis.

This study is mainly concerned with rolling contact fatigue, in the form of pitting, but other failure modes, such as severe wear, caused by micropitting, and scuffing, were also encountered. These same failure modes have, however, been identified on both gear and disc specimens.

Important findings were the greatly enhanced fatigue life exhibited by duplex hardened specimens when compared to their carburised counterparts and how the former exhibited a subsurface origin of failure, as opposed to the usual surface initiated failure. The reason for this was thought to be the reinforcement given to the extreme surface by the nitriding process.

Acknowledgements

I would like to thank the following people for helping me in various ways throughout my Ph.D. studies.

Dr. A.V. Olver for his supervision and useful advice.

GKN Westland Helicopters for allowing me to use their facilities and their financial support of this project.

The EPSRC (Engineering & Physical Research Council) for their financial support of my studies.

Martin Salzer, Ron Kench, Dave Davies and all the other people at GKN Westland Helicopters for their help and advice.

The members of the Tribology section (especially Matt, Tae, Rich B., Rich H., Derek, Ian, and Susie) for making the past few years entertaining ones and for preventing me from finishing too early.

My family.

CONTENTS

List of Figures 12

List of Tables 18

Nomenclature 19

Glossary 21

Chapter 1 Introduction

1.1 Background 23
1.2 Objectives 24
1.3 Thesis Structure 25

------- PART 1 - REVIEW -------

Chapter 2 Surfaces in Contact

2.1 Smooth Surfaces in Contact 26
2.1.1 Static Contact of Smooth Bodies 27
2.1.2 Moving Contacts on Smooth Bodies 31
2.2 Rough Surfaces in Contact 33
2.2.1 Surface Roughness 33
2.2.2 The Talysurf 34
2.2.3 Static Contact of Rough Bodies 36
2.2.3.1 Analytical Techniques for Rough Surface Analysis 37
2.2.3.2 Numerical Techniques for Rough Surface Analysis 38
2.2.4 Moving Contacts on Rough Bodies 42
2.3 Lubricated Surfaces in Contact 49
2.3.1 Smooth Lubricated Contacts 50
2.3.1.1 Hydrodynamic Lubrication 50
2.3.1.2 Elastohydrodynamic Lubrication 50
2.3.1.3 Mixed Lubrication 52
2.3.1.4 Boundary Lubrication 52
2.3.1.5 Regimes of Lubrication 52
2.3.2 Rough Lubricated Contacts 53
2.4 Conclusions 55

Chapter 3 Rolling Contact Fatigue

3.1 Rolling Contact Fatigue....56
3.2 Factors affecting Rolling Contact Fatigue....59
3.2.1 Material Variables....59
3.2.2 Surface Finish....61
3.2.3 Lubrication....63
3.2.4 Operating Variables....67
3.2.4.1 Load....67
3.2.4.2 Temperature....68
3.2.4.3 Geometry....68
3.2.4.4 Sliding....70
3.2.4.5 Other Variables....72
3.3 The Pitting Mechanism....72
3.4 The Statistical Nature of Fatigue....77
3.5 Fatigue Models and Design Standards....79
3.5.1 Fatigue Models....79
3.5.2 Fatigue Design Standards....81
3.6 Conclusions....81

Chapter 4 Gear Failure Modes

4.1 Gearbox and Gear Failures....82
4.2 Tooth Breakage....84
4.3 Scuffing....85
4.4 Pitting....87
4.5 Micropitting....89
4.6 Other Failure Modes....91
4.7 Conclusions....93

Chapter 5 Gear Materials

5.1 The Basic Requirements for a Gear Steel....94
5.2 The Requirements of an Aerospace Gear Steel....95
5.3 Current Surface Engineering Processes for Gear Materials....96
5.4 The Need for New Materials....102
5.5 The Possible Benefits of New Materials....104
5.6 Hardness and the Effects of the Alloying Elements in Steel....106
5.7 A Brief History of Bearing and Gear Materials....109
5.8 Previously Investigated Gear Materials....112
5.9 The Materials being Investigated....117
5.9.1 BS S156....117
5.9.2 AISI M50NiL....117
5.9.3 32CDV13....118
5.9.4 AISI M50NiL Duplex....118
5.10 Conclusions....119

Chapter 6 Test Methods for Evaluating Gear Steel Pitting Performance

6.1 Techniques for Evaluating Gear Steel Performance 120
6.2 The Use of Discs to Simulate Gears 122
6.3 Why Gear and Disc Tests may not Correlate 123
6.3.1 The Influence of Slide-Roll Ratio 123
6.3.2 Hunting and Integral Ratios 123
6.3.3 Bulk Metal and Flash Temperature Differences 125
6.3.4 Engagement Discontinuities 125
6.3.5 Extended Contact 125
6.3.6 Differences in Properties Due to the Manufacturing Process 126
6.3.6.1 Roughness Effects 126
6.3.6.2 Case Depth 127
6.3.7 The Size Factor 127
6.3.8 Debris Effects 127
6.3.9 Dynamic Loads 128
6.3.10 Misalignment 128
6.4 Conclusions 128

Summary Part 1 - Review 129

---- PART 2 - ANALYTICAL & EXPERIMENTAL RESEARCH ----

Chapter 7 A Description of Experimental Test Rigs and Specimens Employed in this Study

7.1 The Gear Test Rig 130
7.2 The Three Disc Contact Machine 135
7.3 The Axial Fatigue Test Rig 139
7.4 The Design of the Test Specimens 140
7.4.1 The Gear Test Specimens 140
7.4.2 The Disc Test Specimens 147
7.4.3 The Axial Fatigue Specimens 148
7.5 Specimen Properties 149
7.5.1 Roughness 149
7.5.2 Hardness 150
7.5.3 Material Microstructure 152
7.6 Online Monitoring of the Tests 156
7.6.1 Failure Detection in the Gear Rig 156
7.6.2 Failure Detection in the Disc Rig 162
7.7 Test Procedure and Test Piece Preparation 165
7.8 Test Programme 165
7.9 Conclusions 166

Chapter 8 Stress Analysis

8.1 Disc Rig Loading Conditions 167
8.2 Gear Rig Loading Conditions 173
8.2.1 Static Analysis 174
8.2.1.1 Description of Gear Contact Model 174
8.2.1.2 Tooth Contact Neglecting Tip Effects 178
8.2.1.3 Modelling of Pre-engagement 182
8.2.2 Dynamic Analysis 186
8.2.2.1 The Dynamic Factor 186
8.2.2.2 Determination of the Natural Frequencies of the Gear System 187
8.3 Roughness Effects 188
8.4 Stressed Volume 193
8.5 Residual Stress Distributions 195
8.6 Conclusions from the Stress Analysis 197

Chapter 9 Thermal Analysis

9.1 Gear Temperature Measurements 199
9.2 Heat Partition Theory 201
9.3 Disc Temperature Measurements 205
9.4 Flash Temperatures 206
9.5 Conclusions from the Thermal Analysis 210

Chapter 10 Lubrication Analysis

10.1 Lubricant Properties 212
10.2 Lubricant Tests 212
10.3 Sliding and Entrainment Speeds 217
10.4 Film Thickness 219
10.5 Conclusions from the Lubricant Analysis 222

Chapter 11 The Gear Test Experimental Results

11.1 Examination of the Gear Contact Fatigue Test Results 223
11.1.1 The Non-tip Relieved BS S156 Gear Tests 223
11.1.2 The Tip-relieved BS S156 Gear Tests 228
11.1.3 The AISI M50NiL Gear Tests 230
11.1.4 The AISI M50NiL Duplex Gear Tests 231
11.2 Comparison of the Failed Gear Specimens 232
11.3 S-N and Weibull Results for the Gear Fatigue Tests 234
11.4 The Axial Fatigue Test Results 237
11.5 Conclusions from the Gear and Axial Fatigue Tests 239

Chapter 12 The Disc Test Experimental Results

12.1 Examination of the Disc Contact Fatigue Test Results 241
12.1.1 The Chamfered BS S156 Disc Tests 241
12.1.2 The Crowned BS S156 Disc Tests 242
12.1.3 The AISI M50NiL Disc Tests 244
12.1.4 The AISI M50NiL Duplex Disc Tests 246
12.1.5 The 32CDV13 Disc Tests 252
12.2 Comparison of the Failed Disc Specimens 254
12.3 S-N and Weibull Results for the Disc Fatigue Tests 255
12.4 Conclusions from the Disc Fatigue Tests 258

Summary Part 2 - Analytical & Experimental Research 260

------- PART 3 - DISCUSSION ------

Chapter 13 The Gear, Disc, and Axial Fatigue Test Discussion

13.1 The Gear Rolling Contact Fatigue Tests 264
13.1.1 The Non-Relieved Gear Tests 264
13.1.2 The Tip-Relieved Gear Tests 265
13.2 The Disc Fatigue Tests 266
13.2.1 The Crowned Disc Tests 266
13.2.2 The Chamfered Disc Tests 267
13.3 The Axial Fatigue tests 267
13.4 The Materials Tested 268
13.4.1 BS S156 268
13.4.2 32CDV13 268
13.4.3 AISI M50NiL 269
13.4.4 AISI M50NiL Duplex 270
13.5 The Possible Effects on Gearbox Size and Weight 271
13.6 Conclusions 272

Chapter 14 Comparison and Correlation of Gear and Disc Failures

14.1 Comparison of Gear and Disc Failures 274
14.2 Gear-Disc Correlation Factor 275
14.2.1 The Influence of Slide-Roll Ratio 278
14.2.2 Temperature and Film Thickness Differences 278
14.2.3 Stress Concentrations Arising from the Geometry 279
14.2.4 Roughness Effects 279
14.2.5 Stressed Volume 280
14.2.6 Extended Contact 280
14.2.7 Dynamic Loads 280
14.2.8 Other Factors 280
14.3 Conclusions 281

Chapter 15 Conclusions

15.1 Summary of Thesis....283
15.2 Conclusions....284
15.3 Proposals for Future Research....286
15.3.1 Suggestions for Experimental Research....286
15.3.2 Suggestions for Theoretical Research....287

References....288

Appendix
Appendix A Material Specification....305
Appendix B Material Heat Treatment Specification....307
Appendix C Spur Gear Design Specification....309
Appendix D Spur Gear Design Drawing....310
Appendix E Barrel and Ring Design Drawings....311
Appendix F Lubricant Specification....312
Appendix G Dynamic Load Analysis....313
G1 The Dynamic Factor....313
G2 Determination of Natural Frequencies in the Gear System....314
Appendix H Calculations of Gear Tooth Gaps for Pre-engagement....319
Appendix I Pre-engagement Computing Program....325
I1 Program Listing....325
I2 Program Outputs....350
Appendix J Monitoring System Software Program....354
Appendix K Spur Gear Design and Geometry Nomenclature....356
K1 Gear Terminology....356
K2 Gear Design Calculations....357
K3 Profile Correction....359

List of Figures

Figure No.
1.1.1 The Gear-Disc Correlation Factor (ZG_2 from BSI 1986).....23
2.1.1 Elliptical Contact Geometry.....28
2.1.2 Contact Ellipse Showing the Major and Minor Semi-Axes a and b.....28
2.1.3 Stress Distribution at the Surface Caused by Uniform Pressure and Hertz Pressure (Johnson 1985).....29
2.1.4 Contact of Cylinders (Johnson 1985).....30
2.1.5 Surface Stresses due to Friction (Johnson 1985).....32
2.1.6 Contours of Principal Shear Stress Beneath a Sliding Contact (Johnson 1985).....32
2.2.1 A Rough Surface Pressure Profile Contrasted to Hertz Pressure Profile (Webster & Sayles 1986).....33
2.2.2 The Talysurf.....35
2.2.3 The Talysurf Traverse Unit.....35
2.2.4 Output Display on the Talysurf.....36
2.2.5 Output From the Rough Surface Contact Model (Webster & Sayles 1986).....41
2.2.6 Typical Output the Rough Surface Contact Model using "Plasticity" (Webster & Sayles 1986).....41
2.2.7 The Effect of Continued Sliding on Plasticity Index (Greenwood & Williamson 1966).....44
2.2.8 RMS Roughness Versus Correlation Length Map for Abraded Surfaces (Hirst & Hollander 1974).....45
2.2.9 Shakedown Map for the Steady Sliding of Two Cylinders (Johnson & Shercliff 1992).....47
2.2.10 Shakedown Limits (Kapoor & Johnson 1993).....48
2.2.11 Orthogonal Shear Stress Distribution for a Rough Surface (from program by Kim & Olver 1997).....49
2.3.1 Stribeck Curve (Anghel 1998 attributed to Stribeck 1902).....53
3.2.1 Areas of Tension and Compression in a Rolling-Sliding Contact.....71
3.2.2 Direction of the Traction Force on the Driving and Driven Gear Teeth.....71
4.1.1 Fretted Tapered Gear Seat on a Shaft (Tallian 1992).....82
4.1.2 The Effect of Running Conditions on the Failure Mode.....83
4.2.1 Tooth Breakage due to Bending Fatigue on a Helical Gear (Neale 1995).....84
4.2.2 Tooth Root Fracture (Tallian 1992).....84
4.2.3 Fatigue Crack Caused by Stresses at the Root Fillet Leading to Tooth Breakage (AGMA 1980).....85
4.3.1 Scuffing Failure on Gear Teeth (Pitch Line Unaffected) (Drago 1988).....86
4.3.2 Localised Scuffing (Tallian 1992).....86
4.4.1 Pitting in a Helical Gear (Alban 1985).....87
4.4.2 Pitting due to Surface Distress (Tallian 1992).....87
4.4.3 Shape of a Pit (52x) (Bartz & Kruger 1973).....88
4.4.4 Progressive Deterioration of Gear Teeth by Pitting (Alban 1985).....89
4.5.1 Micropitting in Gear Dedendum (Neale 1995).....90
4.5.2 Close View of Micropitting 500x (Graham 1979).....90
4.6.1 Case Crushing (Drago 1988).....92
4.6.2 Abrasive Wear (Tallian 1992).....93

5.5.1 Influence of Test Temperature on the Case Hardness of a Number of Temper Resistant Gear Steels (from Davies & Gittos 1989).....105
5.5.2 Typical Temperature History in a Helicopter Main Gearbox with Time after Oil Loss (from Davies & Gittos 1989) 105
5.8.1 Influence of Tempering Temperature on Conventional and Temper-Resistant Gear Steels (from Davies & Gittos 1989) 115
5.8.2 Comparison of the Impact Resistance of Conventional and Candidate Gear Steels (from Davies 1986) 115
6.2.1 Contact of Involute Spur Gear Teeth (Johnson 1985) 122
7.1.1 The Gear Rig.....130
7.1.2 The Test Gear Lubrication Circuit 131
7.1.3 The Slave Gear Lubrication Circuit.....132
7.1.4 The Mounted Test Gears.....133
7.1.5 Schematic of the Gear Test Rig 134
7.2.1 The Three Disc Contact Machine 136
7.2.2 The Three Disc Contact Machine Layout.....136
7.2.3 The Three Disc Contact Machine Lubrication Circuit 138
7.3.1 The Axial Fatigue Test Rig (Davies 1996) 139
7.4.1 The Seventeen Tooth, Involute Spur Test Gear 140
7.4.2 Calibration Curve for the Gear Test Rig 142
7.4.3 Reduced Radius of Curvature and Tooth Meshing Number Across the Path of Contact 142
7.4.4 The Effect of the Crowning Radius on the Maximum Contact Stress and Contact Half Width for a Torque of 300, 350 and 400 N m 143
7.4.5 Typical Lead Profile for a Test Gear 143
7.4.6 Tooth Load Cycle for a Properly Relieved Gear 145
7.4.7 Long and Short Relief Diagrams for Involute Spur Gear Teeth 145
7.4.8 Transmission Error Diagram for a Loaded Tip Relieved Gear (assuming constant stiffness).....146
7.4.9 Involute Profile for a Test Gear (Tip and Root Relief of about 40 μm).....147
7.4.10 The Chamfered and Crowned Barrels and Ring Specimen 148
7.4.11 The Axial Fatigue Test Specimen 149
7.5.1 The Hardness Profiles of the Gear Specimens 151
7.5.2 The Hardness Profiles of the Barrel Specimens 151
7.5.3 The Hardness Profiles of the Ring Specimens 151
7.5.4 Transverse Section Through a BS S156 Gear Tooth.....152
7.5.5 Transverse Section Through an M50NiL Gear Tooth 153
7.5.6 Transverse Section Through a 32CDV13 Barrel.....154
7.5.7 Transverse Section Through a 32CDV13 Ring 154
7.5.8 Transverse Section Through a Plasma Nitrided M50NiL Duplex Gear Tooth.....155
7.5.9 Transverse Section Through a Plasma Nitrided M50NiL Duplex Barrel.....155
7.5.10 Transverse Section Through a Gas Nitrided M50NiL Duplex Barrel.....156
7.6.1 Signal Average for the Vibrations Detected by the Accelerometers.....157
7.6.2 Frequency Fourier Transform before Failure.....157
7.6.3 Frequency Fourier Transform after Failure.....158
7.6.4 Frequency Fourier Transform of the Bandpass Filtered Signal before Failure 158
7.6.5 Frequency Fourier Transform of the Bandpass Filtered Signal after Failure...158
7.6.6 Schematic Representation of the Gear Rig Control Instrumentation 160

7.6.7 The Gear Rig Monitoring System Display Showing Shutdown After Gear Pitting 161
7.6.8 Schematic Representation of the Disc Rig Control Instrumentation 163
7.6.9 The Disc Rig Monitoring System Display Showing a Typical Shutdown after Failure of a Barrel by Pitting 164
8.1.1 Schematic of Disc Rig Test Piece Layout and Motion 167
8.1.2 Chamfered and Crowned Barrel Specimen Contact Layout 168
8.1.3 Variation of Contact Stress with Applied Pressure for a Chamfered Barrel ... 168
8.1.4 Variation of Contact Stress with Applied Pressure for a Crowned Barrel 169
8.1.5 Variation of Contact Width with Load in the Chamfered Barrel Specimen 169
8.1.6 Variation of Contact Dimensions with Load in the Crowned Barrel Specimen (Major Width, 2*a*, Minor Width, 2*b*) 170
8.1.7 Chamfered Barrel Pressure Distribution 171
8.1.8 Chamfered Barrel Deformed Profile 171
8.1.9 Crowned Barrel Pressure Distribution 172
8.1.10 Pressure Distribution on a Barrel with a 5° Chamfer 173
8.1.11 Pressure Distribution on a Barrel with a 15° Chamfer and Smaller Mesh Size than Figure 8.1.7 173
8.2.1 The Input Page to the Gear Contact Program 175
8.2.2 Schematic Showing the Principle of Gear Tooth Load Analysis 175
8.2.3 The Gear Geometry To Evaluate Tooth Gap, E[N] 176
8.2.4 Program Output Showing the Calculated Tooth Gaps, Deflections, and Load Sharing for Non-Relieved Gear Teeth 177
8.2.5 Program Output Showing the Load Sharing Diagram 177
8.2.6 Variation of Maximum Hertzian Contact Stress on the Gear Teeth at the Lowest Point of Single Tooth Contact with Torque 178
8.2.7 Variation of Maximum Hertzian Contact Stress on the Gear Teeth at the Lowest Point of Single Tooth Contact with Oil Loading Pressure 179
8.2.8 Variation of the Contact Ratio *a*:*b* Along the Gear Tooth Contact 180
8.2.9 Variation of the Contact Stress Along the Gear Meshing Cycle for Three Values of Torque 180
8.2.10 Variation of Contact Stress Throughout the Gear Mesh Cycle with Torque .. 181
8.2.11 Variation of the Major Contact Dimension 2*a* Throughout the Gear Mesh Cycle for Three Values of Torque 181
8.2.12 Variation of the Major Contact Dimension 2*a* Throughout the Gear Mesh Cycle 182
8.2.13 Variation of the Minor Contact Dimension 2*b* Throughout the Gear Mesh Cycle for Three Values of Torque 182
8.2.14 Tooth Interference Causing Pitting (Alban 1985) 183
8.2.15 Load Sharing Diagram using the Extended Contact Analysis for Two Values of Torque 184
8.2.16 The Contact Stresses on a Crowned Non-Tip-Relieved Gear Tooth Suffering Extended Contact at the Extremities of the Mesh Cycle 184
8.2.17 The Effect of Gear Tooth Tip Radius on the Contact Stresses in a Crowned Non-Tip-Relieved Gear Tooth Suffering Extended Contact 185
8.2.18 The Contact Dimensions of a Crowned Non-Tip-Relieved Gear Tooth Suffering Extended Contact at the Extremities of the Mesh Cycle 185
8.2.19 The Two Systems Used to Model the Natural Frequencies of the Gear System 188
8.3.1 The Deformed Surface Profile of the Loaded Chamfered Barrel Profile 190
8.3.2 The Chamfered Barrel Surface Stress Distribution 190

8.3.3 The Crowned Barrel Surface Stress Distribution....191
8.3.4 The Gear Surface Stress Distribution....191
8.3.5 The Distribution of Orthogonal Shear Stress in the Crowned Disc....192
8.3.6 The Distribution of Orthogonal Shear Stress in the Gear....192
8.3.7 The Maximum Orthogonal Shear Stress at Each Depth for the Gear and Disc Specimens....193
8.5.1 X-Ray Residual Stress Profiles Comparing AISI M50NiL and M50NiL Duplex and Shot Peening....196
8.5.2 X-Ray Residual Stress Profiles for AISI M50NiL with Various Shot Peening Treatments....197
9.1.1 Location of the Holes for Thermocouples in the Gear Tooth....200
9.1.2 The Temperature Measurement Set-up on the Gear Rig....200
9.1.3 Gear Tooth Temperature Variation with Time (Increasing Torque Steps)....201
9.2.1 Variation of the Heat Partition Coefficient Along the Gear Path of Contact ..202
9.2.2 The Instantaneous Rate of Heat Conducted into the Gears ($\mu = 0.07$)....203
9.2.3 The Heat Conducted into the Gears per Unit Length per Revolution....203
9.2.4 Heat Conducted into the Gears per Unit Length per Revolution as a Percentage of the Maximum Value....204
9.2.5 An Example of Temperature 'Cross-Over' in a Disc Contact (Paliwal & Snidle 1987)....205
9.4.1 The Flash Temperature Generated Along The Non-Relieved Gear Tooth with Extended Contact at the Extremities of the Meshing Cycle ($\mu = 0.1$)....210
10.2.1 HFR Test (Temperature 70 °C. Stroke Length 1000 μm. Load 200g.)....214
10.2.2 HFR Test (Frequency 20 Hz. Stroke Length 1000 μm. Load 400g.)....214
10.2.3 Principle of Optical Interferometry (Smeeth 1998)....215
10.2.4 Film Thickness Behaviour of Lubricant AN157 with Temperature....216
10.2.5 Film Thickness Behaviour of Lubricant AN157 at 120 °C....216
10.2.6 AN157 Boundary Film Decay After Testing at 120 °C for 30 minutes and 1 hour and then Stopping the Rig....217
10.3.1 Sliding and Entrainment Speeds in the Test Gears....218
10.3.2 Slide-Roll Ratio Variation Across the Gear Teeth....218
10.3.3 Gear and Disc Slide-Roll Comparison Showing Single and Double Tooth Pair Contact....219
10.3.4 The Sliding and Entrainment Speed Along the Non-Relieved Gear Tooth Meshing Cycle Showing the Effects of Extended Contact....219
10.4.1 Film Thickness Variation with Torque in the Gear Tooth Contact....221
10.4.2 The Minimum Film Thickness for a Non-Tip-Relieved Gear Tooth Contact Suffering Extended Contact at the Extremities of the Mesh Cycle....221
11.1.1 Scuffing in a Non-Relieved BS S156 Gear Tooth....224
11.1.2 Close-up of Scuffing Failure on a Gear Tooth (Pitch Line Unaffected)....224
11.1.3 Strong Marking Possibly from Pre-Engagement in the Dedendum of a Non-Tip Relieved BS S156 Gear....225
11.1.4 Closer View of the Marking Shown in Figure 11.1.3....225
11.1.5 Wear Pattern on a Non-Relieved Gear Tooth after Running at Low Load....226
11.1.6 Lead Profiles of Meshing Teeth 1 and 2 in Mating Non-Relieved Gears....227
11.1.7 Scanning Electron Micrograph of the Dedendum of the Gear in 11.1.5 Showing Micropitting (1000x)....227
11.1.8 Pitting in a Tip-Relieved BS S156 Gear Tooth....228
11.1.9 Pit Surrounded by Localised Scuffing in a Tip-Relieved BS S156 Gear....229
11.1.10 Severe Pitting Damage on a Tip-Relieved BS S156 Gear Tooth....229

11.1.11 Transverse Section Through the Dedendum of a BS S156 Micropitted Gear Tooth....229
11.1.12 Scanning Electron Micrograph of the Edge of a Contact in a Tip-Relieved Gear Tooth Dedendum Showing Micropitting....230
11.1.13 Pit in a Scuffed Dedendum of a Tip-Relieved BS S156 Gear....230
11.1.14 Micropitting and Pitting in an AISI M50NiL Gear Dedendum....231
11.1.15 Transverse Section Showing Cracks in an M50NiL Gear....231
11.1.16 An AISI M50NiL Duplex Gear After Ten Million Load Cycles....232
11.2.1 Scanning Electron Micrograph of a BS S156 Gear Dedendum....232
11.2.2 Scanning Electron Micrograph of an AISI M50NiL Duplex Gear Dedendum....233
11.2.3 Scanning Electron Micrograph of a BS S156 Gear Dedendum....233
11.2.4 Scanning Electron Micrograph of an AISI M50NiL Gear Dedendum....234
11.2.5 Scanning Electron Micrograph of an AISI M50NiL Gear Addendum....234
11.3.1 The BS S156, AISI M50NiL, and M50NiL Duplex Gear Fatigue Lives....235
11.3.2 Weibull Plots of the Gear Contact Fatigue Lives....235
11.3.3 The L_{50} Lives for the Gear Contact Fatigue Tests....236
11.3.4 The Tip-Relieved and Non-Tip-Relieved BS S156 Gear Fatigue Tests....236
11.4.1 The BS S156 Axial Fatigue Tests at 150 °C....237
11.4.2 The AISI M50NiL Duplex Axial Fatigue Tests at 150 °C....238
11.4.3 The Effect of Temperature on AISI M50NiL Axial Fatigue Tests....238
11.4.4 Comparison of the BS S156, AISI M50NiL and M50NiL Duplex Axial Fatigue Tests at Zero Mean Stress and 150 °C....239
12.1.1 Scuffing on Chamfered Barrel Run at -0.28 Slide-Roll Ratio....241
12.1.2 Pitted Chamfered Barrel Run at -0.14 Slide-Roll Ratio....242
12.1.3 Micropitted and Pitted BS S156 Chamfered Barrel....242
12.1.4 Pitted and Micropitted Crowned BS S156 Barrel....243
12.1.5 Micropitted Crowned BS S156 Barrel....243
12.1.6 Scanning Electron Micrograph of Micropitting in a Crowned Barrel....243
12.1.7 Progression of Micropitting in Crowned BS S156 Specimens....244
12.1.8 Pits at the Edge of an AISI M50NiL Barrel Track....244
12.1.9 AISI M50NiL Ring with Small Pits at the Edge of the Run Track....244
12.1.10 Scanning Electron Micrographs Showing the Progression of Damage in an AISI M50NiL Barrel....245
12.1.11 Pitted AISI M50NiL Duplex Barrel (Plasma Nitrided)....246
12.1.12 Pitted and Micropitted AISI M50NiL Duplex Barrel (Plasma Nitrided)....246
12.1.13 Scanning Electron Micrograph Showing Micropitting on an AISI M50NiL Duplex Barrel (Plasma Nitrided)....247
12.1.14 Pitted and Micropitted AISI M50NiL Duplex Barrel (Gas Nitrided)....247
12.1.15 Scanning Electron Micrograph Showing Micropitting in an AISI M50NiL Duplex Barrel (Gas Nitrided)....248
12.1.16 Optical and Scanning Electron Micrograph Images of the Same Subsurface Initiated Pit in an AISI M50NiL Duplex Barrel (Gas Nitrided)....249
12.1.17 Crack Morphology in An AISI M50NiL Duplex Pit Showing the Progression of What Appear to be Subsurface Initiated Fatigue Cracks....250
12.1.18 Two Examples of Micropitting in the AISI M50NiL Duplex Rings (Gas Nitrided)....251
12.1.19 Optical and Scanning Electron Micrograph Images Showing Two Examples of AISI M50NiL Duplex Ring Damage....251
12.1.20 32CDV13 Barrel showing Micropitting....252
12.1.21 Transverse Sections of a 32CDV13 Barrel Showing Micropits....252

12.1.22 Three examples of Damage on the 32CDV13 Rings....253
12.2.1 Scanning Electron Micrograph of a BS S156 Barrel Specimen Run at -0.14 Slide-Roll Ratio....254
12.2.2 Scanning Electron Micrograph of an AISI M50NiL Duplex Barrel Specimen Run at -0.14 Slide-Roll Ratio....254
12.2.3 Taper Section of a BS S156 Disc Run at -0.14 Slide-Roll Ratio....255
12.2.4 Taper Section of an AISI M50NiL Duplex Barrel Run at -0.14 Slide-Roll Ratio....255
12.3.1 The BS S156, AISI M50NiL, and M50NiL Duplex Chamfered Barrel Fatigue Lives for Slide-Roll Ratios of -0.026 and -0.14....256
12.3.2 Weibull Plots of the Disc Fatigue Lives....256
12.3.3 The L_{50} Lives for the Disc Contact Fatigue Tests....257
12.3.4 The Chamfered and Crowned BS S156 Disc Fatigue Tests....257
14.2.1 Rolling Contact Fatigue Lives of the Gear and Disc Experiments....276
14.2.2 S-N Plot with L_{50} Lives for the Various Specimens....276
D1 Spur Gear Design Drawing....310
E1 Crowned Barrel Design Drawing....311
E2 Chamfered Barrel Design Drawing....311
E3 Ring Design Drawing....311
G1 The Two Systems Used to Model the Natural Frequencies of the Gear System....315
H1 Gear Teeth Meshing at the First Point of Tooth Contact (on the Path of Contact)....319
H2 Gear Tooth Meshing Simulated by the Crossed Belt Analogy....320
H3 Gear Geometry for Pre-engagement Analysis....321
H4 Specific Geometry....322
H5 Detailed Diagram for the Gear Teeth Pre-engagement Analysis....323
I1 Input Page to the Program....350
I2 Program Output Showing the Calculated Tooth Gaps, Deflections, and Load Sharing for Non-Relieved Gear Teeth....350
I3 Program Output Showing the Load Sharing Diagram....351
I4 The Contact Stresses on a Crowned Non-Tip-Relieved Gear Tooth Suffering Extended Contact at the Extremities of the Mesh Cycle....351
I5 The Sliding Speed Along the Non-Relieved Gear Tooth Meshing Cycle Showing the Effects of Extended Contact....352
I6 The Entrainment Speed Along the Non-Relieved Gear Tooth Meshing Cycle Showing the Effects of Extended Contact....352
I7 The Minimum Film Thickness for a Non-Tip-Relieved Gear Tooth Contact Suffering Extended Contact at the Extremities of the Mesh Cycle....353
I8 The Flash Temperature Generated Along The Non-Relieved Gear Tooth with Extended Contact at the Extremities of the Meshing Cycle ($\mu = 0.1$)....353
J1 Gear Rig Control Program Block Diagram....354
J2 Disc Rig Control Program Block Diagram....355
K1 Rack Form Covering the Range of Modules 1-50 (from BS 436 Part 2 (BSI 1970))....357
K2 Limiting Values of the Sum of the Addendum Modification Coefficients Σx for a Gear Pair from BGA (1992) Chart Modified from BSI (1970)....358
K3 Limiting Values of Addendum Modification Coefficient, x, for a Single Gear from BGA (1992) Chart Modified from BSI (1970)....359
K4 The Profile Tolerance Diagram for the Test Gears (mm)....360

List of Tables

Table No.

5.7.1 Typical Steel Alloy Compositions....110
7.5.1 The Surface Roughness of Specimens....150
8.1.1 Disc Rig Speeds, Slide-Roll Ratios, and Cycles per Hour....168
8.3.1 Radii of Curvature for the Barrel and Gear Specimens....190
8.4.1 Barrel Stressed Volume (p_o = 2.6 GPa, μ = 0.07)....195
8.4.2 Gear Stressed Volume (p_o = 2.6 GPa, μ = 0.07)....195
8.4.3 Disc-Gear Lives for the Stressed Volumes Calculated....195
8.5.1 BS S156 Gear Residual Stress Measurements at the Surface....197
9.3.1 Specimen Temperature at -0.026 and -0.28 Slide-Roll Ratio, Measured by Graham (1979) and the Estimated Temperature at -0.14 and the Bulk Temperatures at the Contact Inlet (p_o = 2.6 GPa)....206
9.3.2 Summary of the Estimated Bulk Temperatures for the Fatigue Tests....206
9.4.1 The Material Properties for the Flash Temperature Calculations....208
9.4.2 The Flash Temperature Calculation for the Chamfered Disc at 2.6 GPa....208
9.4.3 The Flash Temperature Calculation for the Crowned Disc at 2.6 GPa....209
9.4.4 The Flash Temperature Calculation for the Gear at 2.6 GPa....209
9.4.5 The Calculated Contact Temperatures for the Test Specimens....209
10.1.1 Lubricant Specification (Castrol AN157)....213
10.4.1 Minimum Film Thickness and Lambda Ratio for the Fatigue Tests....222
14.2.1 Comparative Fatigue Lives for the BS S156 Tests....277
A1 BS S156 Material Specification....305
A2 M50NiL Material Specification....305
A3 32CDV13 Material Specification....306
A4 BS S156, AISI M50NiL, and AISI M50NiL Duplex Material Properties....306
B1 Material Heat Treatment for BS S156 and 32CDV13....307
B2 Material Heat Treatment for AISI M50NiL and AISI M50NiL Duplex....308
C1 Involute Spur Gear Data....309
F1 Lubricant Specification (Castrol AN157)....312
G1 Values of Effective Pitch Error Used to Calculate K_1 (μm)....314
G2 Factors K_1 and K_2 for the Dynamic Factor....314
G3 Notation for the Natural Frequency Analysis....315
G4 Calculated Values of Mass, Stiffness, and Moments of Inertia....317
G5 Natural Frequencies of the Gear System....318

Nomenclature

a	Major semi-axis of elliptical contact	mm
b	Minor semi-axis of elliptical contact	mm
$BCD1$	Base circle diameter of the pinion	mm
$BCD2$	Base circle diameter of the wheel	mm
CLA	Centre line average roughness	μm
D	Diameter	m
E	Young's modulus	$N\ m^{-2}$
E^*	Reduced Young's modulus of contact	$N\ m^{-2}$
$E[N]$	Gap between mating gear teeth at point N	mm
H	Hardness	$N\ m^{-2}$
H_v	Vickers hardness number	$kgf\ mm^{-2}$
h_o	Minimum EHD smooth body film thickness	m
F_N	Total load on gear teeth	N
k	Yield stress in shear	$N\ m^{-2}$
k_v	The dynamic factor	
L	Length of contact	m
m_n	Module of a gear	mm
N	Rotational speed	rev/min
P	Load per unit length (line contact)	$N\ m^{-1}$
P	Load (point contact)	N
p_o	Maximum Hertzian contact pressure	$N\ m^{-2}$
R	Radius	m
R^*	Reduced radius of contact	mm
RA	Roll angle	°

R_a	Centre line average roughness	μm
RMS	Root mean square roughness	μm
R_q	Root mean square roughness	μm
R_{11}	Maximum principal radius of curvature of body 1	mm
R_{12}	Minimum principal radius of curvature of body 1	mm
R_{21}	Maximum principal radius of curvature of body 2	mm
R_{22}	Minimum principal radius of curvature of body 2	mm
u	Surface speed of body	$m\ s^{-1}$
w	Track width of barrel	m
W'	Load per unit length (line contact)	$N\ m^{-1}$
W	Load	N
α_{tw}	Working pressure angle	°
β^*	Correlation length	μm
λ	Lambda ratio	
λ_a	Average wavelength	μm
μ	Coefficient of friction	
σ	Root mean square roughness	μm
σ_y	Yield stress	$N\ m^{-2}$
$\sigma_1,\sigma_2,\sigma_3$	Principal stresses	$N\ m^{-2}$
υ	Poisson's ratio	
ψ	Plasticity index	

Glossary

AGMA	American Gear Manufacturers Association
AISI	American Iron and Steel Institute
ASME	American Society of Mechanical Engineers
ASLE	American Society of Lubrication Engineers
ASM	American Society for Metals
ASTM	American Society for Testing Materials
BGA	British Gear Association
BSI	British Standards Institution
CVD	Chemical Vapour Deposition
DIN	Deutsches Institut Für Normung
Ed.	Editor
EHD	Elastohydrodynamic
EHL	Elastohydrodynamic Lubrication
EP	Extreme Pressure
HPSTC	Highest Point of Single Tooth Contact
HRC	Hardness Rockwell C
IMechE	Institute of Mechanical Engineers
IOP	Institute of Petroleum
IR	Infrared
J.	Journal
JSLE	Japanese Society of Lubrication Engineers
JSME	Japanese Society of Mechanical Engineers

LEFM	Linear Elastic Fracture Mechanics
LPSTC	Lowest Point of Single Tooth Contact
pp.	Pages
PVD	Physical Vapour Deposition
RCF	Rolling Contact Fatigue
SEM	Scanning Electron Microscope
Trans.	Transactions
VAR	Vacuum Arc Remelting
VIM	Vacuum Induction Melting
Vol.	Volume

Chapter 1 Introduction

1.1 Background

Rolling contact fatigue is widely recognized as a primary failure mode in both gears and rolling element bearings. Surveys of helicopters (US National Materials Advisory Board 1979) have confirmed the phenomenon accounts for a high proportion of the overhaul rejections of gears; and it appears that it may impose a considerable penalty on reliability and cost of ownership. This is not surprising, in view of the little attention given to rolling contact fatigue in the design process of gears.

Most gear design standards assume that gear tooth meshing can be entirely reproduced by the contact of 'equivalent discs' and that rolling contact fatigue cannot occur below a certain value of contact pressure: the 'endurance limit'. However, disc tests are sometimes said to give unrealistically high endurance limits and a 'gear-disc correlation factor' is introduced to account for this (see Figure 1.1.1).

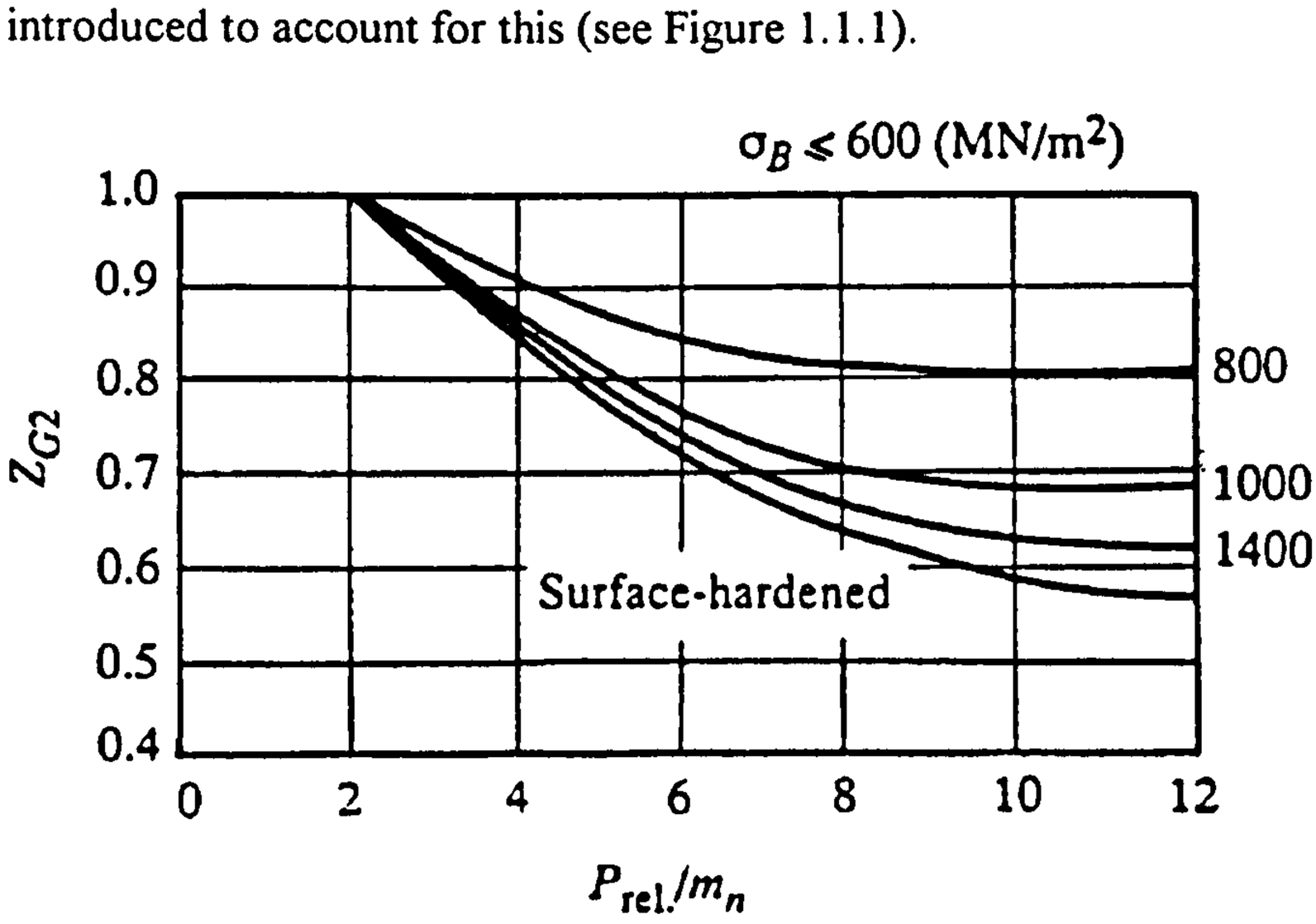


Figure 1.1.1 The Gear-Disc Correlation Factor (ZG_2 from BSI 1986)

The possible reasons for discrepancies between gear and disc tests are numerous. They include:

- The varying, rather than constant, slide-roll ratio present in gears
- Differences in the bulk metal temperatures of the test pieces

- Engagement discontinuities and their associated lubrication effects in gears
- A difference in roughness, material response and case depth due to the manufacturing process
- The size factor
- Debris effects
- Misalignment

These effects are discussed in more detail in Chapter 6. A better understanding of most of them is needed for a more accurate design procedure to be evolved, some of them being scarcely understood at all.

In the last twenty years a range of new materials and processes have become available to gears and rolling bearings. Many are being researched and adopted by the aerospace industry because of the critical nature of this area and the requirement for smaller, lighter, more reliable, and higher temperature operating components. Some of these materials and processes are both complex and costly for conventional gear design. Nevertheless, any significant reductions in size and weight that may be possible in future geared transmissions could validate the use of some of these materials in other areas, particularly in demanding or troublesome applications. The main uncertainty is the impact of these new materials on durability, and in particular on rolling contact fatigue, a facet of their performance which has been little studied.

1.2 Objectives

The aim of this research was to investigate the behaviour of several temper resistant carburising steels, which have been developed to maintain hardness at elevated temperatures.

Four materials were to be tested under high load: a standard carburised steel (BS S156); two temper resistant steels, one carburised (AISI M50NiL) and one nitrided (32CDV13); and a duplex hardened steel (AISI M50NiL Duplex).

Particular attention would be given to the determination of surface endurance limits under a range of operating conditions using both gear and disc specimens.

An analysis of the relationship between the gear and disc tests, used to simulate gears, was also to be carried out, based on accurate analysis of the tooth stresses in gears.

1.3 Thesis Structure

After this introduction the thesis has three main parts, each consisting of several chapters. The first part (Chapters 2-6) is a review of the literature and main aspects relevant to the work presented here. This includes topics such as the study of surfaces in contact, rolling contact fatigue, gear materials and failure modes, and test methods used to evaluate rolling contact fatigue. The second part (Chapters 7-12) includes the analysis and experimental work carried out by the author. The analysis considers the test rigs, the specimens, loading effects, and thermal and lubrication aspects. The results from the experimental research include work on the various materials, test rigs, and specimens used. In part three (Chapters 13-14) a discussion of the results obtained and their significance is given. Aspects such as material differences, gear-disc correlation, and possible effects on gearbox sizing are considered. Chapter 15 contains the main conclusions drawn from the project as well as possible areas for future research.

PART 1 - REVIEW

Chapter 2 Surfaces in Contact

To understand many of the factors affecting the durability of gears, one must understand the interactions taking place at the surface of the teeth. The durability of a gear is essentially determined by the stresses arising from the surface interactions it undergoes in contact. In this chapter some of the literature on surfaces in contact is reviewed. To start with, the simplest assumption of smooth bodies is analysed, this is examined for both static and moving contacts and then, as real surfaces are not smooth in practice, rough body contact is considered. Finally, because most gear contacts are lubricated, the effect of a lubricant in a contact is reviewed.

2.1 Smooth Surfaces in Contact

Replacing sliding by rolling produces a very large reduction in the resistance to motion. For this to be effective, however, the surfaces must be hard, stiff, and relatively smooth (Johnson 1988). The reduction of the resistance to motion by introducing these stiffer surfaces brings about high stress concentration at the point of contact. It is important to be able to evaluate these stresses, arising from the contact between the surfaces of two bodies, in order to determine whether they will be susceptible to fatigue or any other failure mechanism.

The contact between two surfaces can usually be classified as being either conforming or non-conforming. A conforming contact is one in which the two surfaces fit together closely without deforming: an example would be a flange. A non-conforming contact, on the other hand, is one in which the surfaces do not fit together: a gear tooth pair in contact would be a good example of this.

When brought into contact without deformation non-conforming, smooth surfaces come together forming a point or line contact, depending on their geometry. The contact area between these surfaces is small when compared to the radii of curvature of the undeformed bodies themselves; and the contact stresses are, therefore, concentrated

close to the contact area and decline rapidly in intensity with distance from it. These are the conditions which apply to the contacts studied by the author.

2.1.1 Static Contact of Smooth Bodies

The stresses and deformations which arise at the point of contact between two elastic solid bodies were first analysed by Hertz, in 1882, and this analysis was included in an assessment of the topic by Johnson (1985).

The analysis assumed that the surfaces were smooth and approximated them by second order polynomials near the contact point. The stresses could then be calculated by treating each body, except for the initial gap, as a semi-infinite elastic solid bounded by a plane surface, i.e. an elastic half-space.

The following assumptions were made in the Hertz theory of elastic contact:

1. The surfaces are continuous and non-conforming ($a<<R^*$). The significant dimensions of the contact area must be small when compared with the dimensions of each body and relative radii of curvature of the surfaces;
2. The strains are small $a<<R^*$ (the contacting bodies are within their elastic limit);
3. Each solid can be considered as an elastic half-space; and
4. There is no friction between the surfaces (only normal pressure is transmitted between them).

The boundary conditions are such that the normal displacements of the surfaces give no overlap and the pressure is zero outside the contact and positive within it. If the pressure distribution is integrated the total load can be evaluated from the integral, $\int_S pdS = P$.

Using these assumptions and boundary conditions, with the surfaces in contact having radii of curvature of different sizes in different directions (see Figure 2.1.1), Hertz showed that the projection of the contact area on the tangent plane was an ellipse (see Figure 2.1.2) and the pressure distribution was semi-ellipsoidal in this area (see Figure 2.1.3 which shows the pressure distribution and stresses for a Hertzian contact and for uniform pressure). The surface pressure distribution can then be found from the geometry, loads, and elastic properties of the surfaces and can be expressed as:

$$p(x,y) = p_0\sqrt{\left(1-\frac{x^2}{a^2}-\frac{y^2}{b^2}\right)}$$

where p_o is the maximum contact pressure and a and b are the maximum and minimum semi-axes of the contact ellipse respectively.

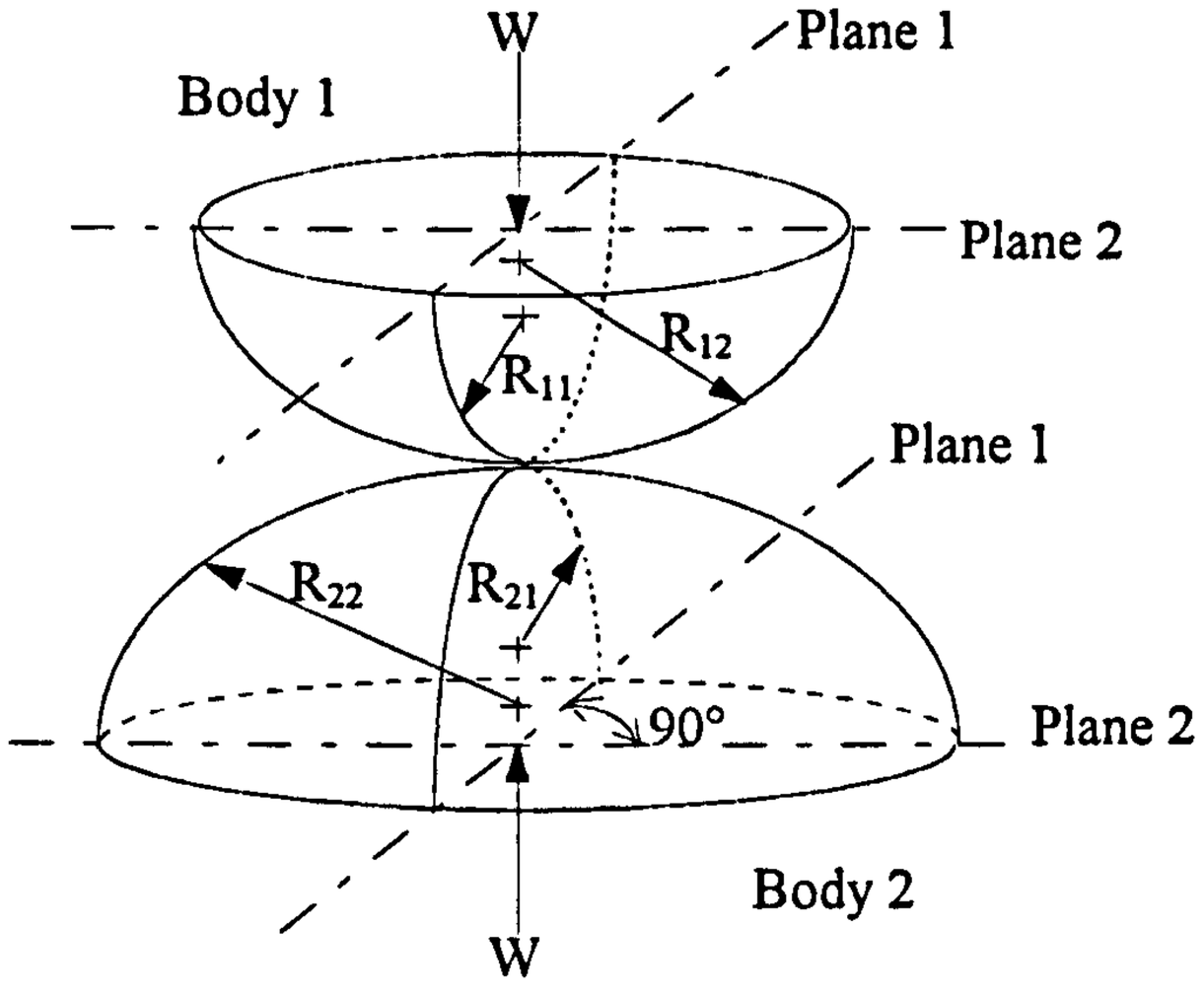


Figure 2.1.1 Elliptical Contact Geometry

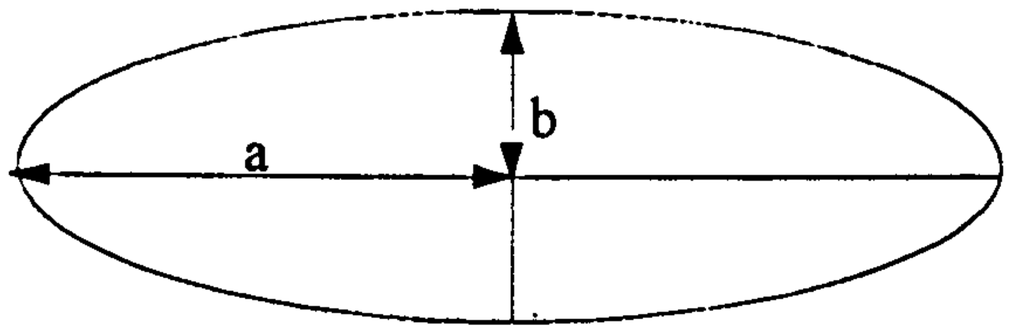
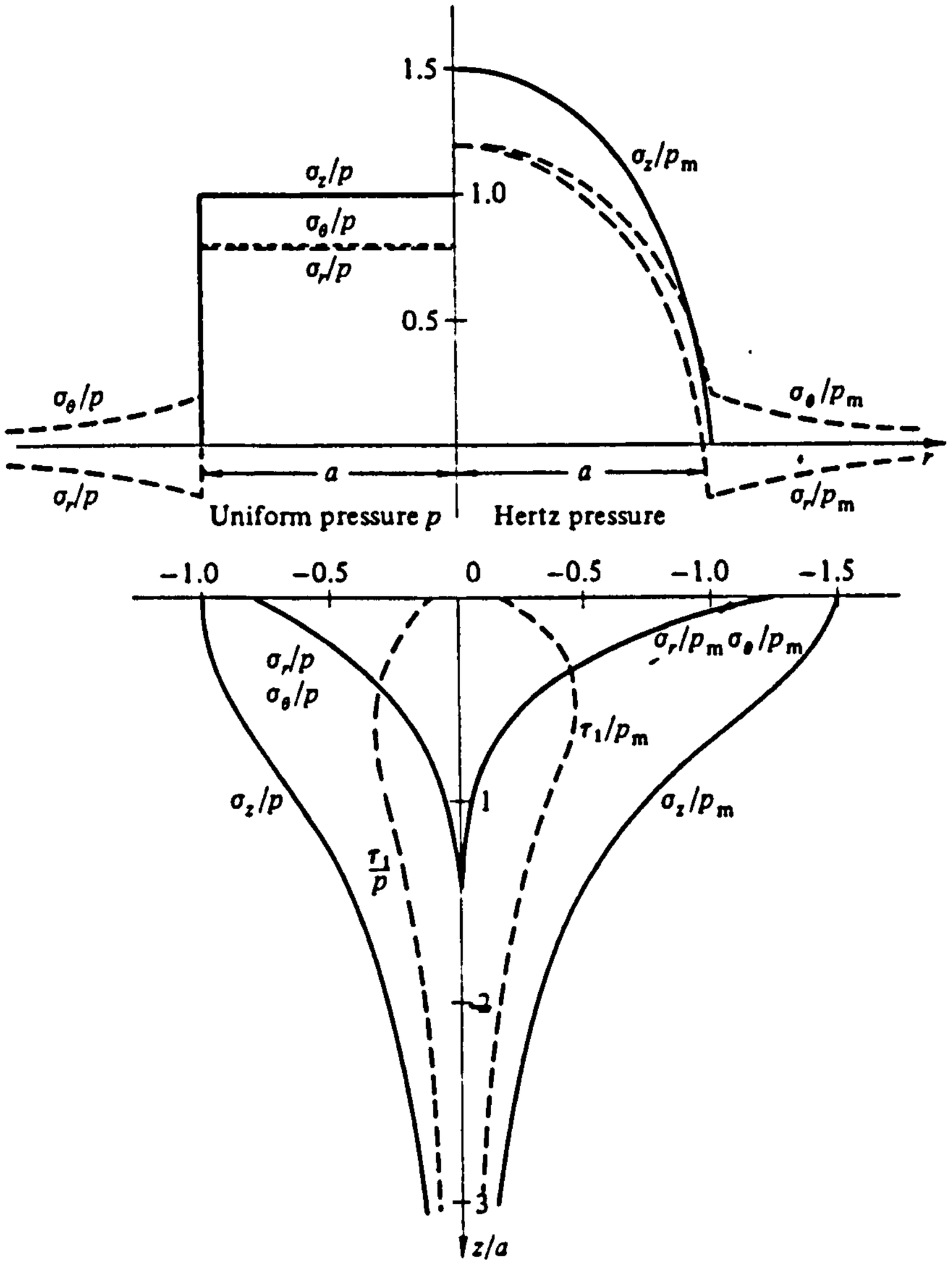


Figure 2.1.2 Contact Ellipse Showing the Major and Minor Semi-Axes a and b

Since the pressure distribution is semi-ellipsoidal and the volume of an ellipsoid is known, one can express the total load in the form, $P=(2/3)p_o\pi ab$.

To determine the value of the maximum Hertzian contact stress and the major and minor semi-axes of the contact ellipse for this general case, one must solve two elliptical integrals (this can be done by using an iteration technique discussed further on).

There are two special conditions which simplify the expression for contact pressure: these are for the contact between two cylindrical bodies with parallel axes and the contact of two spheres, or a sphere and a flat. For these situations the contact solution turns from a three-dimensional problem to a two-dimensional one.



σ_z, σ_θ and σ_r are the direct stresses referred to cylindrical coordinates, τ_1 is the principal shear stress and p_m is the average pressure in the contact

Figure 2.1.3 Stress Distribution at the Surface Caused by Uniform Pressure and Hertz Pressure (Johnson 1985)

For parallel cylinders, as a/b tends to infinity, the contact shape tends towards that of a long rectangular strip of width $2a$ lying parallel to the cylinders' axes. The equations for this line contact are:

$$p(x,y) = p_0\sqrt{\left(1-\frac{x^2}{a^2}\right)}$$

$$p_0 = \sqrt{\left(\frac{PE^*}{\pi R^*}\right)}$$

For a point contact, where the radii are equal:

$$p(x,y) = p_0 \sqrt{\left(1 - \frac{x^2}{a^2} - \frac{y^2}{a^2}\right)}$$

$$p_0 = \left(\frac{1}{\pi}\right)\left(\frac{6PE^{*2}}{R^{*2}}\right)^{\frac{1}{3}}$$

These surface pressure distributions can in turn be used to find the distribution of stresses near the contact using elasticity theory (as shown by Timoshenko and Goodier 1951). A plot of these stress distributions is shown in Figure 2.1.4

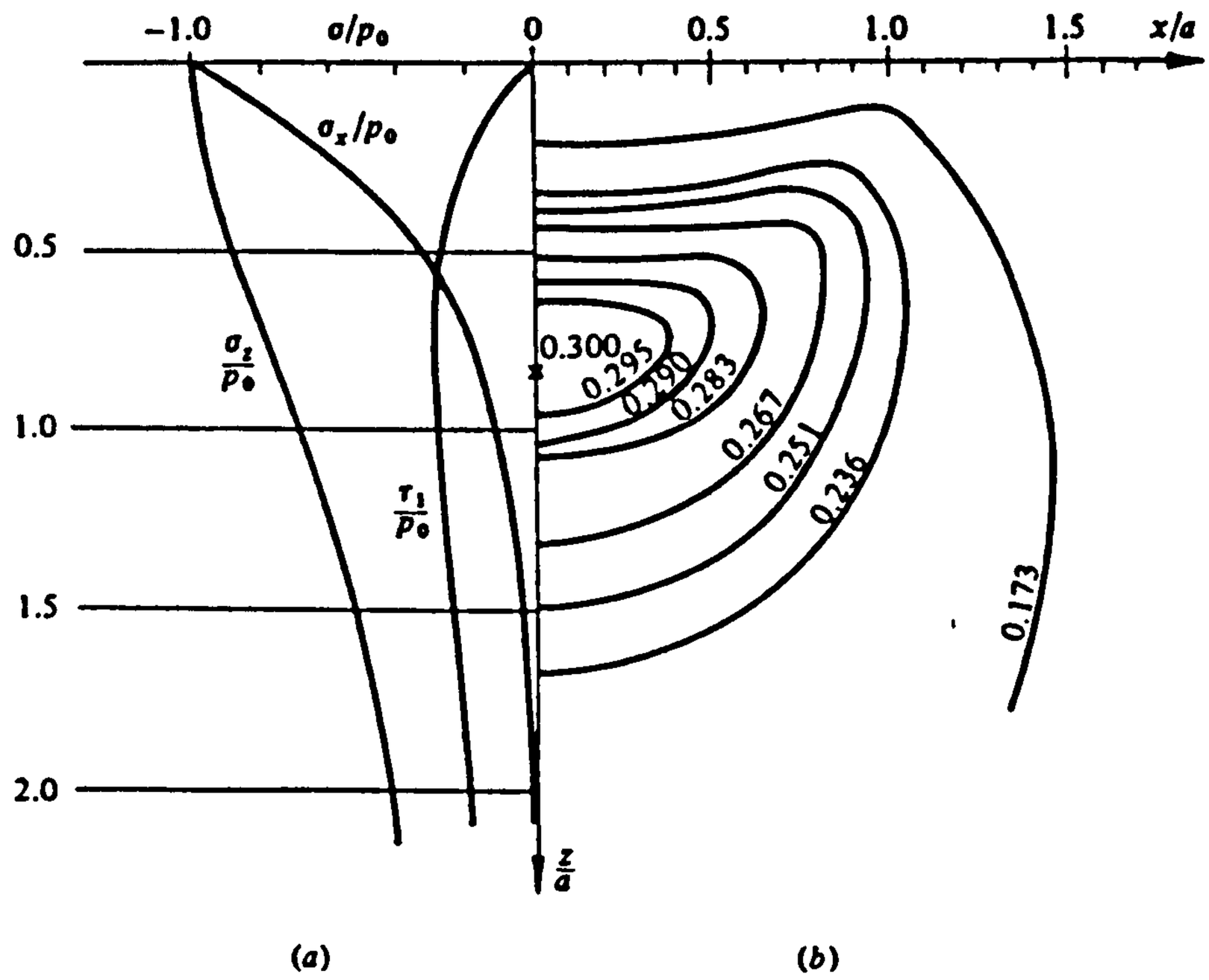


Figure 2.1.4 Contact of Cylinders (Johnson 1985) a) subsurface stresses along the axes of symmetry b) contours of principal shear stress τ_1

Finally, under the topic of static contact of smooth surfaces, one should mention that the above solutions consider an isotropic, homogenous material. An example that would not fulfill these criteria is a coated material, as the coating will, in general, have elastic constants which differ from those of the underlying material and counterface. The surface deflections experienced will not be those of an elastic half space and a different pressure and subsurface stress distribution will result. The contact of smooth, coated bodies was considered by Gupta and Walowit (1974).

2.1.2 Moving Contacts on Smooth Bodies

Gear teeth in motion do not have a static contact point, their surfaces move relative to each other. One can describe the contact pressure on a normally loaded, non-conforming, pure rolling contact, i.e. no sliding, by the Hertz equations (this could apply to the pitch point on a gear). It will, however, tend to increase the contact area and reduce the maximum contact pressure, p_o. The effect of rolling motion in a non-conforming, smooth body contact is to make the Hertzian pressure distribution sweep through the contact. When sliding is included, the area of contact, in the absence of friction forces, would also have dimensions given by the Hertz theory. However, there is bound to be a tangential friction force when there is sliding. This will oppose the direction of motion on both surfaces. Fortunately, for analysis purposes, the shape and size of the contact and normal pressure distribution are unaffected by this friction for materials with similar elastic properties and there is a small effect on the contact of bodies with dissimilar elastic constants. This, then, means that the stresses and deformation due to the normal pressure and the tangential traction are independent and can be superposed. The tangential traction is distributed in direct proportion to the normal pressure when using Amontons' law of sliding friction; $Q=\mu P$, where the constant of proportionality is the coefficient of kinetic friction, whose value is determined by the materials and the physical conditions of the interface. For the case of a cylinder sliding perpendicular to its axis the pressure distribution was shown earlier, the equivalent tangential traction is:

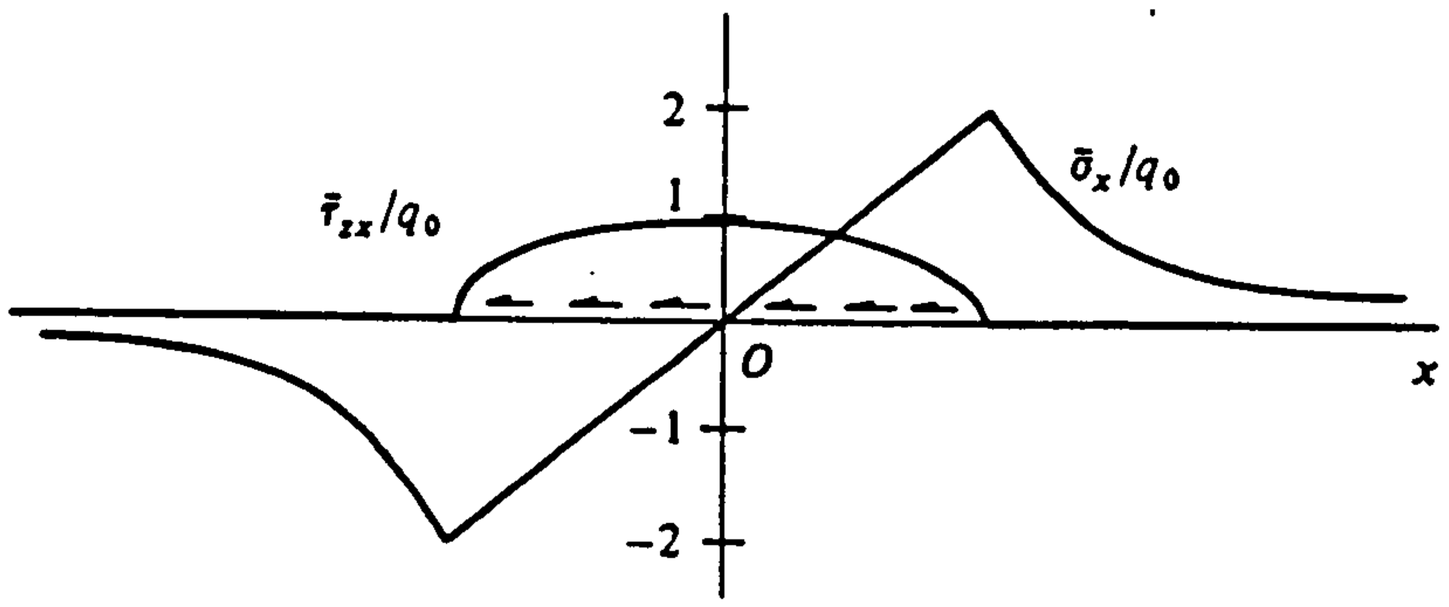
$$q(x) = \pm \mu p_o \sqrt{\left(1 - \frac{x^2}{a^2}\right)}$$

where the negative sign is associated with the positive velocity.

The integrals giving the stress components in a sliding cylinder have been evaluated by Smith and Liu (1953) amongst others. One of the results of introducing traction is to make the direct stress parallel to the surface a maximum compressive at the leading edge of the contact area and a maximum tensile at the trailing edge, both of magnitude $2\mu p_o$, shown in Figure 2.1.5. For a moving load this means that any point coming into contact is subjected to a completely reversing shear stress. A similar analysis on elliptical contacts gives the same trend.

The friction introduces shear stresses into the contact surface which could reach yield if the coefficient of friction were sufficiently high. This is because the onset of plastic yield

in a sliding contact will be governed (using the Tresca yield criterion) by the maximum value of the principal shear stress throughout the stress field. One can therefore calculate the contact pressure that would give rise to yield. The overall effect of friction is to move the maximum principal shear stress closer to the surface than in the static case, as shown in Figure 2.1.6.



τ_{xy} and σ_x are the tangential and normal traction respectively
q_o is the maximum tangential traction

Figure 2.1.5 Surface Stresses Due to Friction (Johnson 1985)

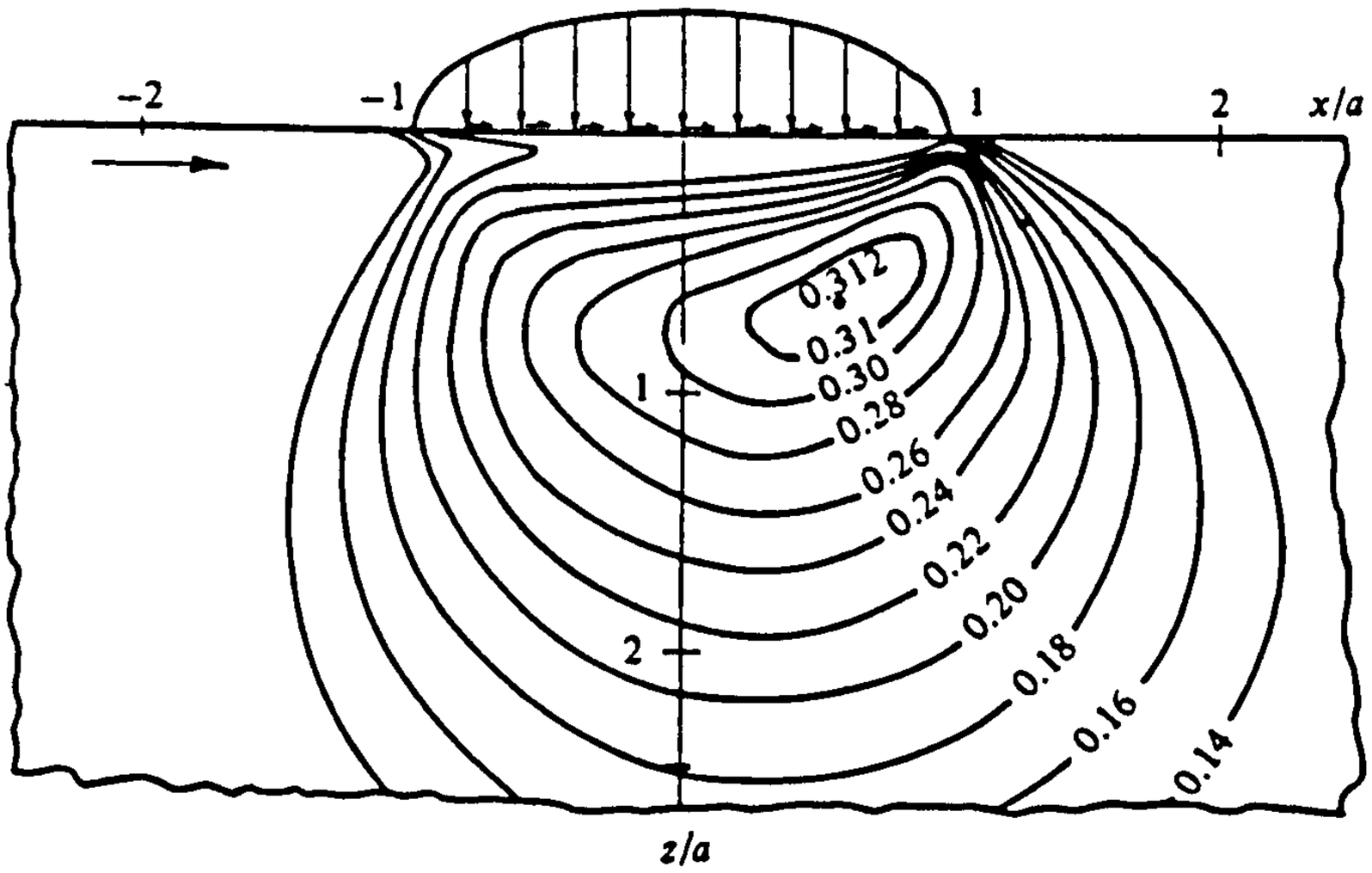


Figure 2.1.6 Contours of Principal Shear Stress, τ_1, Beneath a Sliding Contact (μ=0.2) (Johnson 1985)

It should be mentioned that if the tangential force between the surfaces is less than the limiting friction the contact will be divided into regions of microslip and ones of adhesion (Johnson 1985).

In general, a combination of rolling and sliding will exist in a contact and, provided the surfaces are smooth, the above discussion is valid.

2.2 Rough Surfaces in Contact

In the past, bodies were taken to be smooth when the contact between them was analysed, in the manner shown in the previous section. However, the surfaces of contacting bodies are not topographically smooth and comprise a multitude of peaks, known as asperities, and valleys. This invalidates the use of Hertz theory, which characterises the surfaces by local radii of curvature.

If this roughness is now considered in the analysis of a contact, it means that the contact between surfaces will be discontinuous and the real area of contact will be a small fraction of the nominal contact area. As a direct result of this, the actual pressure distribution does not follow precisely the smooth distribution predicted by the Hertz equation; the local pressures and subsurface stresses tend to be much higher (see Figure 2.2.1).

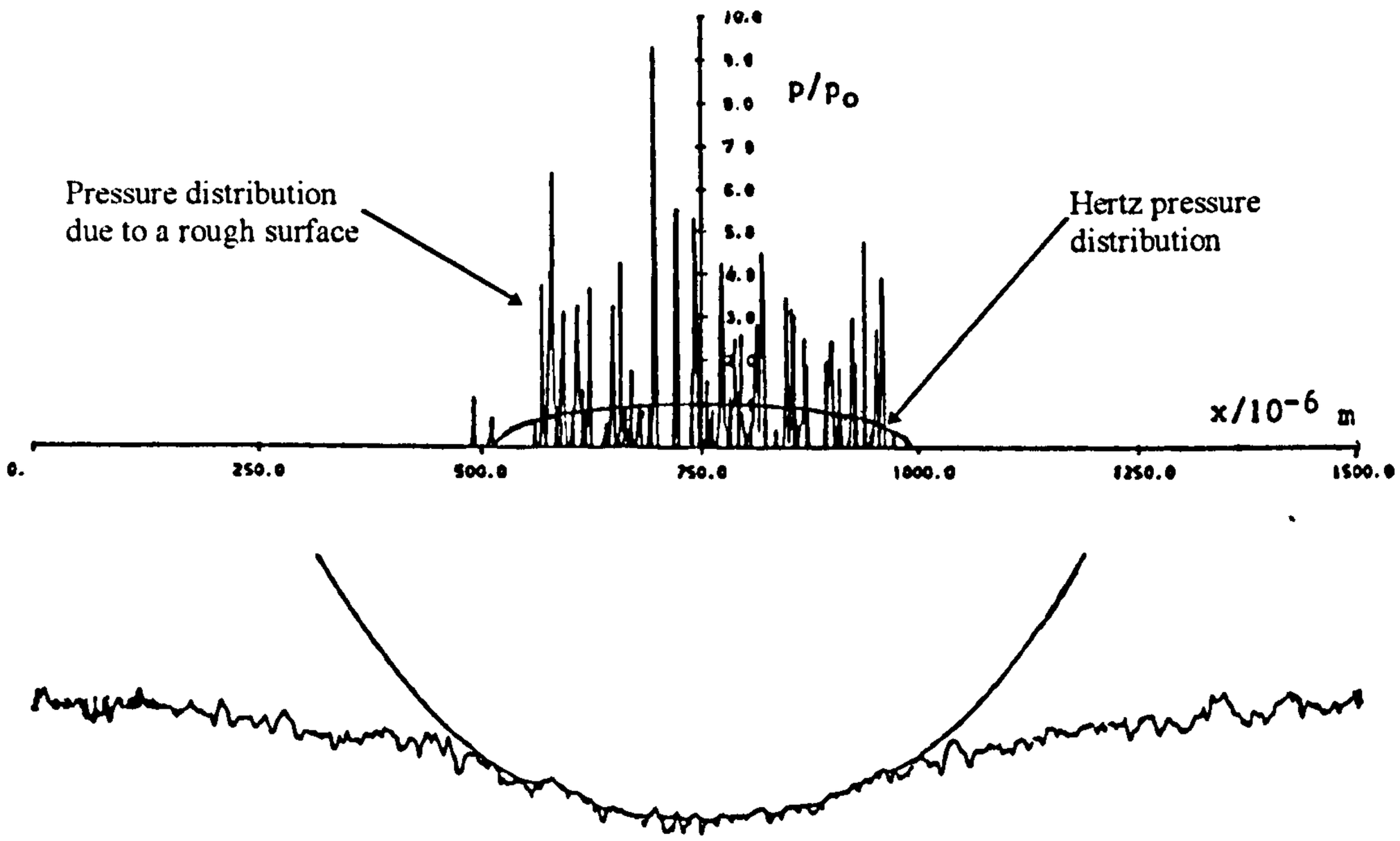


Figure 2.2.1 A Rough Surface Pressure Profile Contrasted to Hertz Pressure Profile (Webster & Sayles 1986)

Surface roughness will now be discussed before explaining some of the methods which can be used to evaluate the contact conditions in rough surfaces.

2.2.1 Surface Roughness

All surfaces are rough. This roughness is usually imparted on components during the machining and finishing processes. In order to predict the performance of a component in

service, particularly its fatigue life, it is important to measure and characterise its surface roughness.

There are many parameters for quantifying surface roughness in two-dimensional profiles, as this is the most frequently used measuring method for surfaces. These parameters can be grouped into two categories, ideally, a parameter from each is needed to adequately describe the surface topography (Sayles 1982):

- Height parameters, and
- Spatial parameters.

Two of the most frequently used height parameters are the centre line average (CLA or R_a) (BS 1134 1961) and the root mean square roughness (R_q or σ) (explained by Thomas 1974, amongst others).

Spatial parameters give an idea of the spacing between asperities. Two common measurements are the average wavelength, λ_a, (explained by Whitehouse 1994, amongst others) and the correlation length, β^*, (Whitehouse & Archard 1970).

The analysis of a surface profile generally involves identifying the irregularities to be measured and separating them from the remainder of the roughness. One can apply a long wavelength filter by limiting the length over which an individual measurement is made: this is known as the 'sampling length' and will cut out waviness if it is not required. The sampling length must be long enough to be representative of the roughness in at least one area of the surface and either short enough to exclude the waviness or long enough to include it, as may be required. The profile can also be filtered once it has been measured using the appropriate equations, this is best done when the profile is digitised in a computer. There are two types of filter: high pass to remove the longer wavelengths and low pass to remove the shorter wavelengths.

One can therefore define a measured profile using the above parameters. The surface profiles used by the author were measured using a Talysurf described next.

2.2.2 The Talysurf

The stylus surface measurement system used in the present work was the Form Talysurf (Figure 2.2.2), which gives a two-dimensional roughness measurement of a surface.

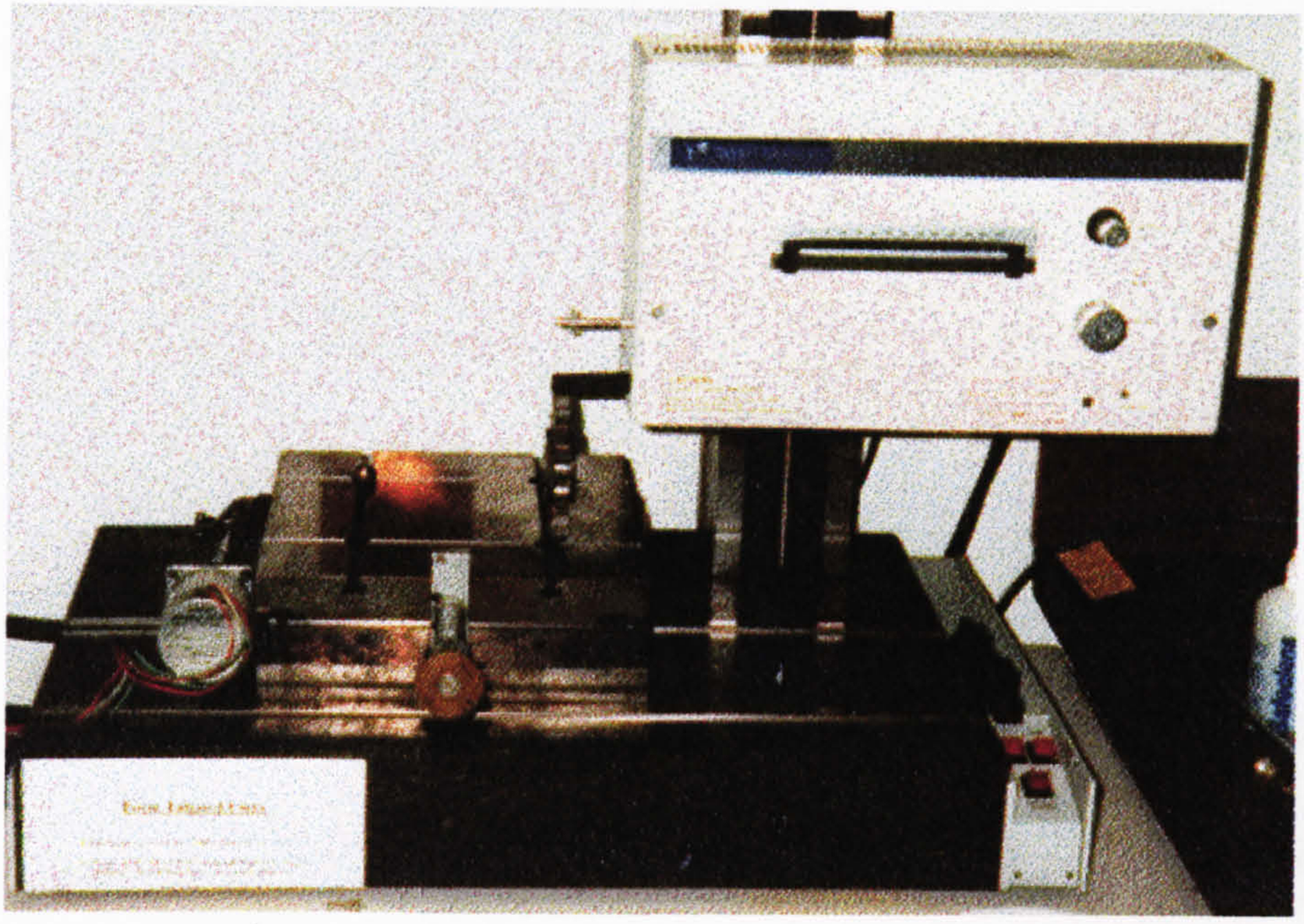


Figure 2.2.2 The Talysurf

This instrument has a traverse unit (Figure 2.2.3) which employs a sharp, 2 μm tip radius, diamond stylus coupled to a two axis laser interferometric transducer. The stylus crosses the surface at a constant speed and produces an analogue voltage signal proportional to its vertical movement. The trace is digitised at a suitable sampling interval and the output is coupled with a computer from which statistical data can be evaluated. The Talysurf itself has two profile filters: a short wavelength one given by the stylus tip radius and a long wavelength given by the sampling length.

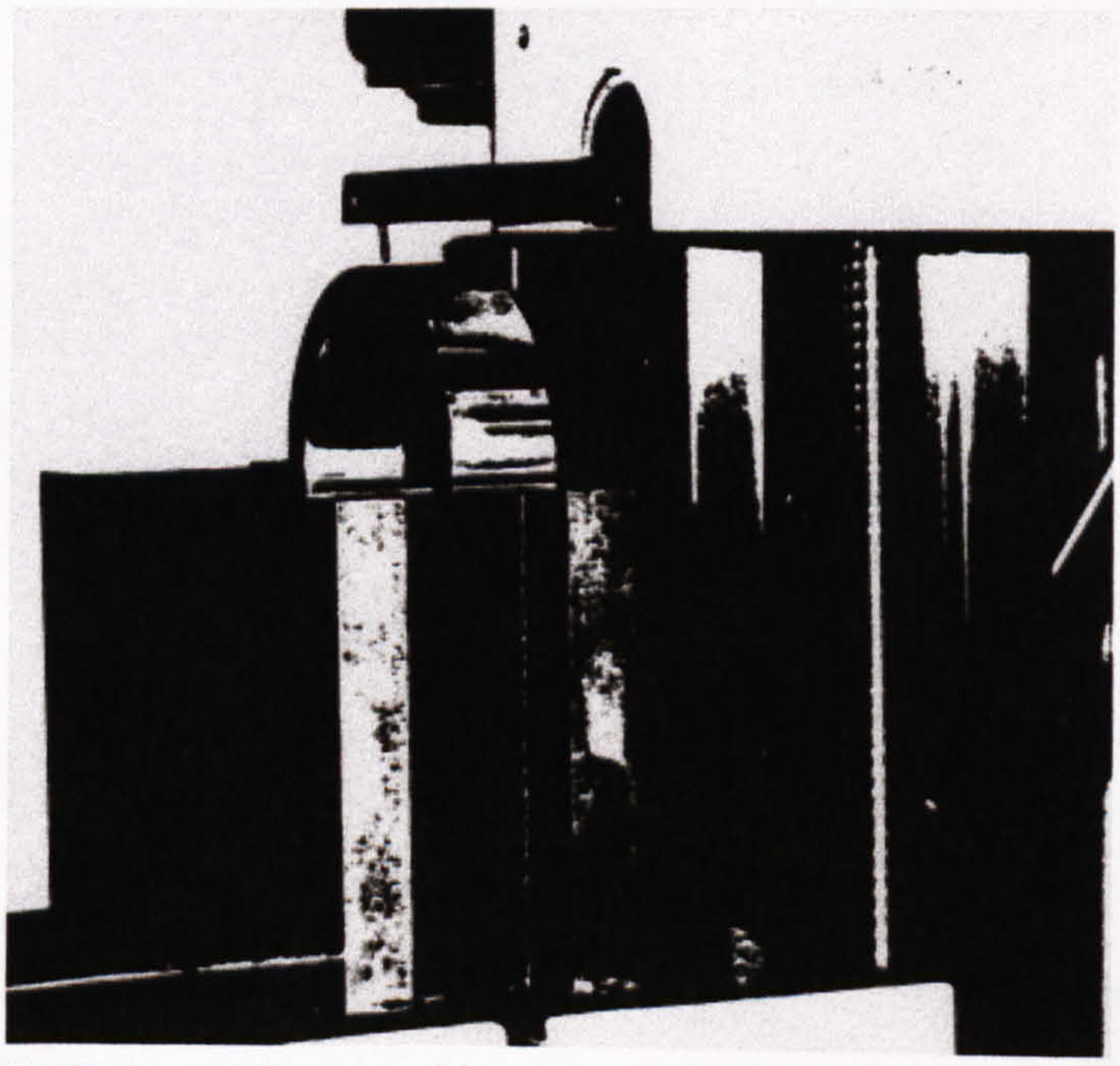


Figure 2.2.3 The Talysurf Traverse Unit

The main source of error in the set-up is that the stylus is not a point, but has finite dimensions. It will, therefore, fail to follow the peaks and valleys exactly and, hence, will produce a distorted record of the surface. The horizontal resolution therefore depends on the stylus' dimensions. The Talysurf has a stylus shaped like a truncated pyramid with 90° included angles between opposite faces, so, a profile containing peaks and valleys of small curvature, or slopes steeper than 45°, could be misrepresented. This, however, is not a problem in the measurement of real surfaces because their slopes are usually low.

The way in which profiles are commonly presented can be misleading; a slope of 1° is almost imperceptible to the human eye. The vertical magnification on profile charts is, therefore, greatly exaggerated over the horizontal (100 times for example, Parsons 1970), giving a false impression of what the surface profile is actually like (Figure 2.2.4).

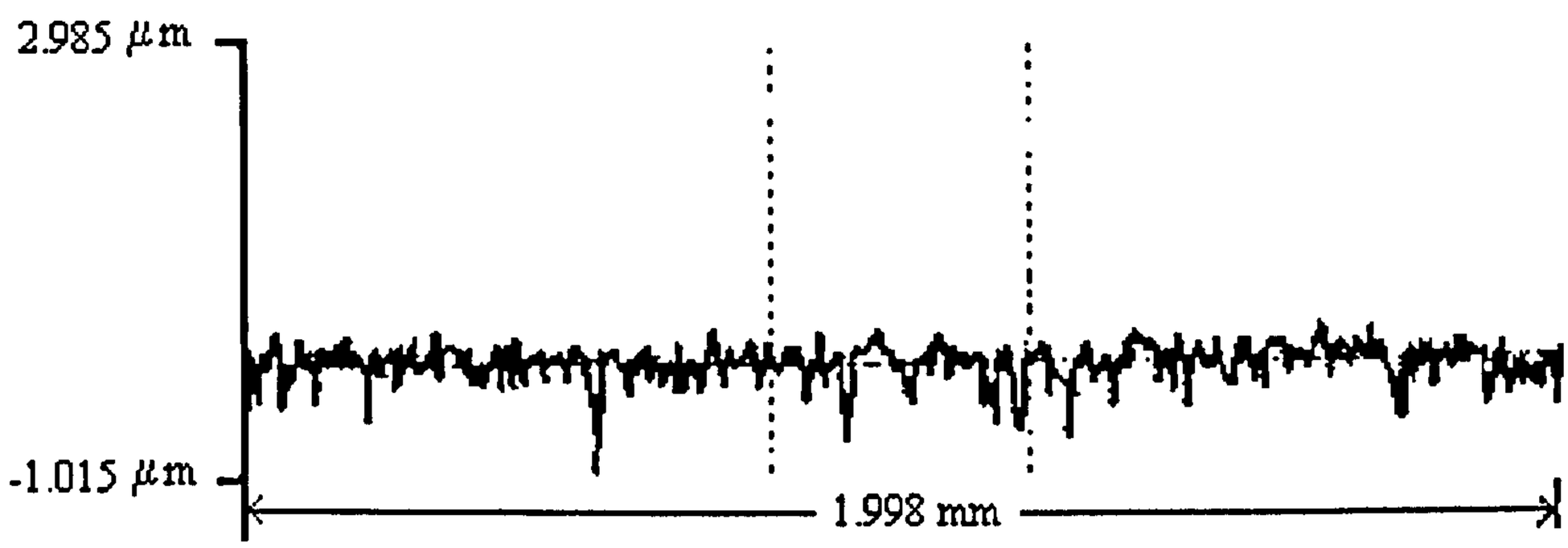


Figure 2.2.4 Output Display on the Talysurf

Finally, it is also worth noting that, the roughness measured will depend on trace direction for anisotropic surfaces, such as ground gear teeth (Thomas 1982).

2.2.3 Static Contact of Rough Bodies

Having seen that real surfaces are rough, a review of the literature on rough body contact is given here. There have been two approaches to the study of the effects of surface roughness and discontinuous contact on the results of conventional contact theory. These are analytical and numerical solution techniques.

- Analytical techniques use the general approach of reducing the measured topography to some statistical properties of the surface, combined with asperity shape to model the real surface; and

- Numerical techniques, which have been developed since the advent of computers, where real measured data can be used as an input for numerical contact analysis. The contact of rough surfaces can be simulated without the need for statistical modelling.

2.2.3.1 Analytical Techniques for Rough Surface Analysis

An example of an analytical approach to model the contact of rough surfaces is work done by Archard (1957). He pointed out that, although it was reasonable to assume plastic flow for the first few traverses of one body over another, one could not assume this for machine parts which experienced millions of cycles during their life. He also suggested that the surface asperities may flow plastically at first, but they must reach a steady state in which the load is supported elastically. He developed a theory which considered an asperity covered in microasperities and each of these with micromicroasperities which gave successively closer approximations to the law stating that the real area of contact was proportional to the applied load. This, perhaps, could be used to explain Amonton's laws of friction, where friction is proportional to load, for elastic asperity contacts. He also showed that the number of asperities in contact was proportional to the load as the scale of the asperities got smaller.

Another important study to determine the elastic-plastic effects in surface contacts was carried out by Greenwood and Williamson (1966). They used a statistical analysis to model a rough surface as spherically capped asperities of constant radius, with heights which varied randomly according to an exponential distribution. They derived the following set of expressions for a rough, nominally flat surface relating applied load, area of contact, and number of contact spots:

- the area of contact was proportional to the load;
- the number of contact spots was proportional to the load; and, finally,
- the average contact size was independent of load.

On this basis they derived a parameter which indicated whether contact would be elastic or plastic: the 'Plasticity index', which was described as a ratio of elastic hardness to the real hardness. They showed that most materials had plasticity indices such that plastic flow of the asperities occurred under the lightest of loads, except for especially smooth surfaces. These values and the definition hold for a particular surface model considered

(Gaussian approximated by the exponential distribution), but they considered that the concept was a general one.

A disadvantage of the above theory is that the model considers all the asperities to be identical except in their heights, which certainly does not represent a real surface. Another drawback of this analysis is the assumption of a constant summit radius of curvature; this leads to an underestimation of the degree of plastic contact because it is the high asperities which suffer the greatest deformation, and these tend to be sharper than the low asperities.

These models yield important results about the average properties of the contact of rough surfaces, but the real pressure distribution and deformed shape is lost due to the statistical nature of the approach. The availability of computers has led to the development of surface measurement and analysis systems in which real measured data is used. The models use numerical solution techniques, which enable the contact of rough surfaces to be simulated without the need for statistical modelling (these solutions were previously impracticable to solve, due to the computation involved).

2.2.3.2 Numerical Techniques for Rough Surface Analysis

If the contact is non-Hertzian, a rough or conforming contact, for example, there is no analytical solution in closed form and one must therefore use a numerical method (as described in Johnson 1985). The aims of these models are to predict the pressure distribution and model asperity contact in an elastic manner; giving individual asperity deformations by using real measured rough surfaces, rather than statistical models of surface topography. The rough surface could come directly from data recorded on the stylus measuring equipment described earlier.

One must determine the distribution of normal pressure which satisfies the boundary conditions at the interface, for a contact area whose shape and size may not be known at the outset.

The starting assumptions for such a numerical contact model (Webster & Sayles 1986) are:

- The strains are small compared to the overall surface geometry, leading to linear elastic theory equations;

- Inside the contact region the penetration is just equal to zero and the surface pressures are greater than or equal to zero;
- Outside the contact region there is no penetration and the normal surface pressures are zero;
- The surface slopes are reasonably small so that forces act normally to the surfaces;
- Tangential stresses and displacements are ignored, i.e. the contact is frictionless, or the surfaces are of equal elastic modulus.

A continuous distribution of pressure is replaced by a discrete set of pressure elements and the boundary conditions are then satisfied at these discrete points. The form of the pressure element has to be decided and the contact surface has to be divided into segments of the appropriate size. The solution then involves imposing rigid body movement to the upper surface vertically downwards to obtain an overlap of the two surfaces. The sum of the deflections in the two bodies, plus the initial gap at any contacting point, is just equal to the geometric overlap.

From the shape and assumed elemental pressure distribution, it is possible to use half space theory to derive expressions for the displacements anywhere on the surface, due to an applied pressure on a particular element. The matrix of displacement coefficients C_{ij} is needed, which expresses the displacement at a general point I due to a unit pressure element centred at point J.

This leads to a set of linear simultaneous equations that relates displacements to pressures. The total load carried by the contact is related to the values of the pressure elements by $P=A\Sigma p_j$, where A is a constant depending on the form and size of the pressure element (for a uniform pressure element A is the surface area of the element). In order to find the values of the adjacent columns of uniform pressure, acting on discrete segments of the body, which best satisfy the boundary conditions a direct, or matrix inversion, method in which the boundary conditions are satisfied exactly at specified matching points, usually the mid-points of the boundary elements can be used. The total displacement at a given point is merely the sum of the displacements due to all the elemental pressures. Once the solution for the elemental pressures has been found the elements where the pressures are negative are removed from the assumed contact region and a new set of contact points are derived for which the simultaneous equations are solved again. The total normal load, calculated by integrating the pressure distribution, is

compared to the desired value and the rigid body overlap adjusted accordingly until a solution giving the required load has been achieved, converging on a particular set of contacting points.

The author has written such a program, based on a solution method by Allwood (1997), using a matrix inversion method in which the boundary conditions are satisfied exactly at specified matching points, in order to find the values of the adjacent columns of uniform pressure acting on discrete segments of the body. The advantages of this particular method are that it solves the derived matrix of equations for all the contact points by Gauss-Jordan elimination (described in Carnahan et al. 1969) once and then minimises the solution time by working out the matrix inversion only for those points which have changed, by either having been assumed to be in contact and not being, or vice-versa. It is the first Gauss-Jordan elimination which takes up the most solution time, subsequent iterations are fast. Assuming one makes an accurate initial estimate of the surface points in contact, this model is a good method for surface contact analysis.

Another example of a numerical solution, used by the author, was that developed by Webster and Sayles (1986). It is similarly a two-dimensional linear-elastic numerical technique which simulates the dry, elastic, frictionless contact of a real rough surface (modelled as an elastic half-space) normally loaded against a smooth cylindrical body. The set of linear simultaneous equations that relates displacements to pressures are solved by Choleski factorisation (described in Carnahan et al. 1969), which takes advantage of symmetry in the matrix. The initial and deformed profiles and the pressure distribution evaluated are stored as a data file. Some of the data evaluated from the analysis of rough surface contacts using this model is shown in Figure 2.2.5.

A three-dimensional numerical technique to model surface deformation and stress, developed by West and Sayles (1988), was also used in this study, and results obtained with it will be discussed in Chapter 8.

The numerical analyses described are, however, specifically for purely elastic contact, where an assumption of no plastic flow is made. There is a need to consider plastic deformation in a complete analysis because in a real surface the roughness is random, and some high, sharp asperities will deform plastically causing permanent surface deformation, even at moderate loads. The full solution of problems involving plasticity are complex, therefore, to make the 2-dimensional model described here more realistic, a

simple plasticity model option was included to simulate the more realistic elastic-plastic mode of contact. An example of the model output using this plasticity criterion is shown in Figure 2.2.6. One can see the shortcomings of the model, as asperities are loaded together to a limiting value of p_y. This approach may be reasonable for isolated asperities with low slopes, in practice the plastic deformation of neighbouring asperities would interact in the sub-surface and asperity persistence must be addressed (Sayles 1994).

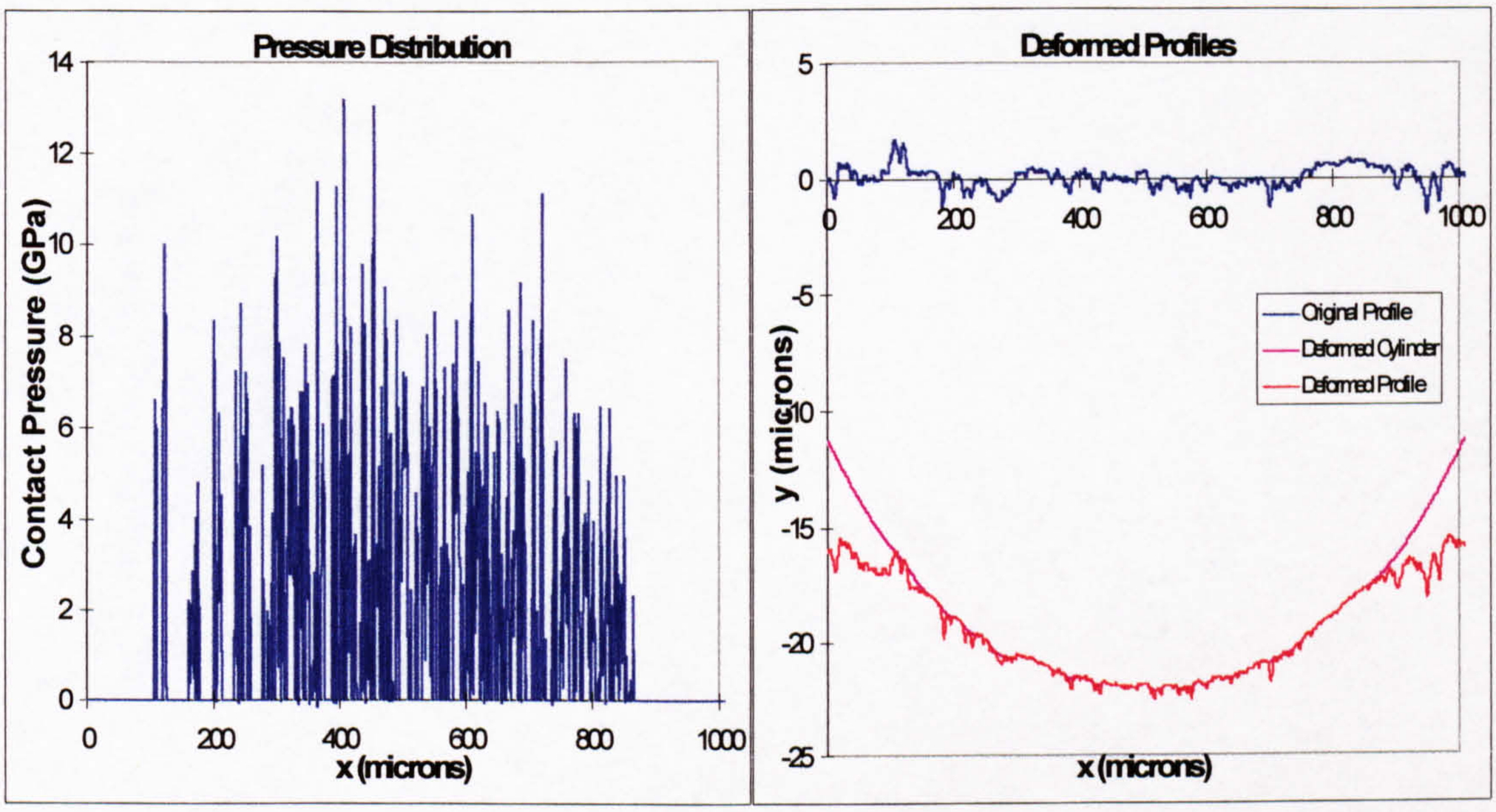


Figure 2.2.5 Output From the Rough Surface Contact Model (Webster & Sayles 1986)

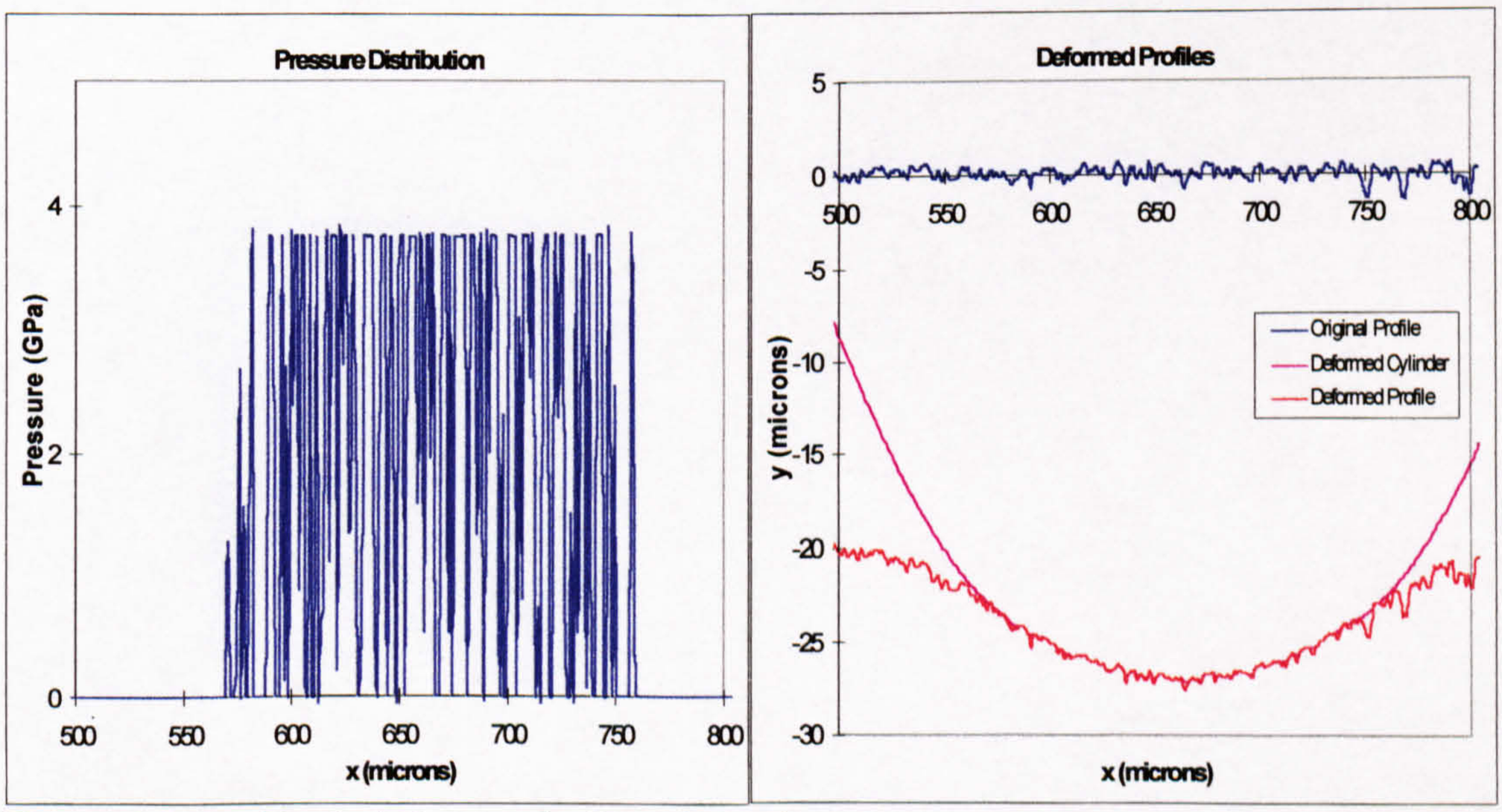


Figure 2.2.6 Typical Output the Rough Surface Contact Model using "Plasticity" (Webster & Sayles 1986)

One must comment on the fact that these models simulate dry contact, which is not the case in most tribological contacts. The models will not precisely reflect the pressure

distributions arising from the lubricated contact of rough surfaces. However, they can be used to give an indication of the contact conditions when the ratio of film thickness to roughness is low and there is considerable surface contact, many gear contacts fall in this category (Olver 1992). The models also allow comparison of the merit of various surface finishing techniques.

Finally, it has also been assumed that the materials being analysed are isotropic and homogeneous, as mentioned for Hertzian smooth surface analysis. The contact of coated, rough surfaces has to be treated differently and this has been analysed by Cole and Sayles (1992). They varied the thickness and the ratio of elastic modulus of the coating and the substrate to examine the changes in the contact pressure. From their results, it can be seen that when the elastic modulus of the coating and the substrate are similar, the presence of the layer has little influence on the pressure distribution, but when the coating layer is stiffer than the substrate, the pressure peaks generated become much more pronounced. However, the surface engineering processes considered in this study (carburising and nitriding) have little effect on elastic properties, so the bodies may be considered homogeneous.

2.2.4 Moving Contacts on Rough Bodies

In this section the literature concerning the effects of motion on rough surface topography and stresses are briefly described and then running-in is given particular attention. The effects on rolling contact fatigue are considered in Chapter 3.

In a normally loaded, non-conforming, pure rolling, rough contact the surface pressure would be similar to that shown in Figure 2.2.7, with pressure peaks at the asperity contacts. The motion would make the pressure distribution sweep through the contact. When sliding is included there will be a tangential friction force opposing the direction of motion on both surfaces. With sliding, a single asperity may make a number of contacts with opposing asperities during its pass through the bulk contact (Hamer et al. 1991). This will create a greater number cycles of stress as individual pressure fluctuations sweep through the contact and are imposed on the main pressure distribution, which also moves along. This phenomenon has been analysed by Hamer et al. (1991) and Kim and Olver (1997) in relation to fatigue life modelling.

If a virgin surface slides past another surface of comparable or greater hardness, its topography will undergo a change, with the roughness of its contacting surface usually decreasing. This is called running-in.

There are two mechanisms that lead to running-in. On the one hand, there is change in surface shape by redistribution of the material due to plastic flow, without any loss of material; and on the other hand, there are the various wear mechanisms, all of which involve net material loss. The alteration of the surface profile, however, is usually the result of both processes taking place together.

Such processes lead to shakedown, with a reduction of friction and the attainment of a stable 'run-in' surface; or, alternatively, to the development of damaging features such as cracks. Shakedown is the process whereby a cyclically loaded structure, which deforms plastically during the first few applications or passages of load, achieves a steady cyclic state in which the deformation is perfectly elastic. During subsequent passes the conformity between the surfaces increases, the contact area is increased, and the contact pressure is reduced. The maximum load for which shakedown occurs is known as the 'shakedown limit'. Loads in excess of this limit would cause repeated plastic deformation in the steady state, leading to fatigue or ductile failure.

Greenwood and Williamson (1966) showed that repeated contact between surfaces, as in normal sliding, leads to the reduction of the plasticity index (described earlier), ψ, from an initial value in the plastic range, to a value in the elastic range (this can be seen in Figure 2.2.7).

However, the wear debris produced in sliding could reverse this trend and, by damaging the surface, could prevent ψ from reaching the elastic range. They concluded that the nature of the deformation is more sensitive to the surface finish than to the applied load.

Rowe et al. (1975) showed that when rough surfaces were lightly loaded, where only the higher asperities exceeded the elastic limit, the running-in process was predominantly one of local plastic deformation and abrasion. They found that if one slider was soft and the other was hard this behaviour would be seen only if the harder member was smooth. They concluded that the initial surface finish of the softer material was of little importance, within practical limits, and that there was no need for a high degree of finish, which entailed a greater danger of seizure. The harder surface finish of the slider, however, should be 'economically optimised'.

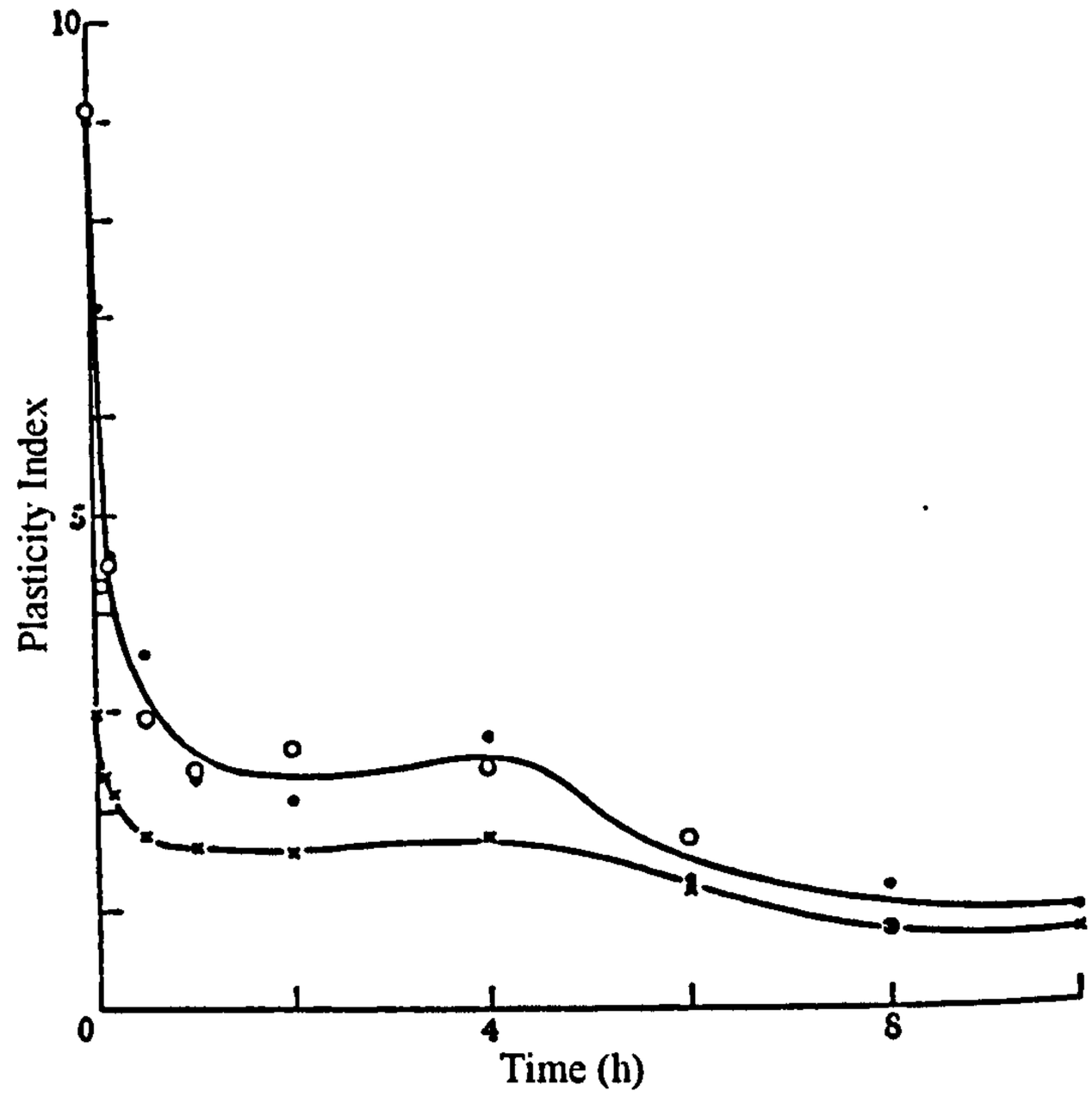
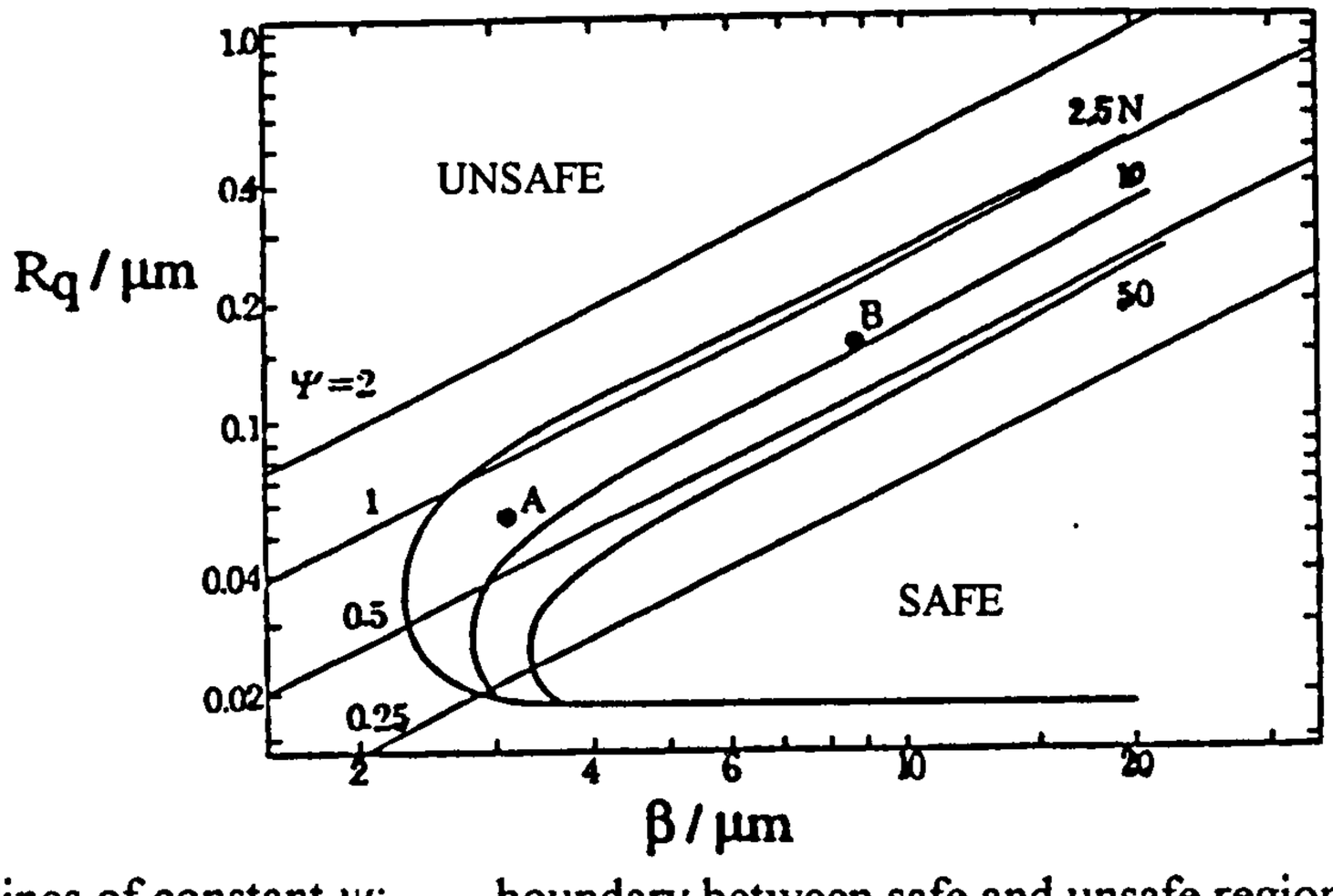


Fig 2.2.7 The Effect of Continued Sliding on the Plasticity Index (Greenwood & Williamson 1966)

Hirst and Hollander (1974) showed that, in the boundary lubrication regime (described later), there could be a large change in friction and wear between two surfaces as the temperature was raised. In the range of temperature and load in which this transition occurred, they suggested that R_q and β^*, the *RMS* roughness and the autocorrelation length respectively, may be important parameters in defining the boundaries for the safe operation of surfaces. By rubbing stainless steel sliders of different roughness (having a wide range of R_q and β^*) they found a region of 'safe' R_q and β^* outside of which severe stick slip occurred (see Figure 2.2.8). The upper boundary was shown to be controlled by the plasticity index, as this represented the transition from a predominantly elastic state to a significantly plastic one in the unsafe region. From this they concluded that rough surfaces could lead to seizure or severe wear, and they must be smoothed by careful running-in. The lower boundary, for very smooth surfaces, e.g. $R_q < 0.02$ μm, was also susceptible to damage if the lubrication failed, as immediate seizure would occur. The reason they suggested for this occurrence was that 'there were no longer any interruptions in the surface to prevent the growth of small adventitious welded junctions'. In conclusion, it is therefore desirable for successful boundary lubrication that surfaces should be neither too rough, nor too smooth.



lines of constant ψ; —— boundary between safe and unsafe region

Figure 2.2.8 RMS Roughness Versus Correlation Length Map for Abraded Surface (Hirst & Hollander 1974)

Poon and Sayles (1992) revisited this research, particularly the unsafe sliding behaviour, irrespective of the correlation length, at low levels of roughness. They confirmed the upper boundary of Figure 2.2.10 but found a different shape to the curves due to the lower boundary actually being dependent on the RMS roughness and β^*. They commented on the difficulty in establishing these 'fuzzy' boundaries. They examined the factors affecting the region two sliding bodies occupied on this diagram. They found that to promote safe boundary lubrication of the contact, an increase in hardness would help avoid plasticity, a modulus increase would avoid excessive contact and roughness could also be controlled to have appropriate values.

Ostvik and Christenson (1968) carried out experiments using a two disc machine to get an insight into the changes which occurred in a surface during the running-in process. Their results showed that surfaces that had been run-in had a much larger load-carrying capacity, or could work more satisfactorily at smaller film thickness. This effect was caused by a gradual conforming of asperities of the two surfaces to each other, which in the preliminary stages was mainly due to a reduction of the height of the highest asperity peaks, but also to an overall reduction in the average slope of the asperities.

Olver et al. (1986) also observed that at a low slide roll ratio, with the three disc contact machine described later on, the roughness of the softer surface tended to be reduced, but that of the harder persisted, even when the hardness difference was less than 10%.

Morimoto and Tamamura (1992) studied the effect of different materials in contact on running-in. Their experimental set-up consisted of a cylindrical steel bar, with a machined surface, being plastically run-in (burnished) under a rolling contact, using a lathe and a ball as the tool. In general, they found the burnishing force applied had a pronounced influence on the roughness of the run-in surface. An extremely small force was insufficient to plastically deform the asperities of the turned surface. In contrast, an excessive force caused swelling on the already burnished surface by means of plastic deformation, the surface roughened and additionally ran a risk of adhesion or seizure.

According to Johnson and Shercliff (1992), running-in is influenced by three factors:

- Residual stresses that are induced by the initial plastic deformation on first loading, act so as to inhibit yielding in subsequent loading;
- Geometric changes arising from initial plastic deformation may change the distribution of load so as to reduce the level of the applied stress; and.
- Strain hardening of the material may raise the elastic limit.

In order to model the behaviour of rough surfaces in sliding contact, the interaction between two cylindrical elastic-plastic asperities was analysed by Johnson and Shercliff (1992). The analysis was based on the hypothesis that the profiles of the asperities deformed plastically in such a way that in the steady state they were loaded to the shakedown limit (or less) of the material throughout the contact period. If the shakedown limit were exceeded at any point during the contact period, then further plastic deformation of the profile would occur to reduce the contact stress.

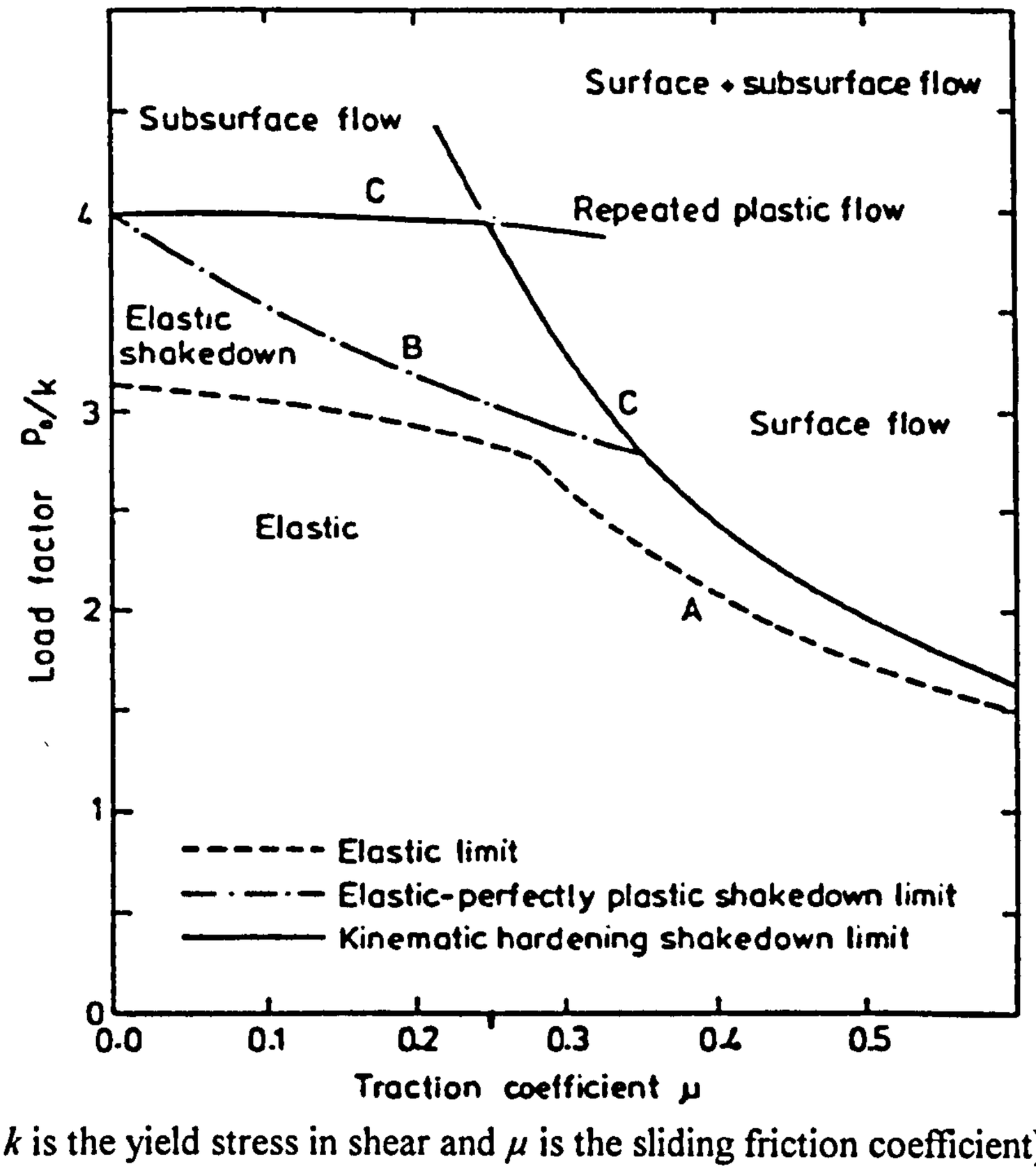
For a long cylinder, rolling and/or sliding on a plane surface, exact shakedown limits have been found for a perfectly plastic solid and for a kinematically hardening solid. These can be seen in Figure 2.2.9 a 'shakedown map'.

It should be noted that for low friction (e.g. μ<0.25), shakedown is controlled by sub-surface stresses and the shakedown limit significantly exceeds the elastic limit. For high friction (μ> 0.25), the material yields at the surface and little protection is then provided by either residual stresses or strain hardening.

This analysis of the shakedown of a pair of lateral asperities was used by Kapoor and Johnson (1993) when developing a theory to describe the plastic 'running-in' process. They considered the repeated sliding contact of a rough surface with two-dimensional

cylindrical asperities of equal radius, but random (Gaussian) height, over a hard regular surface with two-dimensional cylindrical asperities of equal height and radius.

They assumed that during sliding contact all asperities above a certain height developed a contact pressure high enough to undergo plastic deformation because the contact pressure, p_o, exceeded their elastic limit. Residual stresses would develop, asperity height and profile would change, and the material may strain harden. This process continued until the height and shape of the asperities had changed such that the contact pressure did not cause any further plastic flow and the load was carried elastically, the other asperities either did not make contact or did not reach the elastic limit.



(k is the yield stress in shear and μ is the sliding friction coefficient).

- Curve A is the elastic limit / k, below this yield does not occur even on first loading.
- Curve B is the shakedown limit / k for a perfectly plastic material. The difference between A and B shows the influence of residual stresses in promoting shakedown.
- Curve C is for a kinematically hardening material and the difference between curves B and C shows the influence of strain hardening.

Figure 2.2.9 Shakedown Map for the Steady Sliding of Two Cylinders (Johnson & Shercliff 1992)

They admitted that wear in early sliding also assisted the process of shakedown by reducing asperity heights but that, in lubricated sliding, wear reduced significantly after running-in. The predictions of the above theory might therefore be expected to apply, even if there was some wear in the early cycles of sliding.

They examined somewhat idealised conditions:

- Lateral asperities, in which the sliding motion was perpendicular to the lay of the roughness, as in ground gear teeth, and
- Longitudinal asperities aligned in the direction of sliding, as in a lathe-turned journal bearing.

The steady state topography of the deformed rough surface was found and, by integrating the load carried by each asperity in the shakedown state, they found the load carried by the surface in the steady state. The shakedown limits for the different asperity models are shown in Figure 2.2.10.

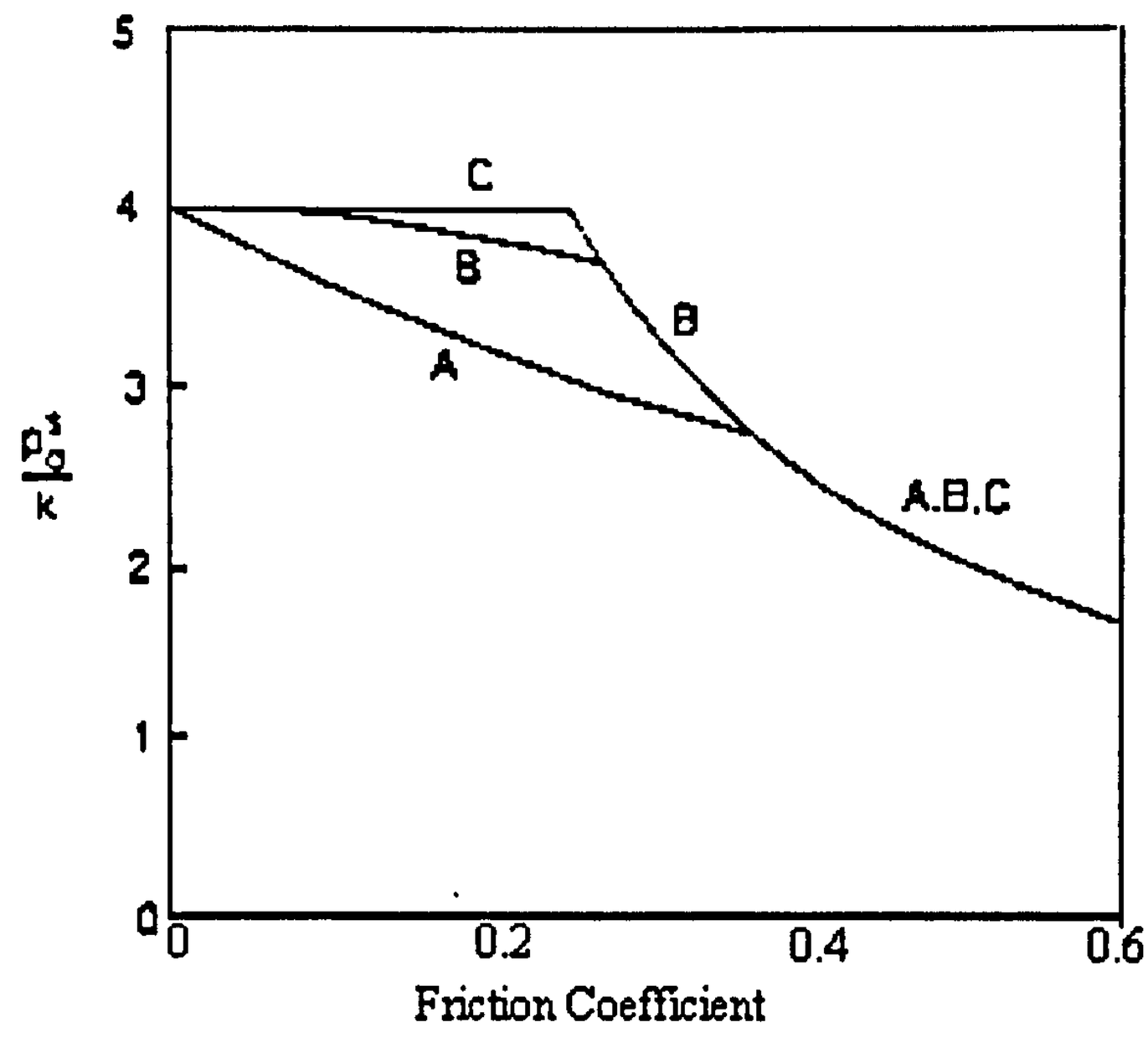


Figure 2.2.10 Shakedown Limits (Kapoor & Johnson 1993)

The literature in this section so far has described analytical techniques for modelling dynamic, rough contacts. There are few numerical models because of the complexity of the analysis. However, the numerical model by Webster and Sayles (1986) has had

subsurface stresses, including those due to any sliding friction, incorporated into it by Bailey and Sayles (1991). Their model produced similar stress fields to those given by Smith and Liu (1953) with smooth surfaces. With rough surfaces it produced high shear stresses concentrated locally near the surface, as a result of localised asperity contacts giving rise to high contact pressures. The typical Hertzian stress field is retained away from the contact (see Figure 2.2.11). This analysis has been further adapted by Kim and Olver (1997) to enable fatigue life modelling.

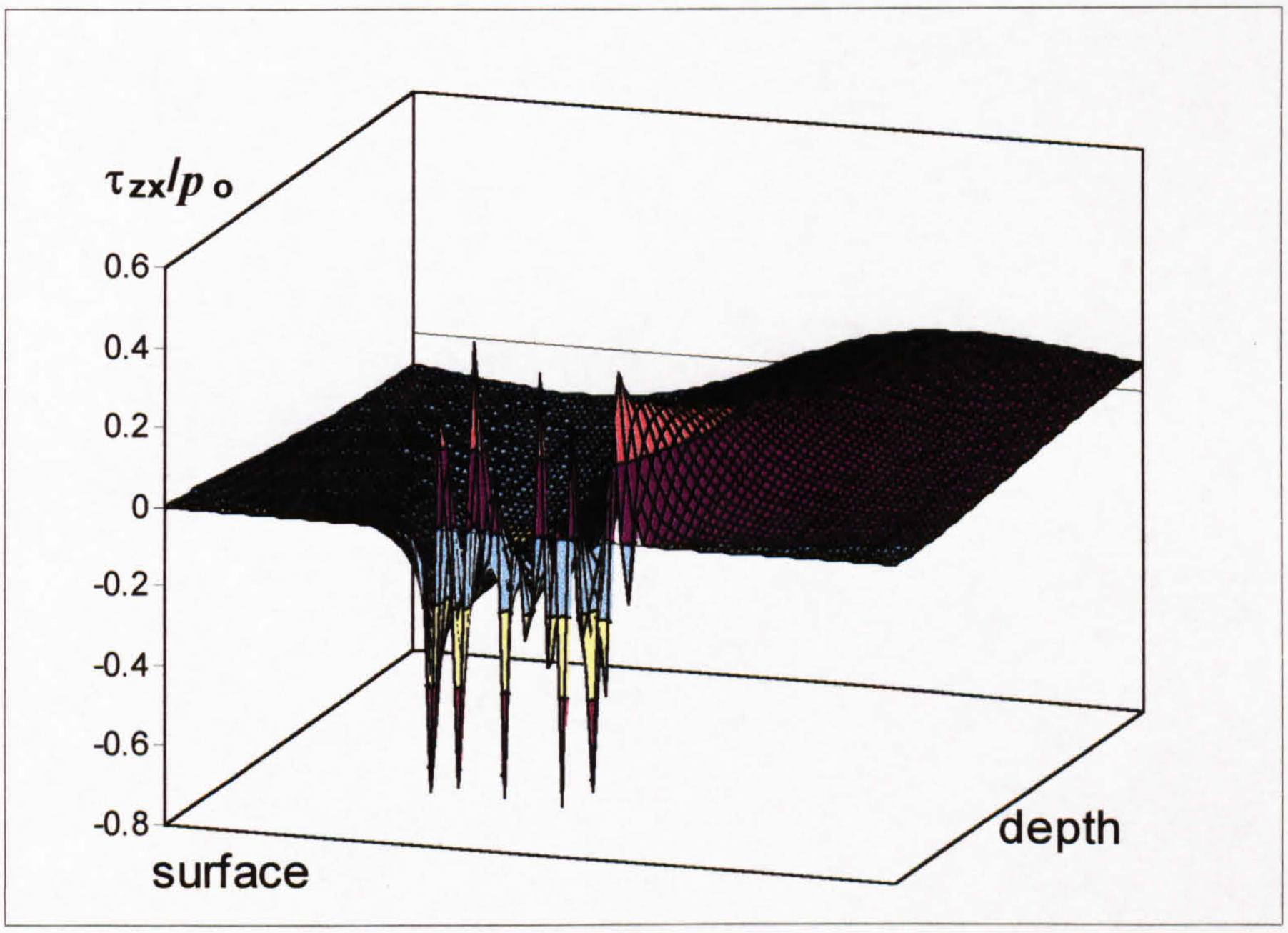


Figure 2.2.11 Orthogonal Shear Stress Distribution for a Rough Surface (using program by Kim & Olver 1997)

2.3 Lubricated Surfaces in Contact

Up to now only unlubricated contacts have been considered, the presence of a lubricant will reduce the contact stresses and friction by separating the two rough surfaces with a low shear strength film.

Bowen (1978) stated that the primary purposes of a lubricant were to reduce friction and remove and redistribute heat. The secondary purposes were to reduce wear, offer satisfactory pitting life, prevent rust and corrosion, and remove wear debris. In Kelly and Lemanski's (1967) review of lubrication of involute gears they suggested the main uses for lubricants between contacting bodies were to reduce friction and surface damage by carrying the load and separating the two surfaces, to remove debris, and cool the

BIBL LONDON

surfaces. Which aspects of lubrication are most important will most probably depend on the application of the lubricant.

Of prime importance in lubricated contacts is the film thickness, which is critically dependent on viscosity, increasing in value with it. It would therefore seem that having a viscous lubricant to give a large film thickness would be the best approach to avoid surface contact, and hence reduce damage. It is, however, not always desirable to have the most viscous lubricant as it may not circulate well, giving heating and debris problems and greater power losses from churning, which in turn produces more heat. Often it is the cold start requirements that limit the maximum working viscosity of most practical lubricants. Viscosity is highly dependent on temperature, so this too is an important aspect when considering the lubricant in a contact.

2.3.1 Smooth Lubricated Contacts

2.3.1.1 Hydrodynamic Lubrication

If one simplifies the Navier-Stokes equations for a fluid element, by neglecting inertial forces, one can derive the Reynolds' equation (Reynolds 1886), which describes the pressure distribution in a fluid between two solid surfaces when the surfaces slide or are squeezed together. The load, friction force, friction coefficient, and flow can all be calculated from these equations for hydrodynamic film geometry, which applies usually to conformal contacts, such as journal bearings. The lubricant film is usually large enough to prevent asperity contact, and the pressures are in the region of hundreds of MPa.

In hydrodynamic lubrication, the friction is dependent on speed, load, and viscosity of the lubricant and is largely insensitive to the nature of the surfaces, or of the lubricant, other than its viscosity (Benedict & Kelly 1961).

2.3.1.2 Elastohydrodynamic Lubrication

If one applies the Reynolds' equation to non-conforming elastic contacts, where the load is distributed over a small area and hence there are high local pressures, an oil film of very low thickness would be derived. It was therefore once thought that these contacts operated in what is known as boundary lubrication. However, it was then realised (Cameron 1954) that the high pressure in a non-conforming contact would have two

beneficial effects on film formation: it would increase the oil viscosity in the contact and elastically flatten the contacting surfaces.

These effects were included in the Reynolds' equation by Grubin and Vinogradova (1949), and realistic film thicknesses in the order of a tenth of a micron, were derived. This was called the elastohydrodynamic (EHD) lubrication regime. The pressure-viscosity relationship assumed was that given by the Barus equation: $\eta = \eta_o e^{\alpha p}$ (Barus 1893), where η is the viscosity at pressure p, η_o is the atmospheric pressure viscosity, and α is the pressure viscosity coefficient. The contact deformation was that given by Hertz theory, described earlier. The Hertz equations are strictly only for static, unlubricated contacts, but in practice they provide good approximations for this lubrication regime.

In EHD there is a central contact region of almost uniform film thickness and there are constrictions at the rear and sides of the contact. The EHD film thickness is almost entirely dependent on the fluid viscosity in the inlet zone, which depends on surface temperature. However, film thickness affects friction, which in turn affects heat generation and bulk temperature, and hence inlet viscosity. Martin (1978) has reviewed friction in EHD, with particular attention given to gears. There is no interaction of asperities, and friction is a function of fluid properties and in certain situations the surface quality.

There are various film thickness equations for EHL which have been derived semi-algebraically or numerically by Grubin (1949), Dowson-Higginson (1977), and Dowson-Hamrock (Hamrock & Dowson 1977); they apply to fully flooded, isothermal systems. They show that film thickness in EHL depends strongly on the lubricant viscosity, entrainment speed, and, to a lesser extent, on the pressure viscosity coefficient. They also show that load and Young's modulus have a minimal effect.

EHD theory makes the basic assumptions that flow in the lubricant film is steady, but also inertialess, isothermal, and incompressible, while the lubricant is considered Newtonian. Two important effects which can reduce film thickness below values obtained from the above equations, are heating of the contact inlet (Murch & Wilson 1975) and starvation (Wedeven et al. 1971, Hamrock & Dowson 1981). One must also realise that the isothermal character of the film flow is probably no longer valid at high sliding velocities of magnitude normally occurring at the tips and roots of gear teeth.

Experimental measurement of films in highly loaded contacts is now possible, the results agreeing with EHD theory down to a few nanometres for pure hydrocarbons (Spikes 1997).

2.3.1.3 Mixed Lubrication

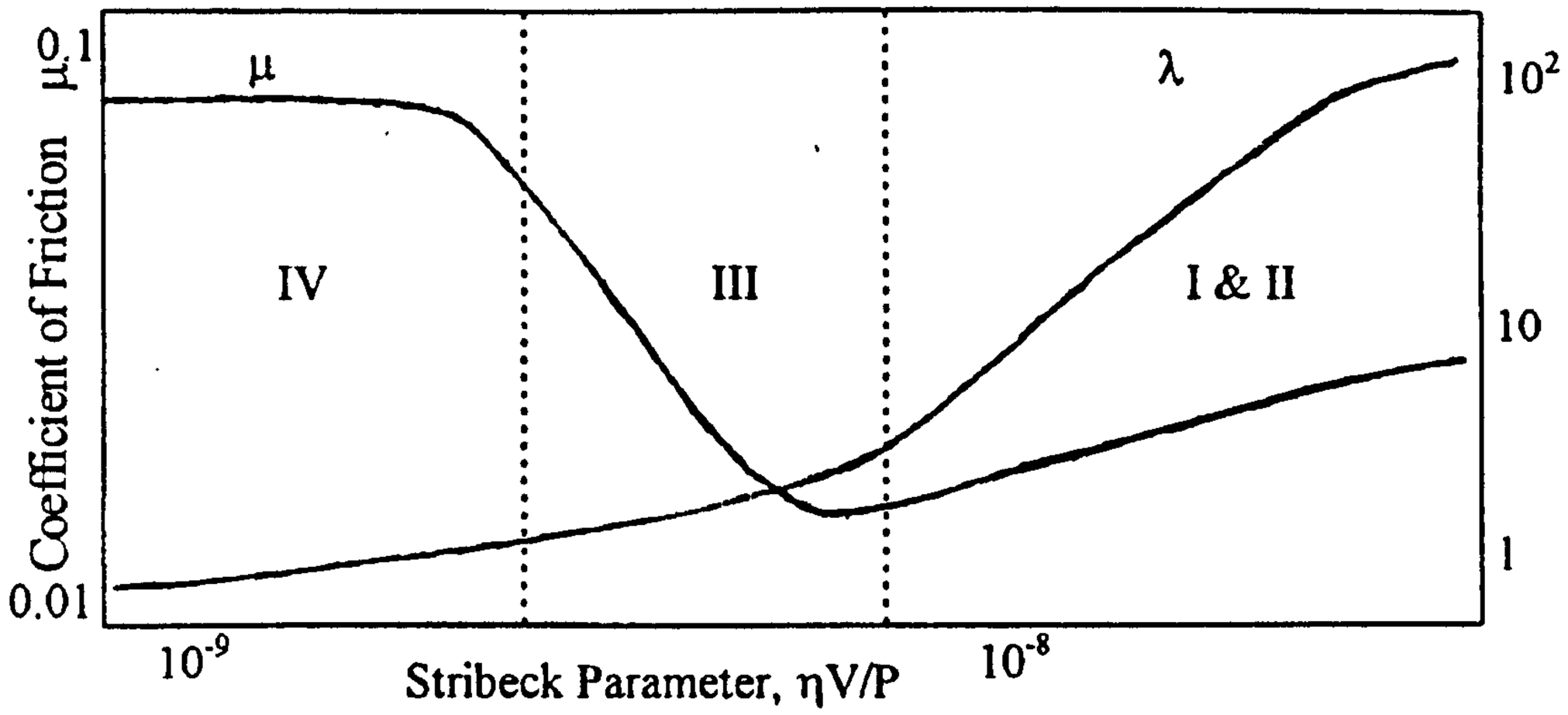
If the load and speeds are such that there is a very small elastohydrodynamic film, the contact moves into the mixed regime. In this regime the load may be carried partly by the lubricant and partly by the surface asperities. Despite there not being a full film, the lubricant greatly reduces friction and surface damage. This effect is extremely important, since many lubricated systems which might be expected, under ideal conditions, to operate under thick film conditions, in fact, spend part of their life in this regime (Martin 1978). This may result from excessive loading or heating, misalignment, poor manufacture, vibration, or continuous stopping and starting. Tallian et al. (1965) found partial, or mixed, lubrication, where load is shared by the asperities and fluid film, operated over a range $1<\Lambda<4$ (Λ, the lambda ratio, is described in Section 2.3.2).

2.3.1.4 Boundary Lubrication

If the film thickness is negligible when compared to the surface roughness, the load is carried mainly by the asperities and by and through the boundary film; the system is in the boundary lubrication regime (Spikes 1993). The subject has been reviewed by Campbell (1969), Spikes (1993), and Martin (1978). The surface characteristics and the properties of any adsorbed films determine the contact friction and the bulk properties of the lubricant, speed and load, have little or no effect (Benedict & Kelly 1961). Martin (1978), however, stated that the coefficient of friction may vary with load, sliding velocity, materials and lubricant, he did confirm that viscosity effects were small.

2.3.1.5 Regimes of Lubrication

The various lubrication regimes, and the effects they have on friction, can be seen in Figure 2.3.1, a Stribeck curve (Anghel 1998 attributed to Stribeck 1902). This relates the Stribeck parameter, a function of viscosity, velocity, and load, to the friction coefficient. The modified Stribeck curve shows the EHD regime on the same plot as the hydrodynamic regime (as in Hutchings 1992), though the friction evolution may be different, particularly at higher speeds (Anghel 1998).



I Hydrodynamic Lubrication
II Elastohydrodynamic Lubrication
III Mixed Lubrication
IV Boundary Lubrication

Figure 2.3.1 Stribeck Curve (Anghel 1998 attributed to Stribeck 1902)

In the full fluid lubrication regime shown in Figure 2.3.1 (on the right side) a fall in friction is due to thermal effects. There is an increase in friction as one moves into the mixed regime as there is occasional surface contact. The friction then levels off when the film is reduced further, corresponding to boundary lubrication. The point of transition from mixed to boundary lubrication is uncertain. A review of friction in gear teeth is given by Martin (1978).

2.3.2 Rough Lubricated Contacts

In conventional EHD theory it is assumed that the lubricated surfaces are perfectly smooth. Dowson and Higginson's (1977) equations are based upon the analysis of a model in which this assumption is made. This assumption of smooth surfaces would seem to be justified, provided that the minimum film thickness predicted by such theories is significantly greater than the height of any surface roughness features. In recent years the term micro-EHL has been used to describe the effects of rough surfaces on the mechanism of EHD lubrication (Chang et al. 1993 and Chang 1995). However, in many heavily loaded contacts, particularly those found between gear teeth and in rolling element bearings operating at high temperatures, the thickness of the oil film, according to smooth surface theory, can be of the same order as, or less than, the surface roughness. Under such conditions, some degree of asperity interaction is expected, and smooth surface theory no longer applies. This type of lubrication is known as mixed, or partial, EHL, as mentioned earlier.

Crook (1961) investigated the effects of running-in with a lubricant; after initial contacts had occurred, the discs ran in to approximately full film conditions (low loads and sliding speeds). It should be noted that this was true in the pure, or near, rolling conditions, where the contact was approximately isothermal. Where there is a large amount of sliding and high load, the film becomes dependent on the load by virtue of the effect of the load on the temperature.

Tallian et al. (1964, 1965) used electrical resistance techniques to examine roughness in EHL. A rolling four ball machine was used along with an electrical conductivity method for counting the number of contact spots with time. The surface profiles of run ball tracks were measured and were used to predict the average duration and frequency of these contacts. The predictions compared well with experimental values. The amount of wear taking place was measured with a radiotracer technique and was shown to be closely related to the amount of metallic contact. In a summary of their results (Tallian 1967), a dimensionless ratio of lubricant film to composite roughness, lambda, was shown to be an influential parameter governing wear and fatigue lives. They found that the lubrication was partial over the range $1<\Lambda<4$.

$$\Lambda = \frac{h_0}{R_{qc}} \qquad R_{qc} = \sqrt{R_{q1}^2 + R_{q2}^2}$$

It is worth noting that in disc machine experiments, the discs are usually finished by grinding in the circumferential direction (surfaces produced in this manner may be considered to have a two-dimensional finish), so that the entrainment of the lubricant is along the direction of the surface finish. This will contrast with the lubrication, on the asperity scale, of a surface with a finish lying perpendicular to the direction of entrainment, such as a gear tooth.

A model by Barragan et al. (1989) considered a theoretical surface with sinusoidal roughness. Their results showed that an increase in temperature in micro-EHL of circumferentially ground rollers had an effect which was similar to that produced by an increase in surface roughness. As temperature was increased, the asperity contacts tended to behave as 'isolated' contacts with the pressure in the valleys falling. The results also showed that in heavily loaded micro-EHL the minimum film thickness could be significantly less than that predicted by the Dowson-Higginson formula, for the same

operating conditions but with smooth surfaces. The model did not account for the nature of real surfaces, thermal effects, or non-Newtonian rheology effects.

The slide-roll ratio in the mixed EHD lubrication regime was shown by Smeeth and Spikes (1996) to not affect the film thickness predicted by EHD theory for slide-roll ratios of less than 30%. At higher slide-roll ratios film thickness was said to decrease with increasing sliding speed by as much as 20% of the value measured under pure rolling.

2.4 Conclusions

This chapter has provided an overview of the current knowledge on surfaces in contact. An idea of the complexity involved in solving the stress distributions on a surface and its consequent performance has been given.

The contact of gear teeth involves motion, roughness, lubrication, and running-in effects; all these aspects have been discussed here. Some simplifications must probably be made to allow an approximate analysis of the contact conditions. One could make the assumption that the contact is static, smooth, or ignore the lubricant.

A review of rolling contact fatigue follows this survey on non-conforming surface contacts, as this phenomenon arises from the cyclic stressing of contacting surfaces and is a major part of the present investigation.

Chapter 3 Rolling Contact Fatigue

Having discussed the interactions of surfaces in contact, the stresses, roughness and lubricant effects, and running-in, it is now appropriate to discuss rolling contact fatigue. This is one of the principal factors affecting the durability of gears, and is the main process being investigated in this research. In this chapter some of the literature on rolling contact fatigue is reviewed regarding definitions, main factors thought to affect it, mechanisms, models, and the statistical nature of the process.

3.1 Rolling Contact Fatigue

Rolling contact fatigue (RCF) is an important cause of failure in loaded, rolling-sliding, lubricated contacts and controls the service life of many components for a given load. Rolling suggests there is no sliding present but, as, in gearing, there is considerable sliding, particularly at the tooth root and tip, it is considered important to include sliding in this review of rolling contact fatigue failures.

According to Scott (1977), 'Rolling contact fatigue is characterised by the sudden removal of surface material and in some cases by the catastrophic fracture due to repeated alternating stress. The process has three phases: preconditioning of the surface prior to cracking, crack initiation, and propagation'. Rolling contact fatigue includes the following failure types: pitting, micropitting, and case crushing, which are described in detail in Chapter 4.

The first major study carried out on RCF was done by Way (1935) using a disc machine, although the phenomenon was known before then. He studied the pitting of rail steels with discs which were subjected to nominally pure rolling contact. Tallian (1967) reviewed RCF and surface distress and outlined four failure modes: wear, plastic flow, fatigue, and bulk or structural failure. Berthe et al. (1980) described 5 types of damage observed near pure rolling conditions: micropitting, sponges and flats (areas of high micropit density), macropits (areas where micropits have joined to leave a shallow trough in the surface), surface wear, and pitting.

The details of the process vary with the material and operating conditions but, in all cases, it manifests itself by the initiation and propagation of cracks in the near-surface

layer until microscopic pieces detach themselves to form a small crater called a 'pit' (Johnson 1988). The pits result from repeated surface or subsurface stress cycles that are beyond the endurance limit of the material. The stress field is predominantly compressive, and rolling fatigue is often preceded by substantial plastic deformation.

Johnson (1994) postulated that the cracks which initiate failure were the result of either low-cycle fatigue due to alternating plastic strain or the exhaustion of ductility by the steady accumulation of unidirectional strain (ratchetting). The threshold of such failures is then the 'shakedown limit', i.e. the contact stress below which steady cyclic loading does not exceed the elastic limit, described in Chapter 2.

Cracks may originate in the subsurface, usually from a non-metallic inclusion, or, more likely, at the surface itself (Johnson 1988, Pearson & Dezzani 1993). If they form at the surface, their orientation is controlled by the direction of the traction force, and they are inclined at a shallow angle (around 20-45°) to the surface (Bartz & Kruger 1973, Hamer et al. 1991, Tallian 1992). The pits are in the range of millimetres wide, appear fan shaped, and are symmetrical about an axis parallel to the rolling direction. At the bottom of a pit a series of curved steps indicating progressive fracture can be observed, this is because pitting is a fatigue phenomenon in which the breakdown of the tooth contact occurs by a process of progressive cracking (Way 1935). Once a pit has formed in a surface there would be high stress concentrations around it when it re-entered the contact probably causing further damage (Sayles & Ioannides 1988).

The onset of pitting is greatly influenced by sliding in the contact (Diaconescu 1975, Graham 1979, Nakajima 1990, and Tallian 1992). The sliding component of the motion produces a traction force which changes the stress picture at the contact (as described in Chapter 2). This results in a failure origin which is somewhat different from that observed under pure rolling conditions, in that it is closer to, and sometimes on or very near, the surface.

In gear teeth, due to the sliding action, failures usually initiate at the surface perhaps through plastic deformation of the asperities, or other surface irregularities, whose height exceed the thickness of the lubricant film (Johnson 1988). The dedendum section of the drive gear is often the first to experience serious pitting damage as the pits tend to form on the slower moving surface (Ichimaru et al. 1980). Once enough stress cycles have

been built up, pitting continues until the tooth profile is completely destroyed by pits of various shapes and sizes, causing rough operation and considerable noise.

Rolling contact fatigue appears to have a high dependence upon the Hertzian contact pressure (this can be evaluated using Hertz's theory of elastic contact between counterformal surfaces as shown in Chapter 2). This is an important design calculation for the risk of pitting, however, there are many other factors which must be taken into account; such as lubrication effects, sliding speed, and stress concentrations caused by asperities. The onset of pitting is characterised by a high degree of scatter in 'identical' tests meaning that a statistical approach to the analysis of results is required.

Micropitting, another form of RCF, has been described and investigated by Berthe et al. (1978), Flamand and Berthe (1978), Berthe et al. (1980), Shotter (1981), Webster and Norbart (1995) and Olver et al. (1986) amongst others. The cavities resulting from this phenomenon are in the range of tens of microns in size, much smaller than pits, and the process can sometimes lead to severe wear. Micropitting is strongly dependent upon surface roughness and seems to occur for roughness ratio (composite surface roughness to EHD film thickness) greater than 1.25 (Berthe et al. 1978, Flamand & Berthe 1978).

Berthe et al. (1978) and Olver (1984), amongst others, associated the failure mode with plastic deformation on the asperity scale, low film thickness, and roughness and hardness of the counterface are also important factors. Berthe et al. (1978) and Flamand and Berthe (1978) found that micropits were formed in the first few (10^5) cycles of operation. The micropits can be localised to over-stressed areas where they tend to redistribute the load by progressively removing areas of high contact stress. They may then stop with this load redistribution, and continued operation may polish the contacting surface and improve the overall appearance (Shotter 1981, AGMA 1980). Olver et al. (1986), however, found there was an incubation period for micropitting, where no macroscopic wear occurred, this was followed by a wear phase in which the diameter of the test specimen decreased linearly with time. When the slide-roll ratio was increased, pitting occurred faster but the wear rate was unaffected. In gears the micropits form at a shallow angle to the surface and reverse direction at the pitch line, where the traction force changes too (Shotter 1981).

Howes et al. (1976) suggested the following eleven factors were important variables in RCF: steel type, processing, surface finish, load, speed, temperature, slip, lubricant type,

viscosity, additives, and humidity. Some other factors that are partly described by the above list, are more precisely: steel hardness, oil film thickness, contact pressure, water content of the lubricant, slide-roll ratio, pressure-viscosity behaviour of the lubricant EHD film, and the viscosity-shear behaviour of the lubricant.

Davies (1996) identified the following factors as important to gearing RCF performance: hardness; component core quality; case quality in carburised steels; grain size, fine grain sizes giving optimum properties, as the grain size coarsens, properties such as ductility and fatigue strength decrease (attributed to Kalner 1973); size, shape, and type of inclusions, since they influence the stress concentration effect (attributed to Cummings et al. 1957).

3.2 Factors affecting Rolling Contact Fatigue

The factors affecting rolling contact fatigue can be grouped into the following major categories.

3.2.1 Material Variables

Way (1935) discovered that nitrided rollers would not pit under conditions that would result in severe pitting for quenched and tempered mild carbon steel rollers. He suggested using a material with a very hard surface and tough interior, as obtained by nitriding, to avoid RCF. This work was done with discs in pure rolling, with low loads, and soft steels (apart from the nitrided specimens). In these respects the conditions differed significantly from those found in most power transmission gears

Cameron (1954) reported that pitting occurred in the majority of soft marine gears, but that it was not regarded as serious, and would quite often disappear after run-in. This again is very different to the processes taking place in surface hardened gears.

The initiation of fatigue cracks is associated with local cyclic plastic deformation. In RCF, cracks may initiate beneath the surface at non-metallic inclusions or microstructural inhomogeneities, or alternatively from the surface at asperities or scratches. When steels were first manufactured one of the major problems was the presence of a large number of metallic inclusions in the steel. Littmann and Widner (1966), showed that these were responsible for the nucleation of microcracks in cyclically stressed components, fatigue cracks then propagated from these points. They also showed that flaws in the surface of a machined component could act as a stress concentration point from which cracks grew.

Martin et al. (1966) observed that improvements in surface finish switched the life limiting region from the surface to subsurface inclusions. Then, as the quality of the steel improved with the introduction of vacuum degassing and other remelting processes, the origins of fatigue shifted back to the surface, as the number and size of oxide particles in the steel were reduced. The initiation period of sub-surface cracks had been extended and early failures almost eliminated by reducing the inclusion content of the steel. An overall life increase of eight times was reported for bearings subject to multiple vacuum remelt (Morrison et al. 1963). Martin and Eberhardt (1967) noted that changes in the surface structure and separation of the grains allowed microcracks to be nucleated in the surface region. Minute surface imperfections such as grinding furrows, pits, and dents all promoted surface pitting. They found plastic deformation in the bulk material of components in areas where calculated stresses were below the "threshold level" for growth of deformation bands. These areas contained defects which promoted regions of plastically deformed martensite in their vicinity and were active or potential failure nuclei. These deformation bands around large non-metallic inclusions created visible butterfly-shaped structures. Nowadays, RCF is mainly a surface initiated process, and surface treatments and finish seem to be the most important material-related variables in fatigue performance.

In Kerrison's (1975) review of the metallurgical factors in pitting, he found that the most significant improvement to rolling contact fatigue was given by increasing the hardness of the material, as this increased the resistance to yield. This, however, may be a problem for the fracture resistance of a component, and in case hardened materials it may not be economically feasible to achieve the greatest depth possible. Sharma et al. (1977) investigated analytically the case depth requirements for carburised gears. It was concluded that the minimum case depth requirement in carburised gears was dictated by case crushing, which occurs when the alternating shear stress exceeds the allowable fatigue strength at the case-core interface.

Winter and Weiss (1981), from results of tests on carburised and hardened gears, found that for surface hardness above HRC 60 (698 kgf mm^{-2}) pitting resistance did not reliably increase. They also found that the resistance to pitting and micropitting of a gear of given hardness may be equalled or surpassed by that of a gear of lower hardness, caused by a given proportion of retained austenite, or by that of a gear of lower hardness which would readily run-in to produce smooth tooth surfaces. The reason given was that the

retained austenite would allow yield without cracking, therefore running-in and distributing load. Hardened gears without retained austenite were found to be more prone to micropitting with decreasing hardness (from 60 to 50 HRC 698-513 kgf mm^{-2}).

Winter and Weiss (1981) found that the resistance to pitting increased with depth of case, to a depth limit beyond which no further increase occurred. This was also reported by Fujita and Yoshida (1981) for case-hardened chromium molybdenum rollers.

Dawson (1962) investigated experimentally the effects of differences in hardness on roller fatigue life. The surface finish of the harder disc was found to be predominant in determining the pitting life.

Finally, Zaretsky and Anderson (in the discussion section of a paper by Howes et al. 1976) commented on the fact that metallurgical variables could be difficult to control when more than a few specimens were to be manufactured for fatigue research. Their experience had shown that metallurgical variations could be more significant in affecting fatigue life than the investigated variables.

3.2.2 Surface Finish

Way (1935) found the nature of the surface finish on rollers, in tests using a disc machine, greatly influenced the specimens' tendency to pit; pitting being prevented on a highly polished surface and accelerated on a rough-machined surface.

In experiments with a disc machine, Shotter (1958) tried to determine the possible influence of surface finish on gear tooth performance. By reasoning that rough discs suffered large amounts of surface deformation, whereas very smooth discs hardly deformed at all, he suggested that pitting may only occur after a given amount of surface deformation had taken place. Pitting and surface deformation were both absent under conditions where there was no metallic contact. He found that, with different hardness discs, the harder disc controlled the roughness of the softer disc. If the harder disc was very rough, then running it against a softer disc would roughen the softer disc; conversely, a hard, smooth disc would flatten the asperities on a rough, soft disc in the first few revolutions and would not harm the surface. When there was a difference in surface finish and hardness, the harder disc was predominant in determining pitting life.

This was consistent with tests carried out on discs connected by gears of 1:1 ratio. More revolutions to pit were required than when gears of non-integral ratio were used. The

important difference was that only where gears of 1:1 ratio were used could a point on one disc always came into contact with the same point on the other. Therefore, during the first few revolutions, the surface roughness and asperities would deform plastically to produce conformity. On subsequent revolutions there would be little further plastic deformation at the surface.

This effect has also been observed by other researchers, particularly Ichimaru et al. (1980), and is discussed separately in Section 3.2.4.5. They also noted that the test conditions were such that asperities deformed plastically, but no correlation between the initial conditions and the surface damage were noted. The final roughness ratio was more significant than the initial on fatigue life. These results tend to indicate that a strong correlation existed between variation of roughness, mode of deformation of the surface, and weakening of the material during the first few cycles of running.

Dawson (1962) also noted that pitting was affected by surface roughness in lubricated contacts, a reduction in surface roughness increased pitting life, and this was probably due to the influence of metallic asperity contact through the oil. Therefore, pitting should be dependent both on the oil film thickness between the surfaces and roughness.

Bailey (1989) investigated the effect of various surface finishing techniques on fatigue life with disc tests. Abral polishing, a vibro-abrasive polishing technique giving a much smoother surface than grinding, showed no significant improvement to fatigue life over ground specimens at -0.026 slide-roll ratio. However, shot peened and Abral polished specimens exhibited a much greater fatigue life. At the higher slide-roll ratios of -0.14 and -0.28, the Abral and Abral and shot peened specimens had similar lives and gave significantly greater lives than ground specimens. Perhaps, only when there was enough sliding present did the roughness degrade the fatigue life, consistent with the mechanism proposed by Kim and Olver (1997). Bailey commented that the ground surface showed significant deformation of the asperity peaks, and this formed numerous cracks. Abral polishing virtually eliminated all evidence of asperity deformation and microcracking and failures originated from isolated areas of local surface distress.

Nakajima and Mawatari (1993) found that for rolling with sliding conditions, pitting life with axially ground discs was very short when compared with circumferentially ground discs, this was attributed to the difference in plastic deformation due to asperity interactions.

3.2.3 Lubrication

Gear teeth roll and slide against each other, and the sliding motion requires a lubricant if any significant forces are to be transmitted through the contact. The presence of a lubricant reduces the stresses either by the reduction of friction or, more significantly, by separating the two rough surfaces. There is no general correlation between wear rate and coefficient of friction, although lubricants will tend to reduce both wear and friction.

It is not simple to select a lubricant for a practical situation except by practical determination of load carrying-capacity in a gear rig. Even so, the results from different types of gear machines and different test procedures must be interpreted with care.

Pitting is related to the inability of the lubricant to prevent asperity-asperity interaction between the two surfaces, though it can eventually occur even in the absence of such interaction. Way (1935) found that, with steel roller tests, a lubricant had to be present if pitting was to take place; when steel rollers were run without lubricant, oxides formed on the surfaces and flaked off. He also found that if the lubricant was of a viscosity above a critical value, dependent on the load, even though metal-to-metal contact was still present, pitting could be prevented. One of the suggestions he gave to avoid pitting was to use no oil, which is not reasonable and would lead to severe wear. Another more feasible method suggested was to increase the viscosity of the oil, even though this may not be practical due to the increased churning losses and possible problems with lubricant circulation.

Crook (1961) measured lubricant film thickness between similar discs for various oils at a range of speeds and devised a relationship between the lubricant and the speed of the surfaces. His experiments proved that increasing oil film thickness had a similar effect to that of reducing the surface roughness.

Using this relationship Dawson (1962) investigated the effects of oil film thickness and surface roughness of rollers on fatigue life, using a disc machine. From this work he proposed that pitting life was dependent upon the degree of metallic contact, expressed as the ratio of the composite surface roughness to the lubricant film thickness, calculated using elasohydrodynamic theory (Dowson & Higginson 1977). Dawson called this the D-ratio (later the use of the reciprocal quantity called the lambda value became more common (Tallian 1967, discussed in Section 2.3.2)), and suggested that below certain D values, no pitting took place because metal-metal contact was prevented. He found by

experiment that under a repeated contact stress of about twice the nominal pitting endurance limit, the pitting life was governed by this ratio. At the same high stress he suggested that, in the complete absence of metallic contact, pitting would not occur at all.

In general it is thought that increasing the viscosity of the lubricant tends to increase the life of components (Scott 1963, Nakajima 1990, Winter & Weiss 1981), however, high viscosity increases churning losses and may hinder debris and heat removal from the contact.

Lubricant behaviour is extremely complex especially in the contact. The chemical and physical properties of the lubricant can be modified, or changed completely, by additives. Additives are used to modify or enhance the physical and chemical properties of the lubricant so that it can meet the requirements of service. They are blended in small quantities, some of the most common being: oxidation inhibitors, friction modifiers, detergents, dispersants, and extreme pressure (EP) additives. One of the main problems with additives, such as EP additives, is that, whilst they may offer good protection against fatigue or corrosion in their designated operating conditions relative to the same conditions without additives; they may under another operating range, enhance corrosion or fatigue (Scott 1977).

The lubricant type is important, whether mineral or synthetic. Rounds (1962) looked at the effects of oil viscosity and chemical composition on the fatigue lives of ball bearings. He found that for naphthenic and paraffinic base oils the fatigue life approximately doubled for a tenfold increase in viscosity at 99 °C, but no further gains in life were encountered with viscosity above 30 cS. Naphthenic base oils consistently gave longer lives (2-2.5 times) than paraffinic oils of corresponding viscosity. Chain branching was suggested as a property of the lubricant that may have some effect on life. Rounds also found that the more stable the lubricant was to oxidation and high temperatures, the longer the fatigue lives obtained. The conclusion drawn from this work was that the chemical reactivity of the lubricant was an important factor.

With EHD theory the pressure-viscosity, viscosity-temperature, and viscosity-shear behaviour of the lubricant have also been recognised as critical parameters in RCF. In concentrated contacts the local pressures are extremely high, resulting in the importance of pressure-viscosity coefficient. The viscosity-temperature behaviour of lubricants has

been characterised by relationships such as that proposed by Vogel (1922). The shear behaviour of the lubricant is dependent upon the rate of shear. At low shear rates, fluids are Newtonian and mineral oils behave as such up to a rate of at least 10^6 s^{-1}.

Another important aspect in EHD is the flash temperature, caused by friction in the contact and largely dependent on the speed, load, and the amount of sliding present. The flash temperature doesn't influence film thickness directly, which depends solely on inlet viscosity and temperature, but will contribute to raising the bulk temperature of the component and hence the viscosity.

The form of the pressure profile in an EHD contact depends on the shear strength of the lubricant. The shear strength proportionality constant, gamma, relates the maximum shear stress in the lubricant to the pressure. According to Jacobsen (1983), the value of gamma determines whether the surface distress will take the form of micropitting, waviness with subsequent micropitting, or direct pitting. If gamma is high for a lubricant, it can sustain a high shear stress at a given pressure. This means that there will be a very steep pressure gradient in heavily loaded contacts, thereby producing very local high shear stresses on the surfaces. These shear stresses combined with the high pressures will lift the maximum von Mises stress to the surface of the metal. In EHL, rolling and sliding contacts lubricated with low shear strength oils will have a maximum von Mises stress deep down below the surface, close to the location of the maximum von Mises stress under a Hertzian, semi-elliptical pressure distribution. From tests carried out on bearings, Jacobsen suggested that there was a value of gamma below which pitting would occur and above which micropitting would take place. However, shear thinning and elasticity may mean that gamma is never reached (Olver & Spikes 1998).

One effect, that has been observed consistently, is the reduction of fatigue life when water is added to a system. Grunberg and Scott (1958) found that premature RCF failures could be caused by a small percentage of water dissolved in mineral oils. They reported that removing the small quantities of water normally contained in oils could produce an increase in mean life of 10 %, but gross contamination with water could easily half the mean life. The detrimental effect of water on RCF was also reported by Schatzberg and Felsen (1968) and Hobbs and Mullet (1968). One speculated mechanism (Grunberg & Scott 1960) was that hydrogen caused embrittlement of the material.

Spikes and Macpherson (1980) measured the dissolved water contents of a number of gearbox lubricants in laboratory experiments, fatigue test rigs, and helicopter test and service gearboxes. It was concluded that the water levels present in test and service gearboxes may be sufficient to reduce rolling contact fatigue lives. A comparison of water content in fatigue test rigs and service gearboxes showed that differences existed between the two which may impair correlation of fatigue lives. It appeared from samples that service gearboxes may often contain a lot more water than fatigue test rigs. Higher levels of water were found in ester oils than mineral oils (a factor of ten difference).

Galvin and Naylor (1964), in non-contacting rotating-bending fatigue tests, concluded that a possible effect of fluid on the fatigue limit, and therefore the crack initiation process, involved chemical reaction between the fluid and the surface of the specimen. The lubricant prevented the re-healing of surface cracks by chemically attacking the crack walls.

Winter and Weiss (1981) stated that the presence of chemical additives had little, if any, influence on pitting resistance but could adversely influence slow speed wear.

A further variable likely to affect RCF is debris contamination of the lubricant. Schlicht and Zwirlein (1980) commented on the fact that less than 10 % of bearing failures in field service were due to subsurface material fatigue, many more were due to pitting caused by foreign particle indentations. If a particle can pass between the surfaces in an oil film without causing plastic deformation, no indentation damage will be caused. Particles of size a little greater than the lubricant film thickness can cause changes to the roughness by indenting the surfaces, this may create stress concentrations in the contact. The life of almost every wearing lubricated surface will be improved by reducing the size and numbers of particles in the oil film with fine filtration, together with clean assembly.

Some of the most important factors affecting wear due to contamination in lubricated contacting surfaces are: oil film thickness, surface finish, the size of the particles in the film, and their hardness. Lowenthal and Moyer (1979) and Sayles and Macpherson (1982), amongst others, have investigated the effects of oil borne debris on rolling fatigue life. Bhachu (1980) examined the influence of filter rating on the fatigue life of a population of roller bearings fed by lubricant from a gear rig, via various filter types and sizes from 1 μm to 40 μm. He found that for bearings with different filter ratings, the life could be increased considerably up to 3 μm filter size. This contrasts with Lowenthal and

Moyer (1979), who found no statistical difference between the lives of ball bearings tested with 3 and 30 μm filtration. Bhachu (1980) also found that the initial period of running was most important, as was shown by the very little improvement when 3μm filtration was introduced to a bearing that had been initially run with 40 μm filtration. This was explained by Sayles and Ioannides (1988) as being caused by the surface damage in the form of indentations reducing the fatigue life, and not the continued presence of the debris in the lubricant. They also stated that the surface damage could vary significantly for different debris, largely depending on its hardness and ductility, and the environment in which deformation took place.

The main ways to maintain the contamination levels below those that can lead to rolling contact fatigue are by increasing the separation performance of the filter, decreasing the contaminant entry rate into the system, and improving the contaminant tolerance of the components.

Finally, in experiments with oil jet velocity and location of oil supply, Borsoff (1959) achieved the highest load carrying capacity with the oil jet supplied directly to the incoming mesh. Load carrying capacity increased with a nozzle giving higher jet velocity and decreased with increasing lubricant supply temperature.

3.2.4 Operating Variables (Load, Temperature, Geometry, Sliding, Other)

3.2.4.1 Load

The load is important in rolling contact fatigue as it determines the maximum Hertzian contact stress in a smooth surface and the stresses in a rough body. These high cyclic stresses are the reason for RCF failures and without them fatigue would not occur. In RCF, increasing the load on a component will result in less cycles to failure, providing the load is above the endurance limit of the material. Load is a very important variable in RCF and equations relating load and component life, such as that given by Lundberg and Palmgren (1947), are plentiful.

However, determining the instantaneous load on a gear tooth pair with sufficient accuracy can be difficult. This is considered in Chapter 8.

3.2.4.2 Temperature

Permissible operating temperatures are influenced by the life of the lubricant, the thermal degradation of which is related closely to its bulk temperature. The life of other components such as seals, bearings, and gear materials can also be seriously reduced by excessively high operating temperatures. The fatigue strengths of gear materials may vary little at normal operating temperatures, but their value can be seriously reduced at high temperatures, as may be encountered in an aircraft gearbox (Davies & Gittos 1989).

The temperature of rubbing components is greatly affected by the frictional heat, which may be generated by the viscous shear in the lubricant film and may also be, at least partially, generated by the boundary friction on contacting asperities (Martin 1978).

The bulk temperature of a component is important, as mentioned earlier, because both the minimum film thickness and the friction in a contact with an EHD film are controlled by the viscosity at the inlet to the film, and this has to be taken at the bulk temperature of the contacting bodies separated by the film. The flash temperature should also be considered. Blok (1970) concluded that it caused a steep thermal gradient on the surface, this could cause non-uniform thermal expansion. This would tend to decrease the effective radius of curvature of either rubbing surface, particularly in the contact zone. Consequently, the contact zone would tend to become narrower, the contact stress higher, and the EHD minimum film thickness smaller than would be the case in isothermal conditions.

3.2.4.3 Geometry

Townsend and Zaretsky (1981) used involute spur gears manufactured to high accuracy (e.g. eccentricity, involute), as experience had shown that it was essential for good reproducibility of results. They found that a higher load carrying capacity was given by a gear with larger diametral pitch (smaller module). This was caused by a difference in actual sliding speeds; a larger diametral pitch meant a decrease in sliding speed between the rubbing surfaces and also a greater contact ratio (for their experiments). Increased errors in tooth spacing and involute form gave the lubricant a lower load carrying capacity. They also found that tip relief caused an increase in load carrying capacity of the gears up to a certain value, then a decrease. This suggested the existence of an optimum value for tip relief.

The aim of tip relief is to compensate for tooth deflection, as well as to relieve load in the high sliding portion of tooth action. (This procedure will be described in more detail in Chapter 7). Tip relief when properly applied will reduce dynamic loading at the tooth tip and will reduce the tip load to zero, by shifting the load to the other tooth pair in contact (the static bending stress on the other tooth will increase). Another form of relief, crowning, may prevent edge loading so, this too, could increase fatigue life.

Profile and lead modifications will play an important role in the capacity of individual gears. While the absolute amount and type of modifications from specimen to specimen will be critical in obtaining maximum capacity from any gear pair, for analysis purposes, consistency of modifications from specimen to specimen or, at least, knowledge of variations, is of far greater importance than their absolute amount or type. This is to try and minimise the scatter inherent in fatigue test results.

Littmann and Widner (1966) discussed geometric stress concentrations caused by deflections and the geometry at the end of line contacts, and the effect they had on fatigue. Fatigue occurred in the narrow band at the end of a line contact in which the contact stresses were more severe. There was evidence that in the earliest stages of failure there were cracks extending to the surface, but they were unsure if the first cracks originated at the surface or slightly subsurface. Crowning could avoid this problem but this is usually designed for a given load, so to operate a component over a range of loads, a compromise to avoid loss of effective contact length is needed. Nakajima (1990) found a rather short fatigue life for very smooth rollers when run with a low viscosity oil, this was attributed to the stress concentrations at the end of the rollers. This 'edge' effect has been analysed by the present author in Chapter 8.

Finally, when mentioning geometry in relation to RCF, one must mention the size factor, a parameter which accounts for the fact that the larger a component is, the greater the probability there is of it having a crack of a certain critical length for fatigue crack initiation. Of particular importance in RCF is the stressed volume (Ioannides & Harris 1985).

Fujita and Yoshida (1981) investigated the effect of relative radius of curvature in case-hardened chromium molybdenum rollers. This was done for specimens where the hardness at the depth of maximum shear stress for a given Hertzian stress were the same. The surface durability of the rollers tended to decrease as relative radius of curvature

increased for a given stress. This could be explained by the stressed volume being smaller for a smaller reduced radius of curvature, and therefore there being less chance of it containing a defect.

3.2.4.4 Sliding

A considerable amount of early work on RCF was motivated by concerns relating to rolling element bearings, which operate under conditions of nearly pure rolling. Way (1935) performed his tests under pure rolling conditions, with both rollers running at the same speed. Gear teeth, however, can have a significant sliding velocity in their contact, which tends to raise failure origins towards the surface.

Dawson (1963) demonstrated that sliding promoted fatigue, so that the slide-roll ratio was recognised as an important factor in fatigue life performance. More recently, work on the effect of sliding in the RCF of hardened steels has been investigated by Diaconescu et al. (1974), Macpherson (1975), Graham (1979), and Nakajima (1990), amongst others. They found the effect of sliding was to cause a reduction in the fatigue life of the roller having the lower surface speed. As mentioned by Olver (1995), this effect persisted even at those higher sliding speeds which were accompanied by a decrease in friction; thus the life reduction could not simply be due to the stresses from sliding friction. He attributed it to the increased number of asperity contacts per load cycle. Nakajima (1981) also reported reduction in RCF life with slide roll ratio, and observed that smooth surfaces showed a lower reduction in life with sliding than rough ones.

When there is sliding in a contact, tangential traction results, giving a tensile stress in the vicinity of the inlet and outlet of the contact zone on the surfaces of lower and higher velocities respectively (see Figure 3.2.1)

The magnitude of the tensile stress produced by sliding in the contact in smooth surface theory is calculated by $2\mu p_o$, where μ is the coefficient of friction and p_o is the Hertzian maximum compressive stress (as shown in Chapter 2). However, the local values will be greater due to stress concentrations caused by asperity interactions. This tensile stress may promote the growth of micro-cracks, probably initiated by asperity interactions, into pitting cracks.

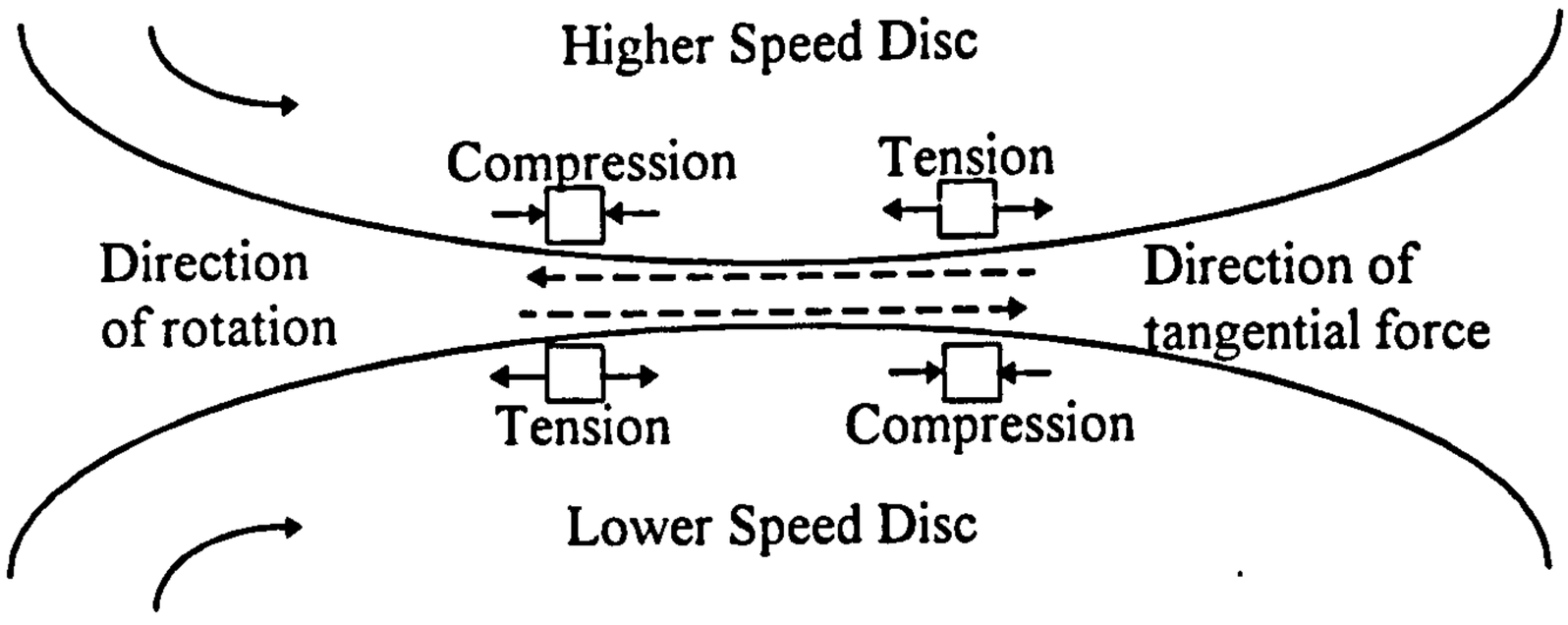


Figure 3.2.1 Areas of Tension and Compression in a Rolling-Sliding Contact

In gears the tangential velocity of the addendum surface of involute teeth is greater than that of the dedendum surface, so that the sliding velocity changes sign at the pitch point (see Figure 3.2.2).

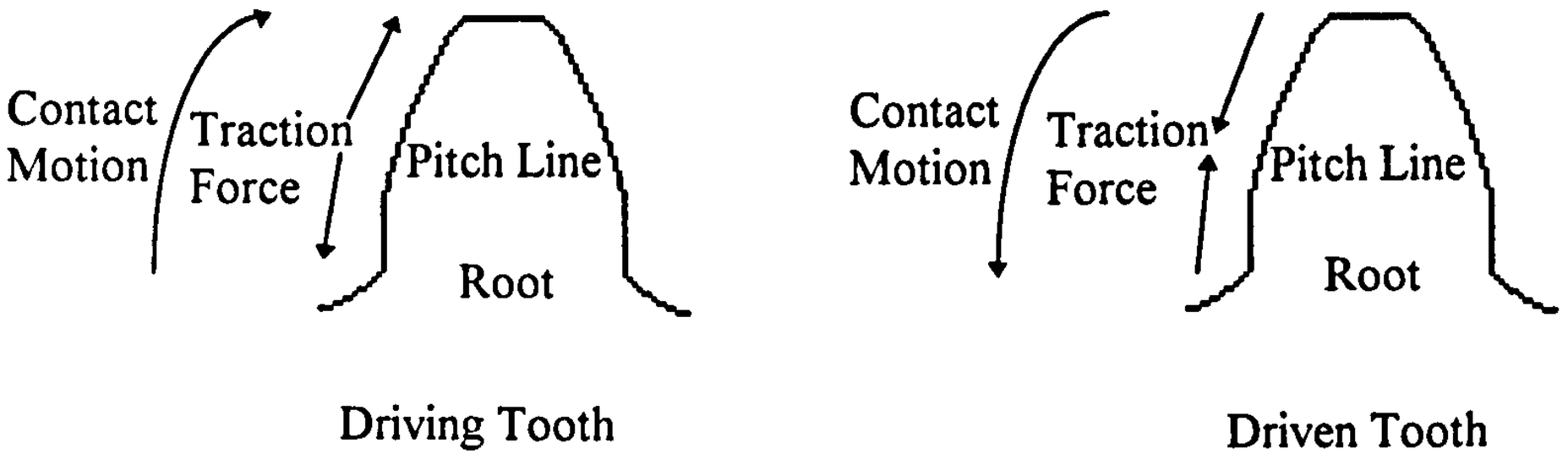


Figure 3.2.2 Direction of the Traction Force on the Driving and Driven Gear Teeth

The slide-roll ratio of the faster moving surface is positive and that of the slower moving surface is negative. When the contact is inside the pitch circle the slide-roll ratio is negative, and when outside positive.

Nakajima et al. (1983), in an experimental investigation using rollers, found that pitting occurred under a condition of negative slide-roll ratio and the pitting cracks dipped always in the opposite direction to the rotation of the roller. Pitting made rapid progress when cracks grew along the direction of the plastic flow beneath the surface, but made slow progress when the direction of the propagation of cracks and the plastic flow crossed each other. The ease of growth of crack, therefore, depended on plastic flow but their direction on the direction of rolling.

Weck et al. (1978) carried out experiments on gear teeth and found that damage caused by pitting always occurred in a particular area of the tooth flanks. The maximum of the pitting frequency distribution occurred at a negative slide-roll ratio of 7-8 %. On other materials, case hardened for example, the maximum was determined at higher slide-roll ratios.

Therefore, friction induced by sliding in a contact affects RCF by shifting the maximum shear stress towards the surface, increasing tensile forces in the contact, asperity stress cycles, and temperature and may also promote debris damage.

3.2.4.5 Other Variables

One should mention work done by Ichimaru et al.(1980), Ishibashi and Tanaka (1981), Nakajima (1981), and Nakajima and Morodomi (1986) studying contacting bodies with integral and hunting ratios. They found a significant difference in fatigue life between the two, with integral ratios giving longer lives than hunting ratios. The reason given for this effect was that in an integral ratio the same regions of the contacting surfaces came into contact with each other with successive revolutions, making the asperities conform better and causing less plastic deformation. In contrast, in a hunting ratio different regions of the contacting surfaces came into contact with each other on successive revolutions.

Nakajima (1981) defined an 'asperity interacting frequency', the number of contact positions on the surface of a high hardness roller with different microgeometries engaging with any one spot on the surface of lower hardness roller. Fatigue tests on rollers were carried out on normalised steel rollers by Nakajima (1981) and on surface hardened rollers by Nakajima and Morodomi (1986). A large value of asperity interacting frequency caused severe wear and retarded occurrence of pitting, especially when sliding was introduced. The main cause of pitting was explained to be the repetition of the plastic deformation due to these asperity interactions.

3.3 The Pitting Mechanism

Way (1935) showed by analysis that a small crack in the surface, if filled with oil, would tend to grow, providing it had a certain initial direction. This strongly suggested that oil penetration of very small surface cracks with a certain initial direction was the reason for the growth of cracks, until a particle was separated from the main body of material, leaving a pit. This also explained his observations on the effects of lubricant viscosity and surface roughness on pitting. The viscosity of the lubricant had to be low enough to penetrate the crack, and make it grow; and the rougher the surface finish, the greater the likelihood of larger initial cracks which could lead to pitting.

The initiation of fatigue cracks represents one of the most important stages in the pitting process. Sites and modes of fatigue crack initiation depend on the microstructure of the

material, type of applied stress, and micro/macro-geometry of the specimens. The origin of a fatigue failure always depends on the outcome of a competition between failures, initiating at the most severe surface or subsurface stress raiser (Martin & Eberhardt 1967).

Considering the material microstructure, micro-cracks can be initiated along slip bands by dislocation motion (Lin et al. 1986), along grain boundaries, or along interfaces and inclusions (Martin & Eberhardt 1967). Depending on the roughness and the cleanliness of the steel and the magnitude of the stresses involved, micro-cracks are formed in the surface or subsurface region. The asperity interactions promote the opening of small micro-cracks in the surface region of the contact. Some of these micro-cracks on the contact surface will stop growing or disappear due to sliding wear, however, when a crack grows sufficiently large, it will not disappear and will remain on the contact surface and continue growing. The crack will incline towards a direction perpendicular to the direction of main stress, this has usually been taken as either the maximum shear stress, maximum orthogonal shear stress, or the surface tensile stress (Diaconescu 1975). The crack will then branch and continue to grow at an ever increasing rate until fracture occurs and a whole section of metal breaks off to leave a cavity. If fatigue cracks can be prevented from forming or growing to the critical size, then fatigue could perhaps be controlled.

Paris and Erdogan (1963) originally described three stages to crack propagation. The first part was called Region I crack growth, or initiation, and begins immediately upon the onset of cyclic stressing and is concluded by the formation and growth of a micro-crack to the point where it becomes self-propagating. In the second part, Region II crack growth, or propagation, the crack has reached a critical size and constant rate crack propagation occurs and continues until achieving a size large enough to undermine the component and initiate rapid growth. The third region of crack growth is occupied by rapid growth, or fracturing, until the pit forms. Region II, which is approximately constant, is covered by the Paris law of crack growth which relates crack growth rate to variation in stress intensity factor:

$$\frac{dc}{dN} = C\Delta K^m$$

where dc/dN is the crack extension per cycle, the stress intensity range $\Delta K = K_{max}\text{-}K_{min}$, and C and m are constants (m~ 2.5-4).

These equations tend to work well when based upon experimental data but cannot be extrapolated far beyond the original material and are dubious when a chemically aggressive environment is present (Foroughi & Spikes 1988).

The time to initiation, the initiation stresses, and the steady state crack propagation rate can all be affected by the lubricant as shown by Lockwood et al. (1986).

It is difficult to study initiation and propagation in rolling contacts as the actual contact conditions are unknown. One method of separating initiation from propagation is to pre-crack the samples so that the initial crack is greater than the critical crack size, therefore, region II cracking develops at once. The time to failure of the pre-cracked and non-cracked specimens is measured and, from the difference in the two results, the time to initiation can be calculated, assuming the critical crack size can be reasonably estimated.

Lundberg and Palmgren (1947), in their study of rolling element bearings, suggested that in mineral oils the initiation stage took 99% of the time to failure and the propagation stages were very short. Yoshioko and Fujiwara (1988), who studied the acoustic emission of bearings in an effort to measure the times of initiation and propagation, reported results that agreed with Lundberg and Palmgren.

Linear elastic fracture mechanics (LEFM) is the study of the propagation of cracks. The main practical concern in applying fracture mechanics to rolling contact fatigue is to calculate the stress intensity factors (SIFs), K_I and K_{II}, at the crack tips. Another important aspect is the likely directions of crack propagation, which may be a function of the SIFs.

Conventional fatigue situations have had LEFM applied with success, but these involve mode I propagation under the action of a cyclic stress. In rolling contacts, tensile stresses are small, leading to the suggestion that cracks propagate in mode II under the action of cyclic shear stress (Johnson 1988). However, this is difficult as crack face friction will reduce the stress intensity factor, K_{II}, at the crack tip. This will be compounded by the compressive stress that will act to keep the crack closed. The mechanism by which such cracks may propagate has been the subject of much work, Keer et al. (1982), Keer and Bryant (1983), Kaneta and Murakami (1987), and Bower (1988), to quote a few. These studies have suggested three mechanisms, involving the penetration of fluid in the cracks, that could influence surface crack propagation. These are:

i) The reduction of crack face friction. The cycle of shear stress can cause mode II (shear) propagation, provided the crack faces are not locked together by the normal compression. The influence of crack face friction on the propagation of subsurface cracks was investigated by Hearle and Johnson (1985) and Sheppard et al. (1987). It was shown that the trailing crack tip has a higher stress intensity range, ΔK_{II}, than the leading tip, which is consistent that subsurface cracks tend to propagate faster from the trailing tip (Yoshimura et al.1984).

ii) The transmittal of the contact pressure to the tip of the crack by pressurised oil from the contact, although this would require elastic deflection and consequent oil flow within the crack. Pressurised cracks have been investigated by Keer and Bryant (1983) and Bower (1988) by using the method of distributed dislocations and by Kaneta and Murakami (1987) by using the body force method. Large values of mode I stress intensity, K_I, were predicted on the assumption that the contact pressure was transmitted to the crack tip without attenuation, but the results did not explain why propagation is only observed to occur in the direction of motion of the load and on the slower moving surface.

iii) A fluid entrapment mechanism, in which the crack is filled with fluid just before the contact area reaches the mouth of the crack. The contact then closes the crack mouth and pressurises the trapped fluid so as to generate a mode I stress intensity at the crack tip and keep the crack faces apart. This hypothesis of fluid entrapment has been examined by Bower (1988). The mechanism can only operate if the mouth passes under the load before the tip, which explains why the crack propagates in the direction of motion of the load. The volume of the fluid trapped in the crack is sensitive to the direction of the traction force at the surface: a driving traction opens the mouth before entry to the contact while a braking traction closes it

The following predictions can be made for crack behaviour by using fracture mechanics (Foroughi & Spikes 1988).

i) K_I is always smaller than K_{II}, except with fluid entrapment propagated cracks;

ii) Crack face friction reduces K_{II}; and

iii) An increase in surface friction coefficient will increase K_I but, whilst altering K_{II}, often has little effect on overall ΔK_{II} due to passage of load over the crack.

Polk et al (1975) used an interrupted stressing technique to measure crack propagation rates. Polk and Rowe (1976) followed up this investigation by using an optical microscope method to count cracks and thus measure the extent of branching. From the amount of branching, a crack severity parameter was calculated. This was correlated with the L_{10} fatigue life of the failed examples and found to be a reasonable fit for a variety of steels and conditions. They suggested that this correlation was independent of stress and metallurgy. The important factor affecting the crack branching was the lubricant chemistry.

Rounds (1962) found an optimum wear rate for maximum life, further increasing or decreasing the wear rate from the optimum value decreased fatigue life markedly. This may be caused by the reduced possibility for a unit volume to accumulate enough cycles to fail by fatigue before it is worn away.

Finally, a good review of RCF crack studies has been given by Foroughi and Spikes (1988). They noted that observations on crack morphology in RCF have been variable but a few features appeared to occur reasonably consistently in the literature. The following list they gave covered the main points concerning subsurface and surface RCF cracks.

Subsurface cracks:

i) These tend to be mainly associated with pure rolling and surface compressive stresses, though they may also be observed in mixed sliding-rolling.

ii) Cracks develop and grow parallel to the surface.

iii) Cracks form typically at depth, $h = 0.35a$ to $2.0a$.

iv) Cracks grow faster on the trailing tip (the one that sees the applied load last).

v) For wear only the trailing tip reaches the surface. In fatigue however, where the fatigue cracks are larger, the trailing tip may turn down vertically into the depth of the material.

vi) Cracks grow preferentially in the driven surface.

vii) Cracks grow at approximately 20-30° into the surface in the direction of the moving load, i.e. against the rotating direction in the driven disc. For case-hardened steel branching cracks then propagate at 90° from the original cracks

towards the surface. For bearing steels, a crack then propagates deep into the surface at the trailing tip to be followed by a crack propagating up from the trailing tip of the original crack towards the surface.

Surface cracks:

i) These tend to be associated with highly purified steels, surface residual tensile stresses, and mixed sliding-rolling systems.

ii) Sliding increases the propagation rate but not the initiation rate.

iii) Cracks grow into the surface in the direction of the moving load i.e. the opposite direction to rolling or rotation. They grow preferentially on driven surfaces, where the applied surface traction acts against the direction of the moving load.

iv) Cracks grow typically at 20° to the surface. This angle can be flatter at low sliding and is steeper with high sliding. At depth they may turn parallel to the surface.

v) On the driver, surface cracks may grow initially vertically into the surface.

vi) Cracks propagate faster with low viscosity oils, and chemically aggressive lubricants. Water may increase the crack branch rate.

3.4 The Statistical Nature of Fatigue

Fatigue is a random process that occurs when a varying stress is greater than a limiting value, the failure taking place only above a certain number of cycles. The same applied stress, however, when applied to identical components will give different lives in repeat tests because of the random distribution of defects in the material. The problem with fatigue testing is one has to balance the number of tests to failure to achieve credible results and the cost in time and money. One should, therefore, use statistical methods in planning and interpreting fatigue experiments, in order to arrive at valid decisions concerning times to failure, errors in estimated times to failure, reliability, and confidence limits. An important issue is whether the sample size for a fatigue investigation is compatible with the desired degree of accuracy in the results.

Considerable scatter in fatigue life can be expected even though the specimens are identical and run under the same conditions. This illustrates that any finite collection of

specimens, run under a fixed set of conditions (load, speed and lubricant), belongs to a population defined by the manner in which the fatigue lives of individual members are distributed. Weibull (1951) constructed a distribution function which represented fatigue data well, in particular that of Lundberg and Palmgren (1947) and Tallian (1962) with rolling element bearing tests. The Weibull cumulative distribution function, F(t), the probability that a specimen will fail in time, t, or less, is:

$$F(t) = 1 - e^{-\left(\frac{t}{\theta}\right)^b}$$

where b is the Weibull slope, θ is the characteristic life, and t is the time to failure.

For a Weibull distribution, straight line graphs are obtained for fatigue data by plotting the logarithm of the life, t, as the abscissa and log log $1/(1-F(t))$ as the ordinate.

Often log log $1/(1-\lambda_n(r))$ is plotted as the ordinate, where $\lambda_n(r)$ represents the median rank of the item under consideration. The median rank for individual items of any ordered collection of data takes into account the fact that a set of experiments consists of a finite number of elements, not the entire population (Johnson 1964).

$$\lambda_n(r) = 1 - 2^{\left(\frac{-1}{n}\right)} + \left(\frac{r-1}{n-1}\right) \times \left(2^{\left(1-\frac{1}{n}\right)} - 1\right)$$

n = Number of specimens run

r = Number of the specimen in order of failure being ranked

where $\lambda_n(r)$ is the median rank of the r^{th} value in n

Once we have plotted fatigue results on a Weibull chart, we can then derive from it information such as the mean life and L_{10}, the number of hours up to which 10% of the specimens in a population have failed, which gives a prediction of the occurrence of early failures. On a Weibull plot this will be the value on the abscissa of the point on a Weibull slope whose ordinate reads 10% failed. In fact, one can predict what percentage of specimens will fail within any specified number of hours.

Having estimated values from a Weibull plot it is important to know how accurate these values are, this will depend on the number of failures from which the estimate was made and upon the Weibull slope.

3.5 Fatigue Models and Design Standards

3.5.1 Fatigue Models

To design a component whose surface will come into contact under given conditions of load and slide-roll ratio with a given surface roughness, material, and lubricant, it is important to be able to predict the number of loading cycles it can sustain before the risk of surface pitting.

Lundberg and Palmgren (1947) published the first theoretical model for pitting life prediction of rolling bearings, this was used as a tool for design and material selection. The basis of the method was the assumption that fatigue was initiated at random defects. These defects behaved independently, and the whole assembly failed as soon as an individual region failed. They found that the probability that the material would survive N million stress cycles, $S(N)$ (where $S(N) = 1\text{-}F(N)$), was given by the formula:

$$\ln(1/S)=k_o^c N^e z_o^{l-h} a l$$

where a was the semi-axis of the Hertz contact and l was the circular length of the raceway. The exponents c, e, and h were determined experimentally; and the constant k was found to depend on material state, surface finish, and lubricant parameters.

Their equation is still widely used for prediction of lives in rolling bearings, even though it is empirical. It describes only how the life varies with the stresses and the volume of material over which they act, it considers a pure rolling contact, and takes no account of a lubricant.

McKelvey and Moyer (1963) looked at the relationship between the maximum compressive stress, p_o, and the fatigue lives obtained under rolling contact. They concluded that the relationship given below was approximate (where m ranged from 4.5 to 9):

$$L_{50}=K(p_o)^m$$

Chiu et al. (1969) devised a model of subsurface and surface fatigue life, based on the concept of crack growth as a result of cyclic stressing. Their formula considered matrix parameters; defect characteristics; and parameters of stress, lubrication, and surface topography. This model was developed further by Chiu et al. (1971), Tallian and McCool (1971), and Tallian (1971) by introducing new factors and incorporating an

engineering model for pitting. They also considered material strength, shape defects, an elasticity function, a stress distribution function, a dispersion parameter, and a matrix ductility exponent. Tallian (1976a & b) then included oil contamination parameters in this model and also developed a contact fatigue model to account for the effect of the ratio of lubricant film thickness to surface roughness (Tallian 1982).

An asperity interaction model was developed by Chow and Cheng (1976), who examined the film thickness between lubricated rollers of varying surface roughness. From this they developed a mathematical model based on the interaction of surface asperities and the transient and residual stresses induced in the surfaces. They suggested that the specific film thickness, lambda, was the most important parameter in EHD lubrication. Their model predicted that at low lambda ratios asperities interacted causing severe subsurface plastic flow, which allowed crack growth to occur very easily, and as a result pitting.

Ioannides and Harris (1985) extended Lundberg and Palmgren's theory for rolling bearing life prediction by considering the local stresses region by region. They also proposed simple power laws for the relevant functions resulting in:

$$\ln(1/S) = A \; N^{e} \Sigma(\sigma)^{c} \; \delta V$$

where the sum is to be taken over the whole volume of the component and δV is the elemental volume. Ioannides and Harris introduced a fatigue limit stress, which allowed for infinite lives to be predicted under low enough stresses.

Models incorporating roughness and sliding contacts using the Ioannides and Harris method have been presented by Hamer et al. (1991); and incorporating local material variations by Kim and Olver (1997).

Fracture mechanics has been applied to a variety of crack positions and geometries by Keer et al. (1982) and Murakami et al. (1985), amongst others. Keer et al. (1982) published models for a subsurface horizontal crack, a surface breaking vertical crack, and a combination of the two cracks. They concluded that the propagation of cracks depended on the local stress intensity factors and upon the magnitude of the mode critical stress intensity level. Keer and Bryant (1983) followed up this work trying to model the mechanism postulated by Way. This mechanism suggested that it was lubricant forced into the openings of surface cracks which, when restressed, caused crack extension and propagation. They concluded that there model did not seem to fit this mechanism, but their model might be deficient.

Finite element models have also been used to describe RCF, Bhargava et al. (1985) used a plane strain elastic plastic finite element method to produce pressure distributions for single contacts. Their model was then extended to take into account repeated contacts by reapplying the pressure for each contact.

3.5.2 Fatigue Design Standards

Design standards such as BS 486 Part 3 (BSI 1986), DIN 3990 (DIN 1987) and AGMA 2001-C95 (AGMA 1995) are set out to provide methods for rating gear systems. These standards usually specify that, in gear sets that are adequately lubricated, the strength design of the gear is established based on the bending strength at the tooth fillet and the surface durability on the tooth flank. They evaluate gear tooth capacity based on the major factors affecting these two failure modes. The standards combine experience obtained in designing, manufacturing, and operating gears with analysis, such as that carried out by Hertz (Johnson 1985). The equations derived therefore contain many empirical factors. These standards are fairly complex and time consuming to use, so many have associated computer programs.

3.6 Conclusions

Rolling contact fatigue is the major factor under investigation in this research and has been discussed here, particularly in relation to its effect on the durability of gears. It is a topic that has been given much consideration and there is a vast amount of experimental and theoretical literature on the subject. One of the major problems with fatigue research is the great number of variables affecting it. Material variables, surface finish, lubrication, load, temperature, geometry and sliding have all been discussed here and are amongst the more important variables. It is difficult to incorporate all of these into an investigation and, even if just one is investigated, results from one set of tests may not correlate with similar investigations. This is a problem posed when trying to relate gear and disc tests, and is discussed further in Chapter 6. The statistical nature of the process and the length of the tests add further to the difficulties of fatigue research.

In the next chapter gear failure modes will be reviewed. Some of these are forms of rolling contact fatigue and were encountered by the author in his gear and disc experiments.

Chapter 4 Gear Failure Modes

Having reviewed surface interactions and rolling contact fatigue, it is now convenient to discuss the problems a gear in operation will face. Some of the most common gear failure modes are reviewed here; particular attention is given to those failures encountered in this study and ones determining gear durability.

4.1 Gearbox and Gear Failures

The aim in transmission design is to create a gearbox which can be manufactured at a reasonable cost and which will transmit the design torque, at the design speed, for a specified ratio, with a given reliability during its life. The design may have constraints imposed on it by space, weight and cost, for example.

A gearbox can fail for a number of reasons, such as: failure of the gears, bearings, shafts, seals, or the lubrication system (Figure 4.1.1 shows severe fretting of gear shafts).

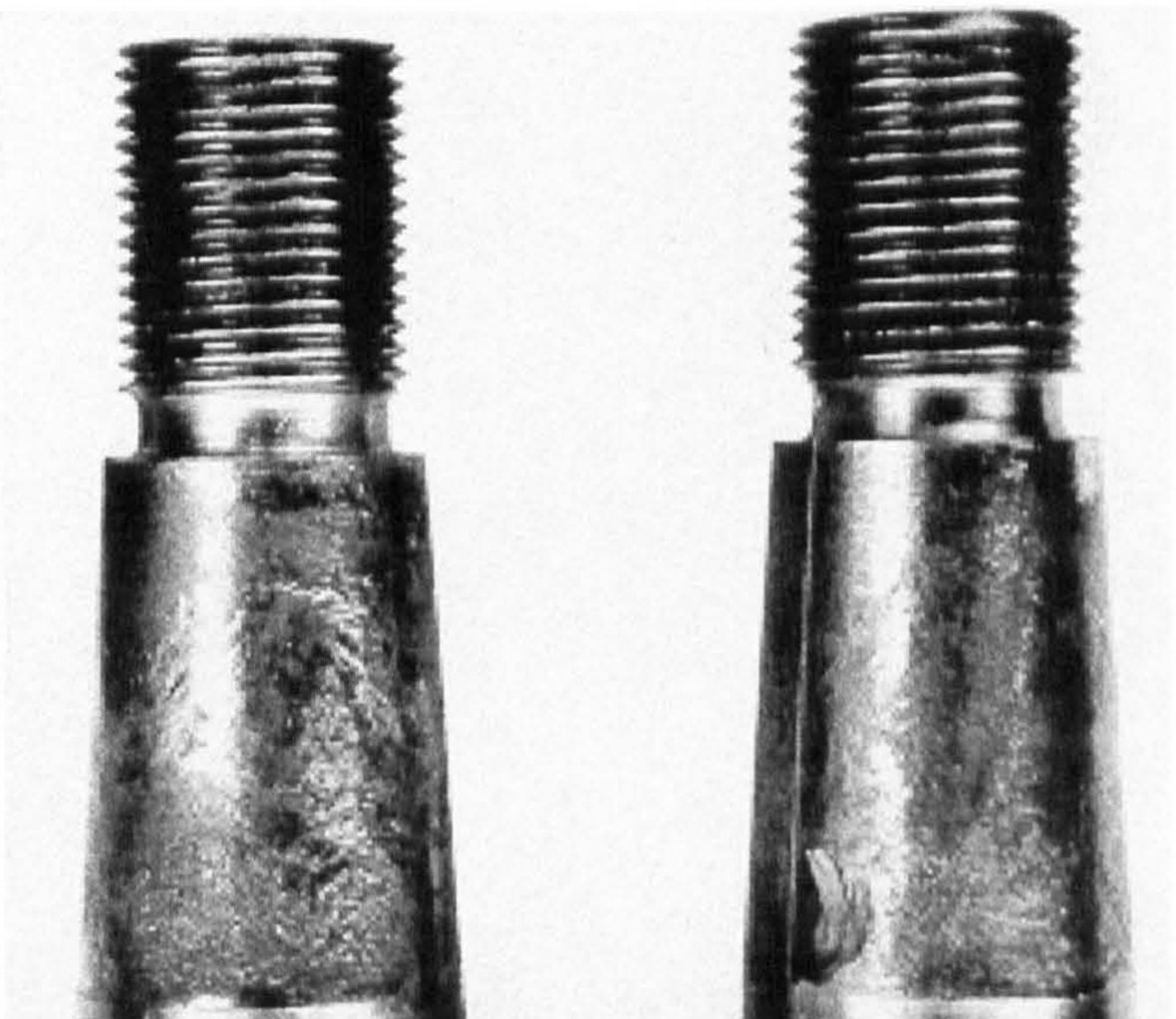


Figure 4.1.1 Fretted Tapered Gear Seat on a Shaft (Tallian 1992)

A gear is said to have failed when it can no longer do efficiently the job for which it was designed (AGMA 1980). AGMA groups gear failures into the following classes: wear, plastic flow, surface fatigue, breakage, and process related gear failures.

The above failures are all possible, however, in the experiments carried out by the author, the gears were operating under certain conditions of contact stress and rolling and sliding speed that made the following failure modes more probable: pitting, micropitting, and scuffing. The gears were designed to minimise risk of tooth breakage by having low bending stresses. These failure modes are described in detail in the following sections, several other failure modes are described in Section 4.6.

The main failure modes are shown plotted on a load versus sliding speed graph, Figure 4.1.2, also known as a failure map, initially proposed by Blok (1958). This can be used as a guide to design, as the effects of running condition on the failure mode can be observed, but it must realised that this applies strictly to a particular gear design and lubricant. The performance is limited by excessive wear at low speeds, due to the low film thickness; scuffing at high speeds, due to the excessive flash temperature; and pitting failure at high loads, where the load is in excess of the endurance limit. This assumes the gears have been designed and manufactured correctly.

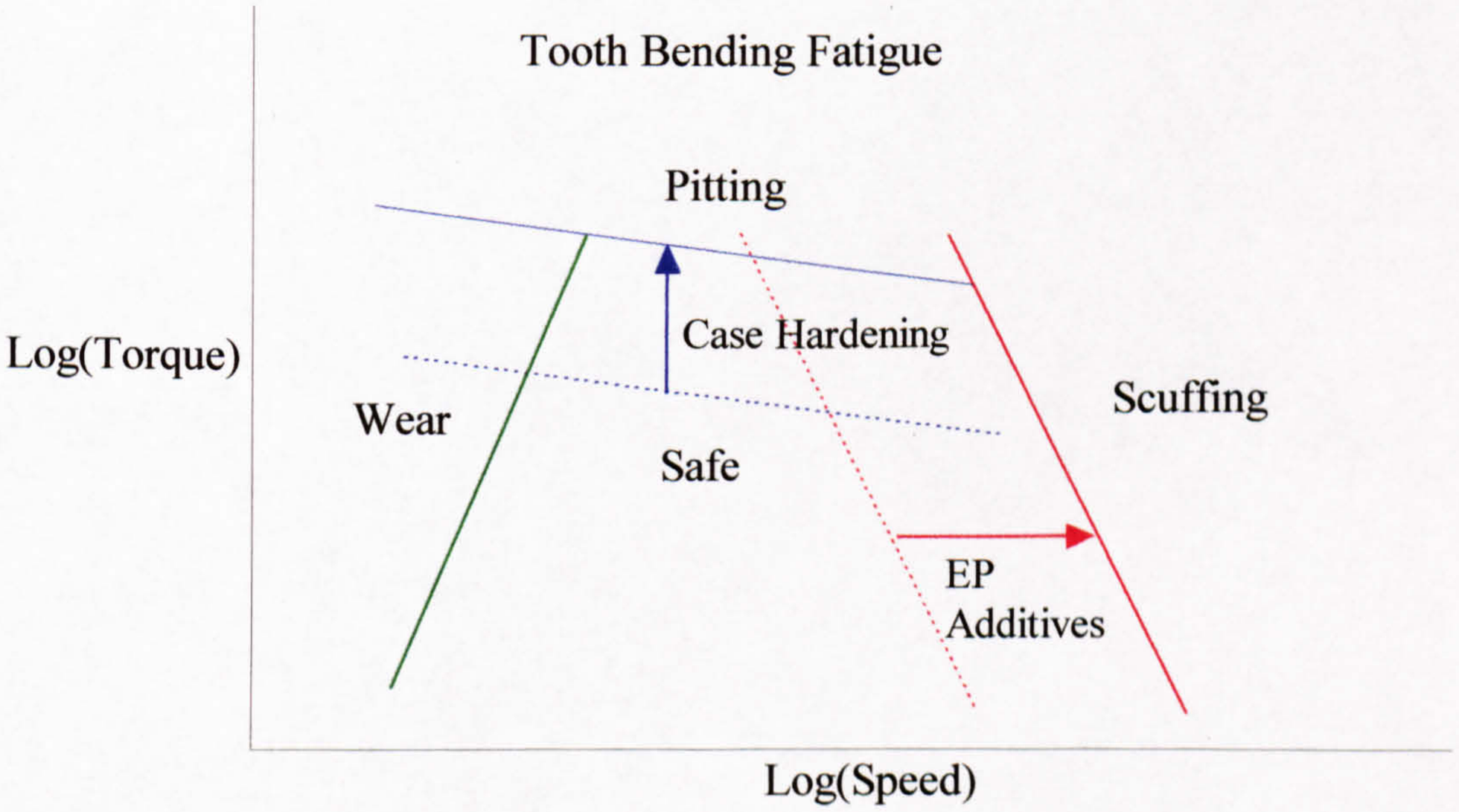


Fig 4.1.2 The Effect of Running Conditions on the Failure Mode

This type of diagram has changed over the years due to improvements in gear tribology. A change from soft to case-hardened gears pushed the pitting limit up significantly, and virtually removed pitting as a significant mode of failure (Johnson 1988). The use of EP additives in lubricants has pushed back the scuffing limit to higher speeds, thereby reintroducing pitting as a mode of failure at higher loads. How this diagram may look for the latest materials and lubricants is a topic requiring investigation.

4.2 Tooth Breakage

This failure mode involves the fracture of part of, or a whole tooth, under operating conditions where the bending stress exceeds the fracture strength, or more commonly, the bending fatigue strength of the gear material (Figures 4.2.1 and 4.2.2).

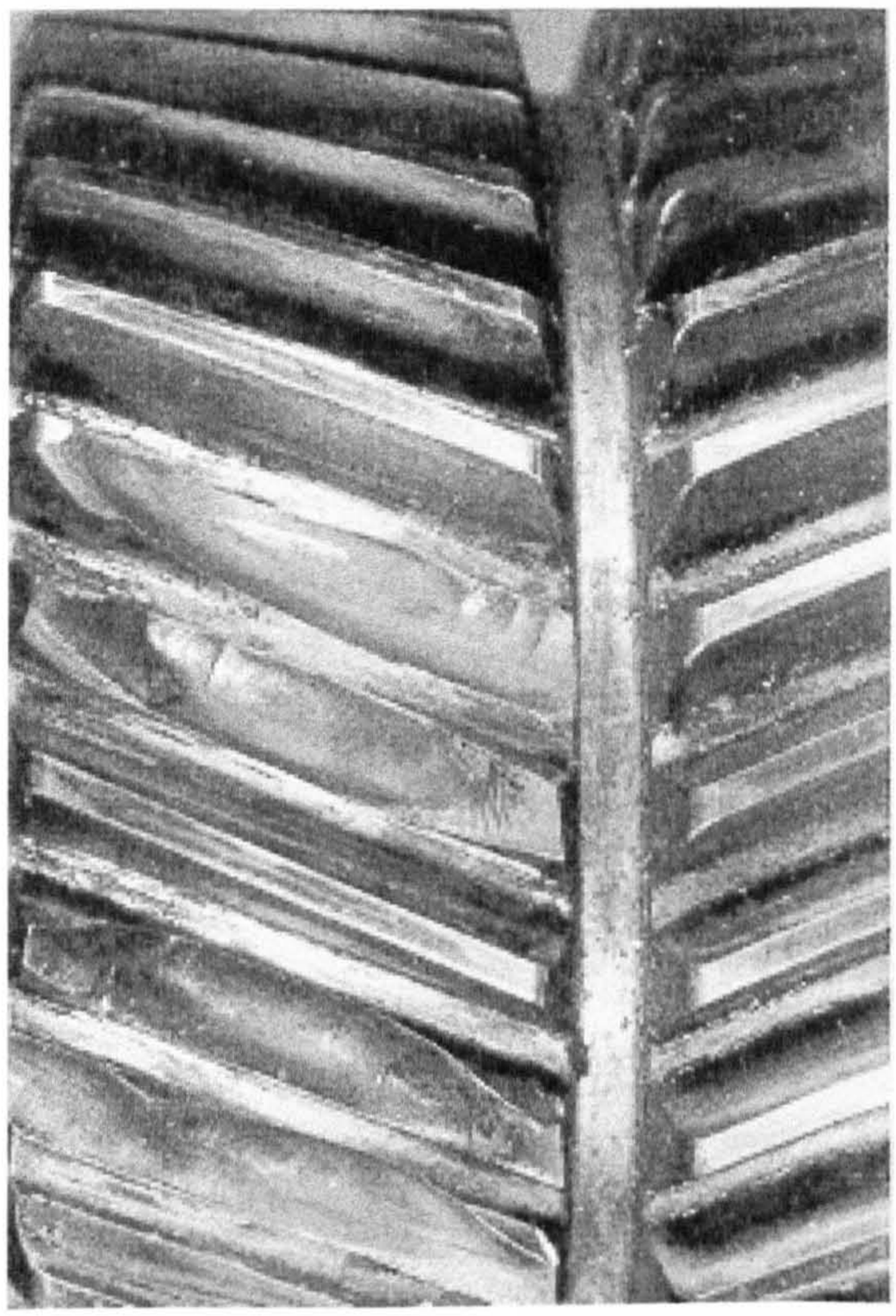


Figure 4.2.1 Tooth Breakage due to Bending Fatigue on a Helical Gear (Neale 1995)

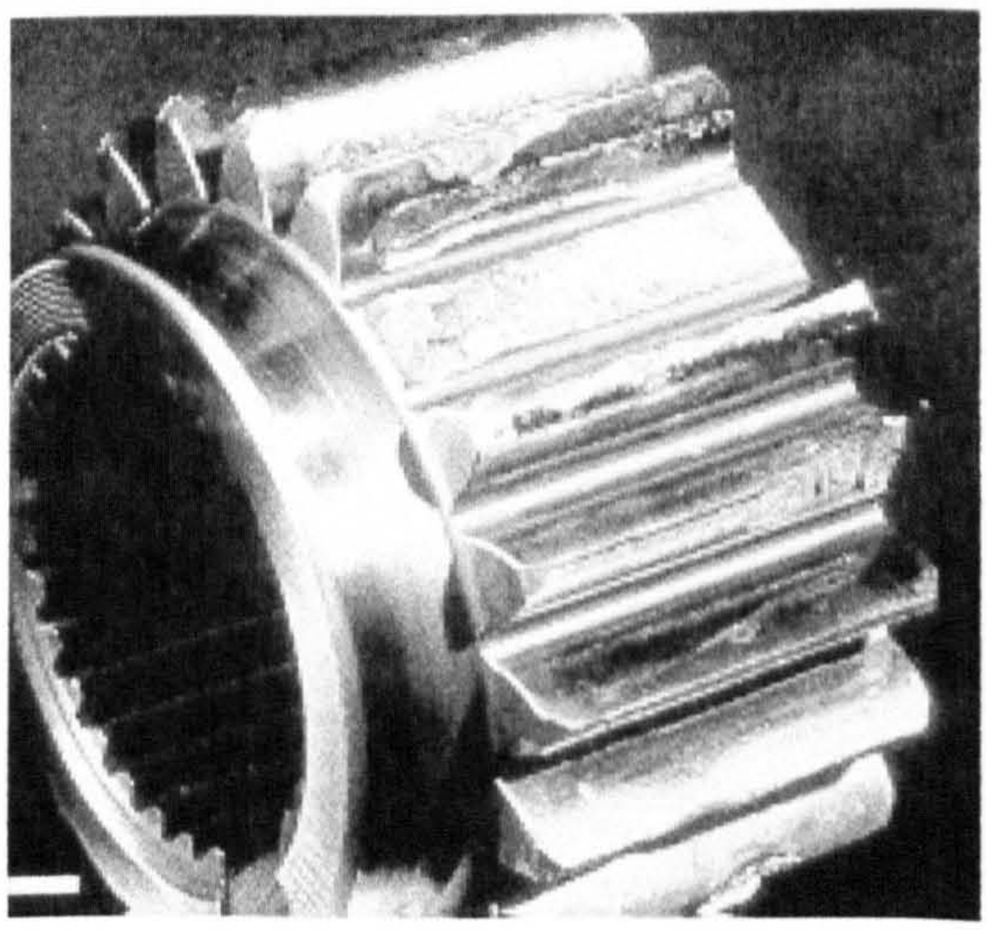


Figure 4.2.2 Tooth Root Fracture (Tailian 1992)

Bending fatigue breakage, due to cyclic stressing of the gear tooth beyond the endurance limit of the material, is generally a consequence of fatigue induced cracks at the tooth

root (Figure 4.2.3). Stress concentrations may help aggravate the running conditions by subjecting the gear to higher root stress levels than would normally be predicted. These stress concentrations can be induced by notches in the root fillet, inclusions, small heat treatment cracks, grinding burns, and residual stresses.

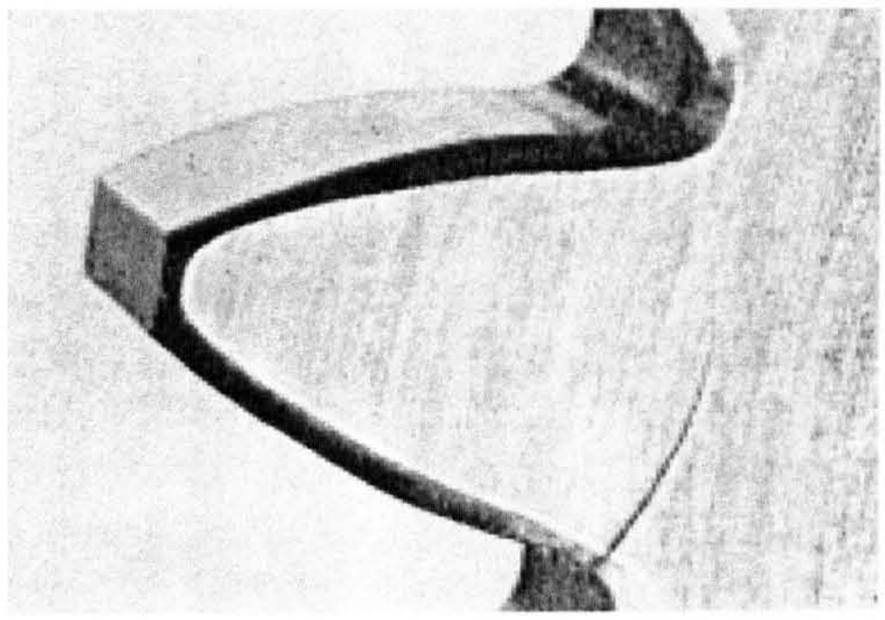


Figure 4.2.3 Fatigue Crack Caused by Stresses at the Root Fillet Leading to Tooth Breakage (AGMA 1980)

Overload breakage, where the load exceeds the tensile strength of the gear material, could result from bearing seizure, failure of the driving equipment, debris passing through the mesh, or from system dynamic loads.

4.3 Scuffing

This involves the instantaneous friction welding and immediate separation, by tearing, of mating gear teeth and, as a consequence, metal is rapidly removed from the surfaces (Neale 1995). Radial scratch and tear marks in the direction of sliding can be observed, and often material has been displaced radially over the tips of the gears. It also appears that considerable material has been removed from above and below the operating pitch line, as this stands out prominently (Figure 4.3.1). The tooth profile is destroyed and the gear is no longer fit for use (AGMA 1980).

The mechanism for this failure is not fully understood and is extremely complex, one supposition is that the time in conjunction must be long enough for a critical temperature to be reached (Kelly & Barnes 1994). Scuffing in a rolling/sliding contact increases in severity with sliding speed, overheating, low hardness, excessive load, and inadequate lubrication (Tallian 1992). Various causes have been postulated: lubricant film failure, inadequate lubrication, or debris contamination, all of which produce localised overheating of the mesh, hence permitting metal-to-metal contact (discussed by Nicolson 1996). It can also be caused by tooth profile modification variations from tooth-to-tooth

and small surface irregularities. These conditions lower the oil viscosity and film strength due to frictional heat and dynamic loads in critical contact areas (AGMA 1965).

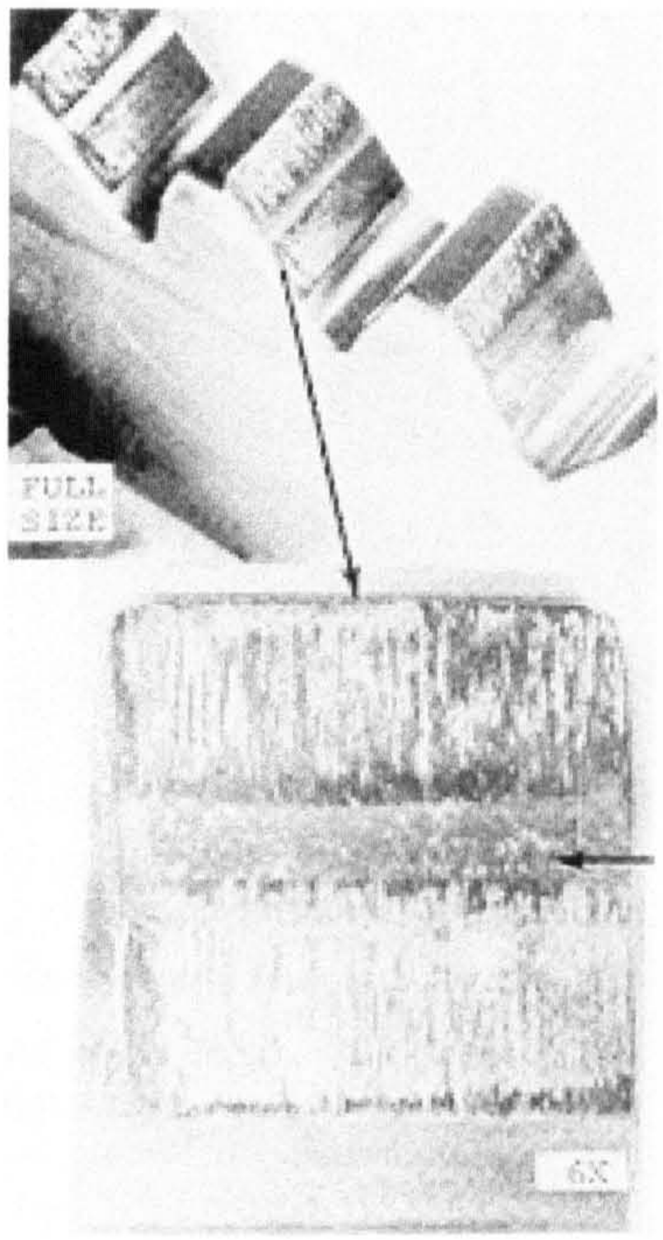


Figure 4.3.1 Scuffing Failure on Gear Teeth (Pitch Line Unaffected) (Drago 1988)

At the moment the effect of parameters such as speed, load, temperature, and lubricant on scuffing for a given geometry, material, and surface finish can be obtained for fixed configurations but are difficult to relate to another test (Tallian 1992).

The critical conditions for scuffing can be delayed, or extended to higher contact loads and speeds, by using EP additives (Johnson 1988).

Localised scuffing can be less serious, as it does not cover the full facewidth (Figure 4.3.2).

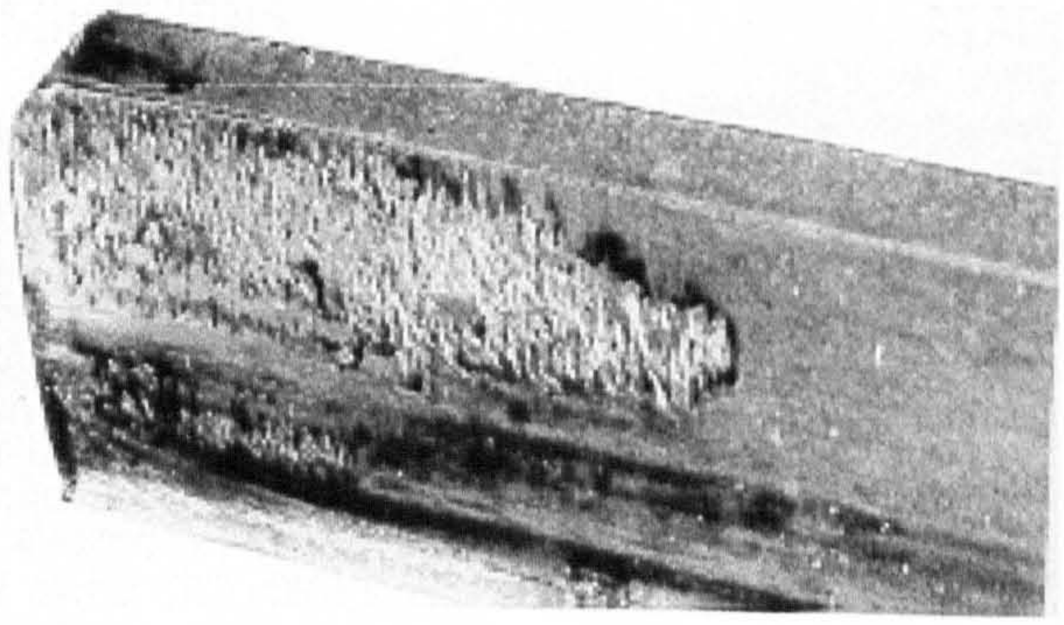


Figure 4.3.2 Localised Scuffing (Tallian 1992)

It is caused by local load concentrations due to bad design or unintentional factors such as: misalignment resulting from manufacture, deflections under load, or temperature

gradients across the face due to non-uniform cooling of the mesh. For example, if the load concentration is near one end of the teeth, the cause is most likely to be misalignment, and the result is more load carried on this portion than the lubricant film can support.

Scuffing is often called scoring (in the US) and sometimes galling (Tallian 1992). Scoring is sometimes seen as a different failure mode (Neale 1995) where lubricant breakdown and welding of the surfaces has not occurred. A good review of scuffing is given by Nicolson (1996).

4.4 Pitting

As mentioned earlier, this is thought to be a form of surface fatigue failure of the material which results from repeated surface or subsurface stress cycles that are beyond the endurance limit of the material. Pitting often occurs when heavily loaded, lubricated surfaces roll together, as in gear teeth and discs (used to simulate gear tooth contact). It takes the form of small craters left as a result of fragments of metal falling out of the surface, normally after a large number of load cycles (Figures 4.4.1 and 4.4.2).

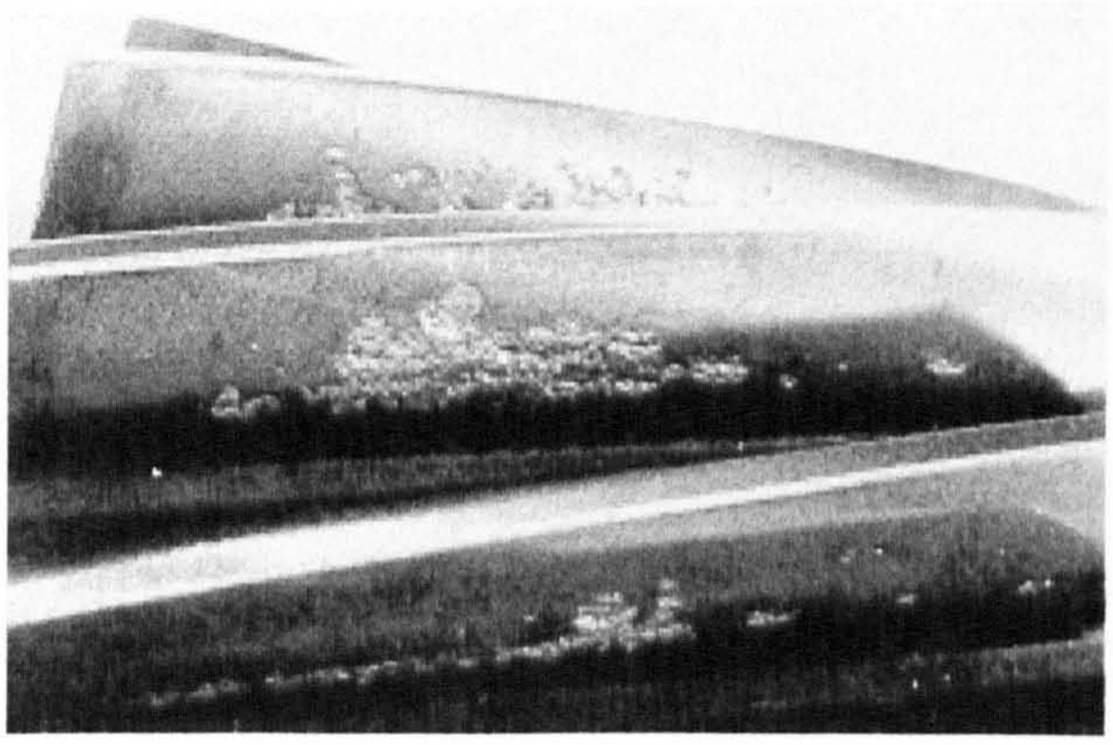


Figure 4.4.1 Pitting in a Helical Gear (Alban 1985)



Figure 4.4.2 Pitting due to Surface Distress (Tallian 1992)

The pits develop from arrowhead cracks that start at the surface and eventually separate a particle from the main body of material; they are fan shaped and are symmetrical about an axis parallel to the rolling direction (Figure 4.4.3). At the bottom of a pit a series of curved steps indicating progressive fracture can be observed. This is because pitting is a fatigue phenomenon in which the breakdown of the tooth contact occurs by a process of progressive cracking. It may originate subsurface from a non-metallic inclusion or, more likely, at the surface itself. In gear teeth it usually manifests itself near the pitch line and is often the life-limiting factor. The onset of pitting is greatly influenced by sliding in the contact, the surface temperature, and the lubricant.

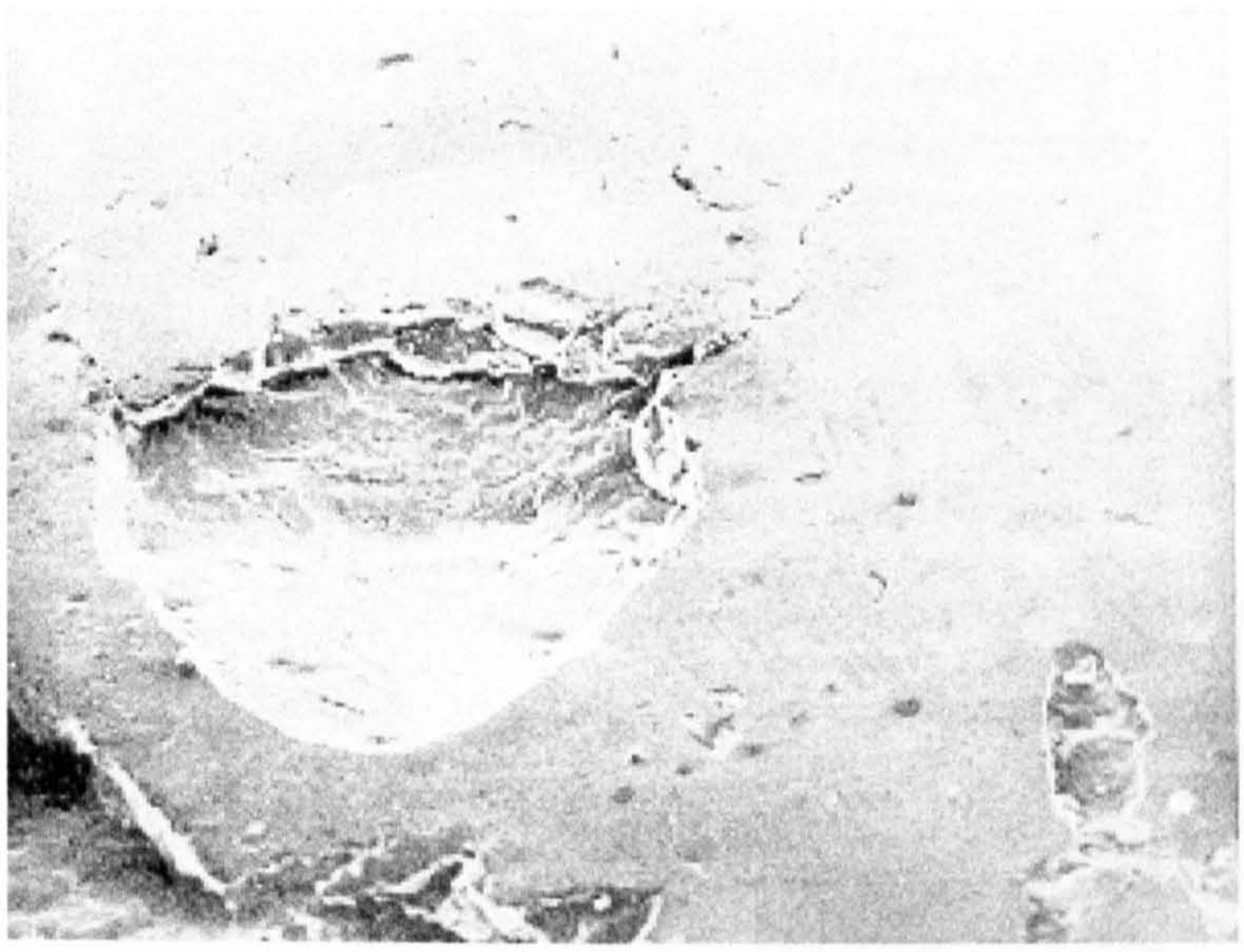


Figure 4.4.3 Shape of a Pit (52x) (Bartz & Kruger 1973)

The dedendum section of the drive gear is often the first to experience serious pitting damage. Once enough stress cycles have been built up, pitting continues until the tooth profile is completely destroyed by pits of various shapes and sizes, causing rough operation and considerable noise. A bending fatigue crack may originate from a pit, causing a tooth breakage failure (Bartz & Kruger 1973, Alban 1985) (see Figure 4.4.4).

Pitting failure can be overcome, or at least delayed, by using smooth gear tooth surfaces; by improving the accuracy of the involute profile; by introducing profile modification to obtain smooth meshing action and a reduction in the dynamic load on the teeth; or by increasing the lubricant viscosity (AGMA 1980). If this does not work, the load cycle on the gear teeth is probably too high. Solutions then involve keeping the load on the surface below the endurance limit of the material or increasing the hardness of the material so that the endurance limit rises to a point where pitting will not take place.

Sometimes pitting can be avoided by increasing the hardness level of only the driving member.

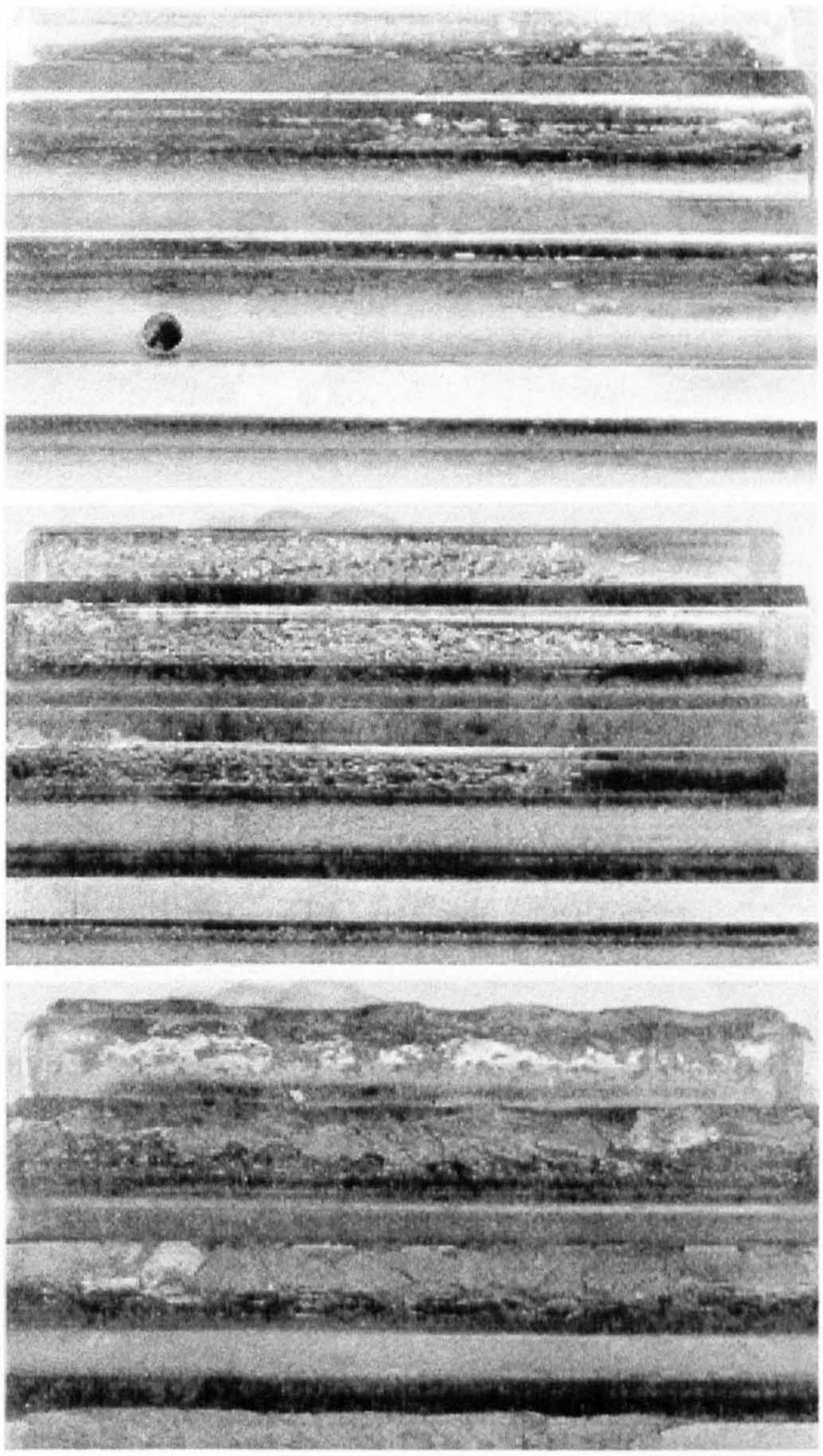


Figure 4.4.4 Progressive Deterioration of Gear Teeth by Pitting (Alban 1985)

The idea behind using a harder material, or reducing the contact stress, comes from the principle that during continuous rolling and sliding contact the initial surface roughness changes due to plastic deformation, therefore, if plastic deformation can be reduced pitting can be prevented.

4.5 Micropitting

Micropitting (Berthe et al. 1980, Shotter 1981, Olver et al. 1986, Webster & Norbart 1995) is another fatigue phenomenon whose initial damage consists of craters roughly 20 μm deep and equal in diameter. These craters (Figures 4.5.1 and 4.5.2) can occur either

isolated or in groups, are initiated at the surface, and are related to asperity interaction. The rate of micropit formation depends on running-in: when running-in takes place, i.e. when the pressure on asperity tips decreases to a value within the elastic limits, the rate of formation of micropits with time tends to zero and the fatigue life is consequently increased (Berthe et al. 1980). They may, however, give rise to severe wear (Olver et al. 1986) or progress into destructive pitting (Berthe 1978). Flamand and Berthe (1978) found that after $15x10^6$ cycles a large density of pits coupled with sliding may sweep away the original surface pattern forming a new surface, micropitting may then stop.

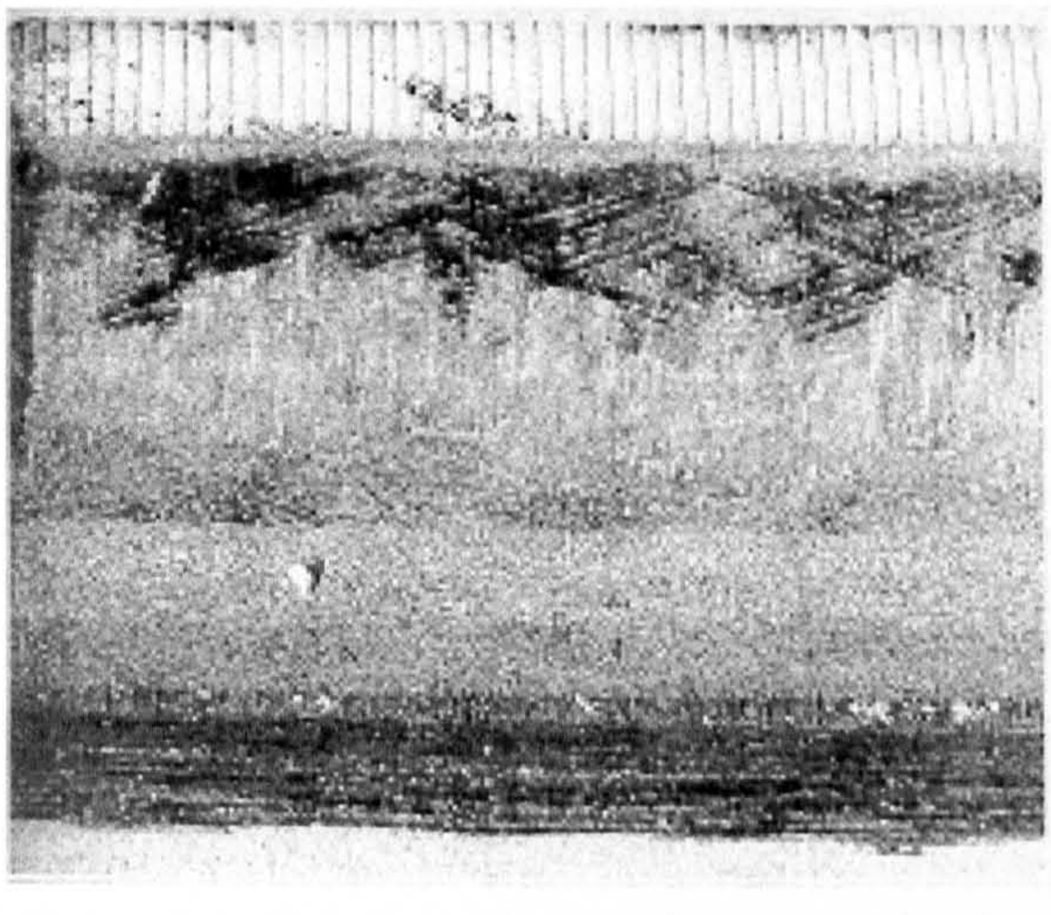


Figure 4.5.1 Micropitting in Gear Dedendum (Neale 1995)

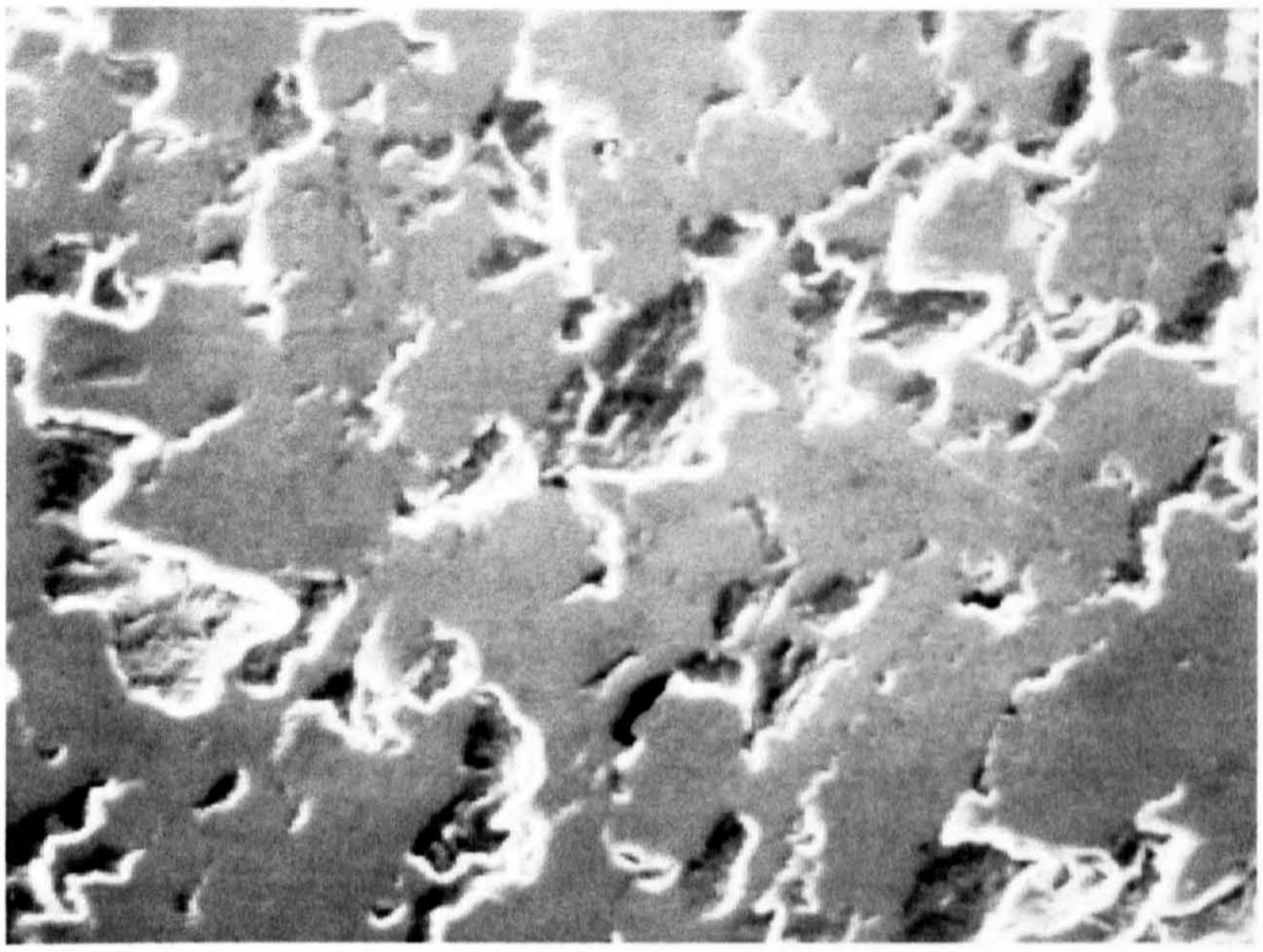


Figure 4.5.2 Close View of Micropitting 500x (Graham 1979)

It appears with both synthetic and mineral oils and with through-hardened and case hardened steels of either carburised or nitrided forms (Shotter 1981). It can be localised

to over-stressed areas, and may tend to redistribute the load by progressively removing high contact zones (AGMA 1980). When the load has been redistributed, it may stop, and continued operation tends to polish the contacting surface asperities and in general improve the overall appearance. It can be a result of minor profile errors, local surface irregularities, or lack of proper alignment.

Olver et al. (1986) associated the wear caused by micropitting with plastic deformation, fatigue cracking, ductile extrusion, and fracture on a scale associated with the asperity contact. The stress raising feature was the roughness producing local plastic deformation, despite the low Hertzian applied stress. They found there was an incubation period where no macroscopic wear occurred, this was followed by a wear phase in which the diameter of the test specimen decreased linearly with time. When the slide-roll ratio was increased, pitting occurred faster, but the wear rate was unaffected. The effect of a small hardness reduction was found to give a very large increase in steady wear rate and decrease the incubation period. This could be removed by making the counterface slightly softer. The various methods suggested to prevent severe micropitting were: both surfaces being as hard as possible; the surface experiencing more cycles should be harder; the harder surface should be made as smooth as possible, this will tend to run-in the other surface; and the lubricant film should exceed the combined roughness height.

The terms surface distress, peeling, fatigue wear, microspalling, frosting, and delamination wear have all been used to describe this phenomenon (Tallian 1992).

4.6 Other Failure Modes

There are various forms of surface fatigue that should be mentioned, due to their importance in gear operation.

Of these, one should mention spalling, as this is seen by some researchers as a different failure mode to pitting and by others the term is used instead of pitting (particularly in the US). The author, however, considers it to be a form of pitting originating from the subsurface.

Case crushing (Drago 1988) is a subsurface fatigue failure which occurs in heavily loaded case hardened gears. Failures of this nature depend on the surface contact stress, a case which is significantly harder than the core, and the application of a large number of stress cycles. Cracks originate in the subsurface area when stresses exceed the

strength of the subsurface material, they propagate towards and along the case-to-core boundary and to the surface of the gear tooth (Figure 4.6.1). When several cracks reach the tooth surface, large, long pieces of the tooth surface break away. The failure is caused by insufficient strength of the material at the depth of the maximum Hertzian shear stress, and high residual stresses in the gear may contribute to this. Solutions to this problem involve increasing the effective case depth or the hardness of the core material.

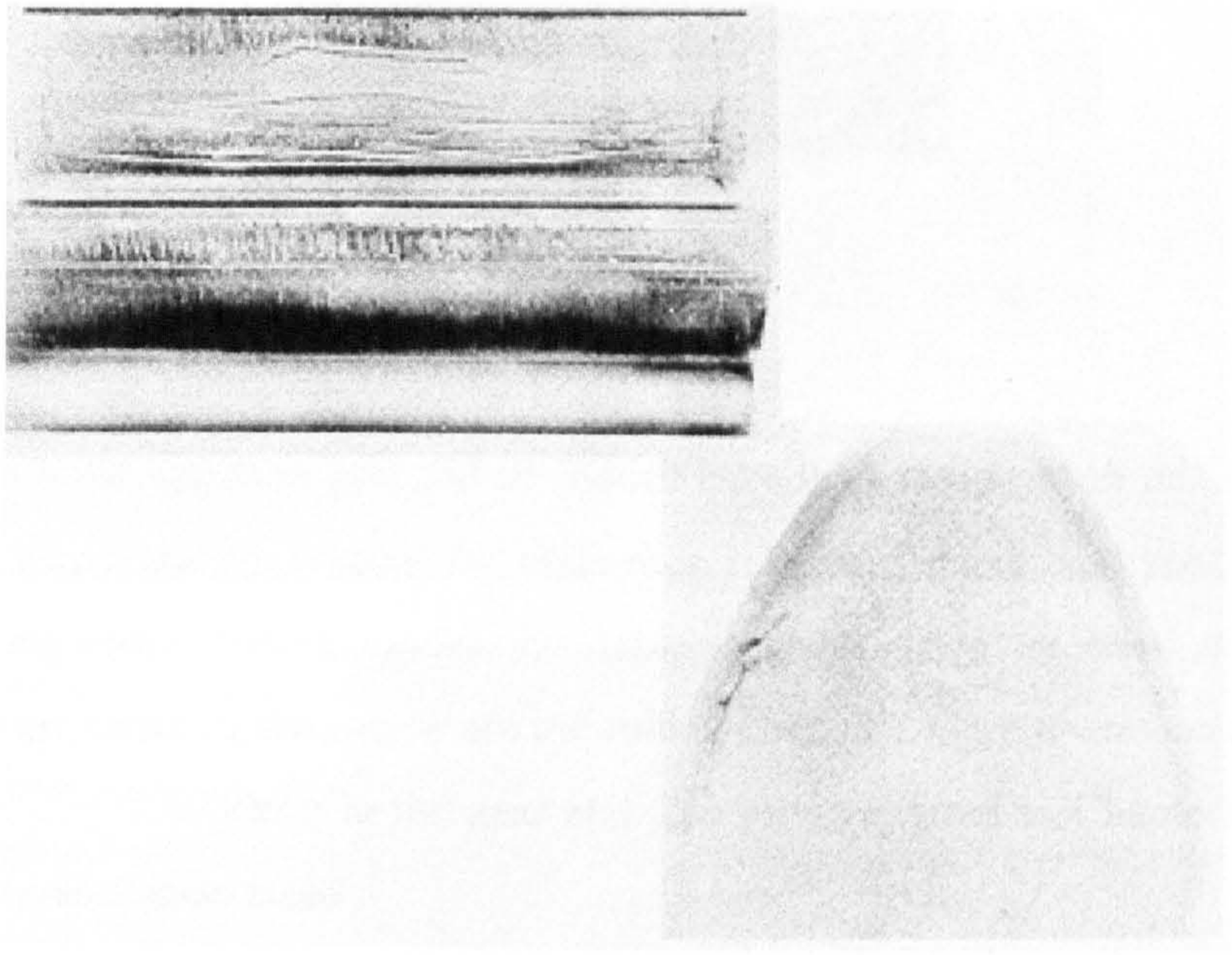


Figure 4.6.1 Case Crushing (Drago 1988)

Plastic flow (AGMA 1980) involves surface and subsurface material deformation and yielding, and is caused by high contact stresses and the rolling and sliding action of the gear teeth. It is usually associated with softer gear materials, although it often occurs in heavily loaded case hardened and through hardened gears. Cold flow, rippling, and ridging are some forms of this failure mechanism.

Finally, there are many forms of wear, defined as the removal of component surface material in the form of loose particles from one or both surfaces. Some forms are not too serious, or are even beneficial, such as polishing, mild, and moderate wear; whereas others can be detrimental, such as abrasive wear (Figure 4.6.2) and corrosive wear (AGMA 1980). The wear rate is greater for more severe stress conditions and sliding, and usually higher for rougher surfaces, higher friction coefficients, contaminated lubricant (three body wear), chemically aggressive environments, bad material combinations, and low hardness (Tallian 1992).

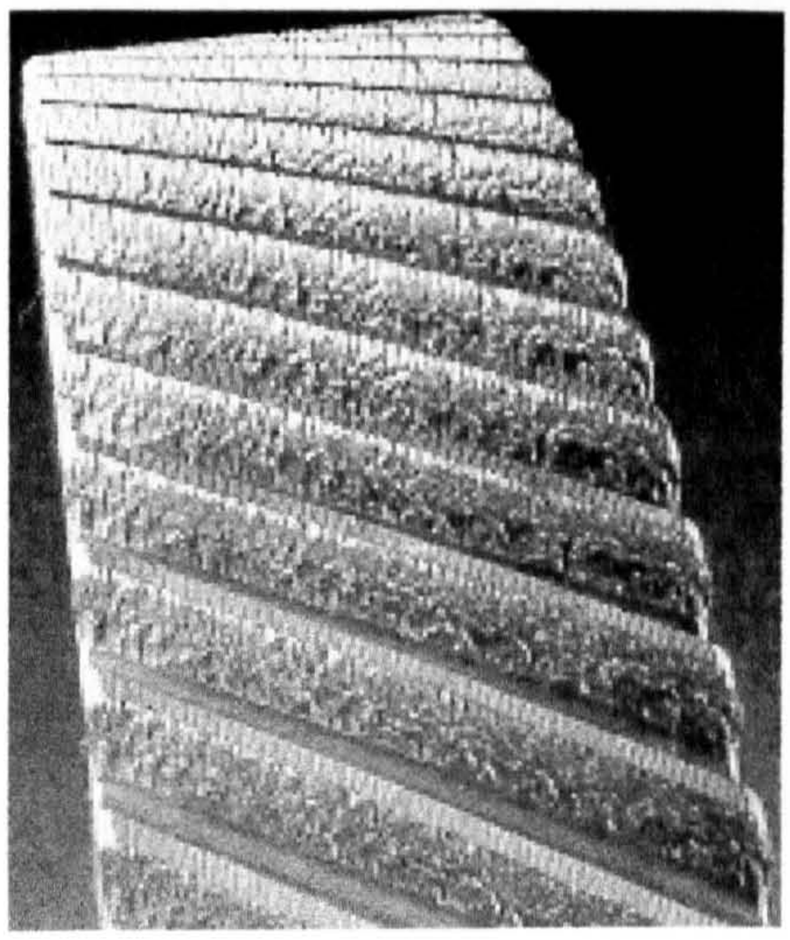


Figure 4.6.2 Abrasive Wear (Tallian 1992)

4.7 Conclusions

Some of the most common gear failure modes have been reviewed in this chapter. The characteristic appearance, reasons for occurring, relative dangers, and possible methods for preventing these failure modes, or delaying them, have all been discussed. Of particular importance to the author are the rolling contact fatigue phenomena pitting and micropitting that took place in the gear and disc tests reported in Chapters 11 and 12, but scuffing was also an issue.

Chapter 5 Gear Materials

This chapter gives an idea of the requirements a gear steel has to fulfil in use, particularly for aerospace applications, and the processes available to tailor a gear material to meet such requirements. The current limitations of gear steels and the possible benefits of some of the more recent materials are discussed, and then some previously investigated steels are reviewed. Finally, the materials and processes investigated by the author are reviewed.

5.1 The Basic Requirements for a Gear Steel

Before discussing the treatments available to steels, it is important to know the requirements a gear steel should meet. The gear application will determine the properties required, material used, and possible heat treatment. The weight, size, and cost of the gears are all important variables to consider, as well as how critical the component is.

Townsend (1983) gave a brief review of the wide variety of gear materials and processes, to improve properties, available to gear designers. Wood, plastic, aluminium, magnesium, titanium, bronze, cast iron, low-, medium-, and high-alloy steels have all been used in gear designs.

A gear steel will probably have a few of the following basic requirements: sufficient static fatigue strength to withstand instantaneous and dynamic loads; adequate toughness to withstand shock loads; adequate resistance to plastic deformation, pitting, scuffing and wear in the tooth contact area; and, finally, ease of manufacture, both thermal and mechanical.

The most important variables that dictate the ability of an alloy to resist the applied bending and rolling contact fatigue loads are surface hardness, core strength, and case depth in a case hardened gear. An essential aspect for optimum rolling contact fatigue performance and wear resistance is a high surface hardness. The high hardness allows the surface to withstand the stresses in the contact without excessive plastic deformation, which would result in rolling contact fatigue (Carter et al. 1960). In Hertzian contacts it is important to have a high material hardness to avoid plastic deformation (the pressure at first yield in a line contact is $1.67\sigma_y$ using the Tresca yield criterion and Hardness $\approx 3\sigma_y$

(Johnson 1985)). In practice, surfaces are rough and the maximum shear stresses are shifted towards the surface and much larger than the Hertzian value.

The subsurface residual stress distribution in a gear can also play an important role. Tensile residual stresses may be detrimental (Davies 1986), increasing the likelihood of fatigue damage, stress corrosion, and fracture; on the other hand, compressive residual stresses are usually beneficial.

Finally, apart from the above mentioned factors, careful heat treatment (Jatczak 1978), grain size, cleanness, and machining are all of prime importance in a gear steel.

5.2 The Requirements of an Aerospace Gear Steel

In addition to the requirements for gear steels, aerospace transmission designs need to remain competitive in terms of weight, cost, and oil loss tolerance.

The high hardness necessary to overcome rolling contact fatigue has the drawback that it also enhances crack propagation. The progression of a surface crack or fracture through the case has a higher probability of changing direction when it reaches a more ductile core (DiRusso 1986). Therefore, the core material in the gear must have a high fracture toughness and resistance to fatigue crack propagation to withstand the cyclic loading.

Jatczak (1978) commented on the fact that ordinarily there is no significant difference in performance between case carburised steels and homogenous high carbon components with regard to rolling contact fatigue, resistance to scuffing, and wear (if the comparison is made at equivalent hardness, microstructures, and surface carbon levels). The static and dynamic load-carrying capacities in Hertzian compression are also essentially equivalent. However, he pointed out that when bending, torsion, and impact stresses were encountered, as in gears, carburised steels always provided significantly higher fatigue strengths. This results from a combination of the higher fracture toughness and impact resistance imparted by the low carbon regions and from the compressive residual stresses produced in the case layers by carburising or nitriding.

An important aspect of case hardening is to create a case which maintains a safe working margin above the induced stresses. To achieve optimum protection against case crushing, it is important to ensure that the case depth exceeds the depth of the maximum Hertzian shear stress. At the same time, the surface hardness has to be as high as possible to overcome the stresses caused by the asperities (discussed in Section 5.3).

It is now widely accepted that improved cleanness of steels by vacuum arc remelting (VAR) and vacuum induction melting (VIM) has improved the fatigue performance of components by reducing inclusion content (Littmann & Widner 1966). These processes are often used for aerospace material production.

It has, therefore, been noted that different properties are needed for the surface and interior of a gear steel for aerospace use. These properties of highest possible yield stress, or hardness, in the surface and high fracture toughness in the core material cannot be achieved without modifications. It can, however, be achieved by one of various methods of surface engineering.

5.3 Current Surface Engineering Processes for Gear Materials

Surface engineering involves modifying the surface properties of a material. It can involve either surface modification or applying a new surface, i.e. a coating. Both can give very different surface properties from the bulk material. Implicit in the decision to engineer the properties of a surface is that some of the existing properties of the substrate material are adequate for the surface to perform satisfactorily (Bell 1993).

The aims of the process can be to improve wear, fatigue, corrosion, impact resistance, or strength at elevated temperature, for example. Aspects such as the surface hardness, bonding strength, component size, thickness of the layer, and cost of the process are all important considerations. The concern in this research is improving rolling contact fatigue performance; this limits the treatments to processes that give a thick, hard layer to overcome the Hertzian and high surface stresses. Consequently, thermal treatments will be discussed here, however, at the end of this section, some coating processes will be mentioned as, although some give a thin case, they can be very hard and could, in the future, be integrated with other processes to give optimum surface characteristics. By determining the critical type of stressing and adapting the material properties to the actual type of stressing, the rolling contact fatigue strength of components, and thus life, can be improved (Schlicht & Zwirlein 1980).

Bell (1993) reviewed a range of surface engineering processes in relation to layer thickness (Figure 5.3.1). The thickness of the engineered surface can vary from several millimetres for surface welding, to a few microns for PVD and CVD coatings. Likewise surface hardness spans a wide range from about 250-350 kgf mm^{-2} for some spray

coatings, to 1000 kgf mm^{-2} for nitrided steels, and up to 3500 kgf mm^{-2} can be achieved for PVD (TiN) coatings.

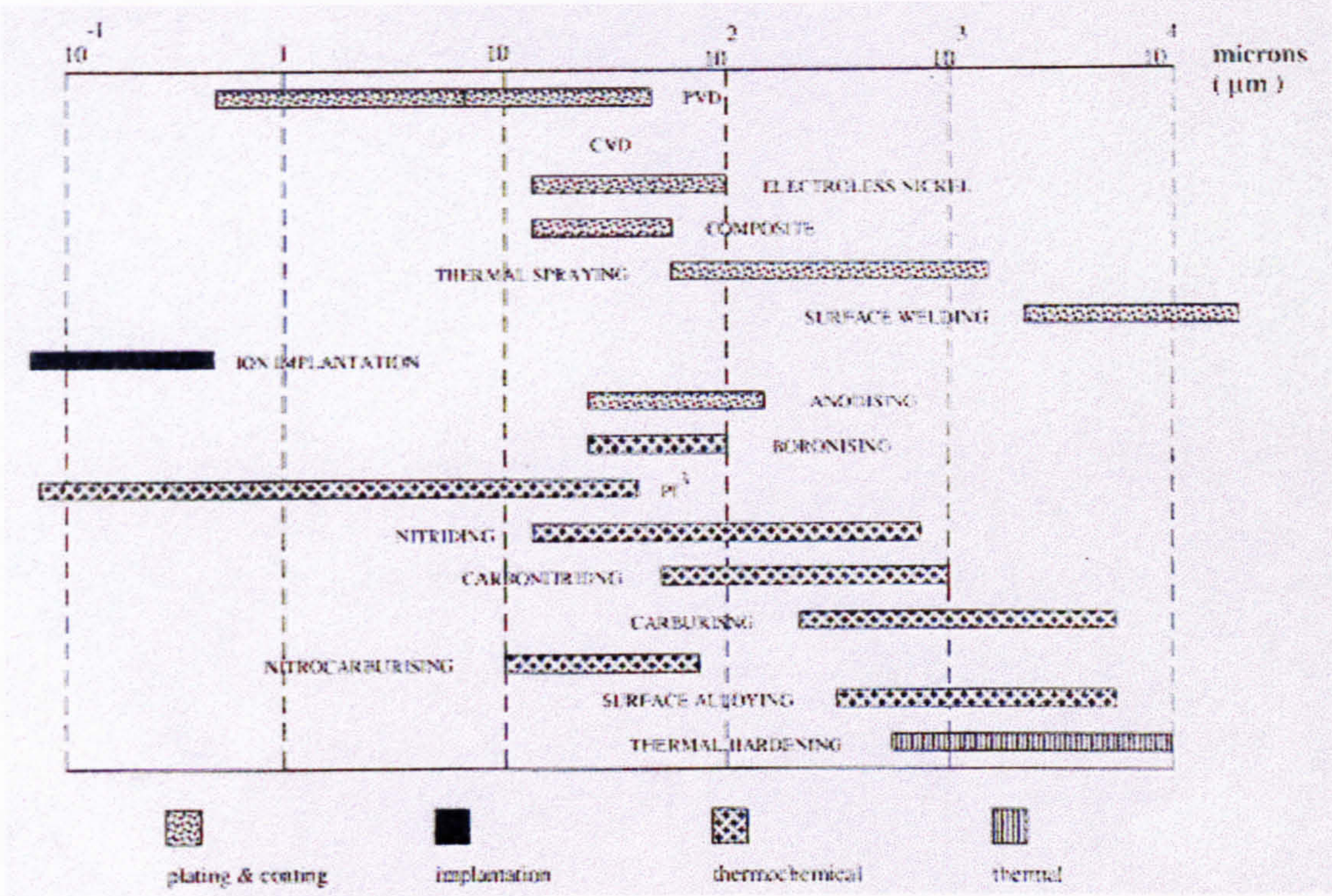


Figure 5.3.1 Classification of the Surface Engineering Technologies as a Function of Surface Modification Thickness (Bell 1993)

Currently the main surface engineering process available to aerospace gear designers involving surface modification is heat treatment. There are three major types of heat treatment: thermal treatments, where temperature variations alone are involved; thermochemical treatment, which involve processes where surface additions or losses take place by diffusion as well as thermal treatment; and thermomechanical treatments, which involve mechanical work during the heat treatment. An in detail description of the thermal processes described in this section can be found in (Bell 1973 and Krauss 1989, amongst others).

The main thermal treatments are annealing, quenching, and tempering. Annealing is used to reduce hardness, improve machinability, and produce a desired microstructure. It requires heating the steel and maintaining it at a subcritical temperature, before cooling it at a suitable rate. Quenching is used to harden an alloy by austenising it and then cooling it rapidly enough so that some, or all, of the austenite transforms to martensite. Tempering is used to impart the best balance of properties and a safe working

temperature on the steel. It involves reheating a quench hardened steel to a temperature below the transformation range and then cooling.

In thermochemical treatments metallic or non-metallic elements are added to produce a hard, wear resistant surface on components that also require toughness. The idea is to improve the fatigue performance of the component and perhaps impart better scuffing and frictional characteristics.

The treatments with non-metals mainly involve carbon and nitrogen, and these can be divided in two main categories: austenitic, where nitrogen and/or carbon are diffused into the steel in the austenite phase; and ferritic, where carbon and/or nitrogen are diffused into the ferrite phase.

The main austenitic processes are carburising and carbonitriding. In carburising carbon is diffused down a concentration gradient into low carbon materials at 900 °C, or higher, for periods between 30 minutes and 16 hours, depending on the case depth required. The carbon may be supplied through a solid, liquid, or gaseous medium and the process must be followed by quenching to harden the case. The increased carbon content in the case increases hardenability by creating more martensite on quenching, so that the resulting case is a mixture of martensite and retained austenite. The high carbon case offers high surface hardness (a maximum Vickers hardness of 900 kgf mm^{-2} can be obtained), but the component has a tougher core than if the whole steel were high carbon steel. A further advantage of the case hardening is that, as a result of the different phase transformation products in the case and core of the material, the case is in a state of compression. The compressive residual stress could be important as it may help rolling contact fatigue endurance and prevent fracture by resisting crack initiation. The majority of carburising steels are low alloy steels of low initial carbon content (0.15-0.2 %). Once hardened the component can be refrigerated, to obtain complete transformation which increases the hardness near the surface and prevents possible dimensional changes occurring in service, and tempered to improve core toughness. In carburising the sides and ends of the gear teeth are at risk of cracking, caused by the expansion of the carburised surface producing excessive tensile stresses in the core material. Reheating can be used instead of direct quenching to refine the structure and reduce the risk of cracking. This involves cooling the steel after carburising to give bainite, then reheating to just above upper transformation temperature and quenching.

In carbonitriding carbon and nitrogen are diffused into the component at 720-925 °C for 1 to 3 hours followed by quenching. The cases are usually shallower than carburising but favourable residual stress and high hardness can also be obtained (Pearson & Dezzani 1993, Bell 1973). The nitrogen increases the hardenability of the surface layer; oil quenching rather than water quenching can therefore be used, reducing the risk of quench-cracking.

The main ferritic processes are nitriding and nitrocarburising. In nitridng nitrogen is added at 500-570 °C from a gaseous or liquid medium, and then the steel is air cooled. Atomic nitrogen forms at the surface and diffuses in, reacting to form nitride compounds as fine precipitates close to the surface, this produces lattice strains high enough to nucleate dislocation which, together with the precipitates, have a strong hardening effect. Compressive residual stress are also obtained in the case. The steels used need to contain one or more of the nitriding elements aluminium, chromium, molybdenum, and vanadium. The hardness produced by nitriding (900-1100 kgf mm^{-2}) is maintained at temperatures up to 500 °C; whereas in the martensitic layers in carburised steels, hardness falls at about 200 °C. The low temperatures involved mean there is little distortion to the component, but the treatment times are longer.

The main problem with nitriding is the formation of brittle nitrogen compounds on the surface of components, this is known as the 'white' layer. It consists of a thin layer of iron nitrides, composed of an outer layer of epsilon iron nitride (typically 10 μm deep), over a layer of gamma-prime nitride (also about 10 μm deep) (Olver et al. 1993). Although it is very hard, it is brittle and cracks easily and can promote fatigue failure (Bell 1973, Braza 1992, and Hutchings 1992). Olver et al. (1993) analysed this white layer and deemed it necessary to remove it, as it offered little substrate protection and could be expected to fail rapidly. It is often removed by grinding or chemical means.

However, in tests described by Winter and Weiss (1981) where the white layer was removed by grinding, the surface stress endurance limit of gears made from two different nitrided materials was reduced by 10-20%. They described the epsilon iron nitride layer as being abrasion and corrosion resistant, and the gamma prime layer as being brittle, and found a tendency for endurance limit to increase with increased epsilon to gamma prime ratio. Davies (1996) suggested there was some evidence to show that a shallow white layer did not adversely effect bending fatigue properties (attributed to Riopelle 1975). In

addition certain investigators have stated that, if the white layer consists of the gamma prime phase, then useful wear properties resulted (attributed to Clayton & Sachs 1977).

In a recent study on the effect of the white layer on micro-pitting and surface contact fatigue failure of nitrided gears, Bull et al. (1998) found that the white layer produced high resistance to micro-pitting and pitting compared to similarly nitrided gears without the white layer. They got a smoother, polished surface when a white layer was present, whereas without it the gears behaved much like carburised gears. They found micropits left cracks behind which enabled further micropitting, this was not observed in the white layer which arrested crack progression. The white layer had a top porous layer and a non-porous one below this. They measured a Vickers hardness of 1000 kgf mm^{-2} in the non-porous layer, while the porous layer had a Vickers hardness of 800 kgf mm^{-2}.

In gas nitriding components are heated to 530 °C in a stream of ammonia gas. The ammonia dissociates forming nitrogen at the surface which diffuses in. In plasma nitriding the component is placed in a chamber with nitrogen and hydrogen at a sub-atmospheric pressure, and a plasma discharge is established by creating an electric potential, with the workpiece as the cathode. The electrical power dissipation heats the steel surface, which is bombarded with nitrogen atoms. The process is faster than gas nitriding and can be operated at lower substrate temperatures (Hutchings 1992).

In nitrocarburising, nitrogen and carbon are added at 500-570 °C then the component is air cooled or quenched. Hardness and wear resistance are given to the surface by a layer of iron carbonitride. A lower hardness than nitriding is achieved (500-650 kgf mm^{-2}), but the process is much faster.

Distortion can be a major problem associated with heat treatment (Davies & Gittos 1989). It is caused by the phase and temperature changes within the material and varies considerably from component to component. Size distortion can be predicted at the design stage and the component can be finish ground. Shape distortion, that occurs particularly in asymmetrical components, can be minimised by avoiding temperature differentials, minimising phase transformations, and avoiding rapid heating and cooling of irregular shapes. Distortion tends to be more of a problem in carburising due to the elevated temperatures invclved, however, as the case is generally deeper than nitriding, finish grinding is not so much of a problem.

Coatings are the other surface engineering process available to modify a component's tribological performance. There is a need to control both the coating and substrate properties and an abrupt change in properties where these meet can lead to potential adhesion problems (DTI 1985). There are, however, a large choice of coating materials available.

The main surface coating groups are electrochemical treatments; chemical treatments; chemical vapour deposition (CVD); physical vapour deposition (PVD); spraying processes; and welding processes.

Electrochemical coatings are produced by electrolysis in an aqueous solution of the coating metal with the component as the cathode. Chromium is the coating mostly used for wear resistance because it combines high hardness (1000 kgf mm^{-2}) with corrosion resistance. The layer is about 0.5 mm (DTI 1985).

In chemical treatment the component is immersed in solution of a salt of the coating metal. After heat treating, the component can have a hardness of 1000 kgf mm^{-2} and a good adhesive wear resistance. Hard particles can be incorporated in both processes (e.g. silicon carbide).

CVD compounds are reacted in the gas phase to form a dense layer on a heated substrate. Titanium nitride and carbide are the most widely used deposits (10 μm depths). The temperatures are high (800-100 °C), this limits the choice of substrate (DTI 1985).

PVD is performed at sub-atmospheric pressures. The coating is generated by thermal evaporation or electrical sputtering of a the chosen material. Titanium nitride is the most popular (1-10 μm depths). Substrate temperatures can be kept below 500 °C.

Spraying processes involve heating particles of the coating material to a molten state and then firing them at the relatively cold substrate. Coating density and strength of bonding to the substrate increase with projection velocity. Certain coatings can be porous and the bond may be less strong than other processes.

Welding processes are used to deposit wear resistant coatings, which range from low alloy steels to tungsten carbide composites. The bond is strong and deposition is fast.

Many of these latter process are not applicable to gears, particularly for aerospace use. The main reasons are: the surface layer may not be thick enough, case crushing and

substrate failures are then possible; the surface layer may not bond strongly enough to the substrate, this could result in peeling and consequent surface failure; the process may not give the gear tooth the right properties (low impact resistance and fracture toughness, for example); too high a processing temperature is needed, this may negatively affect the substrates properties; or the cost of the process may not justify its use. Coatings are viewed with some caution because of fears of exfoliation or delamination (Vanes 1995).

5.4 The Need for New Materials

One should stress that the search for new materials for transmission design is being driven mainly by the aerospace industry because of the high technology nature of this area and the requirement for smaller, lighter, more reliable, and higher temperature operating transmissions. Therefore, some of the materials and processes described here, and in the next sections, are both complex and costly for conventional gear design. Nevertheless, the significant reductions in size and weight that may be possible in future geared transmissions may validate the use of some of these materials in other areas, particularly in demanding or troublesome applications. However, with other gearing factors such as surface roughness improvements by polishing, fine filtration, and lead and profile modifications still needing to be embraced in commercial gearing, perhaps surface hardening by the following techniques is just one of the available methods for improving transmission performance.

The trend in helicopter transmission design has been to increase the torque output to weight ratio and to improve reliability, which affects the cost of ownership. These objectives can only be accomplished with significant changes to transmission design and, as a result, the gears utilised will need to operate at continuously increasing torque or speed and must resist higher operating temperatures. It is considered justifiable, despite increased cost, to use expensive materials and advanced machinery if a higher power to weight ratio, with a high degree of reliability and survivability, is obtained. The weight saved directly relates to fuel capacity, which affects range and cost, and aircraft performance.

Currently, main gearbox input speeds are around 20,000 rev/min, but, in the future, design speeds as high as 27,000 rpm are envisaged; and the maximum operating temperature, currently 100-110 °C, will be up to 150 °C (Davies & Gittos 1989).

Furthermore, there is a desire to manufacture helicopter transmissions that will have an extra oil loss tolerance (this means that gear materials must have the capability of withstanding once-only excursions to 300 °C, this is discussed further in Section 5.5), as a result of battle damage or due to the failure of some critical component. US naval design requirements for severe duty helicopter transmissions require transmittal of functional torque for thirty minutes after loss of primary lubrication (Naval Air Systems Command Specification AS 3684A quoted by Saulnier 1989). The need for fatigue resistance at elevated temperatures is also necessary.

Therefore, the principal property sought in any new gear material for use in helicopters is an increased temperature resistance, while maintaining the other favourable properties previous materials possessed. This would permit higher, more efficient operating temperatures, with a consequent weight saving provided by the smaller gearbox lubrication system required. A side benefit of temper resistance would be the ability of the gearbox to operate for increased time under loss of lubrication conditions, as mentioned earlier. An improved bending and fatigue resistance in a gear material would also allow gearbox size reductions, provided the bearings can carry the increased stresses.

In conventional carburised gear steels, the tempering stage of heat treatment is that in which the best balance of properties and a safe working temperature limit are provided. These steels are usually tempered in the range 140-160 °C, which ensures no microstructural modifications during normal transmission operation (Jatczak 1978). This tempering range, however, when compared to the new temperature requirements, would result in softening of the steel at higher gearbox operating temperatures, together with microstructural modifications and dimensional instability (Davies & Gittos 1989).

This problem cannot be solved by raising the tempering temperature of a conventional carburizing steel to 300 °C, to achieve the desired oil-loss tolerance, because this would reduce fatigue performance (Thorne & Gittos 1985, Small & Gittos 1987). It would also result in an impaired wear resistance, a lower surface hardness, and a reduction in favourable residual stresses in the case (Kirk et al. 1966).

Another aspect of the currently available carburised steels is that they have now been tailored to offer close to their maximum rolling contact fatigue life by producing them to high levels of smoothness and cleanliness, so there are no subsurface initiated failures.

New processes now exist which can offer an increased fatigue life over these carburised steels.

Therefore, conventional steels cannot meet the new requirements placed on aerospace gears. The capability of these steels has become one of the limiting factors in transmission design, restricting any further opportunities for transmission design and development. Further improvements are only possible if changes are made to the gear steels currently used.

5.5 The Possible Benefits of New Materials

As discussed previously, helicopter transmissions have been designed and operated within the restrictions imposed on them by the available materials and lubricants. However, several promising materials have been developed to provide a better gear and/or bearing material for aerospace use.

These materials, known as temper resistant steels, are designed to meet the requirements of transmissions where hardness and surface durability characteristics are maintained at elevated temperatures. This has been achieved in two ways with carburising steels: by retarding the decomposition of martensite with additions of silicon, chromium, and molybdenum to give heat resistance up to 315 °C (Jatczak 1978); and via a process called secondary hardening, which involves precipitation of stable carbides of molybdenum, vanadium, and tungsten to achieve a high case and core hardness, and strength at temperatures up to 500 °C (Mack & Binder 1980).

These temper resistant carburised steels have an increased high temperature hardness (see Figure 5.5.1), which should improve performance, while retaining as many as possible of the advantages currently obtained from conventional carburised steels.

Schmidt (1990) discussed one of the problems caused during the carburisation stage of these steels with high chromium or silicon content. The silicon and chromium formed oxide films on the surface which prevented further carburising. A stage called preoxidation was introduced to reduce oxide adherence before carburising.

A further problem could result from the fact that all these temper resistant gear steels require a significantly higher austenising temperature than conventional carburising steel, this may give rise to distortion problems when heat treating large complex components (Davies 1996).

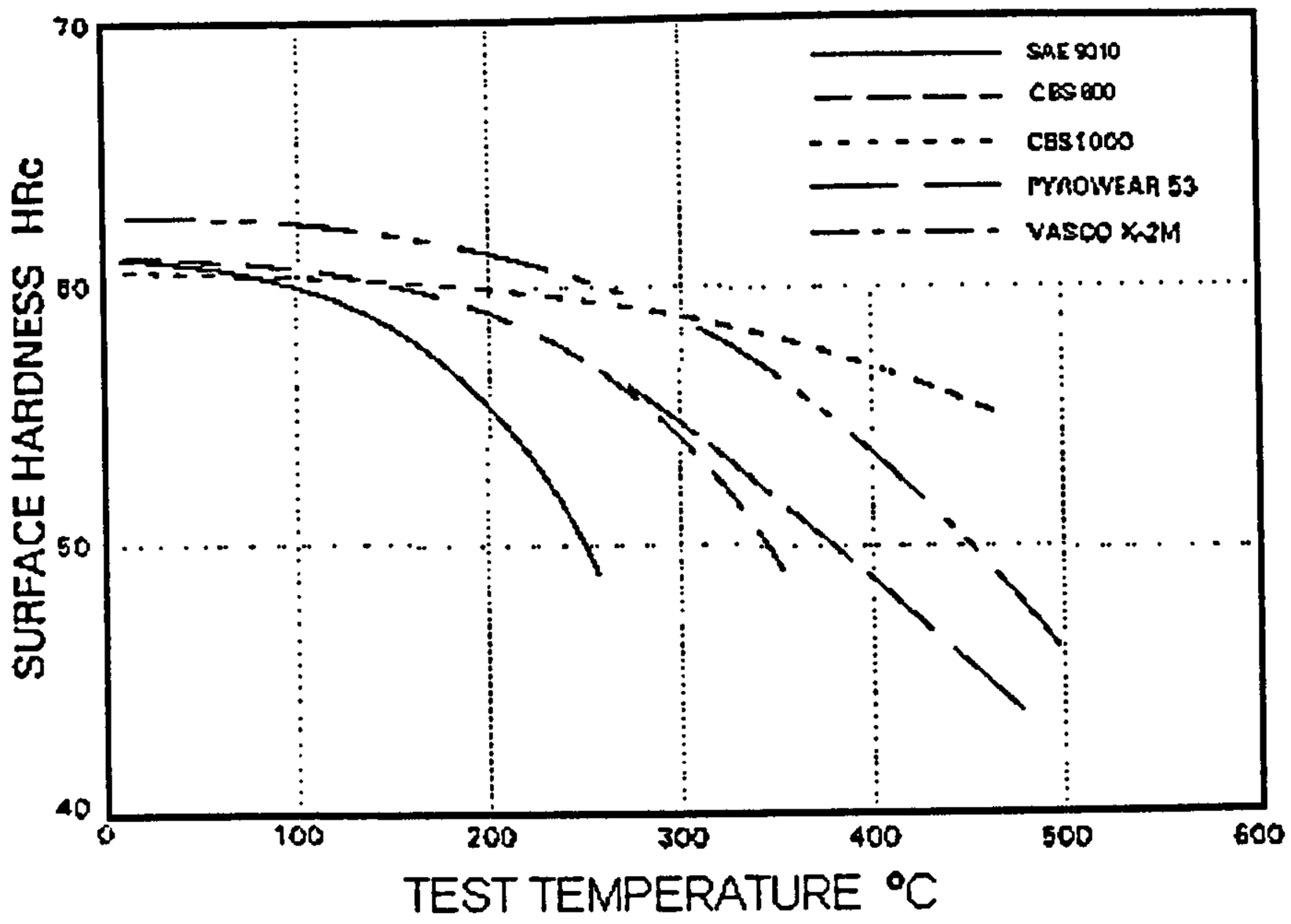
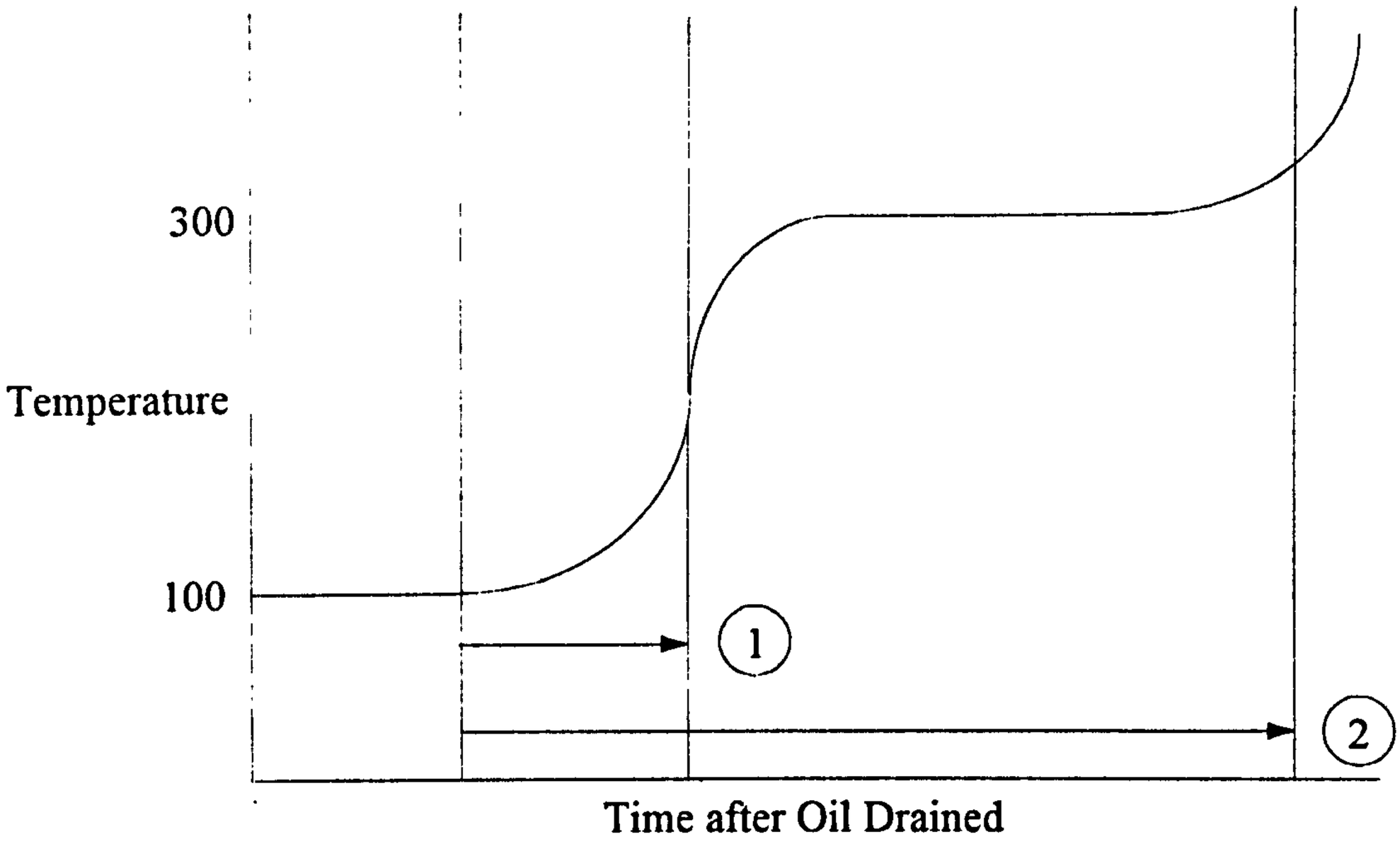


Figure 5.5.1 Influence of Test Temperature on the Case Hardness of a Number of Temper Resistant Gear Steels (from Davies & Gittos 1989)

Destructive tests on conventional gearboxes (Davies & Gittos 1989) have shown that there is an initial rise in temperature after oil loss has occurred, followed by a stable period, prior to a sharp temperature rise, and final failure of the gearbox (Figure 5.5.2).



1 Time to failure of a conventional gear steel
2 Time to failure of a temper resistant gear steel

Figure 5.5.2 Typical Temperature History in a Helicopter Main Gearbox with Time after Oil Loss (from Davies & Gittos 1989)

A survey by Hamlin (1978) found that loss of lubricant from a highly stressed gearbox could cause catastrophic failure within ten minutes, due mainly to loss of bearing clearance. Various methods to overcome this such as bearing improvements, reduction in vulnerability of the gearbox, provisions for an emergency lubrication system, and alternate heat paths to cool high speed bearings were considered.

Some of these temper resistant steels have the potential to be duplex hardened by nitrogen surface treatment (as they have a stable carburised core in excess of 500 °C and contain nitride-forming alloying elements), further enhancing their surface hardness. This should improve rolling contact performance. It is, however, important to control both processes so that the structures and properties resulting from the first process are not deteriorated by the second (Bell 1993).

For high temperature gear applications there are also nitrided steels, these have a high hot hardness and surface hardness. If a sufficient case depth can be obtained in a reasonable treatment time, then nitriding is a good prospect for high temperature operation gears. It gives the added advantage of high compressive residual stresses in the case and low distortion during processing (Pearson & Dezzani 1993).

The advantages of these superior materials can be used in both existing and advanced designs. For existing designs, the result should be an improvement in reliability at normal operating temperatures and also when elevated temperatures are encountered. For advanced designs, weight saving should also be achieved because of the smaller lubrication systems needed.

Finally, those materials which are of particular interest to helicopter transmission designers may be candidates for integral gear and bearing race components, as this offers the advantages of cost and weight reduction.

Temperature resistance and hot hardness are relatively easy to determine, but for a new material to be accepted, all of its other properties must be characterised and found to be equivalent to, or better than, the material it is to replace. The impact of these new materials on rolling contact fatigue failure (pitting) is still an area requiring investigation.

5.6 Hardness and the Effects of Alloying Elements in Steel

Hardness is affected by dislocations on grain boundaries and by the dispersion of particles (carbides). According to Schlicht and Zwirlein (1980), with increasing

tempering temperature the effect of the dislocations on hardness become less important. Secondary hardening starts with the precipitation of carbides at about 440 °C. The increasing secondary hardness reaches its maximum value at about 540 °C. At higher temperatures, there is a drop in hardness promoted by the accelerating precipitation of rapidly coarsening carbides.

In carburising steels the increased carbon content in the case increases hardenability. The hardness capability of a steel is a direct function of its carbon content. The relatively low amount of carbon in carburising steels (~0.10%) accommodates the carburising process, with enough carbon to attain sufficient core hardness, while allowing a large differential of carbon between case and core. The beneficial compressive residual stress which results from carburisation is normally proportional to this differential (Saulnier 1989). The carbon potential should not be set above 1.1 % to prevent formation of massive carbides (Jatczak 1978).

Molybdenum contributes to temper resistant properties (Jatczak 1978). It promotes hardenability by retarding the decomposition of martensite and forming complex carbides, increasing its content requires higher austenising temperatures to obtain proper core hardness (Scott 1967). It causes a loss of impact strength, so a compromise in the quantity used is needed (Saulnier 1989).

Chromium is essentially a hardening element. It too retards the decomposition of martensite by forming a solid solution with both austenite and ferrite iron phases (Jatczak 1978). It is also a strong carbide former and is believed to aid in wear resistance (Scott 1967, Saulnier 1989). As discussed in Section 5.5, high chromium contents can cause carburising problems, but this can be overcome by preoxidation.

Manganese forms carbides in the steel promoting hardenability and stabilises the austenite phase. Fine grained manganese steels can also attain high toughness and strength (Scott 1967). However, due to the volatile nature of manganese during vacuum arc remelting, its quantity is minimised in certain compositions (Saulnier 1989).

Nickel improves strength, roughness and resistance to sub-zero impact loading (Jatczak 1978), but has an adverse effect on room temperature impact loading (Saulnier 1989). It does not form carbides and remains in solution. It improves corrosion resistance and allows strength levels to be obtained at lower carbon contents, thus enhancing toughness and fatigue resistance (Scott 1967).

Silicon is usually used as a deoxidiser in steels. It is a non-carbide forming, solid solution strengthening element, which contributes to core hardenability by retarding the decomposition of martensite (Jatczak 1978).

Copper is believed to improve room temperature impact strength (Saulnier 1989). It is also believed responsible for rehardening caused by a precipitation hardening effect. Its concentration is limited by difficulties encountered during forging.

Vanadium provides grain refinement and minimises grain growth tendencies during thermal processing (Saulnier 1989, Jatczak 1978, Scott 1967). Coarse grain size decreases fatigue strength, fracture toughness and ductility. Vanadium also helps molybdenum with secondary hardening by precipitating stable carbides (Mack & Binder 1980).

Tungsten is another element that can be used to provide secondary hardening in temper resistant steels (Mack & Binder 1980).

To obtain a hard and dimensionally stable carburising case, the total proportions of these elements must be regulated to govern the amount of retained austenite after heat treating (Saulnier 1989).

Case retained austenite will reduce hardness and can be removed by cold treating. This is not usually recommended because some retained austenite has been found to improve contact fatigue life by allowing adjustment in surface contact geometries of mating elements (Jatczak 1978). The changes in dimension of components at operating temperature, due to subsequent transformation of the austenite phase, are imperceptible because only extreme case layers contain retained austenite.

In nitridng atomic nitrogen forms at the surface and diffuses in, reacting to form nitride compounds as fine precipitates close to the surface. This produces lattice strains high enough to nucleate dislocations which, together with the precipitates, have a strong hardening effect. The martensitic matrix is strengthened by solid solution hardening which also generates compressive residual stresses in the case (Vanes 1995). Nitrogen reduces the martensitic reaction temperatures, thus stabilising the austenitic phase. The steels used need to contain one or more of the nitriding elements aluminium, chromium, molybdenum, and vanadium. With nitriding the penetration is inversely proportional to the amount of nitrogen that is precipitated out as alloy nitrides (Davies 1986).

5.7 A Brief History of Bearing and Gear Materials

Since the 1970's many new materials have become available, particularly for aerospace use. Their development has been driven mainly by the requirements placed on high speed, load, and temperature aerospace bearings. There is a continuous search for metals that can withstand higher temperatures in turbines in order to increase power and efficiency. Some of the materials developed for bearings have been recognised as potential gear materials, and new ones specifically for gearing have also been developed. The aim of the designer is to achieve possible weight, space and size improvements, and greater temperature resistance in a transmission. Some of these gear and bearing materials are now discussed. The composition of a few of these alloys is given in Table 5.7.1.

In the 1960's SAE 52100 was the most widely used bearing steel, but there was a search for materials that could resist higher temperatures (Vanes 1995). Tungsten and molybdenum based steels, high speed tool steels, were then adopted due to their increased hardness and ability to operate at higher temperatures (secondary hardening, discussed in Section 5.6, is essentially the mechanism behind this elevated temperature hardness).

After much work to find the best high speed tool steels, T1 was used in the UK and M50 in the USA (Hampshire 1986). As loads increased and fatigue life requirements increased, air-melt steels were replaced with vacuum melting/refining steels. These were then replaced by vacuum induction melted-vacuum arc refined (VIM-VAR) steel processes. The lives of components were of the order of 40 times that of air melted SAE 52100 steel used in the early 1950's (Hampshire 1986).

As mentioned, M50 became one of the predominant materials for use in critical aircraft engine bearings, where high temperature capability was needed. M50 is basically a high speed tool steel which combines high hardness with dimensional stability. It gave an improved fatigue life over previous materials, including under marginal lubrication conditions.

However, it was found that in certain critical jet mainshaft bearings size, and/or speed was limited by the high operational tensile stresses (hoop stresses) which led to inner ring fracture and subsequent catastrophic bearing failure. M50 is a through hardened steel,

Table 5.7.1 Typical Steel Alloy Compositions

Percentages by weight:

Alloying Elements	C	Mn	Si	P	S	Cr	Ni	Mo	Cu	V	W	Fe
SAE 52100	1.05	0.5	0.2			1.3	--	--	--	--	--	Bal.
AISI 9310	0.1	0.65	0.25	0.01	0.01	1.3	3.2	0.11	0.11	--	--	Bal.
BS S156	0.16	0.4	0.2	0.008	0.005	1.15	4.15	0.25	0	0	--	Bal.
M50	0.82	0.09	0.16			4	--	4.15		0.92	--	Bal.
T1	0.7					4				1	18	Bal.
CBS 600	0.2	0.65	0.99	0.006	0.006	1.42	0.05	0.99	--	--	--	Bal.
CBS 1000	0.14	0.52	0.49	0.004	0.003	1.17	2.9	4.18	--	0.4	--	Bal.
Vasco X-2M	0.14	0.31	0.88	0.007	0.001	5	--	1.38	--	0.45	1.36	Bal.
AISI M50NiL	0.13	0.25	0.25	0.006	0.002	4	3.5	4.5	--	1.2	--	Bal.
RBD	0.2					3				0.4	10	Bal.
Pyrowear 53	0.09	0.33	0.96	0.011	0.003	1.05	2.01	3.25	2.19	0.1	--	Bal.
32CDV13	0.34	0.52	0.32	0.009	0.002	2.87	0.12	0.87	--	0.31	--	Bal.

C - Carbon, Mn - Manganese, Si - Silicon, P - Phosphorus, S - Sulphur, Cr - Chromium,
Ni - Nickel, Mo - Molybdenum, Cu - Copper, V - Vanadium, W - Tungsten, Fe - Iron.

and it was the lack of toughness in the core of the material, due to its carbide morphology, that was giving the problem (DiRusso 1986).

Various materials where then developed to overcome the insufficient fracture toughness of components, while maintaining the high hot hardness characteristics of M50. High fracture toughness, carburising tool steels such as RBD and M50NiL were developed, in the UK and USA respectively, to overcome this problem. Both these steels have been used successfully in main shaft applications to overcome cracking problems (Hampshire 1986).

M50NiL was developed to increase both the fracture resistance and fatigue life of gas turbine engine bearings. It had the carbon content reduced from M50's 0.85 % to 0.13 % to provide improved fracture toughness, and a small amount of nickel was added to stabilise the austenite and prevent excessive amounts of ferrite and retained austenite. It was found by Bamberger and Kroeger (1984) and Pearson and Becker (1989) to have an improved fracture toughness over M50 while retaining hot hardness and long bearing fatigue life. Pearson and Becker (1989) found an improvement in rolling contact fatigue, as well as fracture resistance.

Pyrowear 53, a temper resistant carburised steel, was another alternative developed to replace M50 bearing inner races. It was found to be a valid alternative and offered an improved wear and degradation resistance over AISI 9310, a conventional carburised steel (DiRusso 1986).

Bearing manufacturing and steel quality has improved to such an extent that surface flaws, rather than steel inclusions, are a more frequent cause of bearing failure. Bearing life problems now arise when conditions such as higher temperatures, unusual stressing, poor lubrication, and contamination create difficult and demanding applications (Pearson 1995).

As the trend towards higher thrust to weight ratios in gas turbine engines continues, interest is being shown in light weight ceramic bearings. Dezzani & Pearson (1995) have investigated hybrid material combinations (silicon nitride balls and nitrided M50 and M50NiL raceways). Developments in materials such as ceramics has been restricted mainly to rolling elements because of manufacturing difficulties and high tensile stresses in ring components in critical applications.

So far we have discussed material advances carried out mainly to improve bearings. The benefits of material improvements in gears have also been seen, with the possibility of integral races and gears being a great advantage. Having improved steel cleanliness greatly, by the same processes discussed for bearings, research is now pushing for new materials. Since World War II demands for gear designs with very high tooth strengths have been made, there was, however, uncertainty about the upper limits of tooth strength (Seabrook & Dudley 1963).

Although through-hardening high alloy steels perform exceedingly well in bearings, they cannot be safely employed for gears where toughness and resistance to impact and bending are required (Jatczak 1978).

In the 1960's vacuum degassing was used in SAE 52100 gears. This gave an improvement of the order of 3 times on fatigue life (Hampshire 1986). BS S82 was used for its high toughness and fatigue properties to replace SAE 52100 in integral bearing and gear arrangements (Hampshire 1986).

VAR BS S82 had tighter limits on sulphur and phosphorus applied and became BS S156. Gear/bearing and gear assemblies are still made from BS S156, with its limited temperature capability.

However, novel materials, such as Pyrowear 53 (Burd 1984) and deep nitrided 32CDV13 (Chaize & Berthier 1996), have started to find applications in aerospace gearing. All of the materials discussed in this section have been subject to extensive investigation, some of this is discussed in Section 5.8.

5.8 Previously Investigated Gear Materials

Seabrook and Dudley (1963) carried out a large scale flexural fatigue testing programme on many different materials, designs, and processing variables. Gear tooth flexural fatigue strength was investigated as a function of gear tooth geometric shape and material on a non-rotating gear (to avoid the effects of misalignment and dynamic loads). The load was applied at the highest point of single tooth contact by another gear given accurate torque pulsations. They emphasised that dirty or defective material and poor heat treatment and machining could reduce fatigue limits considerably. In general, they found the higher fatigue strengths in gear teeth were given by a case and core configuration, with nitrided and carburised teeth giving the greatest strength and

induction and furnace hardened following these. They also suggested that a material which has a moderate mean strength and little scatter in life associated with it, may be a better choice than a material with a higher mean strength but more scatter.

Averbach et al. (1985) tested fatigue crack propagation in M50NiL and CBS-1000M. They found M50NiL had residual compressive stresses which slowed crack propagation rates. CBS1000M had residual tensile stresses (because of its high retained austenite) which tended to promote crack propagation. Both materials, however, had high fracture toughness and excellent resistance to rolling contact fatigue.

Standard carburised gear materials such as AISI 9310 and BS S156 were once the best choice for aerospace transmissions and are still used extensively (Saulnier 1989). Townsend et al. (1978) and Kotorii (1992), amongst others, have done gear fatigue tests on AISI 9310. AISI 9310 has been found to soften at high temperatures and as a consequence its scuffing resistance in gear teeth for certain applications can be poor (US National Materials Advisory Board 1979).

Spur gear endurance tests and rolling element surface fatigue tests were conducted by Townsend & Bamberger (1991) on VIM-VAR M50NiL and VAR and VIM-VAR AISI 9310 gear material. The VIM-VAR M50NiL gears had surface fatigue lives that were 4.5 to 11.5 times that for VIM-VAR and VAR AISI 9310 gears, respectively. The surface fatigue life of the VIM-VAR M50NiL rolling contact fatigue bars was 13.2 and 21.6 times that for the VIM-VAR and VAR AISI 9310, respectively. M50NiL was also shown to have good fracture resistance. The gears failed by subsurface pitting fatigue, which the present author finds strange in properly heat treated, clean gear steels. The greater difference in bar fatigue tests, when compared to the gear tests, can be explained partly by the hardness differences in the specimens. The gears had a Rockwell C hardness of 61 (720 kgf mm^{-2}) and 60.6 (710 kgf mm^{-2}) and the bars were 61.4 (730 kgf mm^{-2}) and 64 (800 kgf mm^{-2}) for the AISI 9310 and M50NiL respectively. Offset gear teeth were used, they found this did not give edge loading effects, with failures occurring evenly across the facewidth, this was only 3.2 mm so this was not surprising. The material the test bar was run against in the roller tests was not identified, had this been a softer material the difference between the gear and bar tests would be explained.

Townsend and Zaretsky (1981) carried out endurance tests on gears and rolling elements manufactured from AISI 9310, CBS 600, and modified Vasco X-2. CBS 600 is a low

alloy steel that has good machinability, carburises easily, and maintains a suitable hardness at 230 °C for long-term operation and 315 °C for short-term (Jatczak 1978). Modified Vasco X-2 was derived from a through hardened tool steel that had its carbon content reduced in order to make it a case carburising gear steel with a fracture tough core (Drago 1974). CBS 600 gears exhibited longer lives than AISI 9310 ones, but the rolling element tests showed no statistical difference. Modified Vasco X-2 was statistically equivalent to AISI 9310 in both types of tests. An added complication was the case carburisation of Vasco X-2 resulting in rapid fracture at the gear tips when hardened on all sides of the teeth. This was caused by heat treatment cracks. Once again, gear failure by classical subsurface pitting fatigue was reported as well as tooth bending fracture. CBS 600 gave a high fracture toughness, whereas Vasco X-2M had low fracture resistance, this has been confirmed by Davies (1991).

Pyrowear 53 has also been investigated for gearing applications (Burd 1984), and is also being used by certain helicopter manufacturers.

32CDV13, a nitrided steel, has been treated by a novel process called deep nitriding, where case depths of 0.8 mm can now be achieved at a reasonable cost. It has been used in helicopter integral gear and bearing tracks to eliminate fretting between the shaft and bearing and to give a weight saving (Chaize & Berthier 1996).

Davies and Gittos (1989) have investigated the effect of tempering temperature on hardness for some of these new temper resistant materials (see Figure 5.8.1). The initial fall in hardness with tempering temperature in secondary hardening alloys is due to the softening prior to the formation of alloy carbides.

These new steels appear, however, to have a reduced toughness when compared to traditional materials (Figure 5.8.2).

Davies & Gittos (1989) noted that by increasing the tempering temperature beyond 200 °C all the temper resistant gear steels exhibited reduced fracture toughness properties, and in the case of the secondary hardening steels these reductions were significant. By tempering certain steels above 250 °C a process known as tempered martensite embrittlement occurred, due to the production of cementite films at martensite plate boundaries which substantially weakened the matrix. This is usually removed by tempering above 350-400 °C.

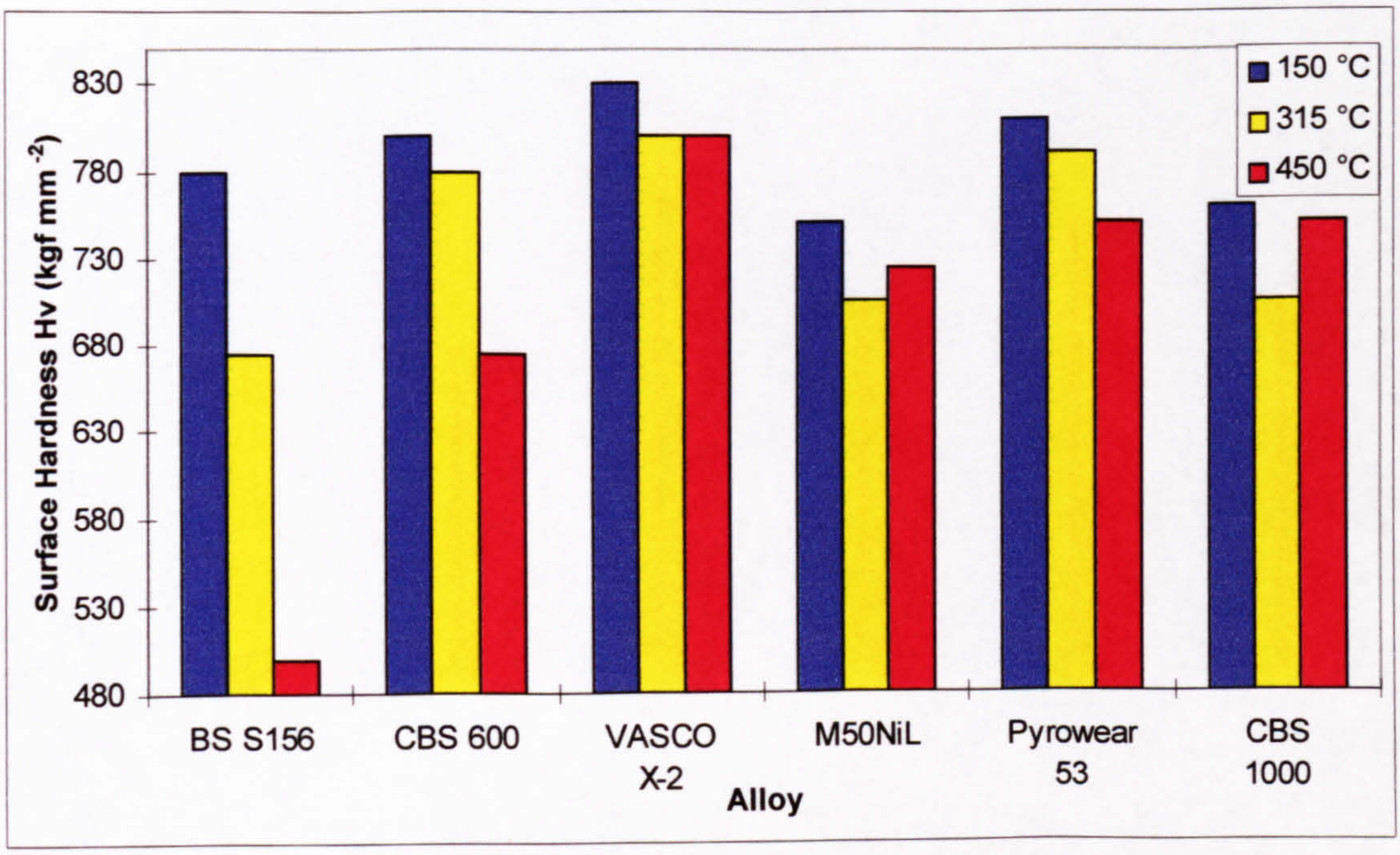


Figure 5.8.1 Influence of Tempering Temperature on Conventional and Temper-Resistant Gear Steels (from Davies & Gittos 1989).

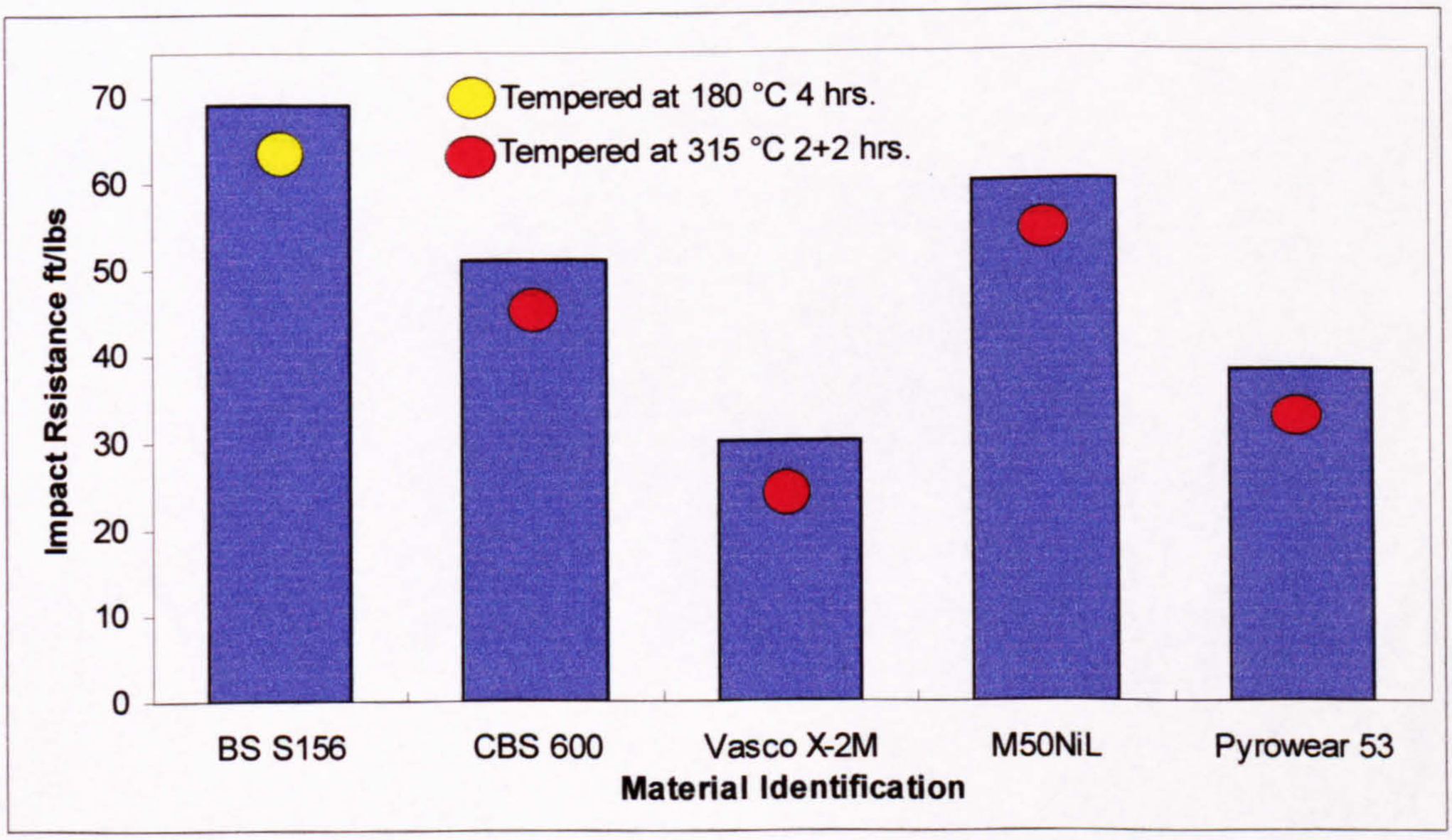


Figure 5.8.2 Comparison of the Impact Resistance of Conventional and Candidate Gear Steels (from Davies 1986)

Duplex hardening is a process involving two surface technologies combined. Their metallurgical interactions play an important role in determining the properties of the resultant composite (Bell 1993). Davies (1991) described it for the nitriding of a previously carburised surface. The process needs a carburised case that is stable above 500 °C and a sufficient quantity of nitride forming elements.

In rotating bend-fatigue tests on duplex and carburised Vasco X-2M, Davies (1991) showed that duplex hardening improved the fatigue endurance by approximately 25%. Axially loaded specimens also showed superior elevated temperature fatigue properties (results of tests at 150 °C) when compared to BS S156.

Olver (1989) showed, on the three disc rig described in Chapter 7, that duplex Vasco X-2M gave a mean life ratio of about 30 times that of carburised Vasco X-2. When compared to previous tests on BS S156, it also had a far higher mean endurance limit. The tests were, however, run against a conventional carburised steel which was softer. Plastic deformation was therefore confined to the counterface, this was confirmed by examination of surfaces. Vasco X-2M has toughness limitations and other materials such as M50NiL should be investigated for this process.

The effects of the white layer thickness and case depth on resistance to scuffing in a nitrocarburised surface was investigated by Vanes (1995) with Falex tests. A medium carbon steel was used as the base material. Removal of white layer was found to improve the anti-scuffing properties of the surface.

Pearson and Dezzani (1993) also investigated the rolling contact behaviour of duplex hardening on M50 and M50NiL surfaces in which the hardness below the nitrided case was HRC 60 (698 kgf mm^{-2}) or higher. The rig consisted of three 52100 steel balls run against a test rod at stresses of 5.42 GPa. They obtained an improvement in fatigue life for both materials over non-duplex specimens of the same material, as well as for low alloy nitrided cases with underlying softer material. Most failures they experienced were from surface not sub-surface origins. L_{50} lives of 6.8, 9.8, 21.5 and 180.3 million cycles were obtained for the M50, M50NiL, nitrided M50, and nitrided M50NiL respectively. Carbide size was given as the reason for differences between M50 and M50NiL, the larger carbides present in the M50 alloy acting as stress raisers. In M50 these large carbide stress raisers could be seen as "butterfly" structures, these may lead to initiation of fatigue cracks. The deep compressive residual stresses of 140-210 MPa in carburised M50NiL were complemented by the higher compressive stresses of 600-800 MPa induced by nitriding, this is thought to be beneficial in preventing crack growth in the surface and near surface zone.

Pearson (1995) and Dezzani and Pearson (1995) discussed tests carried out on hybrid, nitrided M50 (70 HRC, 1075 kgf mm^{-2}), and nitrided M50NiL bearings (68 HRC, 940

kgf mm^{-2}). Full scale bearing tests were done in which the bearings were run for 15 minutes with contaminant to create surface flaws, then cleaned and run with clean oil in partial EHD, in conditions including sliding and temperatures of 150 °C. TDC (thin dense chromium) coated M50NiL bearings showed a marked improvement in life over non-coated M50. Hybrid bearings using silicon nitride balls with nitrided rings were superior at all loads and temperatures. Higher hardness, strength, and residual compressive stresses in the nitride layer were thought to be fundamental in resisting fatigue.

Bell (1993) illustrated the use of duplex hardening when depositing ceramic TiN on top of a plasma nitrided steel. The result was a thin coating of TiN on the surface, with a relatively thick subsurface layer and a ductile core. This duplex structure offered by far the highest wear resistance when compared to TiN coated or nitrided only. Pure sliding tests showed it had a much higher load bearing capacity.

5.9 The Materials being Investigated

The composition of the alloys used is given in Table 5.7.1. The heat treatment procedures of the alloys described below are in Appendix B.

5.9.1 BS S156

This is a conventional carburised gear steel, tempered at 140 °C. This material will be used by the author as a reference material with which to compare the relative performances of other steels. It was produced by gas carburizing, the most common technique, described previously.

5.9.2 AISI M50NiL

AISI M50NiL is a temper-resistant carburised steel that provides elevated temperature performance, in excess of 500 °C, by secondary hardening, and a fracture tough core. Its favourable residual compressive stresses in the zone of subsurface rolling contact stresses should help resist crack initiation and propagation, and contribute to an improved fatigue life, as well as the prevention of fracture. It also possesses a refined microstructure with smaller carbides, to enhance surface finish and improve performance under thin film lubrication.

5.9.3 32CDV13

Nitriding steels offer resistance to elevated temperatures in excess of 500 °C. This gives a higher temper resistance than carburised steels and also provides a higher surface hardness (1000 kgf mm^{-2} nominally), which would be expected to offer improvements to wear and pitting resistance.

There are, however, two major drawbacks in using nitriding steels in highly loaded gears, these are: a substantially shallower case depth and a lower core strength. These two factors dictate the ability of the alloy to resist the applied bending and rolling contact fatigue loads. As mentioned previously, to achieve maximum protection against case crushing it is important to ensure that the case depth exceeds the depth of the maximum Hertzian shear stress. Usually, a nitrided case hardness is greater than a carburised case close to the surface, but its shear strength declines sharply after approximately 0.3 mm.

5.9.4 M50NiL Duplex

Duplex hardening involves nitriding a previously carburised steel. The steel must have certain characteristics for this process to be accomplished: a carburised case that is stable beyond 500 °C and a sufficient quantity of nitride-forming elements. With the development of temper-resistant carburizing steels, the stability of the carburised case can be maintained beyond 500 °C, via secondary hardening, while the presence of nitride-forming alloying elements for temper-resistance, suggest the steel should respond to nitriding treatments. However, the practicality and reproducibility of the proposed treatment in gear manufacturing has yet to be proven, especially in regard to distortion (Davies 1991).

This process applied to M50NiL is not only aimed at oil-loss tolerance but also at achieving an improvement in surface fatigue performance. The enhanced surface hardness will lead to a higher yield stress at the surface; and the superior residual stress distribution attributable to nitriding should improve the steel's pitting and bending fatigue resistance. Similarly, the enhanced case depth attributable to carburizing should maintain a subsurface shear strength sufficient to prevent case crushing.

5.10 Conclusions

This chapter has given an idea of the requirements a gear steel has to fulfil, particularly for aerospace use, and the processes available to tailor a gear material to meet such requirements. The current limitations of gear steels and possible benefits of some of the more recent materials have been discussed. The large number of materials and processes available have led to a large amount of literature on the subject. Many of the previously investigated steels reviewed here have been tested against a lower hardness counterface, the effects of running them against similar counterfaces should be investigated. Finally, the materials investigated by the author have been briefly discussed. The benefits of temper resistant materials and the duplex hardening process are to be investigated on both gears and discs.

Chapter 6 Test Methods for Evaluating Gear Steel Pitting Performance

Having discussed gear failure modes and some of the new gear materials available, ways of evaluating these materials using laboratory performance tests are now considered. The rig used to test a specific property depends on a number of factors: what is being investigated, the time a test lasts, cost, and the repeatability of the results obtained.

Standard tests are developed to test material properties, but their results often bear little correlation with the results obtained from full scale tests, and very often they do not correlate with each other. These tests, however, are usually quick, cheap, and simple to run, and through experience the test may indicate relative levels of pitting, scuffing, or wear resistance (Benedict 1968). They may range from relatively complicated and expensive gear tests to simple and inexpensive tests. It would seem likely that the simpler the test, the less chance there is of obtaining a correlation; perhaps the largest gap in this sequence is between a test using gears as specimens and a test using discs. It is however important to remember, as mentioned by Baber et al. (1968), that in order to not derive erroneous conclusions when conducting gear tests and interpreting the results, the possible effects of the test machine (if of different design), gear material, operating conditions, and atmospheric environment must always be kept in mind. The pitting and scuffing of gear materials is usually studied by gear or disc tests but other test set-ups are used, a few of these tests are mentioned below.

6.1 Techniques for Evaluating Gear Steel Surface Contact Performance

Pitting has been studied with ball machines, when a simulation of rolling bearing behaviour was needed. With balls in contact, very high contact stresses are possible for moderate applied loads. This provides reasonable test times, but one must be careful not to operate in a regime which renders the results inapplicable to the process being studied.

An example of a ball machine is the rolling four ball rig (IOP 1981b), developed for rolling contact fatigue investigations from the sliding four ball wear test rig (IOP 1981a), used to evaluate the ability of lubricants to limit wear in a sliding ball bearing contact. One upper ball is loaded against three lower balls which are free to rotate. The lower

balls are driven by the upper ball and the whole arrangement is lubricated by circulating test lubricant. The test is run until the upper ball pits and, a consequent increase in vibration level, trips the motor. A variation on this rig is the NASA five-ball rig, used by Parker et al. (1974), which is similar to the four ball rig, but has four lower balls instead of three.

Hobbs and Mullet (1968) used a bearing test rig, which used full scale roller bearings, to obtain realistic results for the fatigue lives of bearings. Tests such as these can be expensive and could be very time consuming. Other ball rigs include arrangements such as the ball on cylinder, ball on plate, and ball on ball set-ups.

Non-contacting methods, which do not involve a lubricated contact, can also be used to study fatigue, these include the biaxial-bending, tension-compression, and rotating-bending fatigue rigs, such as the R.R. Moore high-speed rotating beam machine (Hetenyi 1950). These use repeated stressing of the components under different cyclic loads until failure is reached.

Fracture mechanics tests are used to examine crack initiation and propagation in a simpler way to using a full S-N test set-up, the most common arrangement involves plate specimens, notched and stressed to cause strain and cracking at the tip of a notch.

Various forms of disc test machine have been used over the years, historically they were used to provide a simulation for gears in testing for scuffing. Way (1935) and Dawson (1962, 1963) used disc rigs which operated in pure rolling. Benedict (1968) used a geared roller tester to investigate gear fatigue, it used discs pressed onto parallel shafts and linked by gears. The discs were loaded pneumatically, the lower disc being dip lubricated to supply the contact. The hydrostatic disc machine developed by Cameron et al. (1971) was designed to ensure a nominal line contact between the discs. Bearing races were used as test specimens, these were slipped over rigid fixed mandrels with hydrostatic pockets to both locate and load the rings together. A rolling and sliding disc rig used by Graham (1979) was evolved from this last rig, and is the same rig used by the author (described in Section 7.2).

There are many standard gear test machines which all use spur gears as test specimens. The IAE gear test machine (Mansion 1952) uses a pair of spur test gears that are driven by two double helical gears, and both forward and reverse faces are tested. The rig is stopped to apply load by locking torque into it with a loading lever at a coupling. The

FZG tester (IOP 1992) is similar to the IAE rig, both faces of the test gears being tested and the load being applied whilst the rig is static with a load clutch. There is also the 'Ryder' gear test rig (ASTM 1983), which is used mainly for scuffing research. Finally, there is the NASA gear tester (Parker and Zaretsky 1972 and Coy et al. 1975), this was used as the basis for the design of the gear rig used by the author, and described in Section 7.1.

6.2 The Use of Discs to Simulate Gears

The use of disc testers to study pitting instead of gears has been mentioned. It is important to account for the reasons which theoretically enable the simulation of gear tooth contact by equivalent discs.

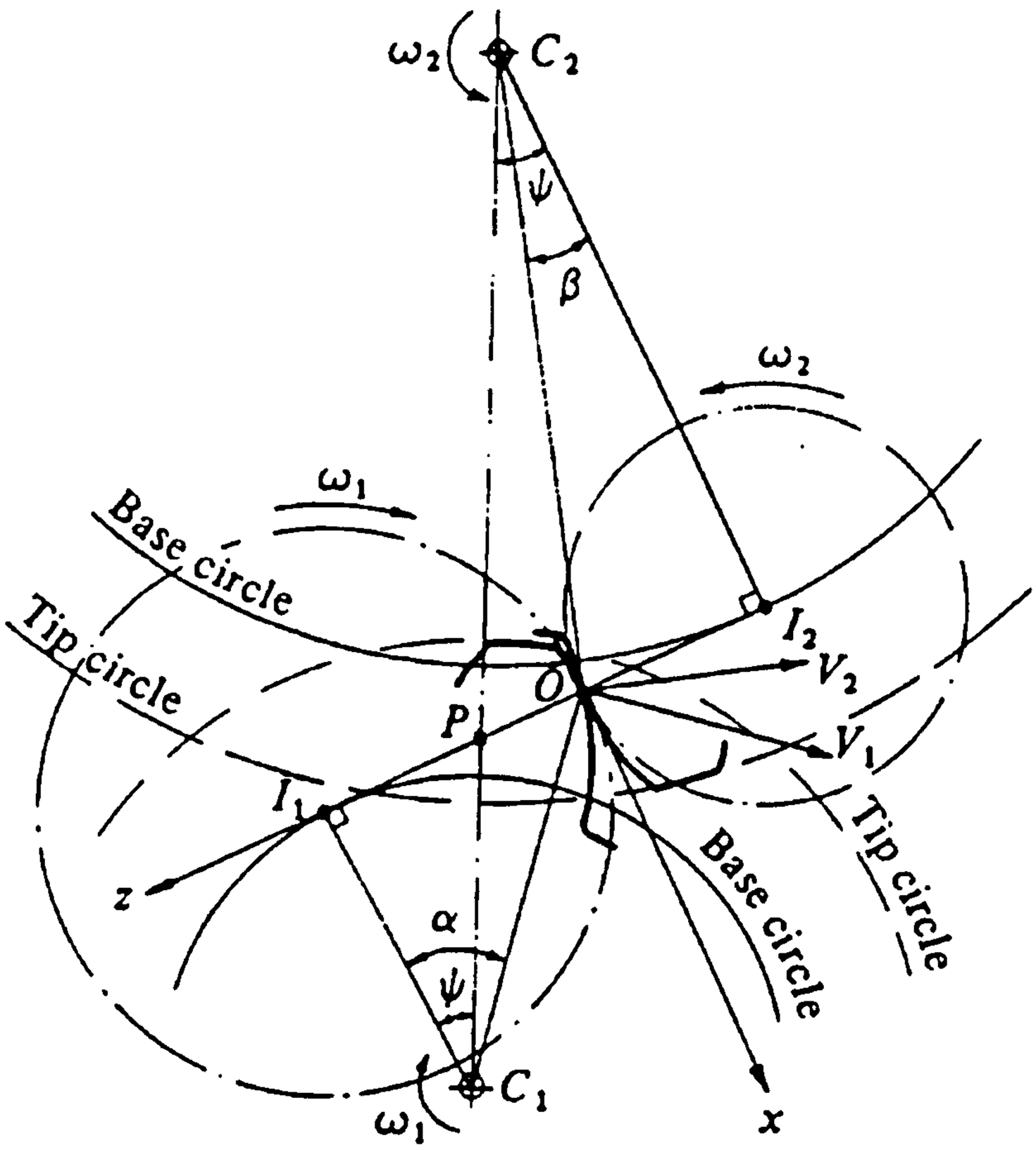


Figure 6.2.1 Contact of Involute Spur Gear Teeth (Johnson 1985)

It can be seen from Figure 6.2.1, that the motion of sliding and rolling at a given instant in the gear tooth meshing cycle can be reproduced by two circular discs of radii I_1O and I_2O, rotating with angular velocities $-\omega_1$ and $+\omega_2$, about fixed centres at I_1 and I_2 (they

are kinematically equivalent). Since the radii of curvature of the involute teeth at O are the same as those of the discs, I_1O and I_2O, the Hertzian contact stresses under a given contact load per unit length are also the same in the disc machine (Johnson 1985).

Hence the disc machine, used by Meritt (1935), has been utilised ever since to simulate the conditions of gear tooth contact in a simple test. The main reasons for using a disc test would be the reduced cost of the test specimens and the ease of manufacturing them to strict tolerances; gears being more expensive because of the consistency of the surface required and more complex manufacturing process.

6.3 Why Gear and Disc Tests may not Correlate

We have seen how discs can be kinematically equivalent to, and also reproduce the same Hertzian stresses as, gears at a given point of the gear tooth contact. There are, however, many reasons for the departure from similarity between gear and disc tests, some of these are discussed here. One should mention that these reasons are for both 'equivalent' discs and discs that don't exactly reproduce the gear contact at a defined point.

6.3.1 The Influence of Slide-Roll Ratio

As mentioned previously, the sliding speed is not constant in gears; this means a varying, rather than constant, slide-roll ratio is present along a gear tooth contact. Hence, disc specimens would have the ability to simulate only one point in the gear tooth meshing cycle. This is of importance because, as mentioned in Chapter 3, sliding has a considerable effect on rolling contact fatigue. In a gear tooth the sliding speeds are greater at the tip and root, but the load there is usually less, so a combination of the load and sliding speed will determine where failure will occur on the tooth if no other effect, such as debris indentation, prevails. To obtain the best correlation perhaps the disc would have to simulate the conditions where failure occurs on the gear tooth.

6.3.2 Hunting and Integral Ratios

This is an effect which has been observed by various researchers, but has been given particular attention by Ichimaru et al. (1980) and Nakajima (1981,1986), in which a difference in fatigue resistance was observed between hunting and integral ratios, the latter giving an extended fatigue life. The reason given for this effect was that for an integral ratio the same regions of the contacting surfaces came into contact with each

other with successive revolutions, making the asperities conform better. Whereas, for a hunting ratio different regions of contacting surfaces came into contact with each other on successive revolutions. The surfaces are likely to change due to local plastic deformation, which occurs because of the high stress concentrations induced by asperity interactions. An increasing conformity between asperities in contact would mean less cycles of plastic deformation, which in turn is likely to increase the fatigue life.

When there is sliding in the contact, the indentations caused by asperities will have their relative locations altered when passing through the contact zone. As a result, when the directions of sliding and roughness are perpendicular, additional plastic deformation may be caused on the asperities, when compared to pure rolling. When the roughness orientation is in the direction of sliding, the asperity interactions accompanied with sliding may be less severe in a 1:1 ratio.

In involute gear tests sliding exists everywhere on the teeth except at the pitch point and the roughness lay is usually perpendicular to the direction of sliding. Hence, one would expect the life to pitting to be shortened by sliding, even in the case of a 1:1 ratio. However, provided the asperities in the high sliding region of the tooth surface have been smoothed out by running-in, any difference in life-to-pitting and oil film formation between an integral and a hunting gear ratio may be caused by the difference in the severity of asperity contact in the small sliding regions around the pitch line, where pitting is likely to take place.

Ichimaru et al. (1980) investigated this with discs of ratios of 1:1, 29:28, and a friction drive. The results they obtained were consistent with gear tests they performed using gear ratios of 1:1 and 27:25. They used one softer roller and an applied load that gave a maximum Hertzian contact stress in excess of the shakedown limit of the softer roller, at least in the initial stages of running. The initial roughness was far greater than the film thickness so severe asperity contact was supposed to occur.

Using a harder roller with regular machining marks perpendicular to the rolling direction and an integral ratio, the EHD film built up gradually in most tests after running-in, probably due to the surface roughness declining. In this case the plastic flow and increase in hardness on, and immediately beneath, the surface of the soft roller was minimal.

With tests with random machining marks on the harder roller and a hunting ratio, pitting occurred after a small number of cycles and an EHD film did not develop. The surface

hardness of the harder roller diminished to some extent and the softer roller suffered considerable plastic flow and an increase in hardness on, and beneath, the surface.

From their results it was seen that pitting was more likely on the surface with lower velocity, and was restrained on the surface with higher velocity. Pitting would take place on the slower disc even though it may be much harder. The EHD film formation was also better in the 1:1 gear ratio than 27:25. After a few cycles the integral ratio gear contact had a fully formed EHD film (due to the decline in roughness) with local breakdown at the highly stressed positions. The 27:25 ratio still had a great amount of metallic contact even after many cycles, this would consequently give a shorter life to pitting. They also examined the effect of surface lay on fatigue performance, this is described in Section 6.3.6.1.

6.3.3 Bulk Metal and Flash Temperature Differences

Discs can be kinematically equivalent to gears, but are not thermally equivalent, giving the two types of specimen different bulk temperatures. This is important because the minimum film thickness and friction in EHD lubricant films in the contact zone are controlled by the representative viscosity, which is defined as the viscosity at the inlet to the film, and this has to be taken at the bulk temperature of the rubbing bodies bounding the film. The film thickness, in turn, will affect friction which will determine the heat generated, bulk temperature, and hence inlet viscosity.

6.3.4 Engagement Discontinuities

The engagement discontinuity in gears, due to the teeth continuously entering and exiting mesh, will have effects which vary from the continuous steady motion of discs. The lubricant film will probably vary considerably across the gear tooth meshing cycle because of this effect whereas, one would assume that, in the steady contact of discs it will not vary much once it is established.

6.3.5 Extended Contact

The presence of extended contact in gear teeth, due to their elastic deflection, may produce premature contact of the gear tooth tip corner in the mating gear tooth root and delayed exit of the root of the gear tooth and the tip of the mating tooth. This may produce higher stress concentrations and flash temperatures, and a lower film thickness

than in discs (Olver et al. 1995). This has been encountered in circumstances where high load has been applied to gears (Kotorii 1992). This phenomenon will be discussed in more detail in Chapter 8.

6.3.6 Differences in Properties due to the Manufacturing Process

These can be mainly classified into roughness and case depth differences, but there may be other factors that have an influence on test results.

6.3.6.1 Roughness Effects

The surface roughness, in general, will be different in gears and discs because of their different production methods. Ground gears tend to have an axial surface finish perpendicular to the rolling direction, as opposed to discs that are finished by cylindrical grinding, which leads to circumferential surface roughness orientation, parallel to the direction of rolling. This will give rise to different lubricant film formation, as shown by Patir and Cheng (1979) and Hua et al. (1987), amongst others. It will also give different surface interactions, as discussed in Section 6.3.2. The test pieces could be manufactured with similar surface roughness lays if, for example, the discs were ground axially. Even then, care would have to be taken to impart similar roughness to the two specimen types if they were prepared by different processes.

Hua et al. (1987) investigated the effects of surface roughness orientation on EHL analytically. They divided surfaces into two main groups: isotropic roughness surfaces and striated rough surfaces. Central and minimum film thickness were affected, increasing as the roughness went from longitudinal to transverse lay. Numerical results showed the film thickness to roughness ratio, lambda, to be important. When Λ>3 the effects of roughness were negligible. An angle parameter, Beta, to describe the roughness orientation was used (Beta goes from 0°, longitudinal, to 90°, transverse). The pressure spike produced in EHD increased as Beta decreased and the its location moved slightly towards the exit point when Beta increased.

Patir and Cheng (1979) derived similar analytical conclusions by using a surface pattern parameter, gamma ($\gamma = \gamma_{0.5x}/\gamma_{0.5y}$), the ratio of x and y correlation lengths of the combined roughness. Purely transverse, isotropic, and purely longitudinal roughness have γ = 0, 1, and infinity respectively. In an analysis of centre film thickness they found the film forming capability increased as the surface roughness parameter decreased from 6 to 1/6,

i.e. from a longitudinal to an isotropic and on to a transverse roughness lay. The effect was found not to affect the centre film thickness until Λ dropped well below 2. Sliding did not have any effect if the surfaces had the same roughness. If the faster moving surface was rougher there was a reduction in nominal film thickness. If the slower moving surface was rougher there was an increase in film thickness. This was ascribed to the effect of the shear flow parameter on the mean flow.

In the tests by Ichimaru et al. (1980) described in Section 6.3.2, when the direction of sliding and the machining marks on the discs were perpendicular to each other, pitting took place after a short running period and the surfaces did not run-in. When the machining marks were oriented in the direction of sliding, the pitting lives were very long and impressions of the rough surface on the softer roller, as well as running-in, occurred.

6.3.6.2 Case Depth

The specimen material may be locally different because of its geometry. For example, in a case hardened material, the case depth may not be the same in differently shaped specimens. There is bound to be some variation in case depth with tooth geometry, whereas, this would not occur in a disc specimen. Therefore, a different ratio of case depth to contact size will probably be present in the gear specimens, when compared to the discs. If they are treated as separate heat treatment batches there is also the possibility of some variation between specimens.

6.3.7 The Size Factor

When one contrasts fatigue test results, one should consider the size factor. This parameter accounts for the fact that the larger a component is, the greater the probability there is of it having a crack of a certain critical length for fatigue crack initiation. Of particular importance is the stressed volume (Ioannides & Harris 1985). If test specimens are of different size this should be considered.

6.3.8 Debris Effects

As discussed previously, rolling contact fatigue can be seriously affected by the presence of debris in the lubricant, if it is greater than the lubricant film thickness and hard enough to cause surface indentations, which create stress concentrations in the contact.

Debris passing through the contact of disc and gear specimens is likely to produce different effects due to the difference in motion and geometry. The size of the debris can be controlled by good filtration, this is a means of extending the life of components.

6.3.9 Dynamic Loads

The dynamic loads are not necessarily the same in the two types of test. Vibratory loads are a common feature to both and need careful evaluation. The use of a hydrostatic disc machine is thought to minimise vibratory loads. Gear testers, in which a pair of test gears are connected directly to a slave gear set of identical ratio to form a power recirculating loop, can experience vibratory loads arising from pitch errors in either the test or the slave gears.

6.3.10 Misalignment

The misalignment in the two types of test may vary and be of a different nature, giving rise to different stress distributions in the specimens and distinct failure modes, or regions. The contact area and distribution of load are affected by machining accuracy, the geometry of the gear and disc specimens, and their mounting system. The effect of misalignment in the axial direction can be alleviated by the use of a crowning radius on both types of test specimens.

6.4 Conclusions

In this chapter we have looked at a few of the most common test rigs for evaluating materials. It has been shown that the test method chosen depends on a number of factors: what property is being investigated, the time a test lasts, cost, and the repeatability of the results obtained. The main testing methods to simulate full scale gear applications are gear and disc tests, but how do they correlate with the actual application? Is it justifiable to carry out cheaper disc tests if these do not give similar trends to gear tests? With this in mind some of the main reasons why disc and gear tests may not correlate have been discussed.

Summary Part 1 - Review

Pitting failures in gears nearly always originate at the surface, nowadays. Increasing the hardness of the surface using a suitable steel-treatment combination is one possible solution used to increase fatigue lives. A range of new materials and processes have become available for gears and rolling bearings in the last years, these will need to be investigated for use in new transmissions if improvements to weight, cost, and oil loss tolerance are desired. One of the uncertainties is the impact of these new materials on durability, and in particular on rolling contact fatigue.

In the literature review these gear steels and processes have been discussed, particularly against the current limitations of steels. The most common gear failure modes have also been reviewed. Their characteristic appearance, reasons for occurring, relative dangers, and possible methods for preventing or delaying them have all been discussed. An idea of the complexity of rolling contact fatigue research has been given. The statistical nature of the process and the length of the tests can be a problem, but the major difficulty is the large number of variables affecting it. Materials, surface finish, lubrication, load, temperature, geometry, and sliding are amongst the more important ones. It is difficult to incorporate all of these in an investigation and, even if just one is investigated, results from one set of tests may not correlate with similar investigations. A few of the most common test rigs for evaluating materials have been reported. The rig used will depend on the property being investigated, the time a test lasts, cost, and the repeatability of the results obtained. The main testing methods to simulate full scale gear applications are gear and disc tests and these are used by the author. It is sometimes difficult to correlate tests by different investigators because many variables are not fully taken into consideration or are not properly controlled or reported. With this in mind and some of the reasons given previously for disc and gear test differences, one can see the problem with correlating the two types of test. This is why, in the present study, both gear and disc tests have been used with a particular emphasis on the correlation between the two.

PART 2 - ANALYTICAL & EXPERIMENTAL RESEARCH

Chapter 7 A Description of the Experimental Test Rigs and Specimens Employed in this Study

Having discussed some of the test rigs used in the past to study materials and failure modes, we can now look at the test rigs used by the author to study the durability of highly loaded, lubricated, case hardened steel gears. The gear and disc rigs and the monitoring systems are described here, as well as the test specimens used, and the test procedure.

7.1 The Gear Test Rig

The gear test rig, shown in Figure 7.1.1, is based loosely on a NASA design (Townsend et al. 1978) which uses the four square principle of applying load to the test gears. This means that the input drive has only to overcome the frictional losses in the system.

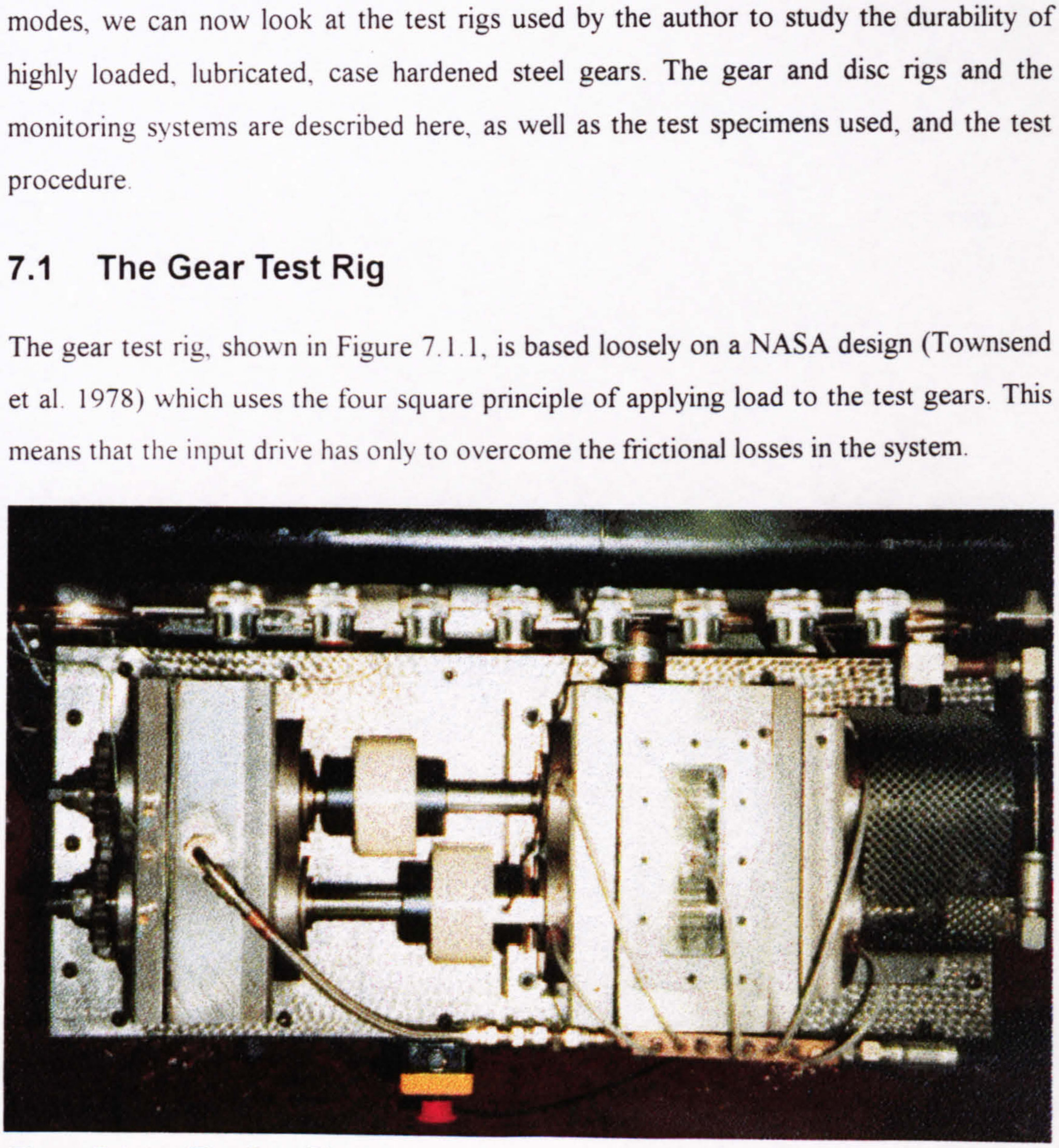


Figure 7.1.1 The Gear Rig

The machine consists of two separate assemblies: the test box and the main box, each with its independent lubrication system (shown in Figures 7.1.2 and 7.1.3 respectively).

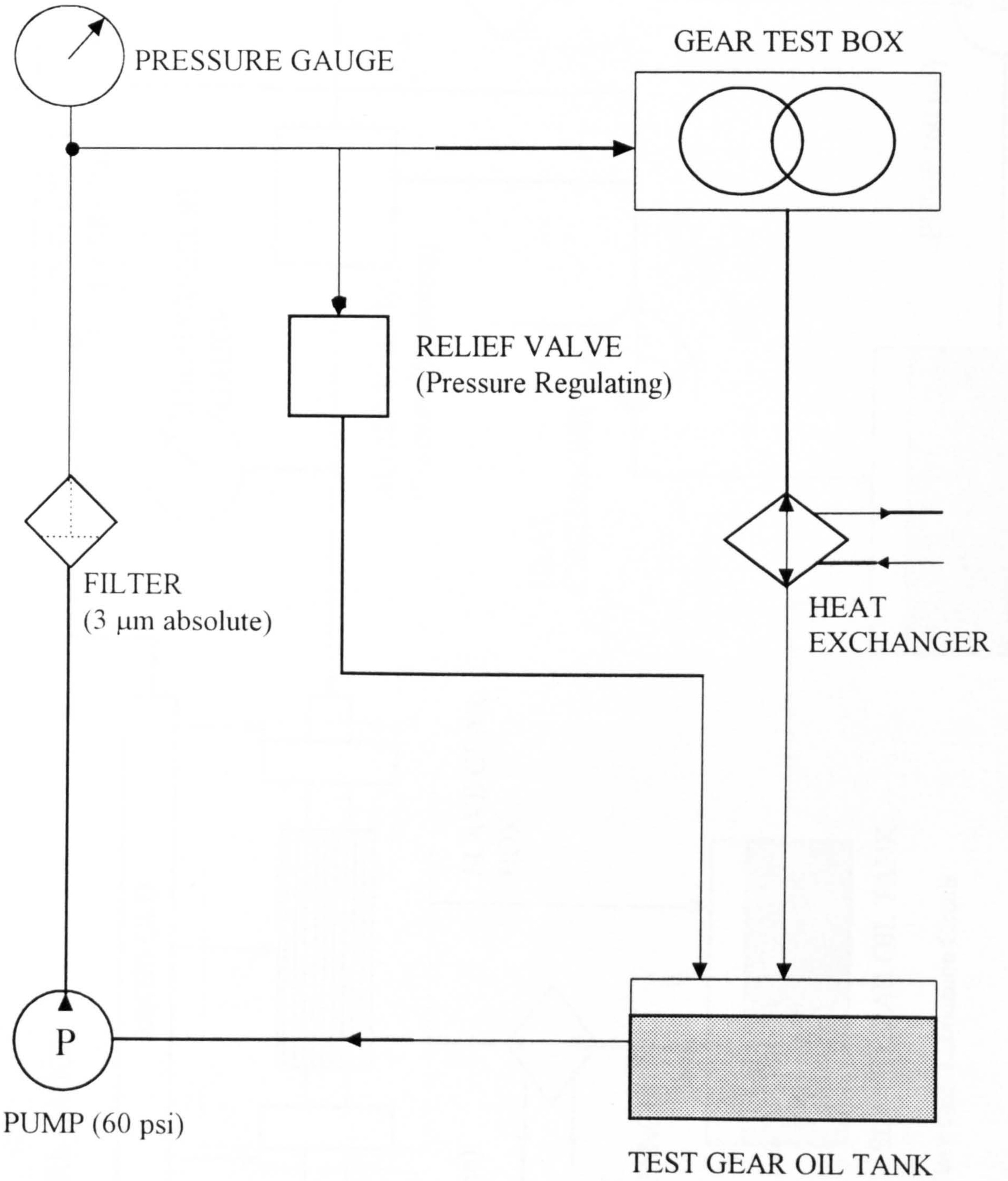


Figure 7.1.2 The Test Gear Lubrication Circuit

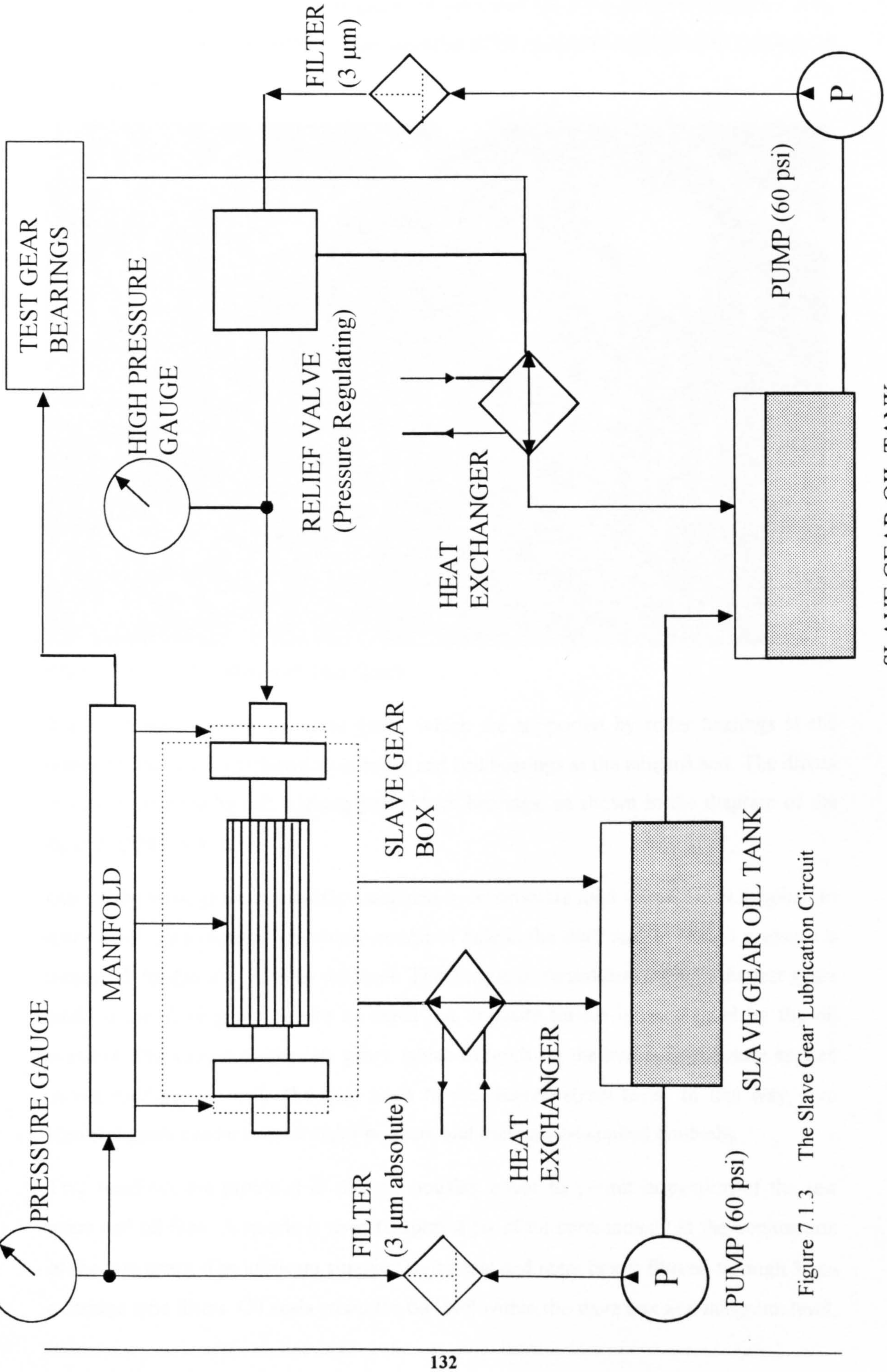


Figure 7.1.3 The Slave Gear Lubrication Circuit

The test box contains the spur test gears that are mounted on keyed shafts (Figure 7.1.4), which are supported by parallel roller bearings at the outboard end and ball bearings at the inboard end.

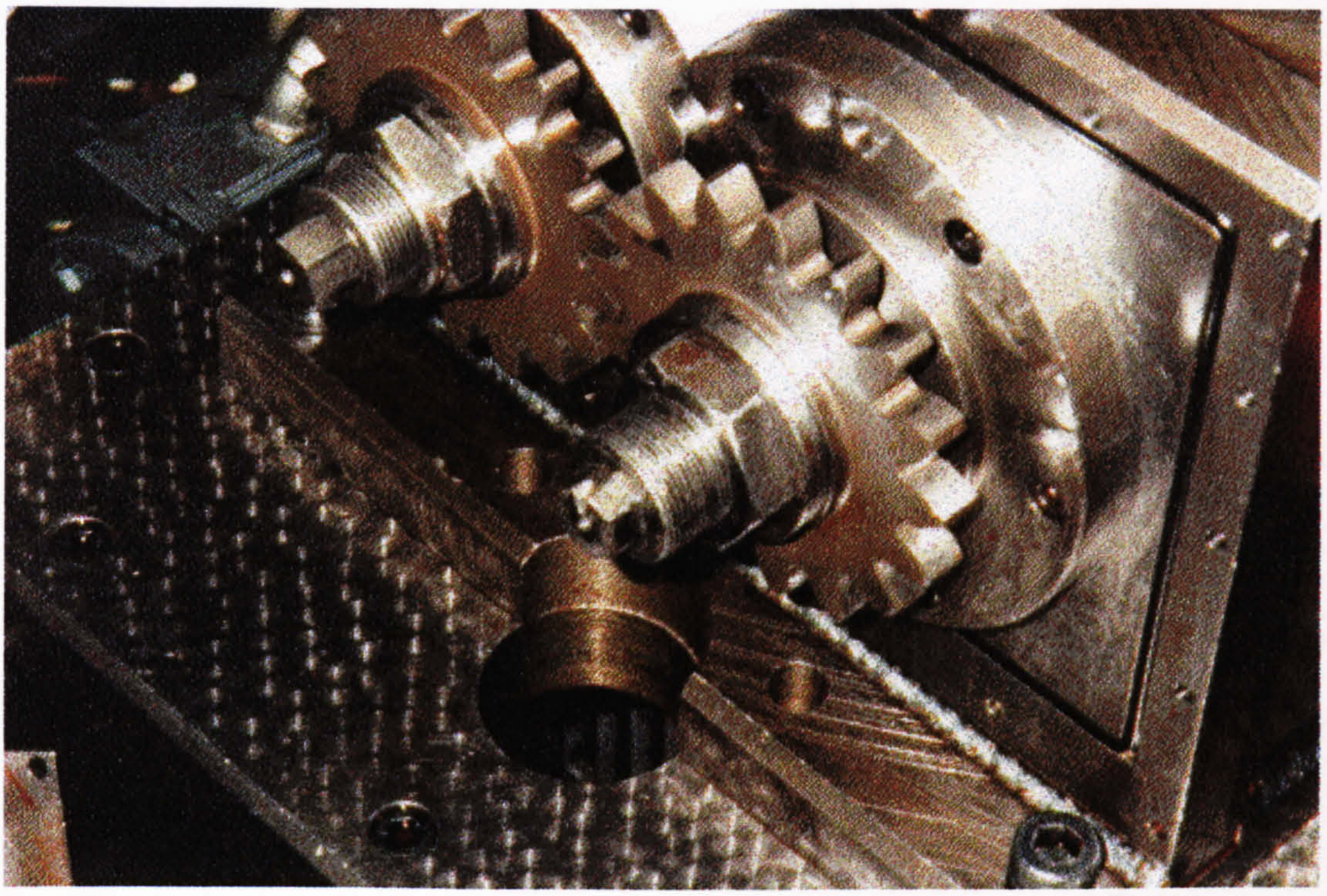


Figure 7.1.4 The Mounted Test Gears

The main box contains the slave gears, which are supported by roller bearings at the outboard end and a combination of roller and ball bearings at the inboard end. The driven shaft is supported by self aligning pillar block bearings, as shown in the diagram of the rig in Figure 7.1.5.

One of the slave gears is specially machined to incorporate load vanes. Oil is supplied to these load vanes through a centrally machined hole in the shaft and, as the oil pressure is increased, torque is applied to the shaft. This torque is transmitted through the test gears back to the slave gears, where an equal but opposite torque is maintained by the oil pressure. The torque on the test gears, which depends on the hydraulic pressure applied to the load vanes, loads the gear teeth to the desired stress level. In this way, two identical gears can be started under no load, and load can be applied gradually.

Two windows are provided in the test housing cover to permit inspection of the test gears and oil flow. A nozzle is used to spray a jet of oil continuously at the conjunction of the two gears. The lubricant supplied to the test and main box is filtered through 3 μm cartridge type filters. Oil seals retain the oil level within the slave box at a minimum level,

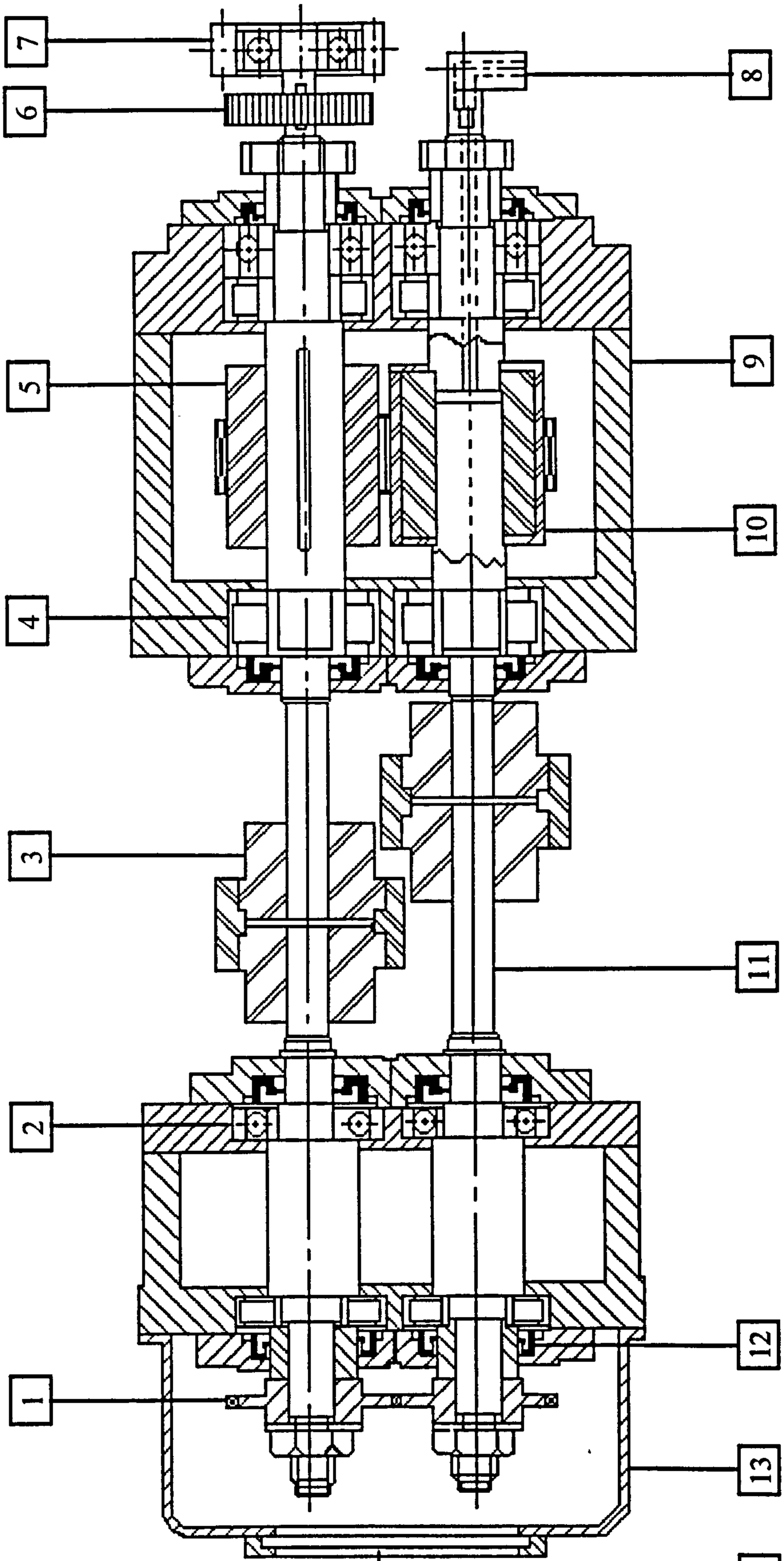


Figure 7.1.5 Schematic of the Gear Test Rig

after which, the oil is fed through coolers before returning to the main tank.

Various modifications were made to the original rig. The test gears were originally offset, so that half the facewidth of one gear would engage with half the facewidth of the mating gear. This was done so as to allow twice as many fatigue tests with the same number of gears. The author, however, did not think this was appropriate because there would be stress concentrations arising from the contact between the edge of the tooth facewidth on one gear and the middle of the facewidth on the other gear's teeth.

The lubrication system was also changed by separating the lubrication to the test gears from the roller bearings supporting the shaft close to them. This was done so that when oil loss tests were carried out on the test gears, the bearings would not be affected. A pressure relief valve was also incorporated, to allow excess oil to the gears to be sent directly back to the sump, and a nozzle was used to direct oil at the test gear mesh.

Filtration was discussed in Chapter 3 as a means of extending gearbox life and improving reliability. As work done by Bhachu (1980) showed that bearing life could be increased considerably by using finer filtration up to a 3 μm filter size, the rig was fitted with filters rated at 3 μm absolute.

7.2 The Three Disc Contact Machine

As mentioned previously, discs are used for the simulation of gear tooth surface distress of various types. A description of the hydrostatic disc machine (Figure 7.2.1), and the associated instrumentation, used in the rolling contact fatigue tests is given here.

The rig consists of three discs of equal diameter mounted 120° apart, with a smaller diameter disc positioned in the middle, contacting with them, and also being supported by them as shown in Figure 7.2.2.

The three larger discs, or rings, are slipped over fixed rigid mandrels, which have hydrostatic pockets that enable the rings to rotate and also load them together against the central disc, or barrel. The rings are driven by shear pins which fit into two slots, diametrically opposed, ground on one side of the ring specimens. These pins are of soft steel so that, if the discs scuff and weld, yield of the pins prevents any risk of damage to the drive system.

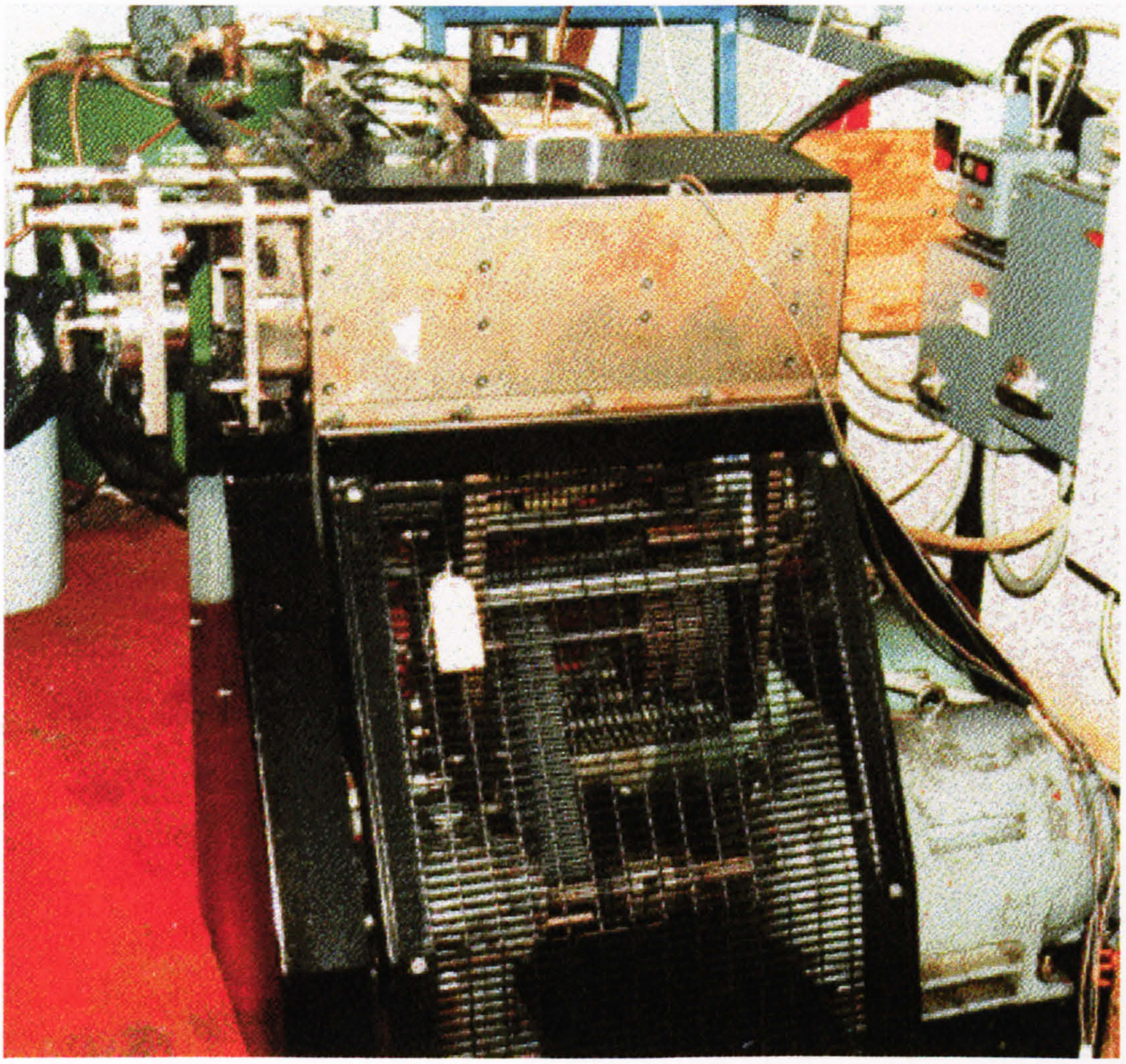


Figure 7.2.1 The Three Disc Contact Machine

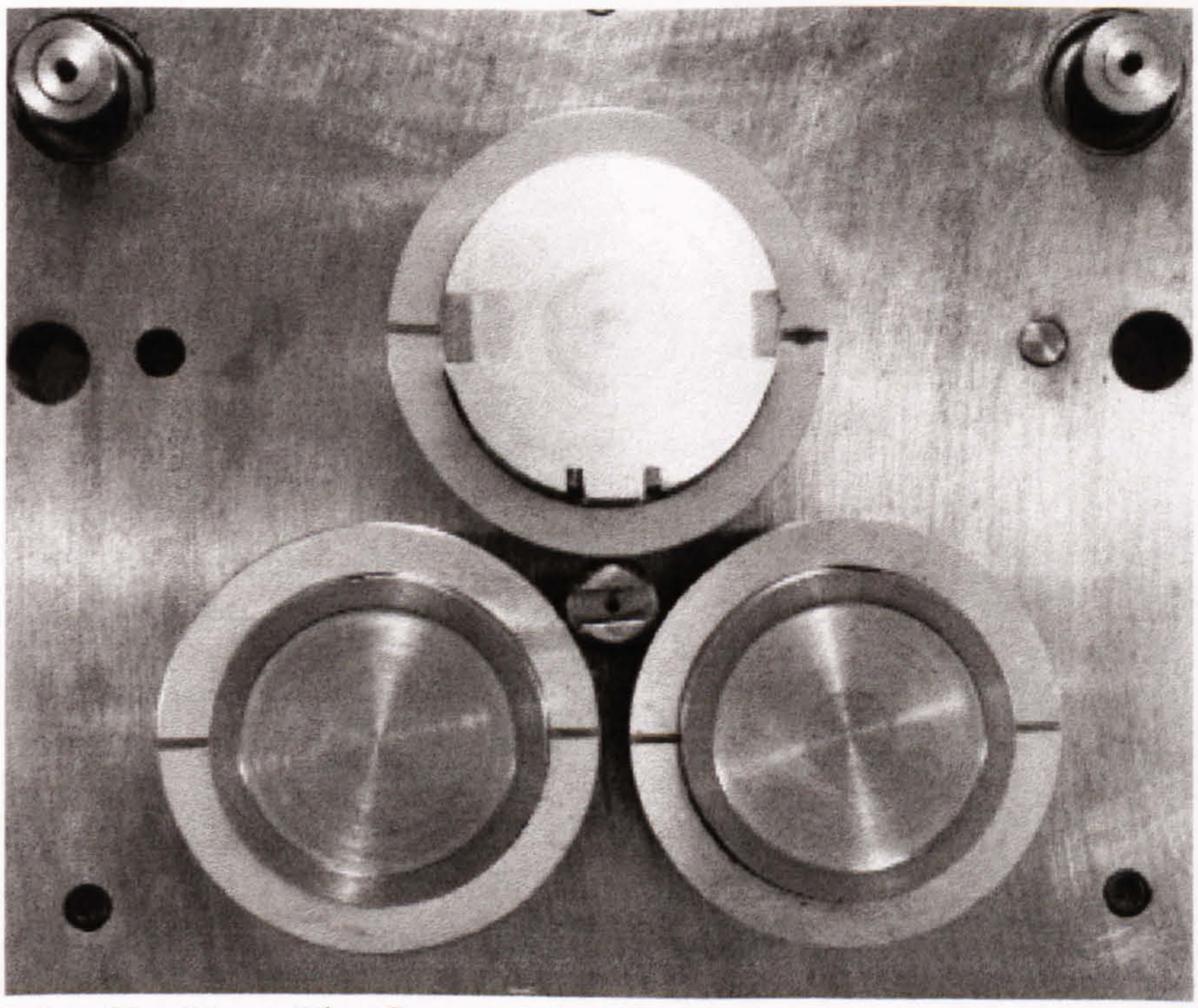


Figure 7.2.2 The Three Disc Contact Machine Layout

The drive system from the motor to the barrel and rings consists of pulleys connected by toothed belts, to give a number of fixed sliding speeds. The motor is coupled to a reverse gearbox to enable the rings and barrel to be driven in opposite directions. The slide-roll ratio can be changed by changing the pulleys and toothed belts, the available ratios are -0.026, -0.145, and -0.282, where the slide-roll ratio is defined as:

$$\text{Slide / Roll Ratio} = \left[\frac{u_1 - u_2}{u_1 + u_2}\right]$$

where u_1 and u_2 are the surface speeds of the ring and barrel respectively.

The test lubricant forms part of the hydrostatic loading system and also the contact supply (Figure 7.2.3). A high pressure pump, for loading, is equipped with a low pressure bleed with which to lubricate the contact. This low pressure inlet supply is temperature controlled by water cooled heat exchangers. Ferrous debris is collected by magnetic filtering in the lubricant supply tank as well as by 3 μm filters.

Trailing thermocouples are used on both the barrel and the discs to give surface temperatures. These thermocouples are complemented by another thermocouple in the lubricant sump, to give control over lubricant temperature.

The load across the facewidth of the contact remains as uniform as possible, by allowing some movement for the specimens to align, thus reducing the probability of edge initiated damage. However, there is an increase in stress at the edges of the track, as will be shown in Chapter 8, and pitting failure tends to take place there.

The specimen shape allows them to be manufactured from any material reasonably cheaply, although quality control and heat treatment are important.

With this test arrangement the barrel undergoes three stress cycles per shaft revolution, making it the element on which failure is expected. In this way, the discs can be reused for other experiments. This factor, along with the high speeds maintained at a fixed slide-roll ratio, can keep experimental test times with surface hardened steels within reasonable limits, at relatively low loads, in keeping with the practical gear situation (Bailey 1989). The rig allows Hertzian contact stresses of up to 3.5 GPa to be achieved with the chamfered barrel specimen and higher with the crowned specimen (these are described in Section 7.4.2).

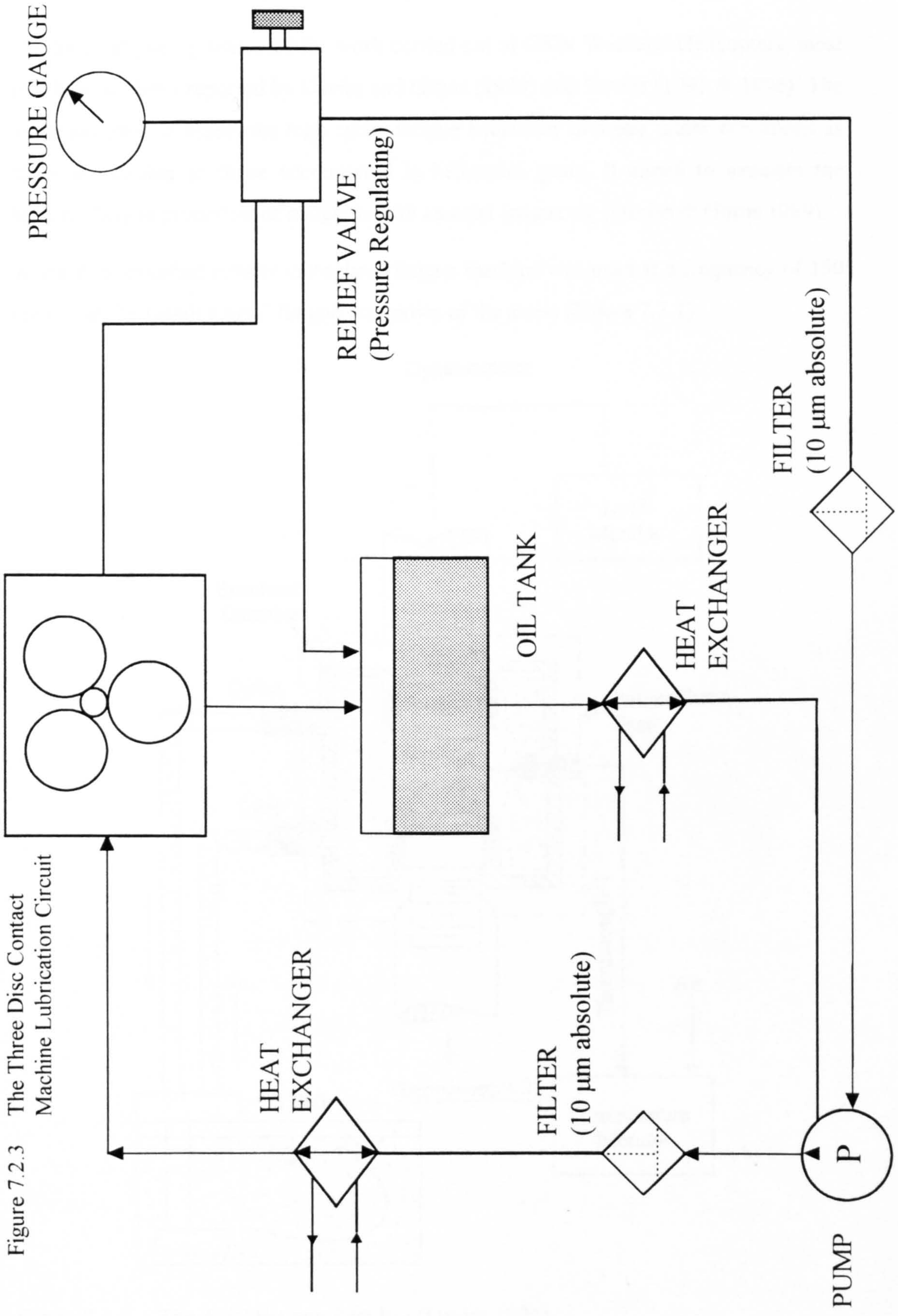


Figure 7.2.3 The Three Disc Contact Machine Lubrication Circuit

7.3 The Axial Fatigue Test Rig

The axial fatigue rig was used for work carried out at GKN Westland Helicopters, most of which has been reported by Davies and Gittos (1989) and Davies (1991 & 1996). The work intended to assess the high cyclic fatigue behaviour of steels under conditions as close as possible to those encountered in helicopter gears. It aimed to simulate the bending fatigue properties of materials with an axial fatigue rig (Davies & Gittos 1989).

A specially modified Amsler vibrophore fatigue machine was used at a frequency of 150 Hz to test the rotating bend-fatigue properties of the steels (Figure 7.3.1).

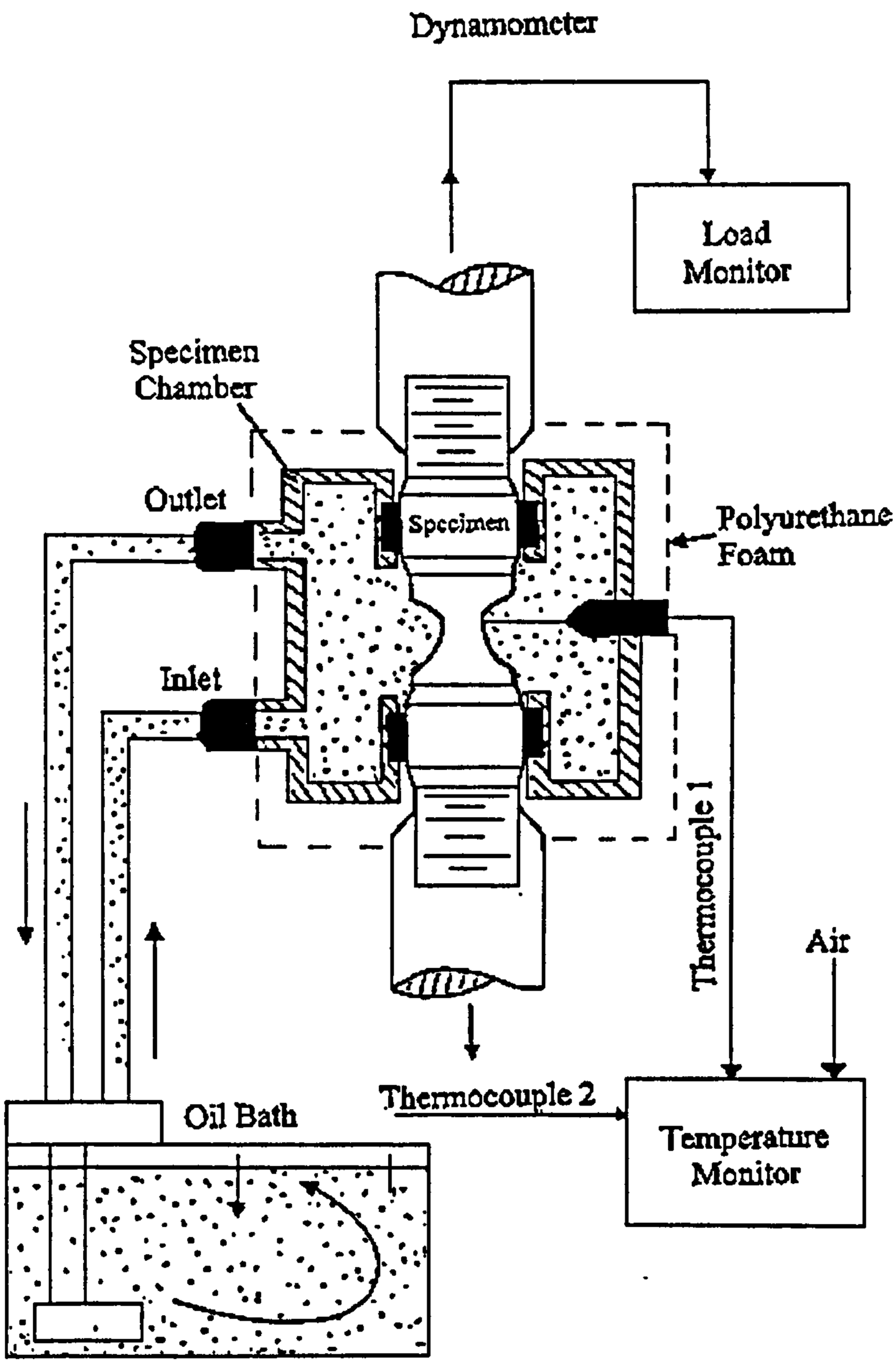


Figure 7.3.1 The Axial Fatigue Test Rig (Davies 1996)

The fatigue specimens were held in position by a threaded grip assembly, while generation and control of the oil temperature was achieved by a combination of methods. The oil temperature was controlled to within ±2 °C of the pre-set 150 °C. The test specimen was held at temperature for 1 hour prior to beginning the test.

7.4 The Design of the Test Specimens

7.4.1 The Gear Test Specimens

The gear test specimens discussed here are for use in the gear test rig described in Section 7.1. They are seventeen tooth involute spur gears (Figure 7.4.1), and were designed to make them more susceptible to pitting failure, rather than bending fatigue.

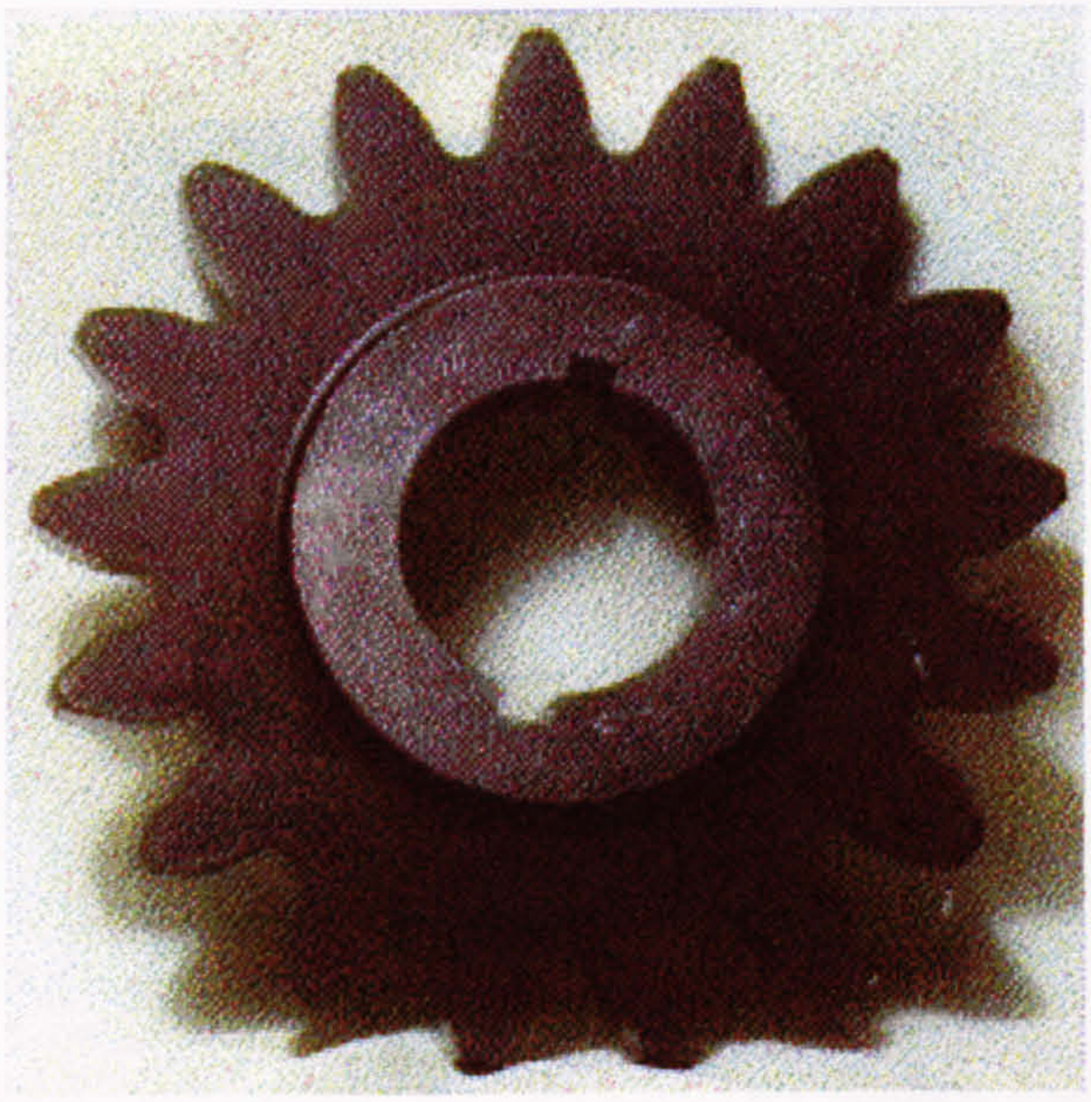


Figure 7.4.1 The Seventeen Tooth, Involute Spur Test Gear

For the gears to fail by pitting, high contact stresses were needed to ensure that the time to failure was not going to be excessive but, at the same time, relatively low tooth bending stresses were required so that tooth bending fatigue failure would not be a problem.

The best way to avoid bending fatigue breakage was to design the gear so that the load transmitted by the teeth would result in bending stresses well within the endurance limit of the material. Care was taken that the material has been properly heat treated, to obtain the best structure, and to minimize any harmful residual stresses. Overload breakage would be harder to design against, but would be unlikely in the gear test rig.

The gear terminology and equations used by the author follow those set out in BS 436 Part 3 (BSI 1986), AGMA 115.01 (1959), and Tuplin (1962). A few basic gearing concepts are mentioned here, for more information on the gear geometry, terminology, and the equations used to design the gears see Appendix K.

The shape of any standard gear can be determined by the basic rack, which is defined by standard proportions. To obtain a particular size gear these proportions have to be multiplied by the module (in millimetres), only specific values being permitted by the standards. The diametral pitch is the Imperial system equivalent of module, it is the reciprocal of the module expressed in inches. The addendum modification coefficient is a non-dimensional number indicating the radial distance the gear cutter reference line and gear reference diameter are apart. It helps determine the shape of the gear teeth, and must be within practical limits to avoid undercutting the teeth or giving them too narrow a crest width.

The gear test rig had a fixed centre distance between the driving shafts of 88.9 mm, and the existing slave gears were thirty-five tooth spur gears. This restricted the options for test gear design; the two test gears had to be 1:1 ratio spur gears. With this in mind, the variables were tooth number and module, the addendum modification coefficient, thence, being determined by the fixed centre distance. This correction factor, however, had to be a reasonable value, lying within an advised range, that suggested by BSI (1970), for example.

A tooth number of seventeen was chosen, more teeth would have presented a risk of bending fatigue due to the finer pitch and less teeth would have posed the problem of tooth undercutting, again being detrimental to bending fatigue resistance. This meant a module of 5.08 mm, or 5 diametral pitch, was appropriate. This gave an addendum modification coefficient of 0.25 for each gear. Having defined the geometry of the gear, the running conditions could be chosen, and, following that, the stresses the gear teeth would experience could be calculated (this is done in Chapter 8).

In order to maintain a high contact stress, but a low bending stress on the gear teeth, the factors to be considered were the running torque and the tooth profile. The maximum torque the rig could output was estimated at 500 N m from Figure 7.4.2. A torque of 350 N m was chosen as the design load, to run the rig within its operating range.

For this value of torque, the maximum contact and bending stresses for the gear teeth could be calculated, assuming that gear teeth were flat along the facewidth, perfectly involute in profile, and that their surfaces were smooth. For the line contact that would exist between the two gear teeth, Hertz theory of elastic contact could be used, as shown in Chapter 2. This was used to calculate the contact stress at the lowest and highest points of single tooth contact (LPSTC and HPSTC), as these were the points where the tooth experienced the highest contact stresses (Figure 7.4.3).

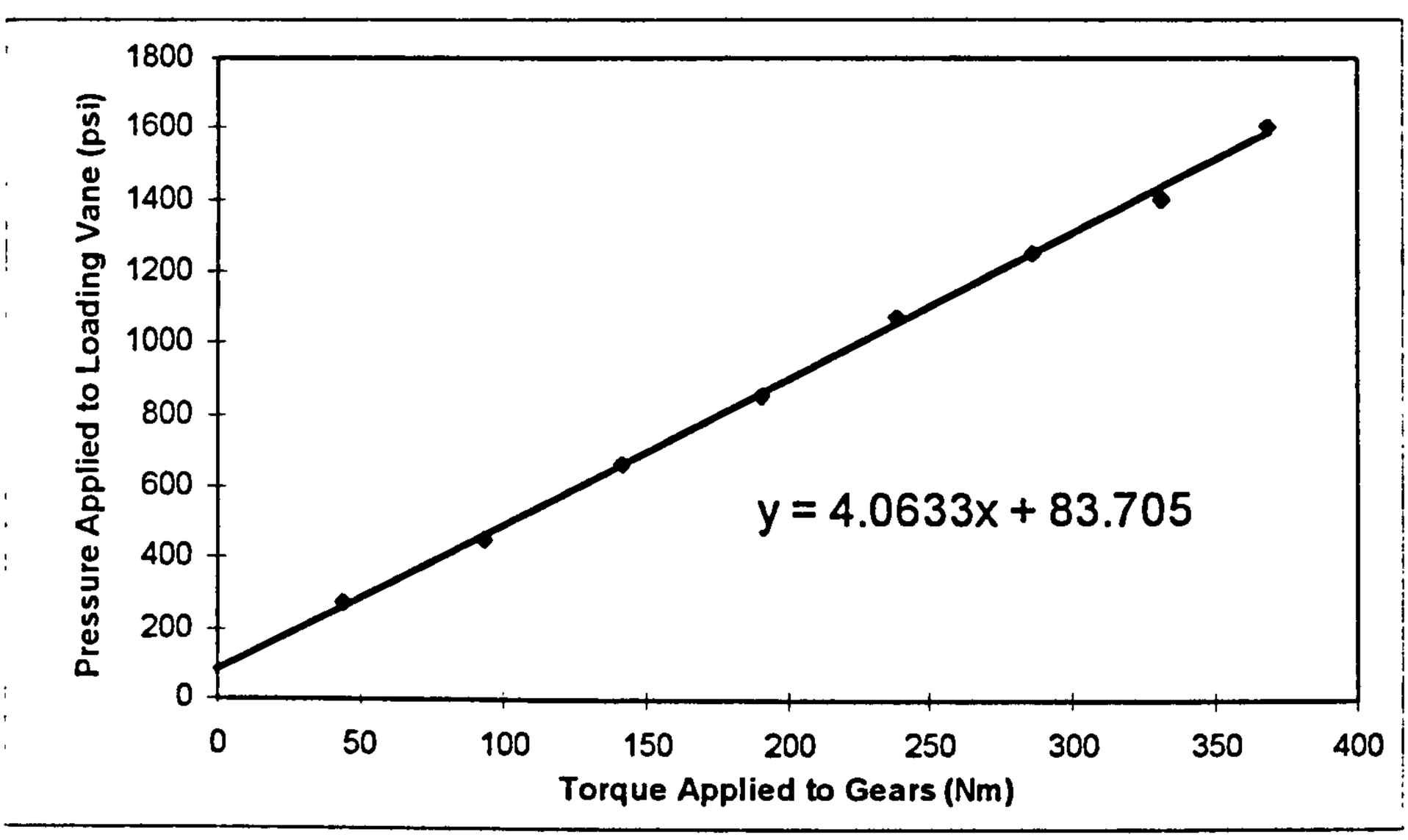


Figure 7.4.2 Calibration Curve for the Gear Test Rig

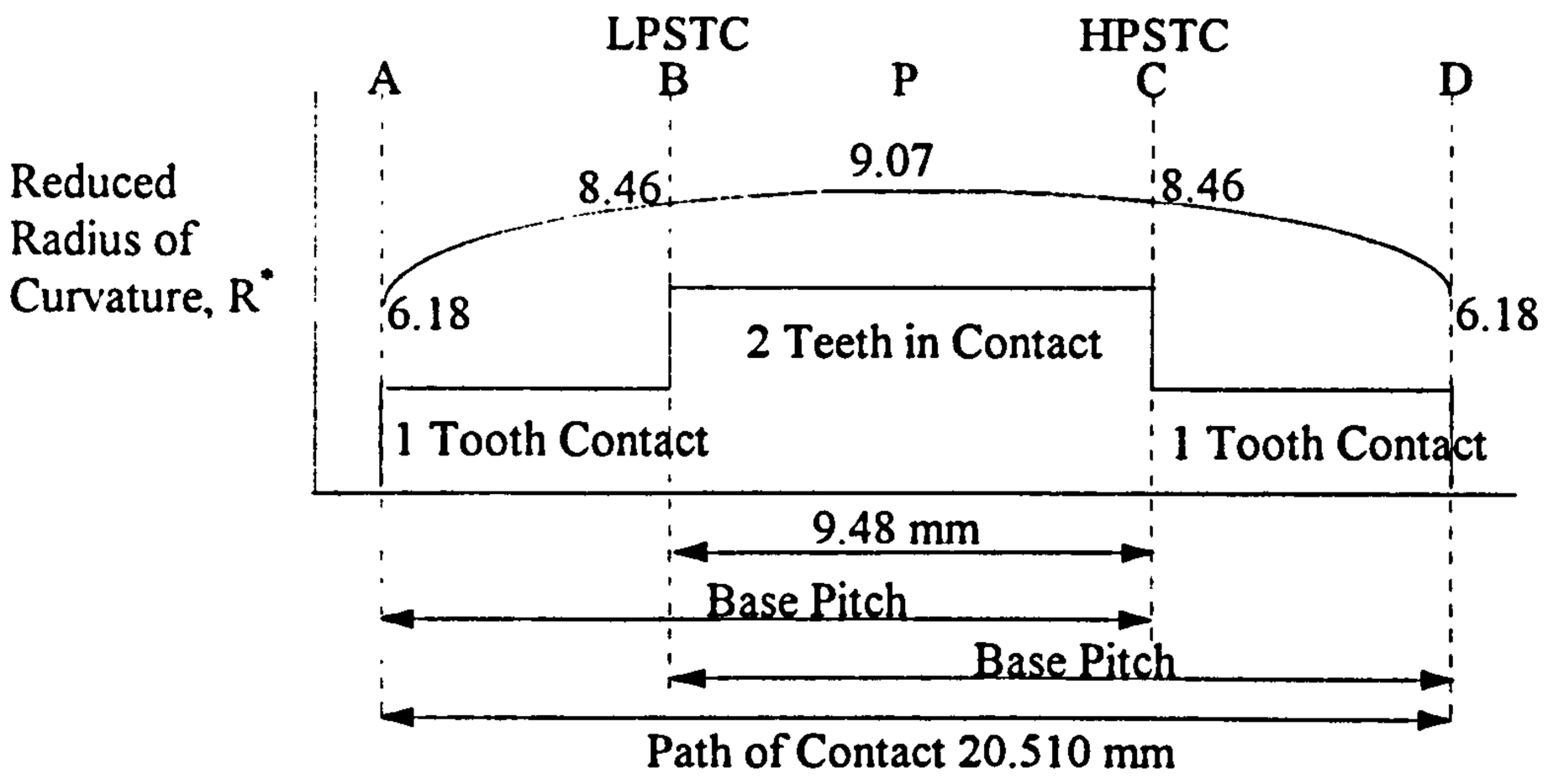


Figure 7.4.3 Reduced Radius of Curvature and Tooth Meshing Number Across the Path of Contact

To increase the contact stress further, without altering the bending stress too much, a crowning radius was applied to the gear teeth. The Hertz solution for two bodies with radii of curvature of different sizes in different directions gives an elliptical contact (as

shown in Chapter 2 see Figures 2.1.1 and 2.1.2). To find the maximum Hertzian contact stress and the major and minor semi-axes of the contact ellipse, the value of two elliptical integrals must be determined. These were evaluated using an iteration technique (Dyson et al. 1989), which yielded the values shown in Figure 7.4.4. It was important that the contact width along the tooth face was less than the facewidth itself for this elliptical contact, for obvious reasons. The crowning applied to the test gears is shown in Figure 7.4.5.

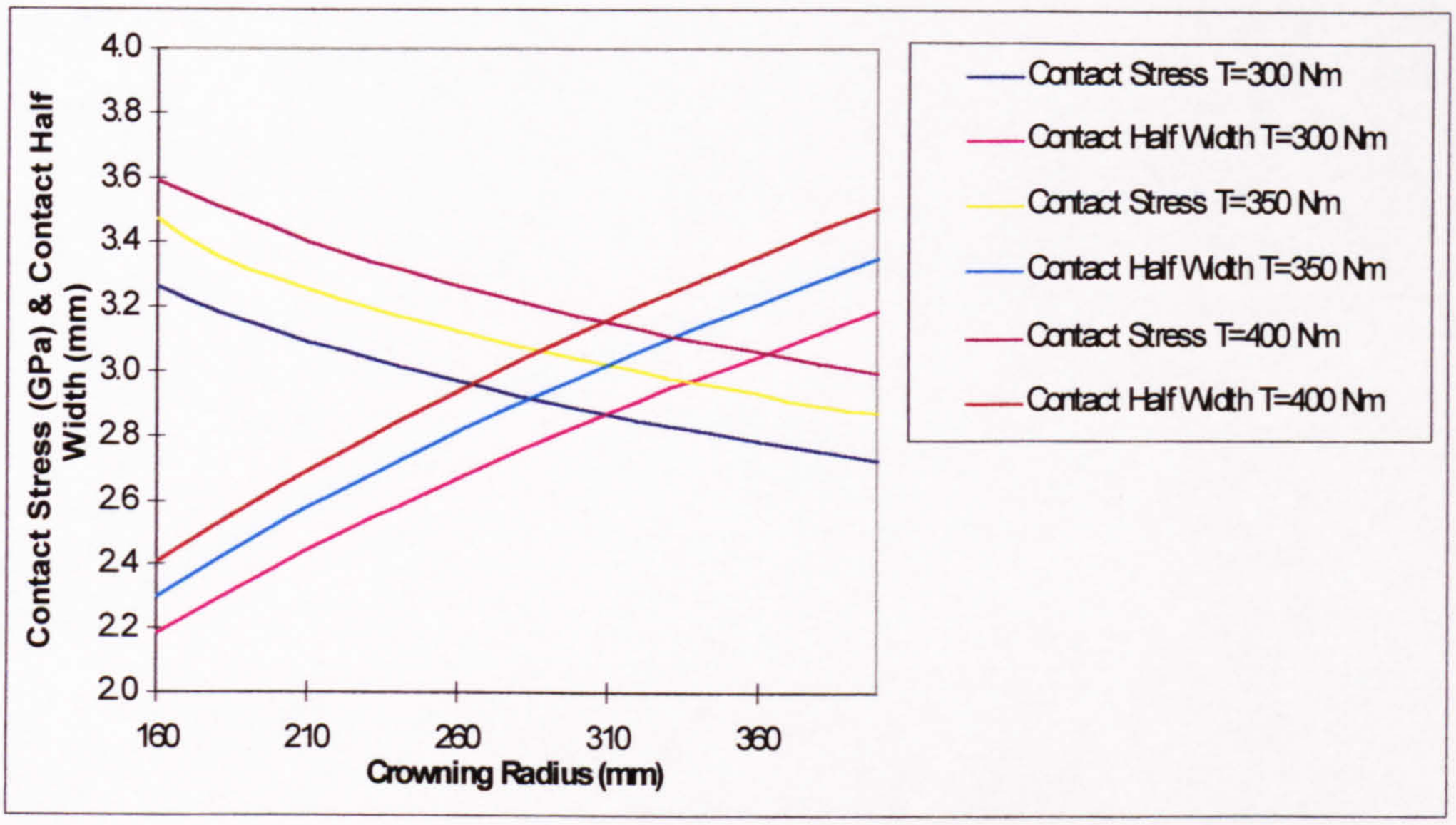


Figure 7.4.4 The Effect of the Crowning Radius on the Maximum Contact Stress and Contact Half Width for a Torque of 300, 350 and 400 Nm

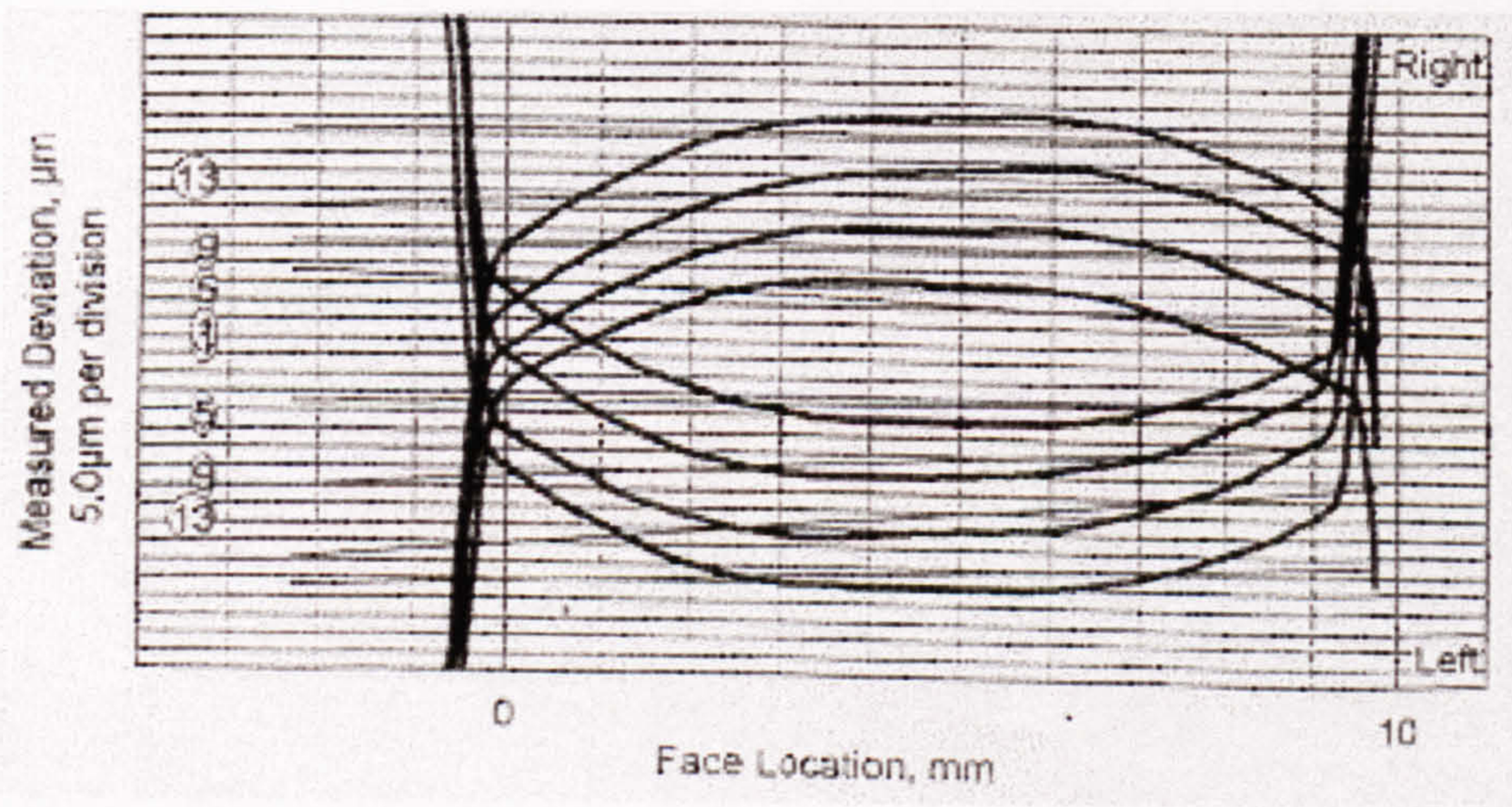


Figure 7.4.5 Typical Lead Profile for a Test Gear

The case depth of the carburised and nitrided test specimens, for these calculated contact stresses, was evaluated using AGMA 246.01A (1971) and AGMA 2001-C95 (1995).

With the design and running conditions determined, there was the problem that scuffing could be the prevailing failure mode at the high loads required. This risk could be compounded by the use of an excessive crown on the gear teeth, that could mean the contact carried more load than the lubricant film could support, leading to film break down and consequent scuffing failure. If this were the case, one could try to avoid it by either reducing the amount of heat in the mesh, which could be achieved by cutting down on the load being transmitted, reducing the speed of the gears, or lowering the inlet oil temperature to the gears; or by using a lubricant with extreme pressure additives. In the author's case, reducing the load and speed were not viable solutions because they were needed to obtain pitting failure within a reasonable time, but the bulk oil temperature of the gears could be controlled. The lubricant plays a very important role in the contact as it must be able to tolerate the load, speed, and temperature conditions of the gear mesh.

Two different gear geometries were going to be used to study the effect of tooth pre-engagement: one with tip relief and one without. The gears without tip relief would give rise to tooth pre-engagement, whereas, the tip relieved ones would not. The tip relief was designed with the aid of a survey on current practices compiled by the BGA (1994).

The idea behind profile relief is for it to compensate for the deflection of gear teeth under load, in order to transmit load smoothly. There is also the added effect that it removes part of the load on the teeth in the high sliding portions, thus avoiding premature failure. It is therefore beneficial in reducing the risk of scuffing and in minimising noise and vibration. Relief can only be correct for a particular applied load and is only worthwhile in good quality gears. In gears where the manufacturing errors are similar to, or greater than, the tooth deflections under load, the advantages may not be gained (it would then be better to improve accuracy).

For geometrically perfect spur gears of infinite stiffness, the contact path for a pair of mating teeth starts at A and finishes at D (Figure 7.4.3). The theoretical tooth load cycle for a tooth pair going through mesh is in the form of a series of steps, however, suddenly applied loads like this are not desirable.

In practice, the gear material is not infinitely stiff, and deflects under load. At point C this will lead to the driving gear rotating slightly in advance of its theoretical position, by an amount equal to the combined deflection of these two teeth. The next pair of teeth should come into contact at A, but because the driving gear has rotated a little ahead of

this position, the teeth at A will be in a slightly different position. This difference in position is called premature engagement. The tooth will also leave contact later than expected, late disengagement. These two processes will combine to produce extended contact of the tooth pair. It can also occur because of manufacturing errors, in particular adjacent pitch errors. Profile relief is carried out in order to prevent this overlapping, but for it to be carried out accurately one needs to know the tooth stiffness. (This will be discussed in detail in Chapter 8).

The loading cycle shown in Figure 7.4.6 is much more desirable than, the previously mentioned, step loading. There is a gradual uptake of load by the incoming pair of teeth and a corresponding release of load by the outgoing pair. The relief must be at least equal to the total deflection of the tooth pair at C to avoid pre-engagement.

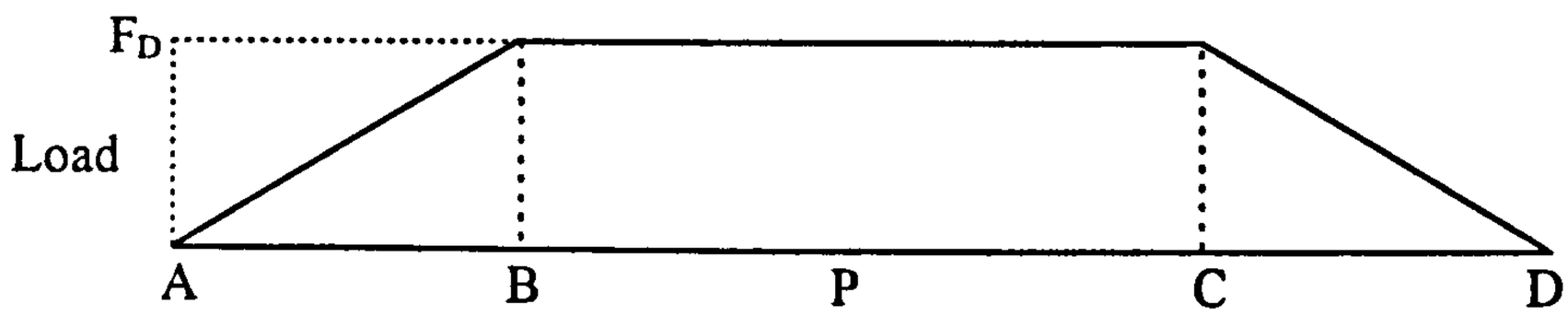


Figure 7.4.6 Tooth Load Cycle for a Properly Relieved Gear

The extent of the profile relief is another aspect to be considered, there are two main types: long correction and short correction, illustrated in Figure 7.4.7.

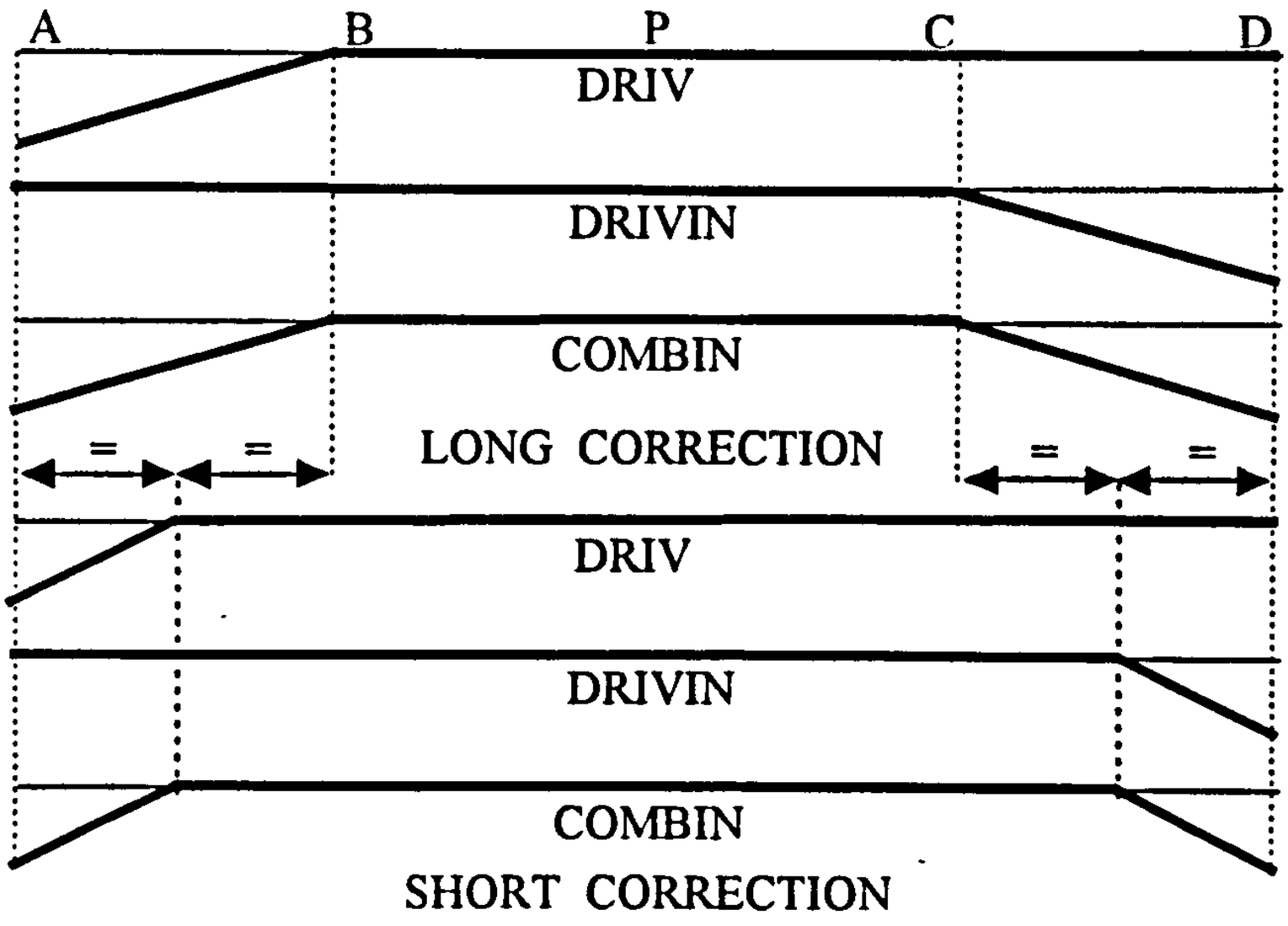


Figure 7.4.7 Long and Short Relief Diagrams for Involute Spur Gear Teeth

The deviation of a gear tooth from its theoretically correct position is called the transmission error, this is a continuous varying function as the gears rotate. A driven gear behind its correct position has a negative error, and vice-versa. The transmission error can be affected by deflections, deviations from the true involute, either in the form of correction or in the form of manufacturing errors, and by pitch errors (it is a sum of all these errors).Transmission error is the best way to derive corrections and tooth load cycles, particularly when random manufacturing errors are present. It is also an important parameter for the evaluation of kinematic accuracy, vibration, and noise.

The transmission error for a gear with no errors, profile relief, and constant stiffness is given in Figure 7.4.8. This also shows the effect of load on the transmission error. (It will increase due to the tooth deflection). If adjacent pitch errors are now taken into account the tooth pair with the pitch error simply has its isolated transmission error moved vertically by the amount of the error. Positive pitch errors (more material) move the curves upwards.

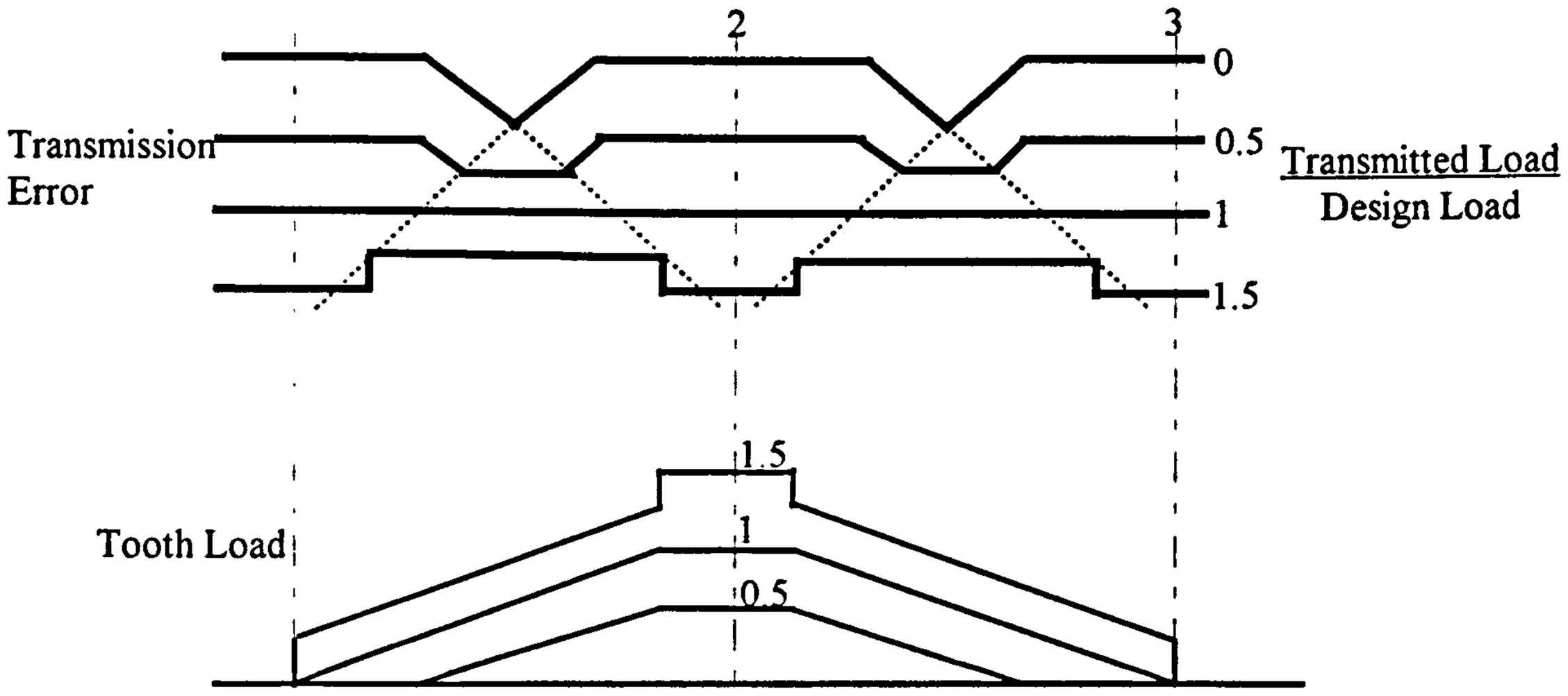


Figure 7.4.8 Transmission Error Diagram for a Loaded Tip Relieved Gear (assuming constant stiffness)

The correction applied depends on what is used as the design load. This was chosen to be the maximum load, since it was thought that the load would be fairly constant during the test. Long correction was thought preferable.

The design procedure adopted was to apply an additional amount of relief equal to the maximum adjacent pitch error. The adjacent pitch error tolerances from the AGMA

standards for a specified gear accuracy were used (AGMA 1988). The tip relief on the test gears is shown in Figure 7.4.9.

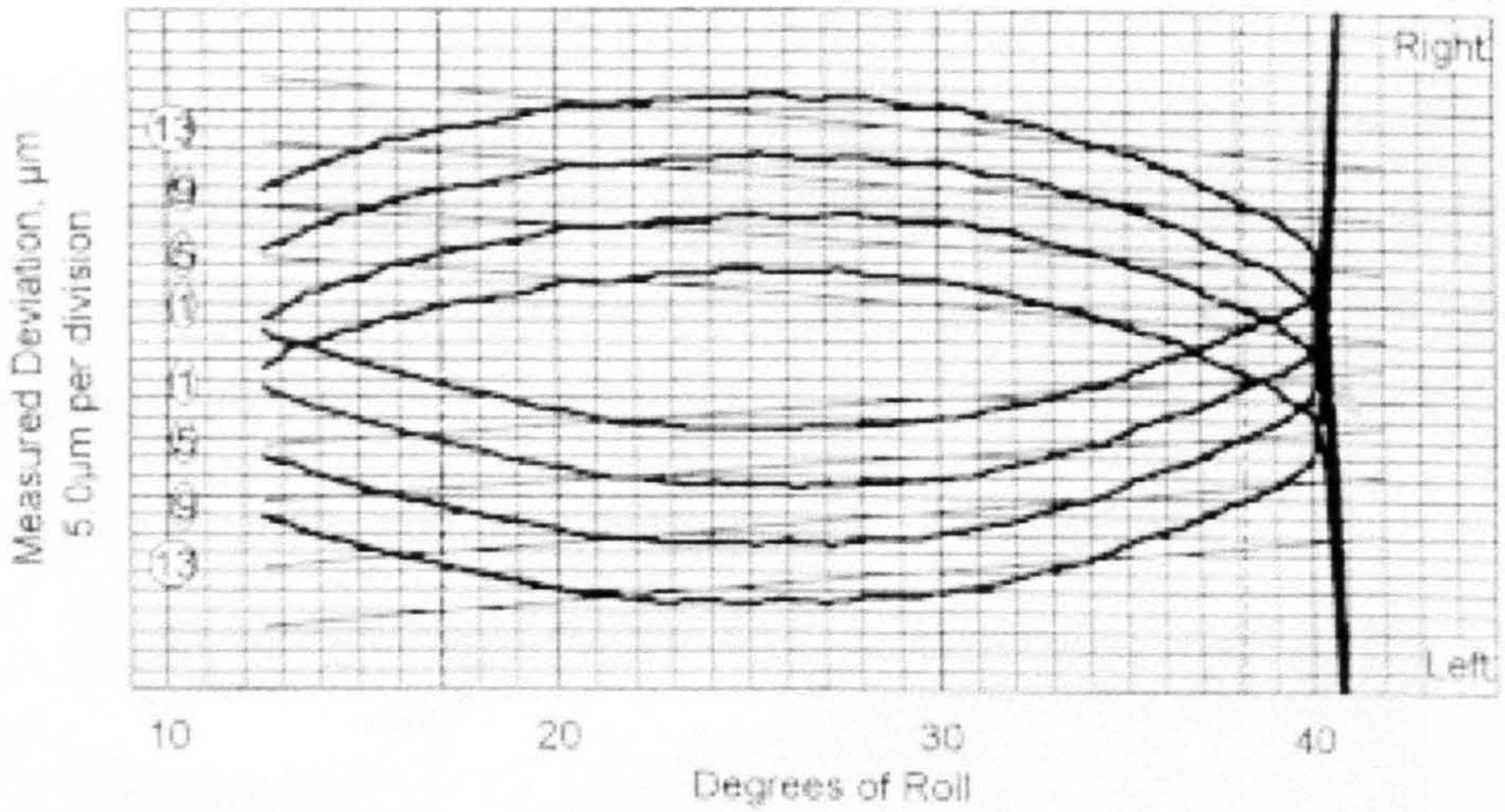


Figure 7.4.9 Involute Profile for a Test Gear (Tip and Root Relief of about 40 µm)

Increasing the amount of tip relief to allow for adjacent pitch errors can have the desired effect when there is a pitch error present by avoiding corner contact and impulsive loading. If there is no error then it can change the design load for which the relief is correct. One must compromise, when choosing the design load, between scuffing risk at high loads and noise and vibration risk at lighter loads.

The gear design specification and drawing are given in Appendices C and D respectively.

7.4.2 The Disc Test Specimens

The disc test specimens were designed for use in the hydrostatic disc machine described in Section 7.2. The geometry of the test specimens was fairly well defined by the test rig layout.

The barrel specimens, manufactured from various materials, were made with two different geometries and tested at a few slide-roll ratios. One type of barrel had a flat face and chamfered edges, and the other type was crowned (as shown in Figure 7.4.10). Failures detected by Bailey (1989) with chamfered specimens indicated that the stress concentration at the edge of the running track determined the pitting life. To alleviate this problem he tried regrinding the test specimens to produce a crowned running track. This, however, introduced the problem that a groove could form in the counterface rings, particularly at high slide-roll ratios. This would reduce the contact stress as the test

progressed. It was thought appropriate therefore to use both types of specimen in this study.

The barrel is chamfered at an angle of 15° to give a track width of 6.35 mm and has a diameter of 18.59 mm, the rings have an outside diameter of 82.93 mm. The crowned barrel specimen was designed with a 45 mm crowning radius, however, this was made with a radius of 22.5 mm, therefore raising the expected stresses in the contact and narrowing the contact width.

The design drawings for these specimens are given in Appendix E.

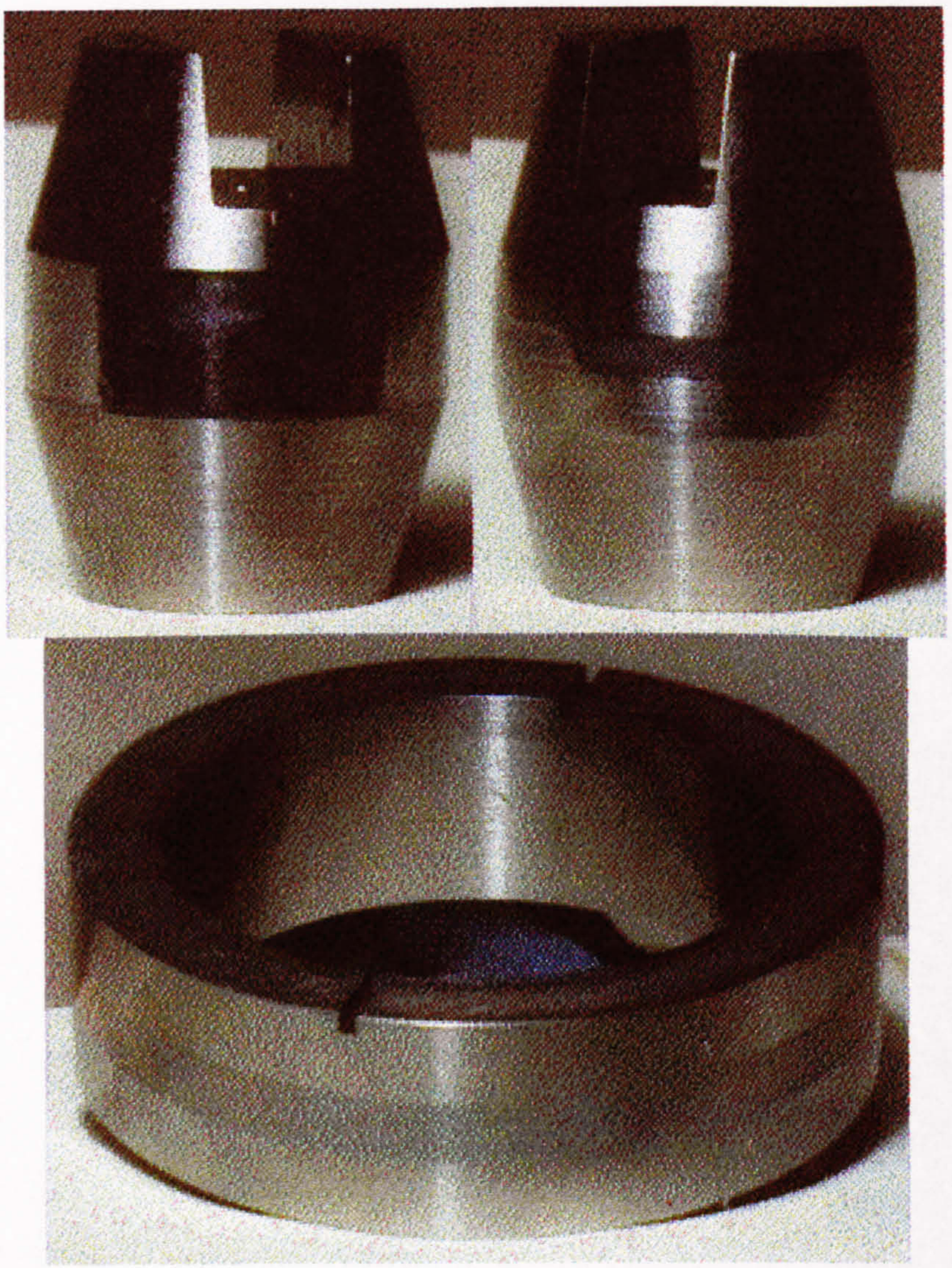


Figure 7.4.10 The Chamfered and Crowned Barrels and Ring Specimen

7.4.3 The Axial Fatigue Specimens

The axial fatigue test specimen was designed to simulate the geometry and stresses experienced by conformal and involute gear tooth roots. The tooth-root stress

concentration, carburised case depth, and applied mean stress were arranged in such a way as to provide a realistic distribution of applied stress, whilst still enabling the use of a simple, axially loaded fatigue specimen. This was achieved by designing a specimen such that the radius at one end of a tapered section simulated the tooth-root stress characteristics of an involute gear (Figure 7.4.11). The results of these axial fatigue tests could therefore be related to the bending fatigue properties of the materials (Davies 1996).

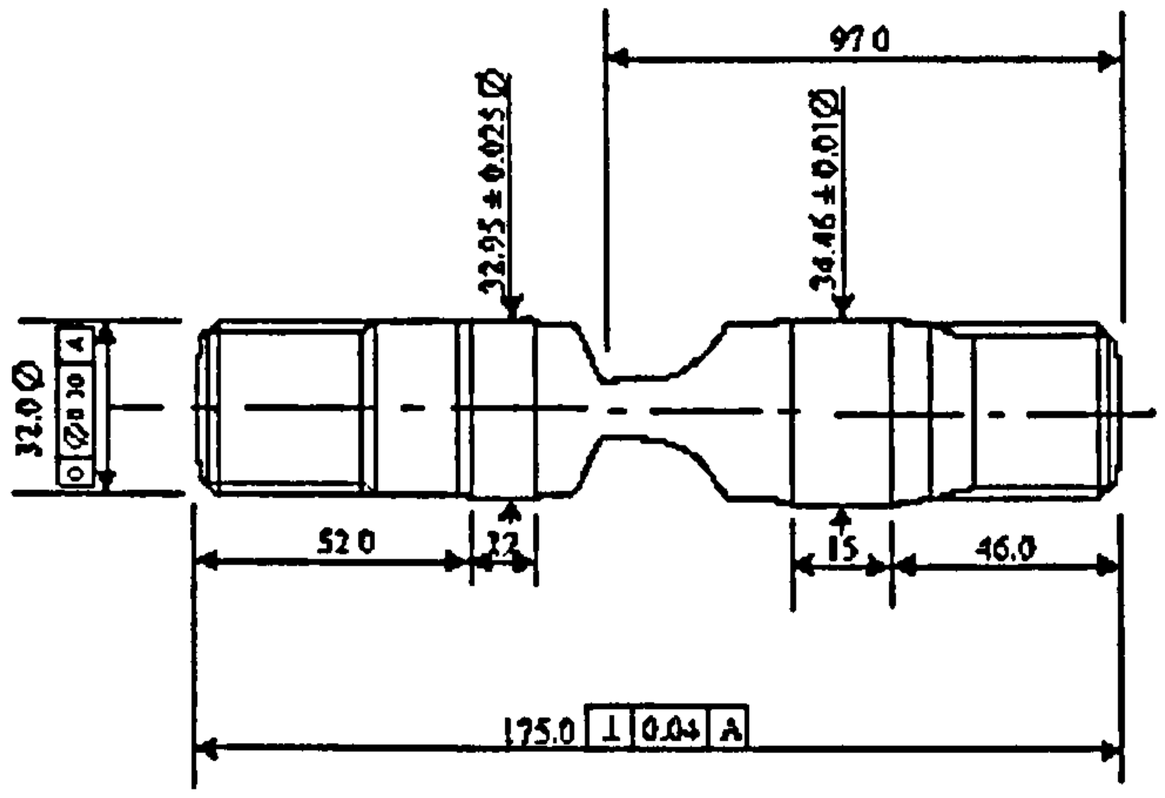


Figure 7.4.11 The Axial Fatigue Test Specimen (Davies 1996)

7.5 The Specimen Properties

The roughness and hardness which are considered to be important in fatigue testing, as discussed in Chapters 2 and 3, are given here. The microstructures of the various materials tested are examined in Section 7.5.3.

7.5.1 Roughness

As explained in Chapter 2, all surfaces are rough. This roughness is usually imparted on components during the machining and finishing processes. In order to predict the performance of a component in service, particularly fatigue life, it is important to measure and characterise its surface roughness. The actual pressure distribution does not follow the Hertz prediction, the local pressures and subsurface stresses tend to be much higher, this was shown in Chapter 2.

The surface profiles used by the author were measured using a Talysurf (described in Chapter 2). Some of the parameters for quantifying surface roughness in two-dimensional profiles were also discussed in Chapter 2. Height parameters and spatial

parameters were both considered important in characterising a surface. The two height parameters used by the author were centre line average, R_a, and root mean square, R_q, roughness. The spatial parameter used was the correlation length, β^*. The statistical parameters of the surface R_a, R_q, and β^* were obtained with the aid of numerical models, developed at Imperial College.

The profiles were filtered once measured. There are two types of filter: high pass to remove the longer wavelengths and low pass to remove the shorter wavelengths. The profile lengths were 1 mm and these were high pass filtered at 0.1 mm.

The roughness was measured axially on the disc specimens and circumferentially on the gears.

Table 7.5.1 The Surface Roughness of the Specimens

Roughness Parameter (μm)	RMS	CLA	β^*
BS S156			
Gear	0.795	0.594	9.792
Chamfered Barrel	0.345	0.268	3.409
Crowned Barrel	0.331	0.250	8.974
Counterface Ring	0.297	0.227	4.201
AISI M50NiL			
Gear	0.458	0.357	9.90
Chamfered Barrel	0.322	0.251	4.26
Counterface disc	0.509	0.381	4.40
AISI M50NiL Duplex			
Gear	0.458	0.357	9.90
Chamfered Barrel	0.527	0.407	4.835
Counterface Ring	0.827	0.643	5.985
32CDV13			
Chamfered Barrel	0.569	0.438	15.61
Counterface Ring	1.045	0.839	15.31

The tabulated values are averages of at least four 1mm profiles high pass filtered at 0.1 mm. (RMS - Root Mean Square Roughness, CLA - Centre Line Average Roughness, β^* - Correlation length.

7.5.2 Hardness

The effective case depth was measured by a Leitz microhardness machine using a 500 gram load on samples which had been diamond polished to 1 μm. The hardness profiles for the gears, barrels and rings can be seen in Figures 7.5.1, 7.5.2, and 7.5.3 respectively. The case depth indicated is that at which the hardness is 520 Hv.

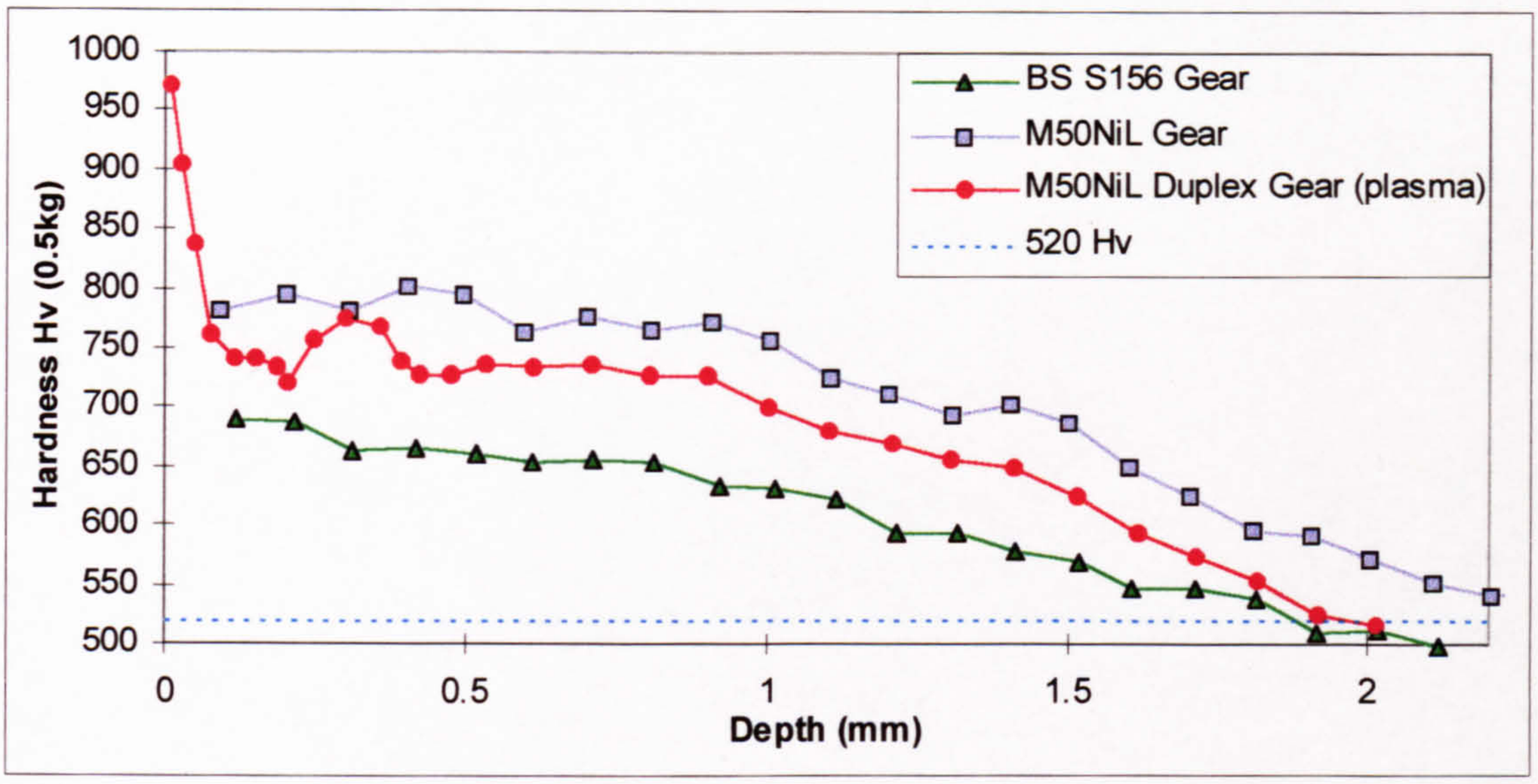


Figure 7.5.1 The Hardness Profiles of the Gear Specimens

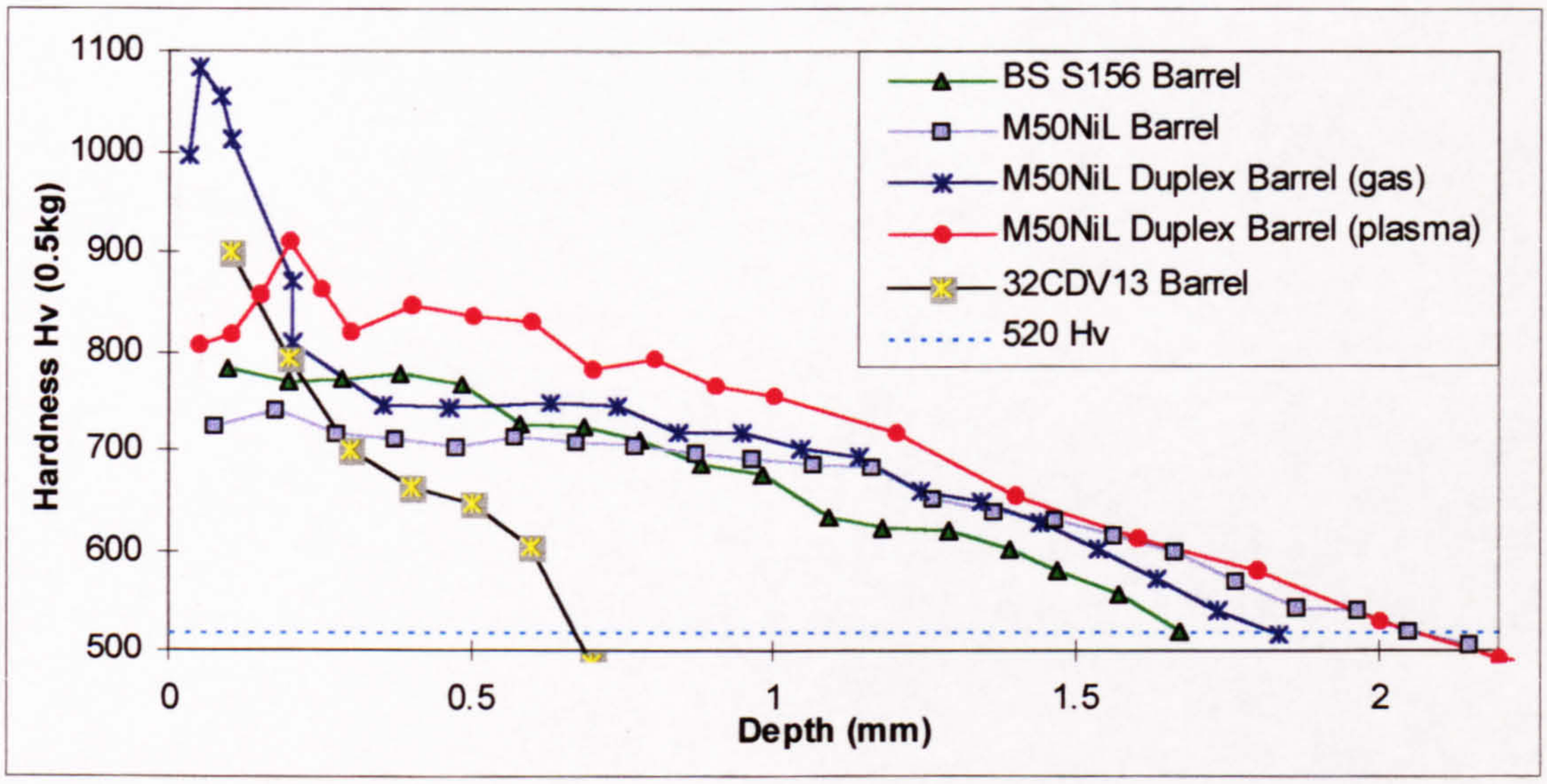


Figure 7.5.2 The Hardness Profiles of the Barrel Specimens

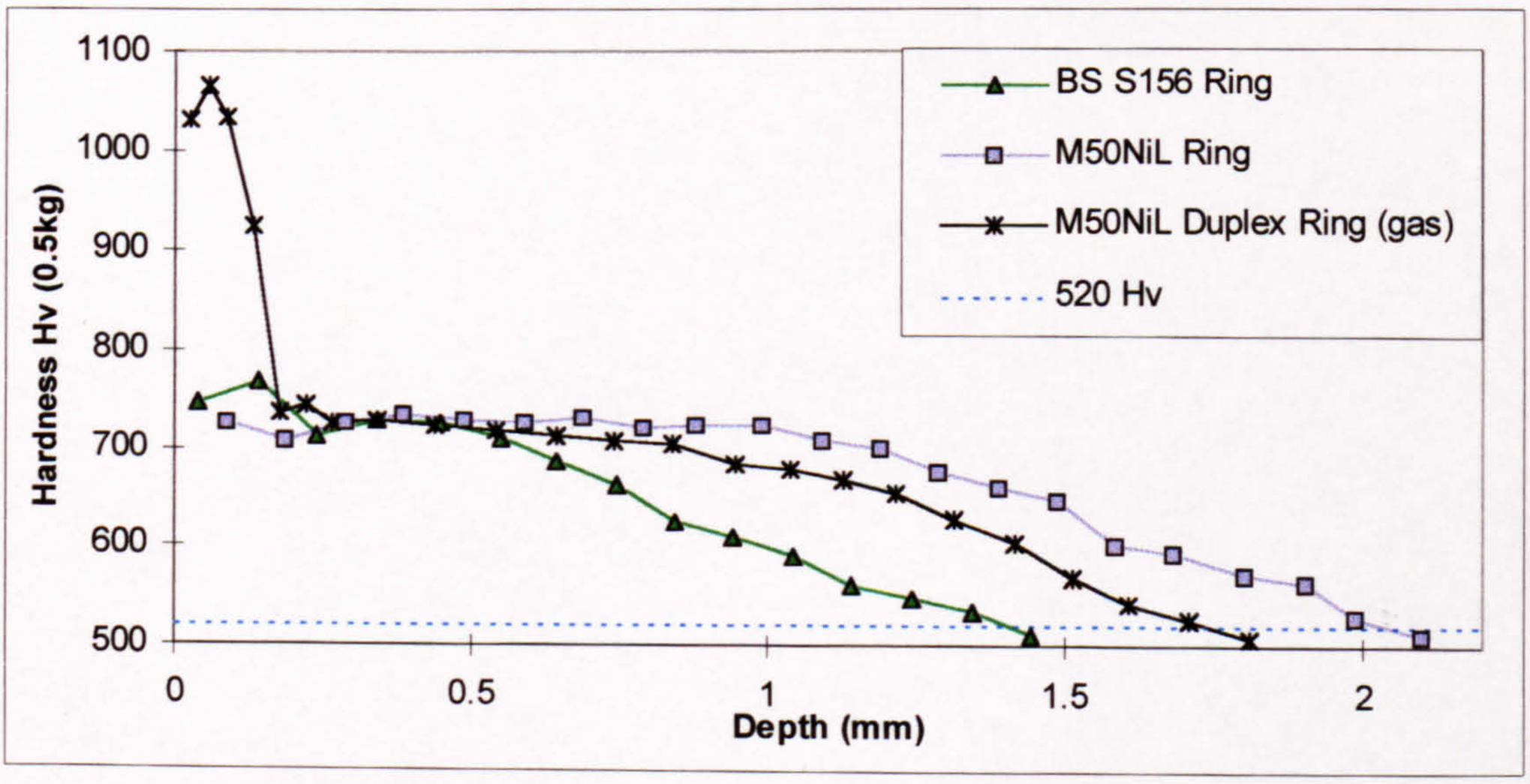


Figure 7.5.3 The Hardness Profiles of the Ring Specimens

The effect of duplex hardening, by plasma nitriding or gas nitriding a carburised steel, can be seen in these figures. The nitriding increases the hardness of the component to a depth of few tenths of a millimetre over that of the only carburised specimens. In this case the plasma nitriding gave a shallower hardening effect than the gas nitriding treatment (in the plasma nitrided barrel specimen it was not possible to measure the hardness close to the surface (Figure 7.5.2), but it was probably similar to that shown for the gear (Figure 7.5.1)). The hardening effect of the nitriding treatment on the 32CDV13 barrel is considerably shallower than that of the carburised cases (Figure 7.5.2).

7.5.3 Material Microstructure

The microstructure close to the surface of the various materials tested is presented here. The BS S156 gear section, shown in Figure 7.5.4, shows a refined martensitic surface microstructure. The AISI M50NiL gear section (Figure 7.5.5) has a coarser microstructure when compared to that of the BS S156 gear, with visible martensite plates and what appears to be a high level of retained austenite. This large amount of retained austenite could have been caused by an excessive carbon content in the material due to carburising. Close to the surface there appears to be less retained austenite. This level of retained austenite may have a negative effect on the performance of the specimen. This will be discussed further in Chapter 13.

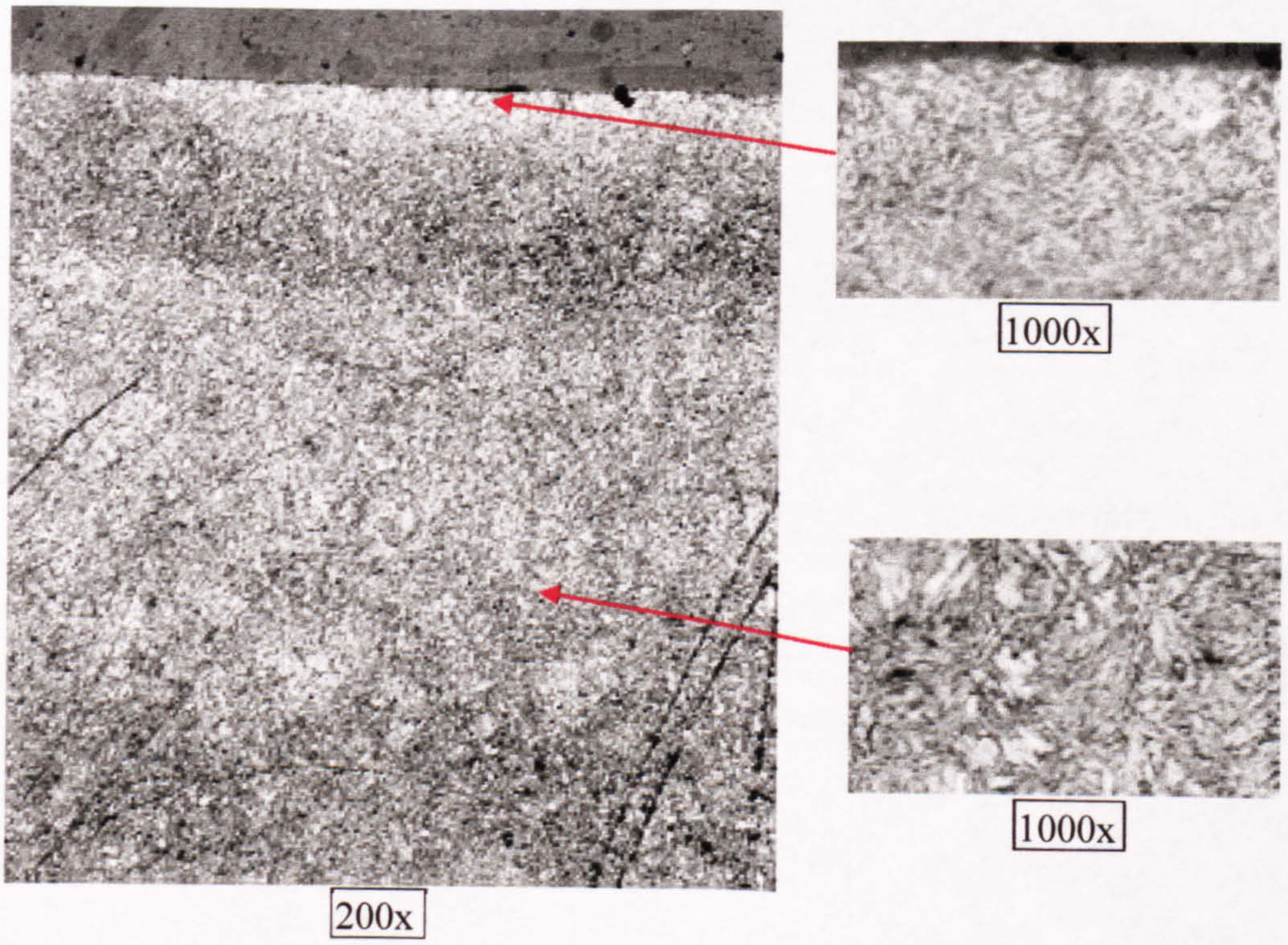


Figure 7.5.4 Transverse Section Through a BS S156 Gear Tooth (5 % Nital Etched)

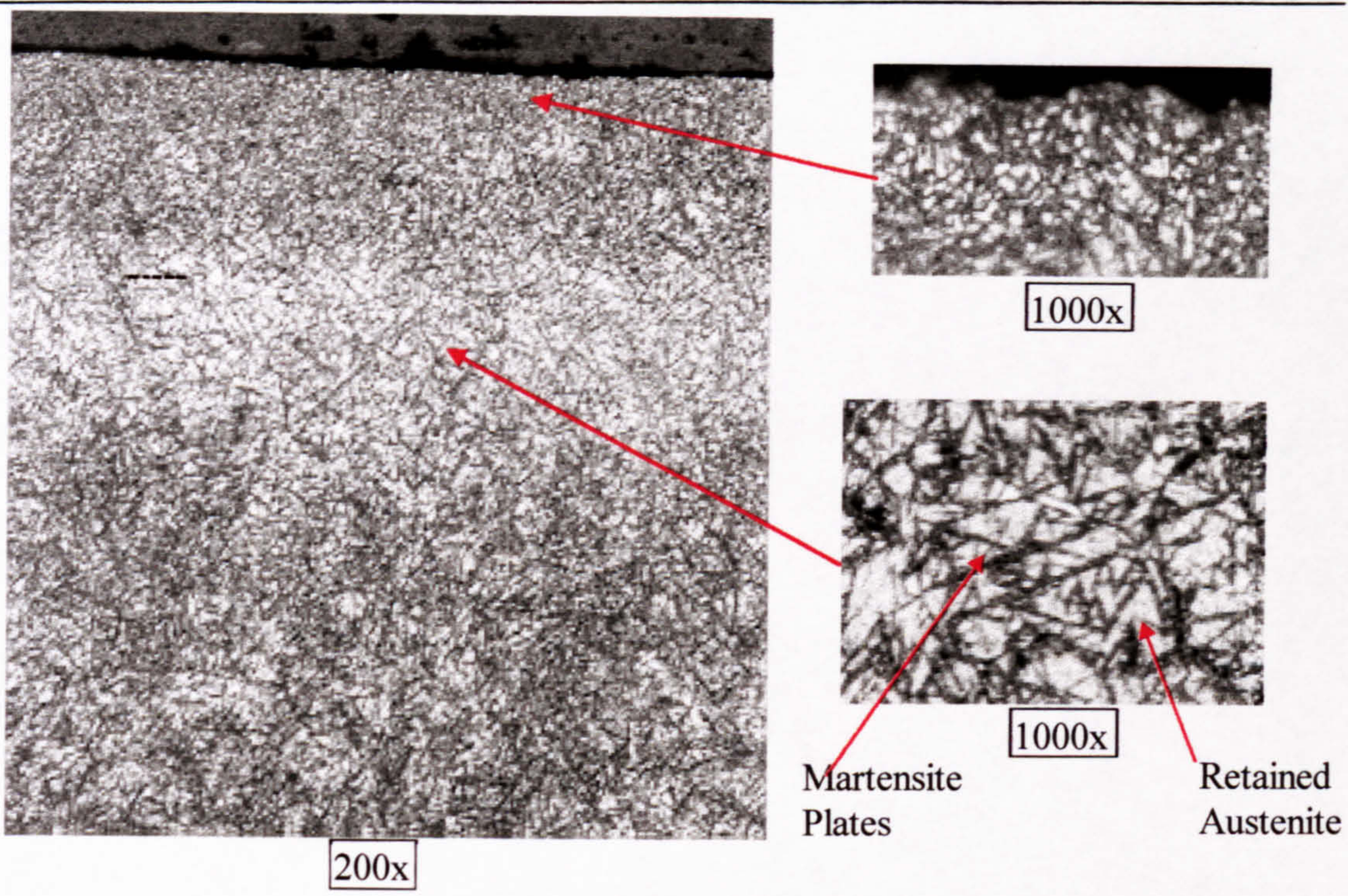


Figure 7.5.5 Transverse Section Through an M50NiL Gear Tooth (5 % Nital Etched)

The nitrided 32CDV13 barrel and ring microstructures are shown in Figures 7.5.6 and 7.5.7 respectively. The white layer on the ring specimen was approximately 36 μm deep. The two phases of iron nitrides, composed of an outer layer of epsilon iron nitride (18 μm deep) over a layer of gamma-prime nitride (18 μm deep), are both visible in Figure 7.5.7. This layer appears to have comparatively large cracks in it and this, coupled with its brittle nature, may have a negative effect on the fatigue life. Approximately half of the white layer was ground off on the barrel leaving mainly the gamma prime-layer. There is also evidence of 'angel hairs' - light nitride complexes of the various alloying elements - deeper in the martensitic structure of the material .

The plasma nitrided Duplex gear specimen microstructure is shown in Figure 7.5.8. There is no evidence of a white layer from the nitriding process. However, there appears to have been a change in the carburised case to a depth of 50 μm, with the top 10 μm having a clearly different appearance from the AISI M50NiL specimens. The carbides can be seen in the microstructure as white specks. The plasma nitrided Duplex barrel specimen shown in Figure 7.5.9, also shows no white layer. Networks of carbides can be seen around the grain boundaries. The nitriding process appears to have reduced the high levels of retained austenite in the AISI M50NiL specimens.

The gas nitrided Duplex barrel shown in Figure 7.5.10 is very different from the plasma nitrided specimens. There is clearly a white layer of approximately 10 μm depth with no distinguishable phases in it. It appears much more intermixed with the underlying material than the white layer in the nitrided 32CDV13 barrel and ring shown in Figures 7.5.6 and 7.5.7.

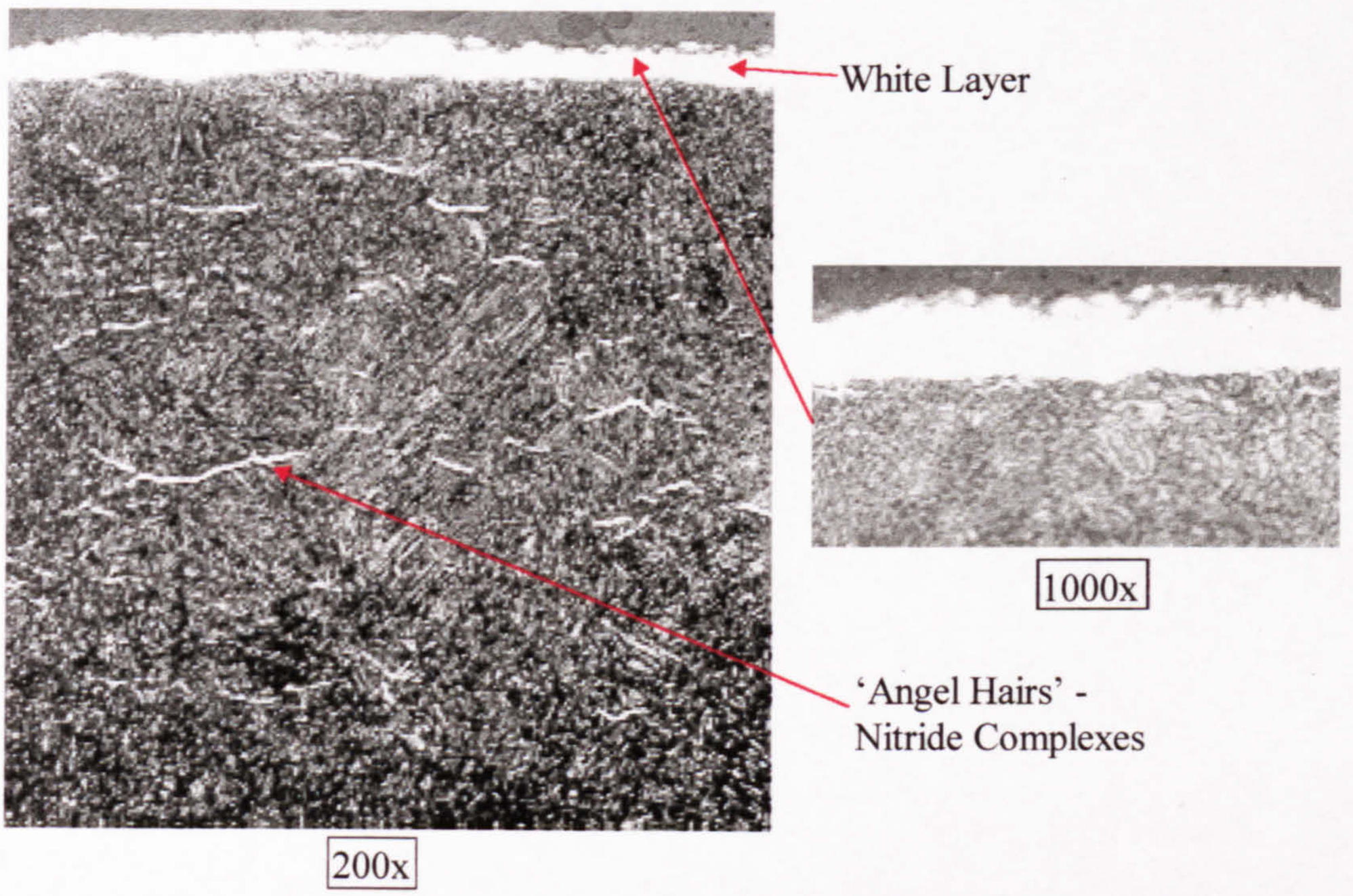


Figure 7.5.6 Transverse Section Through a 32CDV13 Barrel (5 % Nital Etched)

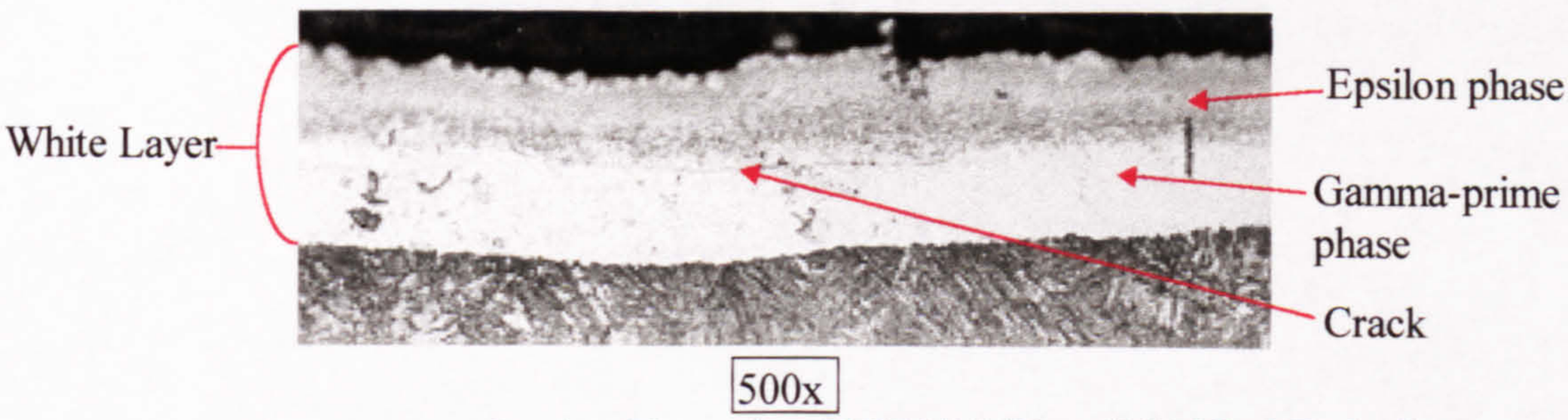


Figure 7.5.7 Transverse Section Through a 32CDV13 Ring (5 % Nital Etched)

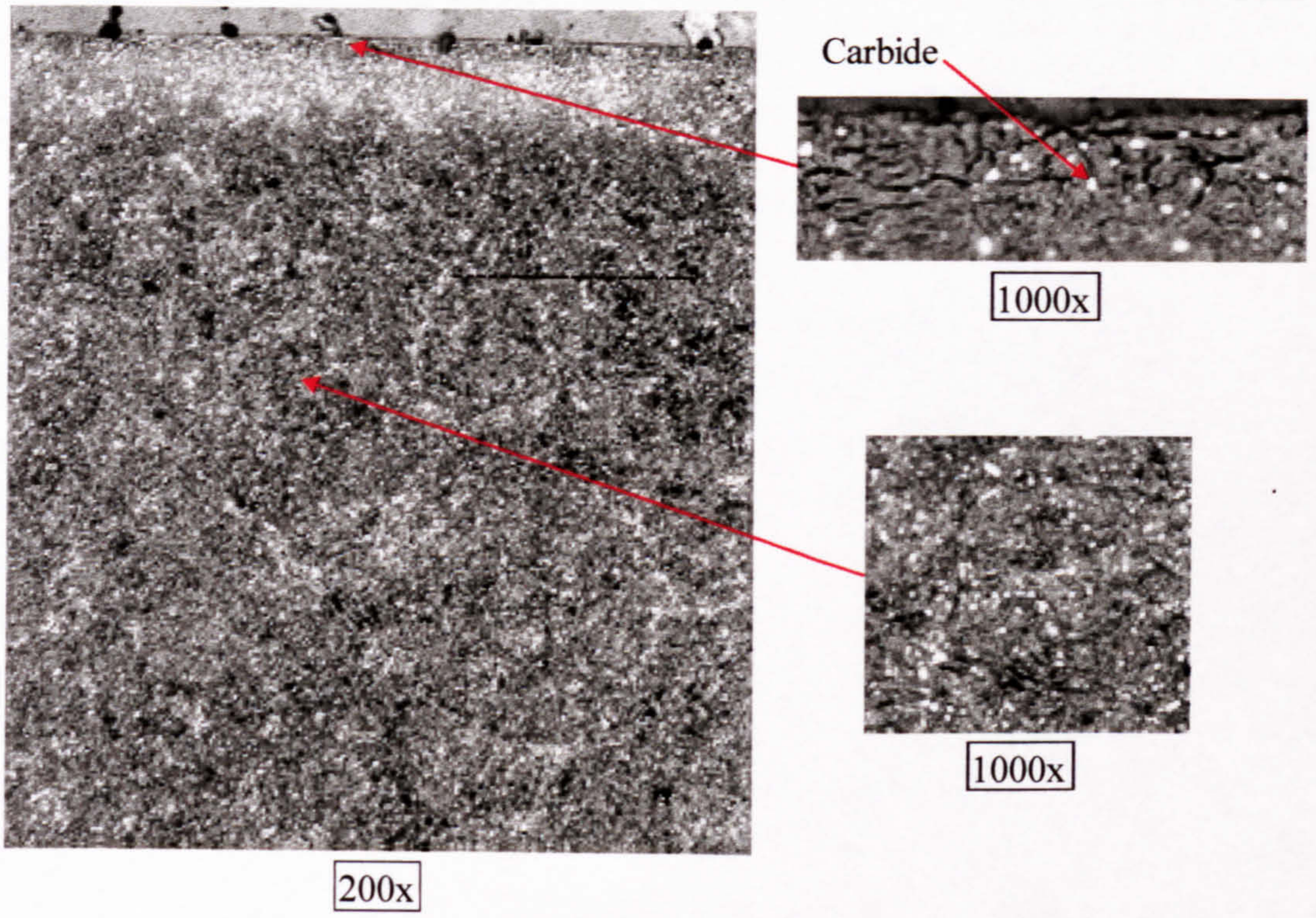


Figure 7.5.8 Transverse Section Through a Plasma Nitrided M50NiL Duplex Gear Tooth (5 % Nital Etched)

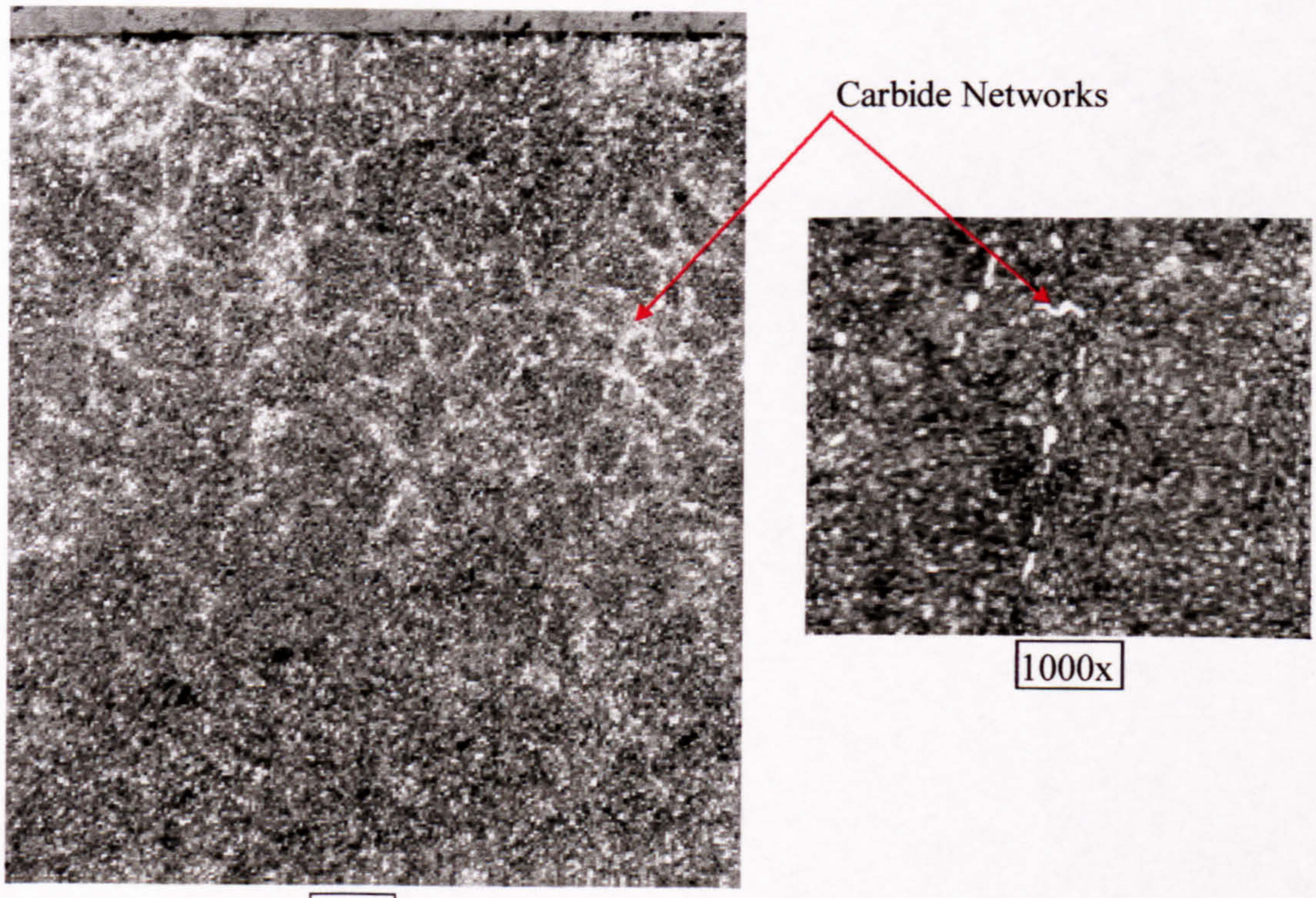


Figure 7.5.9 Transverse Section Through a Plasma Nitrided M50NiL Duplex Barrel (5 % Nital Etched)

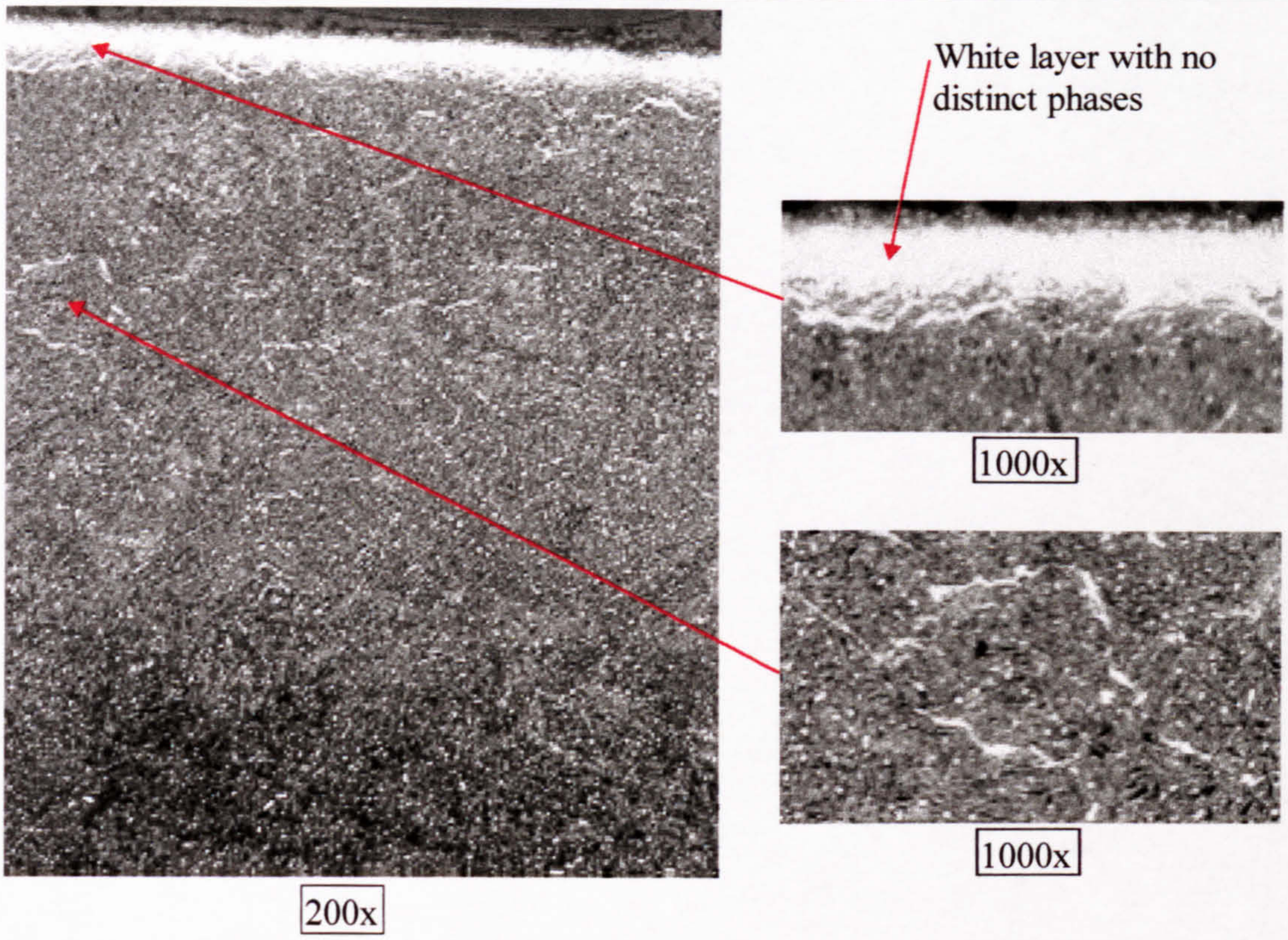


Figure 7.5.10 Transverse Section Through a Gas Nitrided M50NiL Duplex Barrel (5 % Nital Etched)

7.6 On-line Monitoring of the Tests

7.6.1 Failure Detection in the Gear Rig

The gear rig had a monitoring system installed, which would use the signals from two accelerometers mounted on the test gearbox, just above the roller bearings, to determine whether the gears had failed by rolling contact fatigue and, if this was the case, then automatically shut down the test rig. Thermocouples located in different parts of the rig were also used for automatic shutdown if an anomalous temperature rise was detected. This could be due to loss of oil flow to either the slave box or the test gears.

The principles on which the monitoring system worked are described next. The effect of vibration and noise increase as the tooth flank wears, or is damaged by pitting, has been investigated by Kotorii (1992) and Yoshida et al. (1985), amongst others.

The two accelerometers, positioned in the test gearbox housing, picked up vibrations going through the shafts, bearings, and gears. The signal average looked much the same as the schematic shown in Figure 7.6.1.

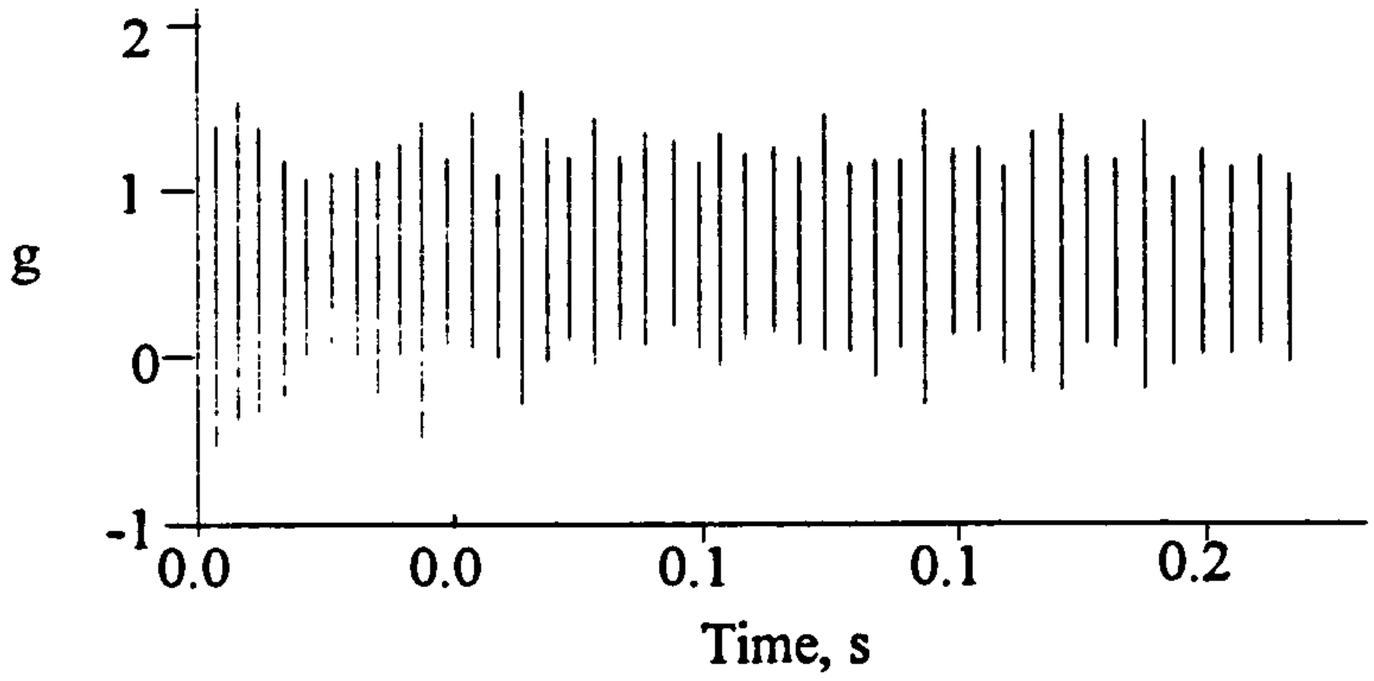


Figure 7.6.1 Signal Average for the Vibrations Detected by the Accelerometers

If, for example, the rig were running at 5000 rpm and seventeen tooth spur gears were used as the test gears, then, there would be 1416.6 tooth contacts per second. Therefore, taking a frequency Fourier transform of the signal output would give a plot similar to that shown in Figure 7.6.2.

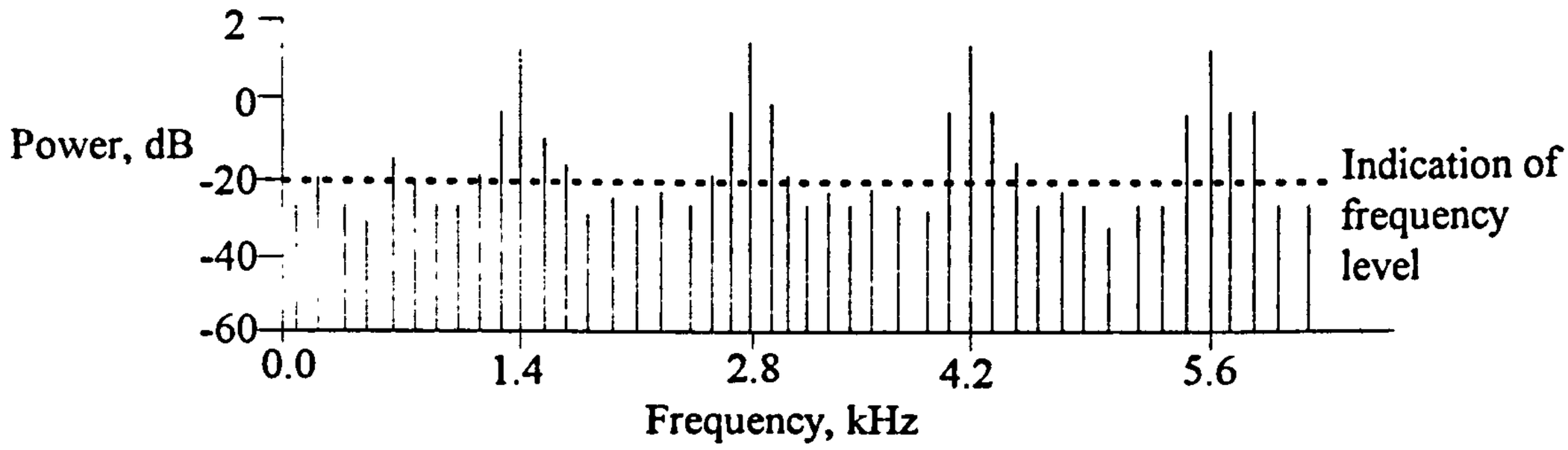


Figure 7.6.2 Frequency Fourier Transform before Failure

The signal peaks at the tooth mesh frequency and at the harmonics and in between these peaks there is noise (vibration coming from other components). This signal would be produced in a smooth meshing gear stage, however, when there is a profile failure, such as that which would occur with pitting, the Fourier transform changes to something like that shown in Figure 7.6.3. The peaks of the meshing frequency are still present, but the level of the noise in between these peaks has risen considerably. Therefore a cut-out was operated when the noise level was excessive, by knowing the root mean square (RMS) value of the noise before and after failure. The best place to observe this rise in noise is probably between the tooth engagement frequency and the first harmonic, i.e. 2833.3 Hz.

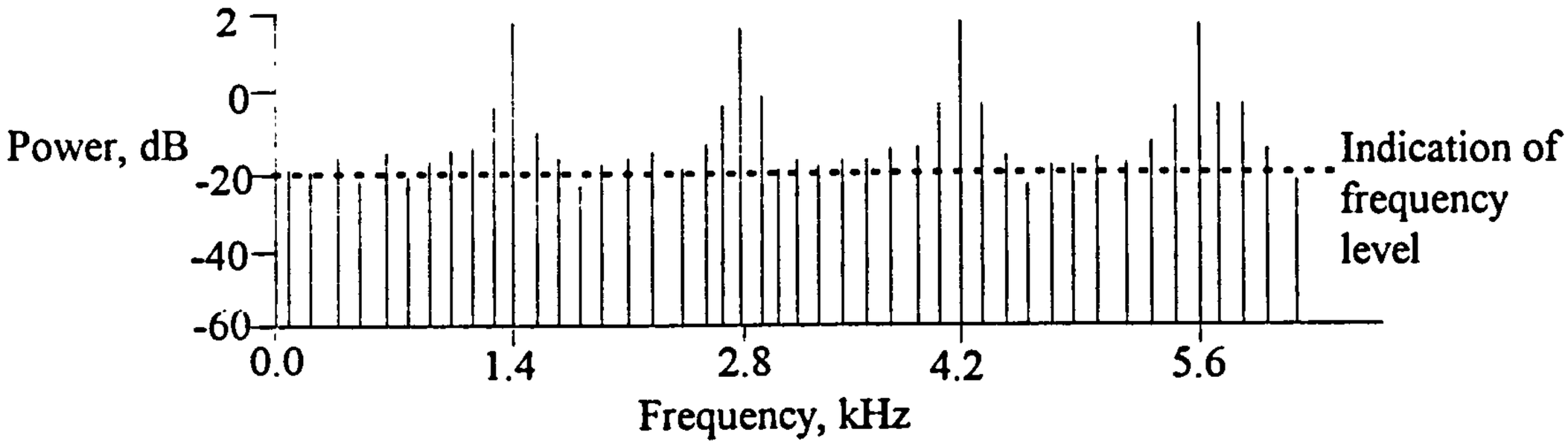


Figure 7.6.3 Frequency Fourier Transform after Failure

The vibration signal was bandpass filtered, so that only the frequencies between 1416 and 2833 Hz could get through, as in Figures 7.6.4 and 7.6.5, and the RMS of this signal was taken. The increase in noise level could then be observed during running. Once a value of RMS had been established, above which the gears have probably failed by pitting, it was used by the control system to shut down the rig via a relay.

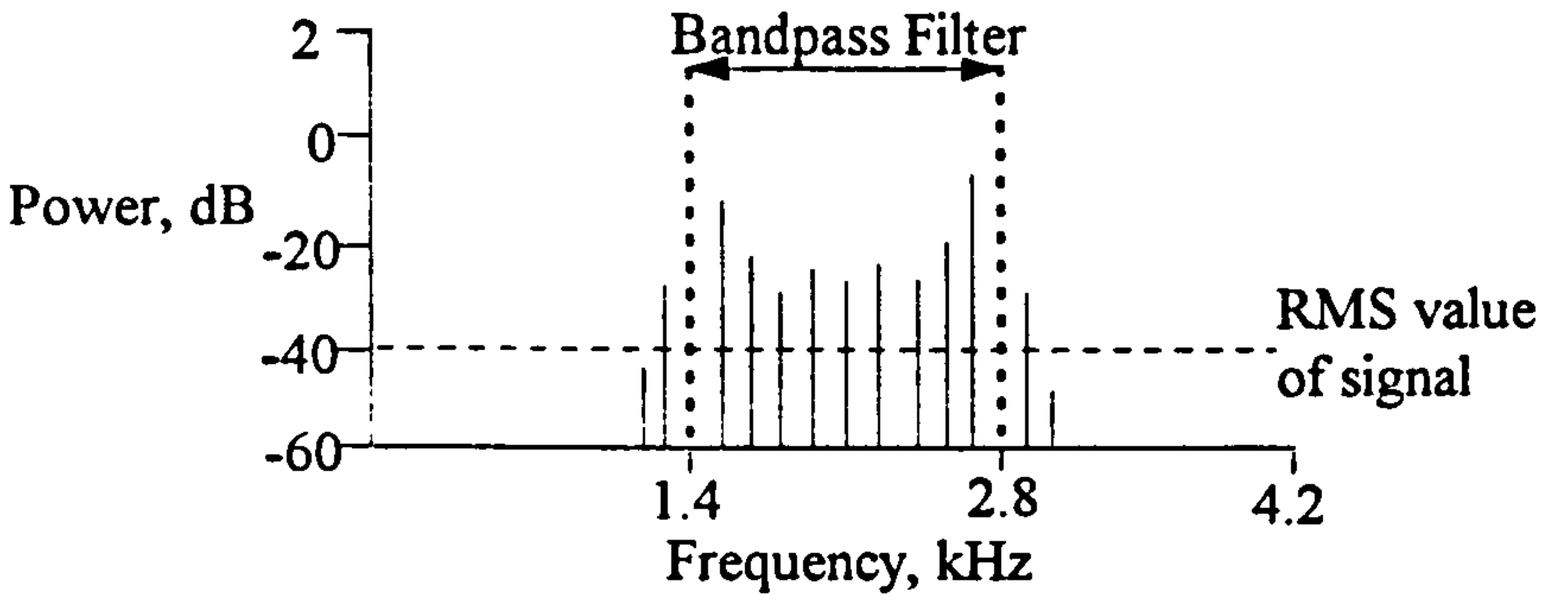


Figure 7.6.4 Frequency Fourier Transform of the Bandpass Filtered Signal before Failure

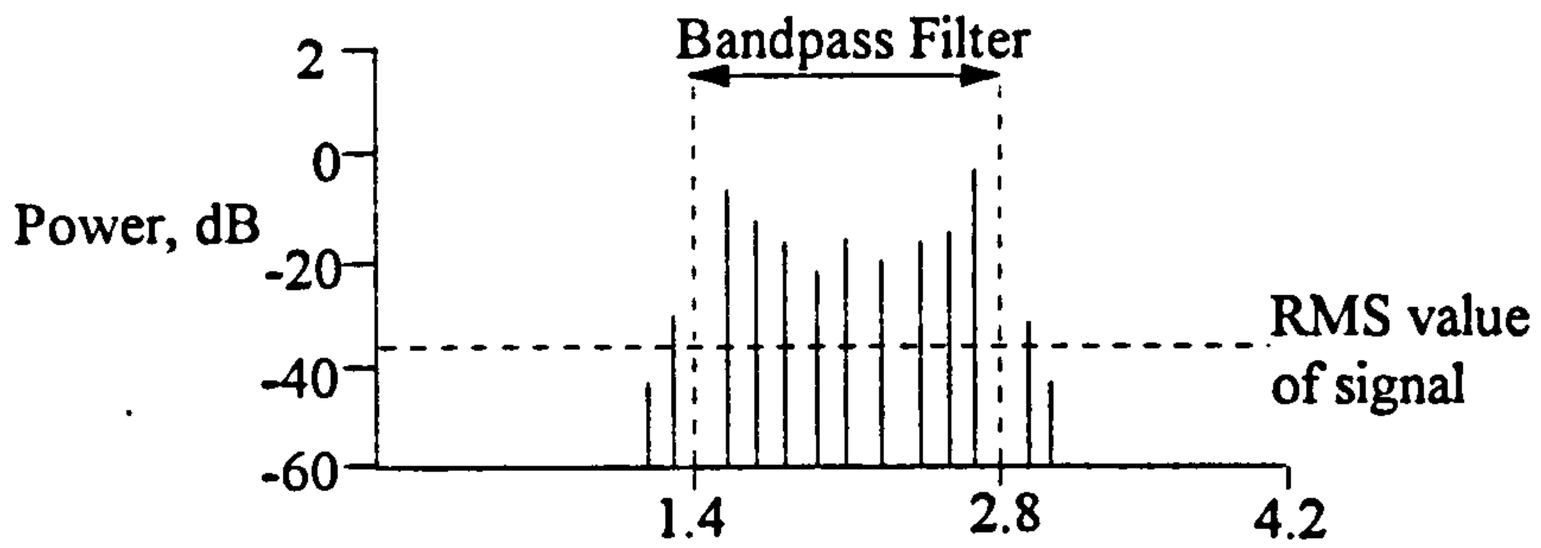


Figure 7.6.5 Frequency Fourier Transform of the Bandpass Filtered Signal after Failure

The system set-up to detect pitting failures in the test gears is shown schematically in Figure 7.6.6. The thermocouples indicated temperatures in various parts of the rig, and

limiting temperature values were assigned to certain areas so that if there were excessive temperature excursions the rig shutdown would be triggered.

The monitoring system was programmed using Labview™ and a typical monitor display is shown in Figure 7.6.7. The increase in vibration level associated with gear failure can be seen at the end of the test shown in this figure.

As mentioned previously, two types of gear specimen were designed, one with tip relief and one without. The vibration levels were found to increase every time the load was increased with the non-relieved gears. The vibration levels were higher in these gears for a given torque when compared to the tip relieved gears. This was due to the greater proportion of the load carried by the tips and roots of the gear teeth, where the teeth first come into contact, generating greater noise and vibration. The tip-relieved gears gave the teeth a more gradual uptake of load, as was discussed in Section 7.4.1.

The tip relieved gears' vibration would increase rapidly initially with the first few load stages and then increase or decrease slightly in level as the load was increased, as would be expected if the relief was designed to carry a larger load. The change in vibration level with load made it hard to determine where to set the vibration cut-out limits, but from experience with the two geometries and observation of the loading stages this was accomplished. Vibration levels did rise suddenly when pitting or scuffing occurred but also varied gradually, from their roughly constant value at load, when micropitting occurred.

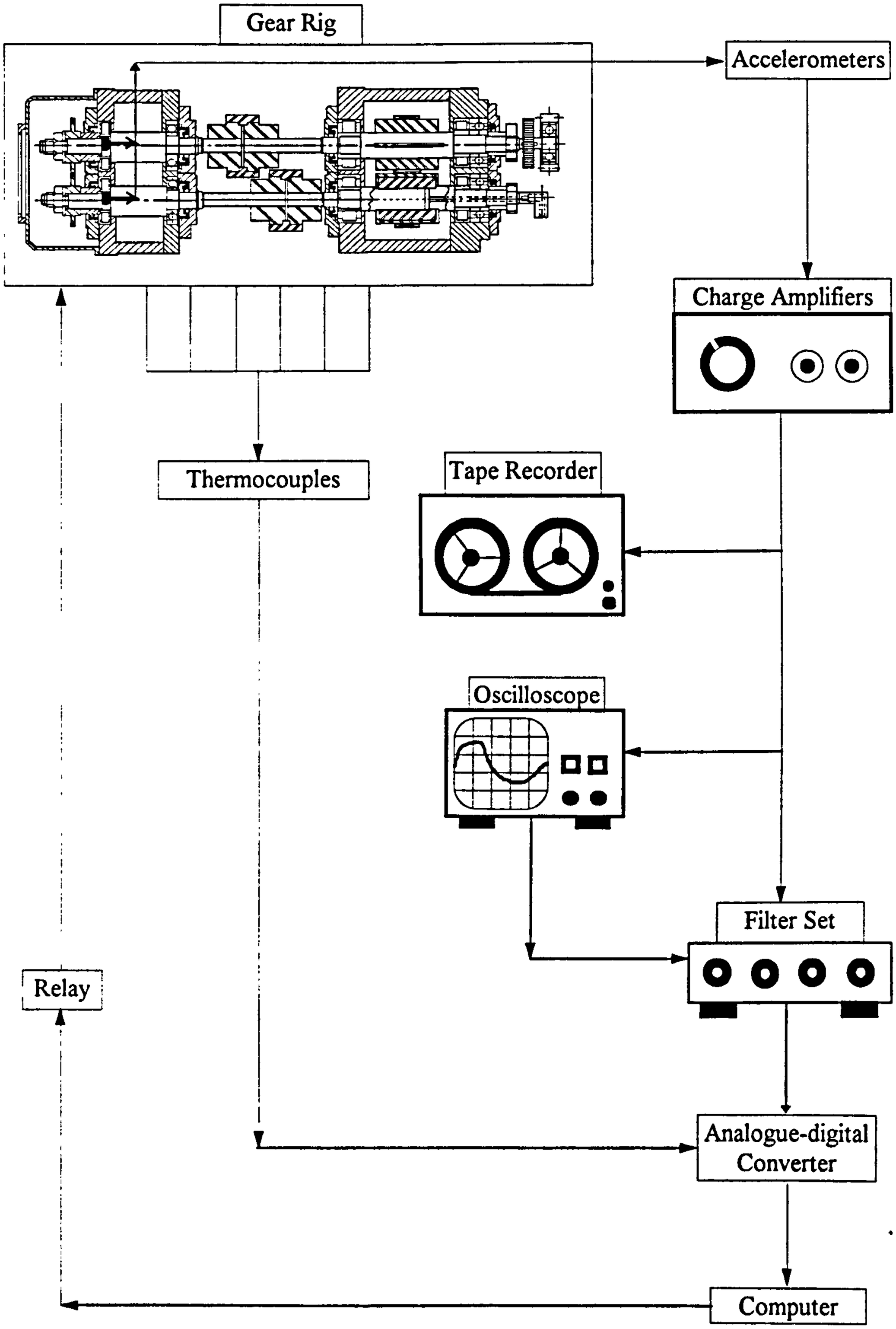


Figure 7.6.6 Schematic Representation of the Gear Rig Control Instrumentation

BEST COPY

AVAILABLE

Variable print quality

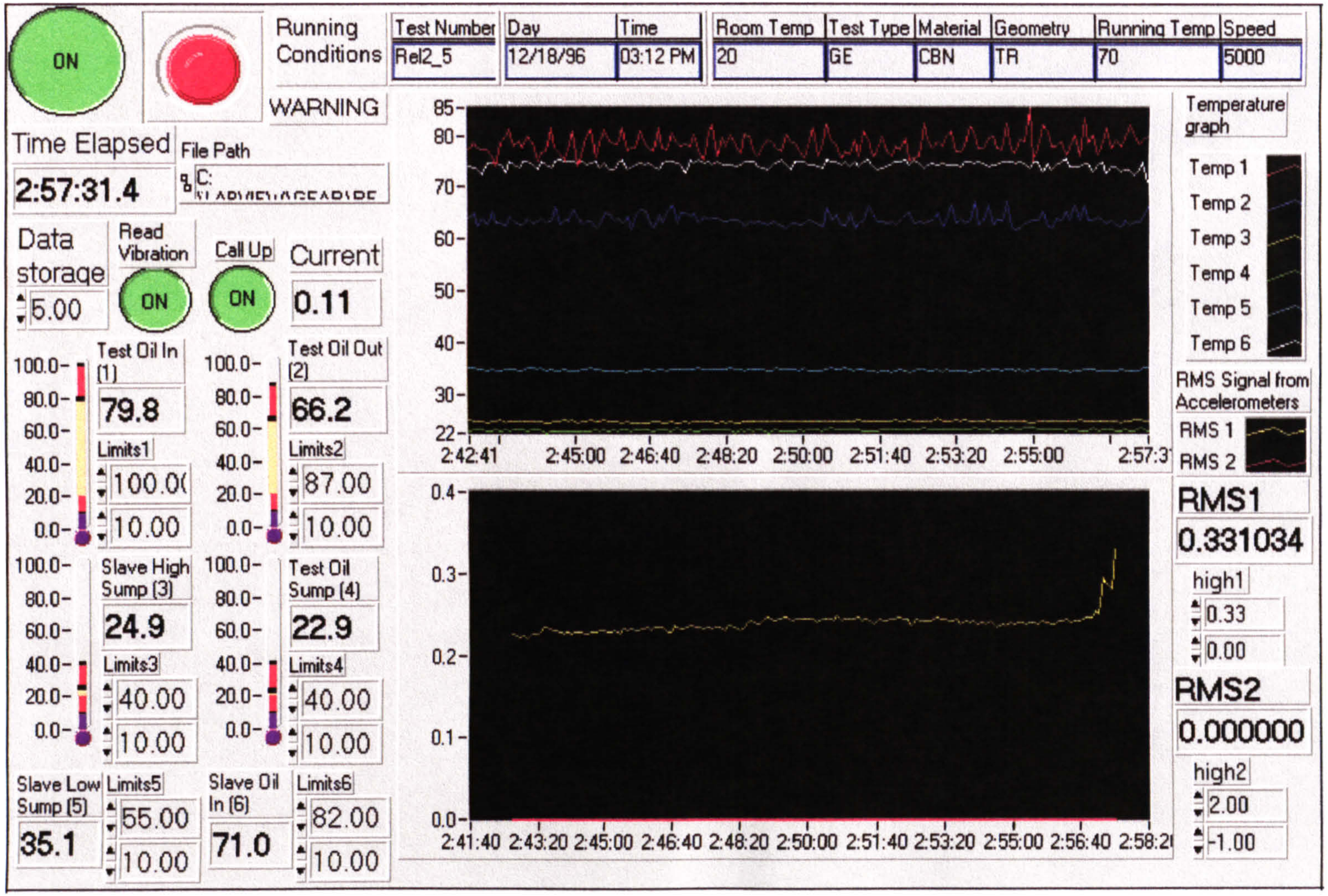


Figure 7.6.7 The Gear Rig Monitoring System Display Showing Shutdown After Gear Pitting

7.6.2 Failure Detection in the Disc Rig

Bailey (1989) used accelerometers mounted on the disc rig test chamber to detect the change in vibration associated with the onset of pitting. The sensitivity of the technique was significantly enhanced by bandpass filtering the vibration signal between 2-6 kHz, as that range was found empirically to be most responsive to the formation of fatigue pits. The RMS value of the band-passed vibration signal was used to trigger the shutdown of the rig. This system was improved and used in the experiments of the present author.

The rig also had a torque monitoring system, which operated via a strain gauge bridge located in one of the drive couplings. Graham (1979) used this system to trigger cut-out when the torque fluctuated beyond a preset limit, as he had noticed that when pitting occurred the torque would fall by 10-14%. This set-up was used as a safety mechanism to stop the motor in the event of a drive train failure.

Thermocouples were used to give the temperature of the barrel and disc specimens and the lubricant sump temperature. If any of these went outside the preset limits, the rig would once again be cut-out.

Finally, a float switch located in the sump would indicate if the lubricant level there was insufficient.

A schematic representation of the disc rig control instrumentation can be seen in Figure 7.6.8. The monitoring system for the disc rig was also programmed using Labview™ and a typical monitor display of the program is shown in Figure 7.6.9. Once again, the increase in vibration at the end of the test, due to pitting failure of the barrel, can be observed in this figure.

The vibration levels for the disc tests were found to be fairly independent of load, varying only slightly as the specimens were brought to full load. This was different from the vibration in the gears which varied with load due to the gear teeth coming in and out of mesh. The level usually decreased slightly with loading indicating, perhaps, running in of the rougher parts of the specimens. Vibration levels would rise rapidly for pitting (Figure 7.6.9) and would rise fairly rapidly for the form of scuffing encountered in the tests. Micropitting could also be detected at a very early stage because of the gradual rise in vibration level from the constant value at load. This was not the case in previous set-ups of operators of this rig.

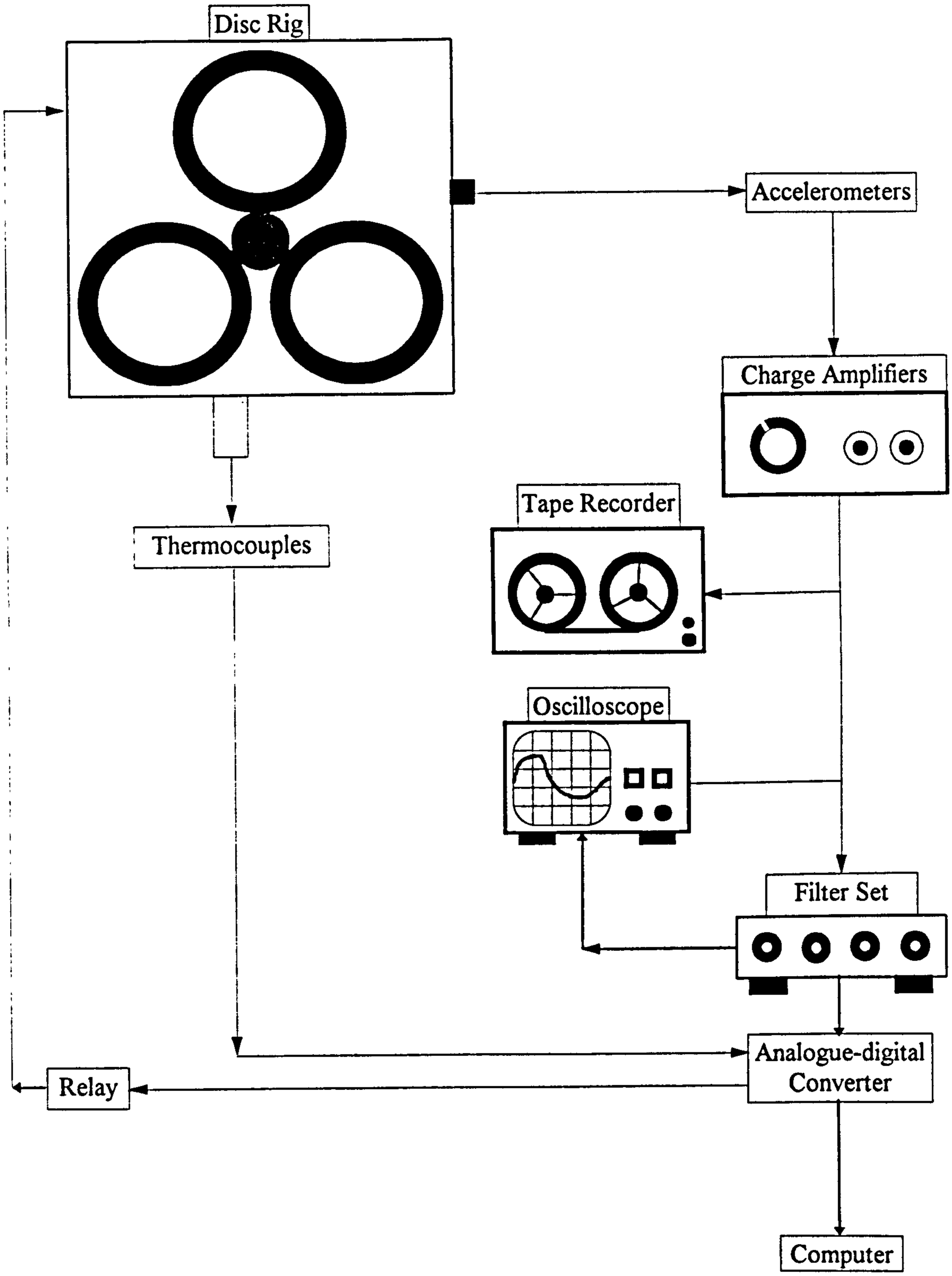


Figure 7.6.8 Schematic Representation of the Disc Rig Control Instrumentation

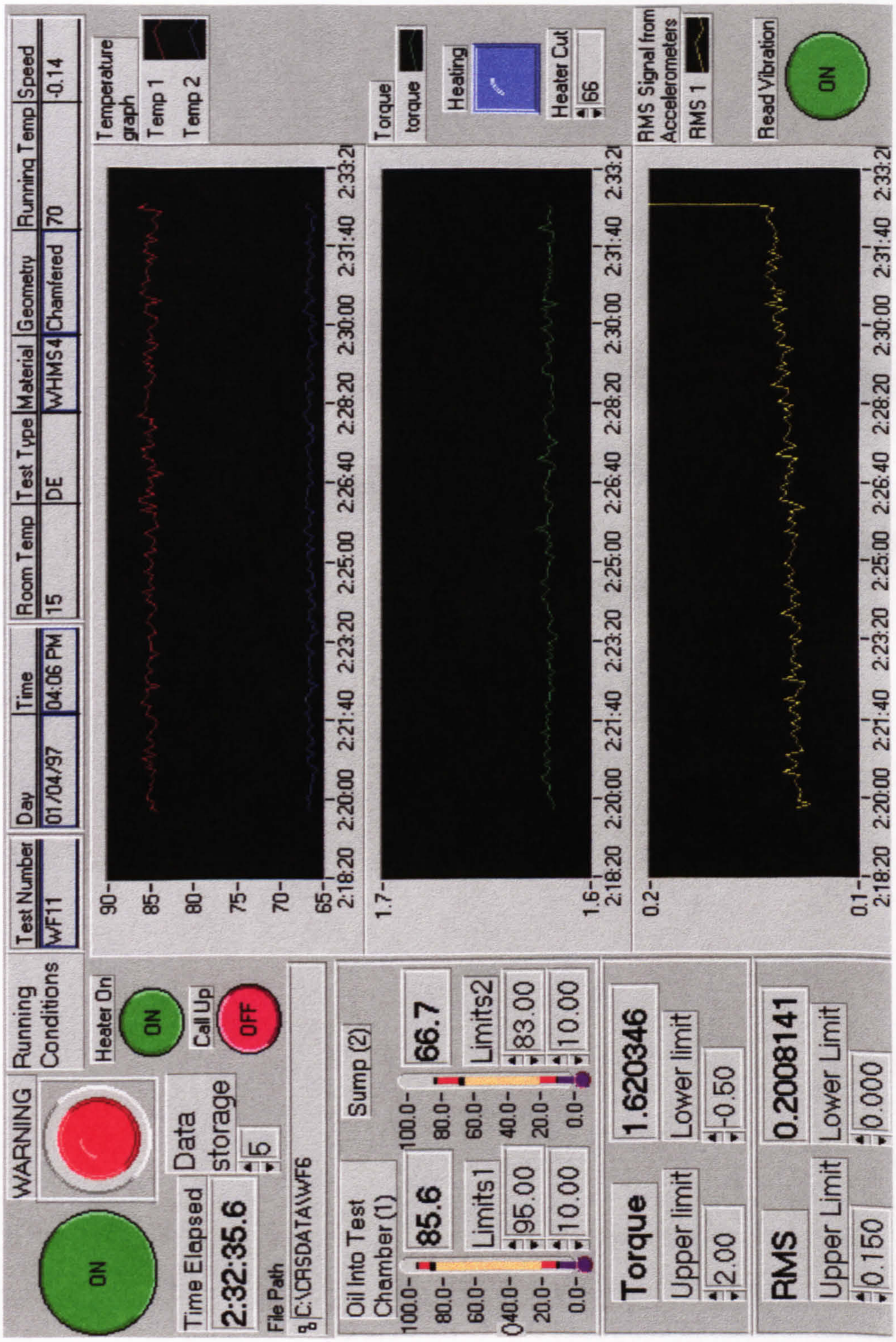


Figure 7.6.9 The Disc Rig Monitoring System Display Showing a Typical Shutdown after Failure of a Barrel by Pitting

7.7 Test Procedure and Test Piece Preparation

The specimens were cleaned and mounted in their respective rig. In the disc rig, the lubricant pump, which loads and supplies lubricant to the contact, was switched on and the lubricant warmed before starting the run. In the gear rig, on the other hand, the pumps were all switched on, but no oil heating before the test started was undertaken. Both tests were run under a no-load condition initially and then the load was gradually increased in steps to the designated running load, allowing a stabilising time in between each load step. This was to ensure a gradual run-in for the specimens. The temperature of the oil sumps was kept constant.

Failure criteria in rolling contact fatigue research have always been slightly dubious. Whether a gear judged to have failed in a test, would actually be rejected in service depends on the application, extent of the damage, and the risk of catastrophic failure. Bartz and Kruger (1973) considered pitting as negligible if the pits were few and small in number, on the other hand, large pitting fatigue was probably going to result in rapid destruction of tooth surface. Winter and Weiss (1981) deemed a gear to have failed in a test when the pitting area covered 1% of the total active surface area of the gear teeth or covered 4% of the active surface of any one tooth. The author used the accelerometer vibration signal to stop the rigs when they reached a threshold value and then inspected the surfaces.

7.8 Test Programme

The four materials described in Chapter 5 were to be tested under high stress conditions, with the specimens and test rigs described in this chapter. The aim of the programme was to research their behaviour, particularly their fatigue performance under a range of operating conditions, using both gear and disc specimens. The effect of load, geometry, and the consequent variation in failure mode would all be investigated.

The gear test programme would investigate the various materials and failure modes, as well as the effect of tip relief on the standard carburised steel (BS S156). This would show whether tip pre-engagement occurred, and whether it had a damaging effect.

The disc test programme would also test the materials, but in greater depth because of the shorter test times and ease of manufacture of the specimens. The two geometries,

crowned and chamfered, would be investigated only on the standard carburised steel (BS S156).

The two types of test would also help establish the existence of any relationship between gear and disc tests.

7.9 Conclusions

The gear and disc test rigs used by the author and the monitoring systems, as well as, the test specimens design and the test procedure have all been described in this chapter.

The residual stresses of the test specimens and a stress analysis of the specimens are reported in Chapter 8.

Chapter 8 Stress Analysis

Having described the test specimens and their respective rigs, it is now appropriate to present the analysis of the stresses the gear and disc specimens experience when running. To fully understand the results obtained in the rolling contact fatigue tests, the running conditions for both the gear and disc tests had to be characterised. In particular, the stresses on the test specimens were determined, as these were shown to have an important effect on rolling contact fatigue in Chapter 3. This will help interpret the results for each rig, and will be used to correlate the two test types in Chapter 14. Results from this analysis will be used in the discussion of the gear and disc fatigue test results in Chapter 13.

8.1 Disc Rig Loading Conditions

Here the loading of the disc rig specimens is discussed. The disc rig was described in detail in Chapter 7 and a schematic of the specimen layout is shown in Figure 8.1.1. The three running conditions available on the rig, shown in Table 8.1.1, were obtained by changing the barrel drive pulley.

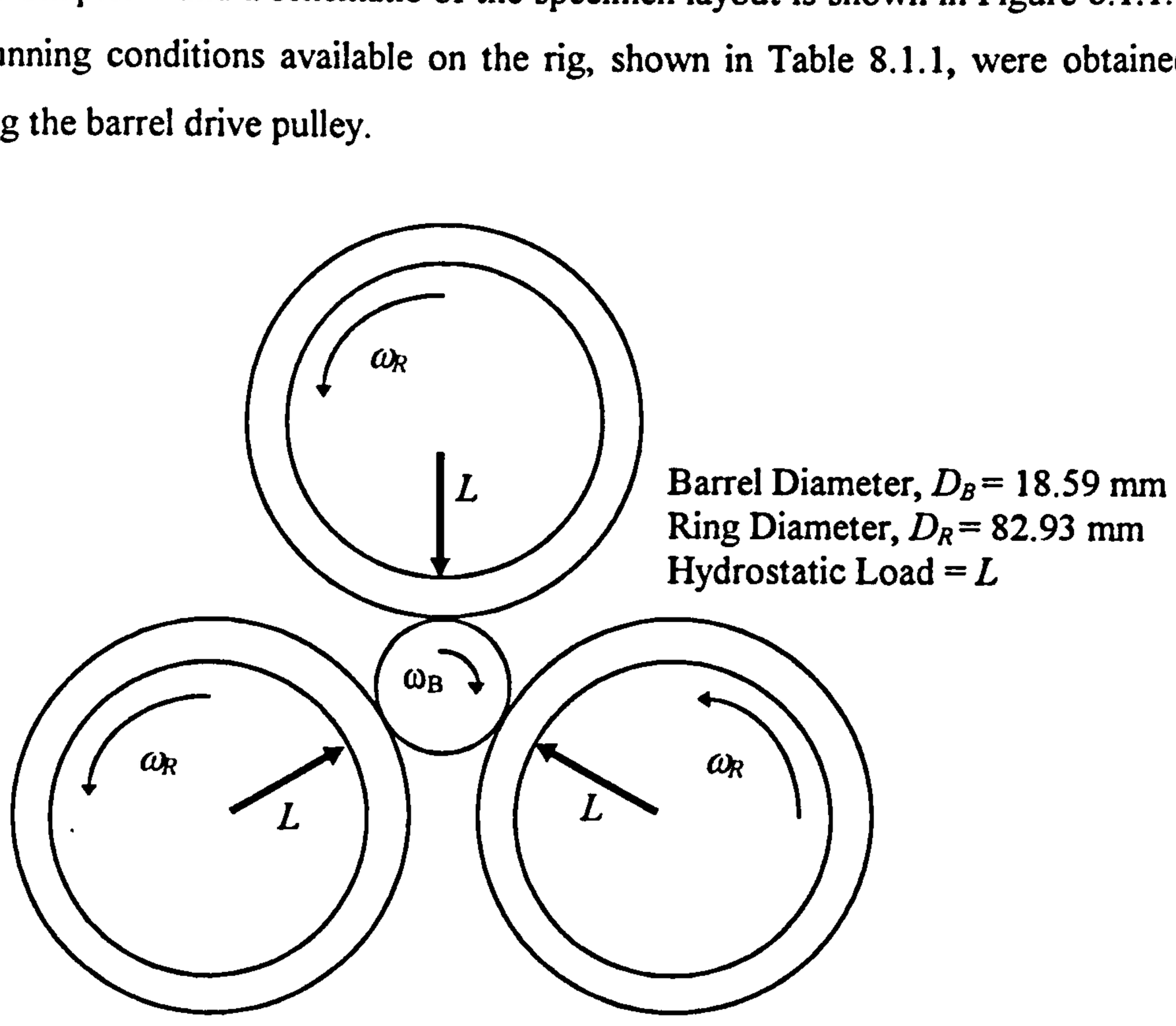


Figure 8.1.1 Schematic of Disc Rig Test Piece Layout and Motion

Table 8.1.1 Disc Rig Speeds, Slide-Roll Ratios, and Cycles per Hour

Barrel (ω_B rev/min)	Ring (ω_R rev/min)	Slide-Roll Ratio	Cycles per hour (x10^3)
3000	1200	-0.282	540
4000	1200	-0.145	720
5060	1200	-0.026	910.8

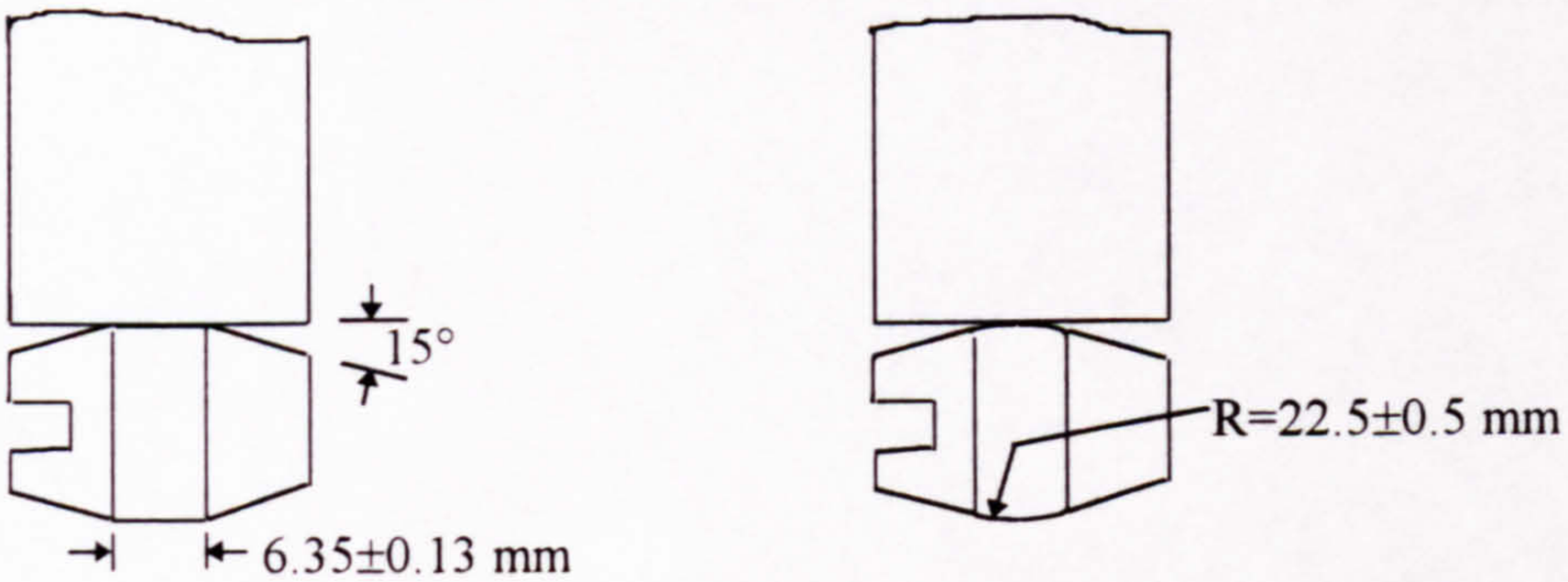


Figure 8.1.2 Chamfered and Crowned Barrel Specimen Contact Layout

The specimens were loaded hydrostatically by a piston of known area inside one of the ring supports. The Hertz contact pressures on the two barrel geometries, crowned and chamfered (shown in Figure 8.1.2), can be calculated for an applied oil pressure, as shown in Figures 8.1.3 and 8.1.4. The value of Young's modulus, E, used was 200 GPa and the Poisson ratio, ν, 0.3.

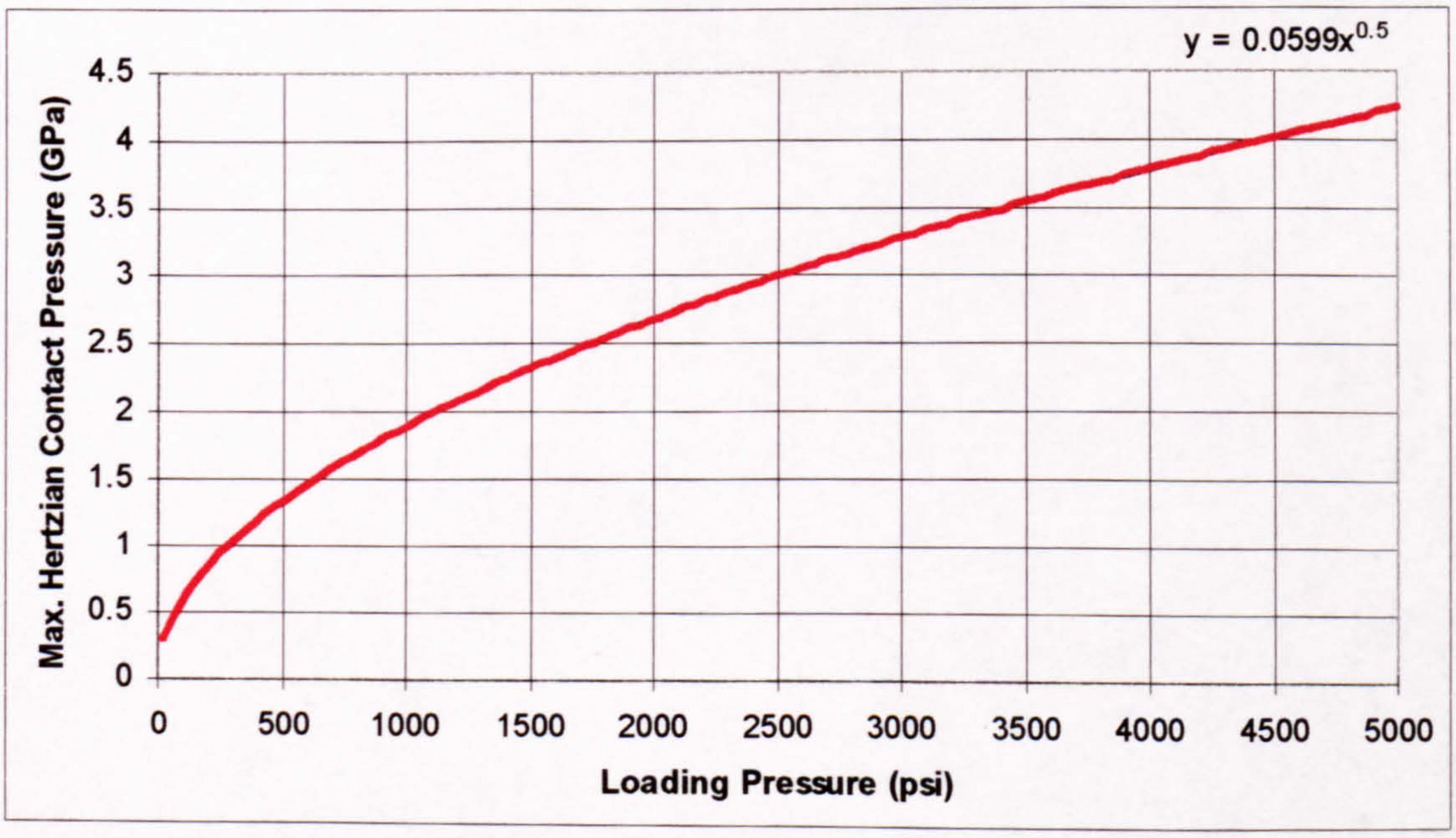


Figure 8.1.3 Variation of Contact Stress with Applied Pressure for a Chamfered Barrel

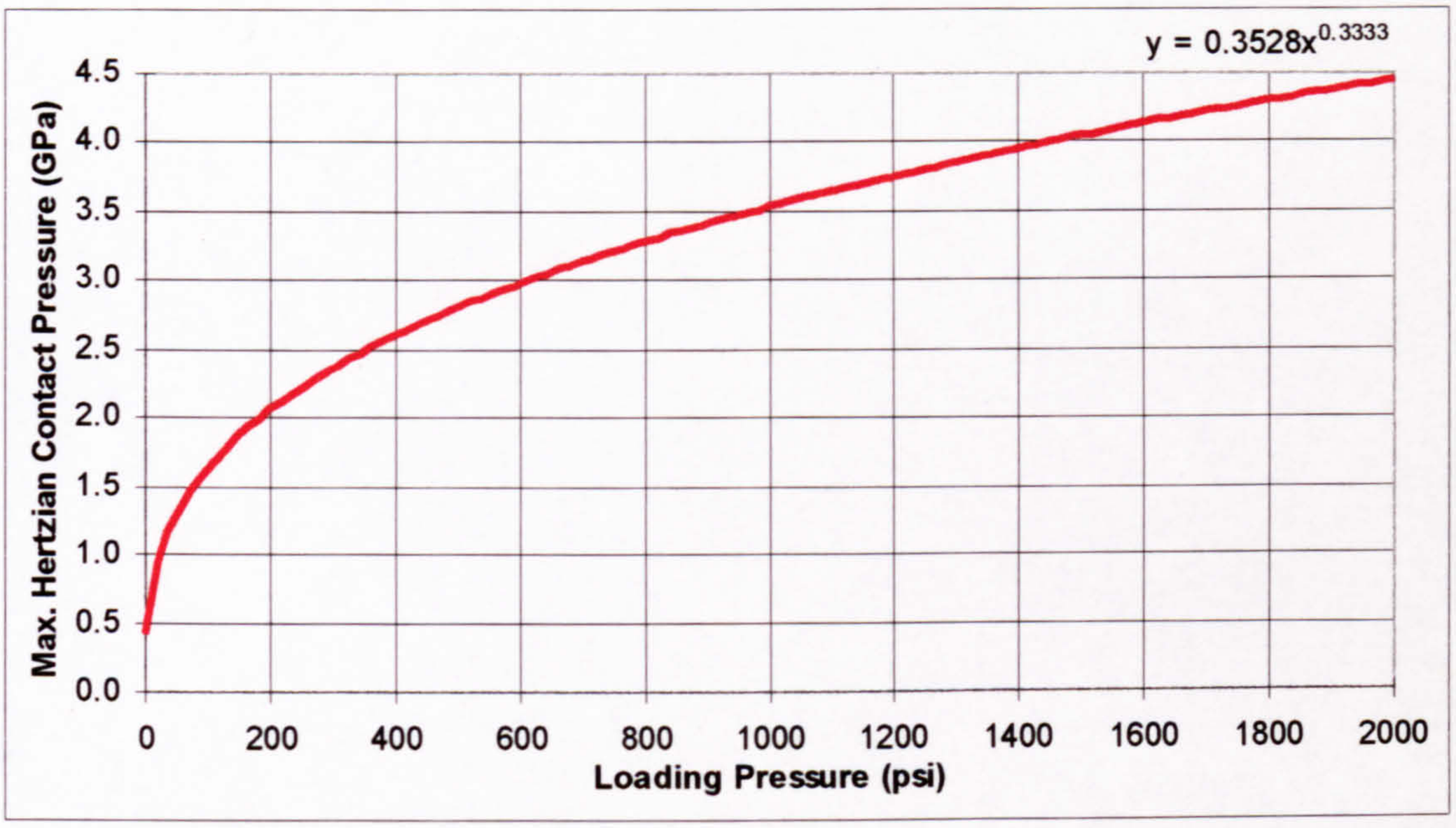


Figure 8.1.4 Variation of Contact Stress with Applied Pressure for a Crowned Barrel

A much smaller applied pressure is needed to achieve high contact stresses in the crowned specimens, as opposed to the chamfered specimen, as would be suggested by the smaller area of contact (discussed in Chapter 2). The crowned specimen produced an elliptical contact when in contact with the ring and the chamfered specimen a line contact. These calculations, however, do not take into account the edge contact occurring in the chamfered barrel, but this is discussed later.

The contact width in the direction of roll for the chamfered barrel is shown in Figure 8.1.5 and the dimensions of the contact in the crowned barrel are shown in Figure 8.1.6.

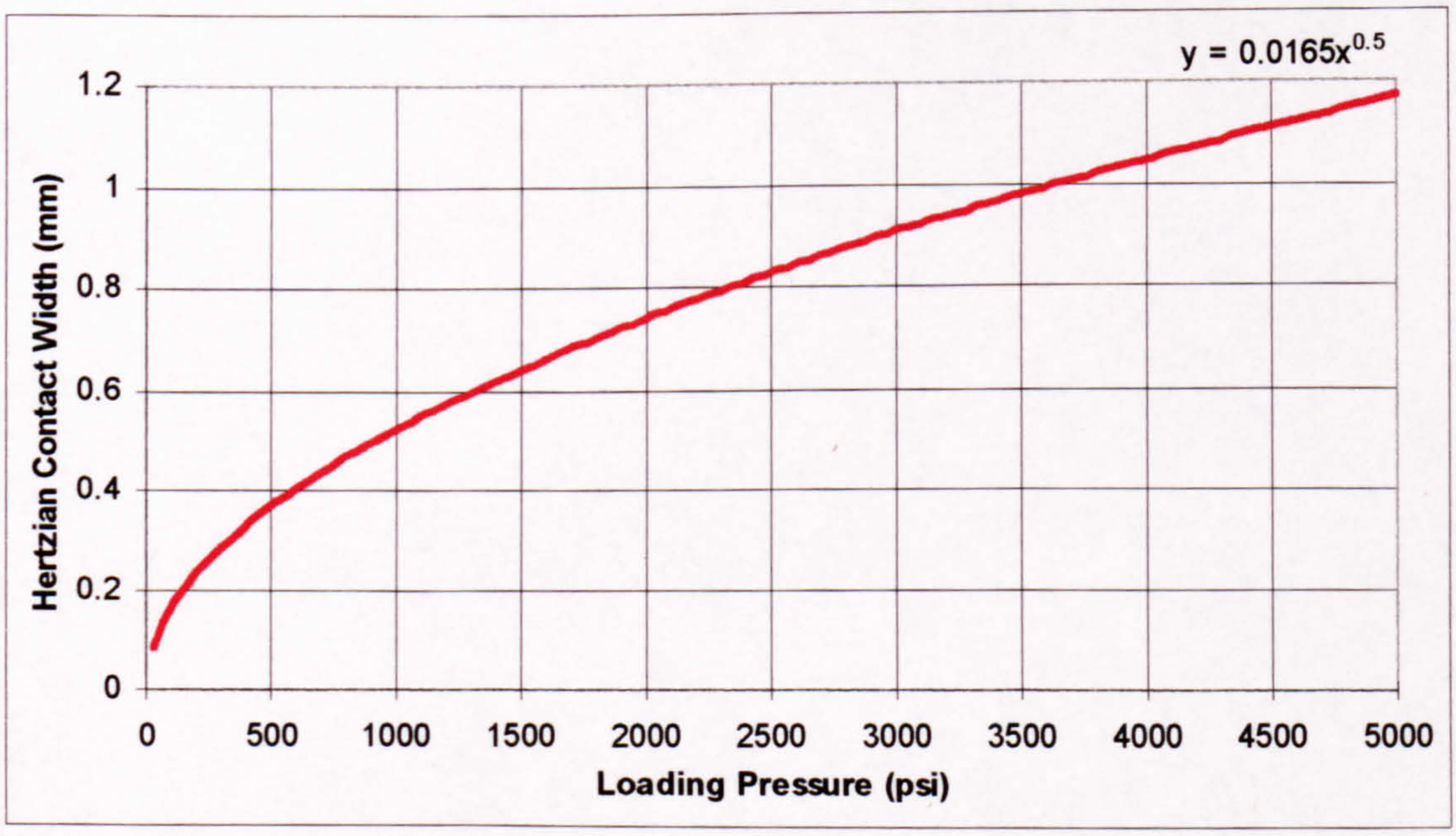


Figure 8.1.5 Variation of Contact Width with Load in the Chamfered Barrel Specimen

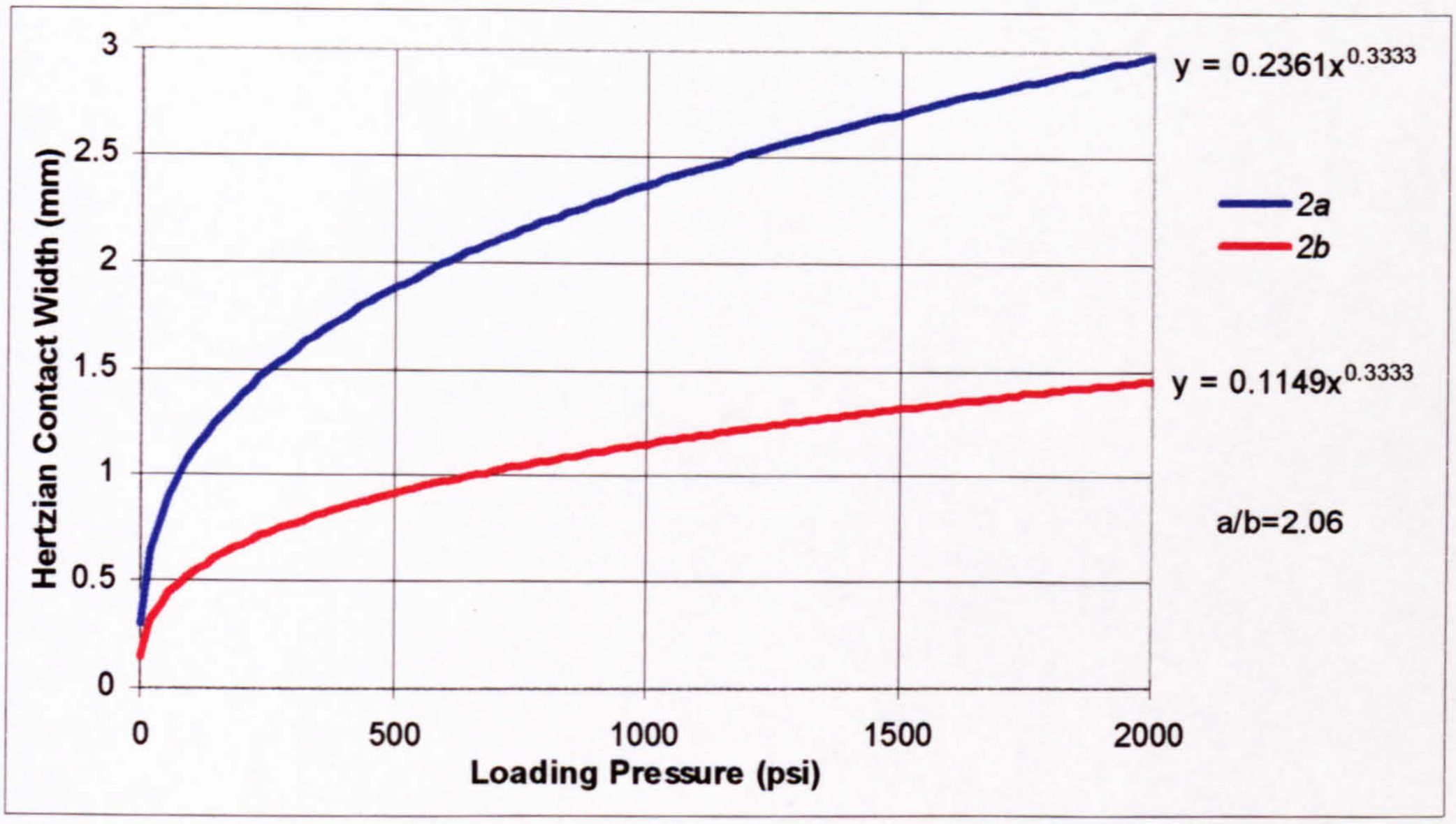


Figure 8.1.6 Variation of Contact Dimensions with Load in the Crowned Barrel Specimen (Major Width, 2*a*, Minor Width, 2*b*)

As mentioned previously, the crowned barrel experiences a greater contact stress than the chamfered one for a given applied load, using the Hertz equations and excluding the effect of edge contact at the extremes of the track. By using a three-dimensional surface contact analysis (West & Sayles 1988), the pressure distribution and deformed surface geometry under a given load were predicted for both the chamfered and crowned barrels. Real surface measurements can be used for analysis or, as done in this case, theoretically smooth ones. Here the model was run using solely elastic contact, so the stresses produced may be above the yield stress of the material. There is a local increase in stress at the edge of the track of the chamfered barrel, as shown in Figure 8.1.7. The deformed surface of part of the barrel can be seen in Figure 8.1.8.

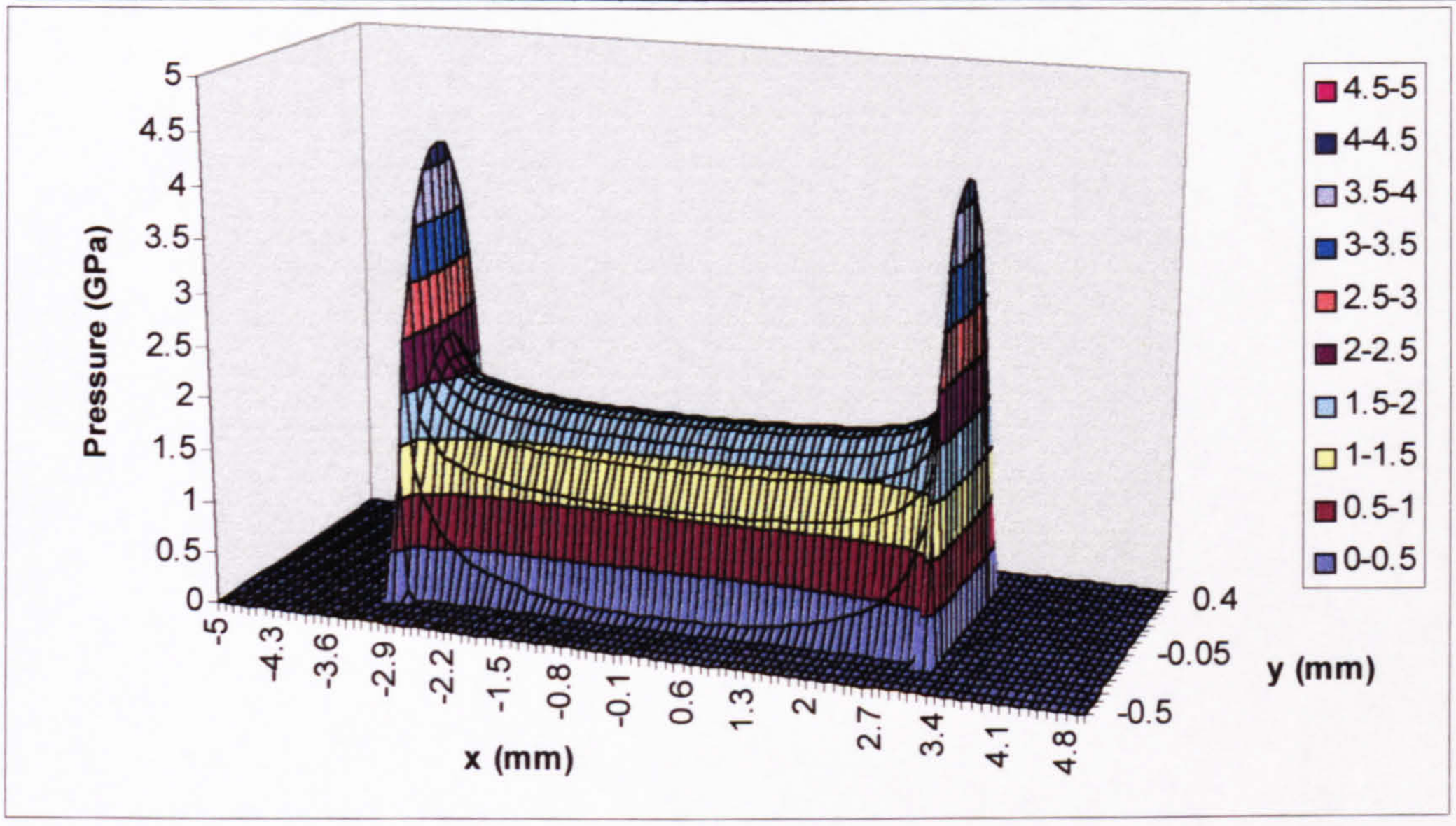


Figure 8.1.7 Chamfered Barrel Pressure Distribution
(Using model by West & Sayles 1988)

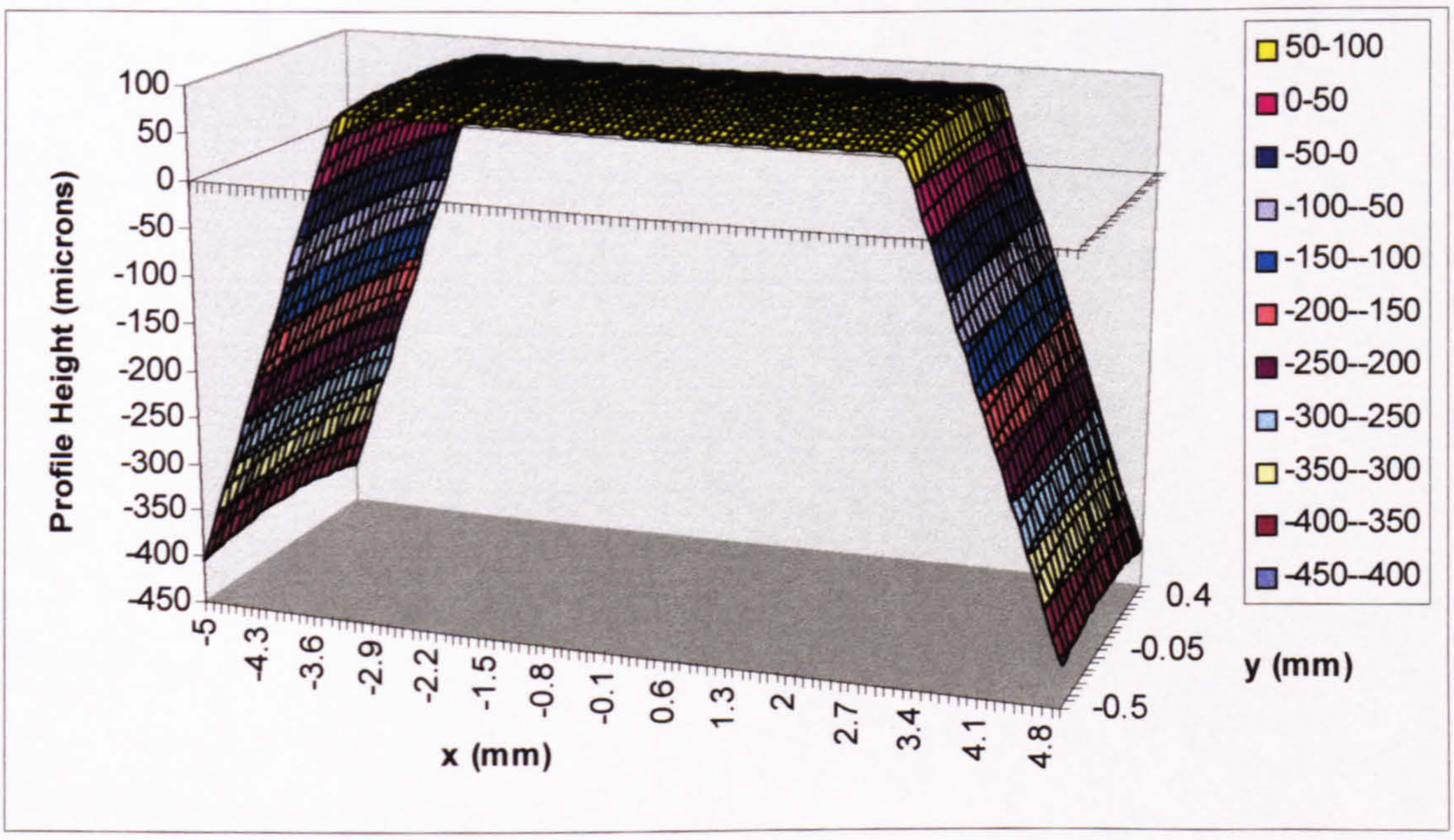


Figure 8.1.8 Chamfered Barrel Deformed Profile
(Using model by West & Sayles 1988)

The numerical analysis was run with the crowned barrel geometry, as shown in Figure 8.1.9. Higher stresses are indeed obtained for an applied load than for the chamfered contact in the central track area, but the stress concentrations that occur at the edge are absent.

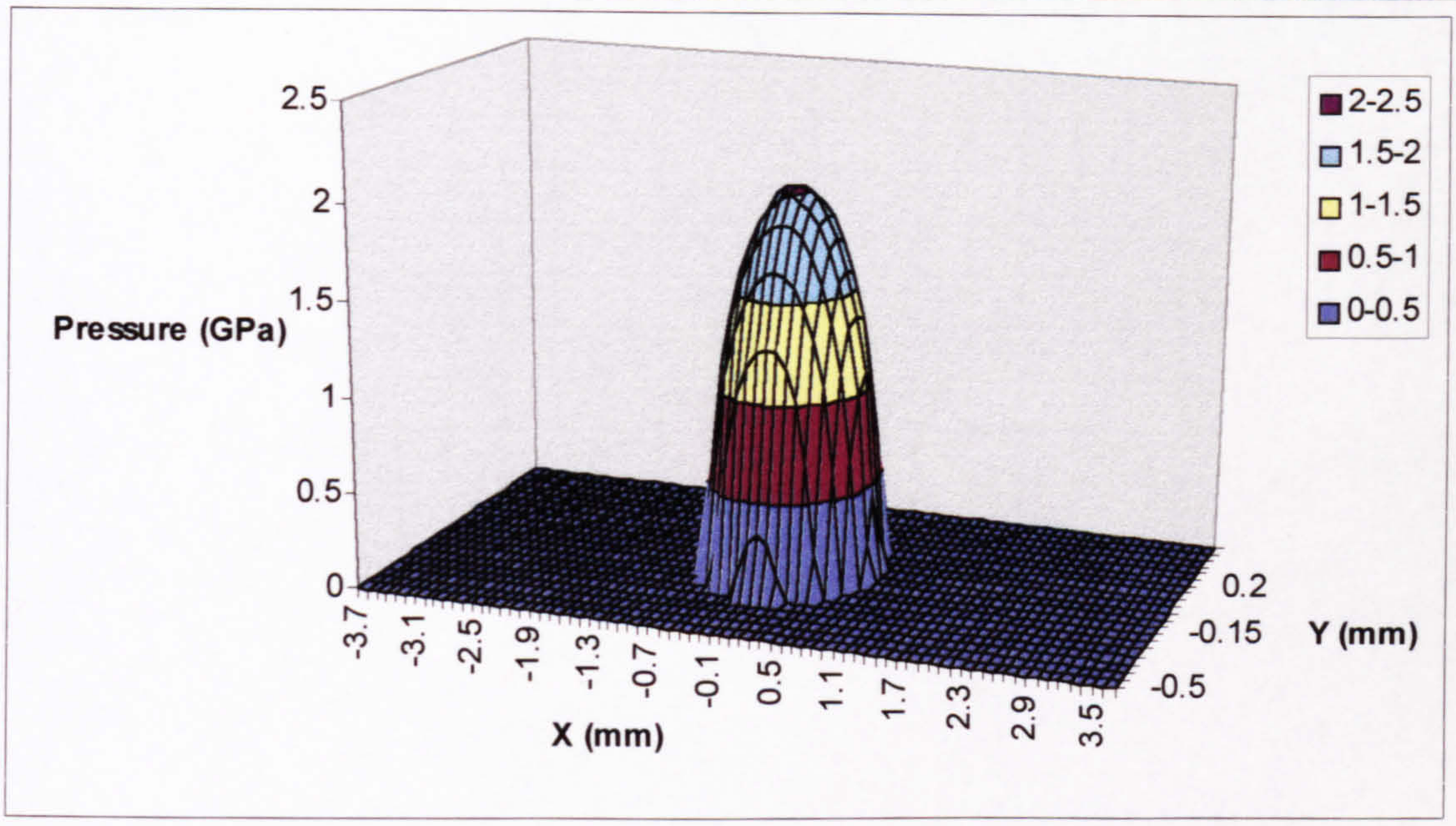


Figure 8.1.9 Crowned Barrel Pressure Distribution
(Using model by West & Sayles 1988)

The number of elements into which the contact is divided for the analysis is important. The more elements, the longer the solution time, but the greater the accuracy. If one refines the mesh size, the stresses existing at the edge in the chamfered barrel analysis increase, suggesting that as the mesh size tends to zero the contact stress tends to infinity there. In practice if the stresses were too high the edges of the barrel would deform plastically to accommodate this, therefore reducing the stress concentration. In addition to this, the barrel would probably not have a perfect chamfer.

Another analysis was done on a barrel with a chamfer of 5°. The result shown in Figure 8.1.10 indicates that the central portion of the barrel is at the same surface pressure as the 15° specimen but the effect of the edge seems to be less severe. This was done using the same mesh size for both models.

When a smaller mesh size was used, increased edge stresses were obtained (Figure 8.1.11). Therefore, whether the effect of the chamfer angle is still relevant at smaller mesh sizes has to be determined.

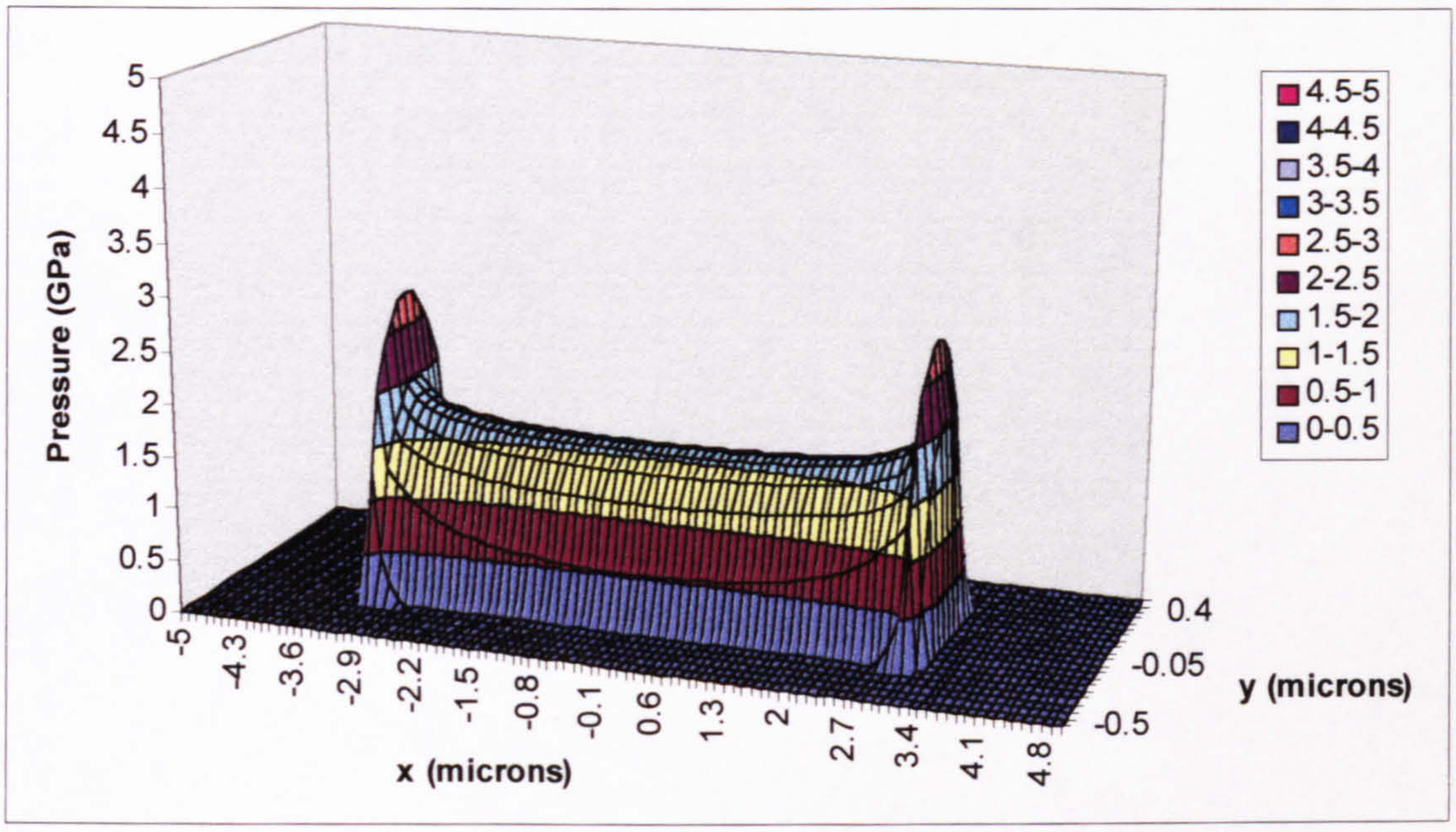


Figure 8.1.10 Pressure Distribution on a Barrel with a 5° Chamfer (Using model by West & Sayles 1988)

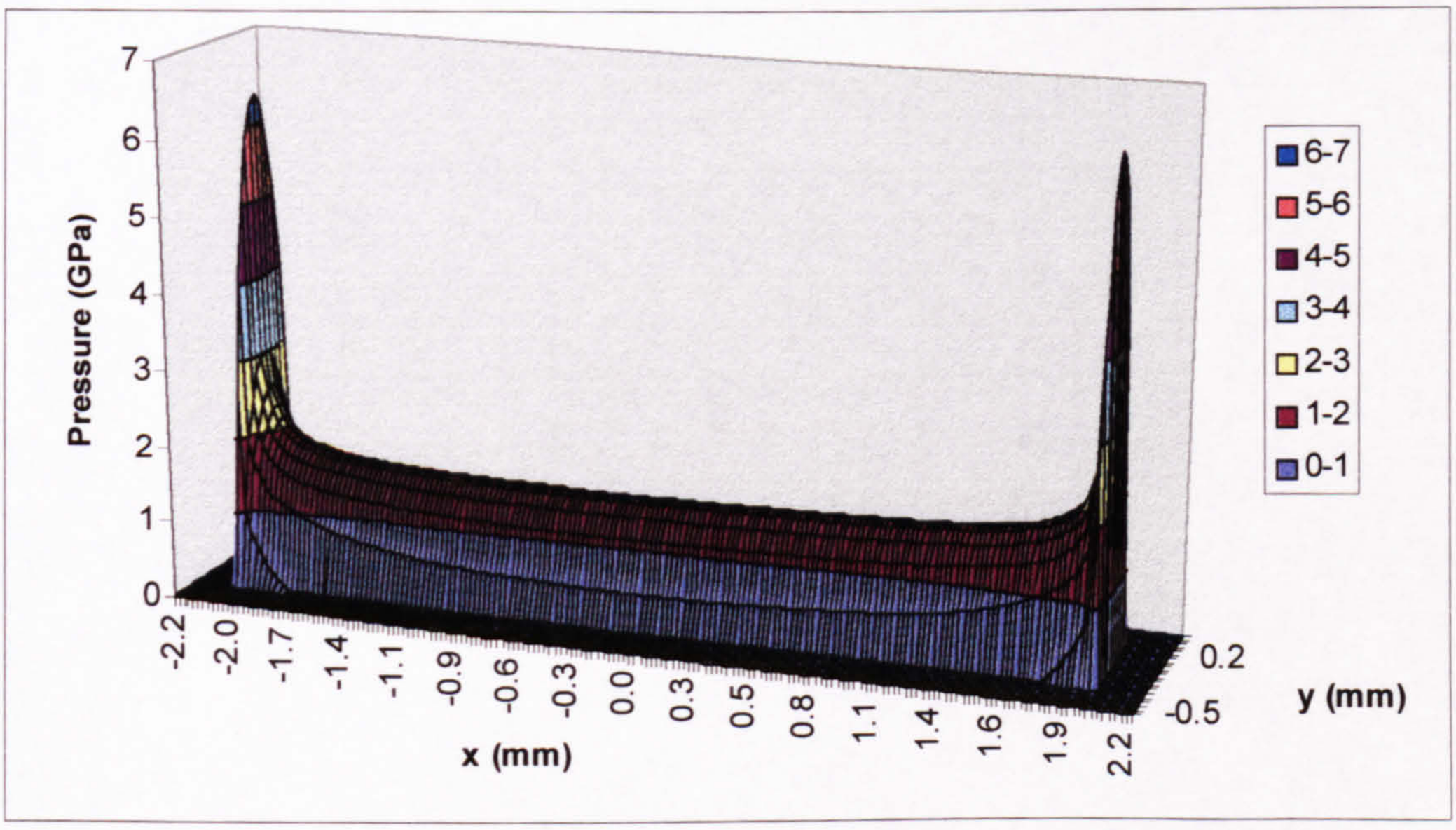


Figure 8.1.11 Pressure Distribution on a Barrel with a 15° Chamfer and Smaller Mesh Size than Figure 8.1.7 (Using model by West & Sayles 1988)

8.2 Gear Rig Loading Conditions

The gear specimens, described in Chapter 7, have a more complex loading analysis than the discs just discussed. The loading is complicated by the engagement discontinuity in gears. The mesh cycle will have effects which vary from the continuous steady motion of discs. The fact that the tooth load can be shared by two pairs of teeth, or all on one pair,

and the varying radius in the tooth contacting path (see Figure 7.3.3), all add to the analysis complexity.

To work out the load variation through the path of contact it is necessary to determine the load sharing between the teeth pairs. This was done with the aid of a computer model written by the author. The load analysis is divided into two parts: a static analysis, where the theoretical loading is predicted for a statically loaded gear; and a simple dynamic analysis, to evaluate any influence of the rig on the actual loading of the gear.

8.2.1 Static Analysis

To evaluate the surface contact pressures through the gear tooth mesh and the risk of extended contact due to elastic deflection of the gear teeth, an analysis of the gear tooth loading was undertaken. The computer model used for this analysis is described next (the program listing is in Appendix I), and then some results are given.

8.2.1.1 Description of Gear Contact Model

A model was developed to find the load sharing characteristics and effects of extended contact (discussed in Section 6.3.5) for spur gears. Gear data was entered to the program (Figure 8.2.1) and it calculated load sharing, contact stresses, film thickness, and flash temperatures. An assumption that the gear teeth were perfectly smooth with no manufacturing errors (i.e. perfect involute), was made.

The number of teeth in contact at any one time and the relative stiffness of the tooth pairs in contact were needed to calculate the load sharing between teeth. The tooth pair combined stiffness varied as the teeth moved along the path of contact. It was important to evaluate the stiffness value as it determined the load sharing between teeth pairs, deflections of the gear teeth, and the extent of extended contact.

The stiffness was calculated using equations in BS 436 Part 3 (BSI 1986). The bending and shear stiffness for each gear tooth, as the load moved along the tooth, were calculated and added to obtain a tooth stiffness for the load at a particular position. This stiffness value was then combined with the mating gear tooth stiffness at that point to find k_1 and k_2, the tooth pair stiffnesses. Once the stiffness of the two tooth pairs were calculated, if one pair was in contact then that tooth pair stiffness was used, if two pairs were in contact they were treated like a pair of springs in parallel, as shown in Figure 8.2.2.

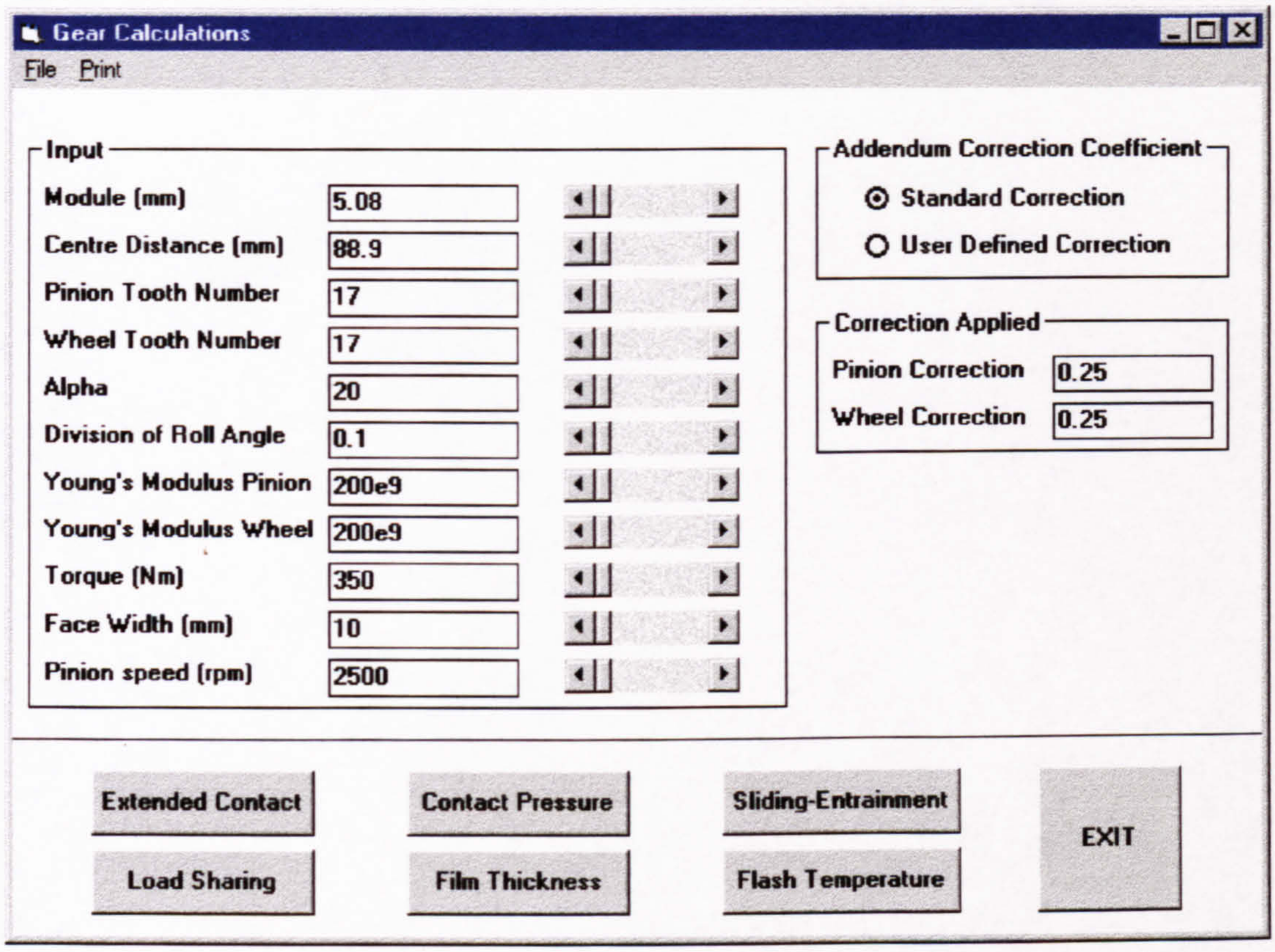
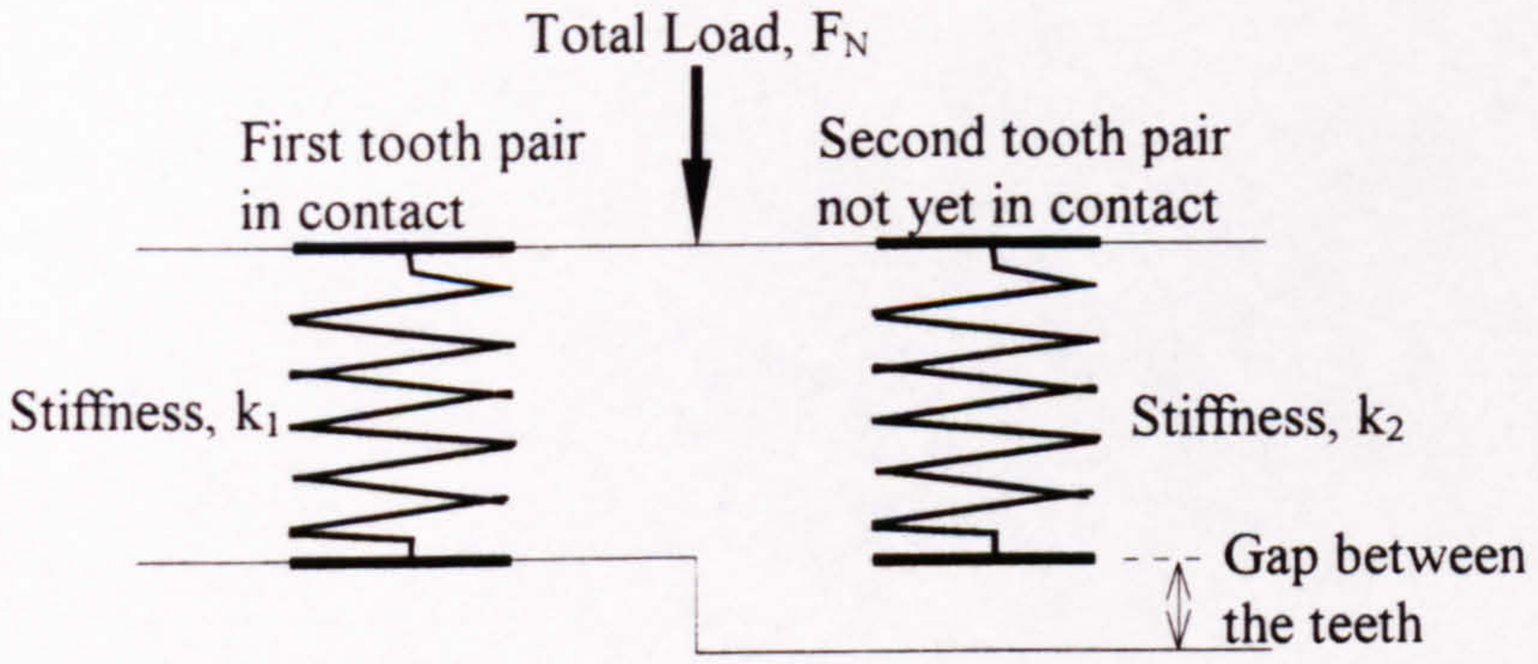
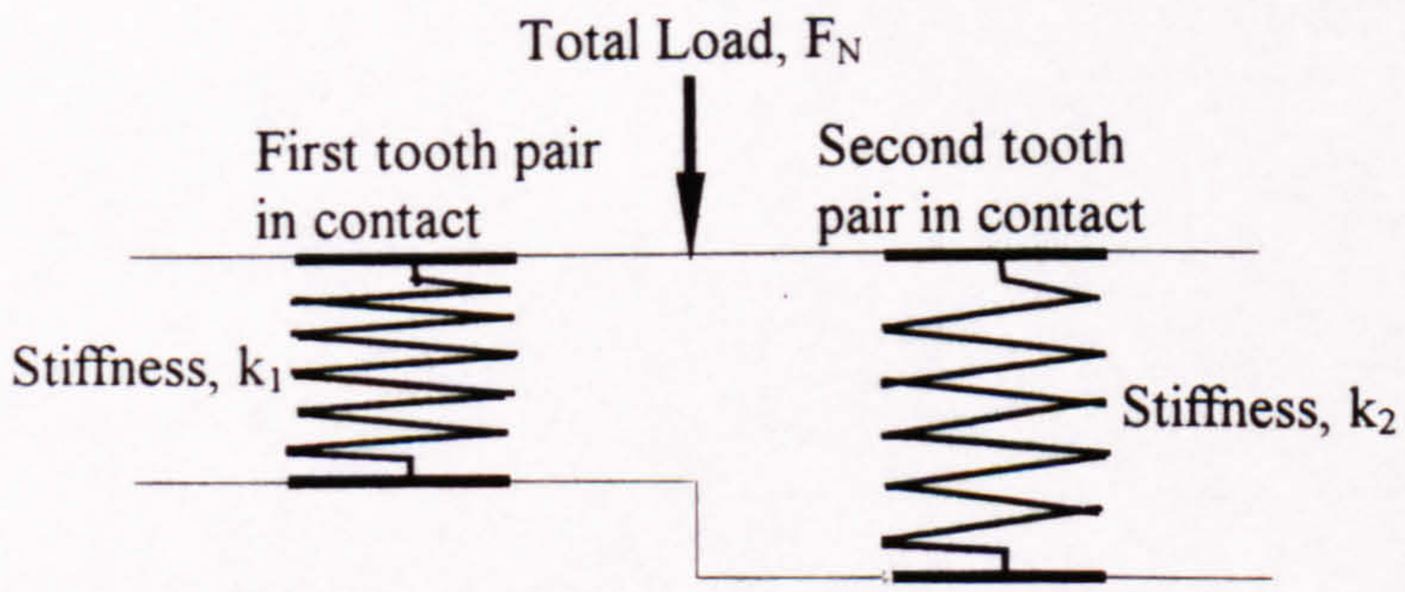


Figure 8.2.1 Input Page to the Gear Contact Program



Two Tooth Pairs, with Only One in Contact



Two Tooth Pairs, with Both in Contact

Figure 8.2.2 Schematic Showing the Principle of Gear Tooth Load Analysis

The model was also used to investigate the effect of extended contact. This was done by assuming the gear teeth were rigid and calculating the size of the gap between the mating teeth before they came into contact (for pre-engagement) and after they had left (for delayed-disengagement). A complete analysis of how the gap size, shown in Figure 8.2.3 as E[N], was calculated is given in Appendix H. This gap at a particular roll angle was compared to the elastic deflections of the gear teeth at that point, to determine whether pre-engagement occurred. The table shown in Figure 8.2.4 is an output of the computer model, showing the size of the gaps between mating teeth and tooth deflections with varying roll angle.

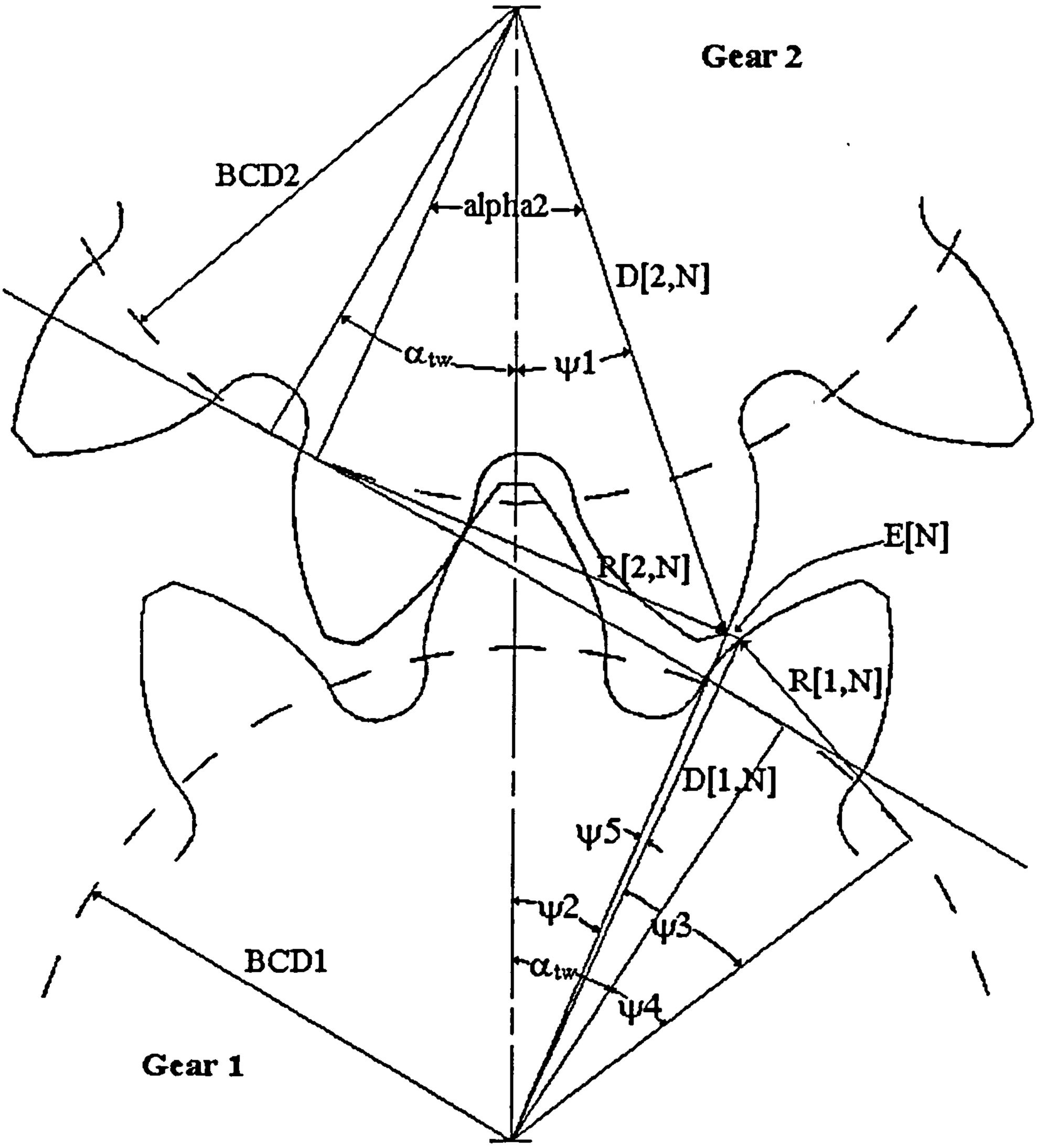


Figure 8.2.3 The Gear Geometry To Evaluate Tooth Gap, E[N]

Extended Contact Results

Print Close

Step	Roll Angle (°)	Gap 1 (mm)	Gap 2 (mm)	Deflect.1 (mm)	Deflect.2 (mm)	Load Sharing
43	9.447	0.0603645	0.0000000	0.0000000	0.0121023	0.0000000
44	9.547	0.0533704	0.0000000	0.0000000	0.0120167	0.0000000
45	9.647	0.0468192	0.0000000	0.0000000	0.0119311	0.0000000
46	9.747	0.0407083	0.0000000	0.0000000	0.0118453	0.0000000
47	9.847	0.0350352	0.0000000	0.0000000	0.0117596	0.0000000
48	9.947	0.0297972	0.0000000	0.0000000	0.0116739	0.0000000
49	10.047	0.0249919	0.0000000	0.0000000	0.0115882	0.0000000
50	10.147	0.0206168	0.0000000	0.0000000	0.0115027	0.0000000
51	10.247	0.0166694	0.0000000	0.0000000	0.0114173	0.0000000
52	10.347	0.0131473	0.0000000	0.0000000	0.0113321	0.0000000
53	10.447	0.0100480	0.0000000	0.0000000	0.0107132	0.0474726
54	10.547	0.0073693	0.0000000	0.0000000	0.0094790	0.1508205
55	10.647	0.0051087	0.0000000	0.0000000	0.0084376	0.2383692
56	10.747	0.0032640	0.0000000	0.0000000	0.0075864	0.3099949
57	10.847	0.0018329	0.0000000	0.0000000	0.0069225	0.3655745
58	10.947	0.0008133	0.0000000	0.0000000	0.0064434	0.4049850
59	11.047	0.0002030	0.0000000	0.0000000	0.0061462	0.4281047
60	11.147	0.0000000	0.0000000	0.0060283	0.0000000	0.4348127
61	11.164	0.0000000	0.0000000	0.0060288	0.0000000	0.4350469
62	11.181	0.0000000	0.0000000	0.0060293	0.0000000	0.4352814
63	11.199	0.0000000	0.0000000	0.0060299	0.0000000	0.4355162
64	11.216	0.0000000	0.0000000	0.0060304	0.0000000	0.4357513
65	11.233	0.0000000	0.0000000	0.0060309	0.0000000	0.4359866
66	11.250	0.0000000	0.0000000	0.0060314	0.0000000	0.4362222
67	11.268	0.0000000	0.0000000	0.0060320	0.0000000	0.4364581
68	11.285	0.0000000	0.0000000	0.0060325	0.0000000	0.4366942

Figure 8.2.4 Program Output Showing the Calculated Tooth Gaps, Deflections, and Load Sharing for Non-Relieved Gear Teeth

The load sharing diagram can be seen in Figure 8.2.5 for the non-relieved spur gear geometry described in Chapter 7. The data was entered in the front panel shown in Figure 8.2.1. Here, however, no effects of pre-engagement are shown.

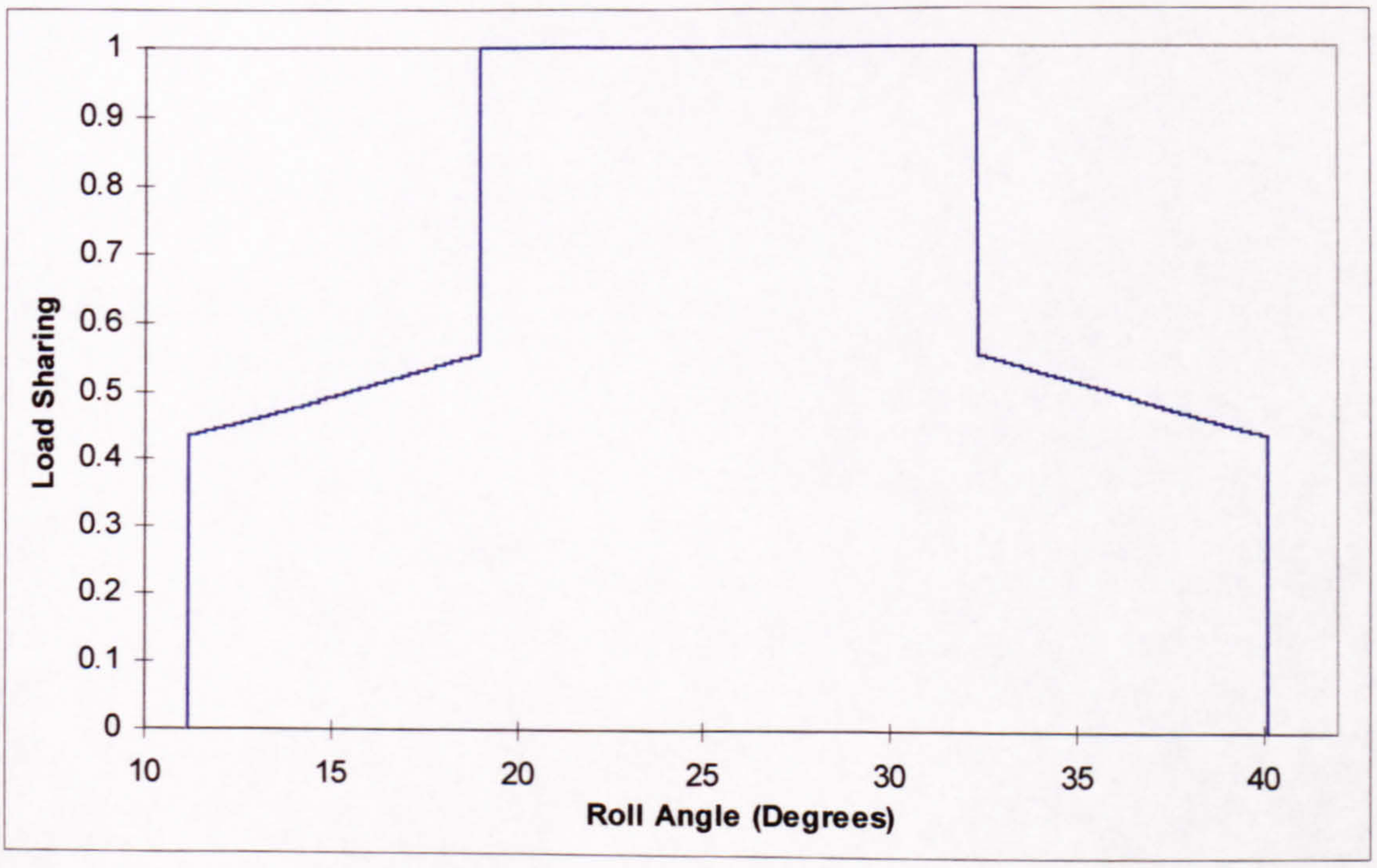


Figure 8.2.5 Program Output Showing the Load Sharing Diagram

8.2.1.2 Tooth Contact Neglecting Tip Effects

The gear rig described in Chapter 7 has a hydraulic loading system, the relationship between the hydraulic pressure and the torque applied to the test gears, or calibration curve, is shown in Figure 7.4.2. The test gears were designed to run at about 350 Nm and were given a controlled crowning radius, as shown in Chapter 7. The geometry of the gears was known and, assuming they were perfectly smooth with no manufacturing errors (i.e. perfect involute), the maximum Hertzian stress on the individual gear teeth for an applied torque was calculated (Figure 8.2.6). This was evaluated at the lowest point of single tooth contact, as this is where the load on an individual gear tooth was the greatest. These contact stress calculations assume there is no extended contact of the gear tooth tips and roots, where even a small load may result in a high stress due to the small tip radius of the gear (discussed in Section 8.2.1.3). The variation of maximum Hertzian contact stress with the loading pressure is given in Figure 8.2.7.

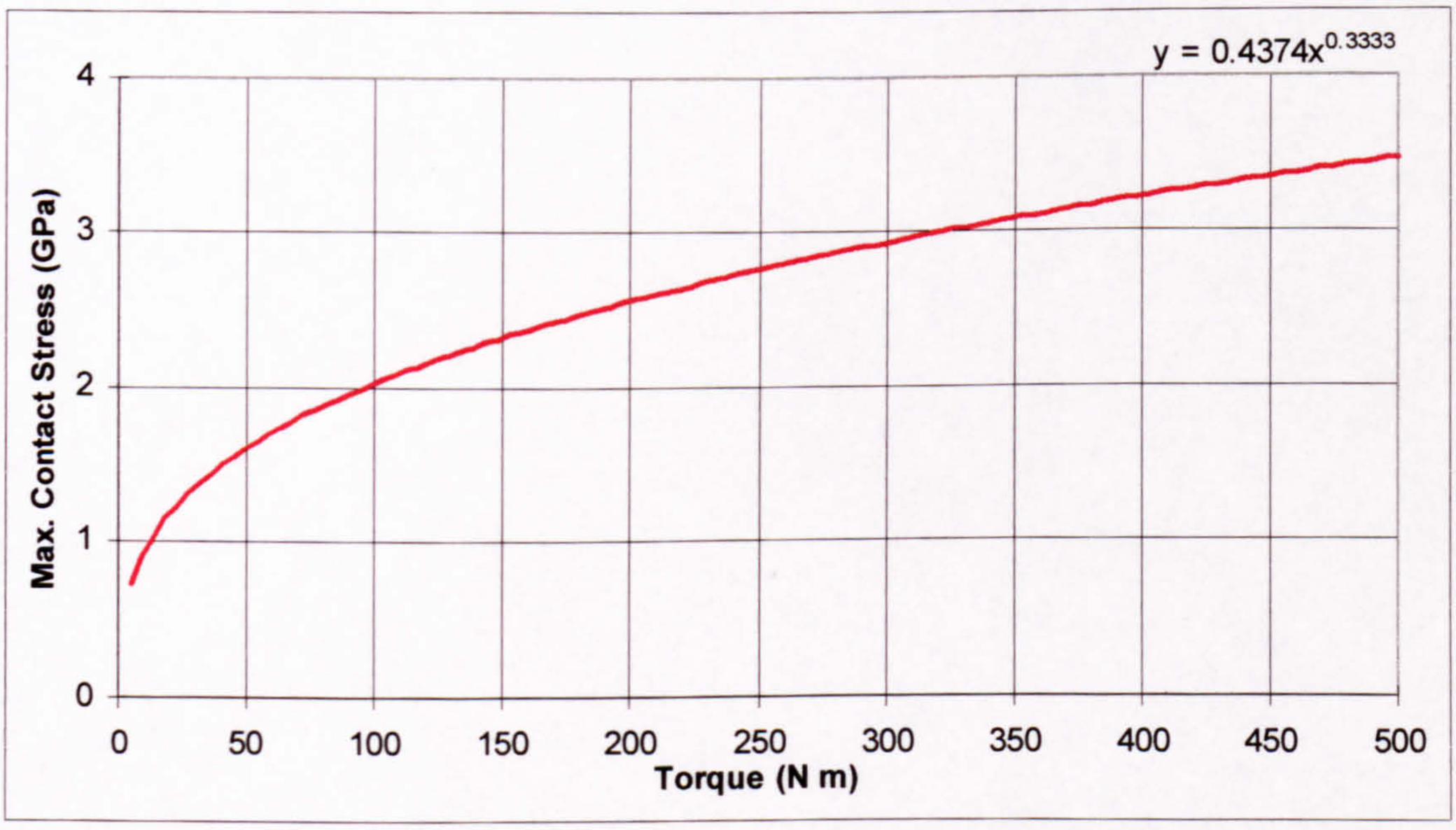


Figure 8.2.6 Variation of Maximum Hertzian Contact Stress on the Gear Teeth at the Lowest Point of Single Tooth Contact with Torque

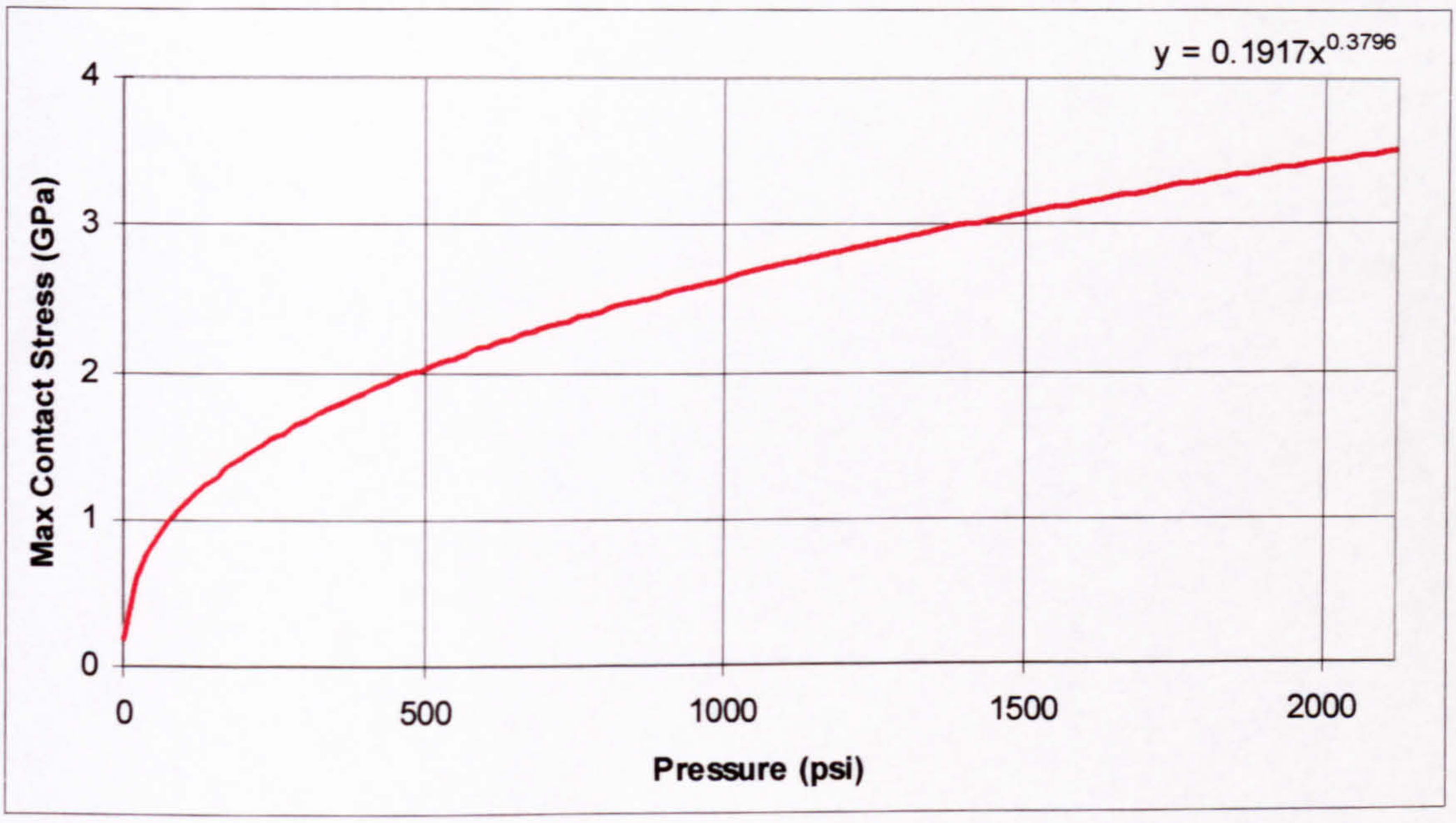


Figure 8.2.7 Variation of Maximum Hertzian Contact Stress on the Gear Teeth at the Lowest Point of Single Tooth Contact with Oil Loading Pressure

The gear teeth will come together producing an elliptical contact area, as described in Chapter 2, but because the radius of curvature is constant in the axial, or lead direction (the crowning radius), but varying in the direction of motion, or profile direction, the shape of the contact ellipse will vary. This is different from the crowned disc tests where the ratio a to b of the major and minor semi-axes of the elliptical contact is constant. The contact dimensions are important in fatigue testing because they will affect the stressed volume (discussed in Chapters 3 and 6). Figure 8.2.8 shows the variation of the ratio a:b along the gear tooth contact. The lowest and highest point of single tooth contact are indicated on the graph because, for pitting correlation, these are probably the points where the gear test should be compared to the disc test (an individual disc test being only capable of simulating one point in a gear tooth contact).

The variation of contact stress across the tooth mesh can also be calculated. This is shown for three different values of applied torque in Figure 8.2.9. It takes into account gear tooth load sharing (Figure 8.2.5), using values from the software program discussed in Section 8.2.1.1. It shows that the contact stress is indeed greatest at the highest point of single tooth contact. A three dimensional plot of the contact stress variation with position along the tooth contact and applied torque was constructed with these values, as shown in Figure 8.2.10.

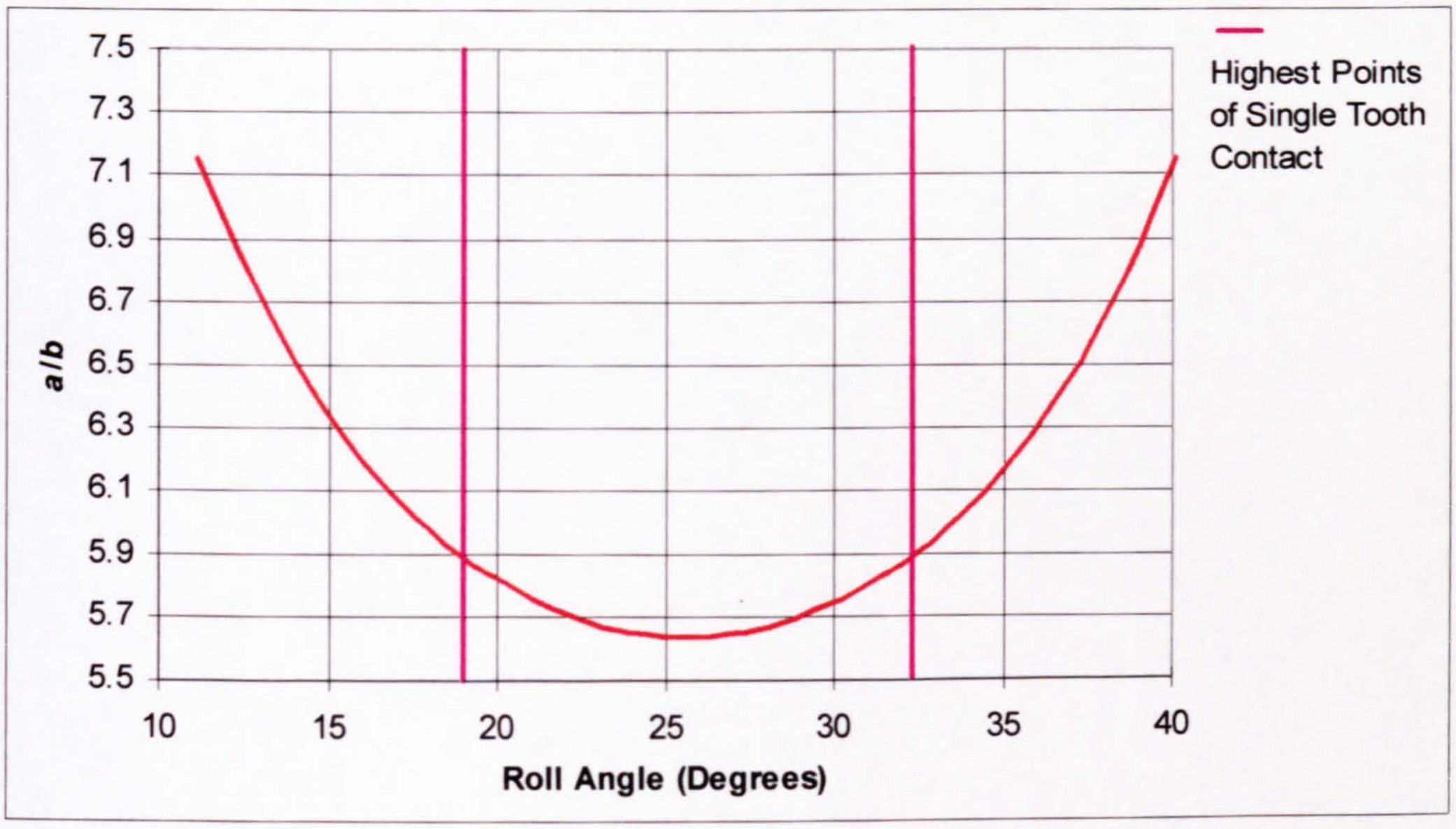


Figure 8.2.8 Variation of the Contact Ratio *a*:*b* Along the Gear Tooth Contact

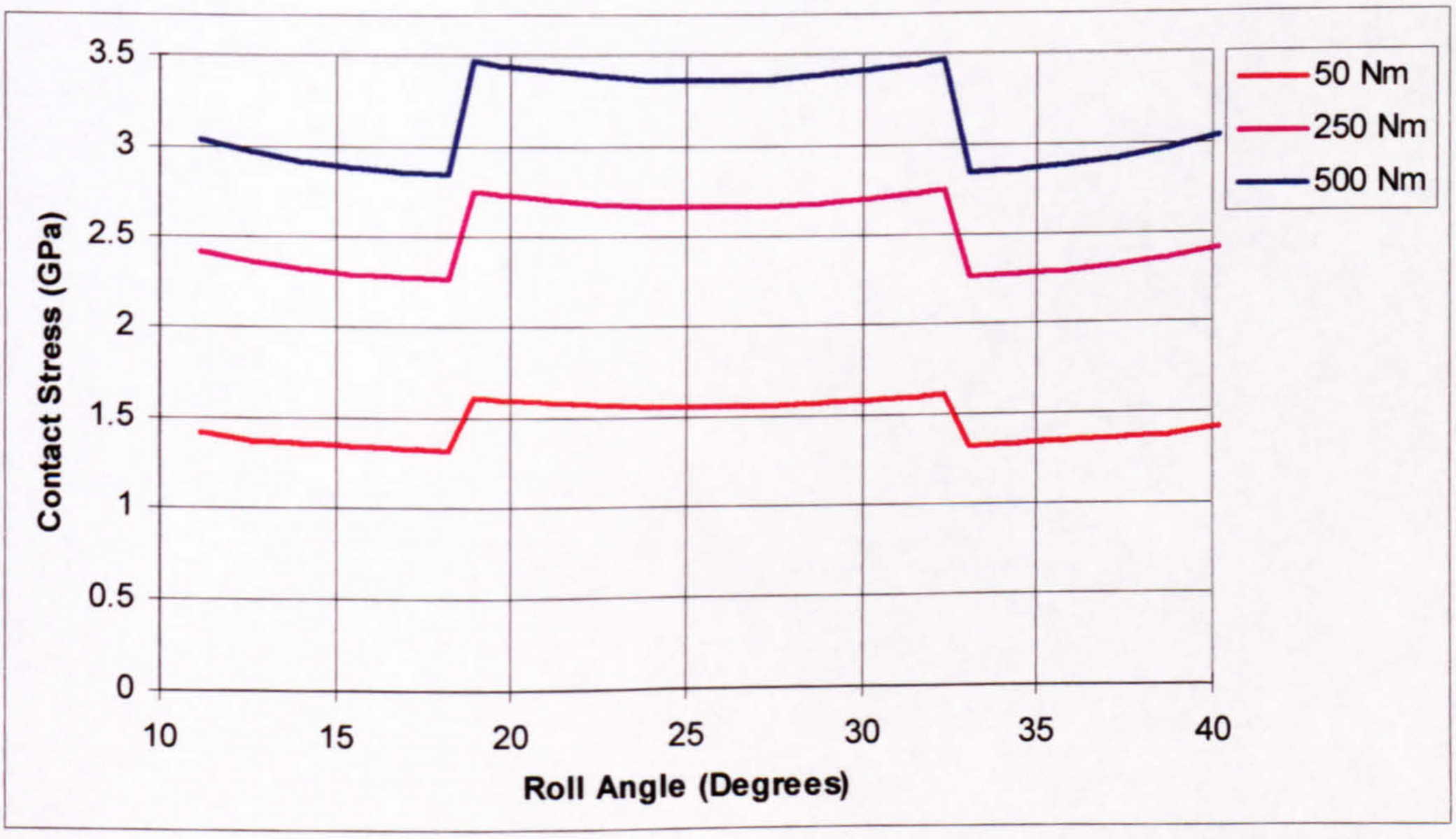


Figure 8.2.9 Variation of the Contact Stress Along the Gear Meshing Cycle for Three Values of Torque

The values of both the contact dimensions $2a$ and $2b$ can be calculated individually and are displayed in Figures 8.2.11 and 8.2.13 respectively, and in three dimensional form in Figure 8.2.12.

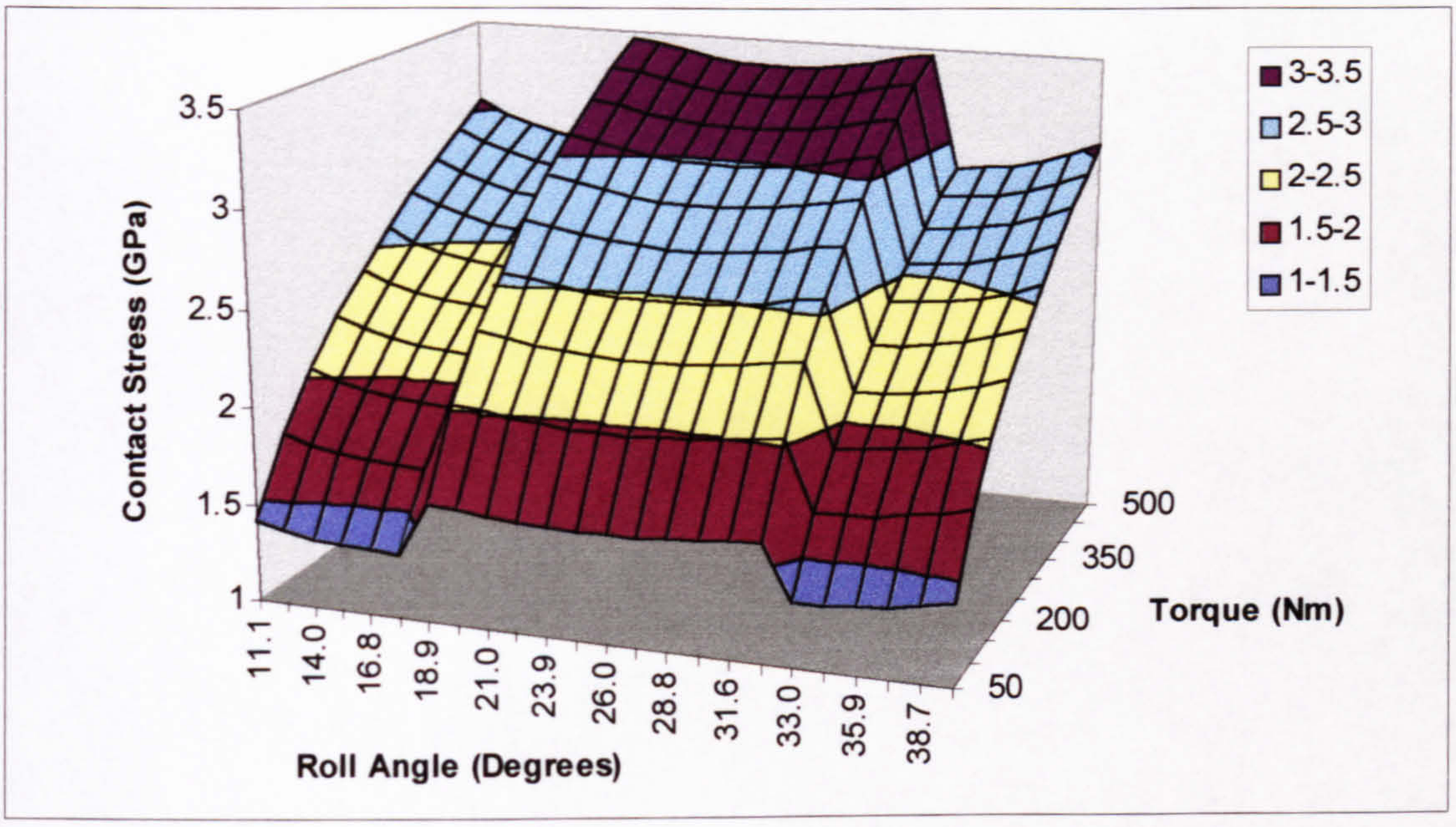


Figure 8.2.10 Variation of Contact Stress Throughout the Gear Mesh Cycle with Torque

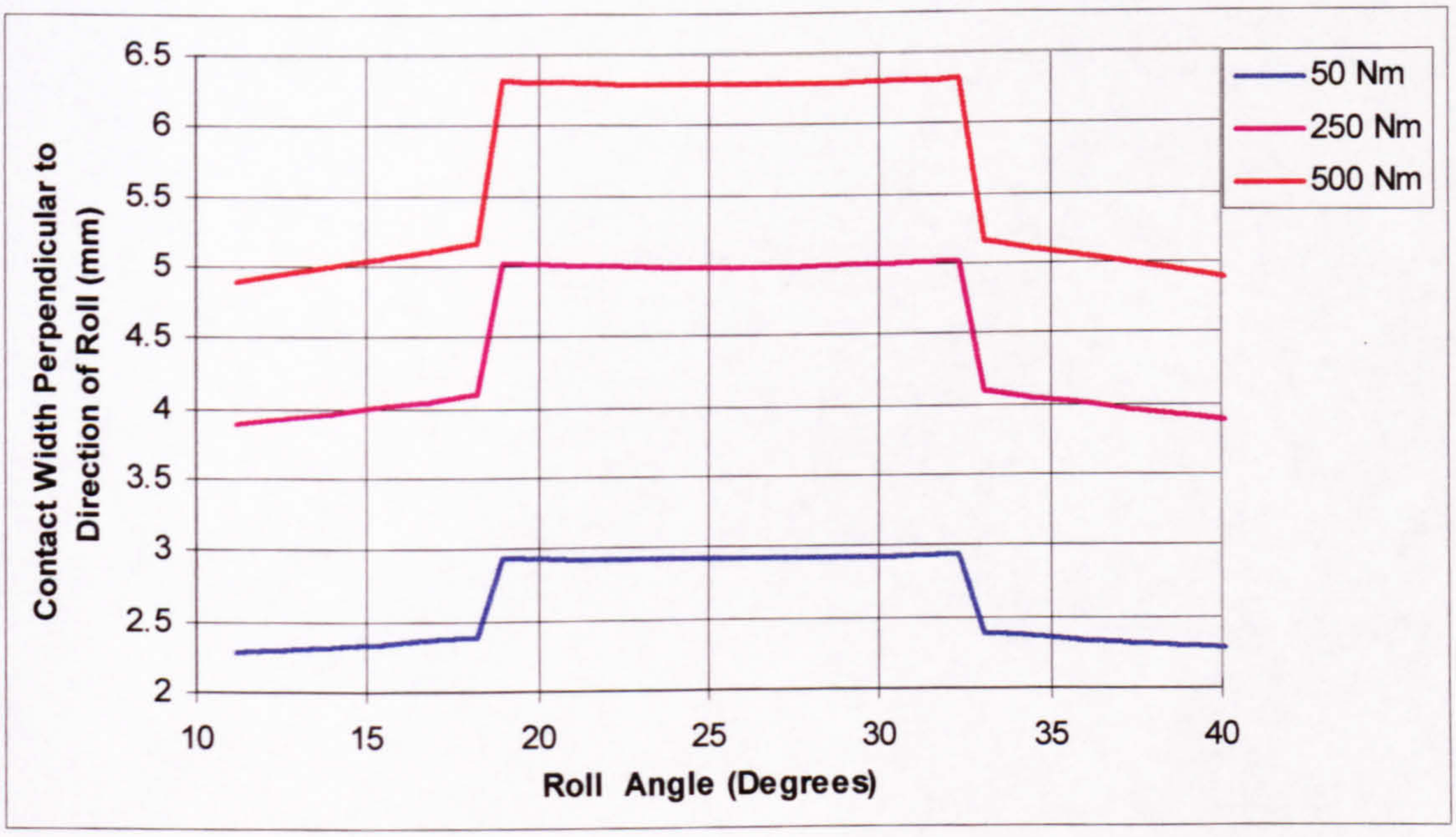


Figure 8.2.11 Variation of the Major Contact Dimension 2*a* Throughout the Gear Mesh Cycle for Three Values of Torque

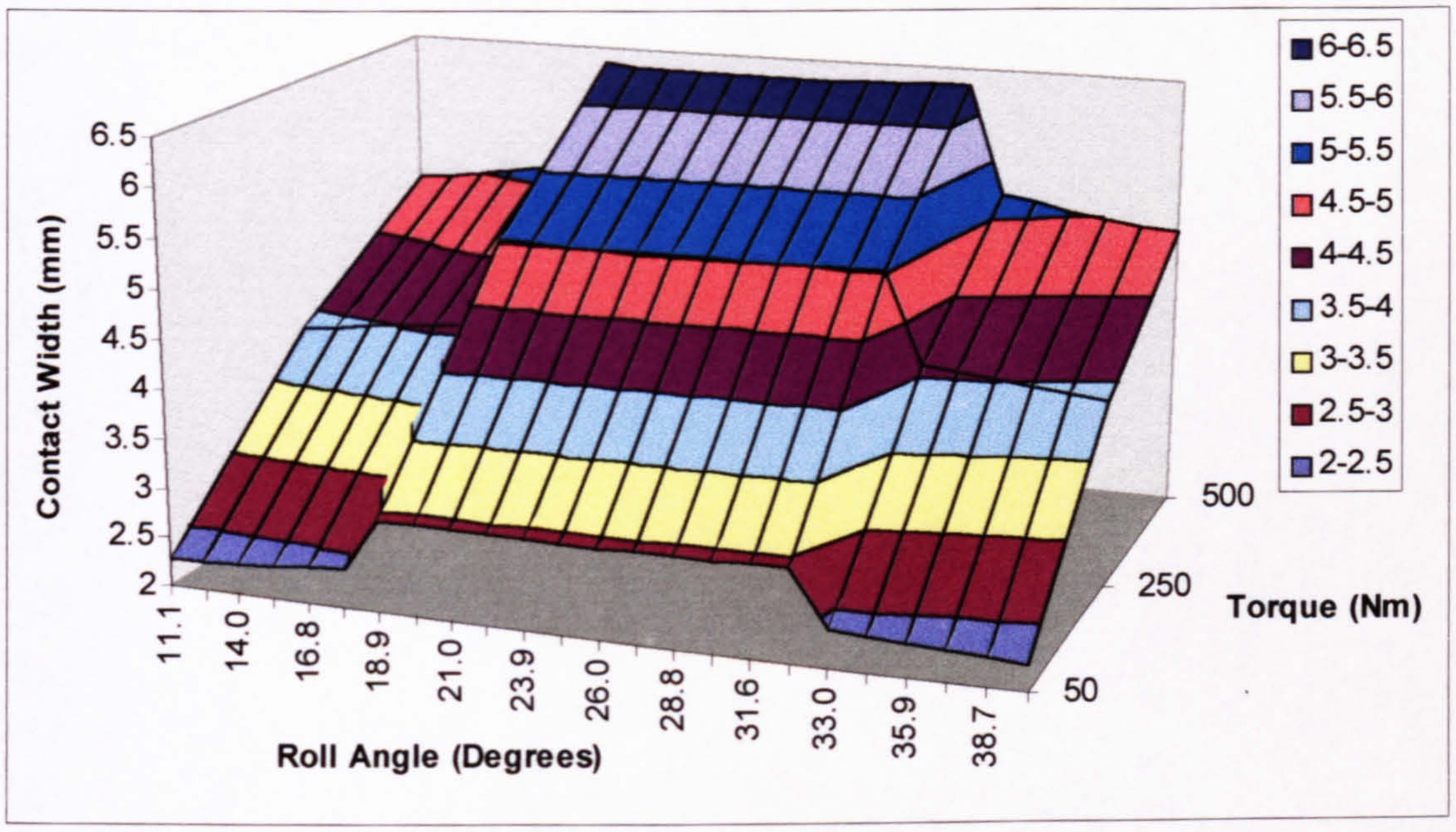


Figure 8.2.12 Variation of the Major Contact Dimension 2*a* Throughout the Gear Mesh Cycle

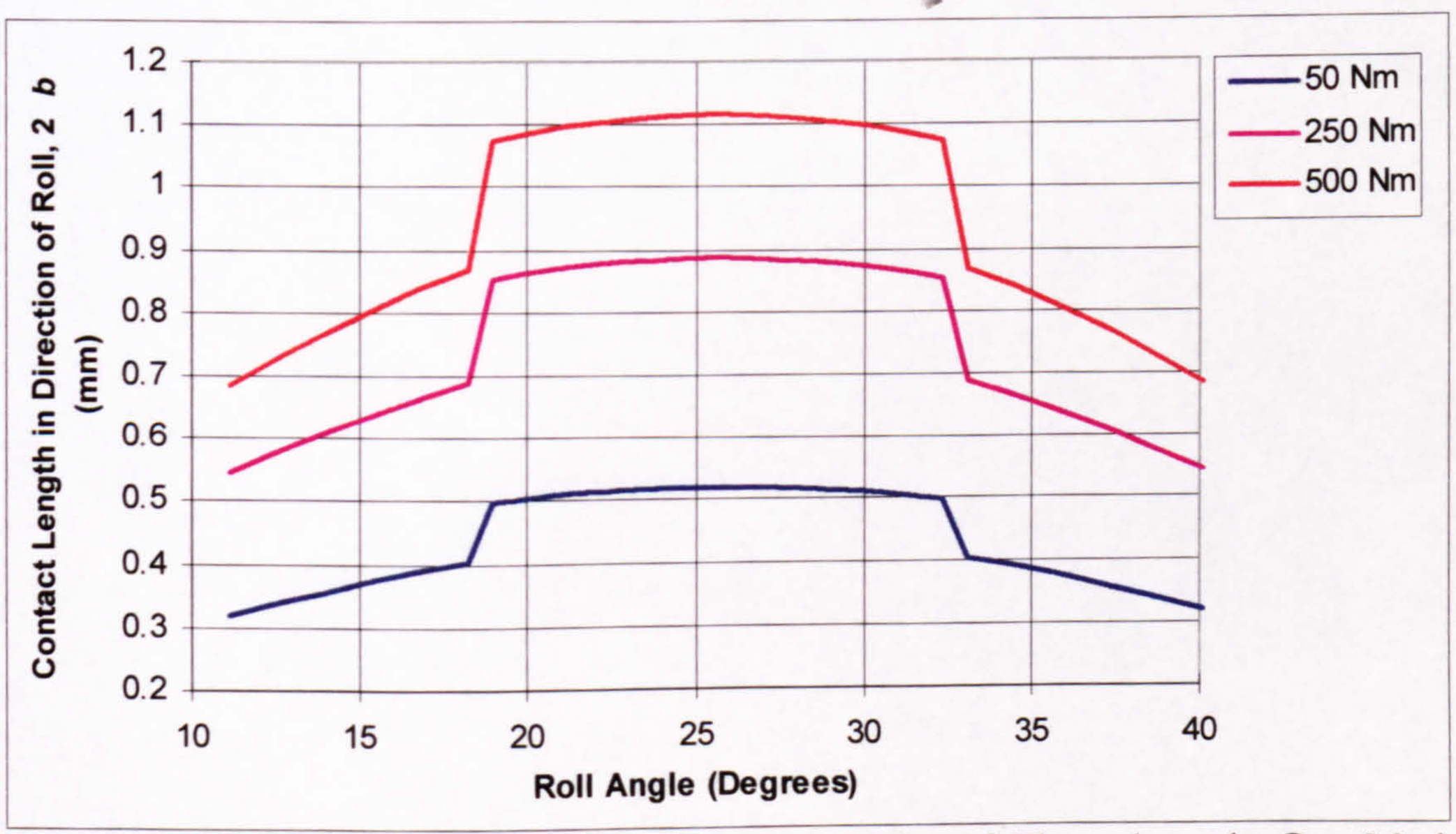


Figure 8.2.13 Variation of the Minor Contact Dimension 2*b* Throughout the Gear Mesh Cycle for Three Values of Torque

8.2.1.3 Modelling of Pre-engagement

One of the explanations given for the difference between gear and disc test results was extended contact of the gear teeth. This phenomenon arises as a consequence of the elastic deflection of the gear teeth and leads to a tooth pair, that should come into contact on the path of contact, engaging prematurely and disengaging later than expected - i.e. extended contact. The result of this could be load applied at the tooth tip, where

there is a small radius of curvature and consequently higher stresses, lower film thickness formation, and higher flash temperatures could result. This process can damage the gear teeth as shown in Figure 8.2.14. It should be mentioned that this effect will probably not take place in properly tip-relieved gears.



Figure 8.2.14 Tooth Interference Causing Pitting (Alban 1985)

The computer model described in Section 8.2.1.1 was used to evaluate the risk of extended contact due to the elastic deflections of the gear teeth. The load sharing between the two pairs of mating gear teeth was evaluated and is shown for two values of torque in Figure 8.2.15. As the torque increases, the tooth deflections also increase and the gear tips remain in contact longer. This modifies the load sharing diagram by making the transitions between one and two tooth contact more gradual.

To get an approximation of the effects of pre-engagement on the surface stresses, a radius was assigned to the gear tooth tip (this was chosen as 0.5 mm for the results presented here because this was thought to be a reasonable value). The stresses at the points where extended contact took place were calculated using Hertzian contact between the tip radius and the radius of the mating gear tooth just below the start of contact. The effect of this extended contact, shown in Figure 8.2.16, is to create pressure spikes at the edges of the mesh cycle. If the radius of the tip is increased the values of these spikes decrease, as shown in Figure 8.2.17. The tips of the gears could not withstand the high pressures shown in Figure 8.2.16 elastically, and there would be some plastic deformation of the tip of the gear tooth or the root of the mating gear tooth. This would reduce contact pressures, but the risk of failure would still be present, particularly by scuffing, since there is high sliding velocity in that area and a reversal of entrainment of the lubricant, leading to a drop in the film thickness (discussed in Chapter 10). The

presence of extended contact would, therefore, appear to be damaging to gear teeth, not only because of the high contact stresses, but also due to the low film thickness and high flash temperatures present there (discussed in Chapter 9), all of which could lead to scuffing.

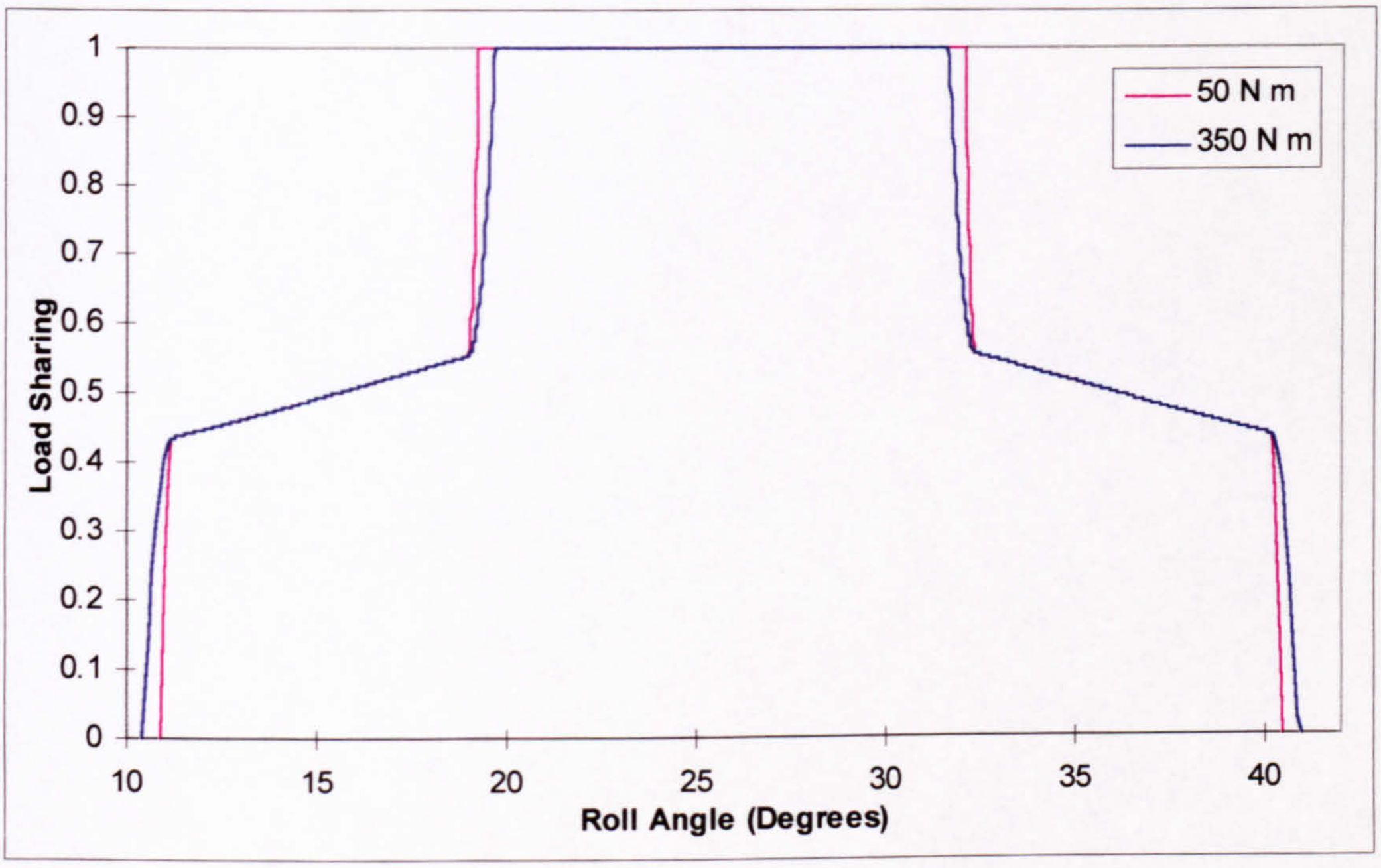


Figure 8.2.15 Load Sharing Diagram using the Extended Contact Analysis for Two Values of Torque

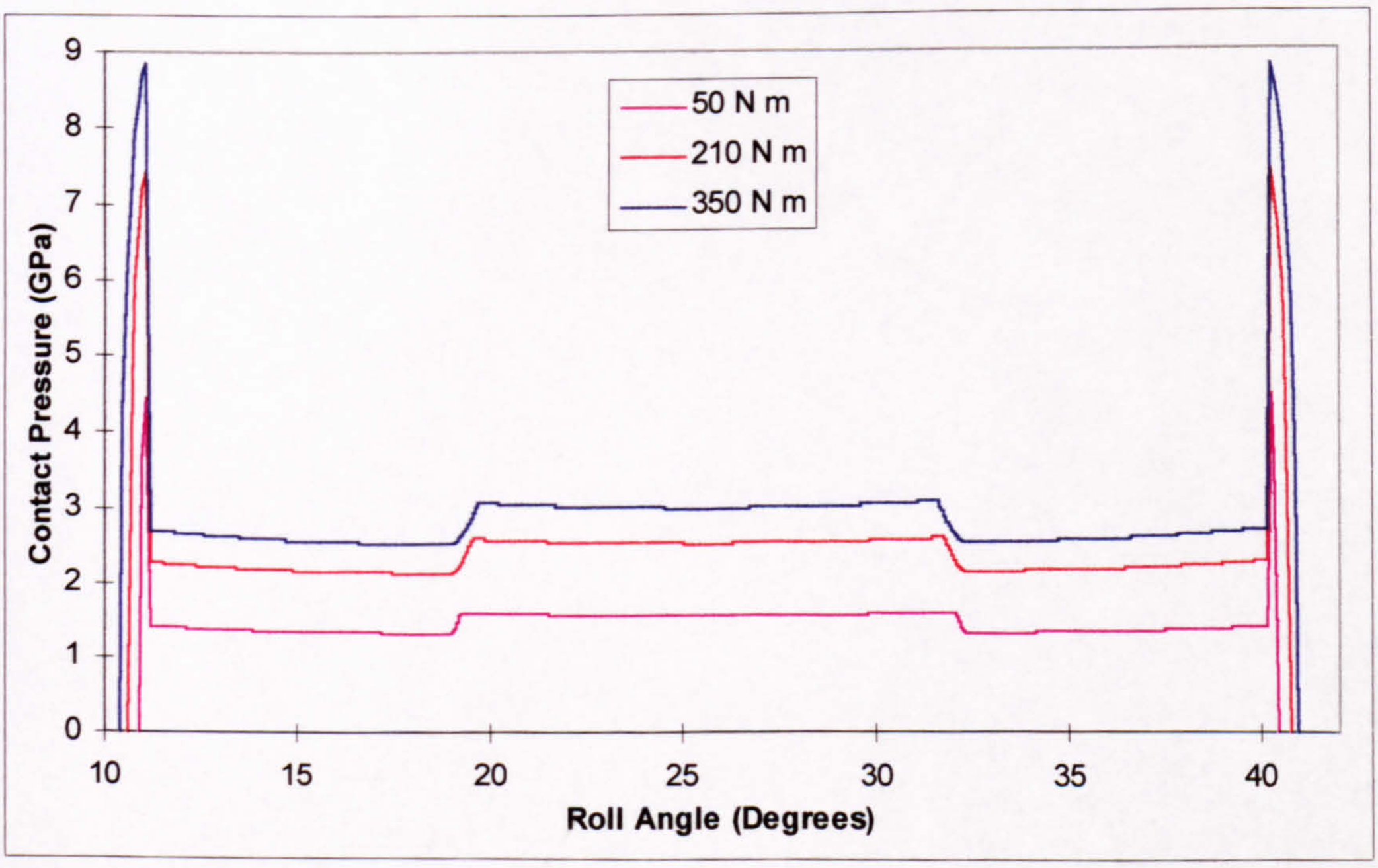


Figure 8.2.16 The Contact Stresses on a Crowned Non-Tip-Relieved Gear Tooth Suffering Extended Contact at the Extremities of the Mesh Cycle

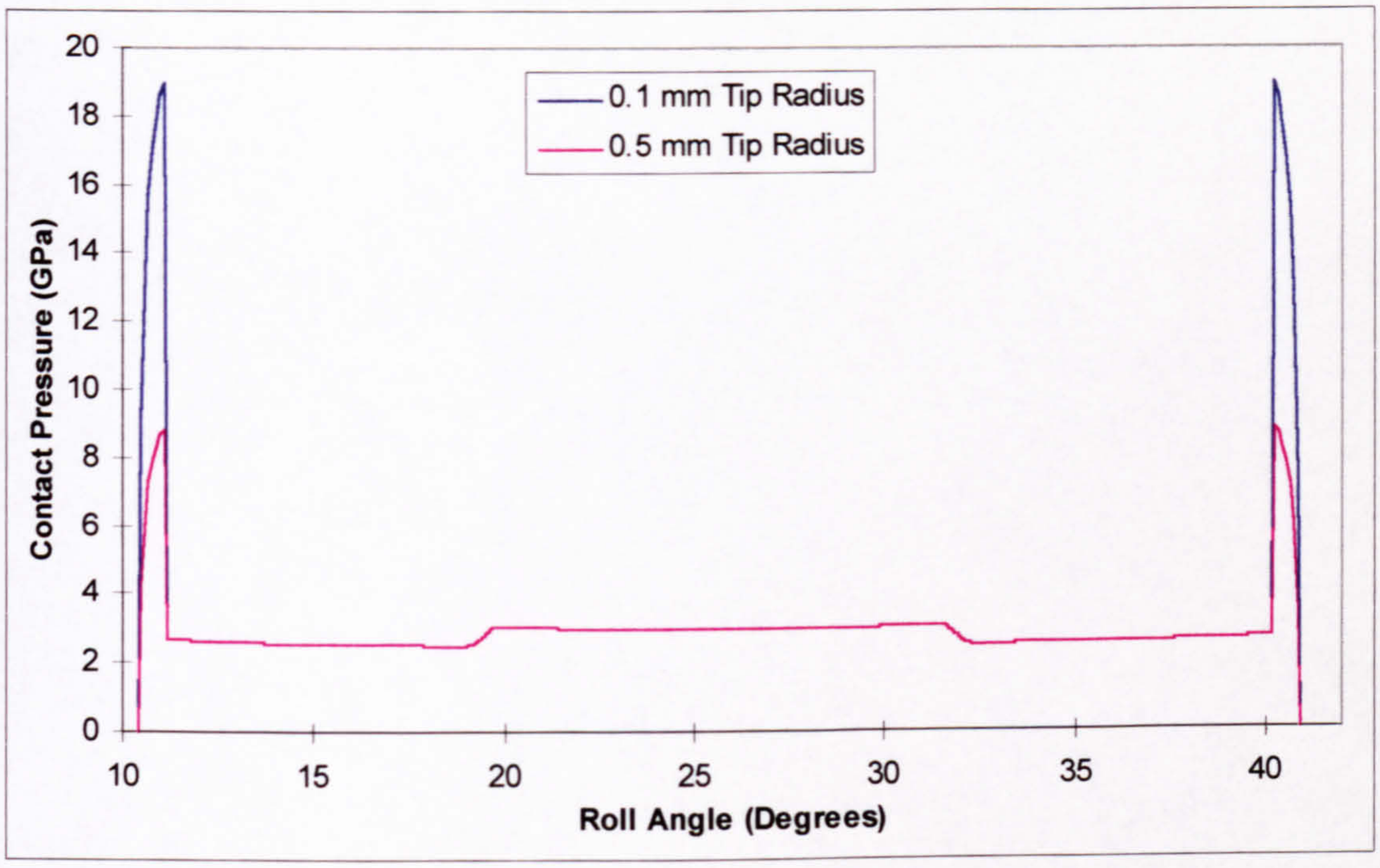


Figure 8.2.17 The Effect of Gear Tooth Tip Radius on the Contact Stresses in a Crowned Non-Tip-Relieved Gear Tooth Suffering Extended Contact

The contact dimensions for a gear tooth pair suffering extended contact, calculated with the aid of the model, are shown in Figure 8.2.18. The contact width in the lead direction would appear to widen at the points were extended contact occurred between a tooth pair. The gear tests, described in Chapter 11, would hopefully help confirm some of the observations made from this theoretical analysis.

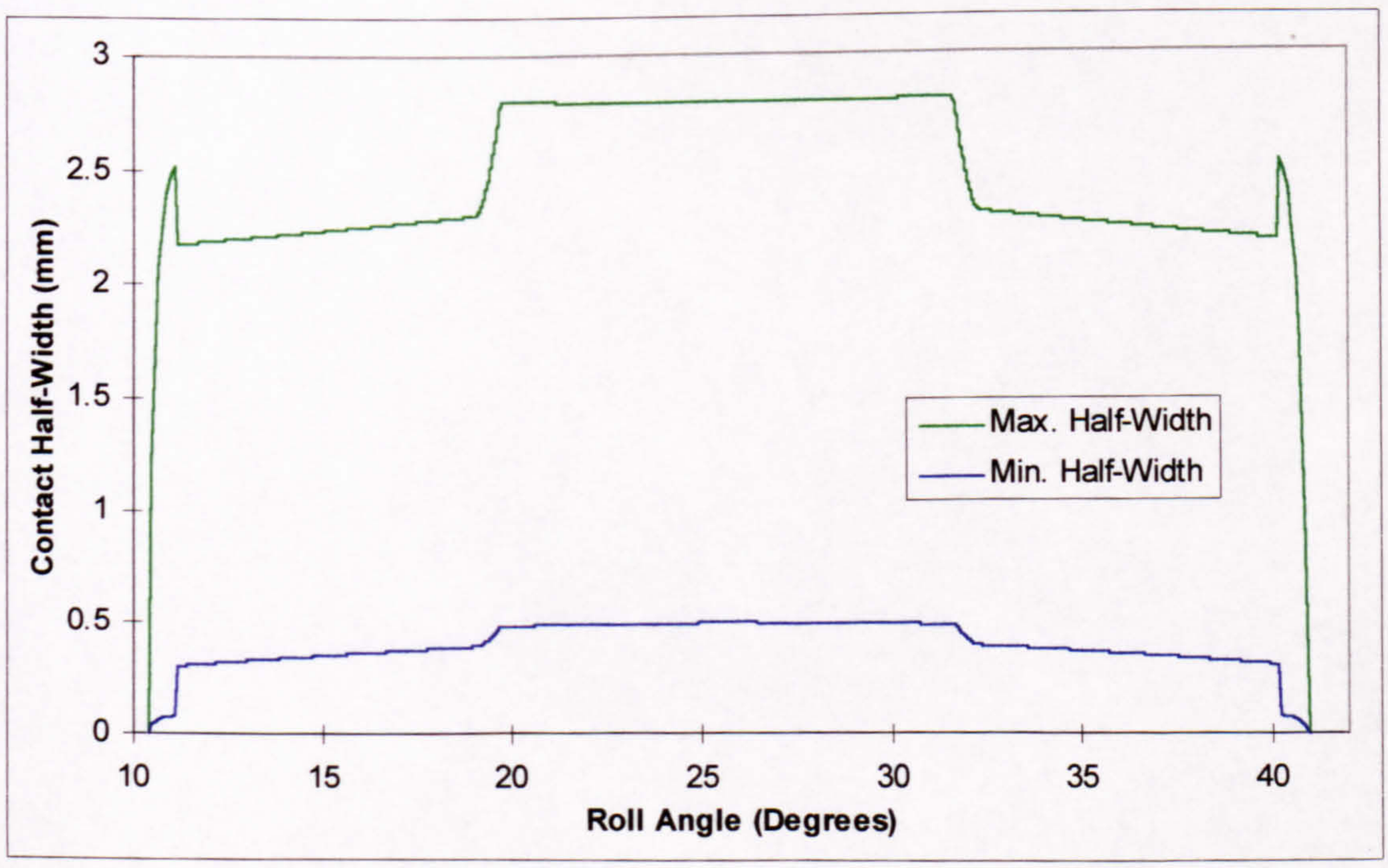


Figure 8.2.18 The Contact Dimensions of a Crowned Non-Tip-Relieved Gear Tooth Suffering Extended Contact at the Extremities of the Mesh Cycle

8.2.2 Dynamic Analysis

The previous analysis was carried out neglecting dynamic loads. These will be imposed on the static load causing fluctuations.

The dynamic loads are not the same in the two types of test, vibratory loads are common in gears. Gear testers, in which a pair of test gears are connected directly to a slave gear set of identical ratio to form a power recirculating loop, can experience vibratory loads arising from pitch errors in either the test or the slave gears. Dynamic loads will have less of an effect on the disc rig. Two simple analyses were carried out to determine dynamic effects on the gears tested by the author.

8.2.2.1 The Dynamic Factor

The dynamic factor, K_v, is the ratio of peak load occurring in the gear mesh at running speed to the load that would exist if all gear elements had zero inertia. It does not take into account the dynamics of the whole drive system, but assumes that the driving and driven machine are de-coupled from the gear pair. The internal dynamic loads depend on the gear geometry (tip and root relief, pressure angle), the mesh stiffness, the pitch and profile errors, the mass of the gears and the dynamic characteristics of the bearings and gear case (BGA 1992).

The calculation of K_v is only valid for gears running well below torsional resonance, defined by the mesh stiffness and the inertia of the mating gears, and if the pinion and wheel are solid. Method C from DIN 3990 (1987) can be used for its calculation.

For gears running below resonance,

$$v \cdot z_1 \sqrt{\left(\frac{u^2}{1+u^2}\right)} < 1000 \text{ ms}^{-1}$$

where v is the peripheral velocity, z_1 the number of teeth on the pinion, and u is the gear ratio. The dynamic factor can then be calculated by the following,

$$K_v = 1 + \left(K_1 \cdot \frac{b}{F_{tD}} + K_2\right) \cdot \frac{z_1 v}{100} \cdot \sqrt{\frac{u^2}{1+u^2}}$$

where b is the facewidth, d is the gear reference diameter, and F_{tD} is the design tangential load. K_1 and K_2 were taken from tables G1 and G2 given in Appendix G (from BGA (1992) for the appropriate gear quality to BS 436 Part 2 (BSI 1970)).

The dynamic factor was calculated as, $K_v = 1.06$

The real contact stress, σ_H, is related to the nominal contact stress, σ_{HO}, by the equation

$$\sigma_H = \sigma_{HO}\sqrt{K_v \cdot K_{HB} \cdot K_{H\alpha}}$$

where K_{HB} is the face load distribution factor for contact stress (which accounts for unequal load distribution across the facewidth due to lead errors and misalignment) and $K_{H\alpha}$ is the transverse load distribution factor (to allow for the effect of pitch and profile errors on load sharing between teeth in mesh).

Neglecting the two parameters K_{HB} and $K_{H\alpha}$, the real contact stress will have fluctuations of up to 2.8 % of the nominal contact stress. Therefore, theoretically, the dynamic loads did not contribute excessively to the gear contact stresses, and they were not added to the values calculated for the maximum static contact stress.

8.2.2.1 Determination Of Natural Frequencies Of The Gear System

An analysis was carried out to determine the natural frequencies of the gear rig and make sure that these were far from the operating frequencies of the rig, in order to avoid any excessive dynamic effects.

The natural frequencies were calculated by two methods: translational and rotational methods, to check they gave the same results. The full analysis is given in Appendix G.

The tooth mesh excitation frequencies for the test gears and slave gears were 708 Hz and 1417 Hz respectively. The shaft frequency was 42 Hz.

The gear rig was treated as a system consisting of two masses, representing the gears, connected by three springs, the two lateral ones representing the shafts and the central one representing the meshing gear stiffness (Figure 8.2.19).

It was uncertain how the hydraulic loading system, described in Chapter 7, behaved (whether this was perfectly rigid, allowing no motion at the end of the shafts, or was totally flexible, or something in between). Two approaches were taken to model the system, a flexible loading assumption with the stiffness k_B being taken as zero, and offering no stiffness, and a rigid loading assumption where the stiffness of the shaft was considered. The calculation of the masses, m, moments of inertia, J, and stiffness values, k, are shown in Appendix G. These were approximated from measurements on the rig.

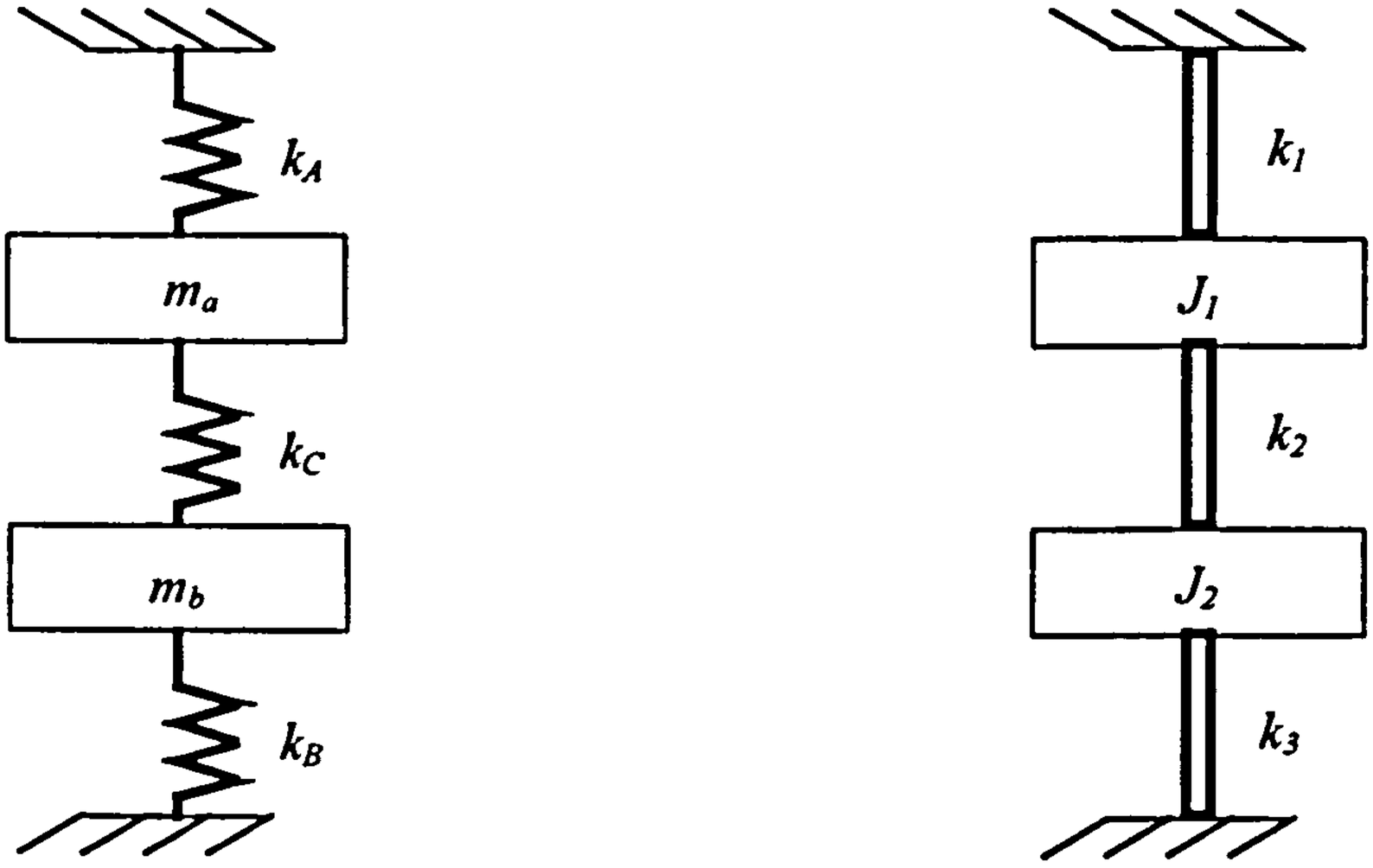


Figure 8.2.19 The Two Systems Used to Model the Natural Frequencies of the Gear System

For the first assumption of a loading system with great flexibility, the resonant frequencies obtained were $f_1 = 2115$ Hz and $f_2 = 242$ Hz

The mode shape for the first frequency would give the shafts a vibratory motion in opposite directions to each other, imposed on the normal motion of the shafts. The second frequency would give a vibratory motion in the same direction, imposed on the normal motion of the shafts.

For the second assumption of a rigid loading system, the resonant frequencies obtained were $f_1 = 2129$ Hz and $f_2 = 344$ Hz. The first frequency would give the shafts a vibratory motion in opposite directions and the second frequency would give a vibratory motion in the same direction.

Both assumptions gave natural frequencies which were far from the test and slave gear meshing frequencies and the shaft frequency. This indicated that resonance induced by tooth mesh excitation or by shaft imbalance should not be a problem, and that the test gears were effectively isolated from the slave gears.

8.3 Roughness Effects

As explained in Chapter 2, all surfaces are rough. This roughness is usually imparted on components during the machining and finishing processes. The surface roughness, in general, will be different in gears and discs because of their different production methods. The gears had an axial surface finish, perpendicular to the rolling direction, as opposed to

the discs that were finished by cylindrical grinding, which led to a circumferential surface roughness orientation, parallel to the direction of rolling. This will give rise to different lubricant film formation. Film thickness has been predicted to increase as roughness goes from a longitudinal to a transverse lay, for lambda values less than about 3 (Patir & Cheng 1979 and Hua et al. 1987). This could be beneficial to the gear contact.

The actual surface pressure distribution does not follow the Hertz prediction due to the surface roughness, the local pressures and subsurface stresses tend to be much higher. The surface profiles used by the author were measured using the Talysurf, described in Chapter 2. In this section the rough surface contact model, developed by Webster and Sayles (1986) and described in Chapter 2, was used to compare the roughness effects of the gear and disc specimens. This model can be used as an aid to predicting the performance of a component and give an indication of the contact conditions when the ratio of film thickness to roughness is low, and there is consequently considerable surface contact. The real rough surface is normally loaded against a smooth cylindrical counterface. The counterface roughness was, therefore, not included (it could, however, all be incorporated on one surface). Finally, the analysis is two dimensional and the crowning radius on the gear teeth or edge effects on the barrel are not taken into account.

The representative roughness profiles were in the circumferential direction, that of contact motion, for the gears and in the axial direction, perpendicular to the contact motion, for the discs. The rough surface profiles were filtered to remove any overall radius of curvature, the curvature was all put onto the smooth cylinder.

This surface curvature was applied all on one surface by using the equation below:

$$R^* = \frac{R_1 \times R_2}{R_1 + R_2}$$

where R_1 and R_2 are the barrel and ring radius for the disc rig, whereas, for the gear rig they were taken as the radii of the mating gear teeth at the lowest point of single tooth contact (these values are given in Table 8.3.1). The load per unit length was chosen to give a Hertzian contact stress of 2.6 GPa in both contacts. The Young's modulus was taken as 2×10^{11} N m^{-2}.

The deformed profile of the chamfered barrel surface under loading can be seen in Figure 8.3.1. One can see that the gear surface produces higher surface contact pressures

(Figure 8.3.4) than both the crowned (Figure 8.3.3) and chamfered barrel (Figure 8.3.2) and would, therefore, be liable to suffer more asperity plastic deformation and consequent fatigue failure.

Table 8.3.1 Radii of Curvature for the Barrel and Gear Specimens

Radius	Barrel Specimen (mm)	Gear Specimen (mm)
R_1	9.30	13.41
R_2	41.47	22.89
R^*	7.59	8.46

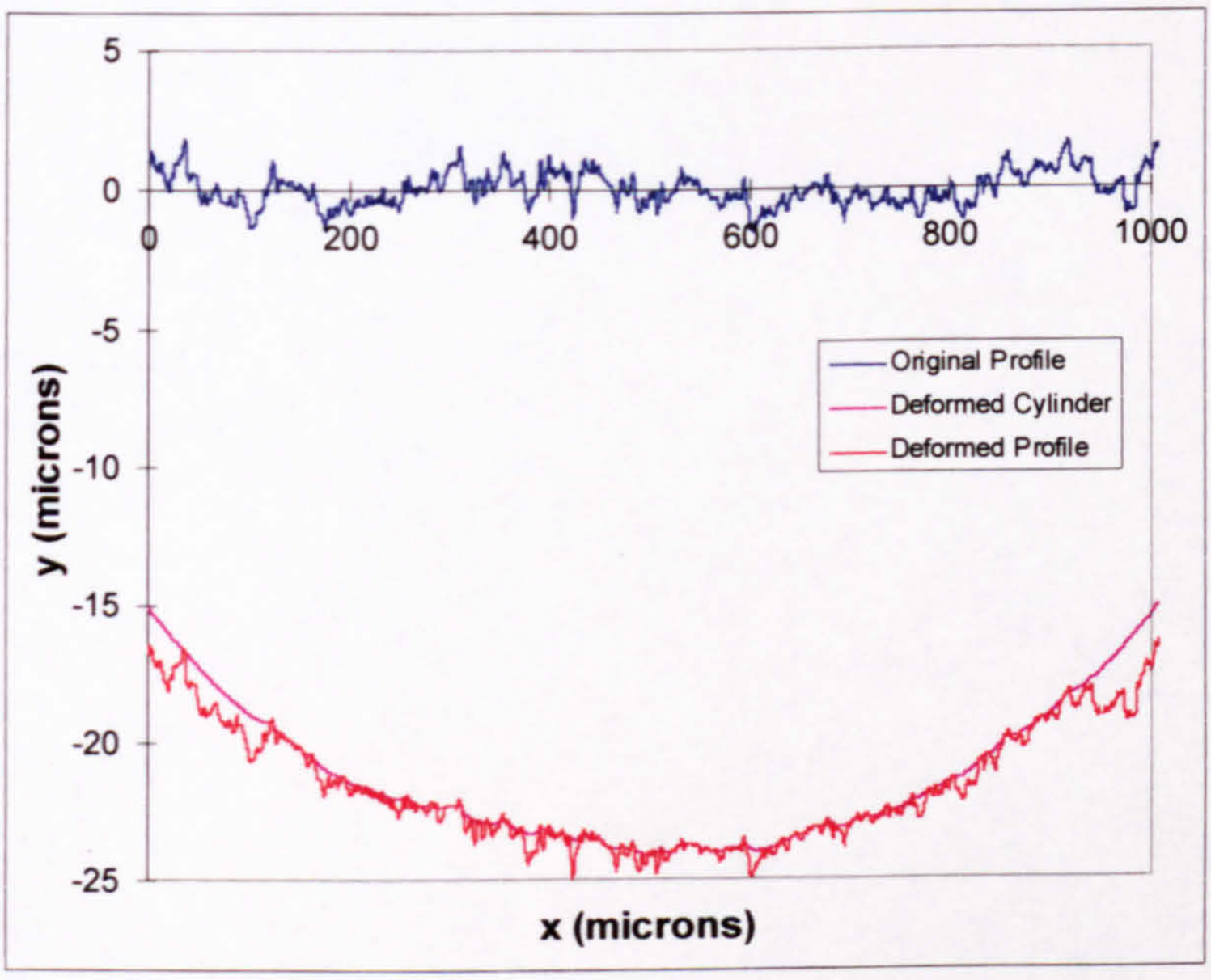


Figure 8.3.1 The Deformed Surface Profile of the Loaded Chamfered Barrel Profile

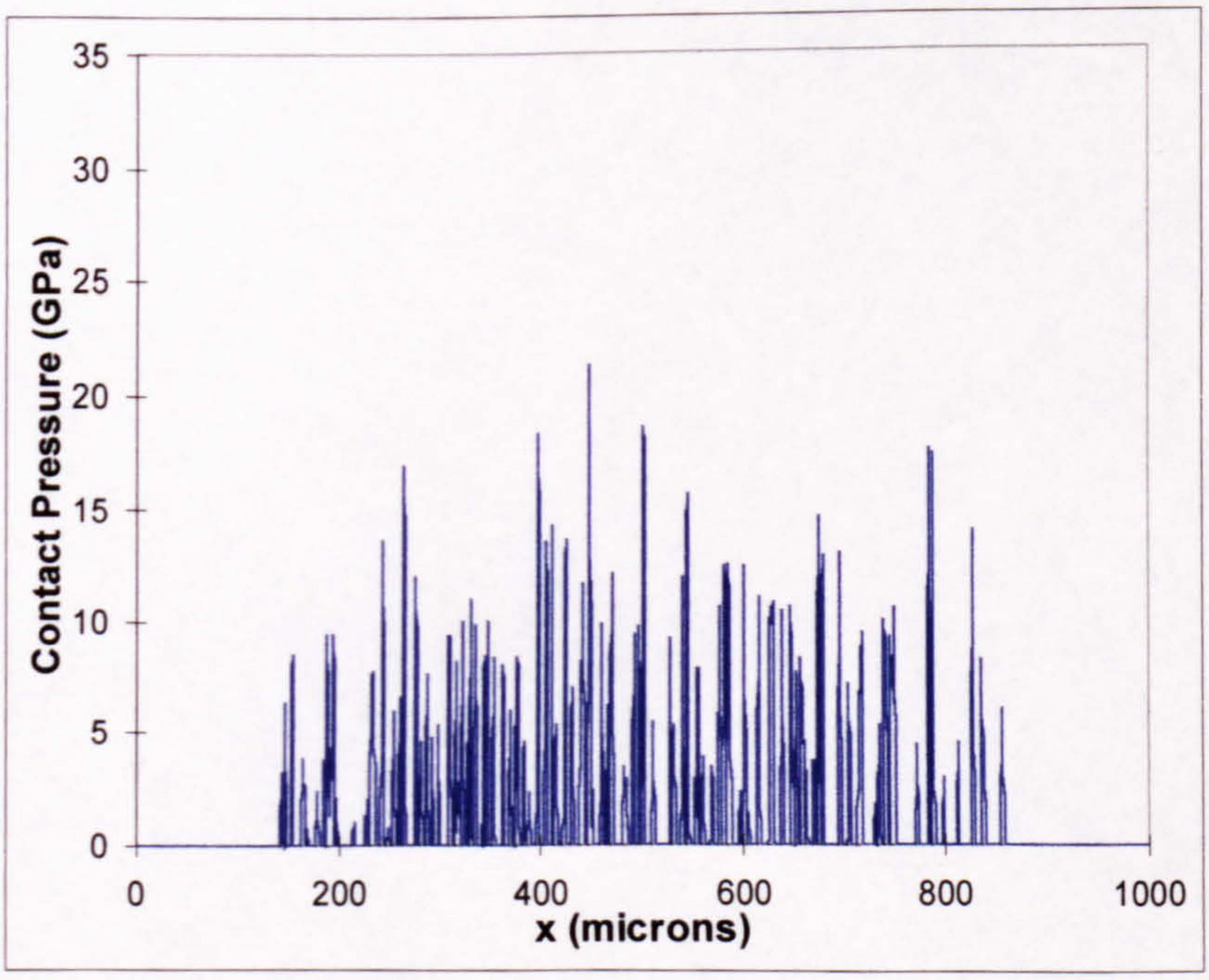


Figure 8.3.2 The Chamfered Barrel Surface Stress Distribution

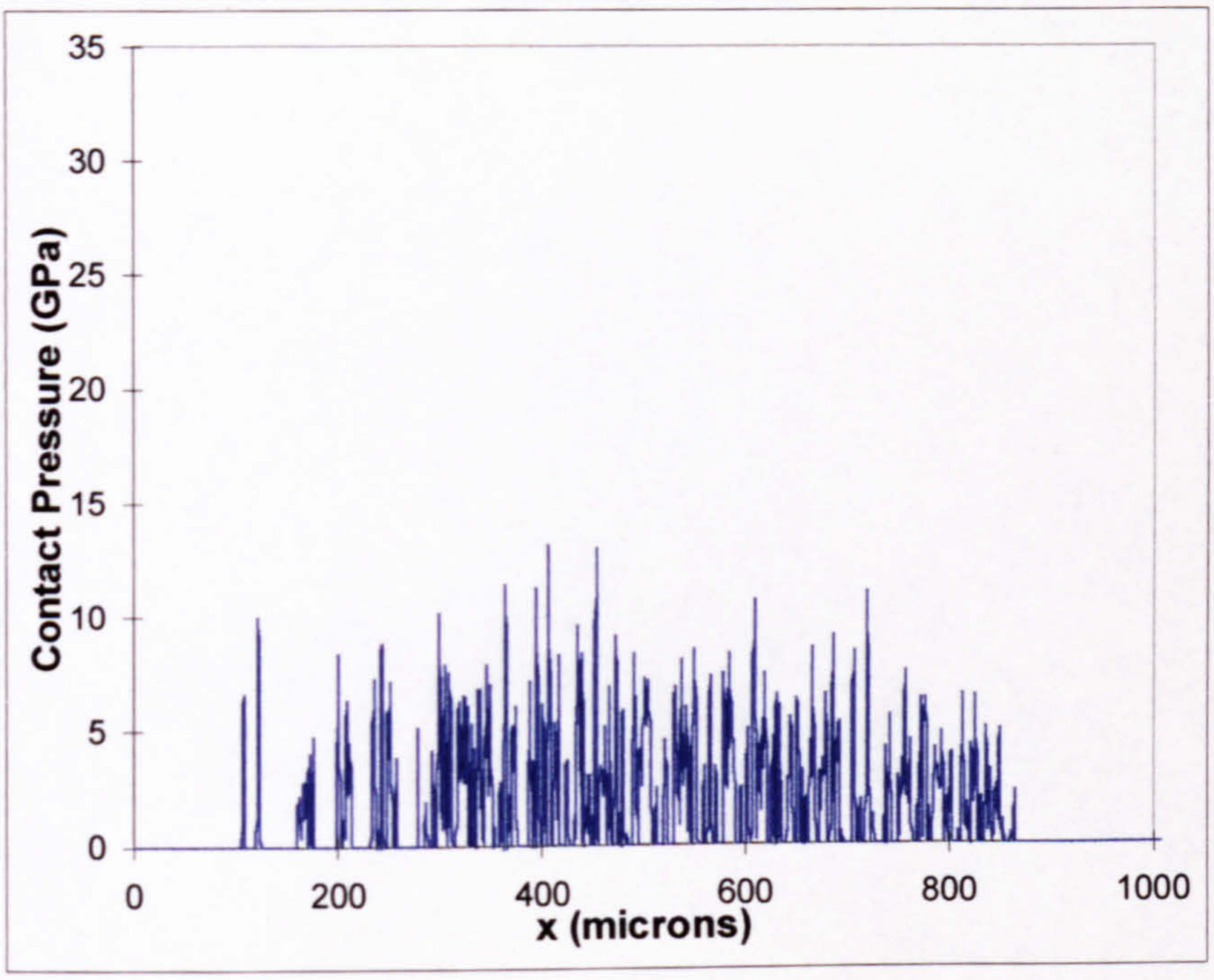


Figure 8.3.3 The Crowned Barrel Surface Stress Distribution

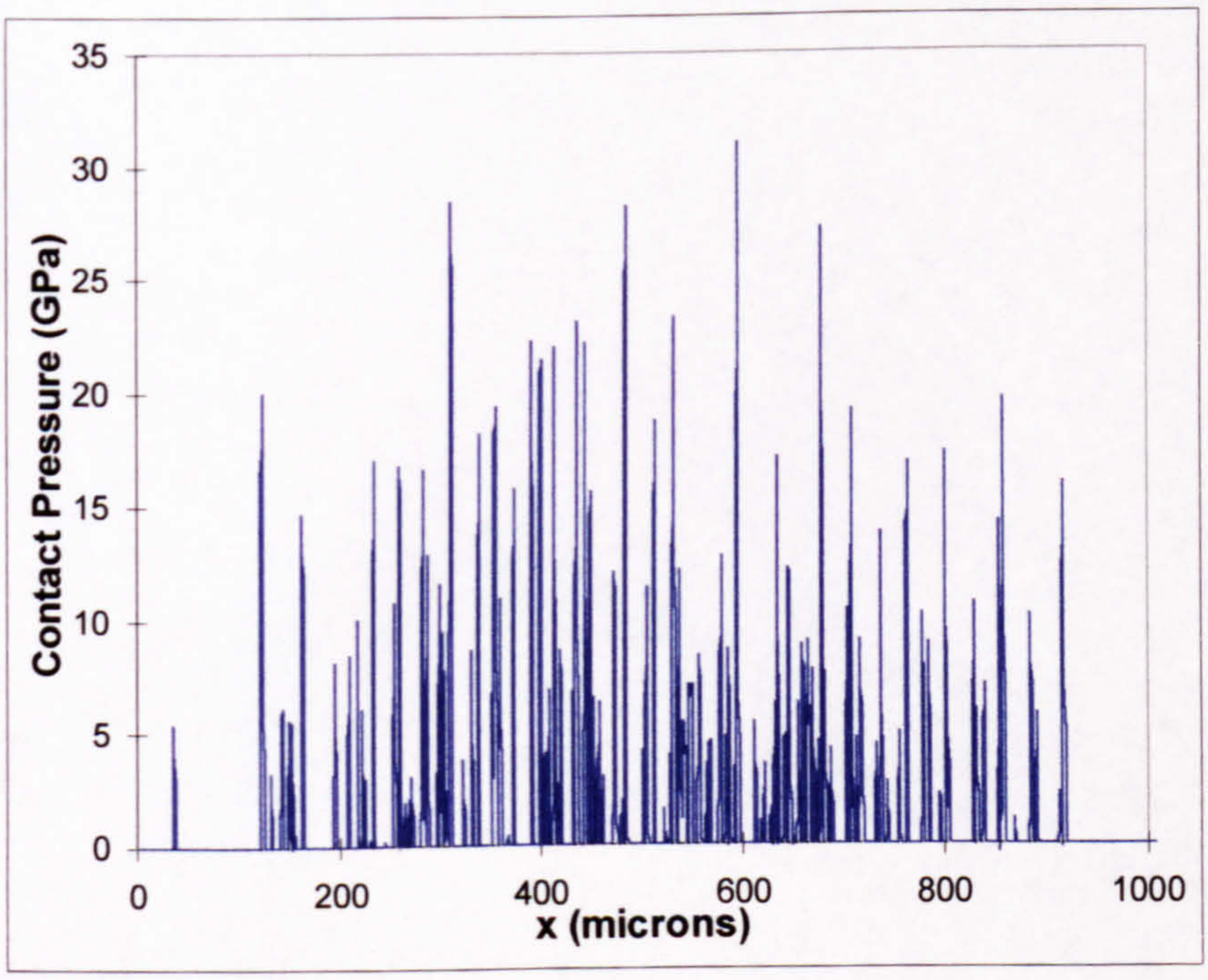


Figure 8.3.4 The Gear Surface Stress Distribution

These pressure distributions were then used with a model, developed by Bailey and Sayles (1991) and adapted by Kim and Olver (1997), to evaluate the orthogonal shear stress distribution for the components (as a ratio of the maximum Hertzian contact pressure, calculated for an equivalent smooth surface). Figure 8.3.5 shows the crowned barrel subsurface stress distribution and Figure 8.3.6 is a similar plot for the gear. Figure 8.3.7 shows the maximum value of orthogonal shear stress at each depth for each

specimen type, up to a depth of 20 μm where the influence of roughness is less significant. The higher subsurface shear stress distribution for the gear, when compared to the crowned specimen, may negatively affect the fatigue lives of the gears.

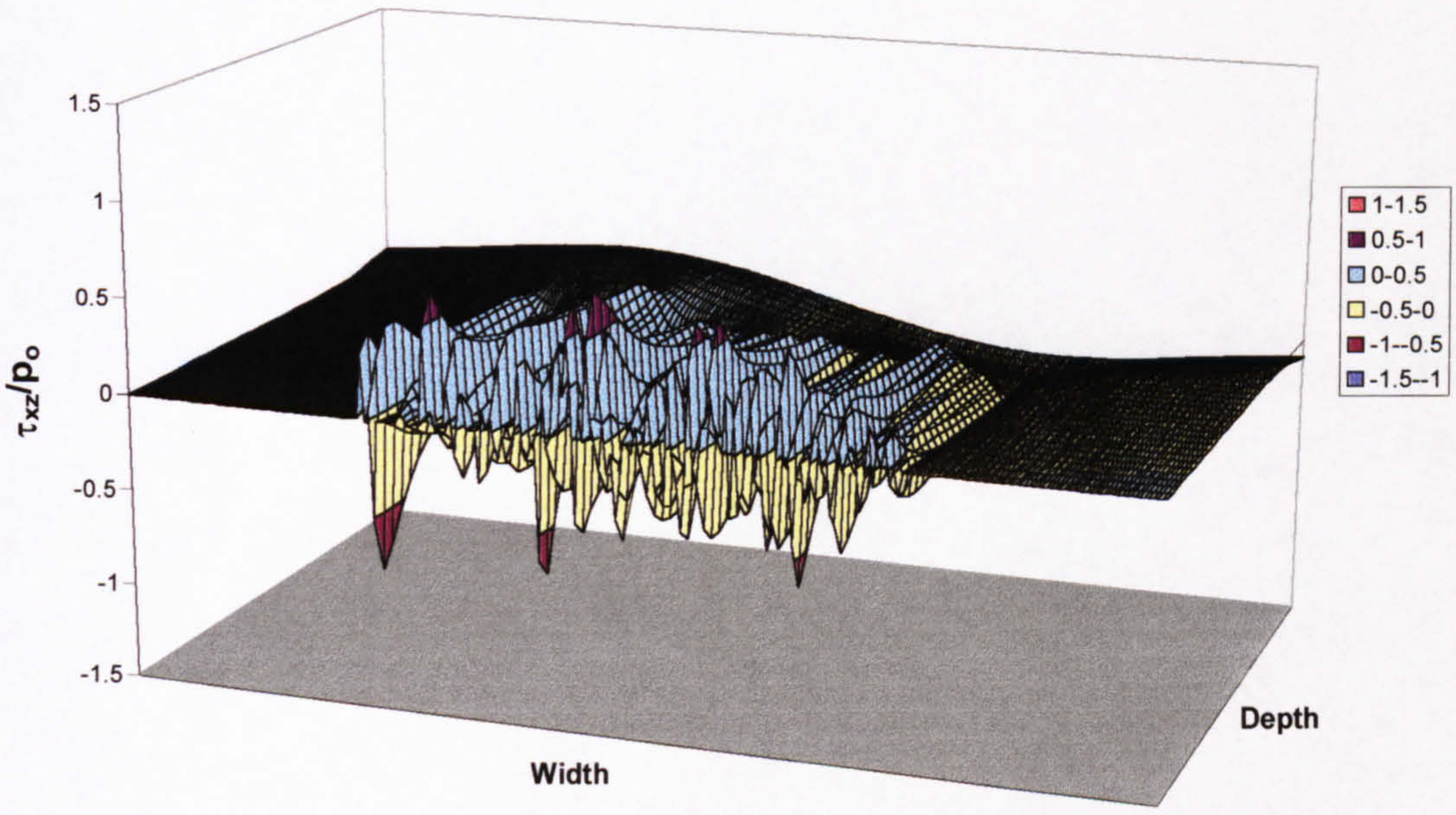


Figure 8.3.5 The Distribution of Orthogonal Shear Stress in the Crowned Disc

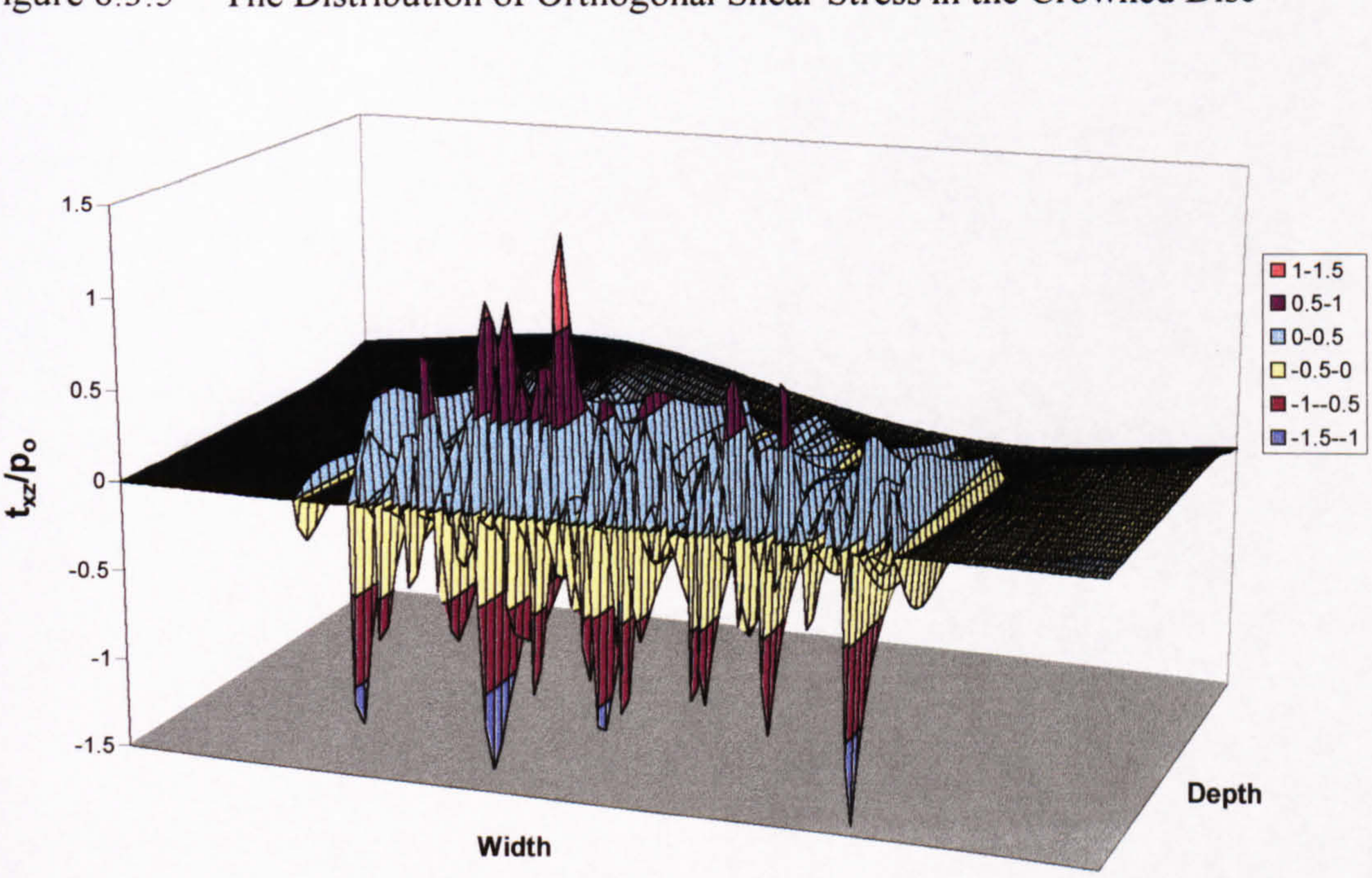


Figure 8.3.6 The Distribution of Orthogonal Shear Stress in the Gear

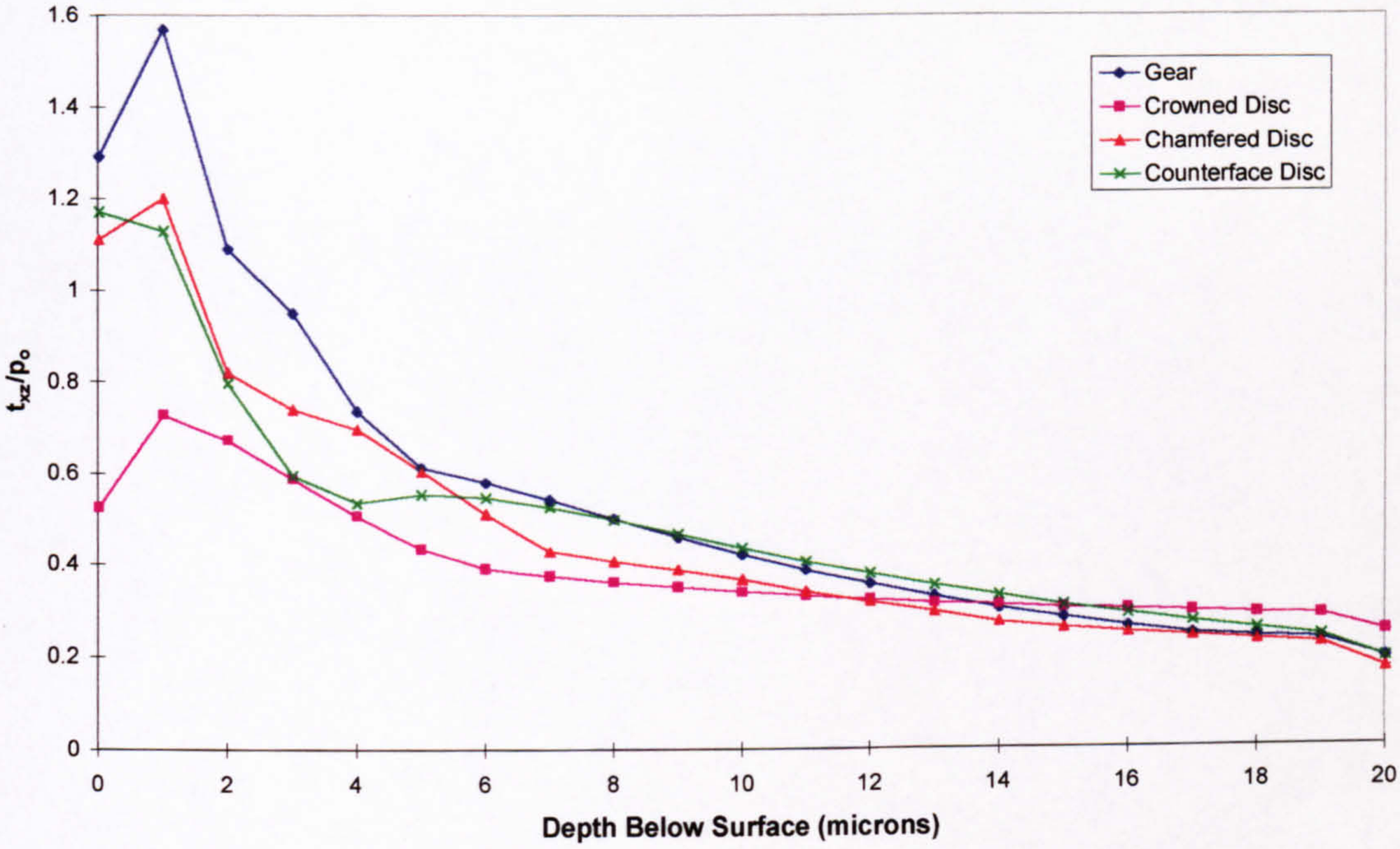


Figure 8.3.7 The Maximum Orthogonal Shear Stress at Each Depth for the Gear and Disc Specimens

The roughness parameters used to characterise roughness values for the different specimens and materials were given in Chapter 7, for both the gear and disc test specimens.

8.4 Stressed Volume

As mentioned in Chapters 3 and 6, when contrasting fatigue test results, the size factor should be considered for specimens of different shape or size. This parameter accounts for larger component having a greater probability of containing a crack of a certain critical length for fatigue crack initiation. The theoretical model for pitting life prediction of rolling bearings, given by Lundberg and Palmgren (1947), and described in Section 3.5.1, incorporates a stressed volume parameter.

$$\ln(1/S)=k(N^e \iota_o^c V)/z_o^h$$

where V is the stressed volume, S is the probability of surviving N cycles of load at a maximum orthogonal shear stress of ι_o. The exponents e, c, and h were determined experimentally as 10/9, 31/3, and 7/3 respectively; and the constant k was found to depend on material state, surface finish, and lubricant parameters.

The stressed volume, V, was given by,

$$V = az_oC$$

where a is the Hertzian contact half-width, z_o is the depth of maximum orthogonal shear stress, and C is the circular length of the bearing raceway.

This equation can be used in this form to calculate the stressed volume in the barrel specimen, but has to be modified for the gears, where the stress and radius of curvature vary through the meshing cycle.

For the gears it was assumed that, as the stress has a very important effect on fatigue life (as seen by the exponent c having a value of 31/3), only stresses above a certain value would influence the fatigue life. From Figure 8.2.9, it can be seen that the stresses drop considerably when there are two gear teeth in contact. Therefore, the portion of the gear contact where only one tooth was in contact was used as the critical length. This was then multiplied by the number of gear teeth to obtain the stressed volume.

The values of a and z_0 were calculated with a model developed by Kim and Olver (1997) to analyse subsurface stresses in rough bodies. Here, however, smooth surfaces were used, and a maximum Hertzian contact stress of 2.6 GPa and friction coefficient of 0.07 were applied to both specimens. The values obtained are quoted in Table 8.4.1 for the barrel specimens, and in Table 8.4.2 for the gears. For the chamfered test specimen, the edge effect was not considered in the analysis, and half the track width was used for a.

To get an approximate idea of the effects of stressed volume on the possible difference in life between gear and disc specimens, the equations below can be used (the subscript D is for disc, and G for the gear).

$$N \propto \left(\frac{1}{V}\right)^{\frac{1}{e}}$$

$$\frac{N_D}{N_G} = \left(\frac{V_G}{V_D}\right)^{\frac{1}{e}}$$

The exponent e was given as 10/9 for rolling bearings by Lundberg and Palmgren (1947). This is the slope of the Weibull plot for fatigue failures [log log(1/S) = e log(N)]. The value of e for the gear and disc fatigue tests conducted by the author was not 10/9, 3 is a more accurate value. Both values have been used for the results shown in Table 8.4.3.

Table 8.4.1 Barrel Stressed Volume (p_o = 2.6 GPa, μ = 0.07)

Parameter	Crowned	Chamfered
Contact half width, a (mm)	1.208	3.175
Depth max. Orthogonal shear, z_o (mm)	0.185	0.185
Diameter (mm)	18.593	18.593
Circumference (mm)	58.412	58.412
Stressed volume, V_D (mm^3)	13.058	34.310

Table 8.4.2 Gear Stressed Volume (p_o = 2.6 GPa, μ = 0.07)

Parameter	Gear
Contact half width, a (mm)	2.366
Depth max. Orthogonal shear, z_o (mm)	0.195
Relevant length of roll / per tooth (mm)	11.03
Number of gear teeth	17
Total length of roll relevant (mm)	187.51
Stressed volume, V_G (mm^3)	86.519

Table 8.4.3 Disc-Gear Lives for the Stressed Volumes Calculated

Parameter	Crowned		Chamfered	
V_G/V_D	6.63	6.63	2.52	2.52
e	1.11	3	1.11	3
N_D/N_G	5.48	1.88	2.30	1.36

The stressed volume is smaller for the disc specimens when compared to the gears, particularly the crowned barrels. As a result, the disc tests could have longer fatigue lives than the gears, for equivalent Hertzian contact stresses, and assuming all other parameters that influence fatigue life to be the same. From Table 8.4.3, the life of a crowned barrel specimen could be around 2 times that of a gear and that of a chamfered barrel 1.4 times that of a gear, at a contact stress of 2.6 GPa, all other factors being the same.

8.5 Residual Stress Distributions

Residual stress distributions, discussed in Chapter 5, are important in determining the fatigue life of a component (Seabrook 1946 and Mattson & Roberts 1959). The features of the distribution which can be of importance include the stress at the surface, the maximum compressive stress, the depth of the compressive layer, and the location and magnitude of the maximum residual tensile stress.

Compressive surface stresses can be enhanced by a process called shot peening, where the surface is bombarded by spherical, uniform sized, hard steel balls under controlled velocity. Shot peening is generally thought to improve the structural fatigue strength of metal components at the surface. The improvements result from a combination of strain hardening and the inducement of residual compressive stresses in the surface of the component. The effect of these residual stresses is to impede crack propagation. Seabrook (1946), in flexural fatigue testing of gears, found that shot peening was beneficial in all cases except that of shot peening a nitrided steel surface.

The type and velocity of the shot and relative hardness of the shot and specimen will be important in determining the residual stresses induced in the surface. It is standard practice to shot peen the root radii of highly stressed gears to improve the tooth bending fatigue strength. Many gears in helicopter transmissions are treated this way. This was not the case for the gears and discs used in this study.

The residual stress measurements for the axial fatigue test specimens, discussed in Chapter 7, were measured at GKN Westland Helicopters. Figure 8.5.1 shows the effect on the residual stress distribution of duplex treating (nitriding) AISI M50NiL. The negative stresses indicate compressive stresses. Figure 8.5.2 shows the effect of shot peening M50NiL, the number is the size of the shot in ten-thousands of an inch (110H and 230H are 0.0110 and 0.0230 inches respectively).

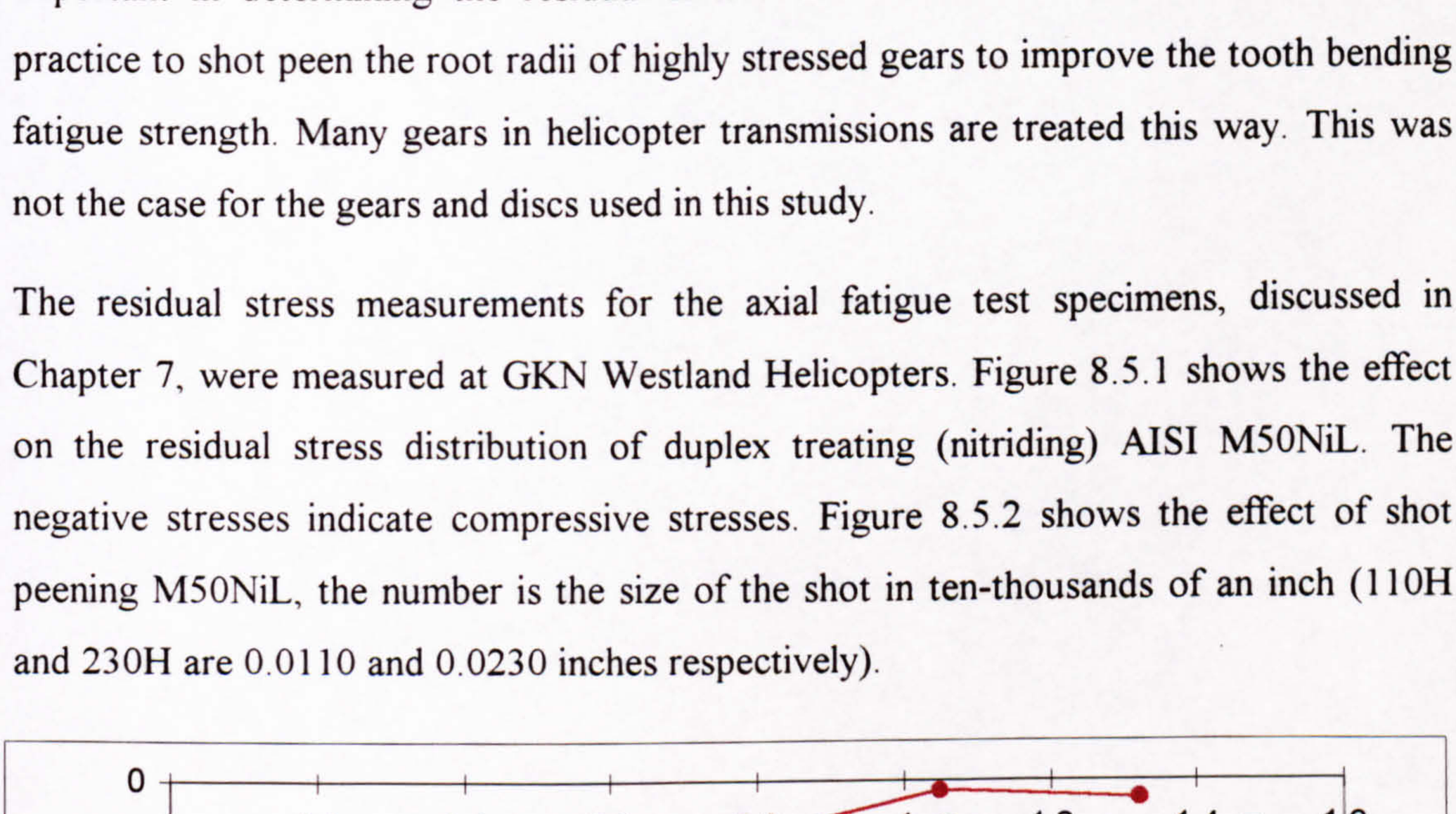


Figure 8.5.1 X-Ray Residual Stress Profiles Comparing AISI M50NiL and M50NiL Duplex and Shot Peening

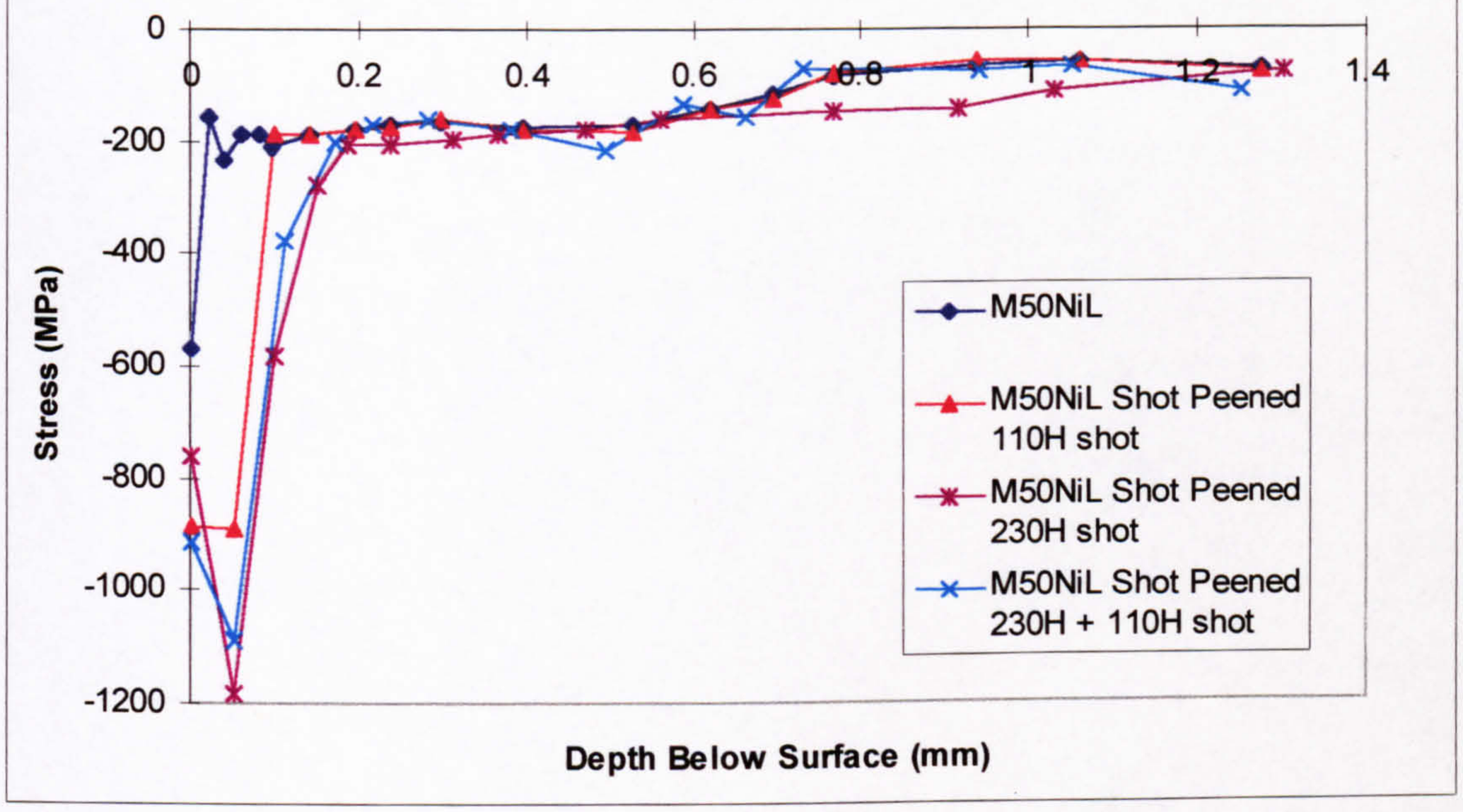


Figure 8.5.2 X-Ray Residual Stress Profiles for AISI M50NiL with Various Shot Peening Treatments

The residual stress was also measured on the surface of a few carburised BS S156 gears, as shown in Table 8.5.1.

Table 8.5.1 BS S156 Gear Residual Stress Measurements at the Surface

Component	Residual Stress MPa
Tip Relieved Virgin	-499
Tip Relieved Pitted	-387
Tip Relieved Pitted	-405
Non-Tip Relieved Micropitted	-264

8.6 Conclusions from the Stress Analysis

This chapter has dealt with the stress analysis of both test rigs, to determine any differences that might arise between them.

- The crowned barrel has a theoretically elliptical contact area, the chamfered barrel a line contact. The chamfered barrel has a stress concentration at the track edge.

- The gear specimens had a more complex loading analysis than the discs, but also have an elliptical contact area. However, the load can be shared by two pairs of teeth or all on one pair, and the radius of the teeth along the meshing cycle also changes. This will give rise to varying contact stresses and contact dimensions through the tooth meshing cycle.

- A computer model was developed to find the load sharing characteristics and effects of extended contact in spur gears. It showed that non-tip-relieved gears could suffer extended contact, due to the elastic deflection of the gear teeth, which may damage the root. The contact pressure would increase, and the contact width would expand at points were extended tooth pair contact occurred.

- A simple dynamic load analysis to find K_v gave a value of 1.05, indicating that dynamic loads would not contribute excessively to the gear loading.

- A theoretical analysis of a simplified model of the gear rig showed that it would not be operating near the natural frequencies of the system and that the slave gears were isolated from the test gears.

- The gear surface produced higher surface contact pressure and higher subsurface shear stress distributions than both the crowned and chamfered disc. This may give the gears a shorter fatigue life.

- The stressed volume is smaller for the disc specimens when compared to the gears, particularly the crowned barrels. As a result, the disc tests could have longer fatigue lives than the gears, for equivalent Hertzian contact stresses, and assuming all other parameters that influence fatigue life to be the same.

- The residual stress distribution showed that duplex treatment by nitriding AISI M50NiL would appear to improve the residual compressive stresses near the surface. This could help reduce fatigue damage.

Chapter 9 Thermal Analysis

As mentioned in Chapter 6, one of the distinguishing features between gear and disc tests was that they may not be thermally equivalent to gears. The two types of specimens would then have different bulk temperatures. This is important because the minimum film thickness and friction in EHD contacts are controlled by viscosity at the inlet to the contact, and this is likely to be at a temperature close to that of the bulk temperature of the rubbing bodies. The film thickness will affect the friction and heat generated and therefore the bulk temperature, and this in turn will affect the inlet viscosity. All these properties will affect the operating performance of the test piece. It was therefore thought important to carry out a thermal analysis on the gear test rig, in which gear tooth temperatures were measured experimentally and compared to values obtained for the disc rig. This chapter contains a description of the gear temperature measurement experiments, a discussion of the results obtained using heat partition theory, the disc temperature measurements, and a flash temperature analysis. Results from this thermal analysis will be used in the discussion of the gear and disc fatigue test results in Chapter 13.

9.1 Gear Temperature Measurements

A tip-relieved gear was mounted in the test chamber, with thermocouples embedded at various heights along a gear tooth (Figure 9.1.1). These thermocouples were connected to a slip ring arrangement (Figure 9.1.2), which allowed the signals to be recorded by a computer and monitoring program, that sampled the gear temperatures at roughly one second intervals. An infrared sensor, which was also used to allow a comparison between the measurement techniques, was mounted pointing at one of the gears, directed so as to see most of the tooth surface.

The temperature readings were recorded as the load was gradually increased (Figure 9.1.3). The numbers 1, 2, 3, and 4 in the chart correspond to the holes in the gear tooth in which the thermocouples were placed, 1 being the hole closest to the gear tooth tip.

It would appear that the infrared measurement gave higher temperature readings than the thermocouples. This seems logical as it was pointed at the surface and, therefore,

obtained surface temperatures, as opposed to the thermocouples that were relying on heat conducted into the gear tooth by a thermal gradient. The thermocouple deep in the gear tooth base (4) always gave the lowest temperature reading and had a slower response time to changes in load. This time lag was probably due to the heat having to conduct further into the gear tooth. Of the other temperatures it would seem that position 3 started hottest but then was caught up and overtaken by 1 and 2 at higher loads, 2 having initially caught up with 1.

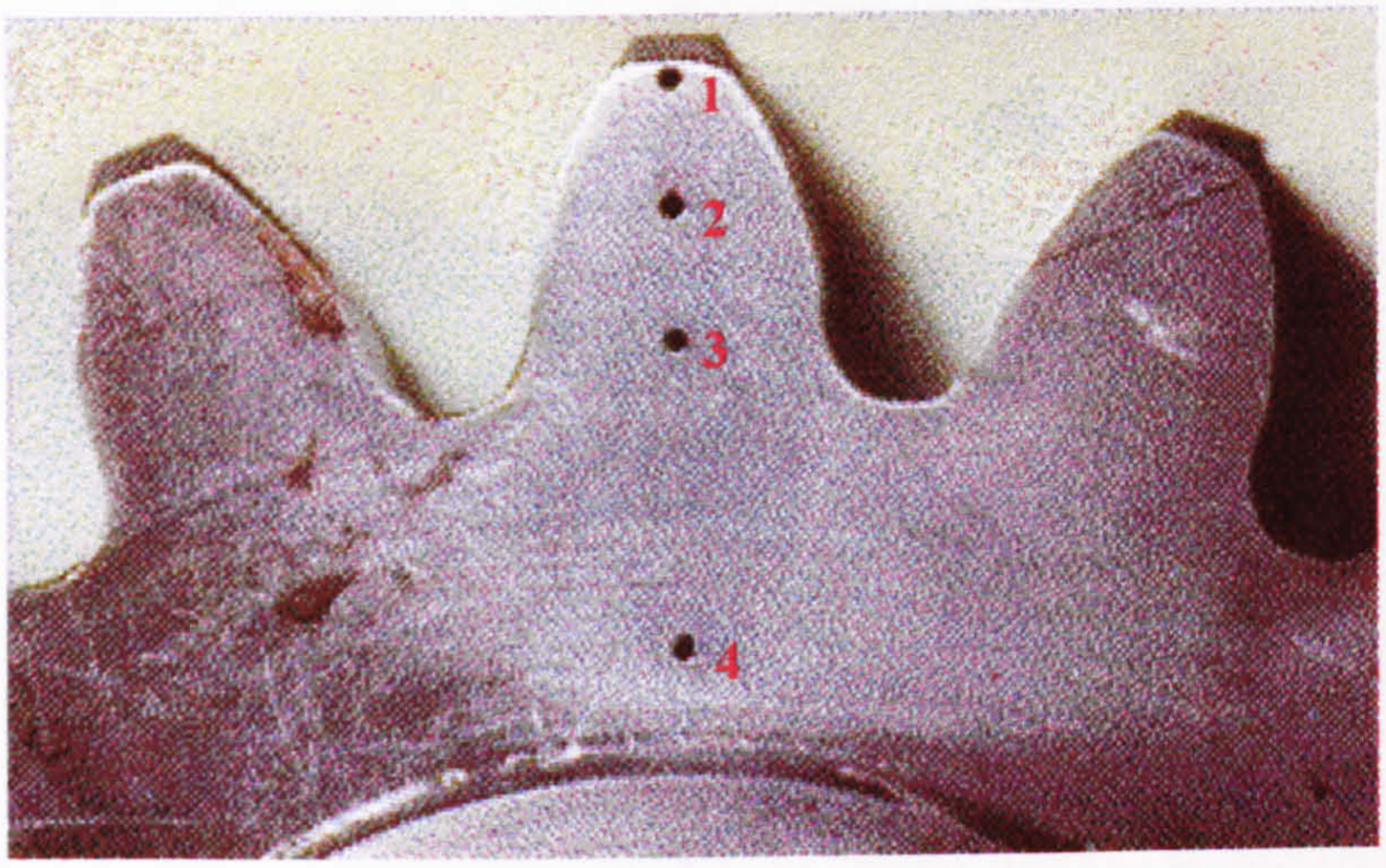


Figure 9.1.1 Location of the Holes for Thermocouples in the Gear Tooth

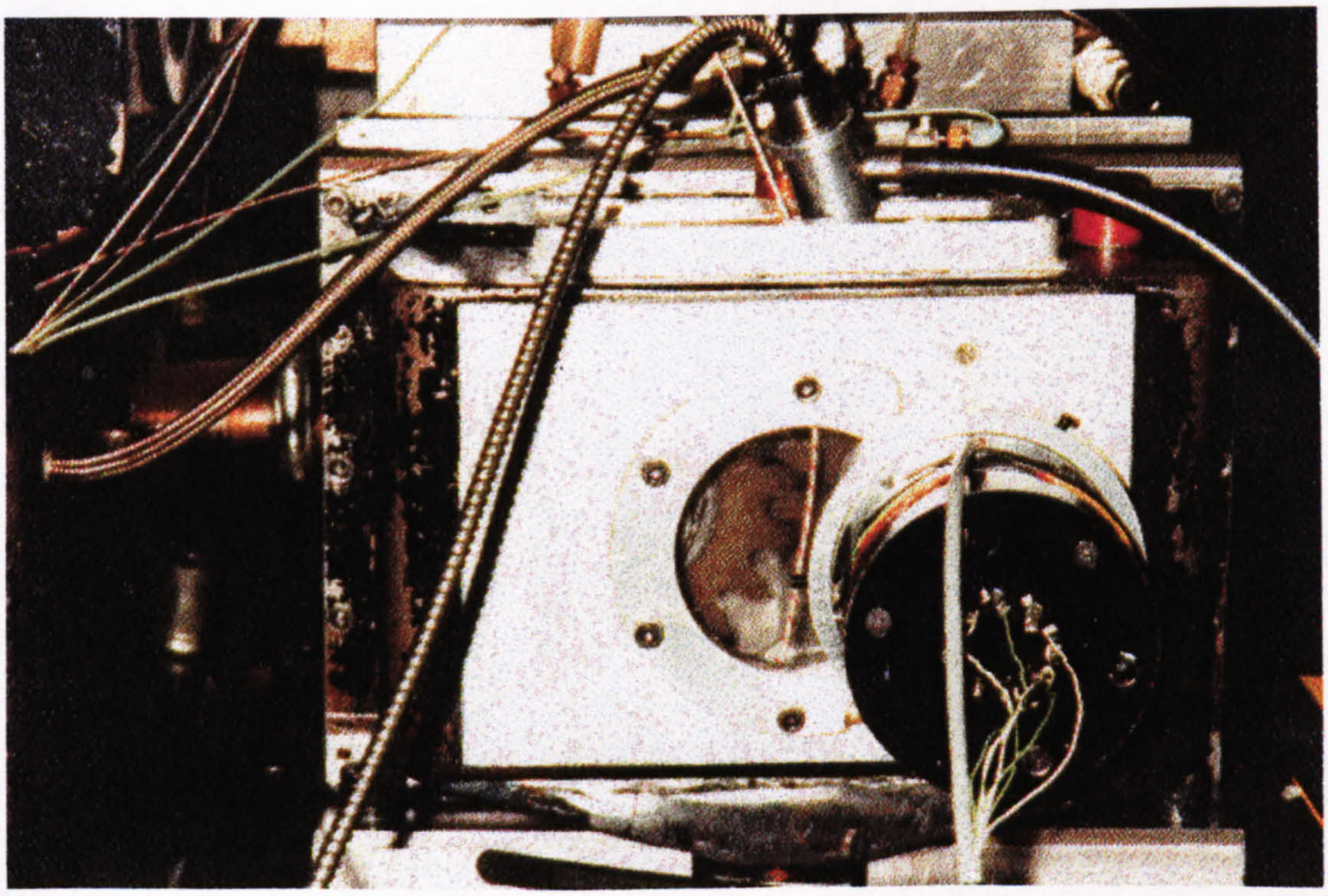


Figure 9.1.2 The Temperature Measurement Set-up on the Gear Rig

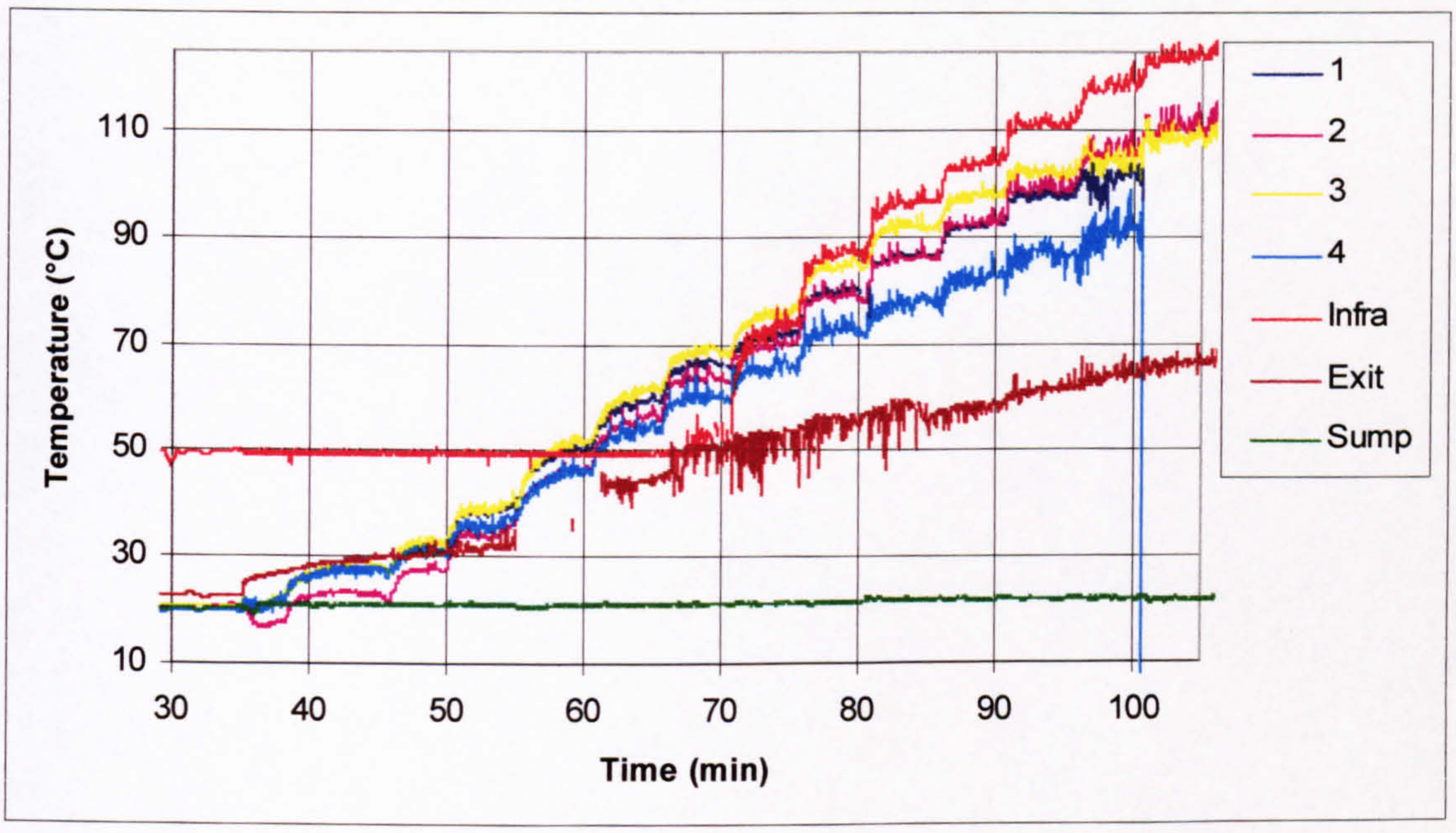


Figure 9.1.3 Gear Tooth Temperature Variation with Time (Increasing Torque Steps)

9.2 Heat Partition Theory

If we now consider heat partition theory, we can attempt to explain the results obtained. The rate of heat generation is given by:

$$\dot{q} = \mu W \Delta V$$

where μ is the coefficient of friction between the mating gear teeth, W is the contact load, and ΔV is the sliding speed. To determine how this generated heat flows out of the contact into the surroundings, we assume that it is conducted into the mating bodies and is then convected into the surroundings by the temperature gradient in the body. When we consider the presence of a lubricant film separating the surfaces in the contact, as in EHD lubrication, we can assume it behaves as a solid, with all the slip occurring on one plane, if the load and sliding are great enough to cause limiting shear stress friction. We can also assume the heat stored in the lubricant is negligible, if the contact is large and the film thin.

With these assumptions, one can determine the heat partition coefficient, α, which is the ratio of the amount of heat generated going to each body in the contact. By modifying the Jaeger moving hot spot equation (Carlslaw & Jaeger 1959) and correcting it for the presence of a film, we obtain an expression for the heat partition coefficient:

$$\alpha = \frac{1.06B_2 + (\frac{\beta h}{k_{oil}A}) + M_2}{1.06(B_1 + B_2) + (\frac{h}{k_{oil}A}) + (M_1 + M_2)}$$

where h is the lubricant film thickness, k is the conductivity, β defines the ratio of lubricant film adhering to each body (dependent on where the film shears), M is the steady state thermal resistance of bodies 1 and 2, and B is an expression taking into account the contact speed and area, material conductivity, and specific heat.

By assuming that the lubricant film sheared in the middle and the thermal resistance, M, was the same for the two bodies, the heat partition coefficient for the gears was calculated, and is shown in Figure 9.2.1. It is important to realise that the left of the chart, where the path of contact values are small, corresponds to the root of gear 1 and the tip of gear 2. What is apparent from this graph is that at the lower load, or more importantly temperature, the heat partition coefficient is fairly uniform across the tooth contact, with roughly half the heat generated going into each surface. However, if we now look at the higher load, or temperature, the heat partition coefficient varies considerably across the contact with the heat partition being less than half in the root and more than half in the tip. The faster moving surface tends to have the higher heat partition coefficient, so that more of the heat generated goes to this surface.

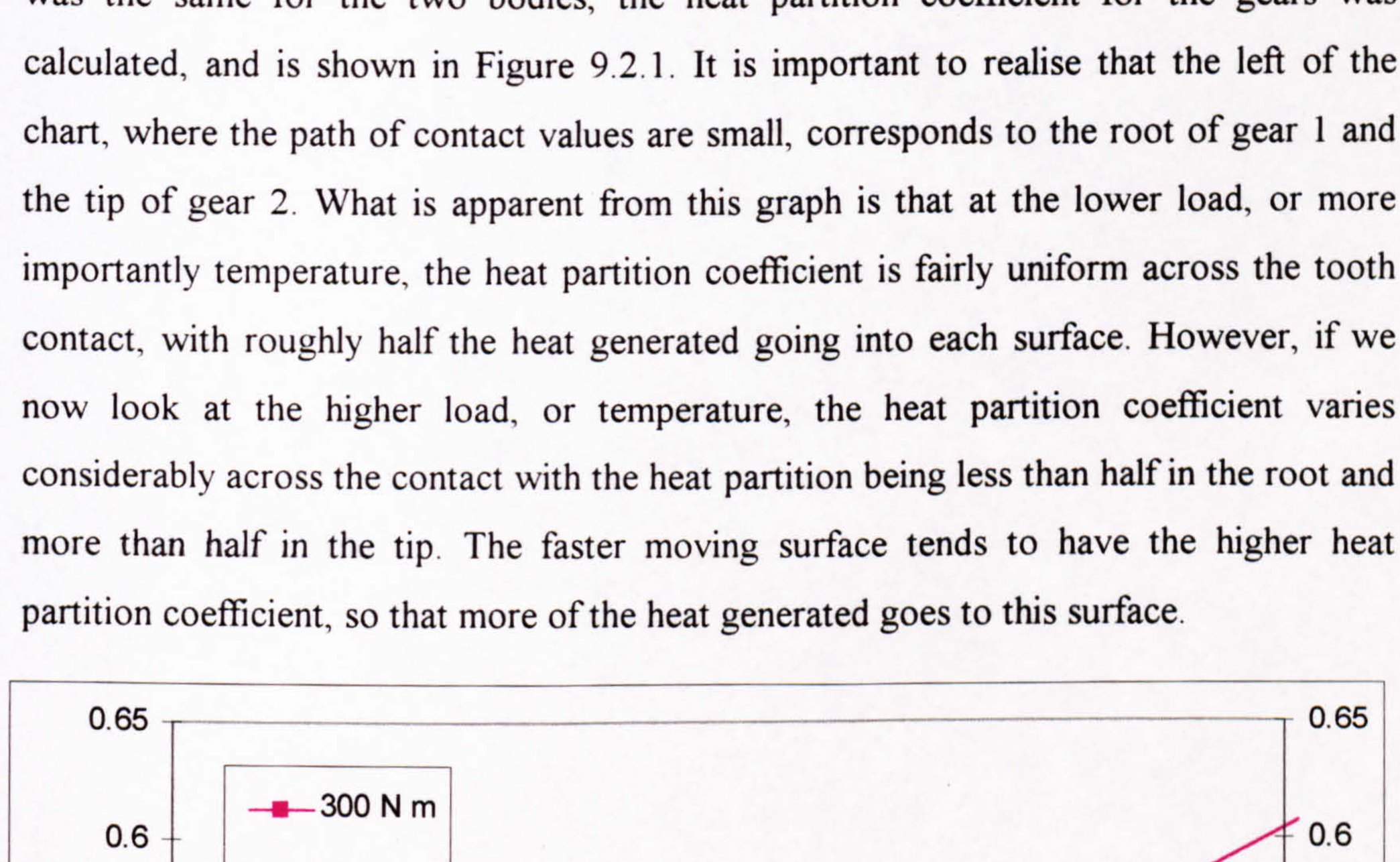


Figure 9.2.1 Variation of the Heat Partition Coefficient Along the Gear Path of Contact

If we plot the instantaneous rate of heat conducted into the gears by assuming a value of coefficient of friction between the gear teeth, as shown in Figure 9.2.2, we can see that for the faster body at high temperature the heat conducted is greater than the slower surface but at lower temperatures this is no longer the case.

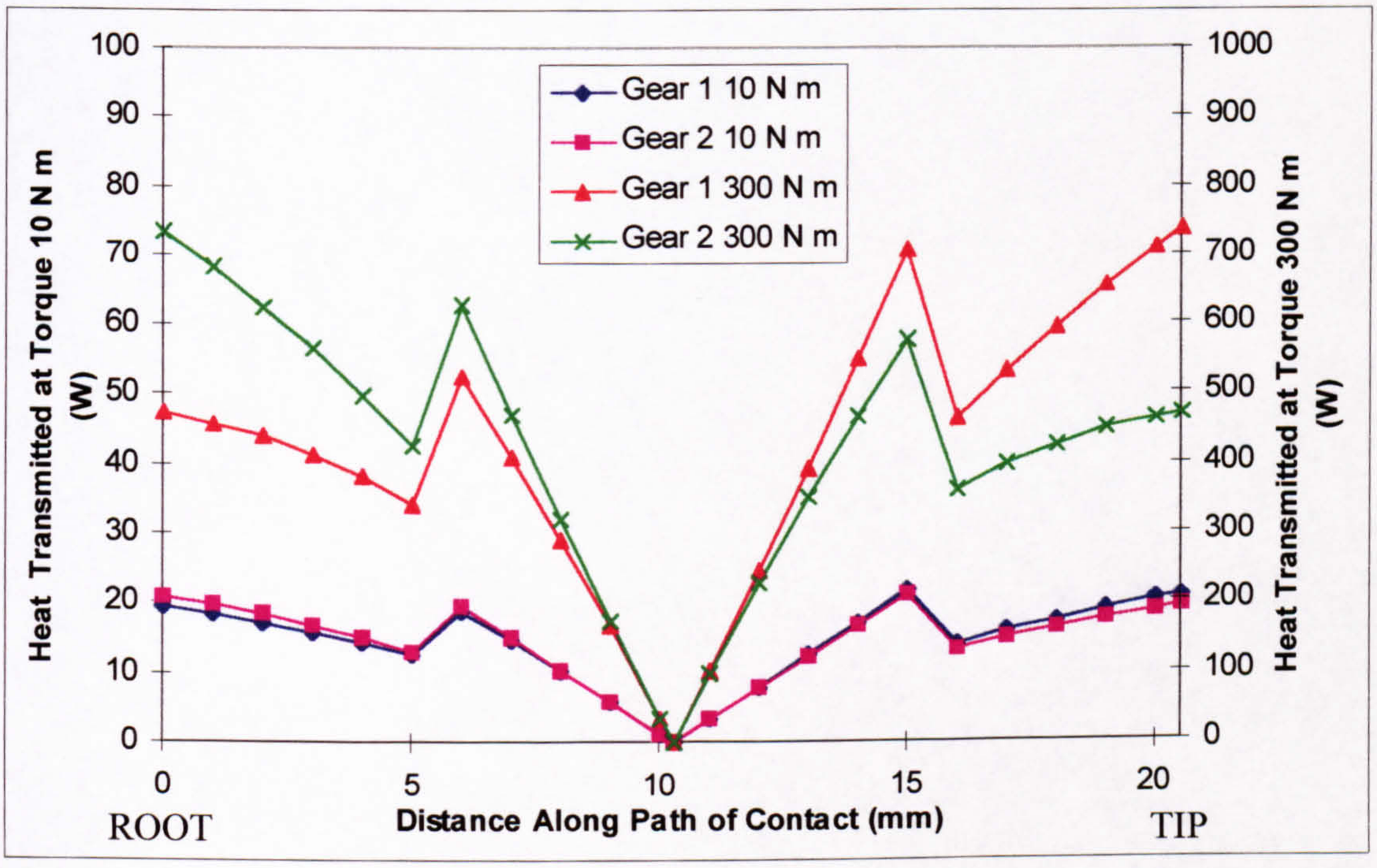


Figure 9.2.2 The Instantaneous Rate of Heat Conducted into the Gears ($\mu = 0.07$)

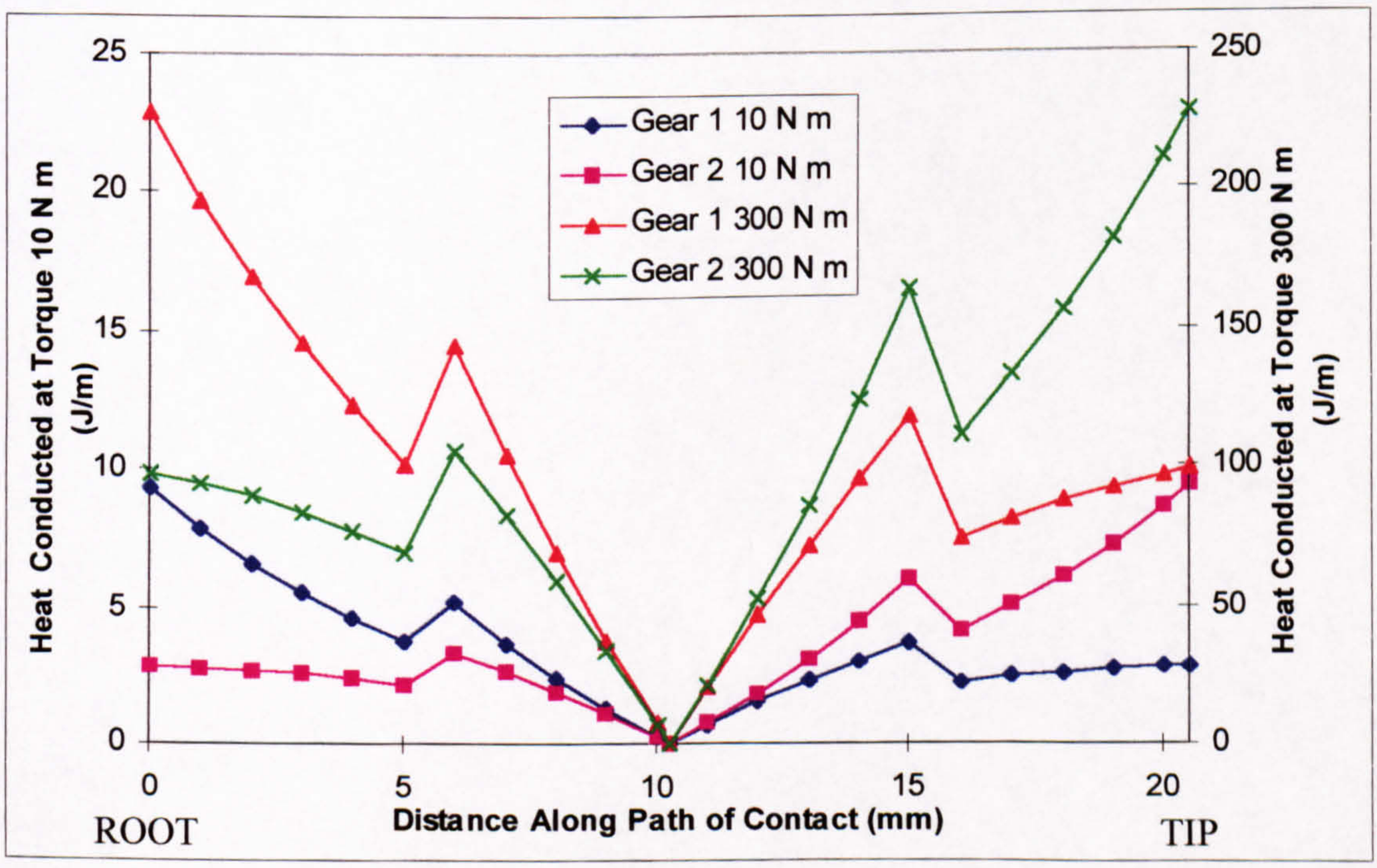


Figure 9.2.3 The Heat Conducted into the Gears per Unit Length per Revolution (μ=0.07)

However, this does not give the complete picture, as the instantaneous rate of heat conducted in the bodies shown in Figure 9.2.2 does not take into account that, although the rate of conduction is greater in the faster body, the contact is also sweeping across this body faster than the mating body. If we now calculate the heat conducted into the bodies per unit width per revolution we obtain a different picture, as shown in Figure 9.2.3. The slower body is actually taking in a greater amount of heat per unit area because it is moving more slowly, even though its heat partition coefficient may be less than 0.5. If we now plot this chart as a percentage of the maximum value of heat conducted we obtain the chart displayed in Figure 9.2.4.

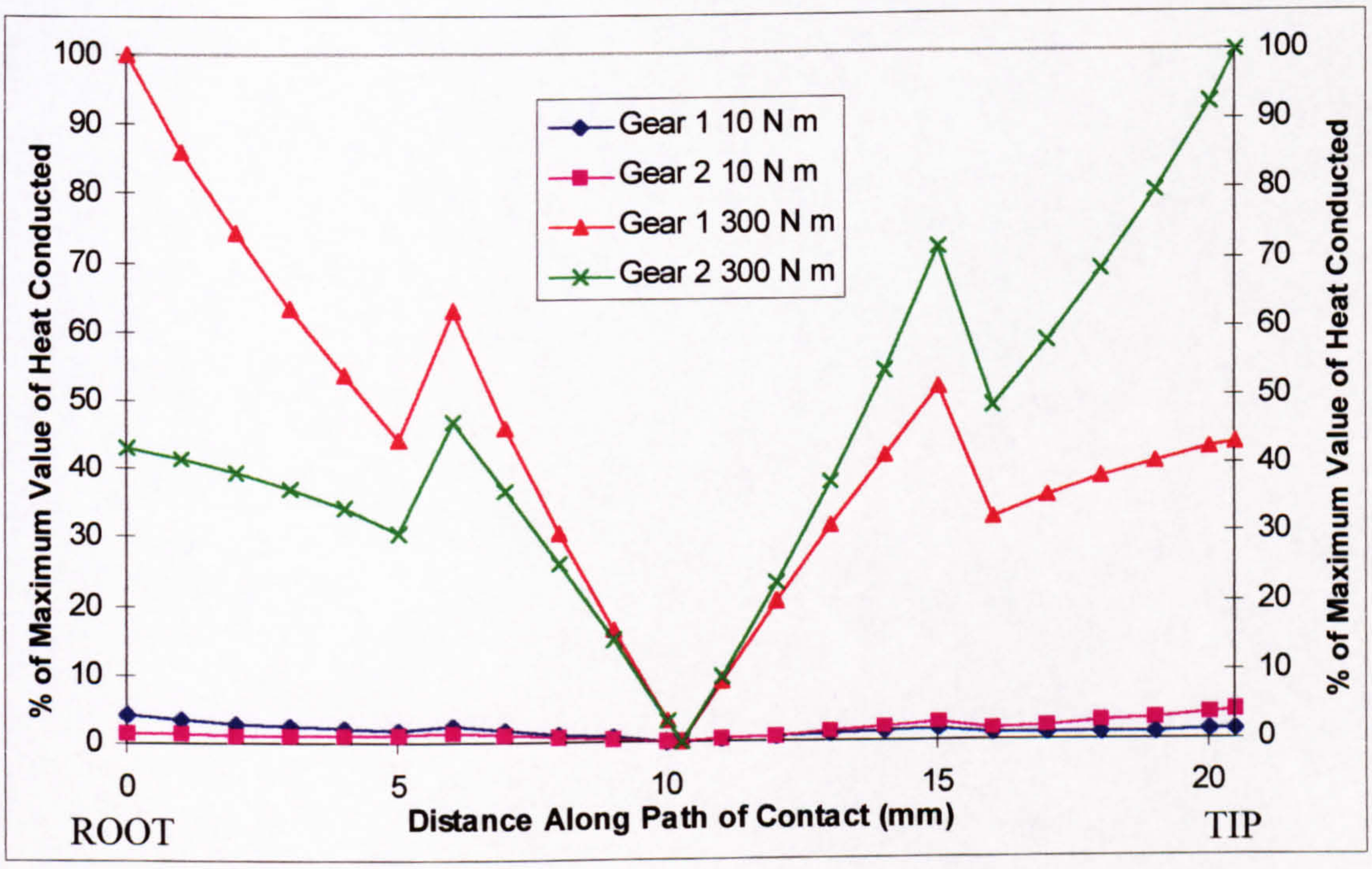


Figure 9.2.4 Heat Conducted into the Gears per Unit Length per Revolution as a Percentage of the Maximum Value

The outcome of the effects of heat partition, load, and contact speed on the gear tooth temperature are, therefore, difficult to predict. An iterative computer model should probably be used (Olver 1994) due to the complexity that the analysis entails. The analysis presented here, however, may help explain how temperature 'cross-over' (temperatures changing at different rates at different points) can occur as gear teeth are loaded (as shown by thermocouple readings 2 and 3 presented in Figure 9.1.3). Another example is shown in Figure 9.2.5 for disc tests. The faster disc is initially colder than the slow one at low loads, because its thermal diffusivity is greater and it is probably receiving only half the heat generated. At the higher loads, the temperature increases and the faster disc becomes hotter than the slow one because it now has a heat partition

coefficient greater than half. The faster disc takes in more heat than the slower disc and, because of the discs' geometry of unbroken contact, this heat raises the bulk temperature above that of the slow disc.

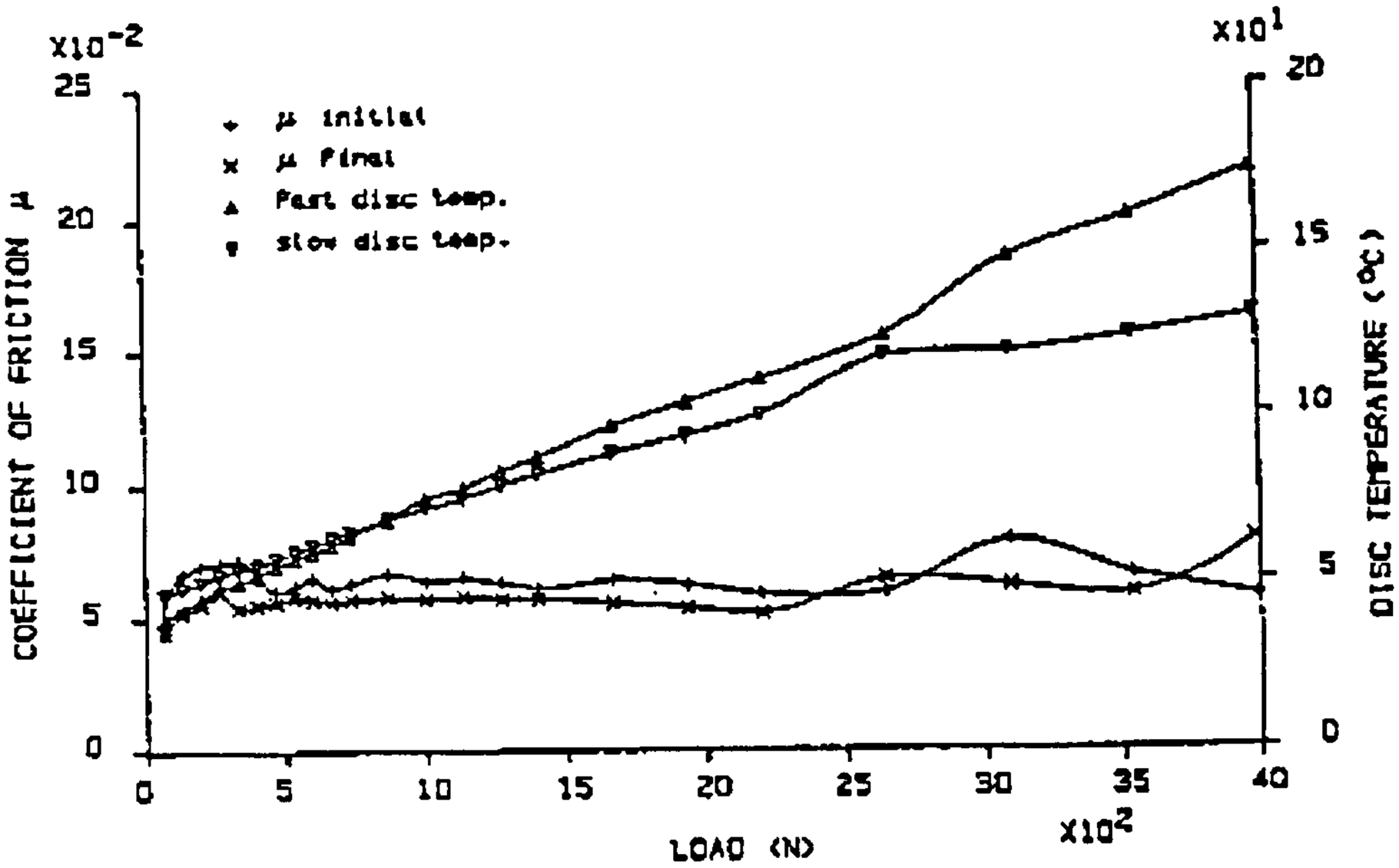


Figure 9.2.5 An Example of Temperature 'Cross-Over' in a Disc Contact (Paliwal & Snidle 1987)

9.3 Disc Temperature Measurements

A higher temperature is expected in the barrel than the rings. This is because this specimen has less time to cool due to its low out of contact time, the three heat inputs per revolution, and its relatively small mass. With three discs, high loads, and high slide-roll ratios, large temperature rises can be expected.

The disc test temperatures will depend on the slide-roll ratio used, increasing with increasing slide-roll ratio. Graham (1979) measured the temperature of the chamfered barrels and rings described in Chapter 7 with spring loaded trailing thermocouples. The barrel and ring temperatures were measured at 60° and 90° from the contact respectively, for slide-roll ratios of -0.026 and -0.28. These values, quoted in Table 9.3.1, were used by the author to calculate the specimen temperatures at the -0.14 slide-roll ratio and to estimate the mean bulk temperatures at the contact inlet for a Hertzian contact stress of 2.6 GPa. The bulk temperatures at the contact inlet were estimated with the equation:

$$T_{BULK} = \left[\frac{T_B V_B + T_R V_R}{V_B + V_R} \right]$$

where T_B and T_R are the temperatures and V_B and V_R are the speeds, of the barrel and ring specimens respectively.

Inlet temperatures of 91, 116 and 128 °C were calculated for a Hertzian contact stress of 2.6 GPa at slide-roll ratios of -0.026, -0.14 and -0.28 respectively. Slightly lower temperatures were estimated for the crowned specimens (Table 9.3.2). From these results, it can be seen that the estimated bulk temperature of the discs and the actual barrel temperature at a slide-roll ratio of -0.28 are much higher than that of the gears for equivalent contact stress.

Table 9.3.1 Specimen Temperature at -0.026 and -0.28 Slide-Roll Ratio, Measured by Graham (1979) and the Estimated Temperature at -0.14 and the Bulk Temperatures at the Contact Inlet (p_o = 2.6 GPa)

	Slide Roll Ratio		
Specimen Temperature °C	-0.026	-0.14	-0.28
Chamfered Barrel, T_B	106	153.1	188
Ring, T_R	78	87.8	95
Bulk, T_{BULK}	92	116	128

Table 9.3.2 Summary of the Estimated Bulk Temperatures for the Fatigue Tests

Specimen	Slide-Roll	Contact Stress GPa	Temperature °C
Gear	Variable	2.6	102
Disc Chamfered	-0.026	2.6	91
Disc Chamfered	-0.14	2.6	116
Disc Chamfered	-0.28	2.6	128
Disc Crowned	-0.026	3.95	88
Disc Crowned	-0.14	3.95	111

9.4 Flash Temperatures

Blok's flash temperature criterion (Blok 1937) has been widely used as an aid to predicting scuffing. This predicts that, for a given material-lubricant combination, scuffing occurs when the maximum instantaneous surface temperature in the contact reaches a critical value. The temperature in the contact, T_C, is the sum of the bulk temperature, T_{BULK}, and the flash temperature rise due to frictional heating, ΔT_F.

$$T_C = T_{BULK} + \Delta T_F$$

This is not a reliable method as both μ and T_{BULK} are hard to obtain accurately, and it does not predict the scuffing performance for lubricants containing EP additives. It has, however, been used here to compare the gear and disc specimen temperatures.

As mentioned earlier, the rate of heat generation in the contact is given by

$$\dot{q} = W\mu|V_2 - V_1|$$

where W is the load, and V' is the surface speed.

Then, using Jaeger moving hot-spot theory (Carlslaw & Jaeger 1959), the speed of the contact on each surface must be calculated. For a high speed surface contact,

$$\beta = \frac{Vb}{2\chi} > 5$$

$$\chi = \frac{K}{\rho\sigma}$$

where b is the contact half-width, K is the thermal conductivity, and σ is the specific heat. The gear and disc contacts are all high speed for both contacting surfaces.

For line and square contacts the average, T_{fa}, and maximum, T_{fm}, flash temperatures are given by:

$$T_{fa} = \frac{1.064\dot{q}}{AK}\left(\frac{\chi b}{V}\right)^{0.5}$$

$$T_{fm} = \frac{2\dot{q}}{AK}\left(\frac{2\chi b}{\pi V'}\right)^{0.5}$$

where A is the contact area.

Assuming the heat is divided between the surfaces in proportions determined by the heat partition coefficient, α, then the following can be assumed:

$$T_{fa1} = 1.064\frac{\alpha\dot{q}}{AK_1}\left(\frac{\chi_1 b}{V_1}\right)^{0.5}$$

$$T_{fa2} = 1.064\frac{(1-\alpha)\dot{q}}{AK_2}\left(\frac{\chi_2 b}{V_2}\right)^{0.5}$$

$$\alpha = \frac{\frac{1}{K_2}\left(\frac{\chi_2 b}{V_2}\right)^{0.5}}{\frac{1}{K_1}\left(\frac{\chi_1 b}{V_1}\right)^{0.5} + \frac{1}{K_2}\left(\frac{\chi_2 b}{V_2}\right)^{0.5}}$$

This expression can be substituted into the equation for maximum flash temperature, to give:

$$T_{fm1} = \frac{2(2b/\pi)^{0.5}(\dot{q}/A)}{(V_1\rho_1\sigma_1 K_1)^{0.5} + (V_2\rho_2\sigma_2 K_2)^{0.5}}$$

$$T_{fm1} = \frac{1.128(W/A)|V_1 - V_2|(2b)^{0.5}}{(V_1\rho_1\sigma_1 K_1)^{0.5} + (V_2\rho_2\sigma_2 K_2)^{0.5}}$$

This equation was used with the material properties quoted in Table 9.4.1 to calculate the maximum flash temperatures for the chamfered barrel (Table 9.4.2), crowned barrel (Table 9.4.3), and gear specimens (Table 9.4.4), at a Hertzian contact pressure of 2.6 GPa.

Table 9.4.1 The Material Properties for the Flash Temperature Calculations

K (W/m K)	52
ρ (kg m^{-3})	7850
σ (J/kg K)	460
μ	0.07

Table 9.4.2 The Flash Temperature Calculation for the Chamfered Disc at 2.6 GPa

Slide-Roll Ratio	-0.026	-0.14	-0.28
R_B (mm)	9.297		
R_R (mm)	41.466		
N_B (rev/min)	5060	4000	3000
N_R (rev/min)	1200		
V_B (m s^{-1})	4.926	3.894	2.921
V_R (m s^{-1})	5.211		
h (mm)	0.359		
β_B	61.5	48.6	36.4
β_R	65.0		
W (N m^{-1})	1467657		
ΔT_{fm} (°C)	19.95	97.62	181.05

Table 9.4.3 The Flash Temperature Calculation for the Crowned Disc at 2.6 GPa

Slide-Roll Ratio	-0.026	-0.14	-0.28
R_B (mm)	9.297		
R_R (mm)	41.466		
N_B (rev/min)	5060	4000	3000
N_R (rev/min)	1200		
l'_B (m s^{-1})	4.926	3.894	2.921
l'_R (m s^{-1})	5.211		
b (mm)	1.208		
a (mm)	0.375		
β_B	64.1	50.7	38.0
β_R	67.8		
W (N)	2465.93		
ΔT_{fm} (°C)	17.3	84.6	156.9

Table 9.4.4 The Flash Temperature Calculation for the Gear at 2.6 GPa

R_1 (mm)	13.408
R_2 (mm)	22.891
N_1 (rev/min)	2500
N_2 (rev/min)	2500
l'_1 (m s^{-1})	3.510
l'_2 (m s^{-1})	5.993
b (mm)	0.402
a (mm)	2.366
β_1	48.8
β_2	83.2
W (N)	5177
ΔT_{fm} (°C)	163.1

The maximum gear flash temperature was calculated at the highest point of single tooth contact, which is reasonable for a tip-relieved gear.

These flash temperatures were combined with the bulk temperature values, calculated previously, to obtain the temperature in the contact for the various specimens, as shown in Table 9.4.5.

Table 9.4.5 The Calculated Contact Temperatures for the Test Specimens at 2.6 GPa

	Temperature °C		
Specimen	T_{BULK}	ΔT_{fm}	T_C
Gear	102	163	265
Chamfered Barrel -0.026	91	20	111
Chamfered Barrel -0.14	116	98	214
Chamfered Barrel -0.28	128	181	309
Crowned Barrel -0.026	88	17	105
Crowned Barrel -0.14	111	85	196

The highest flash and contact temperatures (181 and 309 °C) were given by the barrel at the -0.28 slide-roll ratio. These would be even higher if the bulk temperature had not been taken as an average with the ring specimen (Table 9.3.1). The gear contact temperature is 265 °C, which is probably more accurate than the barrel value, as the bulk temperature of the gears was easier to define.

The effect of extended contact on flash temperature for a non-relieved gear tooth was calculated with the model described in Section 8.2.1.1, and is shown in Figure 9.4.1. This predicted extremely high temperatures at the extremities of the gear tooth meshing cycle, where extended contact took place. This combined with the high contact stresses at these points, as mentioned previously, could be a scuffing risk.

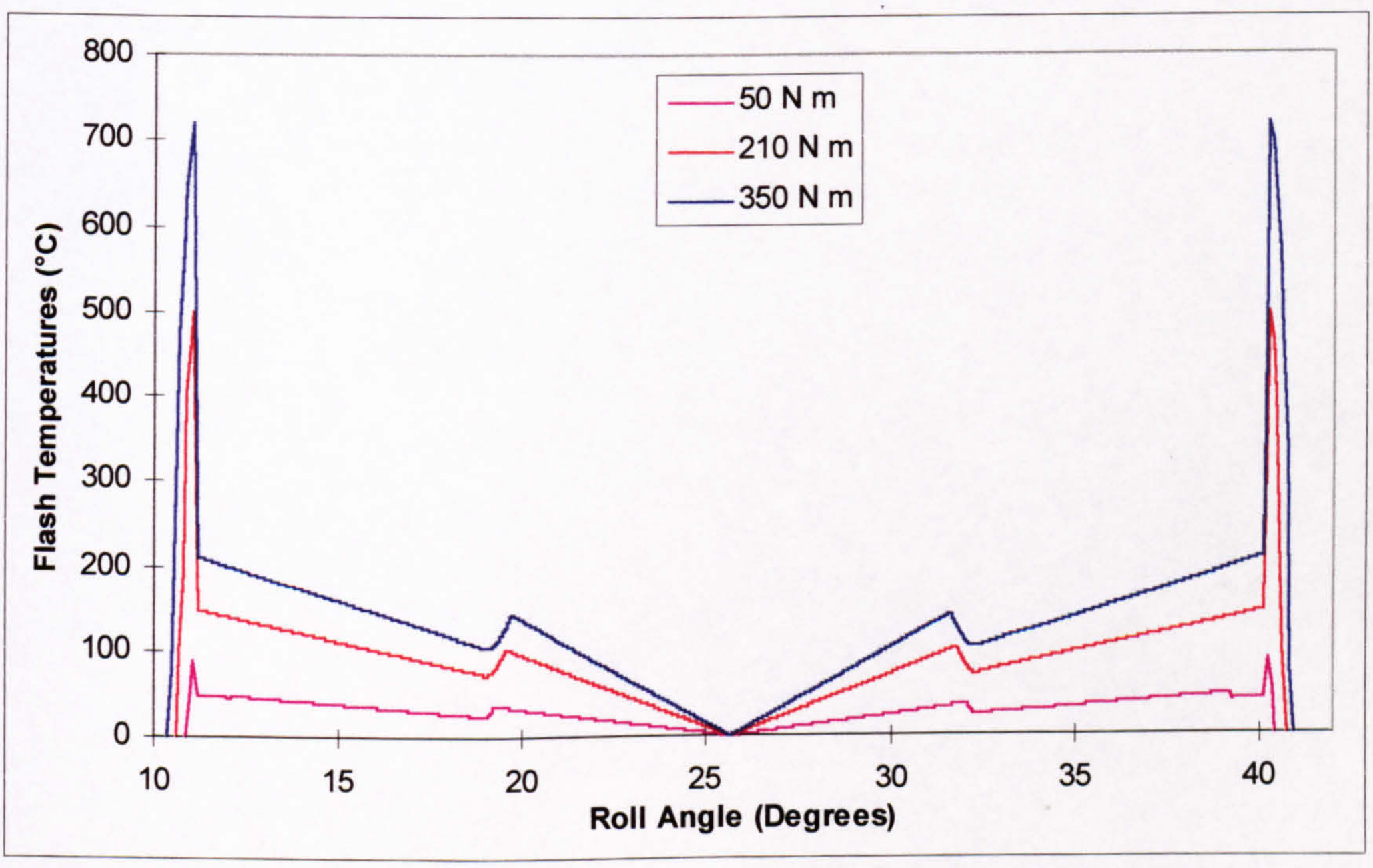


Figure 9.4.1 The Flash Temperature Generated Along The Non-Relieved Gear Tooth with Extended Contact at the Extremities of the Meshing Cycle ($\mu = 0.1$)

9.5 Conclusions from the Thermal Analysis

From the tests and analysis one can make the following conclusions.

The experimental results showed that:

- The gear temperature significantly exceeded the oil supply temperature at high torque.
- The gear tip gets relatively hotter as torque (temperature) increases.
- The infrared temperature reading exceeded all thermocouple temperatures.

- The bulk temperatures of the discs increased with increasing slide-roll ratio.
- The bulk temperature of the discs, and particularly the actual barrel specimen temperature, at a slide-roll ratio of -0.28 was much higher than that of the gears.

The heat partition theory showed:

- The faster surface receives more heat if there is a thin lubricant film (high torque / temperature).
- The heat partition coefficient, α, is 0.5 if the film is thick (low torque / temperature).
- This effect can lead to temperature 'cross-over' with load (as shown in Figures 9.1.3 and 9.2.5).

Flash temperature theory showed:

- The highest flash and contact temperatures were given by the barrel at the -0.28 slide-roll ratio.
- Using the gear contact model extremely high flash temperatures (500 °C) were predicted at the extremities of the non-relieved gear tooth meshing cycle, where extended contact was taking place. This combined with the high contact stresses at these points, could be a scuffing risk.

Chapter 10 Lubrication Analysis

Having investigated the temperatures in the tests, an analysis is now presented of the lubricant properties and the theoretical film thickness occurring in the gear and disc tests. Determination of film thickness in a concentrated contact is important as this determines the extent of asperity contact and affects wear, fatigue, and friction losses. Results from this analysis will be used in the discussion of the gear and disc fatigue test results in Chapter 13.

10.1 Lubricant Properties

The lubricant used for all the fatigue tests discussed in Chapters 11 and 12 was Castrol AN157, a synthetic ester (some properties are given in Table 10.1.1 others are shown in Appendix F). This was chosen because it was developed specifically for helicopter gearboxes and was thought to offer a reasonable resistance to scuffing. Most aerospace lubricants have a low viscosity (~5 cS at 100 °C) and offer low scuffing resistance, so running high load tests with such lubricants could have been a problem.

10.2 Lubricant Tests

A high frequency reciprocating (HFR) rig was used to test the friction and film forming properties of the lubricant. The rig consists of a 6 mm diameter steel ball held in a fixed position and oscillated, at a designated frequency and stroke length with an applied load, against a 10mm diameter steel flat. The contact is fully immersed in lubricant. Another lubricant Castrol Aerojet 5 (a standard aerospace lubricant: 26.6 and 5.04 cS at 37.8 °C and 98.9 °C respectively) was tested as a comparison. Figure 10.2.1 shows the variation of film formation (measured by an electrical method) and friction with time, at a constant temperature of 70 °C for the two lubricants and two different reciprocating frequencies. The increased reciprocating frequency gives rise to the faster formation of a full lubricant film and the reduction in friction. Figure 10.2.2 shows the variation of film formation and friction with increasing temperature. Castrol AN157 would appear to offer improved film formation at elevated temperatures when compared to Castrol Aerojet 5.

Table 10.1.1 Lubricant Specification (Castrol AN157)

Chemical Composition:
Pentaerythritol Ester of Heptanoic Caprylic and Capric Acids
Trimethylolpropane Ester of Heptanoic Caprylic and Capric Acids
Tri(isopropylphenyl) Phosphate
Triphenyl Phosphate
Triphenyl Phosphorothionate
Appearance: Clear and bright straw coloured fluid with blue bloom

Property	Sample A	Sample B
Specific Gravity, 15/15 °C	0.9867	0.9854
Kinematic Viscosity, cS		
at 100 °C	8.96	9.00
at 40 °C	52.24	52.65
at -32 °C	12667	10593
% Change after 72 hrs at -32 °C	1.93	-
Viscosity Index	-	152
Low Temperature Viscosity at -29 °C. cP at 30 rpm	-	4130
Pour Point, °C	-	-56
Flash Point (Closed) °C (IP 34)	-	227
Specific Heat Capacity		
ASTM D 3947 at 50 °C	-	1.78
J/g °C at 100 °C	-	1.77
Ryder Gear Test, 100 °C		
Relative Rating, % Herco Lube A	204.7	
Average Reference Oil Rating lb/in	(2007)	
Load Carrying Capacity FZG, Failure Load Stage	13/13+	
AN157 successfully completed all of schedules 1 and 2. In schedule 3 it gave a normal gear failure, i.e. every third tooth scuffed at a load of 1342 m		

	Author's Measurements
Density at 40 °C, kg m^{-3}	968
Density at 76 °C, kg m^{-3}	942.5
Kinematic Viscosity, Cs at 40 °C	53
Kinematic Viscosity, Cs at 100 °C	15.93
Load Carrying Capacity FZG, Failure Load Stage	11/12

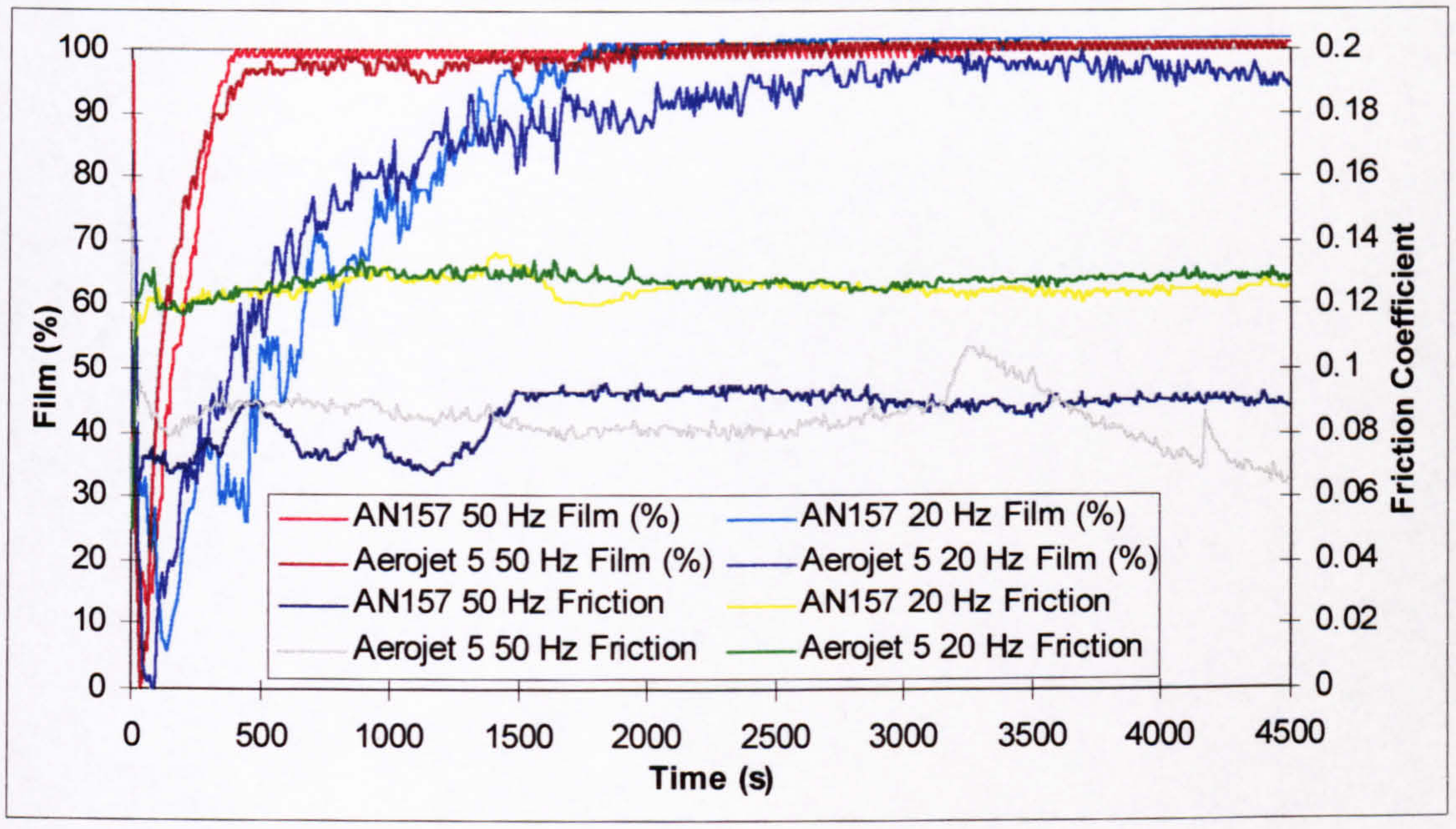


Figure 10.2.1 HFR Test (Temperature 70 °C. Stroke Length 1000 μm. Load 200g.)

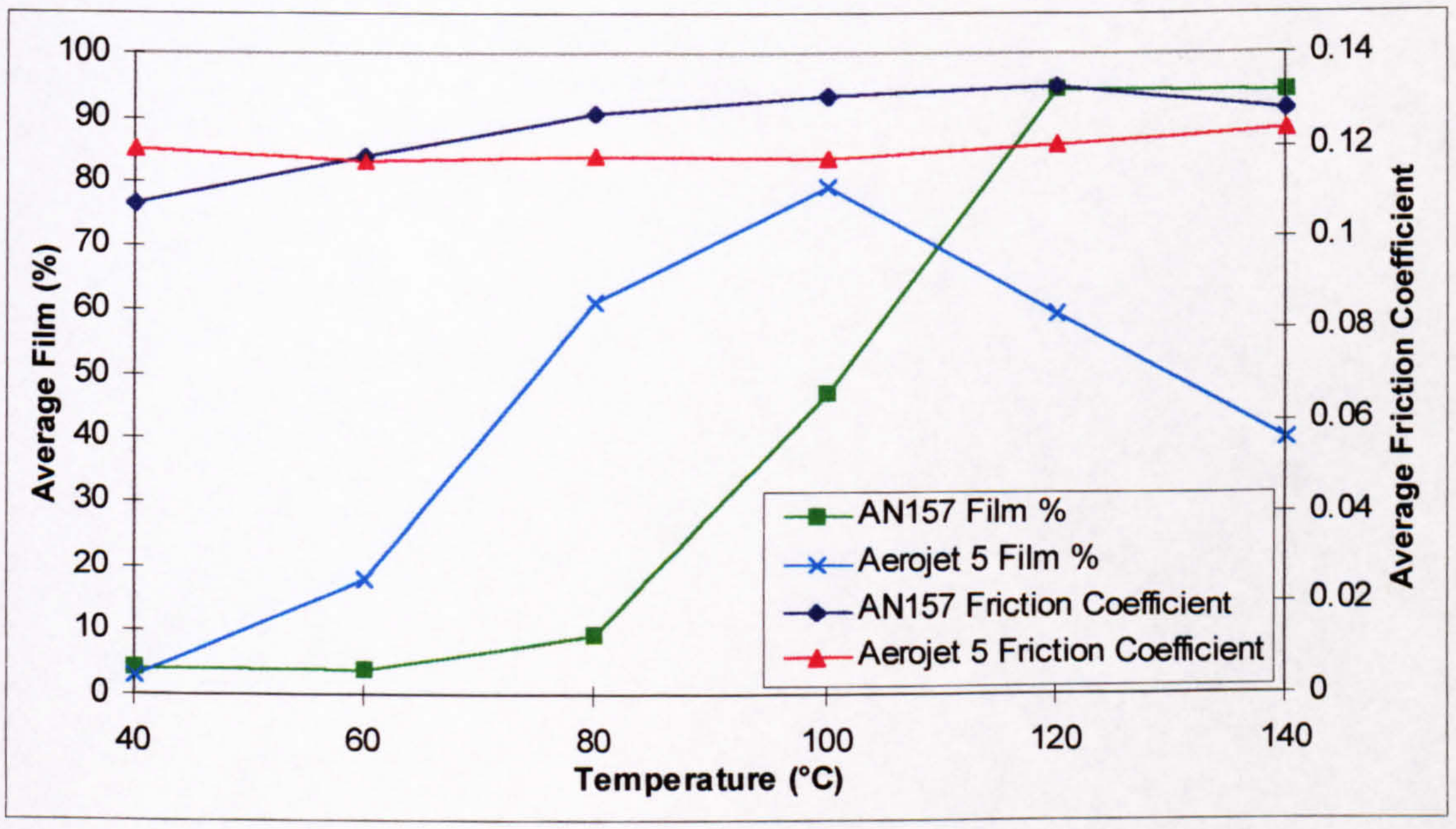


Figure 10.2.2 HFR Test (Frequency 20 Hz. Stroke Length 1000 μm. Load 400g.)

The film thickness can also be measured by optical interferometry. The set-up used consists of a smooth reflective ball which is loaded against a flat transparent disc, the underside of which is coated with a semi-transparent layer of chromium. Light is shone onto the contact and some of it will pass through the oil film and be reflected back from the ball, whilst the remainder will be reflected back from the chromium layer. Interference fringes will therefore be produced by the recombined light waves (Figure 10.2.3).

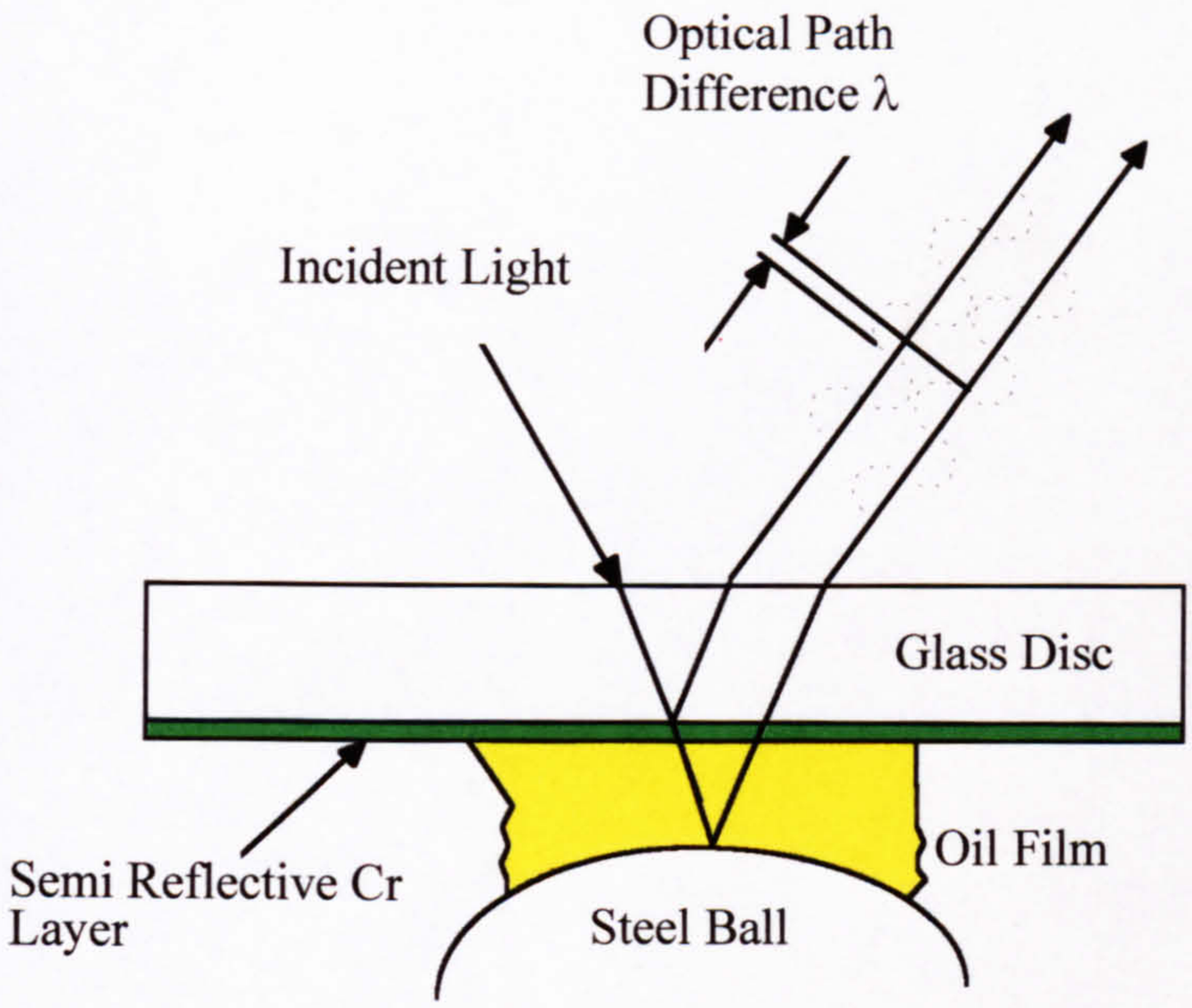


Figure 10.2.3 Principle of Optical Interferometry (Smeeth 1998)

Conventional interferometry suffers two limitations: it is impossible to measure very thin films and the greatest resolution is 25 nm. To overcome this, ultra-thin interferometry was developed (Johnston et al. 1991). A transparent layer of silica (not shown in Figure 10.2.3) is deposited on top of the chromium layer which essentially acts like a solid layer of oil, giving a measurable film thickness at zero speed. The thickness of the silica layer can be measured at the beginning of the test and subtracted from all subsequent readings to give true film thickness (Smeeth 1998).

The results of the film thickness measurement at temperatures of 40, 80 and 120 °C are shown in Figure 10.2.4. Overall, they showed a drop in film thickness with temperature and an increase with entrainment speed, which is to be expected. At 120 °C the decrease in film thickness with decreasing disc speed levels off at the slower disc speeds because of the formation of a boundary film on the contact surface. The variation of the film at these lower speeds with the time the lubricant was kept at 120 °C is shown in Figure 10.2.5. The lubricant was then tested at 120 °C and stopped after 30 minutes and 1 hour and the film left to decrease. The film was then measured with no motion and is shown in Figure 10.2.6. This was the boundary part of the lubricant film, and it did not appear to decrease with time after the test was stopped. This boundary film could have resulted from EP additives reacting with the hot metal surfaces and forming an inorganic layer which prevented seizure, possibly at the expense of high wear.

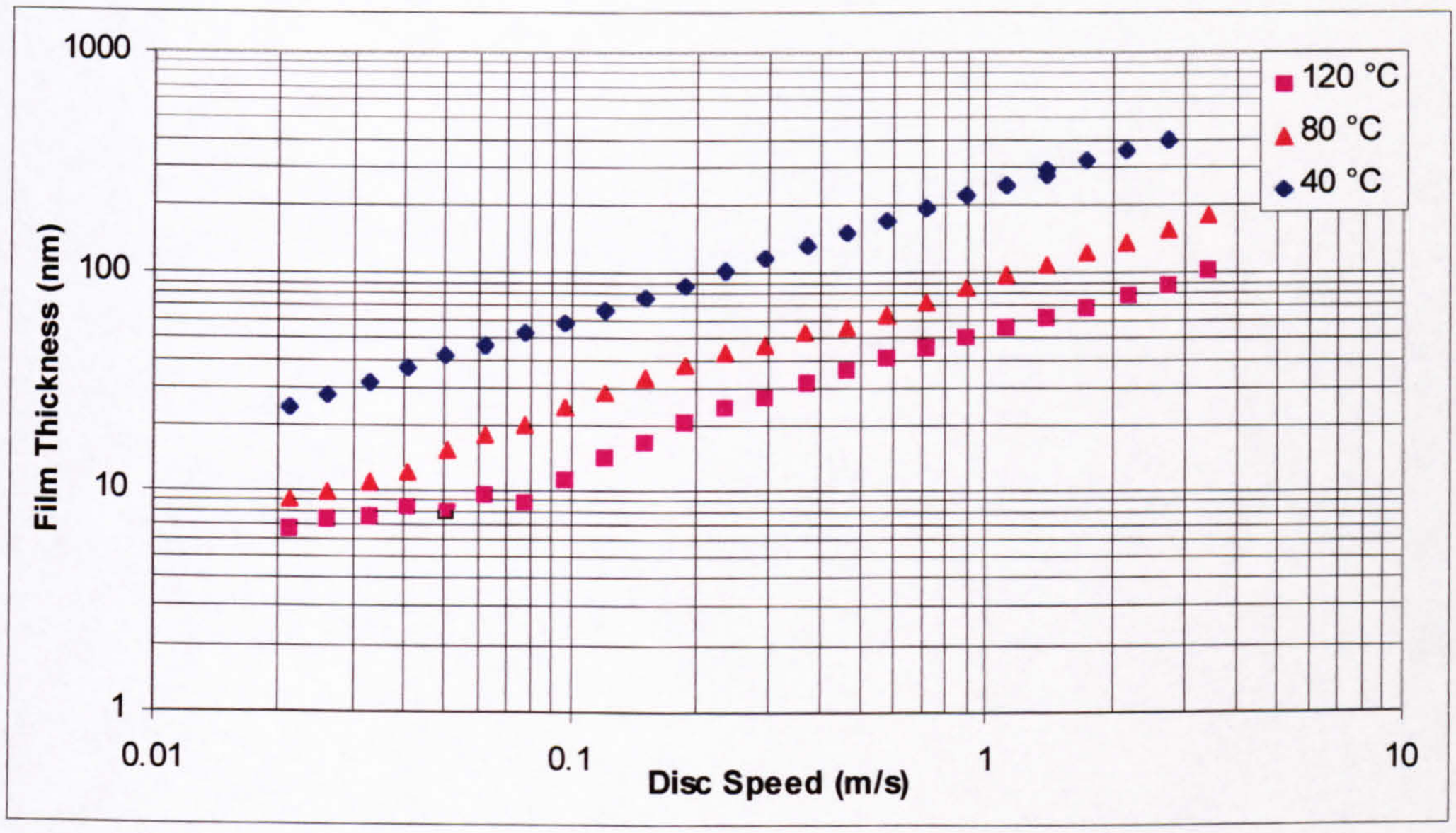


Figure 10.2.4 Film Thickness Behaviour of Lubricant AN157 with Temperature

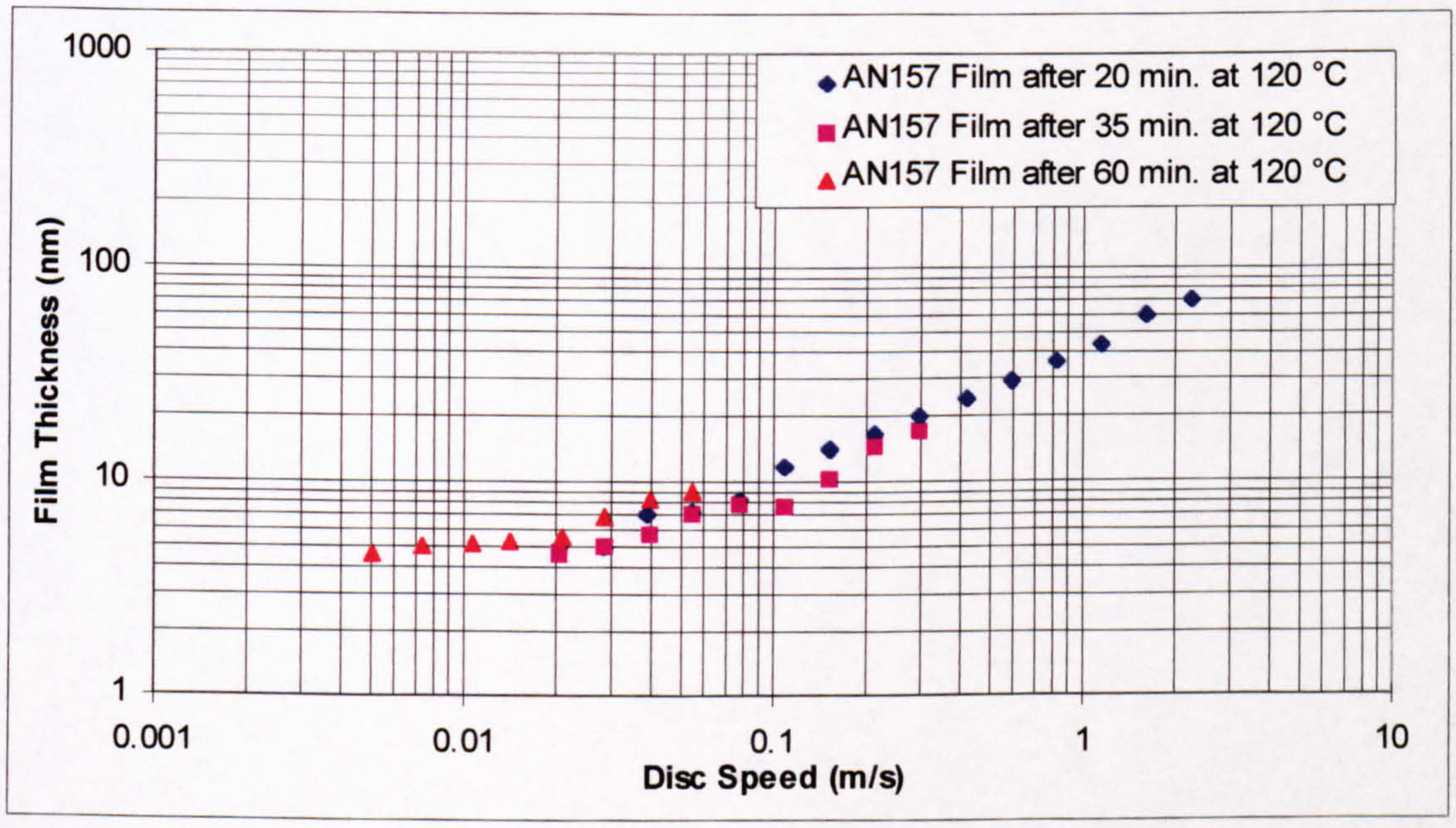


Figure 10.2.5 Film Thickness Behaviour of Lubricant AN157 at 120 °C

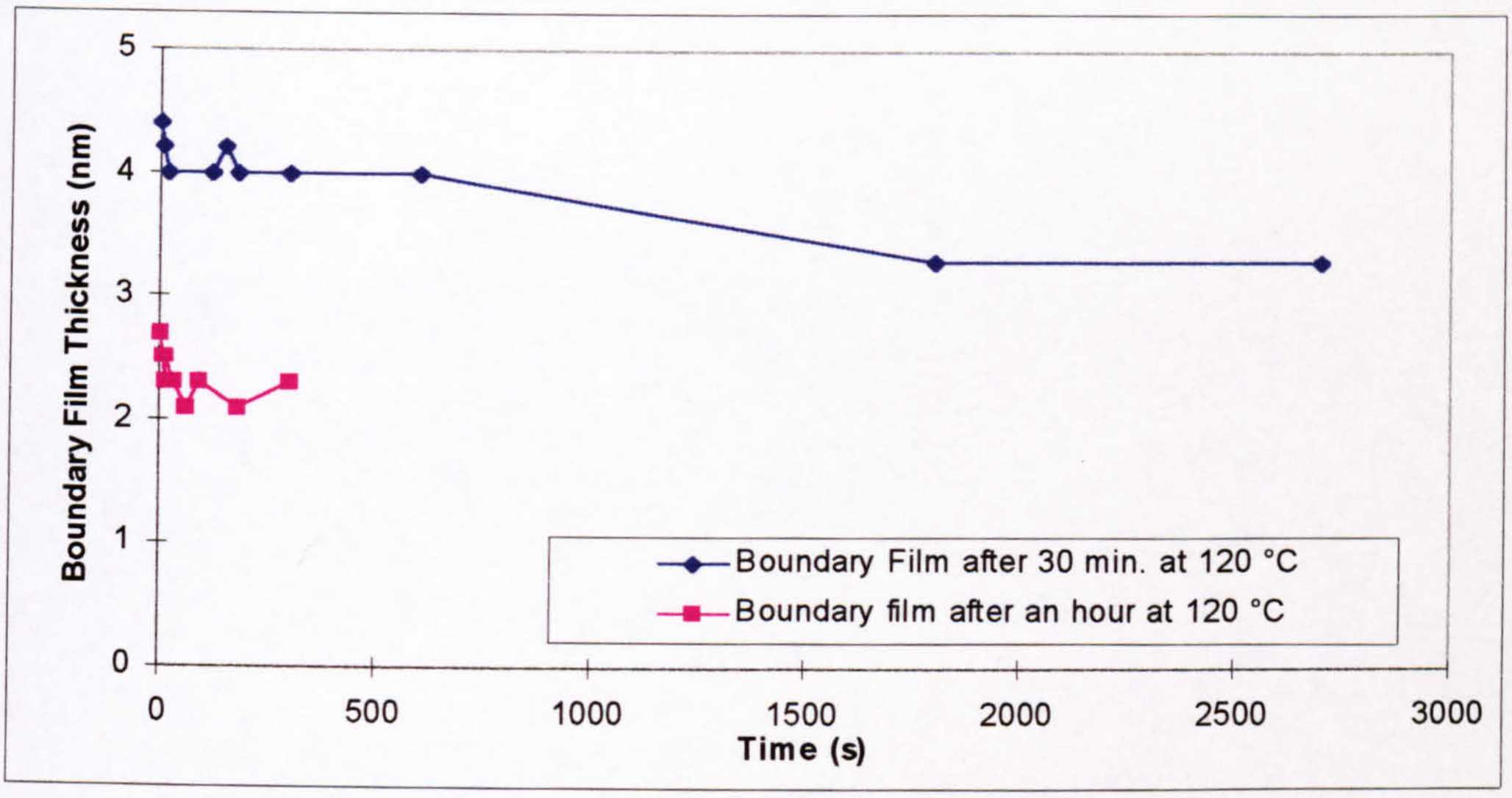


Figure 10.2.6 AN157 Boundary Film Decay After Testing at 120 °C for 30 minutes and 1 hour and then Stopping the Rig

10.3 Sliding and Entrainment Speeds

The sliding speed is a key factor in rolling contact fatigue as discussed in Chapter 4 and can also affect other failure modes such as scuffing. The entrainment speed is that which determines the size of an elastohydrodynamic lubricant film in the contact, which again will play a vital role in the performance of a component. Therefore, in order to understand the test results, an evaluation is now presented of the entrainment and sliding speeds in both tests.

The involute spur gears are kinematically complicated with teeth continually coming in and out of mesh. Sliding changes in magnitude and sign every cycle, the radii of equivalent cylinders will vary through the meshing cycle and, the contact load will vary due to load sharing between teeth pairs in contact. From Figure 10.3.1 one can see the sliding is a maximum at the gear tip and root and there is no sliding at the pitch point. This is a possible reason for scuffing taking place in the tip and root and not on the pitch point, as shown in Figure 3.3.2. The entrainment speed in the gears is a constant across the mesh (except where there is extended contact) because they are of 1:1 ratio. The slide-roll ratio is shown in Figure 10.3.2 for the gears and varies across the tooth contact, while it is a constant value for the disc tests. A comparison between the two types of test is shown in Figure 10.3.3, where each slide-roll ratio available in the disc rig is represented by a discrete point on the chart, whereas, the range of conditions experienced by the gear tooth is represented by the horizontal line. The slide-roll ratio of

-0.28 in the disc rig appeared to offer the closest match to the lowest point of single tooth contact in the gear, where the slide-roll ratio was -0.26.

The computer model developed to investigate extended contact, was used to calculate the entrainment and sliding speeds for non-tip relieved gears with extended contact at the entrance to, and exit from, mesh of the tooth pairs. The result is shown in Figure 10.3.4. The entrainment is shown to stop and reverse in direction in the area of extended contact. This could be damaging due to its effects on film thickness. However, it does occur very rapidly and may not allow the collapse of the fluid film.

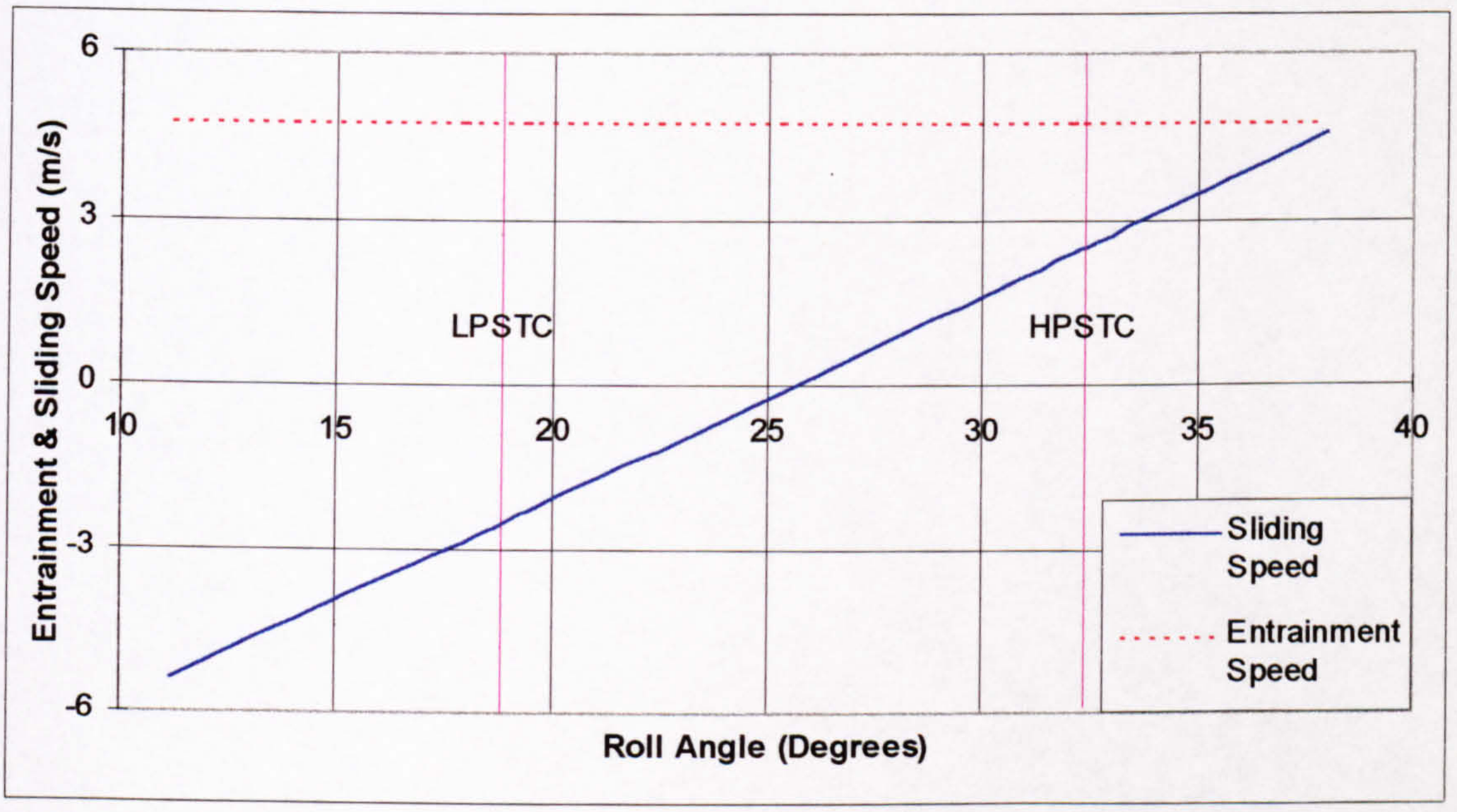


Figure 10.3.1 Sliding and Entrainment Speeds in the Test Gears (L & HPSTC - Lowest & Highest Point Single Tooth Contact)

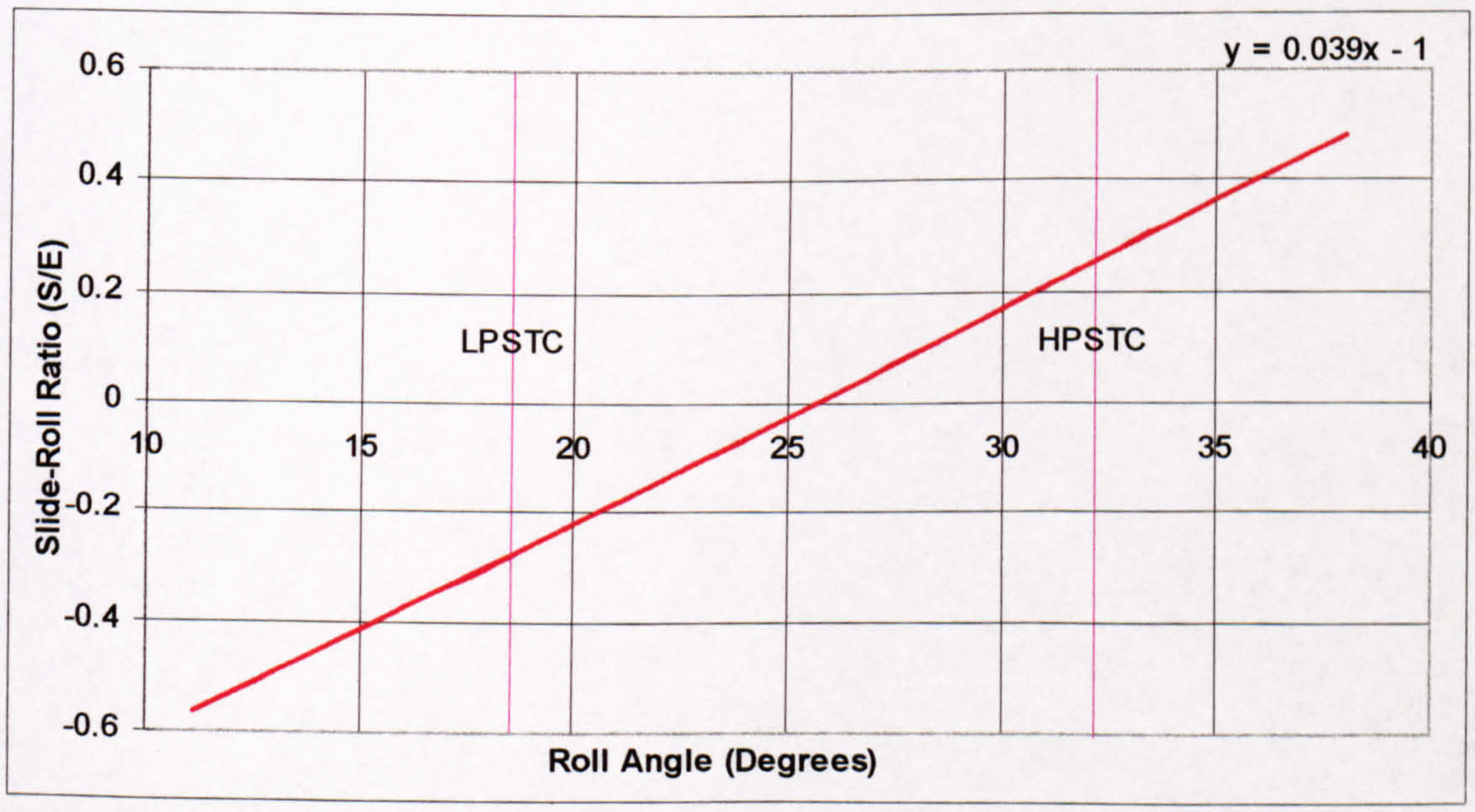


Figure 10.3.2 Slide-Roll Ratio Variation Across the Gear Teeth

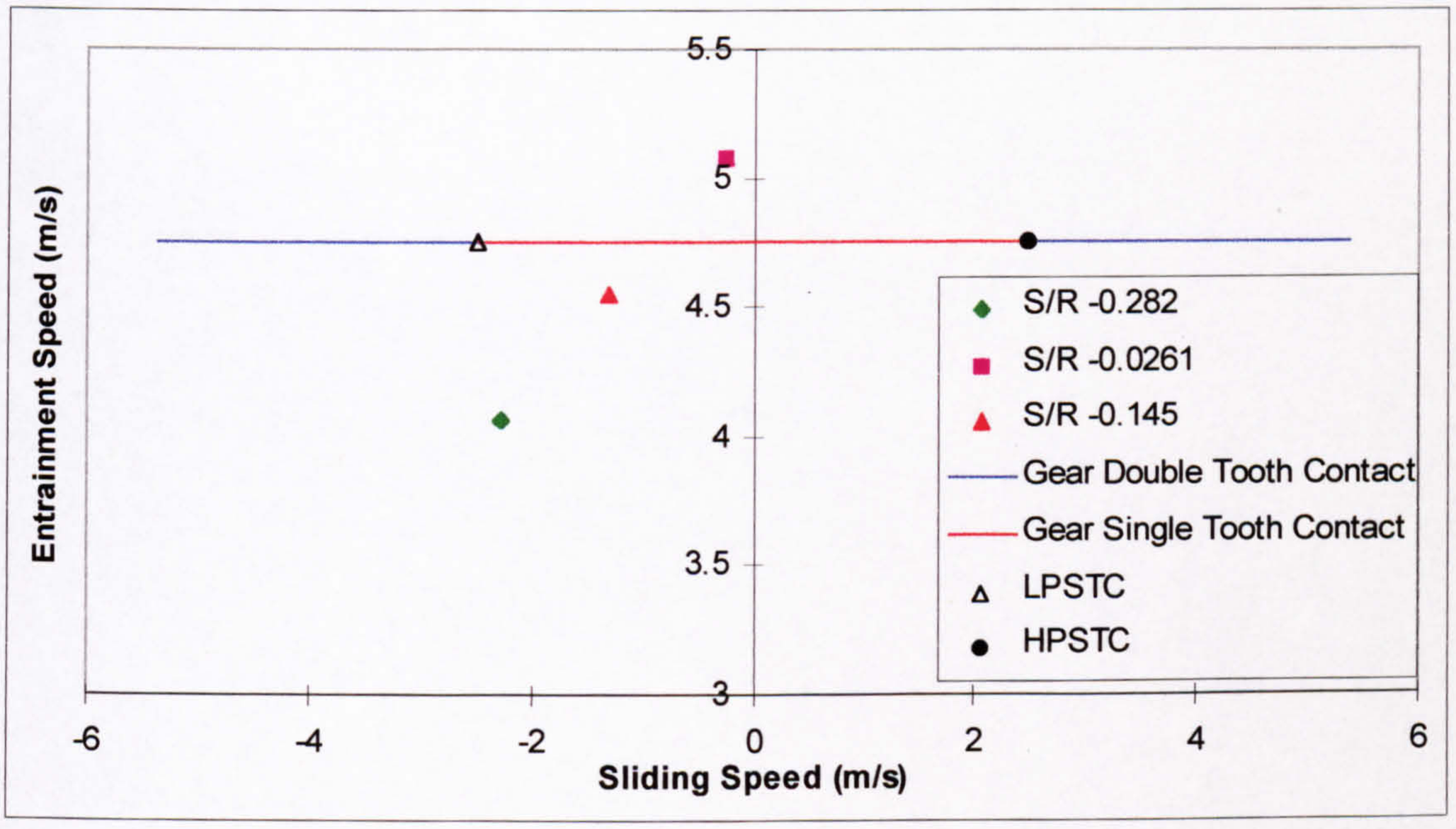


Figure 10.3.3 Gear and Disc Slide-Roll Comparison Showing Single and Double Tooth Pair Contact

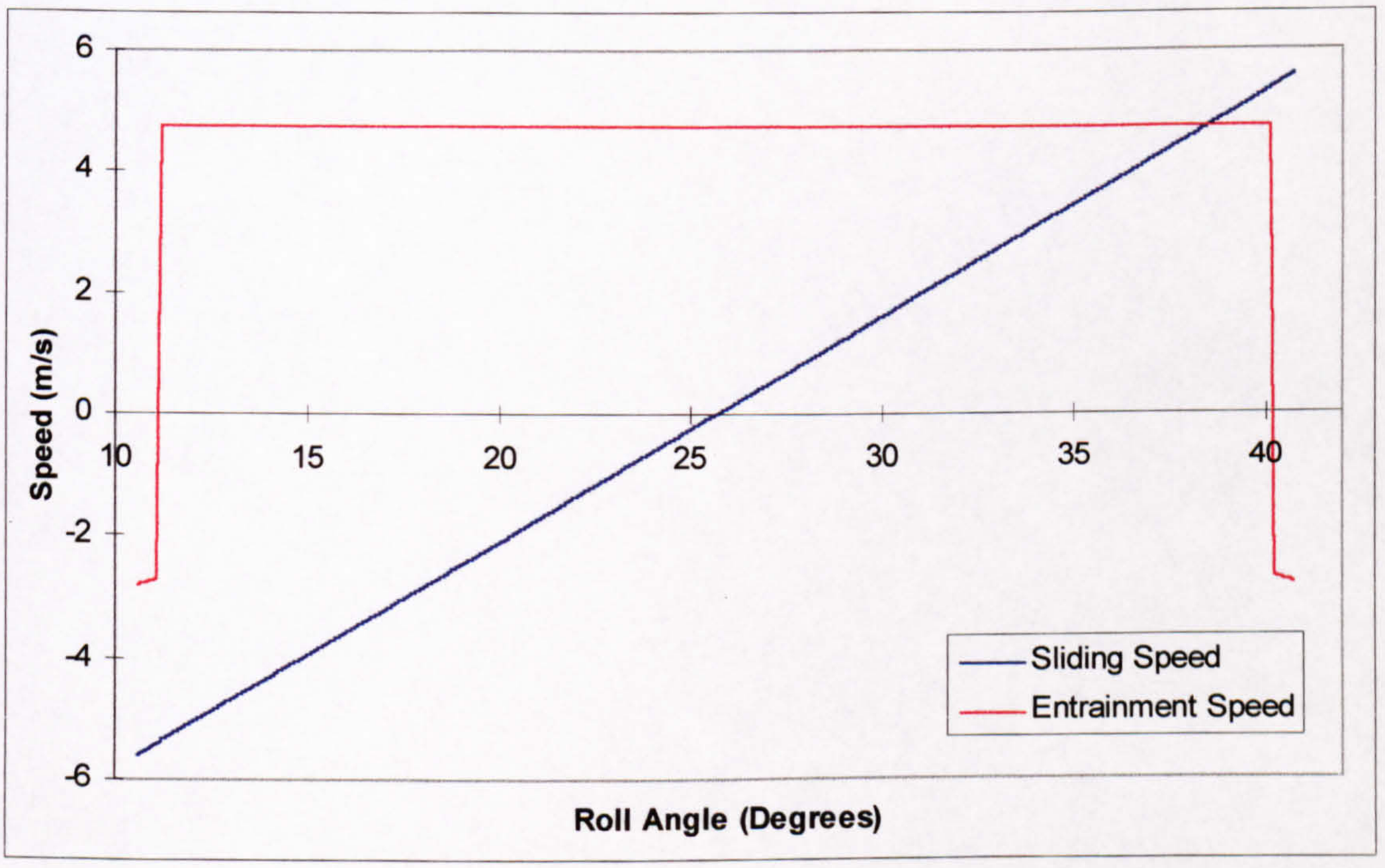


Figure 10.3.4 The Sliding and Entrainment Speed Along the Non-Relieved Gear Tooth Meshing Cycle Showing the Effects of Extended Contact

10.4 Film Thickness

The minimum film thickness and friction in EHD lubricant films in the contact are controlled by viscosity at the inlet to the contact, and this is likely to be close to that of the bulk temperature of the rubbing bodies evaluated in Chapter 9.

The EHD film thickness equations used were those of Dowson and Hamrock (Hamrock & Dowson 1977) (derived from a numerical model):

$$\frac{h_c}{R_x^*} = 2.69\left(\frac{u\eta_o}{E^*R_x^*}\right)^{0.67}\left(\alpha E^*\right)^{0.53}\left(\frac{W}{E^*R_x^{*2}}\right)^{-0.067}\left(1-0.61e^{-0.73k}\right)$$

$$\frac{h_o}{R_x^*} = 3.63\left(\frac{u\eta_o}{E^*R_x^*}\right)^{0.68}\left(\alpha E^*\right)^{0.49}\left(\frac{W}{E^*R_x^{*2}}\right)^{-0.073}\left(1-0.61e^{-0.68k}\right)$$

where k is the ellipticity parameter

$$k = 1.03\left(\frac{R_y^*}{R_x^*}\right)^{0.64}$$

and u is the entrainment speed, α the pressure viscosity coefficient, η_o the effective viscosity in the contact inlet, E^* the reduced Young's modulus, R_x^* the reduced radius, and h_c and h_o are the central and minimum film thickness respectively.

These equations are, in theory, only valid for steady rolling, isothermal conditions. The load and relevant radii change through the gear mesh, but in general using the film thickness equations will only introduce small errors (Hooke 1994). At the pitch line there is pure rolling and the value calculated for film thickness is probably more accurate. Further away from the pitch point, relative motion contains a significant amount of sliding, this may not influence the film thickness provided the correct temperature is applied to the equations (Dowson & Higginson 1977) and shear thinning, viscosity decrease with increasing shear rate, does not occur. However, the unsteady conditions at first contact and the non-involute geometry near the mesh extremes will probably invalidate the use of these equations in these areas.

Using the information from Figure 9.1.3 one can calculate the lubricant inlet viscosity (assuming this is at the temperature of the gear tooth) and hence the elastohydrodynamic film thickness. The results of these calculations are shown in Figure 10.4.1, where the effect of load on temperature, and hence film thickness can be seen. The pitch point has a slightly greater film thickness than the start and end of active profile due to the geometry and load differences at these points.

In gears with no tip relief, the entrainment speed reverses in the areas where extended contact takes place (Figure 10.3.4). This was predicted to have a negative effect on film

thickness, as shown in Figure 10.4.2. The Dowson-Hamrock equations presented earlier were applied throughout the mesh cycle. This, most probably, was not valid, particularly in the area of extended contact, where there is a predicted reversal of entrainment and the calculated film thickness was zero. It was done, however, to get an approximate idea of the conditions at these points. In practice, the film would not collapse at the point of entrainment reversal (Hooke 1994), particularly because of the speed with which it takes place.

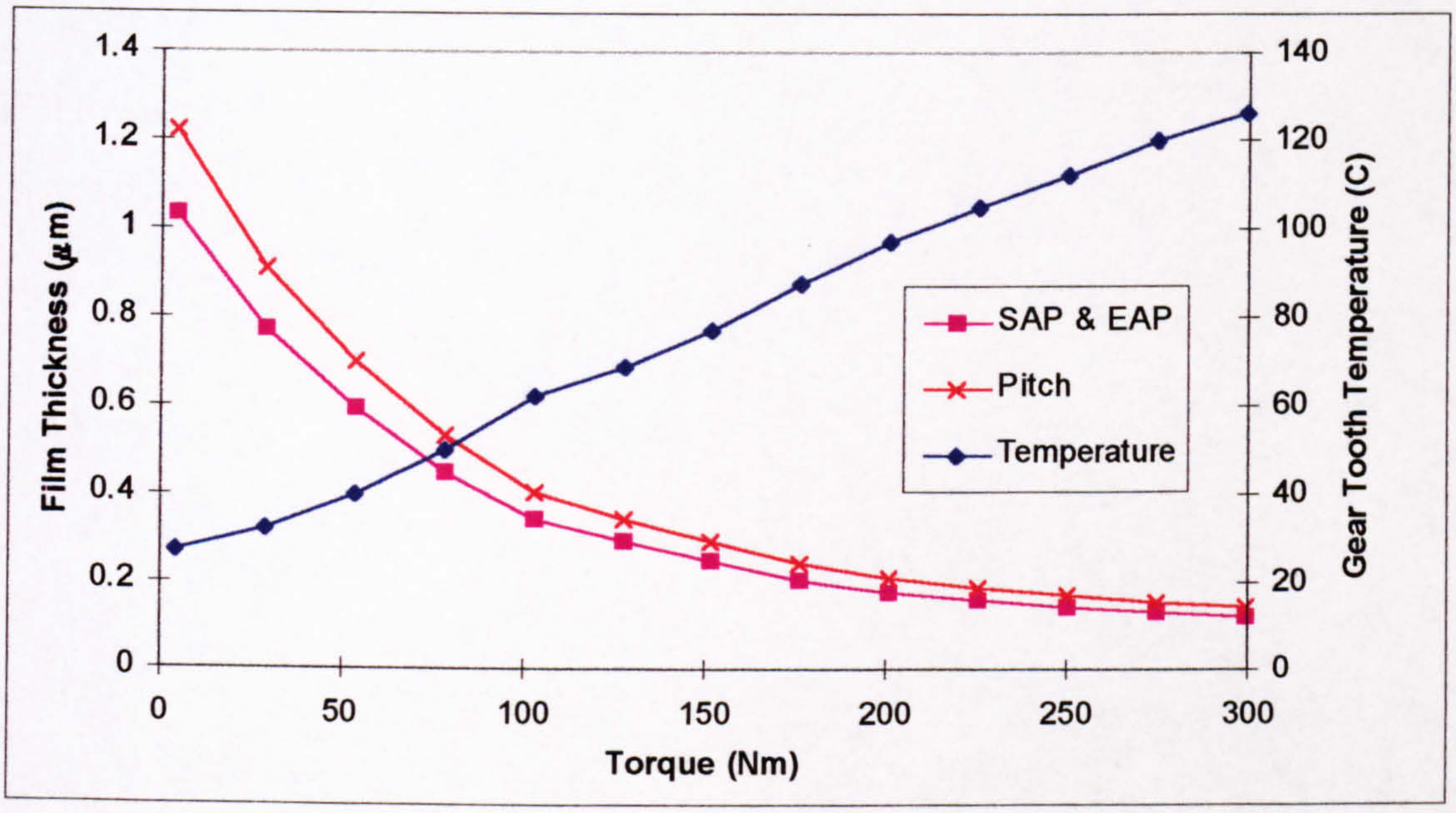


Figure 10.4.1 Film Thickness Variation with Torque in the Gear Tooth Contact

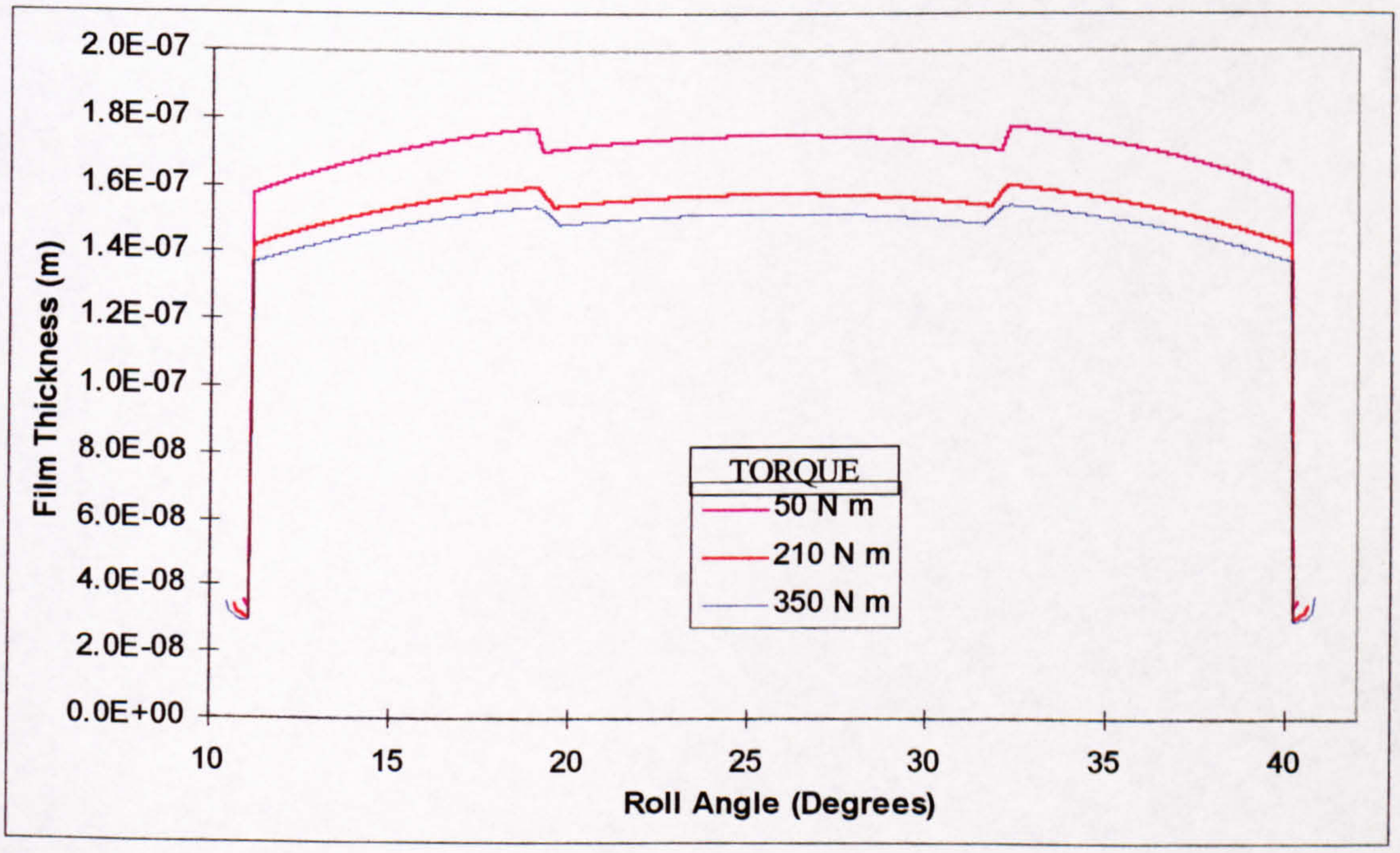


Figure 10.4.2 The Minimum Film Thickness for a Non-Tip-Relieved Gear Tooth Contact Suffering Extended Contact at the Extremities of the Mesh Cycle

The film thickness and the lambda ratio were calculated for the gear and disc specimens at 2.6 GPa (Table 10.4.1). The lambda ratio was calculated using the roughness values quoted in Table 7.5.1. From these results it would appear that the severity of asperity interaction on the gear tooth surfaces will be greater than that on the disc specimens. However, all the values are low and whether these affected the results is debatable.

Table 10.4.1 Minimum Film Thickness and Lambda Ratio for the Fatigue Tests

Test	Slide-Roll	Stress GPa	Temp. °C	h_o µm	Λ ratio
Gear	Var.	2.6	102	0.16	0.15
Disc Chamfered	-0.026	2.6	91	0.18	0.41
Disc Chamfered	-0.14	2.6	116	0.12	0.27
Disc Crowned	-0.026	3.95	88	0.15	0.34
Disc Crowned	-0.14	3.95	111	0.10	0.23

10.5 Conclusions from the Lubricant and Film Thickness Analysis

From the analysis and tests one can conclude:

- The AN157 lubricant appeared to form a relatively solid boundary film at high temperatures.
- The calculated lambda ratio was lower for the gear than the discs, but they were all low. Whether this difference would have any effect on fatigue life is debatable.
- The gears have a constant entrainment speed due to the 1:1 ratio (except for extended contact). The sliding speed is a maximum in the gear tip and root and there is no sliding at the pitch point. In non-tip-relieved gears suffering extended contact at the extremities of the tooth meshing cycle, it was predicted that there would be a reversal of entrainment.
- The gears have a varying slide-roll ratio along the contact path, whereas, the discs can be run at only one slide-roll ratio at a time.
- The slide-roll ratio of -0.28 in the disc rig appeared to offer the closest match to the lowest point of single tooth contact in the gear, where the slide-roll ratio was -0.26.

Chapter 11 The Gear Test Experimental Results

Having analysed the running conditions, loading, and lubricant properties, results are now reported of the gear and disc tests. In this chapter the gear tests described in the test programme in Section 7.8 are reported, the disc tests are reported in Chapter 12. The discussion of the results presented here is given in Chapter 13.

11.1 Examination of the Gear Contact Fatigue Test Results

As mentioned previously, two types of gear specimen were designed, one with tip relief and one without. The BS S156 material was used to investigate the differences between tip-relieved and non-tip-relieved gears, all the other gear materials were investigated with tip-relieved gears. The results of these tests are described next.

11.1.1 The Non-Tip Relieved BS S156 Gear Tests

The non-tip-relieved gears were made solely from BS S156, a carburised steel described in Chapter 5. If the operating load was too high on these gears, scuffing problems were encountered, as shown in Figures 11.2.1 and 11.2.2. It was detected by an increase in vibration measurements and visually by smoking from the test-box. This was known to be scuffing, of the form described in Section 4.3, because there were radial scratch and tear marks in the direction of sliding, material had been displaced over the tips of the gears, and the operating pitch line stood out prominently. This scuffing at the tip and root could be expected because these points, where the sliding speed was highest and hence heat generated was a maximum, carried a considerable amount of load. This effect could also have been worsened by the extended contact of the gear tip in the root of the mating tooth. The limiting maximum Hertzian contact stress to avoid scuffing, was found to be around 2.3 GPa, calculated at the lowest point of single tooth contact.

Scuffing still occurred in the non-relieved gears at lower stresses if they were loaded too quickly. An interesting fact was that as the gears were of 1:1 ratio they could scuff on a few teeth and not on others, which would not occur on a hunting ratio gear system, and enabled the observation of progressive deterioration on different teeth.

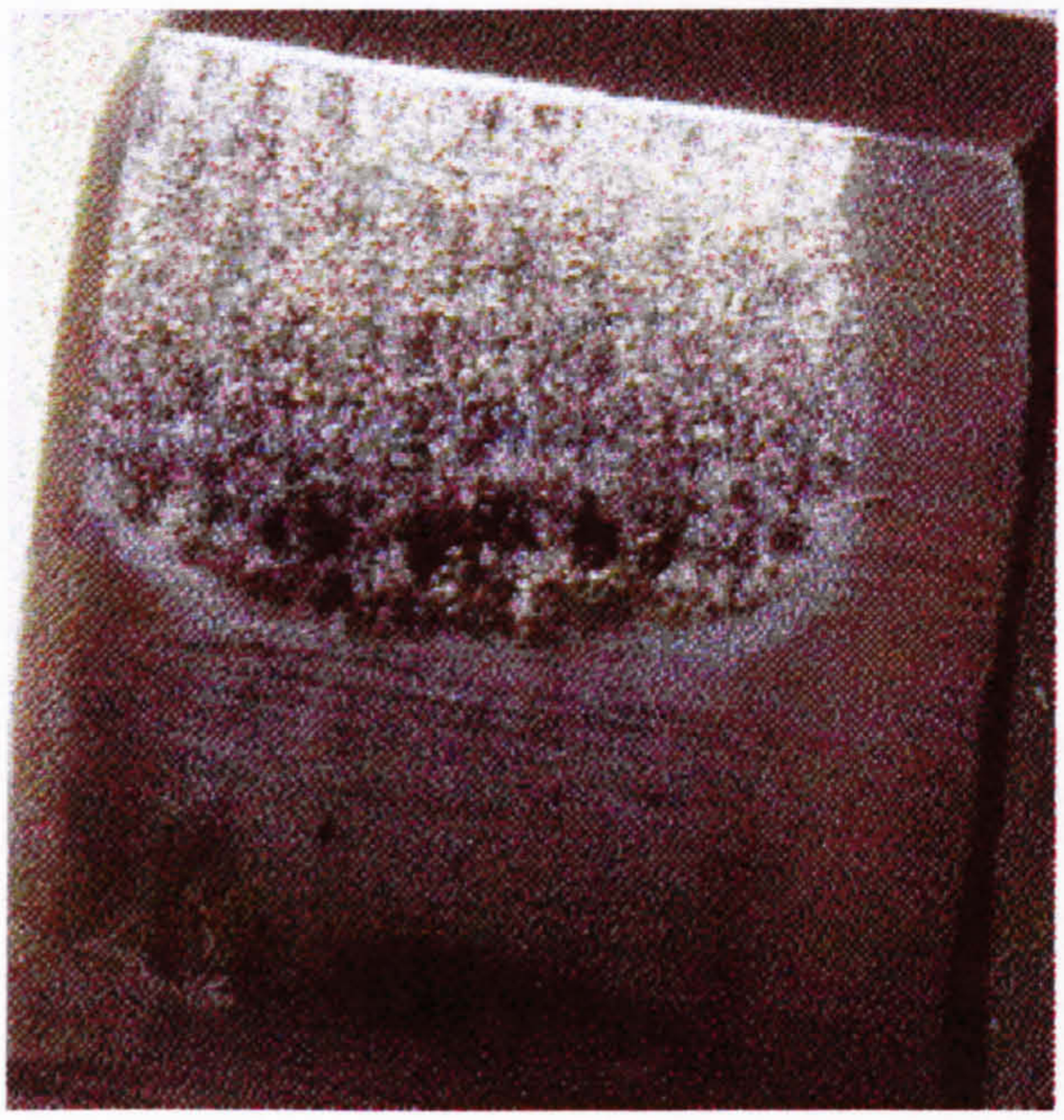


Figure 11.1.1 Scuffing in a Non-Relieved BS S156 Gear Tooth

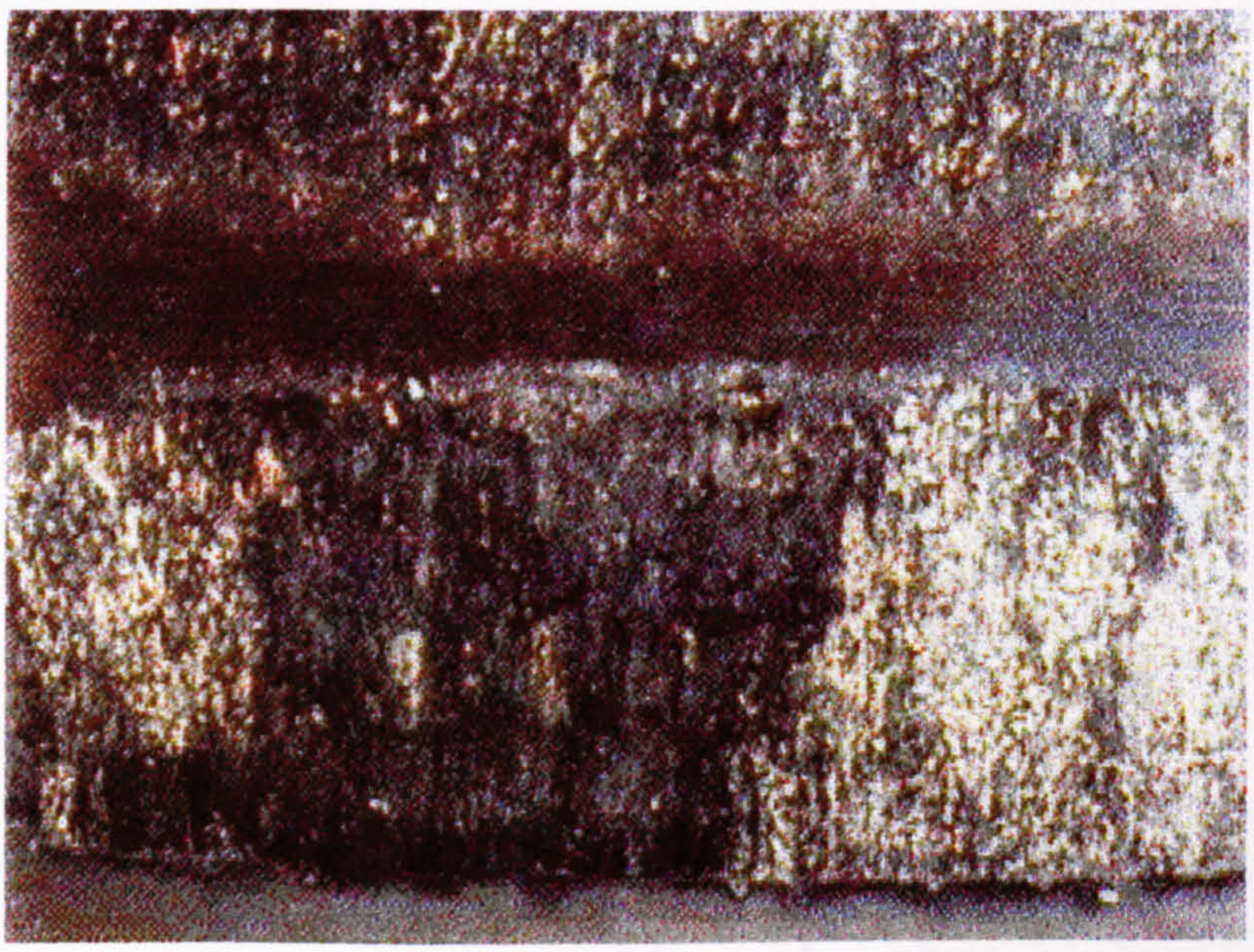


Figure 11.1.2 Close-up of Scuffing Failure on a Gear Tooth (Pitch Line Unaffected)

The non-tip-relieved gear teeth suffered from localised damage caused by the tip of the gear tooth interfering with the root of the mating tooth, i.e. extended contact (Figures 11.1.3 and 11.1.4). The contact width also tended to expand at the tip and root of the tooth unlike the contact pattern in the tip-relieved gears. The maximum operating torque for the non-tip-relieved gears was lower than that achieved in the tip-relieved gears.



Figure 11.1.3 Strong Marking Possibly from Pre-Engagement in the Dedendum of a Non-Tip Relieved BS S156 Gear.

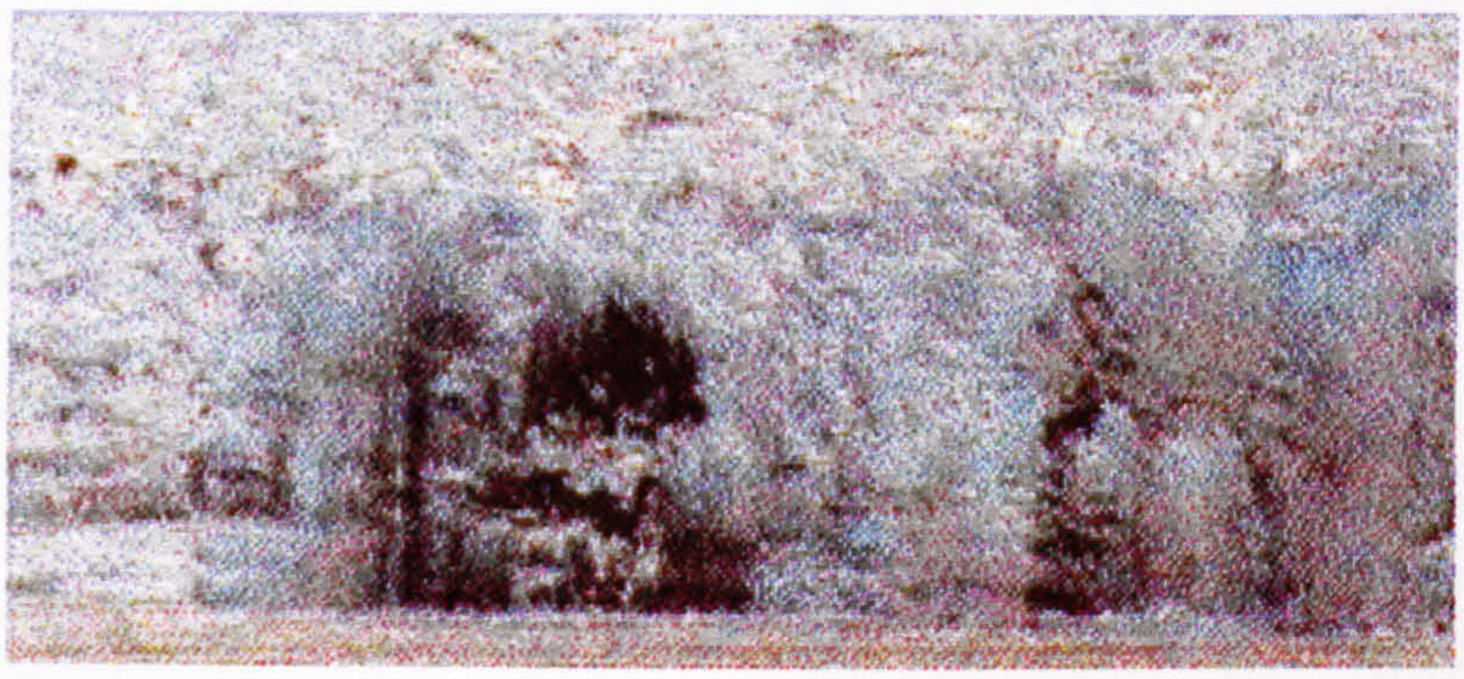


Figure 11.1.4 Closer View of the Marking Shown in Figure 11.1.3

If these non-relieved gears were loaded gently and kept at low loads for a long time, the contact pattern would broaden due to excessive wear on the tooth flank (Figure 11.1.5). The wear was of greatest depth near the limits of single tooth contact in the dedendum. This can be seen from the lead tooth profiles shown in Figure 11.1.6. Broadening of the pattern occurred in both dedendum and addendum, the latter due to wear on the mating gear, so the contact patch developed a 'waisted' appearance (Figure 11.1.5). This made the gear contact more conforming (lower contact stresses) and enabled the load to be increased considerably (Figure 11.1.6). It was found that this excessive wear was caused by micropitting (Figure 11.1.7). This was known as there was evidence of cracking, plastic deformation, and flake-like particle formation, similar to that described by Berthe et al. 1980, Shotter 1981, and Olver et al. 1986 as micropitting wear, and discussed in Section 4.5.

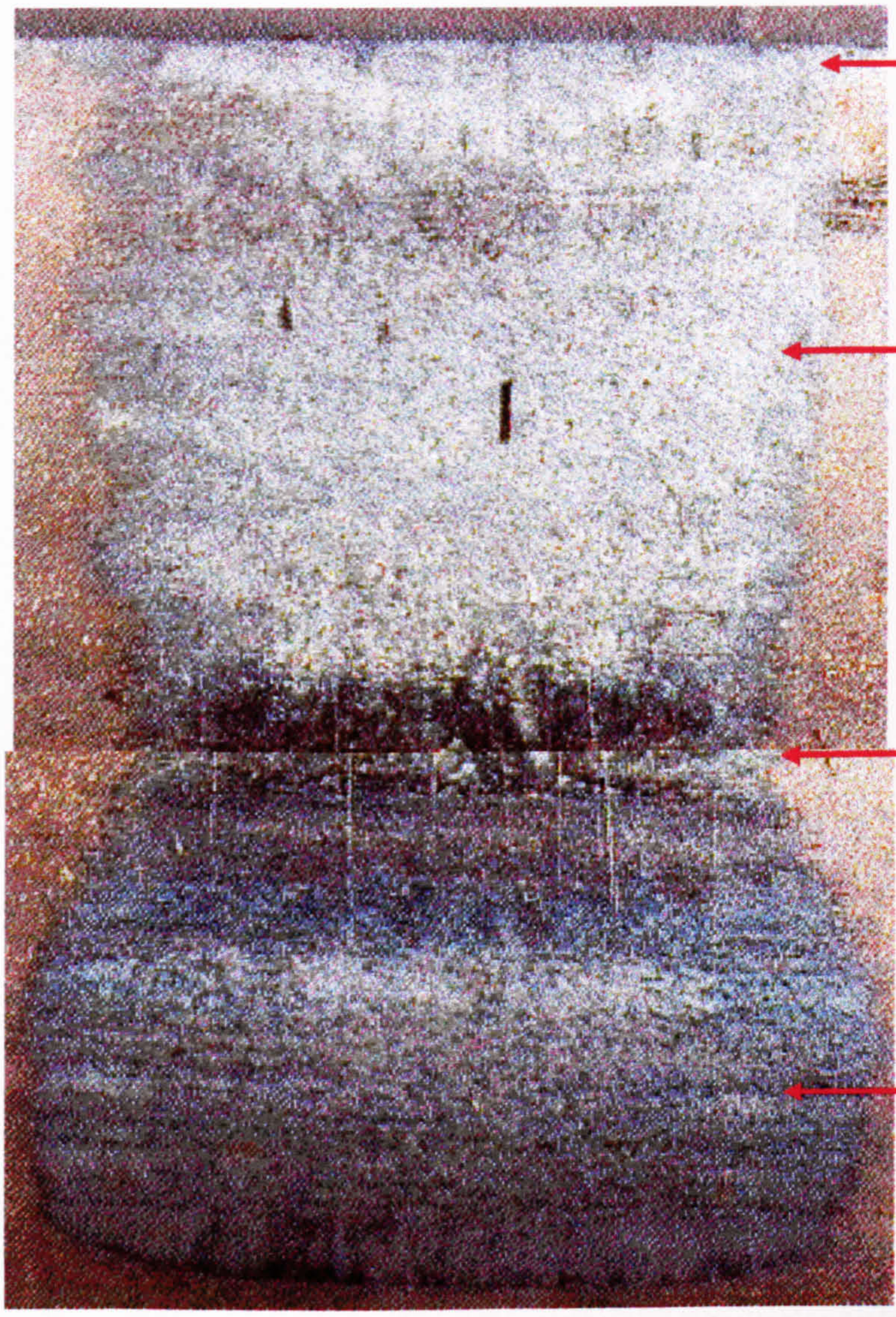
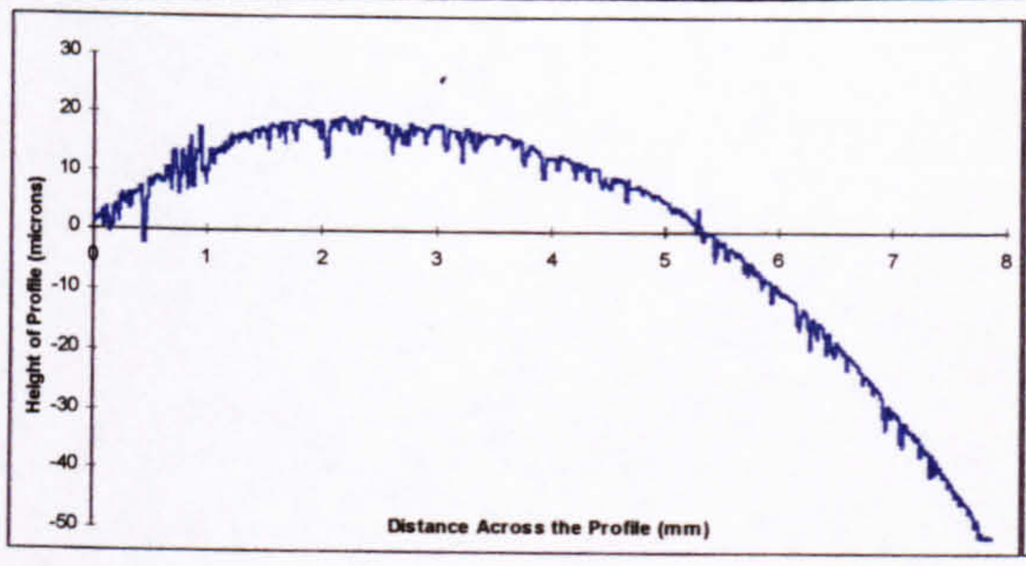


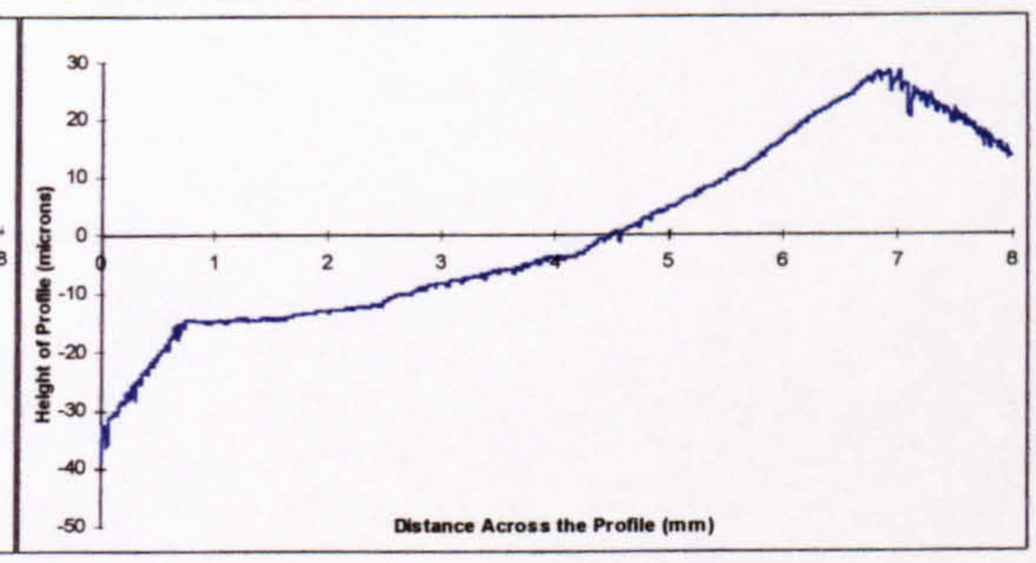
Figure 11.1.5 Wear Pattern on a Non-Relieved Gear Tooth after Running at Low Load

The lead profiles for a non-tip relieved gear, Figure 11.1.6, show about 40μm wear in the dedendum. The vibration levels increased gradually as this test progressed and the cut-out operated a few times. A visual examination of the gears was carried-out before the test was continued. Tests were only suspended due to micropitting for non-tip-relieved gears, as the amount of wear for relatively low loads was large (compared to the tip-relieved gears). Usually a combination of the vibration level and visual inspection of the gear contact pattern was used to determine whether the gear run should be suspended. This particular test was stopped (Figure 11.1.6), however, in a practical application it would depend on the use the gear was being put to, as to whether it would be judged to have failed or considered still capable of operating.

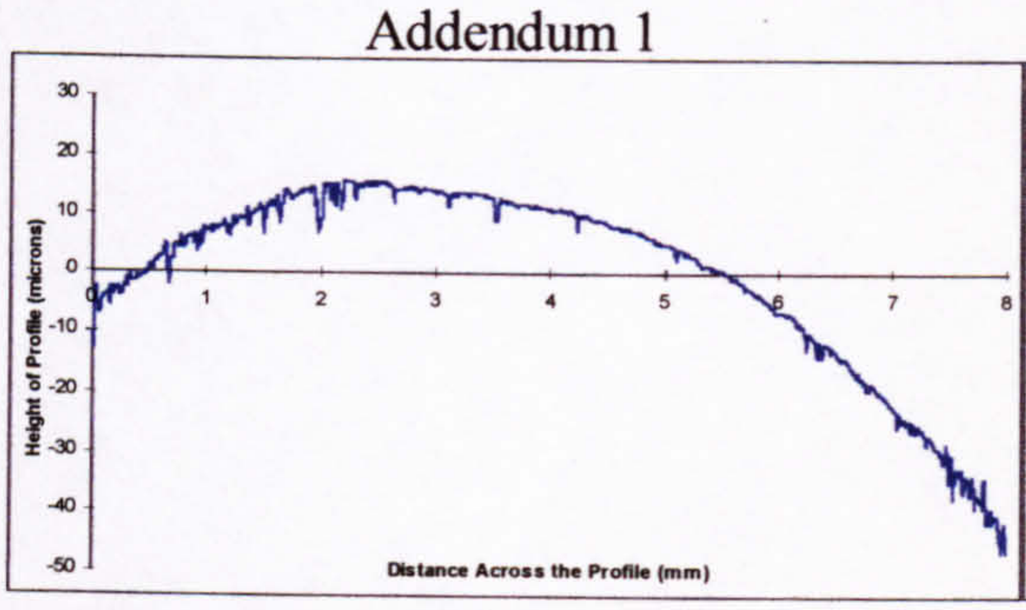
Once a limiting load was determined at which the gears could operate without scuffing, micropitting tended to be the cause of failure, however, pitting was also obtained.



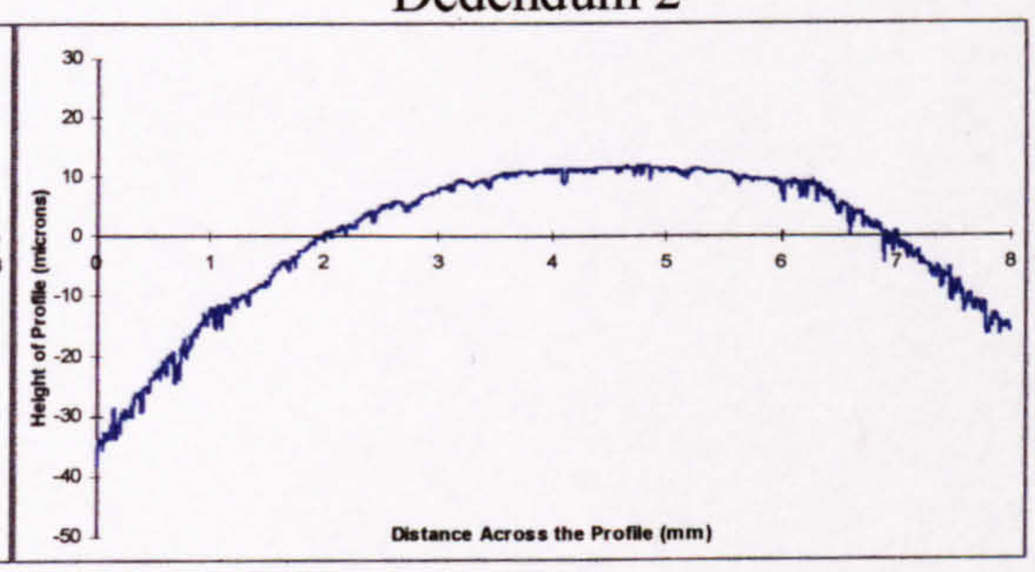
Addendum 1



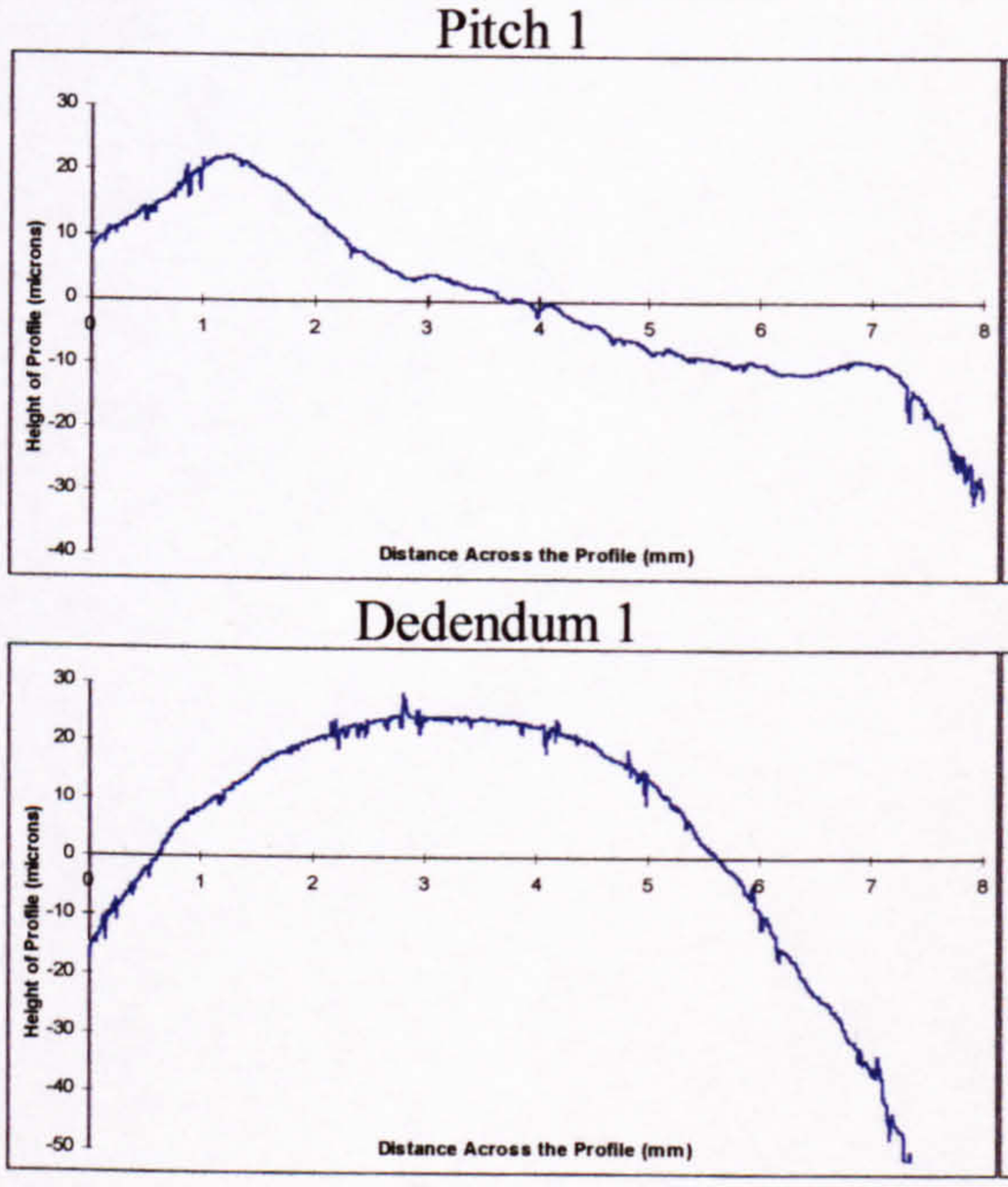
Dedendum 2



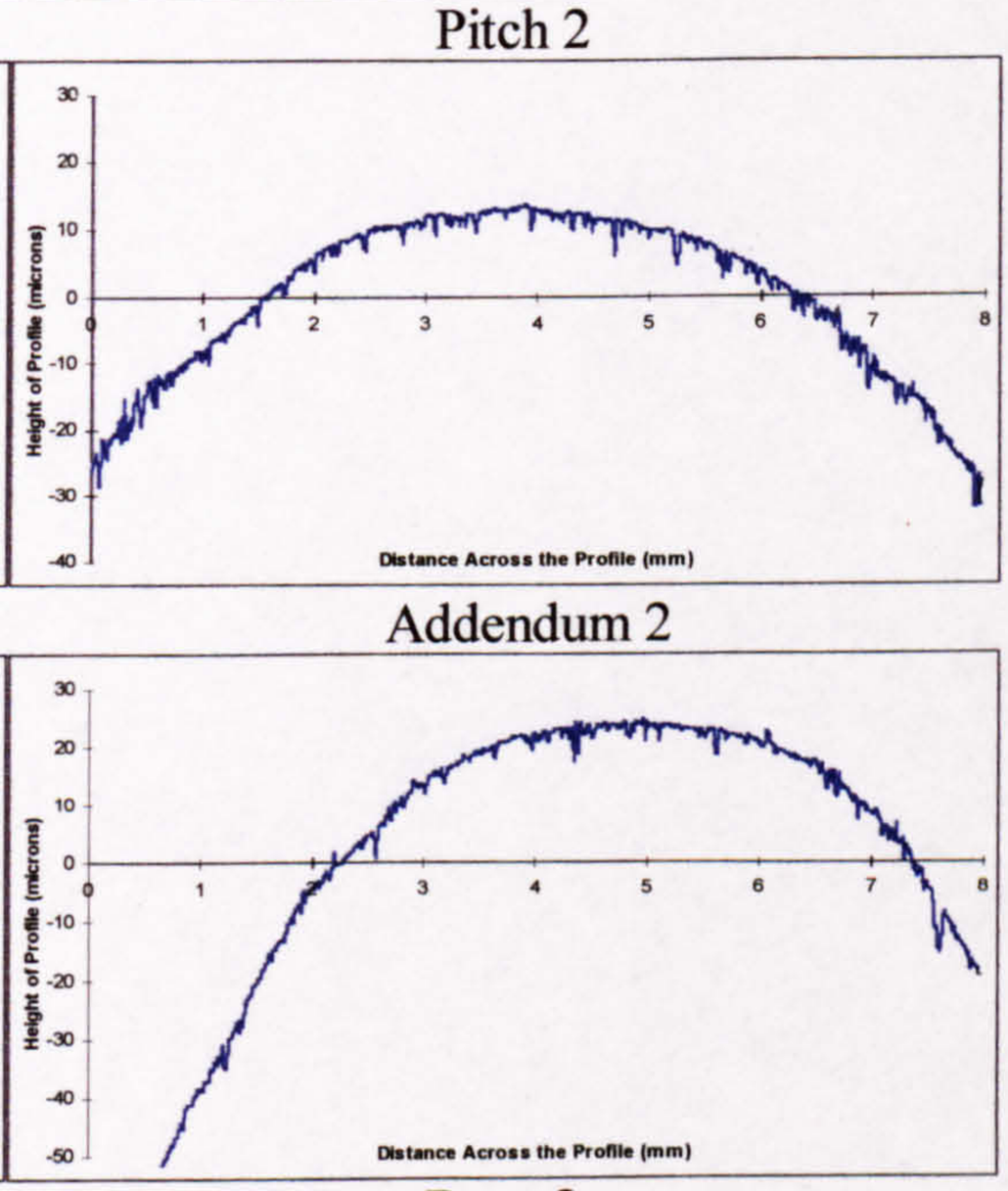
Pitch 1



Pitch 2



Dedendum 1



Addendum 2

Root 1

Root 2

Figure 11.1.6 Lead Profiles of Meshing Teeth 1 and 2 in Mating Non-Relieved Gears

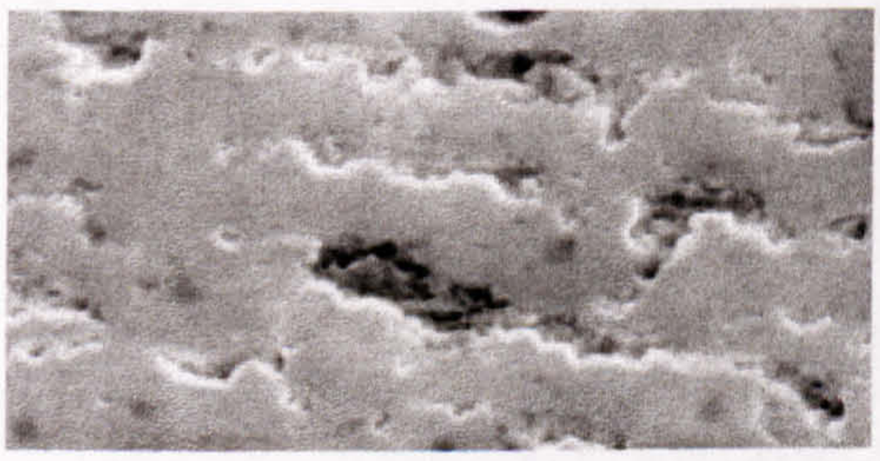


Figure 11.1.7 Scanning Electron Micrograph of the Dedendum of the Gear in Figure 11.1.5 Showing Micropitting (1000x)

11.1.2 The Tip-Relieved BS S156 Gear Tests

The relieved gears gave less problems with scuffing. The load could be increased to higher values than was possible with the non-relieved gears. The tip-relief was designed for a maximum operating torque of 350 Nm, a maximum Hertzian contact stress of 3 GPa at the lowest point of single tooth contact. There was no hard marking in the gear root and the tooth surface pattern was more rounded (Figure 11.1.8). Pitting failures were obtained, most pits occurring on the driving gear even though 1:1 ratio gears were used. This was identified as pitting, described in Section 4.4 and observed by Way (1935), amongst others, as it took the form of small fan shaped craters left by fragments of metal falling out of the surface. The pits were located close to the theoretical lowest point of single tooth contact (Figure 11.1.8), where the contact stresses were highest, so the idea that the disc tests should be considered relative to this position on the gear tooth seemed reasonable (this is discussed further in Chapter 13). The running contact stresses quoted for the gears were calculated at this point for this reason.

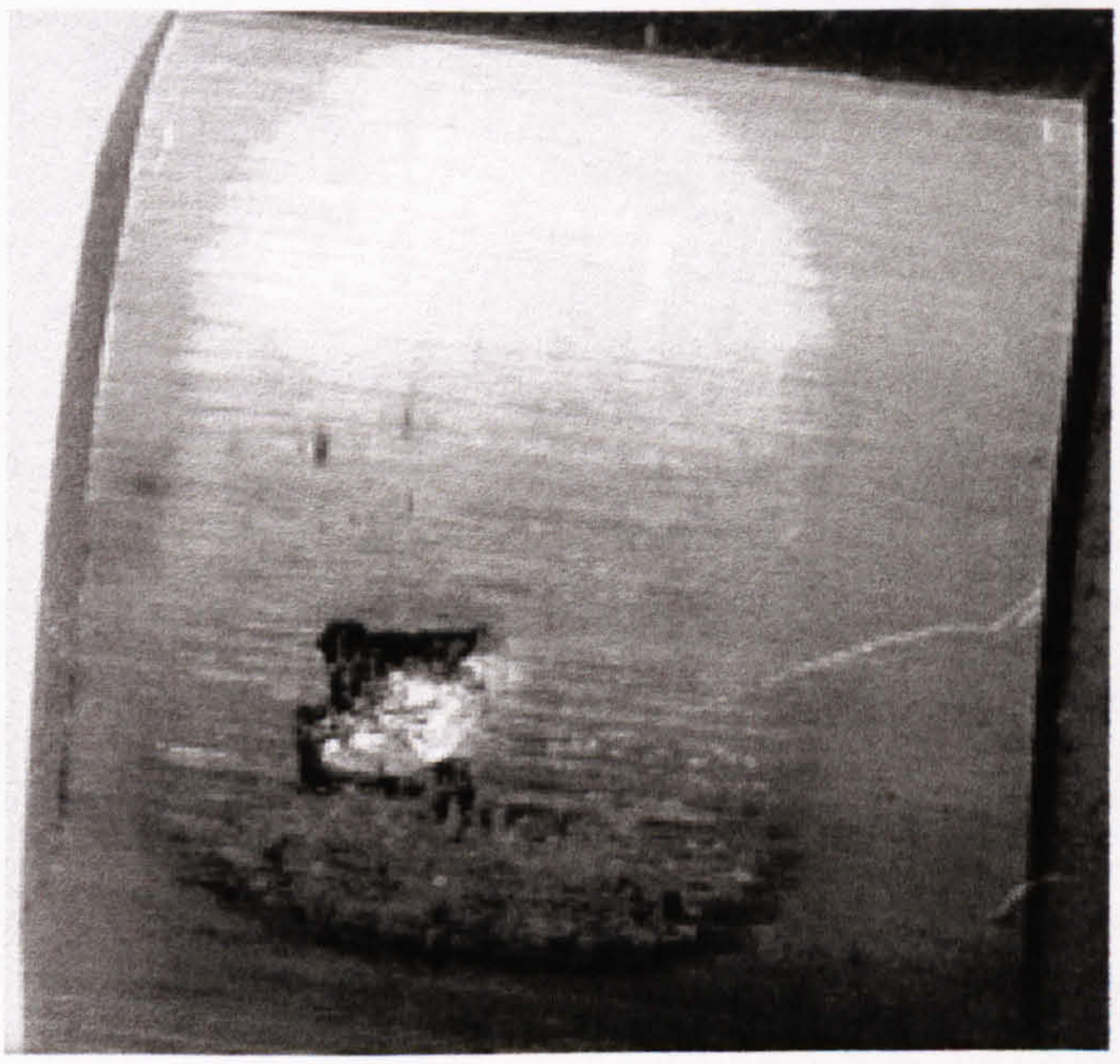


Figure 11.1.8 Pitting in a Tip-Relieved BS S156 Gear Tooth

Some of the pits had localised scuffs round them, possibly due to the stress concentrations caused by the edges of the pit (Figure 11.1.9).

The pitting damage would progress if the test was continued after initial pitting, and individual pits would join together causing severe damage to the tooth, as shown in Figure 11.1.10.

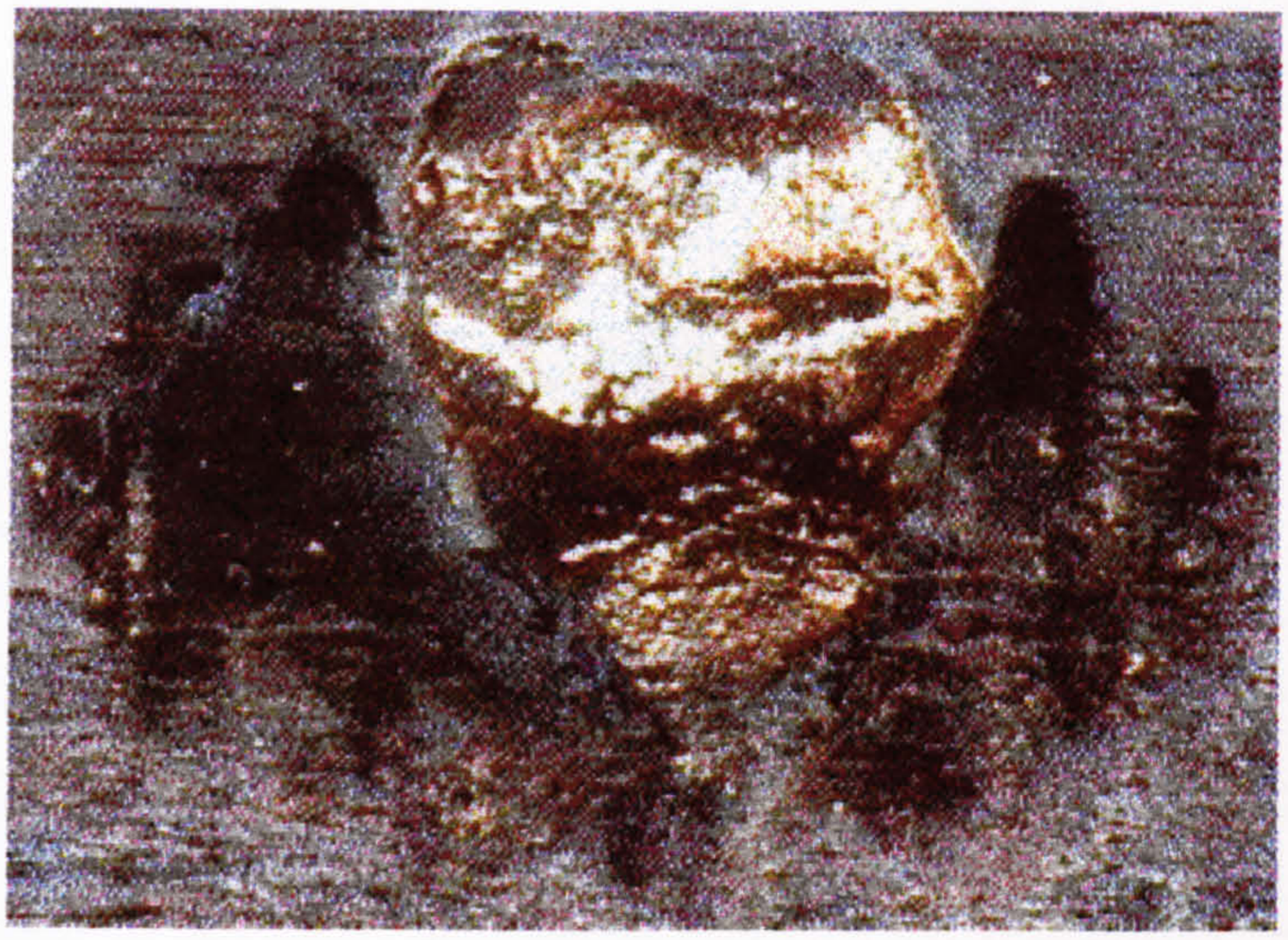


Figure 11.1.9 Pit Surrounded by Localised Scuffing in a Tip-Relieved BS S156 Gear

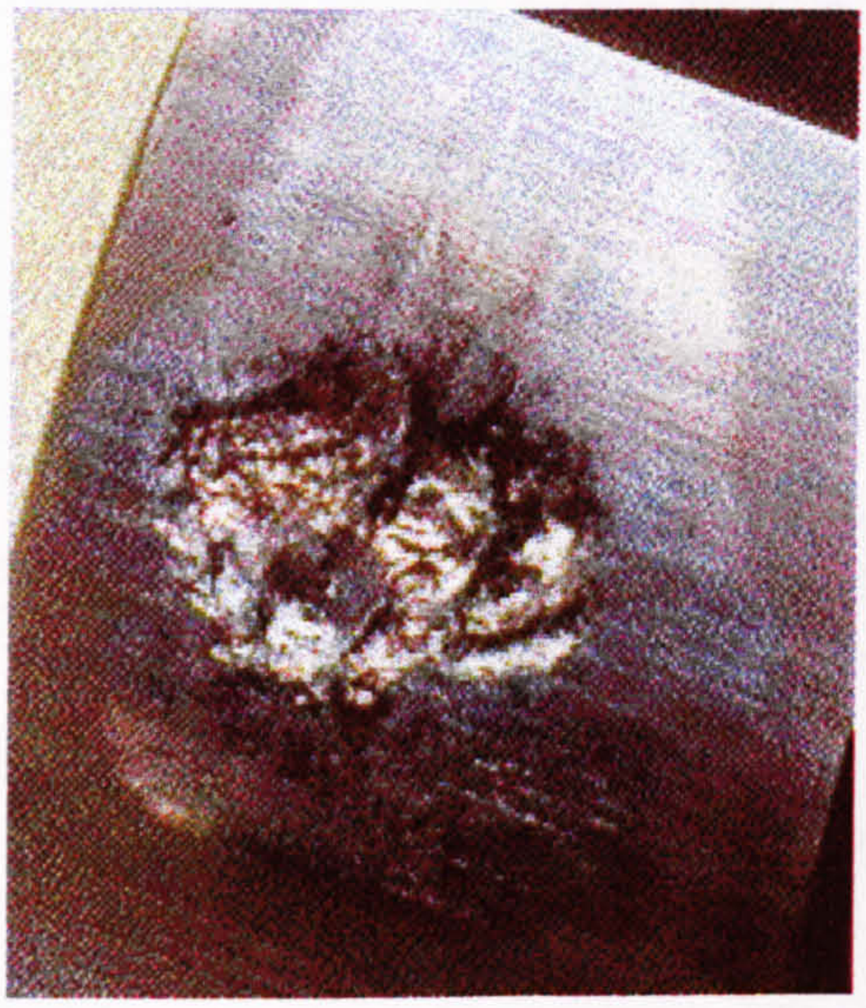


Figure 11.1.10 Severe Pitting Damage on a Tip-Relieved BS S156 Gear Tooth

The gear teeth did not only suffer from pitting damage but also exhibited micropitting mainly in the gear dedendum (Figures 11.1.11 and 11.1.12).



Figure 11.1.11 Transverse Section Through the Dedendum of a BS S156 Micropitted Gear Tooth (Etched in 2 % Nital) (500x)

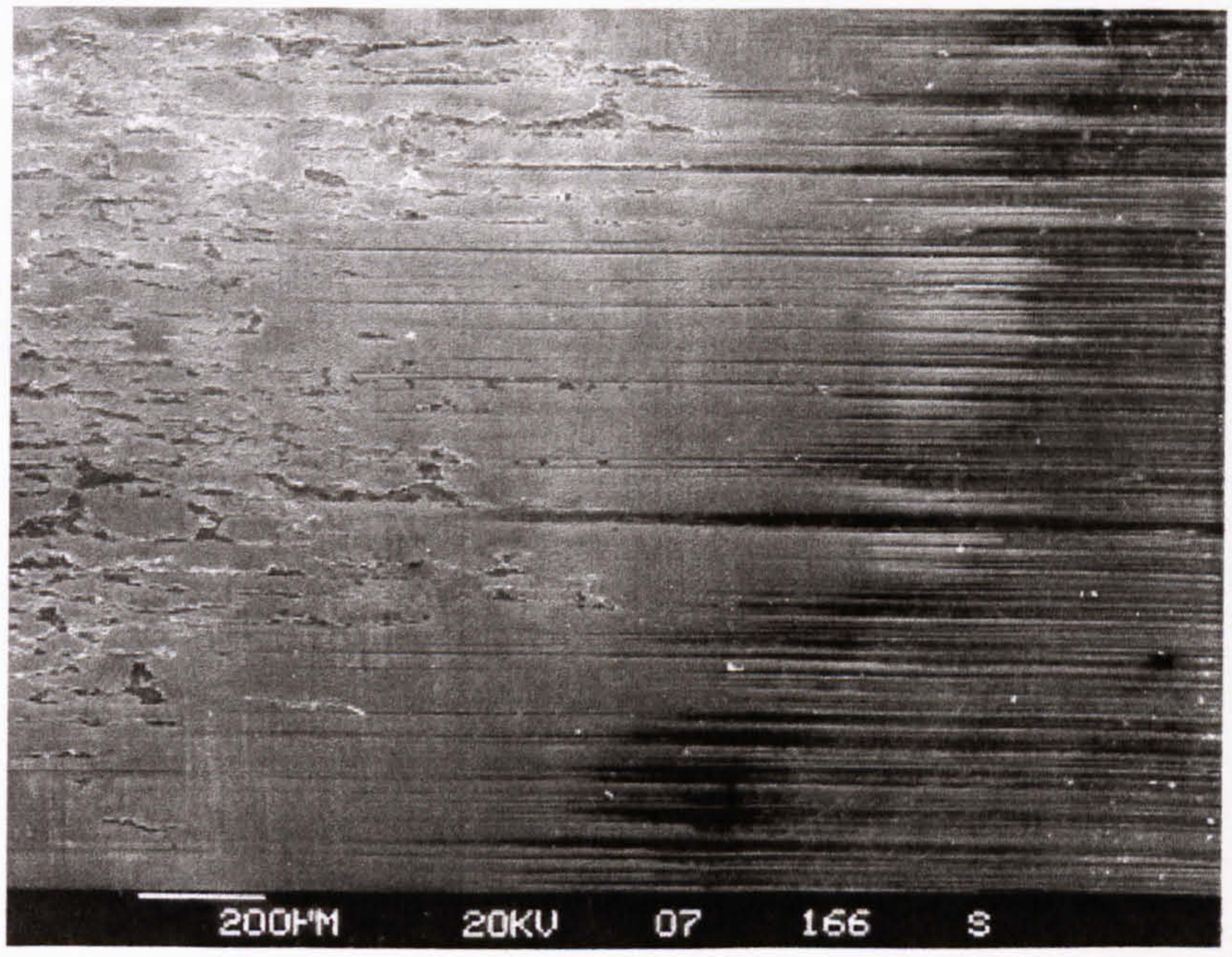


Figure 11.1.12 Scanning Electron Micrograph of the Edge of a Contact in a Tip-Relieved Gear Tooth Dedendum Showing Micropitting

Other gear teeth had pits in a fully scuffed addendum, as seen in Figure 11.1.13. To know which occurred first is difficult, but it is most likely that the scuff took place rapidly after pitting.

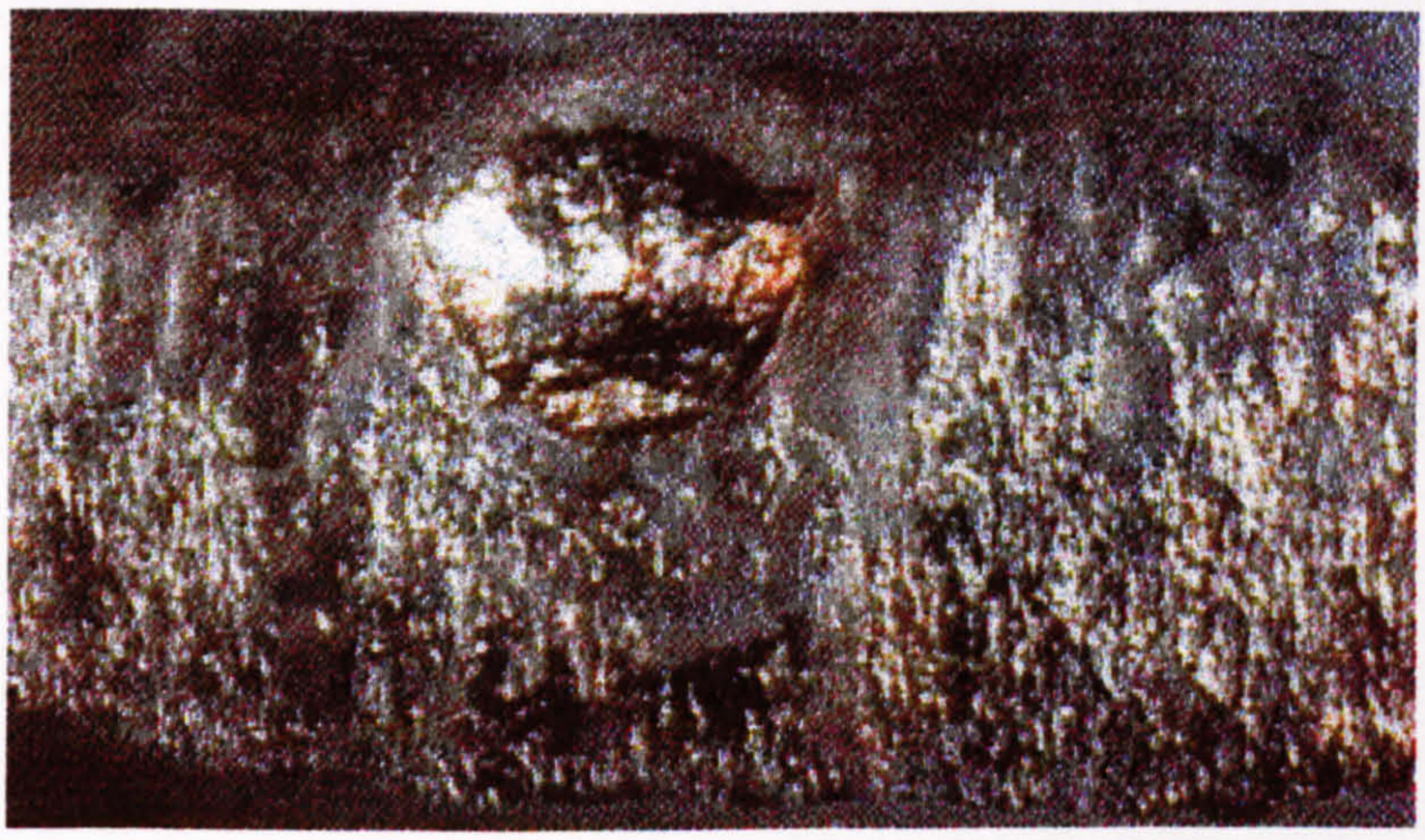


Figure 11.1.13 Pit in a Scuffed Dedendum of a Tip-Relieved BS S156 Gear

11.1.3 The AISI M50NiL Gear Tests

The AISI M50NiL gears, which were all tip-relieved, failed in a similar fashion to the tip-relieved BS S156 gears, exhibiting both pitting and micropitting, mainly in the dedendum (Figure 11.1.14). They had a shorter average life and the damage on the gears appeared to be greater with more severe cracks (Figure 11.1.15).



Figure 11.1.14 Micropitting and Pitting in an AISI M50NiL Gear Dedendum

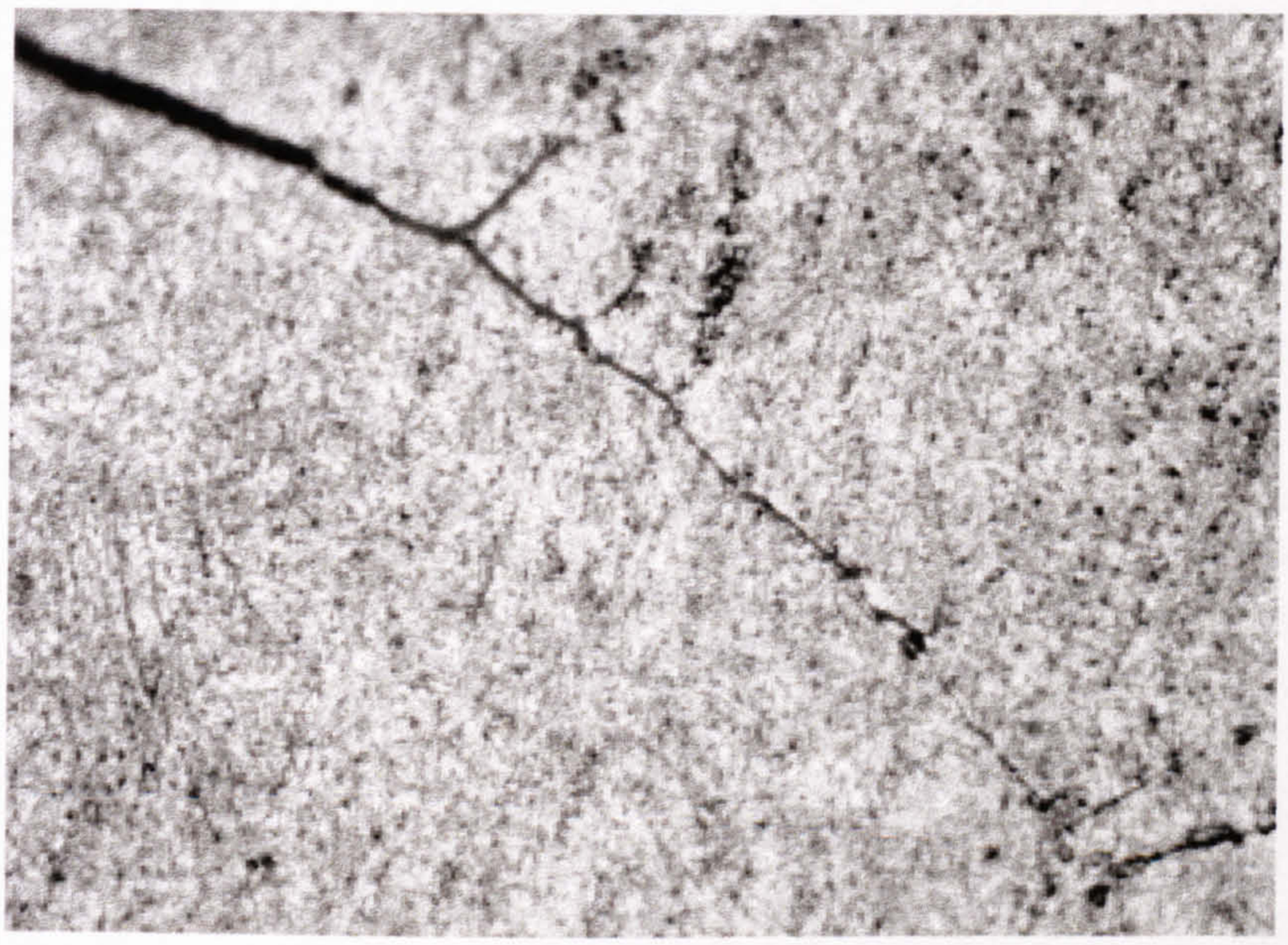


Figure 11.1.15 Transverse Section Showing Cracks in an M50NiL Gear
(Etched in 2 % Nital) (400x)

11.1.4 The AISI M50NiL Duplex Gear Tests

The AISI M50NiL Duplex gears were treated by plasma nitriding carburised AISI M50NiL tip-relieved gears. These duplex gears had a greatly improved pitting life when compared to the AISI M50NiL and BS S156 gears. After running them for about ten million cycles they did not exhibit pitting failures even at higher contact stresses. There was some micropitting concentrated mainly in the dedendum (Figure 11.1.16).

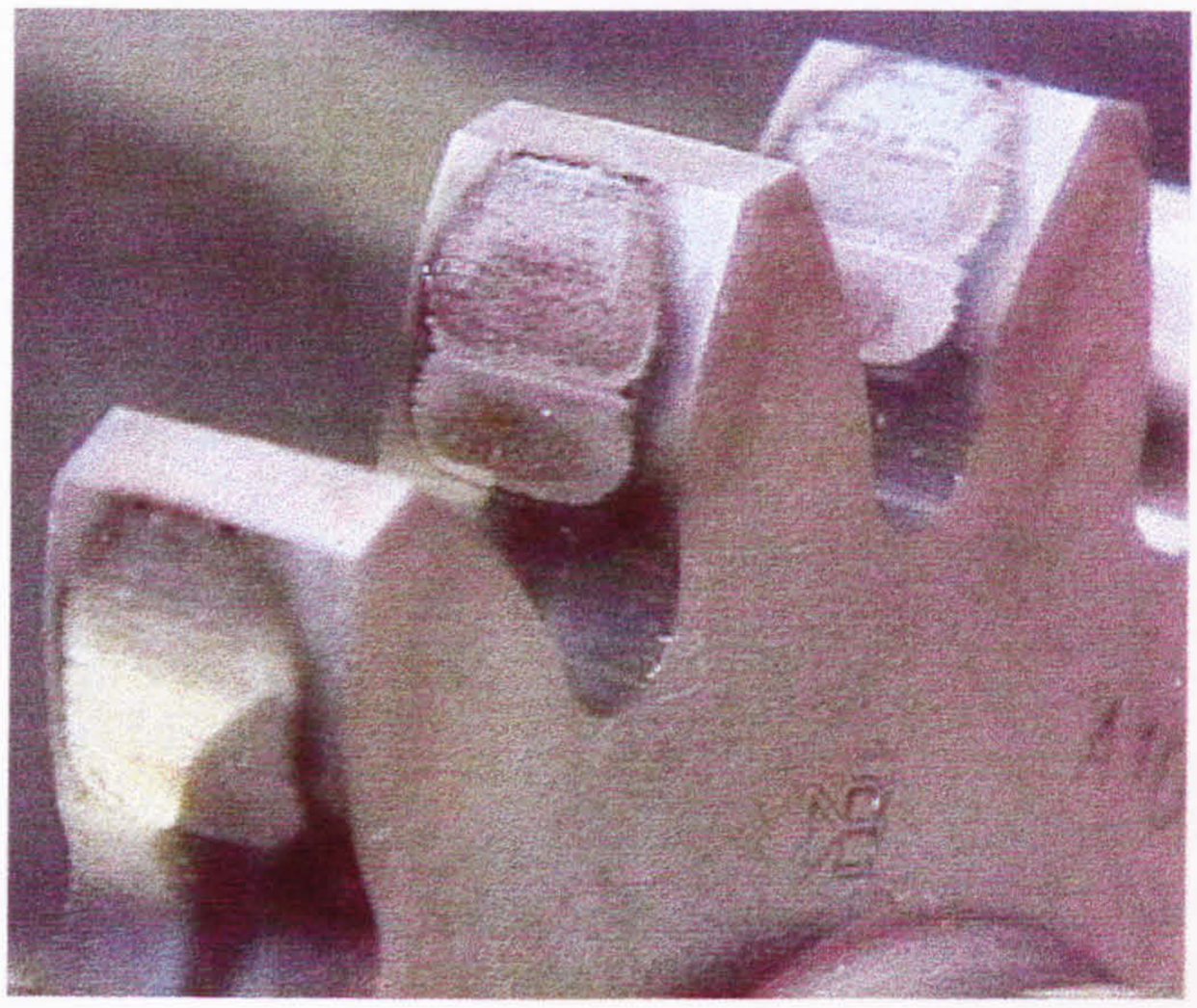


Figure 11.1.16 An AISI M50NiL Duplex Gear After Ten Million Load Cycles

11.2 Comparison of the Failed Gear Specimens

The relative damage to the gear tooth surfaces can be contrasted in Figures 11.2.1 and 11.2.2 for BS S156 and duplex AISI M50NiL gear dedenda, and in Figures 11.2.3 and 11.2.4 for the BS S156 and AISI M50NiL gear dedenda. The M50NiL duplex damage appears shallower in nature than either the M50NiL or S156. The damage on the dedendum and addendum of an AISI M50NiL gear can be compared in Figures 11.2.4 and 11.2.5.

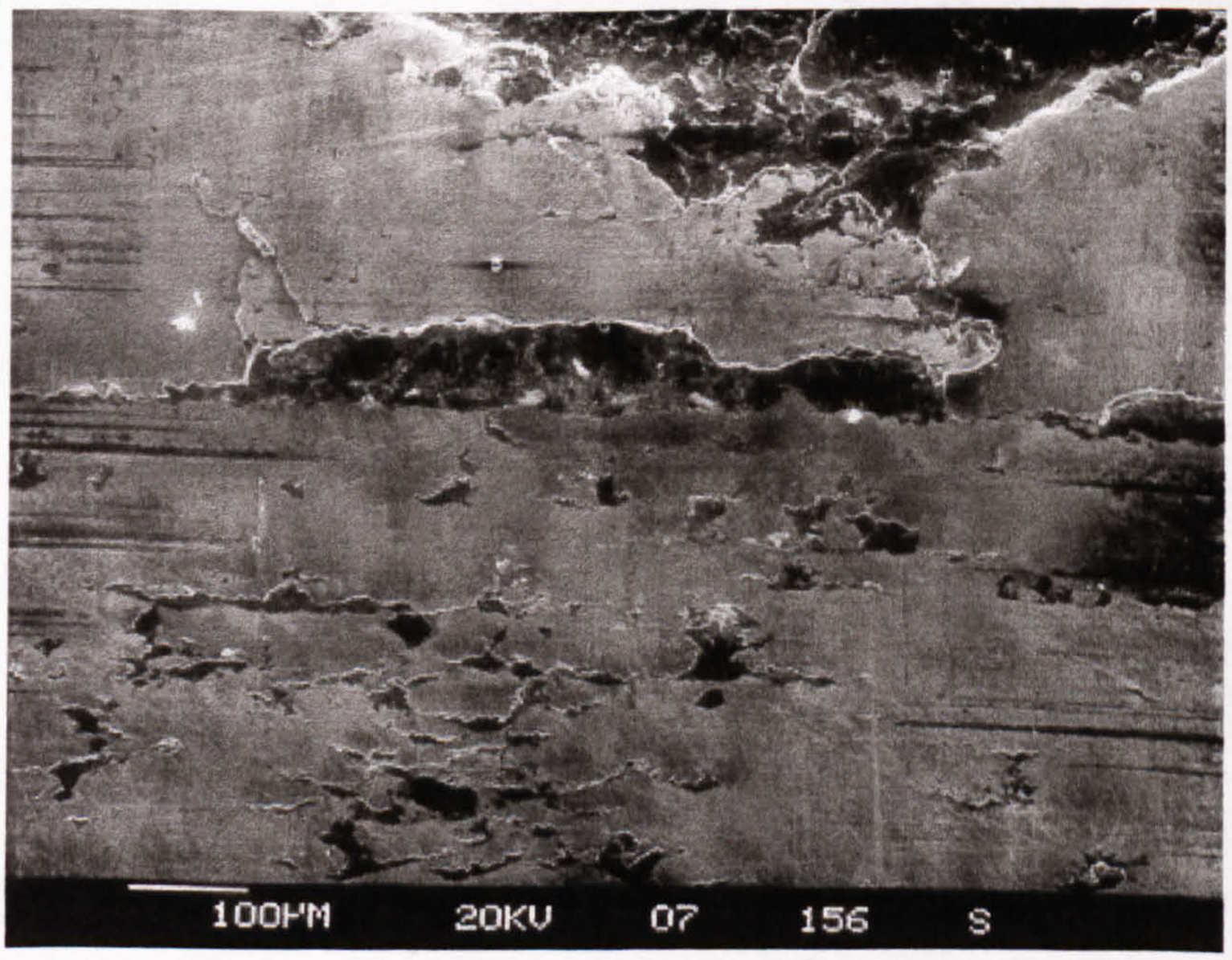


Figure 11.2.1 Scanning Electron Micrograph of a BS S156 Gear Dedendum ($0.5x10^6$ cycles at 2.6 GPa)

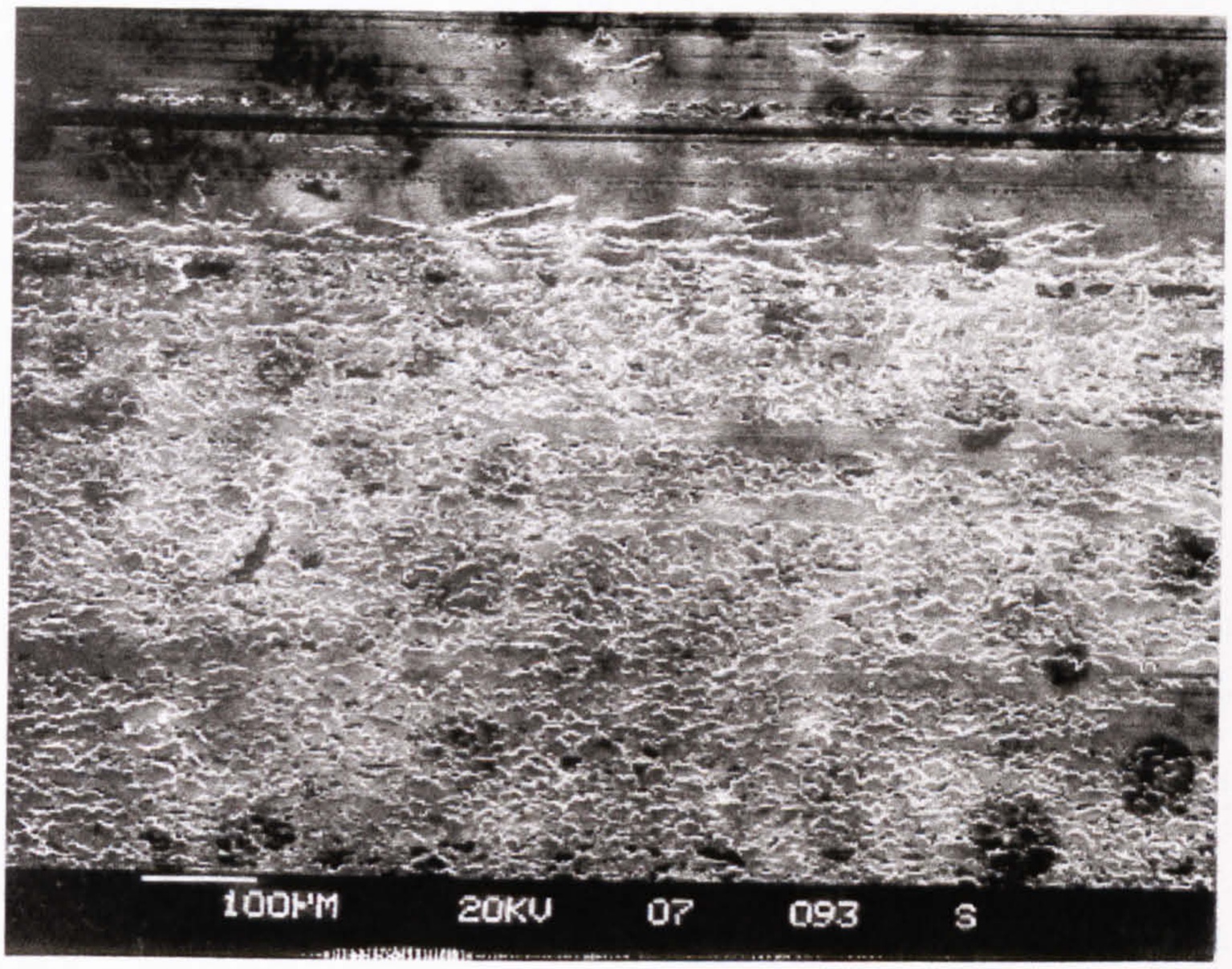


Figure 11.2.2 Scanning Electron Micrograph of an AISI M50NiL Duplex Gear Dedendum ($7.7x10^6$ cycles at 3 GPa)

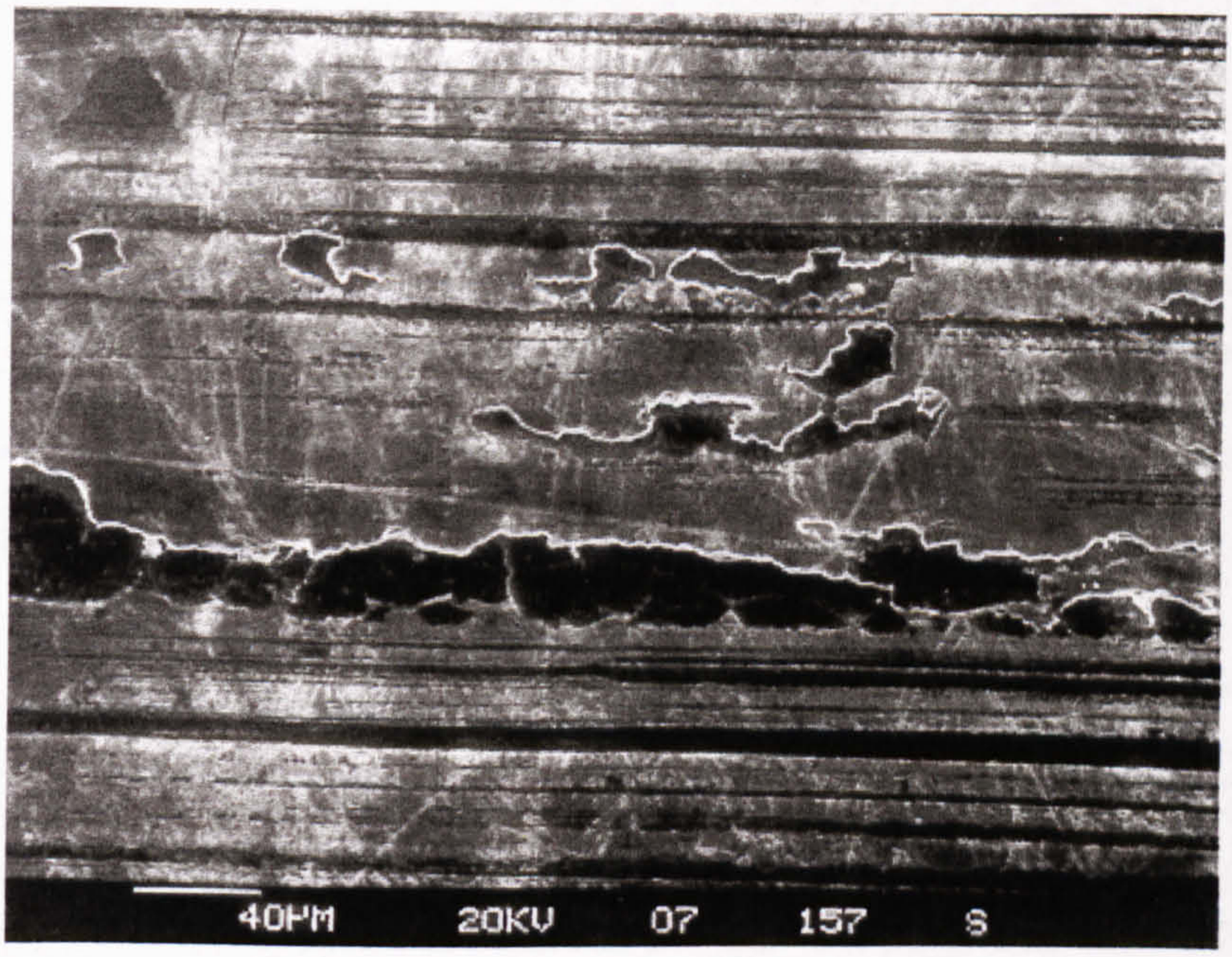


Figure 11.2.3 Scanning Electron Micrograph of a BS S156 Gear Dedendum ($0.4x10^6$ cycles at 2.6 GPa)

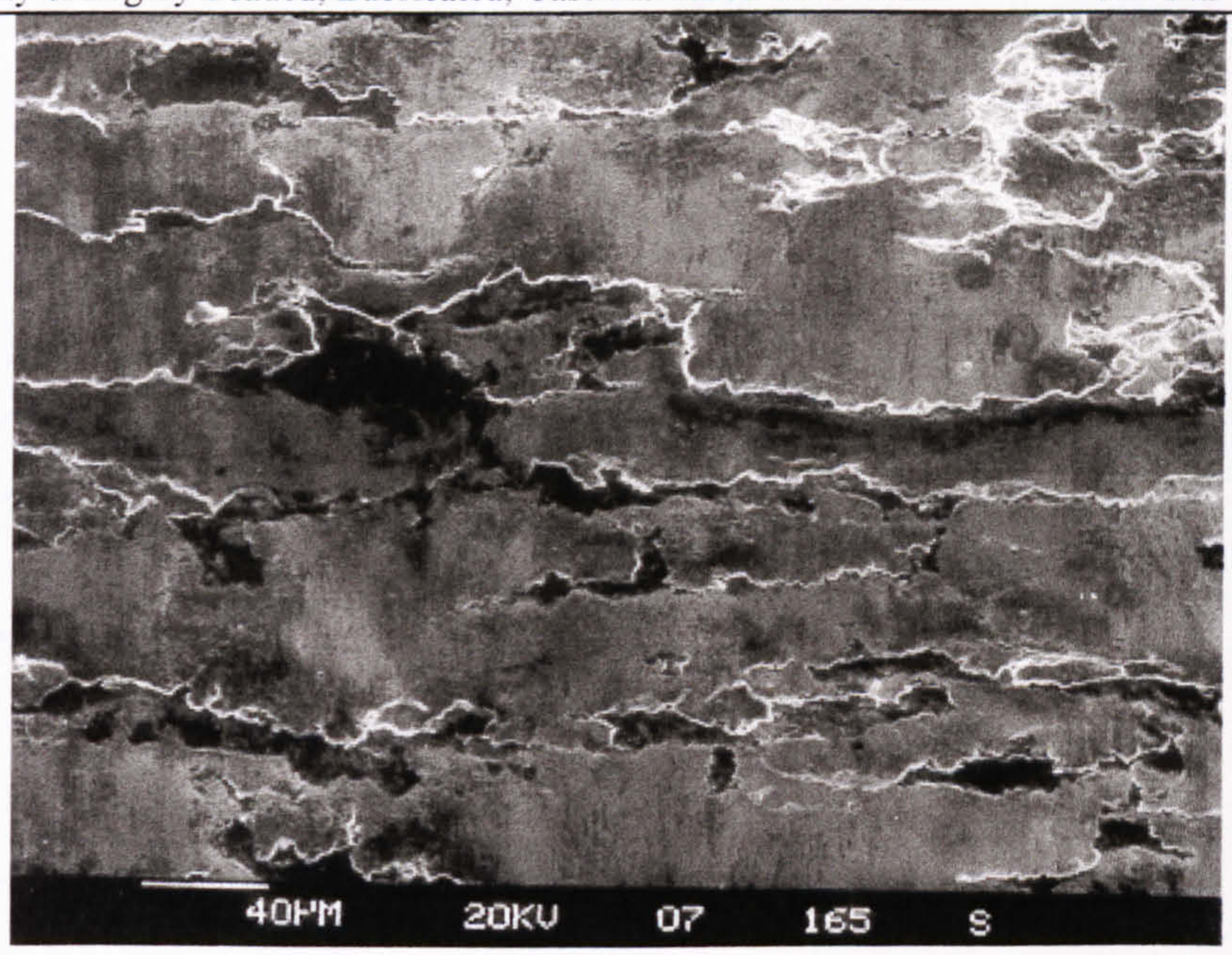


Figure 11.2.4 Scanning Electron Micrograph of an AISI M50NiL Gear Dedendum ($0.5x10^6$ cycles at 2.6 GPa)

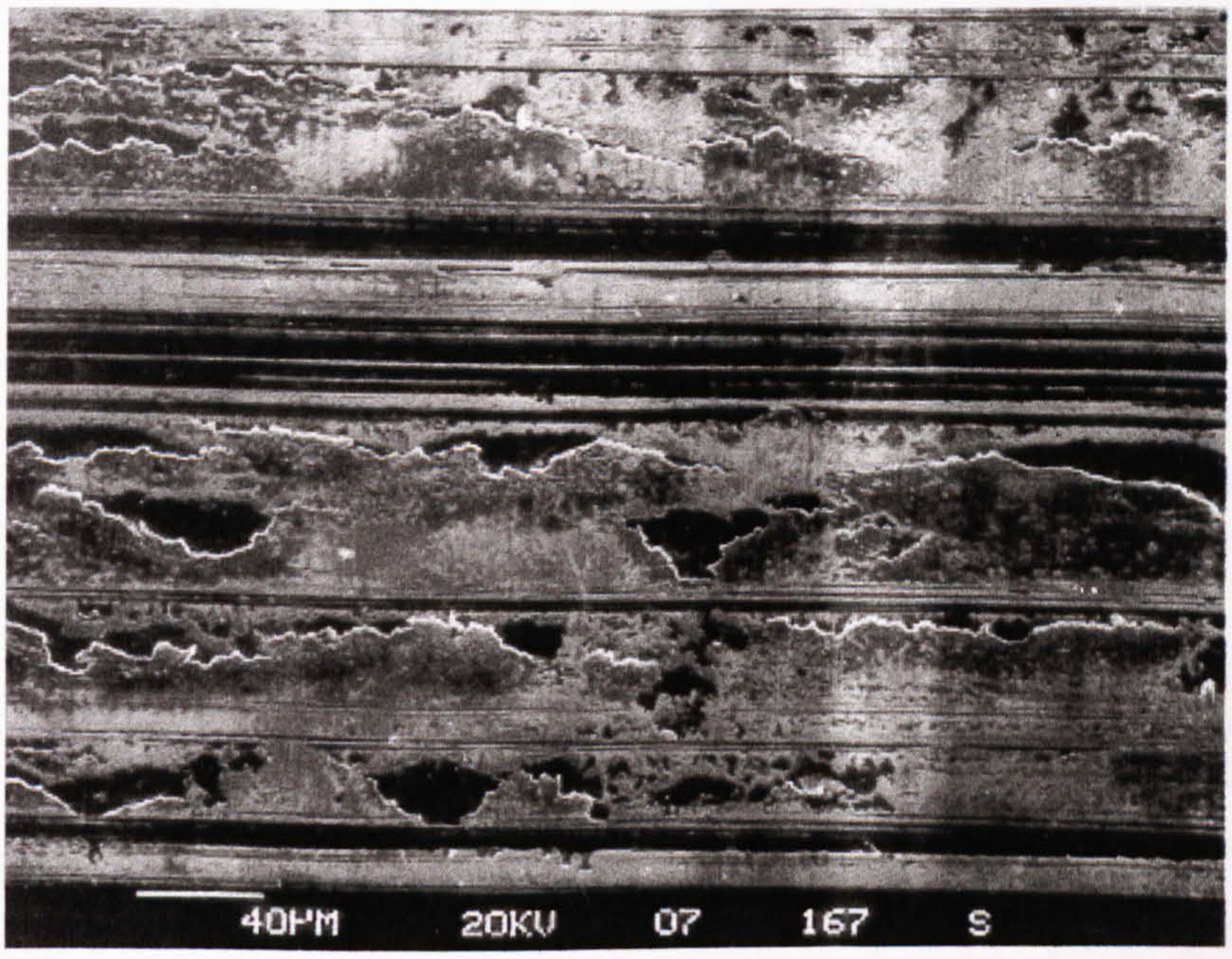


Figure 11.2.5 Scanning Electron Micrograph of an AISI M50NiL Gear Addendum ($0.5x10^6$ cycles at 2.6 GPa)

11.3 S-N and Weibull Analysis for the Gear Fatigue Tests

As mentioned the AISI M50NiL Duplex had a greatly improved rolling contact fatigue life when compared to the M50NiL and BS S156 gears. The fatigue lives for the gears are shown in Figure 11.3.1, one can see the AISI M50NiL Duplex offered improved rolling contact fatigue resistance as they were stopped without pitting failures.

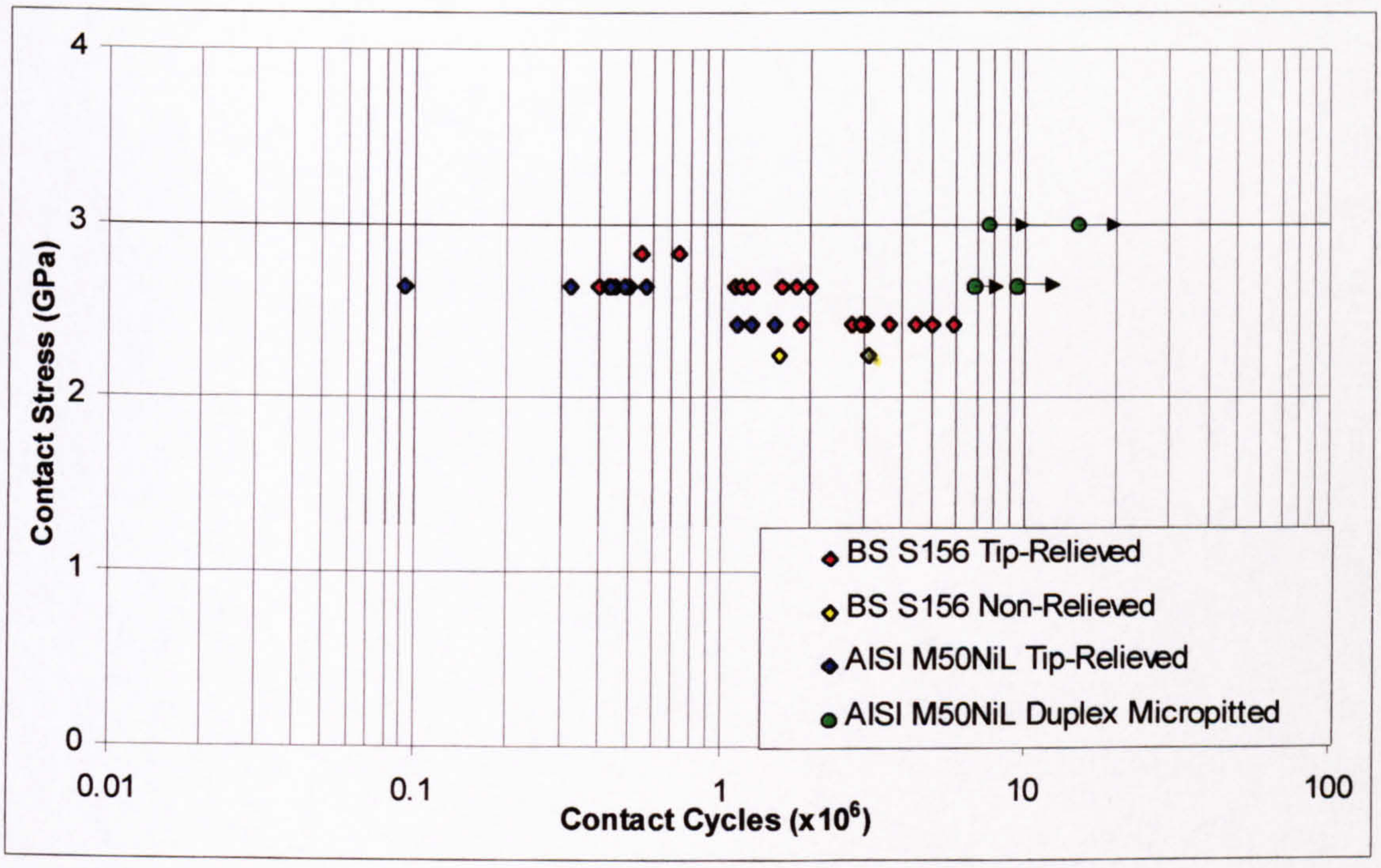


Figure 11.3.1 The BS S156, AISI M50NiL, and M50NiL Duplex Gear Fatigue Lives

The fatigue results were plotted on a Weibull chart (Figure 11.3.2), only tests carried out at similar contact stresses can be compared in this chart. The chart has a couple of tests carried out on the duplex gears at 3 GPa included, although they had not failed, and therefore should not be plotted on a Weibull chart.

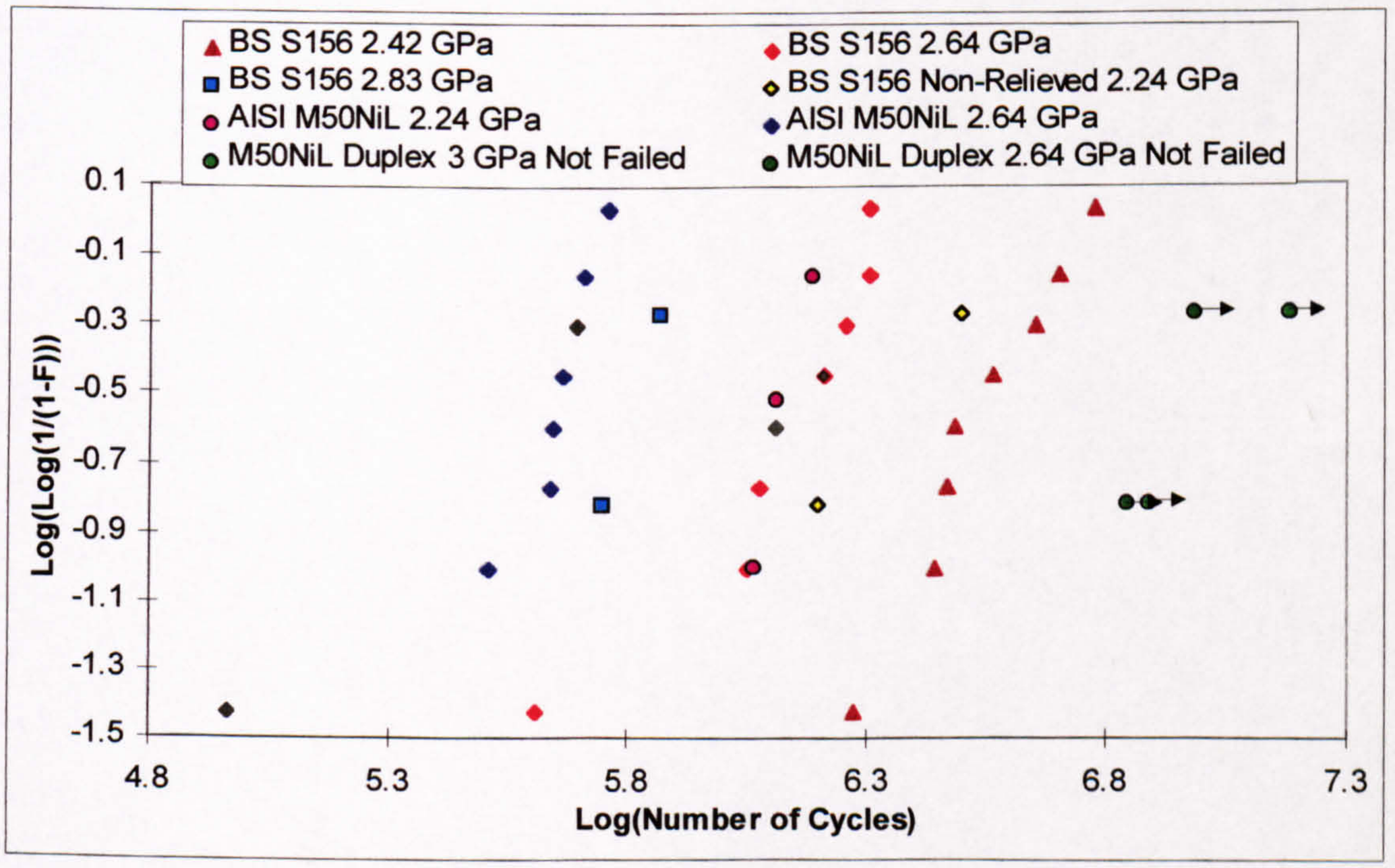


Figure 11.3.2 Weibull Plots of the Gear Contact Fatigue Lives

L_{50} lives were obtained for these fatigue tests and plotted on an S-N chart (Figure 11.3.3) to allow comparison of the different test specimen lives'.

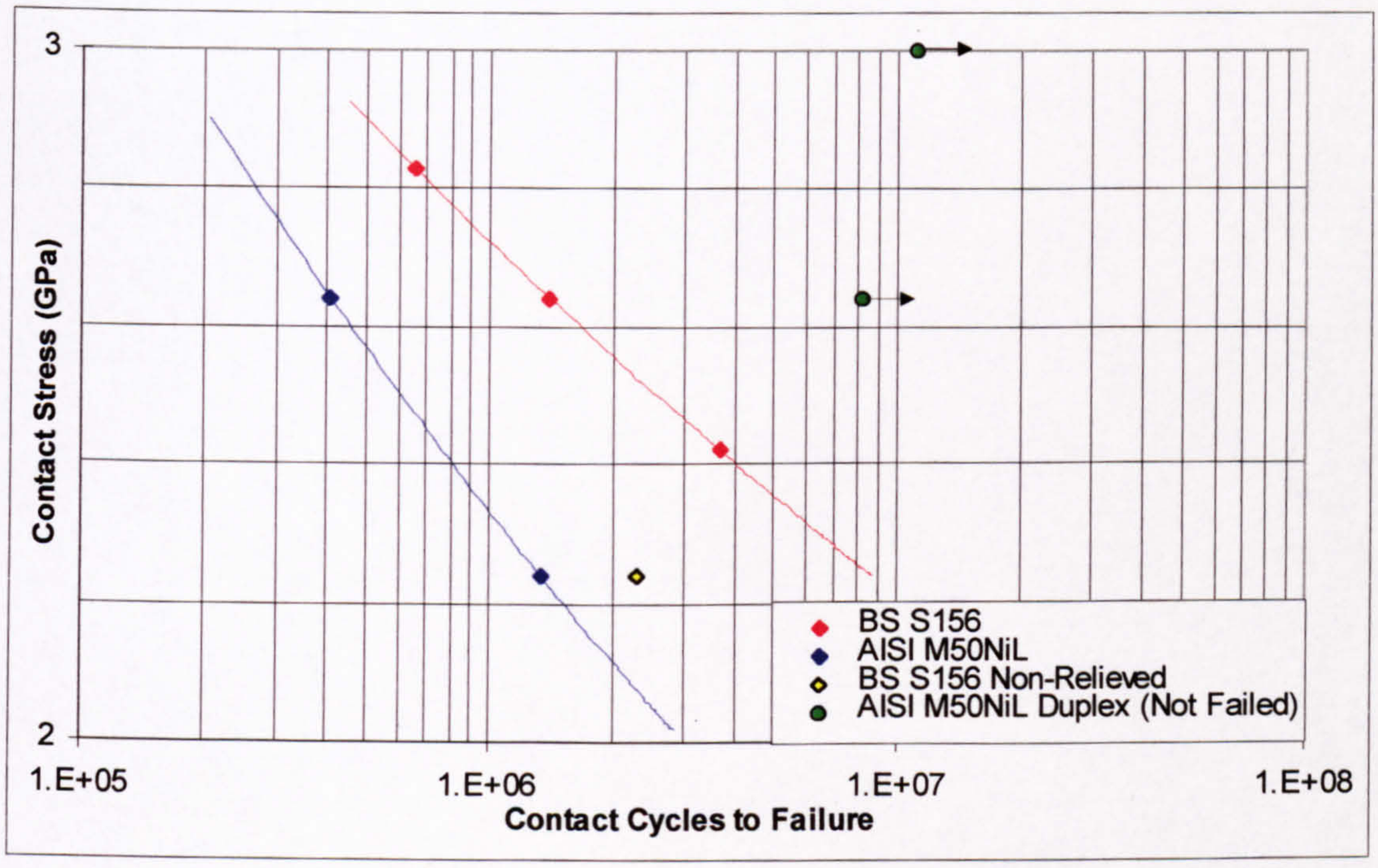


Figure 11.3.3 The L_{50} Lives for the Gear Contact Fatigue Tests

The comparison of the relieved and non-relieved gear tests is given in Figure 11.3.4. These tests were only done with specimens manufactured from BS S156.

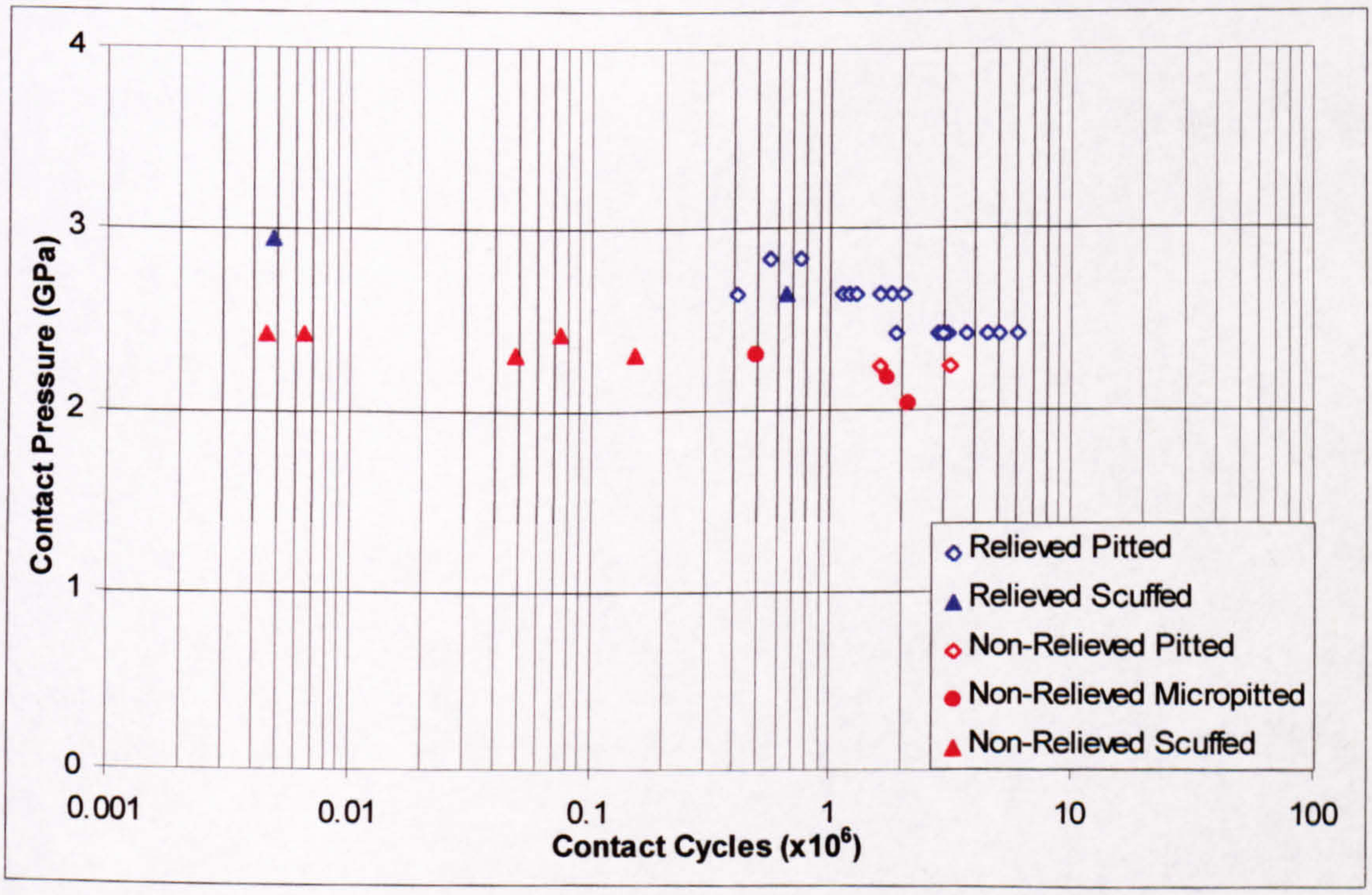


Figure 11.3.4 The Tip-Relieved and Non-Tip-Relieved BS S156 Gear Fatigue Tests

11.4 The Axial Fatigue Test Results

Testing of the axial fatigue specimens was carried out at GKN Wetland Helicopters under tensile, zero and compressive mean stress conditions, using mean/alternating stress ratios of 0.5 (P±2P), 0 (0±P), and -0.185 (-P±5P) at elevated temperature (150 °C) and 0 (0±P) at room temperature. These mean/alternating stress ratios were chosen to simulate the tooth root stresses in idler gears (0±P), conformal gears (-P±5P), and most other gears (P±2P).

Regardless of alloy composition, the highest endurance stress was obtained with a compressive mean stress and the lowest endurance stress with a tensile mean stress (Figures 11.4.1 and 11.4.2). The type and proportion of each failure was found to depend on the applied mean stress, there being more core-originated failures in the compressive stress regime and vice-versa (Davies 1996).

In order to investigate the gear steel performance at elevated temperatures, tests were carried out at 150 °C in an oil environment. Raising the test temperature reduced the fatigue lives regardless of alloy composition (Figure 11.4.3).

When the axial fatigue tests are compared (Figure 11.4.4), the duplex treated AISI M50NiL specimens performed better than both the AISI M50NiL and the BS S156.

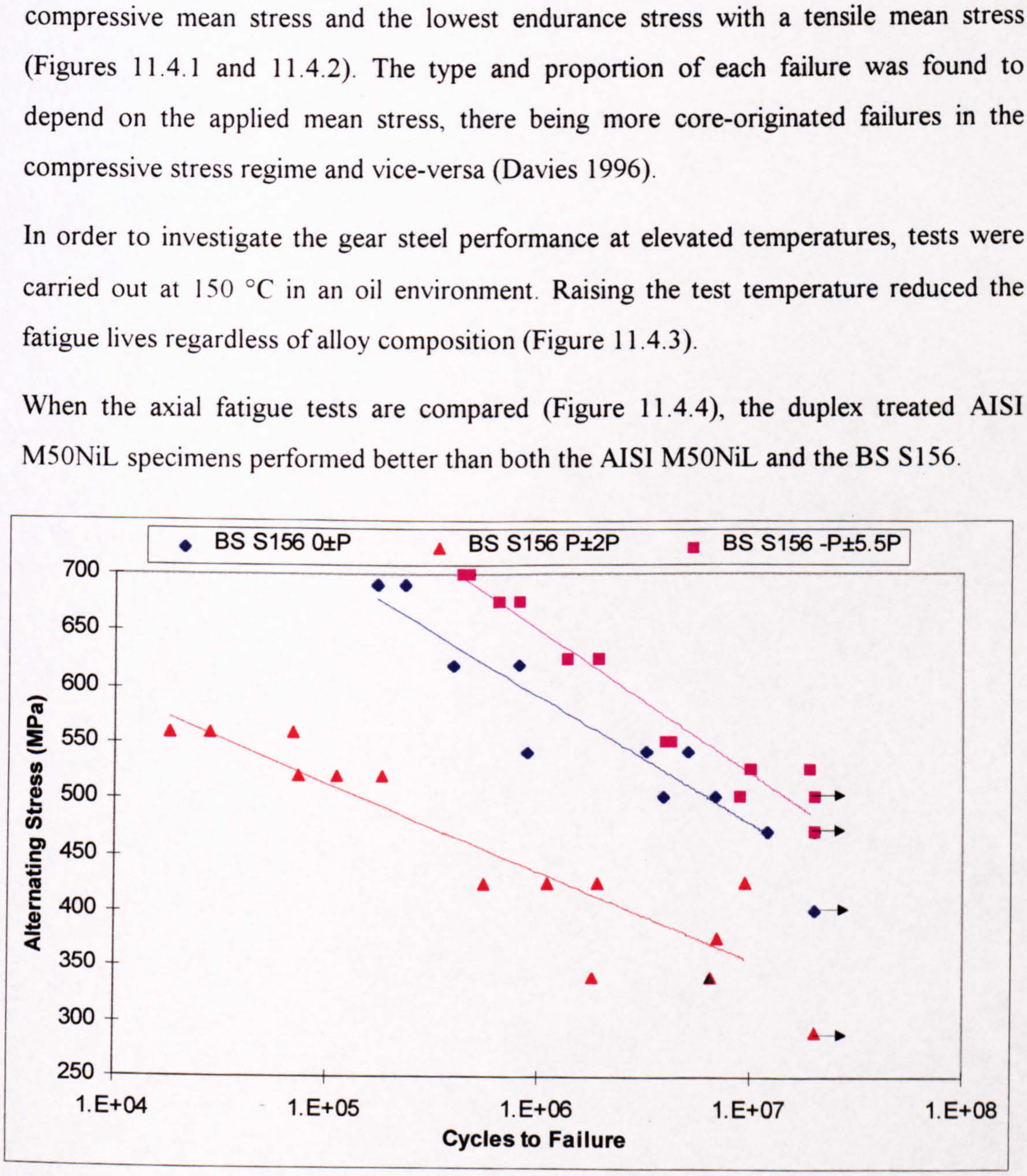


Figure 11.4.1 The BS S156 Axial Fatigue Tests at 150 °C

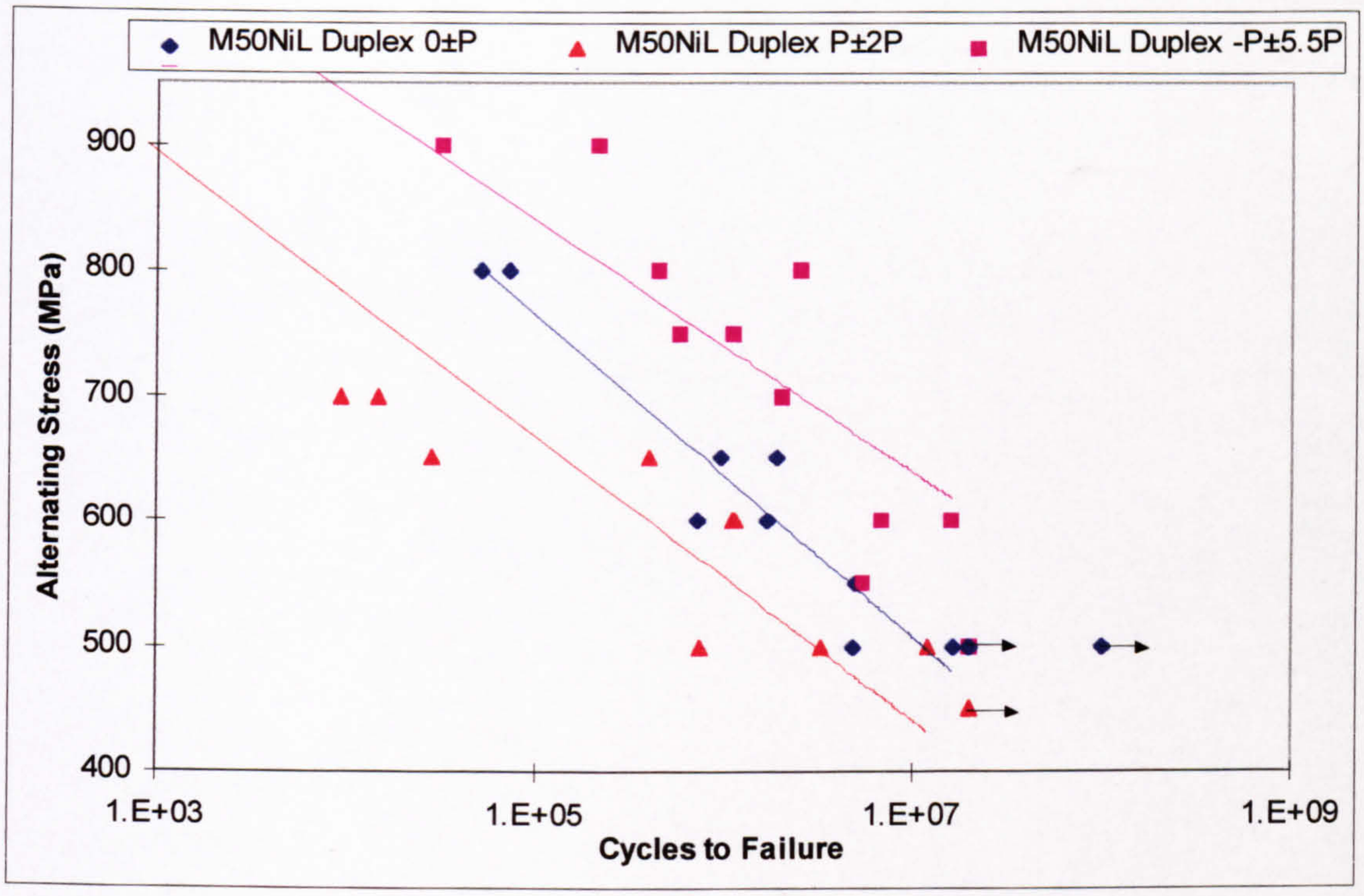


Figure 11.4.2 The AISI M50NiL Duplex Axial Fatigue Tests at 150 °C

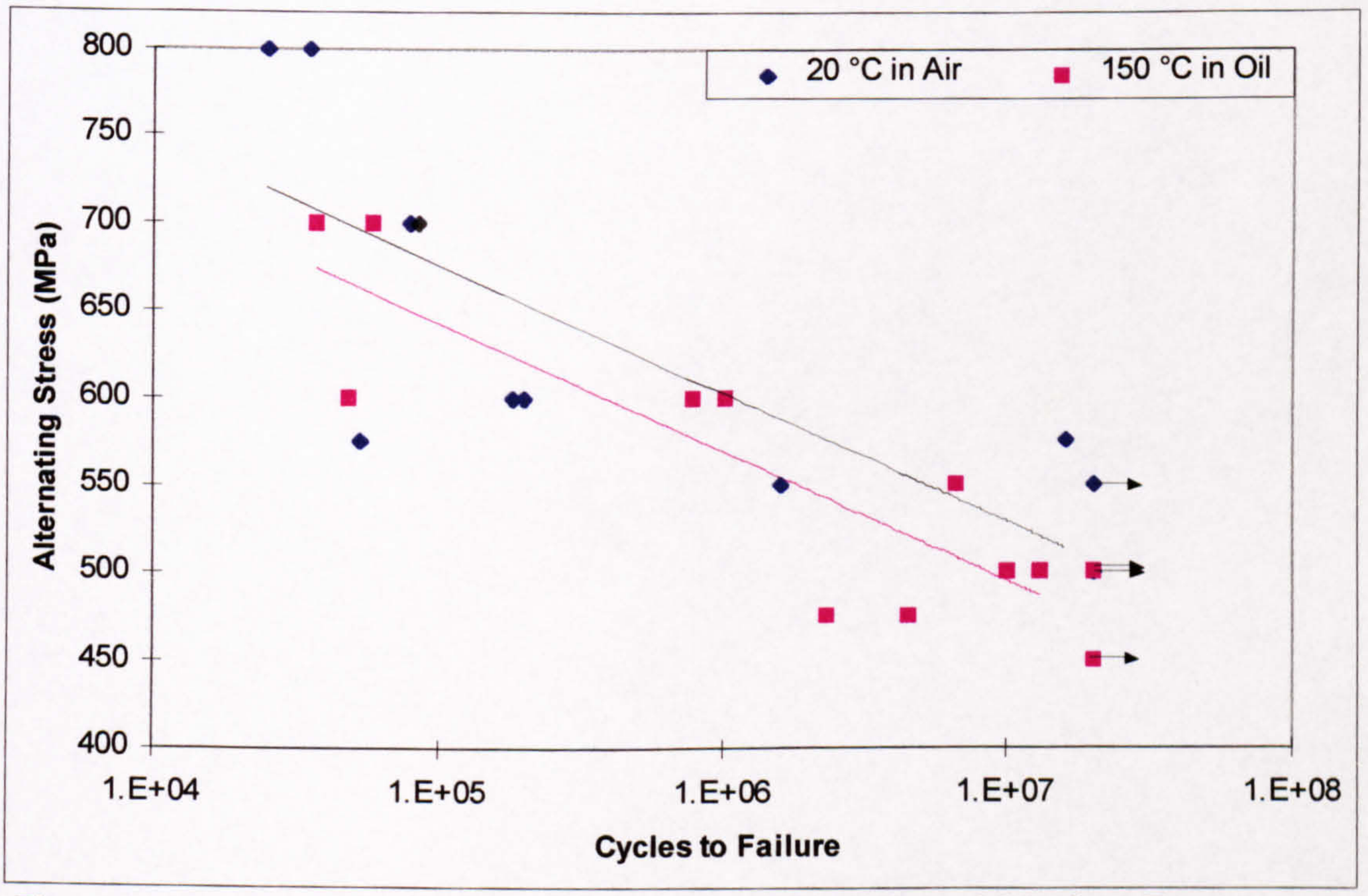


Figure 11.4.3 The Effect of Temperature on AISI M50NiL Axial Fatigue Tests

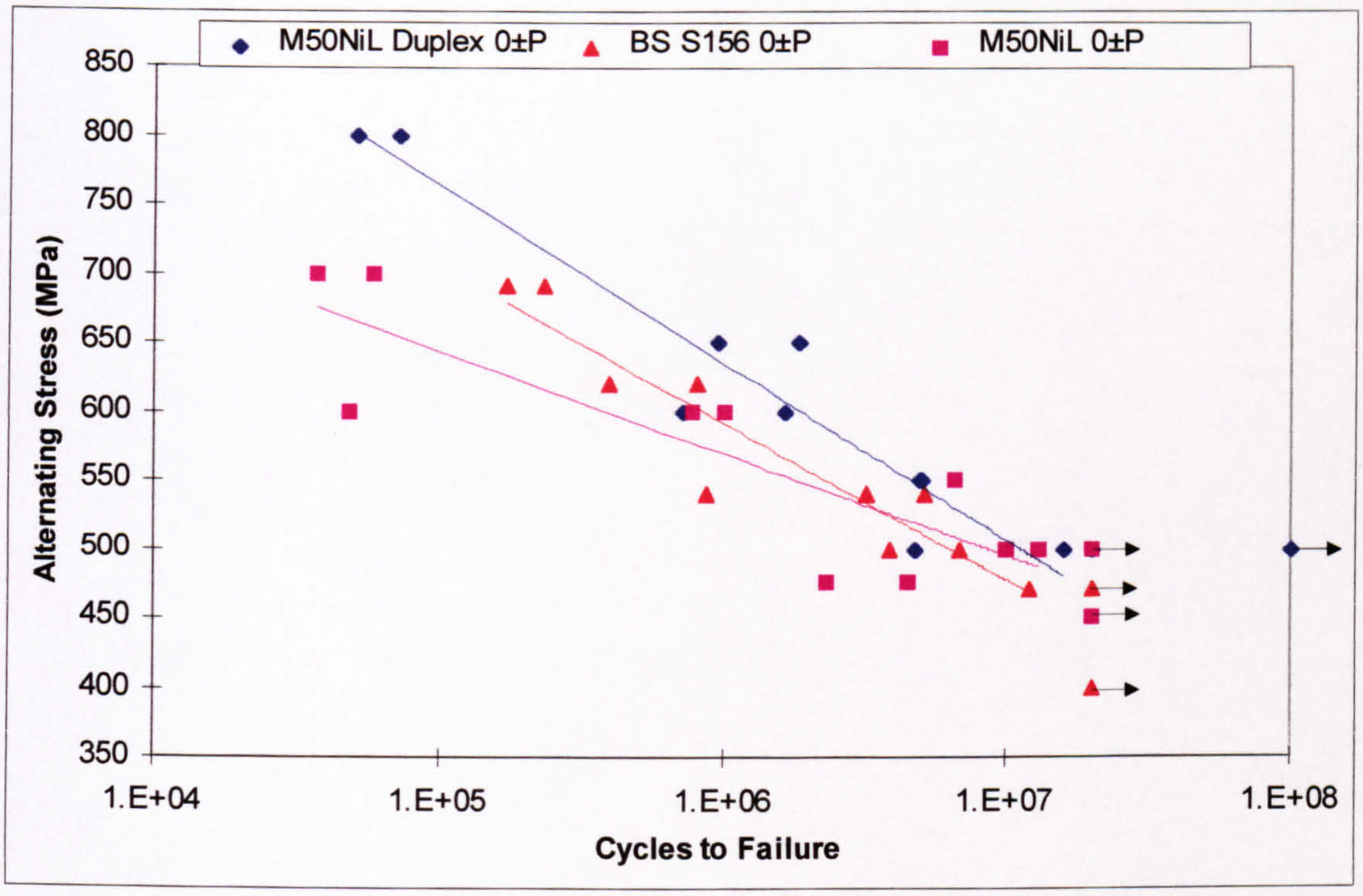


Figure 11.4.4 Comparison of the BS S156, AISI M50NiL and M50NiL Duplex Axial Fatigue Tests at Zero Mean Stress and 150 °C

11.5 Conclusions from the Gear and Axial Fatigue Tests

- The tip relieved gears could be run at higher loads than the non-relieved gears without scuffing. Scuffing occurred in the non-relieved gears if they were loaded too quickly, or too much (a limit of around 2.3 GPa was found). The tip-relieved gears could run at contact stresses of up to 3 GPa.

- The non-tip-relieved gear teeth suffered from localised damage caused by the tip of the gear tooth interfering with the root of the mating tooth, i.e. extended contact. The contact width also tended to expand at the tip and root of the tooth, unlike the contact pattern in the tip-relieved gears which had no hard marking in the gear root and was more rounded.

- If the non-relieved gears were loaded gently and kept at low loads, the contact pattern would broaden due to excessive wear on the tooth flank. This made the gear contact more conforming (lower contact stresses) and enabled the load to be increased considerably. It was found that this excessive wear was caused by micropitting.

- Pitting failures were obtained in the tip-relieved gears, most pits occurring on the driving gear, even though 1:1 ratio gears were used. The pits were located close to the theoretical lowest point of single tooth contact, so the idea that the disc tests

should be considered relative to this position on the gear tooth seems reasonable. The running contact stresses quoted for the gears were calculated at this point.

- The AISI M50NiL Duplex (plasma nitrided) gears had a greatly improved rolling contact fatigue resistance when compared to the AISI M50NiL and BS S156 gears. The AISI M50NiL gears failed in a similar fashion to the BS S156 material, exhibiting both pitting and micropitting, mainly in the dedendum, but had a shorter average life. The Duplex specimens did not fail by pitting within ten million cycles, but suffered some micropitting in the dedendum.

- In the axial fatigue tests, regardless of alloy composition, the highest endurance stress was obtained with a compressive mean stress and the lowest endurance stress with the tensile mean stress. The type and proportion of each failure was found to depend on the applied mean stress, there being more core-originated failures in the compressive stress regime and vice-versa. Raising the test temperature reduced the fatigue lives regardless of alloy composition.

- When the axial fatigue tests were compared, the AISI M50NiL Duplex specimens performed better than both the AISI M50NiL and the BS S156 ones.

Chapter 12 The Disc Test Experimental Results

In this chapter the results of the disc fatigue tests described in Chapter 7 are reported. The discussion of the results presented here is given in Chapter 13.

12.1 Examination of the Disc Contact Fatigue Test Results

Two designs of barrel specimen were run with the three counterface rings, one with a crown in the axial direction and one with a chamfered edge, as discussed in Chapter 7. The BS S156 material was used to investigate the differences between the chamfered and crowned barrels, all the other disc materials were investigated with chamfered specimens. The tests conducted on both types of barrel specimen are discussed here.

12.1.1 The Chamfered BS S156 Disc Tests

A few tests were carried out with BS S156 chamfered barrels at the high slide roll-ratio (-0.28). These scuffed, not in a violent manner, but the surface progressively deteriorated as seen in Figure 12.2.1. The vibration signal gradually edged upwards during the final stages of loading and the test was stopped. The initially smooth aspect of the surface had been altered, becoming striated in appearance.

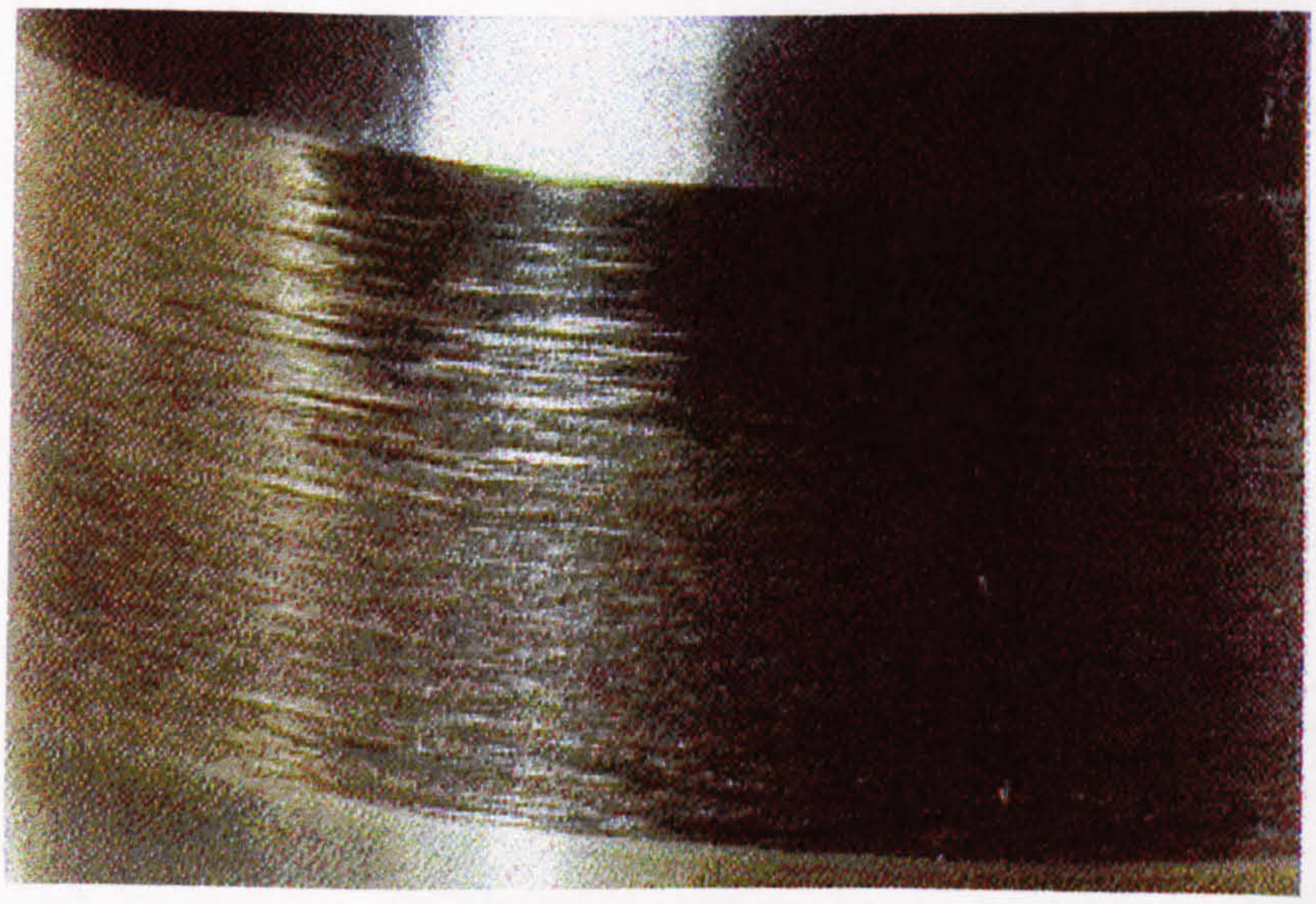


Figure 12.1.1 Scuffing on Chamfered Barrel Run at -0.28 Slide-Roll Ratio

The slide-roll ratio was then lowered (-0.14 and -0.026) to avoid this failure. At these lower slide-roll ratios pitting and micropitting occurred in the chamfered specimens. Pitting always took place on the track edge in these specimens (Figures 12.1.2).

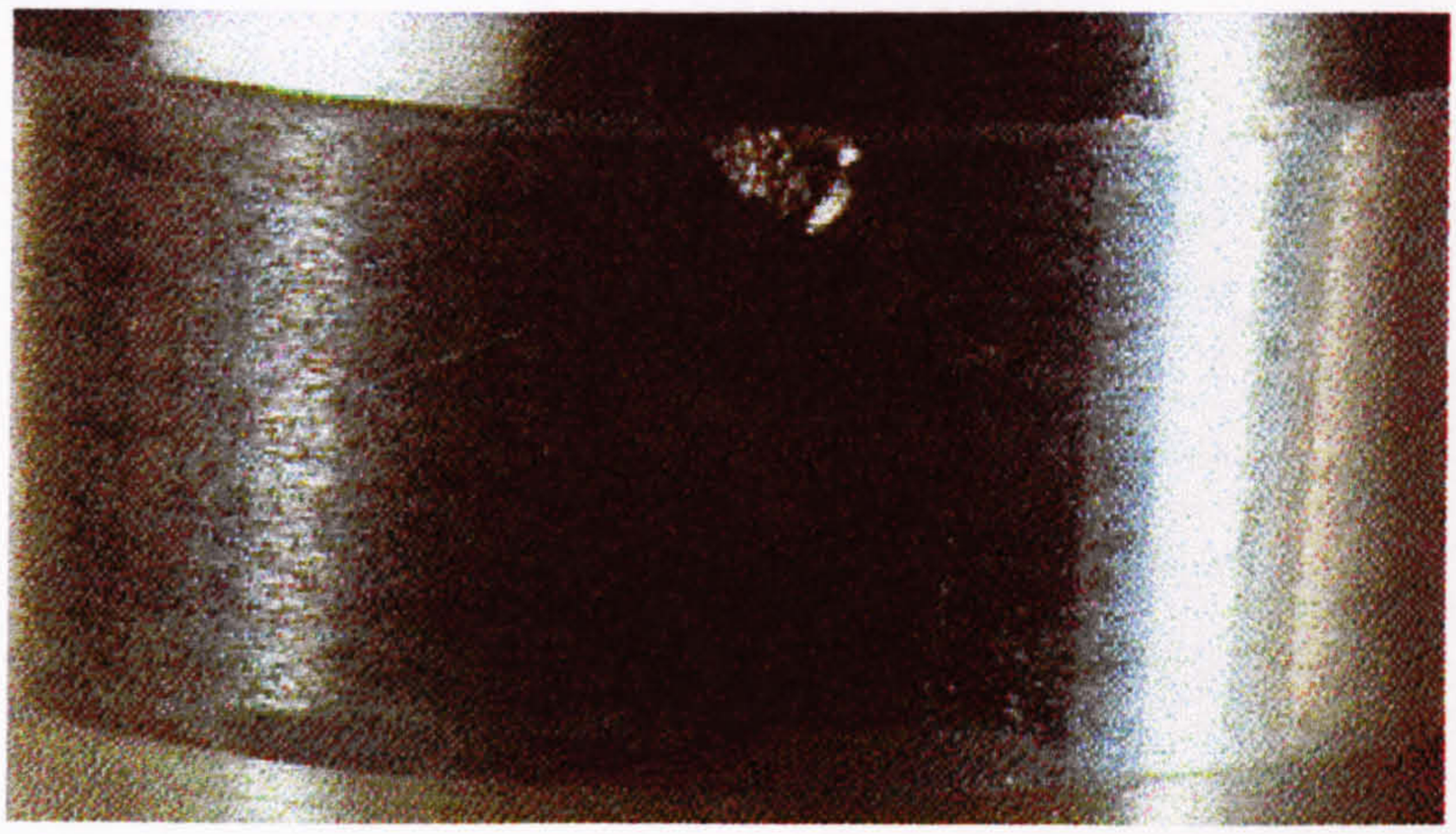


Figure 12.1.2 Pitted Chamfered Barrel Run at -0.14 Slide-Roll Ratio

Many specimens failed by pitting but also suffered from micropitting, as seen in Figure 12.1.3. The specimens that micropitted appeared to have longer lives than specimens that only pitted, as observed by Olver (1995).

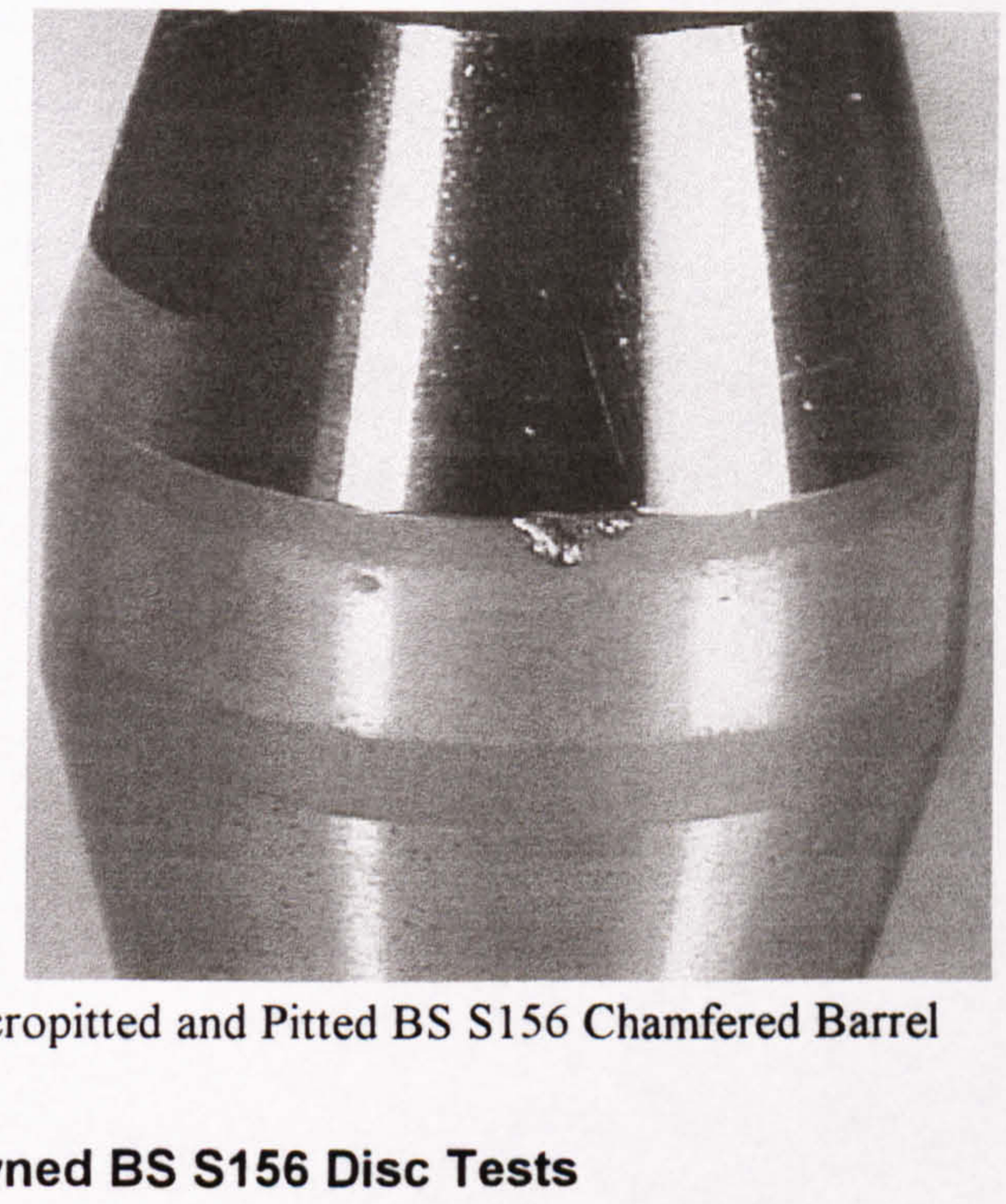


Figure 12.1.3 Micropitted and Pitted BS S156 Chamfered Barrel

12.1.2 The Crowned BS S156 Disc Tests

The crowned BS S156 specimens run at slide-roll ratios of -0.14 and -0.026 also exhibited pitting and micropitting failures. Unlike the chamfered specimens the damage was located in the middle of the track and had a different shape (Figure 12.1.4). The

track width was much narrower than the chamfered barrel because of the crown, and there was no edge contact. The maximum Hertzian contact pressure required to obtain pitting in these specimens was higher than in the chamfered specimens. Most of the barrels looked like that shown in Figure 12.1.5, which when observed closely (Figure 12.1.6) was micropitting.

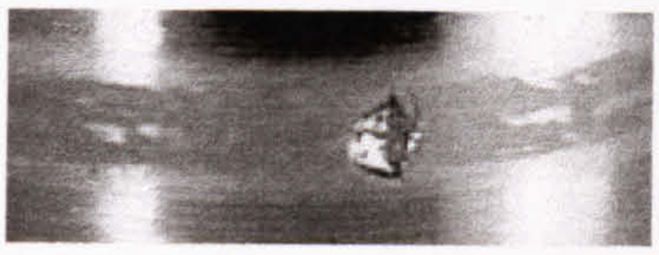


Figure 12.1.4 Pitted and Micropitted Crowned BS S156 Barrel

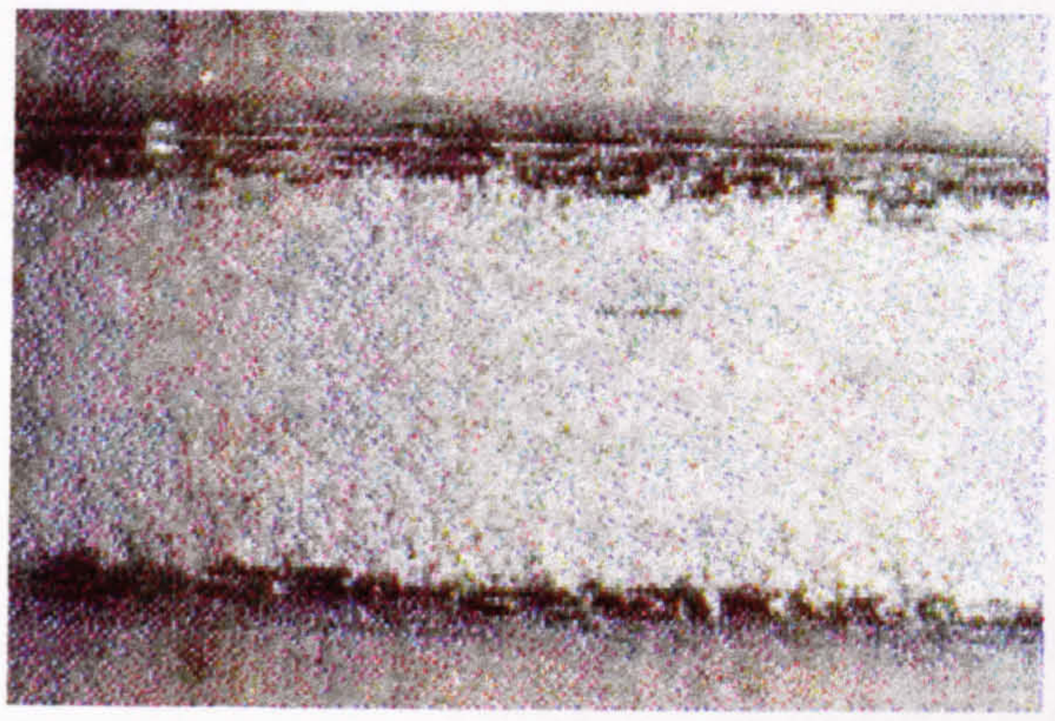


Figure 12.1.5 Micropitted Crowned BS S156 Barrel

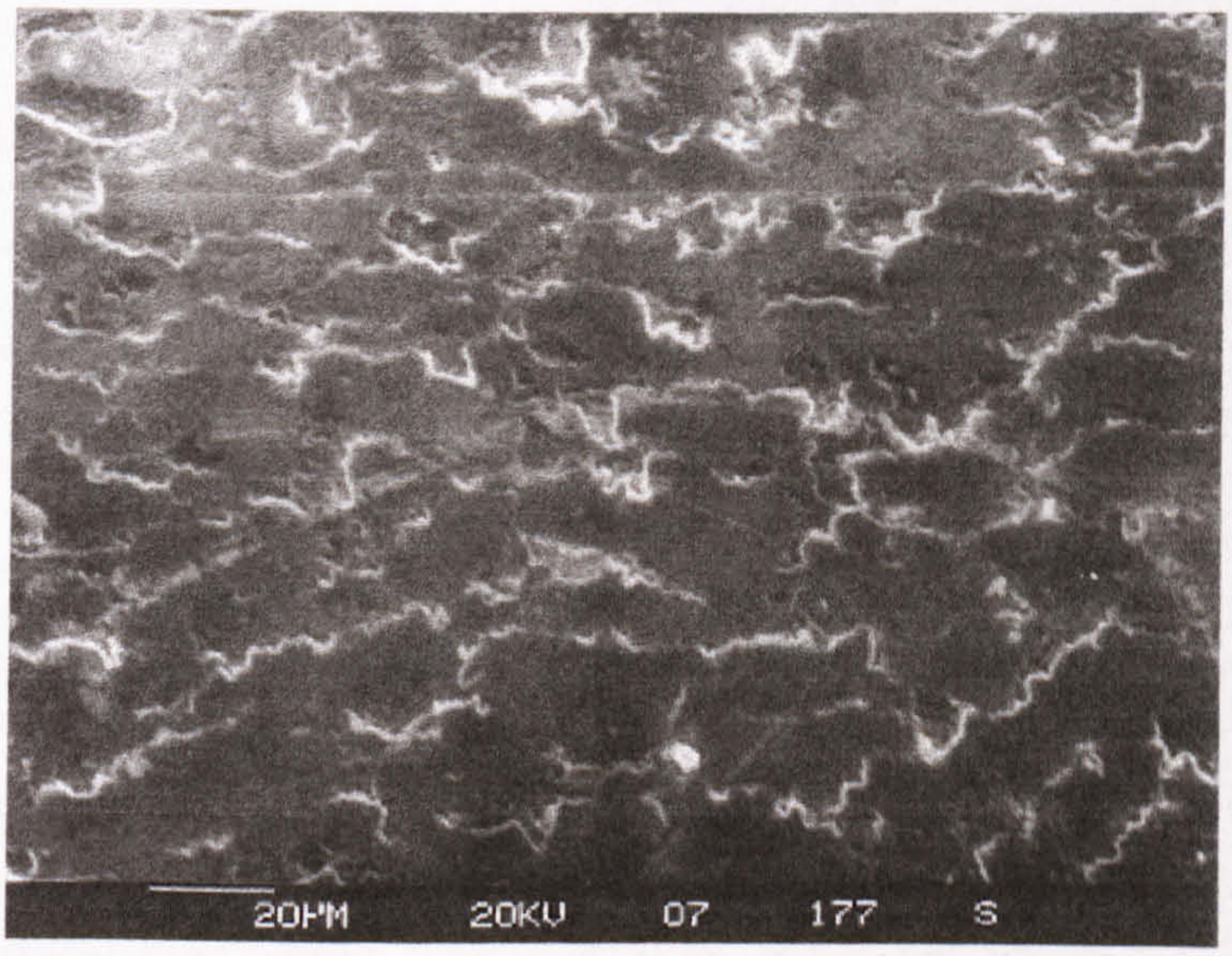


Figure 12.1.6 Scanning Electron Micrograph of Micropitting in a Crowned Barrel

The crowned specimens all suffered micropitting, and as this progressed the radius of curvature of the specimen and the track width were increased (Figure 12.1.7). There was a tendency for the longer life specimens to show a lower tendency to fail by pitting.

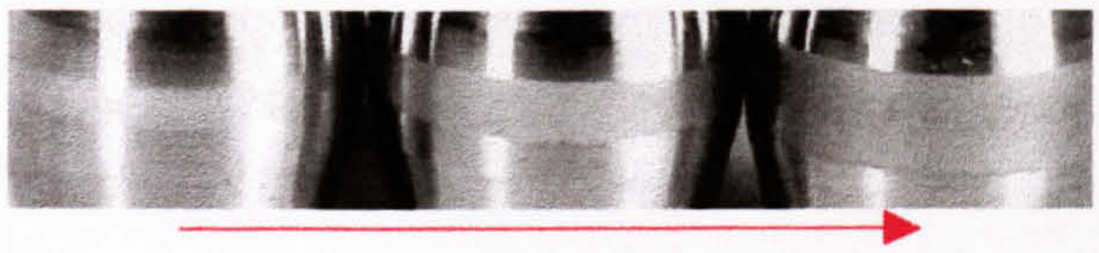


Figure 12.1.7 Progression of Micropitting in Crowned BS S156 Specimens

12.1.3 The AISI M50NiL Disc Tests

The AISI M50NiL barrels were all chamfered. These specimens exhibited similar failures to the BS S156 specimens, with pitting occurring on the chamfered barrel edges. The damage, however, was more extensive in the M50NiL specimens (Figure12.1.8).

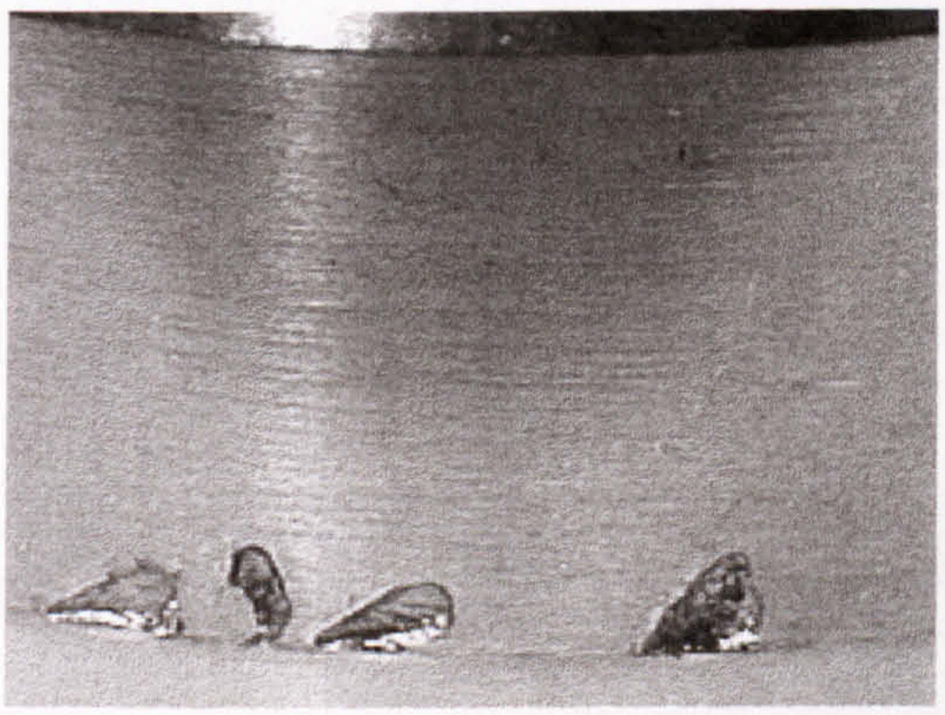


Figure 12.1.8 Pits at the Edge of an AISI M50NiL Barrel Track

Several of the AISI M50NiL rings also had some damage on the edge of the track as seen in Figure 12.1.9.

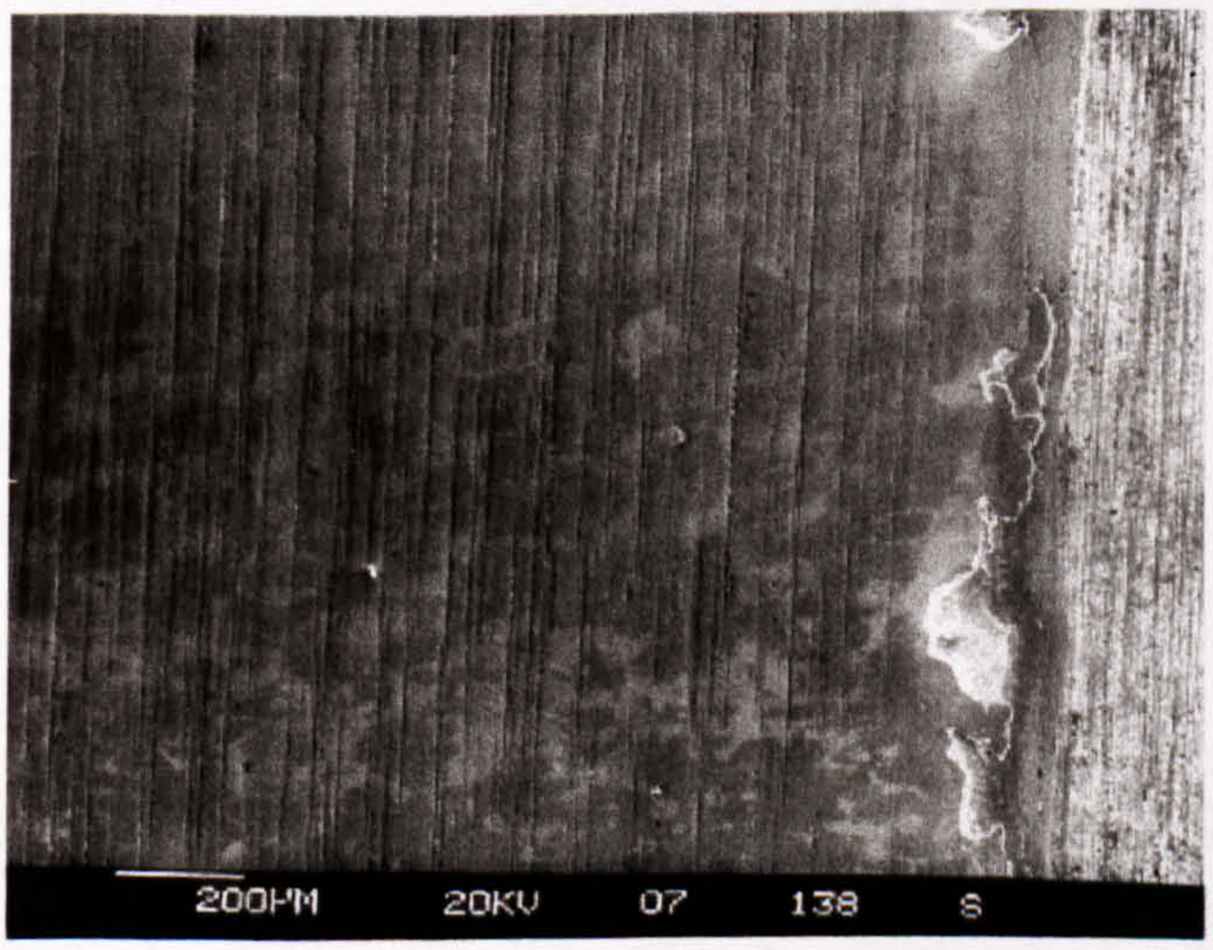


Figure 12.1.9 AISI M50NiL Ring with Small Pits at the Edge of the Run Track

The progression of pit formation in the AISI M50NiL discs can be observed in Figure 12.1.10. Small pits originating from cracks near the edge of the running track appear to be responsible for the nucleation of larger pits in this case.

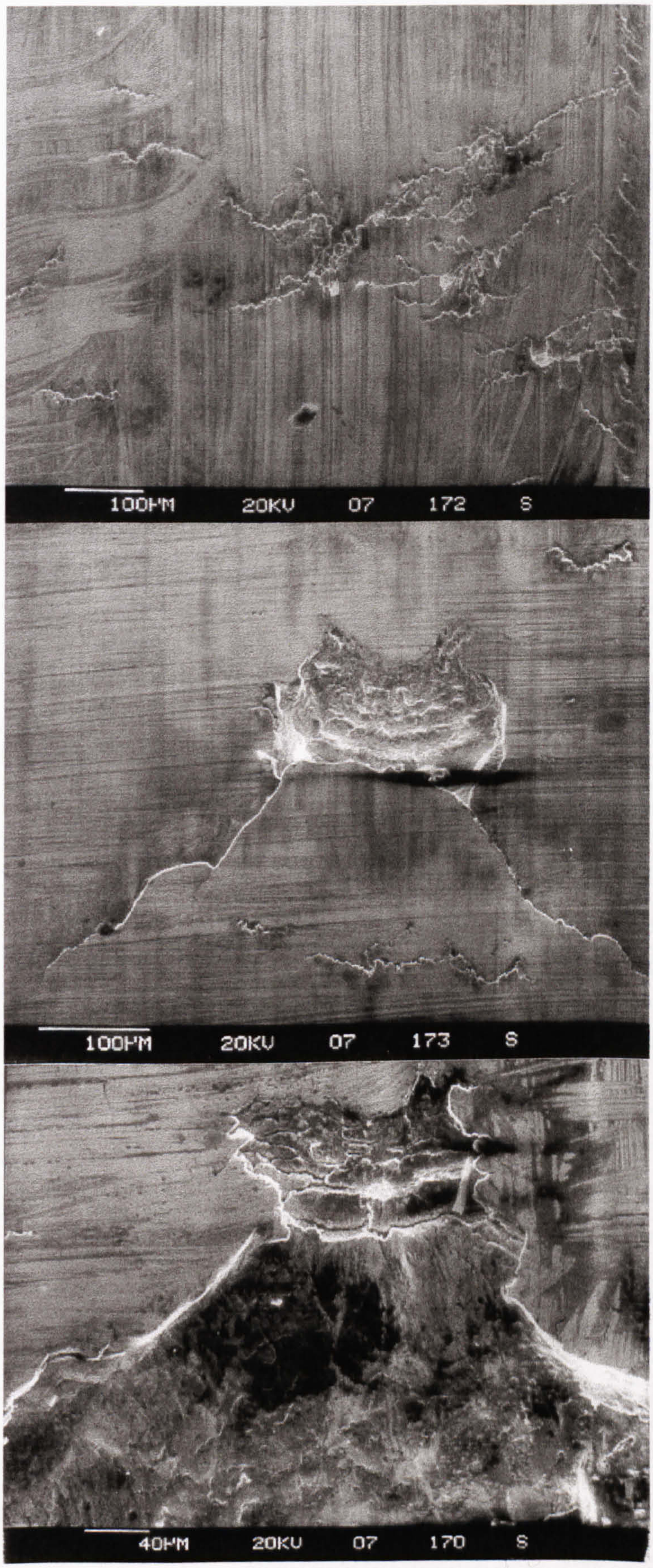


Figure 12.1.10 Scanning Electron Micrographs Showing the Progression of Damage in an AISI M50NiL Barrel

12.1.4 The AISI M50NiL Duplex Disc Tests

The AISI M50NiL Duplex disc specimens were produced by two methods, plasma and gas nitriding. These behaved differently in rolling contact fatigue, with the plasma duplex showing no significant improvement over the AISI M50NiL specimens and the gas duplex specimens performing considerably better.

Some plasma nitrided specimens had shallow, reasonably large pits (Figure 12.1.11) and others failed with small edge pits and micropitting (Figure 12.1.12). A patch of this micropitting on the barrel contact surface is shown in Figure 12.1.13.

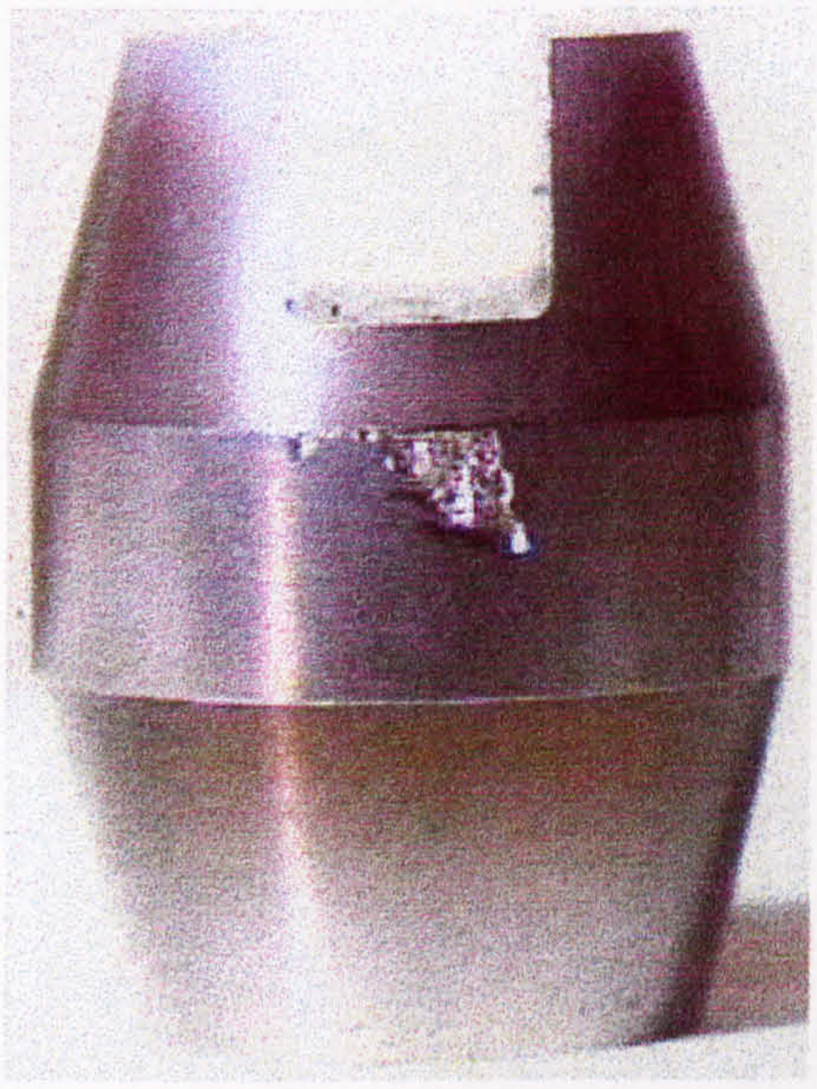


Figure 12.1.11 Pitted AISI M50NiL Duplex Barrel (Plasma Nitrided)

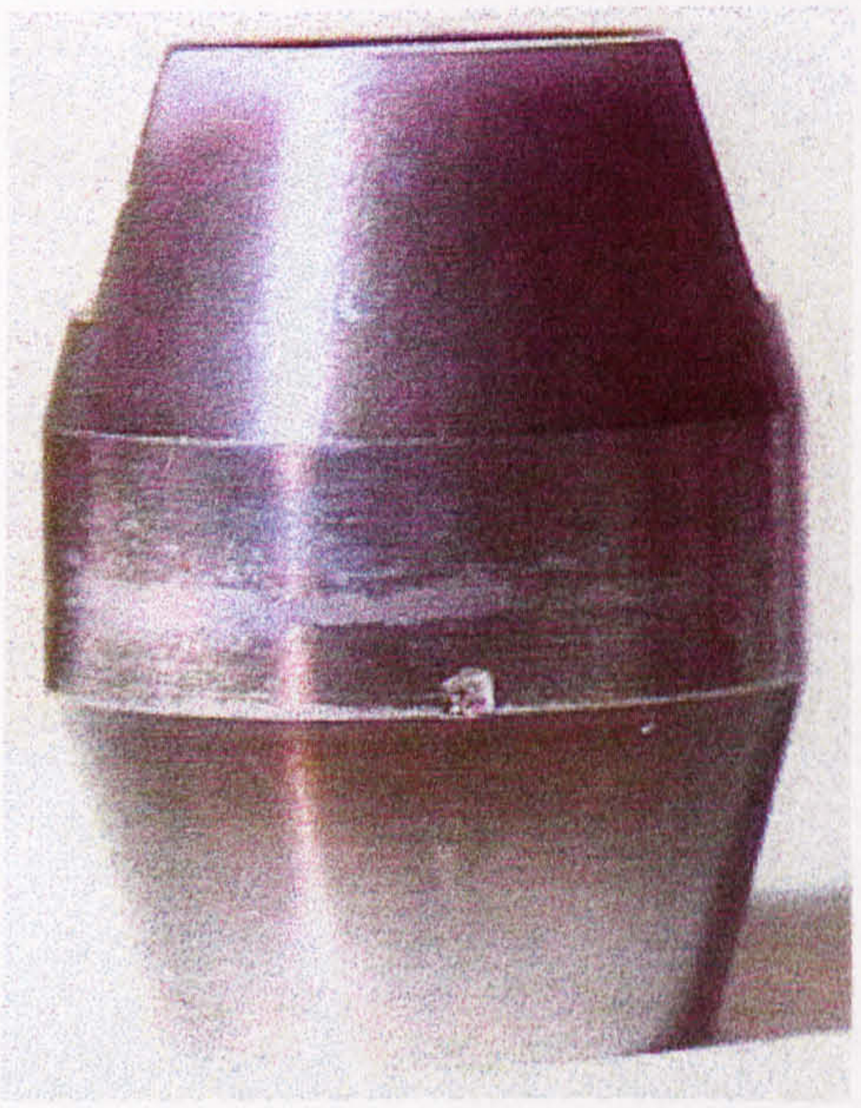


Figure 12.1.12 Pitted and Micropitted AISI M50NiL Duplex Barrel (Plasma Nitrided)

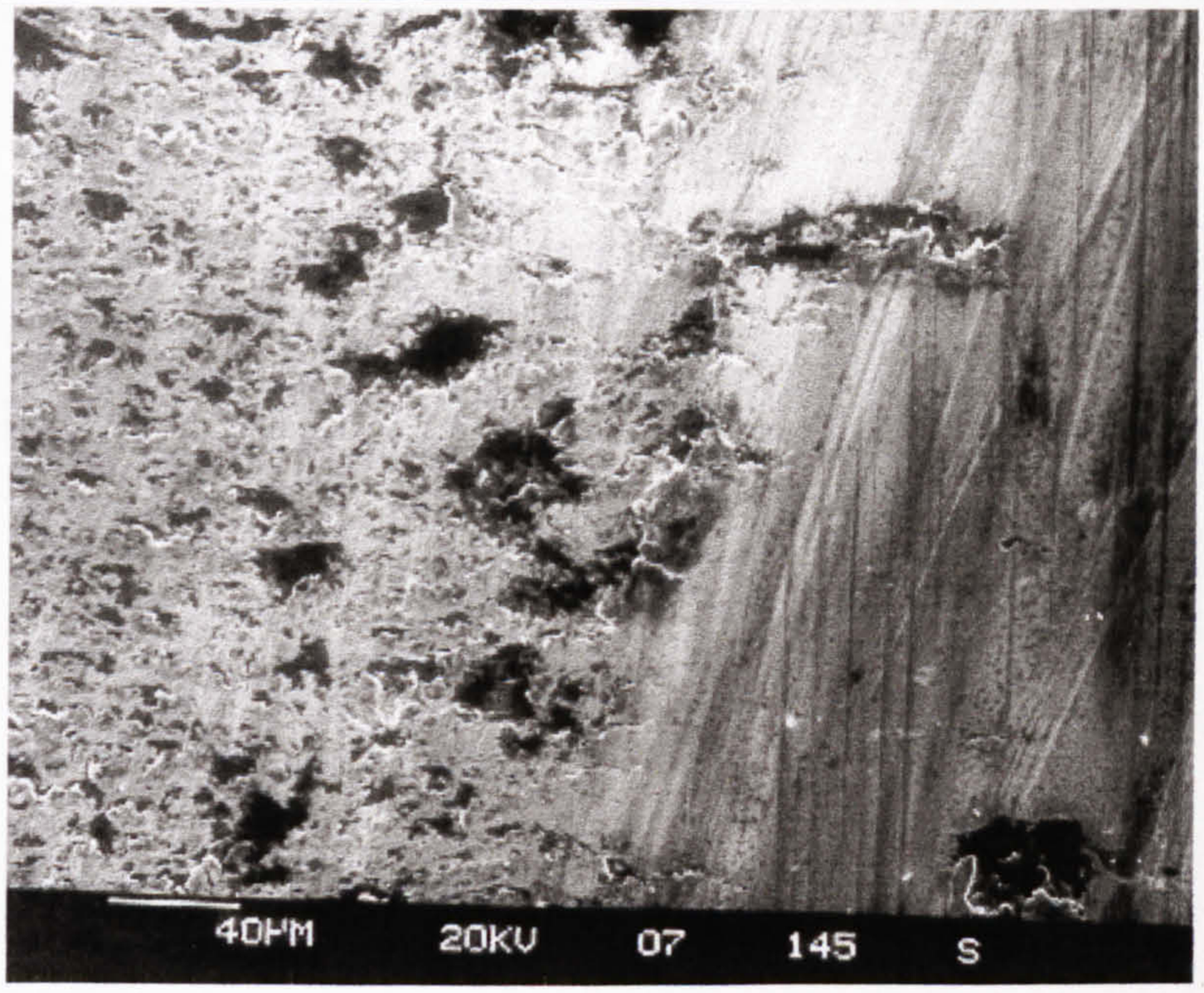


Figure 12.1.13 Scanning Electron Micrograph Showing Micropitting on an AISI M50NiL Duplex Barrel (Plasma Nitrided)

The gas nitrided AISI M50NiL Duplex specimens exhibited a different failure mode to the BS S156 and AISI M50NiL specimens. They failed by pitting after extended lives with micropitting also having taken place (Figures 12.1.14 and 12.1.15). The failure did not occur at the edge as is characteristic of the specimens but in the track, with what appeared to be subsurface initiated fatigue (Figure 12.1.6). A couple of these fatigue cracks morphologies, which appear to initiate from the subsurface, can be seen in Figure 12.1.17.

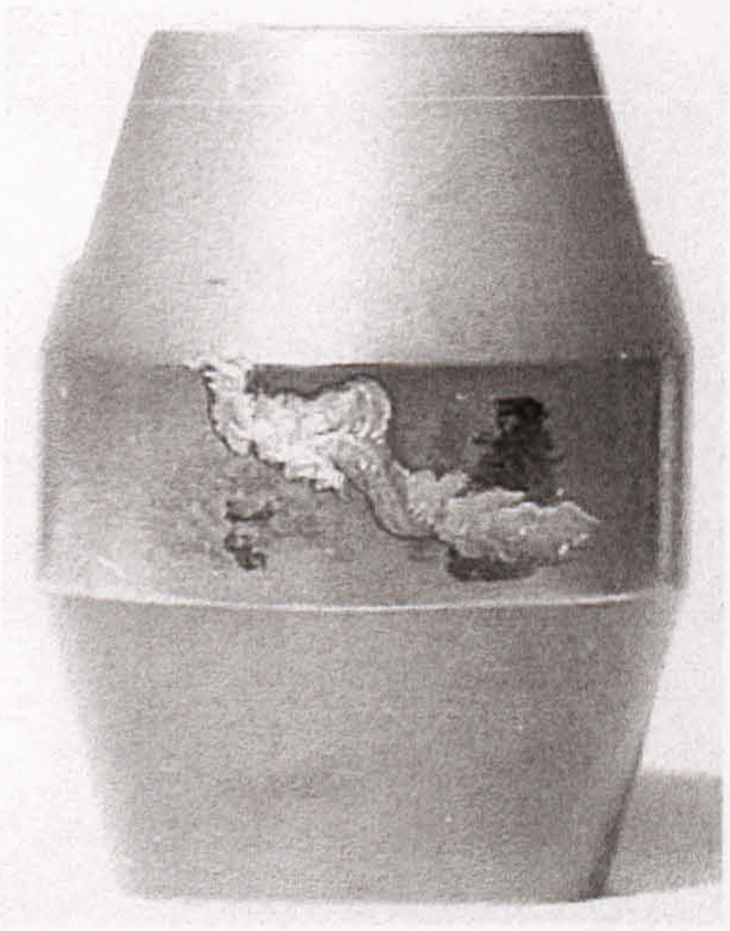
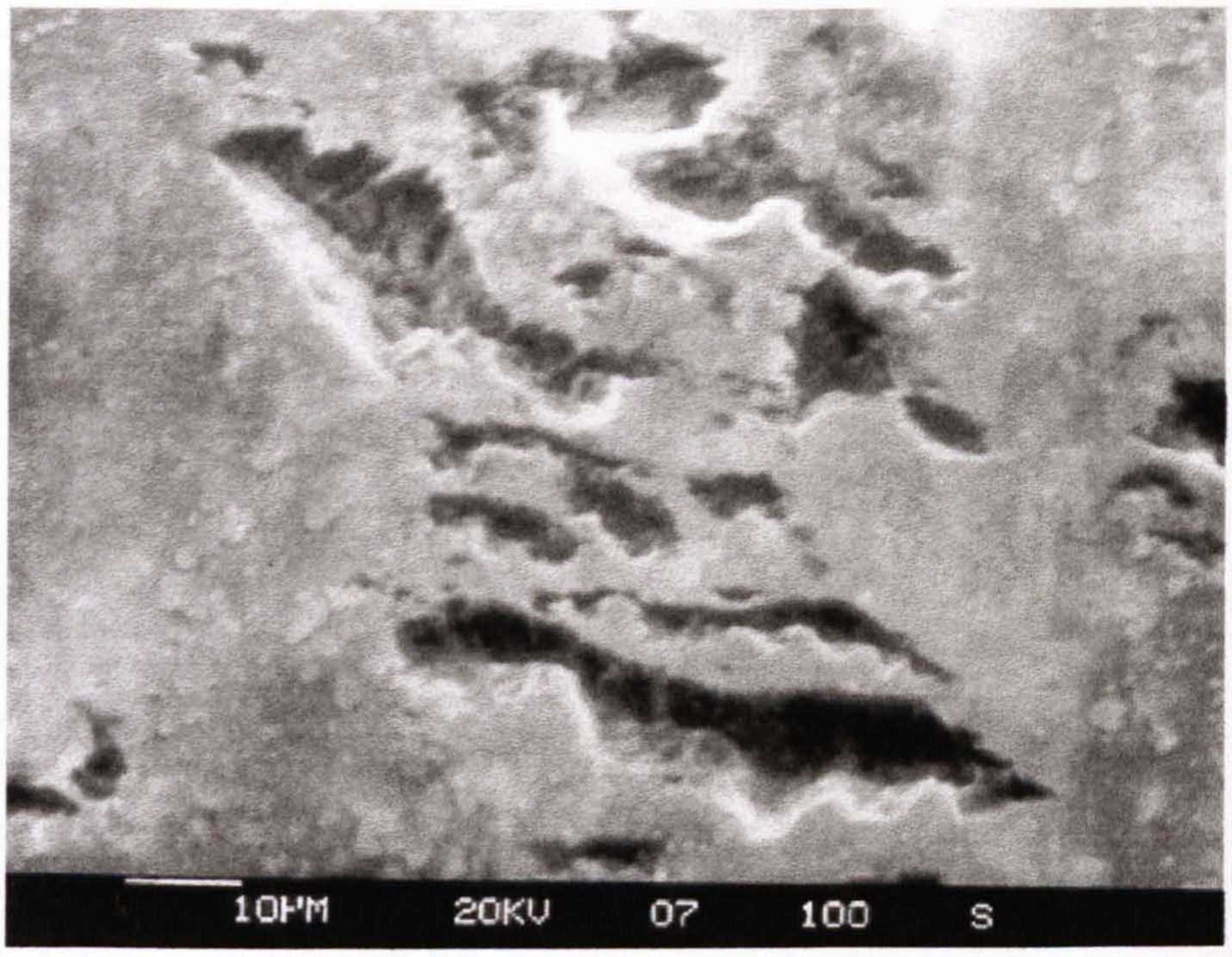


Figure 12.1.14 Pitted and Micropitted AISI M50NiL Duplex Barrel (Gas Nitrided)



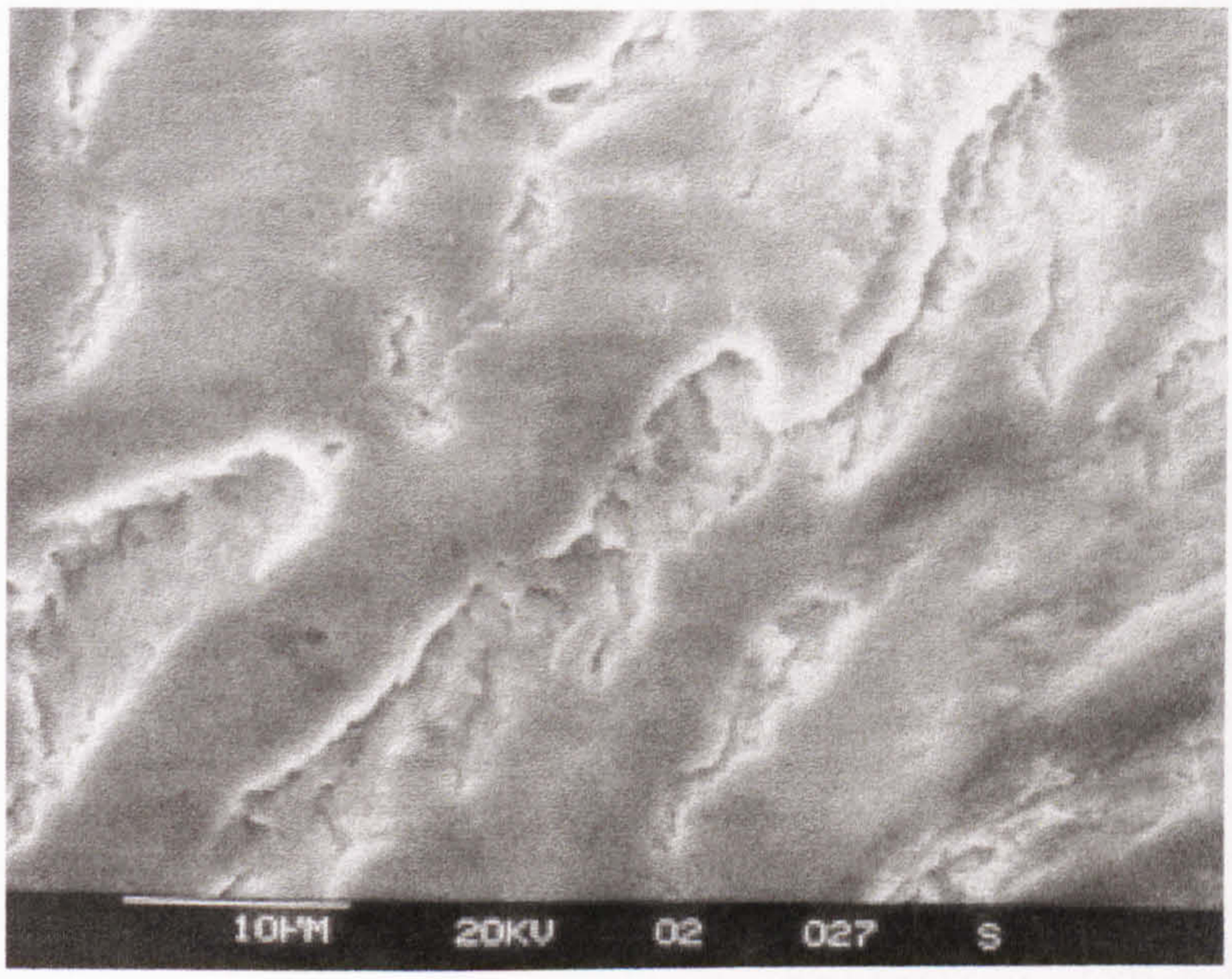


Figure 12.1.15 Scanning Electron Micrograph Showing Micropitting in an AISI M50NiL Duplex Barrel (Gas Nitrided)

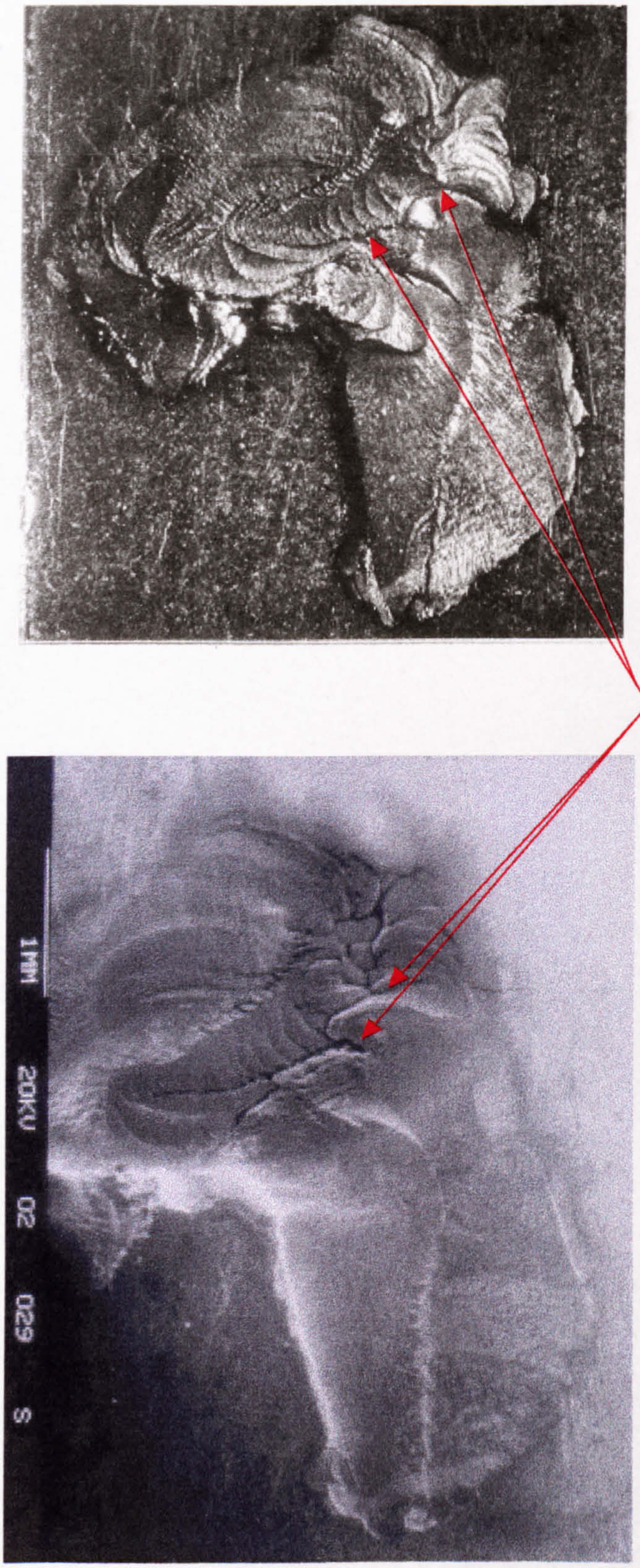
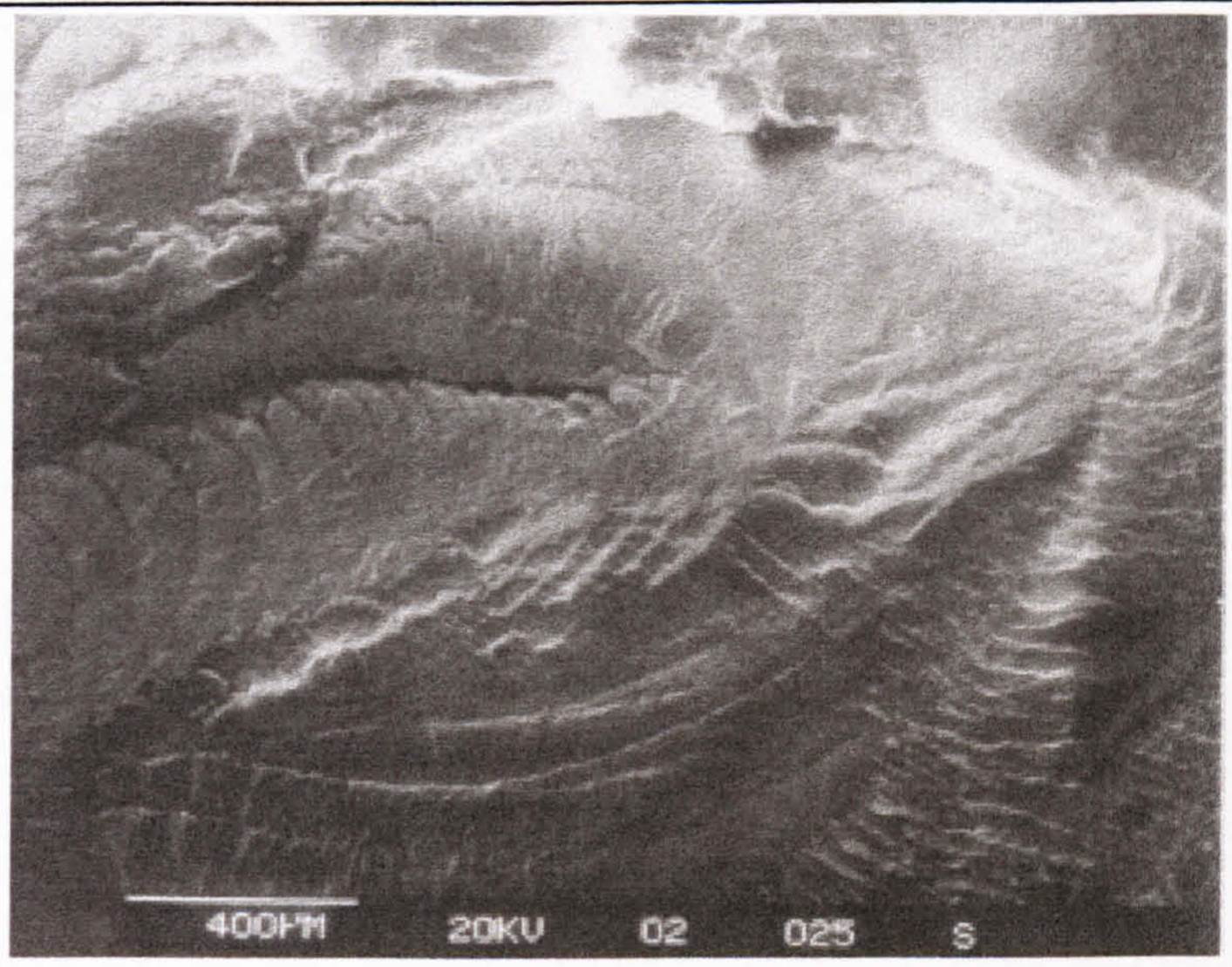


Figure 12.1.16 Optical and Scanning Electron Micrograph Images of the Same Subsurface Initiated Pit in an AISI M50NiL Duplex Barrel (Gas Nitrided)



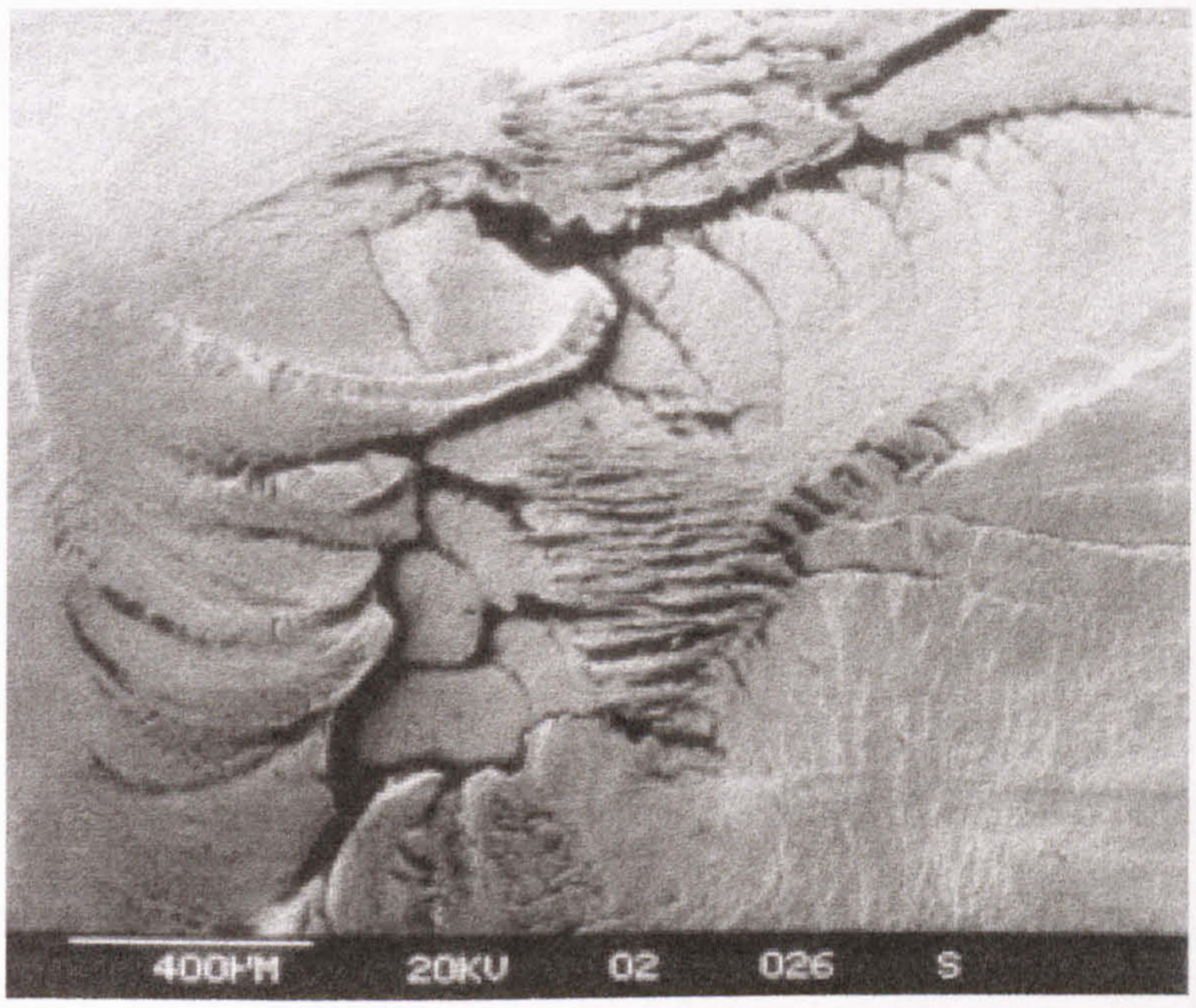


Figure 12.1.17 Crack Morphology in An AISI M50NiL Duplex Pit Showing the Progression of What Appear to be Subsurface Initiated Fatigue Cracks

The rings also suffered some micropitting (Figure 12.1.18) and in a few cases developed some extensive, but very shallow pits (Figure 12.1.19).



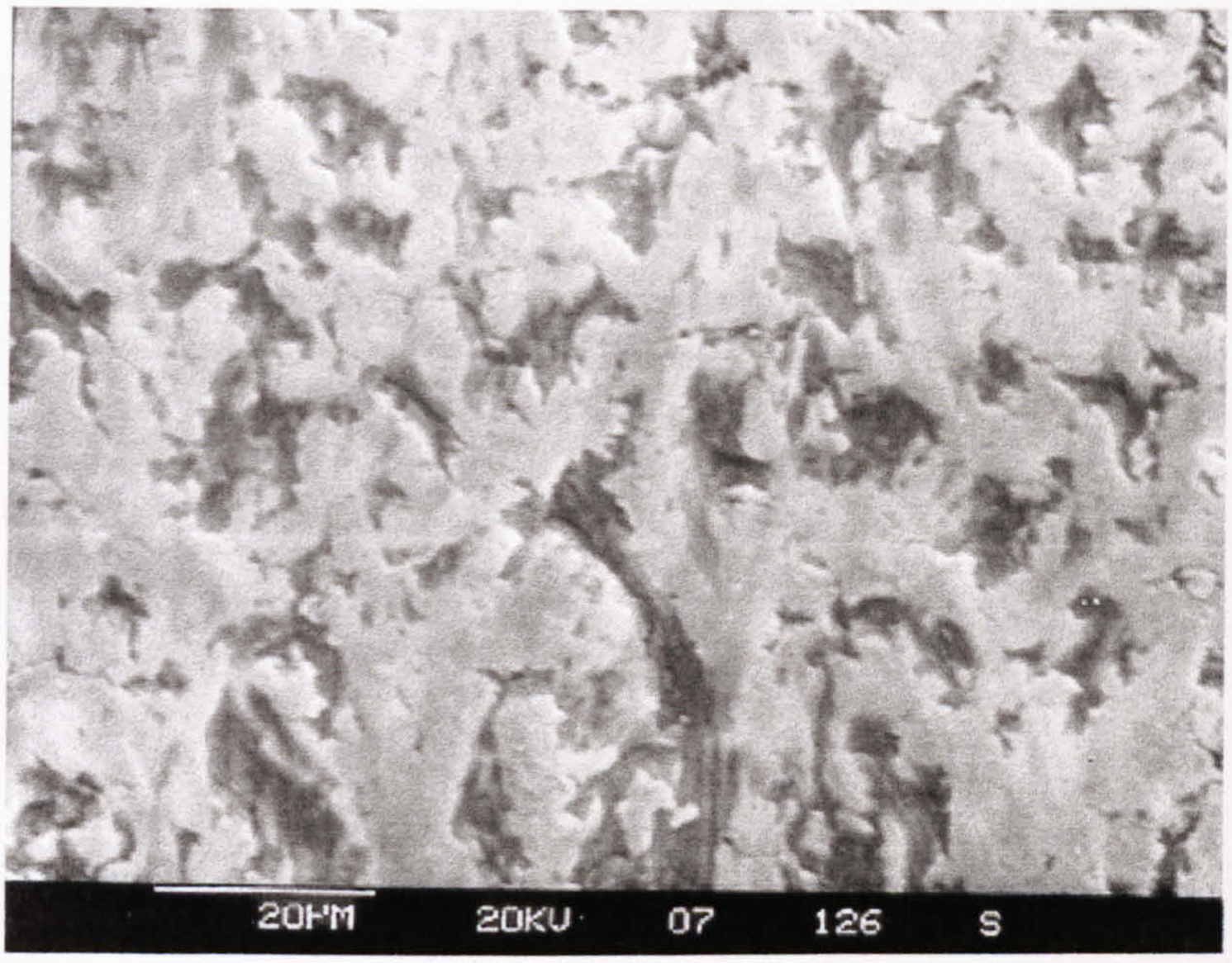
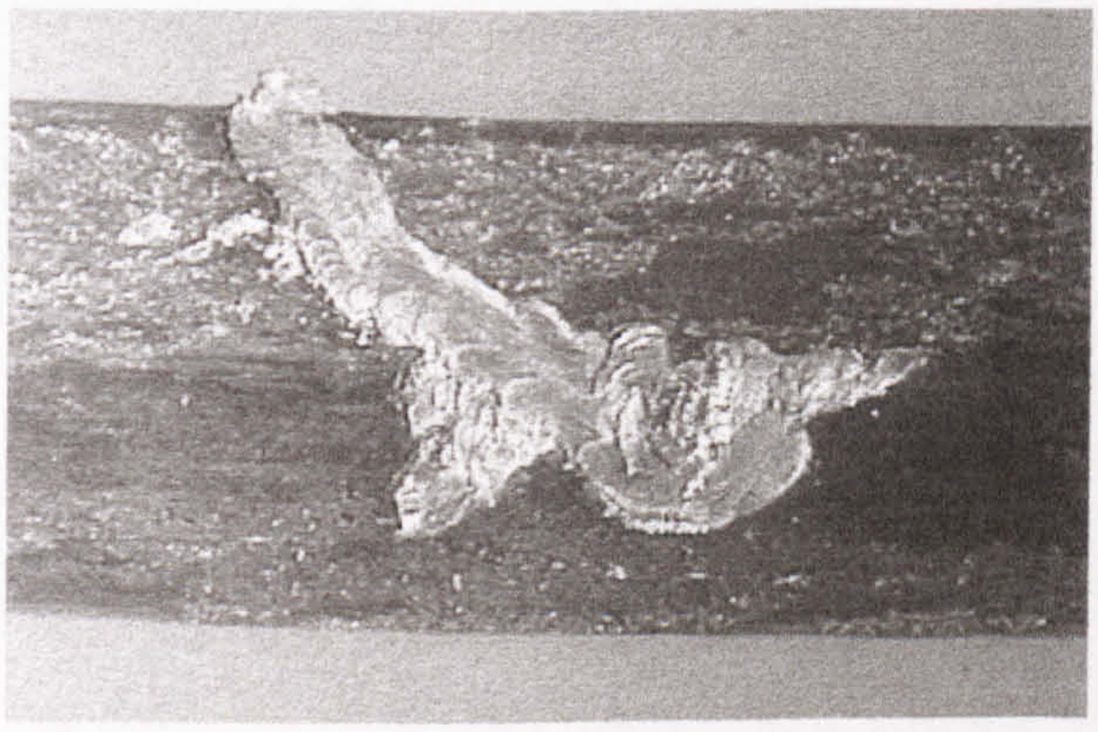


Figure 12.1.18 Two Examples of Micropitting in the AISI M50NiL Duplex Rings (Gas Nitrided)



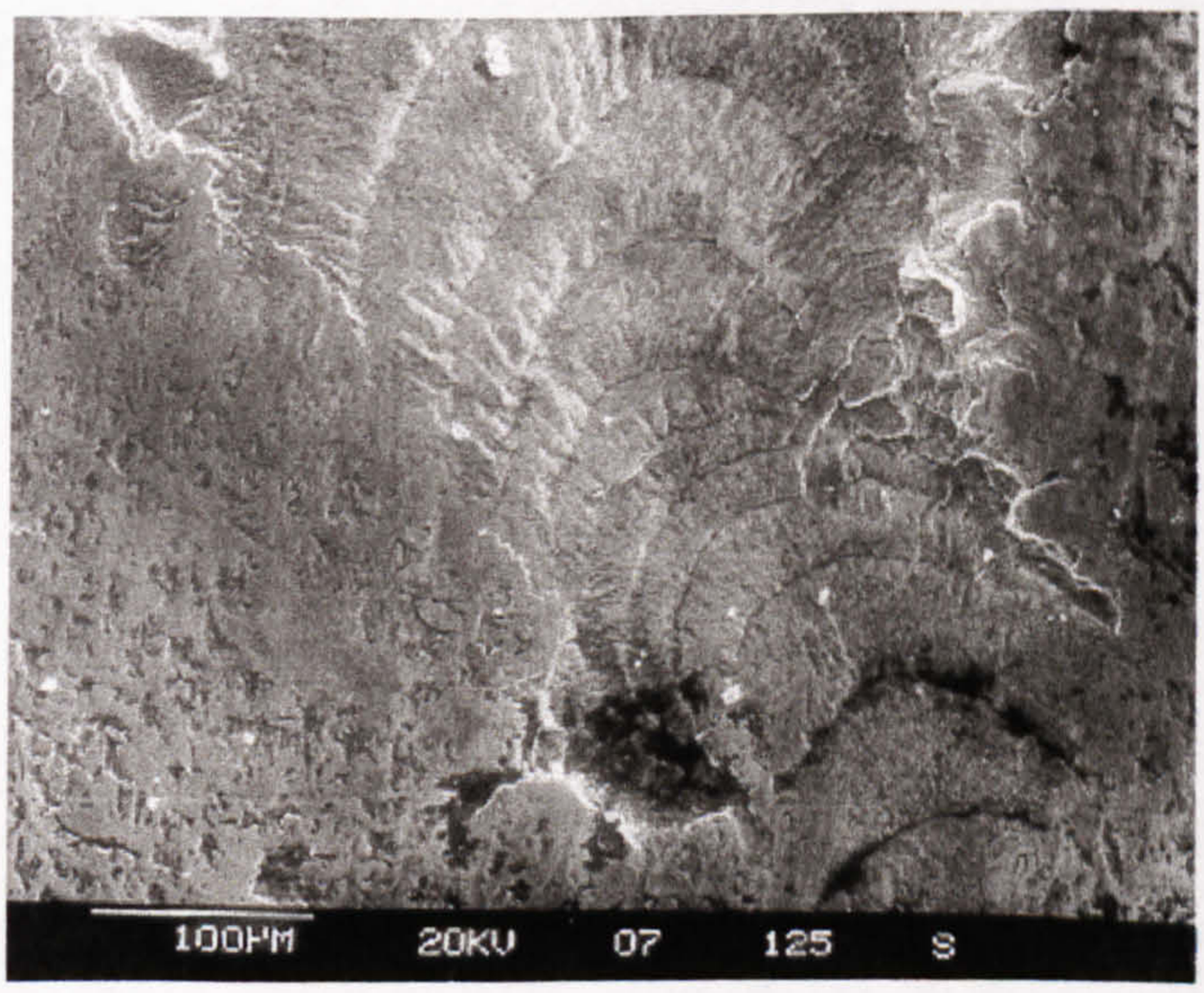


Figure 12.1.19 Optical and Scanning Electron Micrograph Images Showing Two Examples of AISI M50NiL Duplex Ring Damage

12.1.5 The 32CDV13 Disc Tests

The rolling contact fatigue test results of the 32CDV13 disc specimens were very poor. The vibration levels rose rapidly during loading and the tests were stopped before reaching the running load. The 32CDV13 barrels were nitrided and then finish ground to remove part of the 'white' layer, the properties of which were discussed in Section 5.3. The white layer was approximately 36 μm thick and about half of this was removed in the barrel specimens, as shown in Figure 7.5.9. The ring specimens were not finish ground. The barrels appeared heavily micropitted as shown in Figures 12.1.20 and 12.1.21 and the rings were even more severely damaged, with large shallow pits destroying the run surface (Figure 12.1.22).



Figure 12.1.20 32CDV13 Barrel showing Micropitting

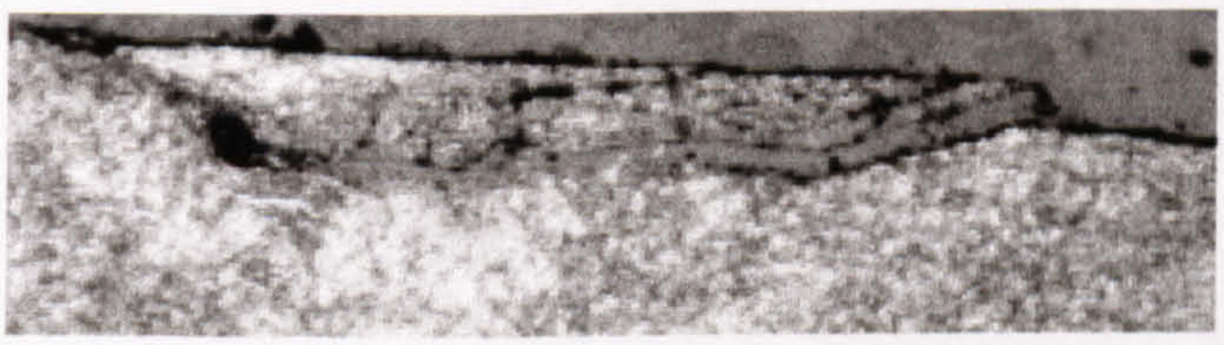




Figure 12.1.21 Transverse Sections of a 32CDV13 Barrel Showing Micropits (200x and 300x respectively)



Figure 12.1.22 Three examples of Damage on the 32CDV13 Rings

Due to the poor performance of the 32CDV13 specimens, these results were not used in the fatigue life analysis presented in the next section. However, reasons for these very low fatigue results will be discussed in Chapter 13.

12.2 Comparison of the Failed Disc Specimens

A comparison of the BS S156 and AISI M50NiL duplex (gas nitrided) disc specimen surface damage can be seen in Figures 12.2.1 and 12.2.2.

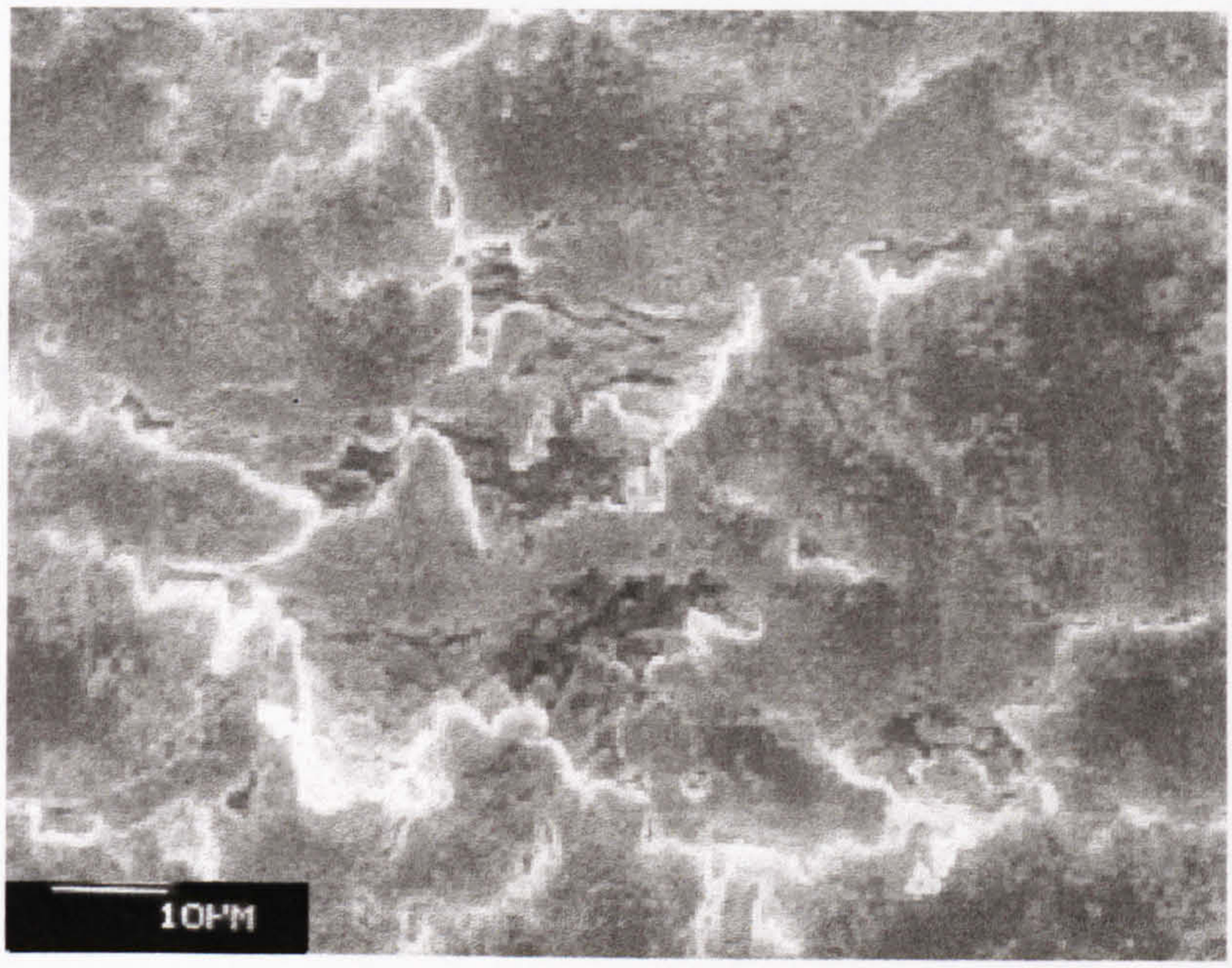


Figure 12.2.1 Scanning Electron Micrograph of a BS S156 Barrel Specimen Run at -0.14 Slide-Roll Ratio ($8.0x10^6$ cycles at 2.5 GPa)

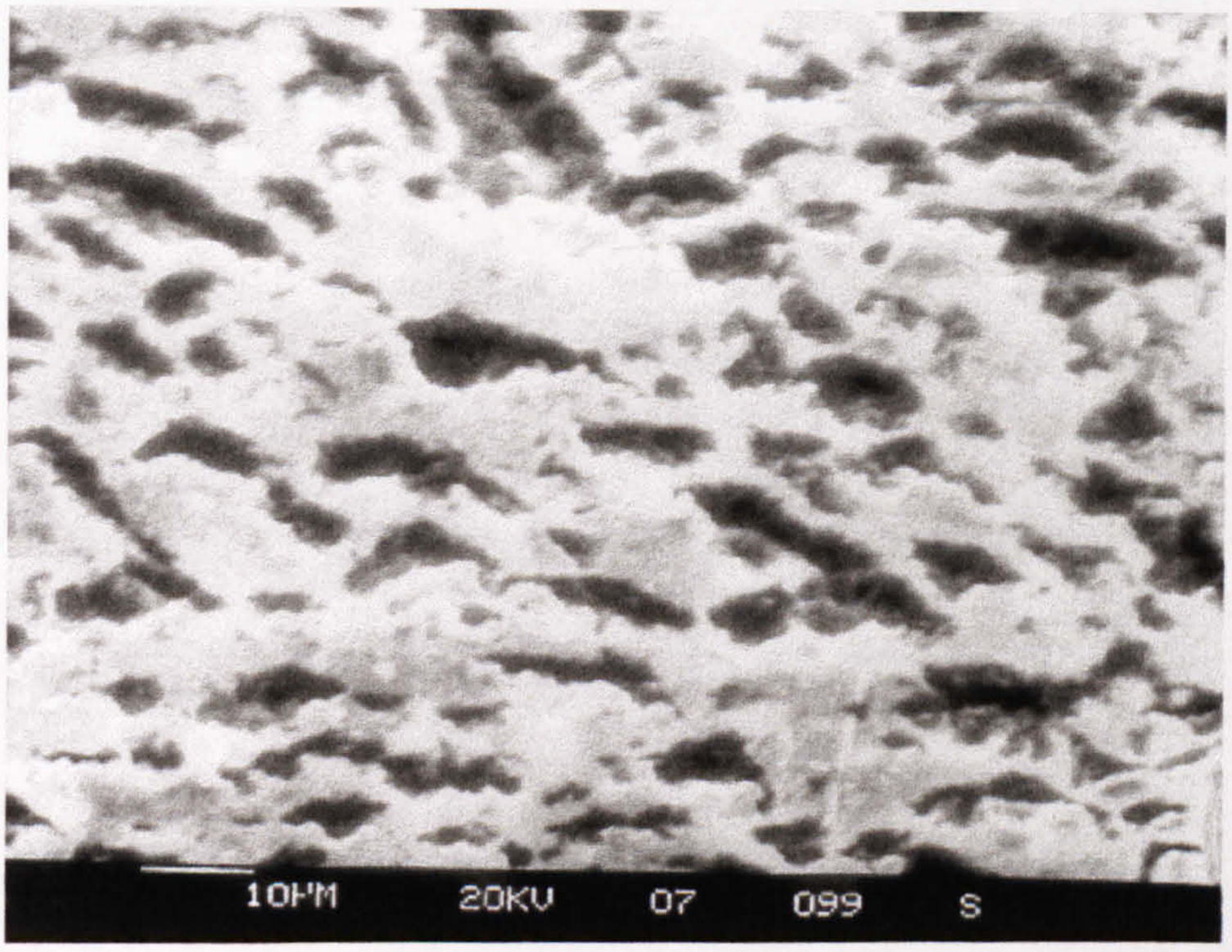


Figure 12.2.2 Scanning Electron Micrograph of an AISI M50NiL Duplex Barrel Specimen Run at -0.14 Slide-Roll Ratio ($22.1x10^6$ cycles at 2.5 GPa)

Figures 12.2.3 and 12.2.4 show the microstructures of the BS S156 and AISIM50NiL duplex specimens. It appears that in this specimen, most of the micropits are confined to the white layer, which was approximately 10 μm from Figure 7.5.8.

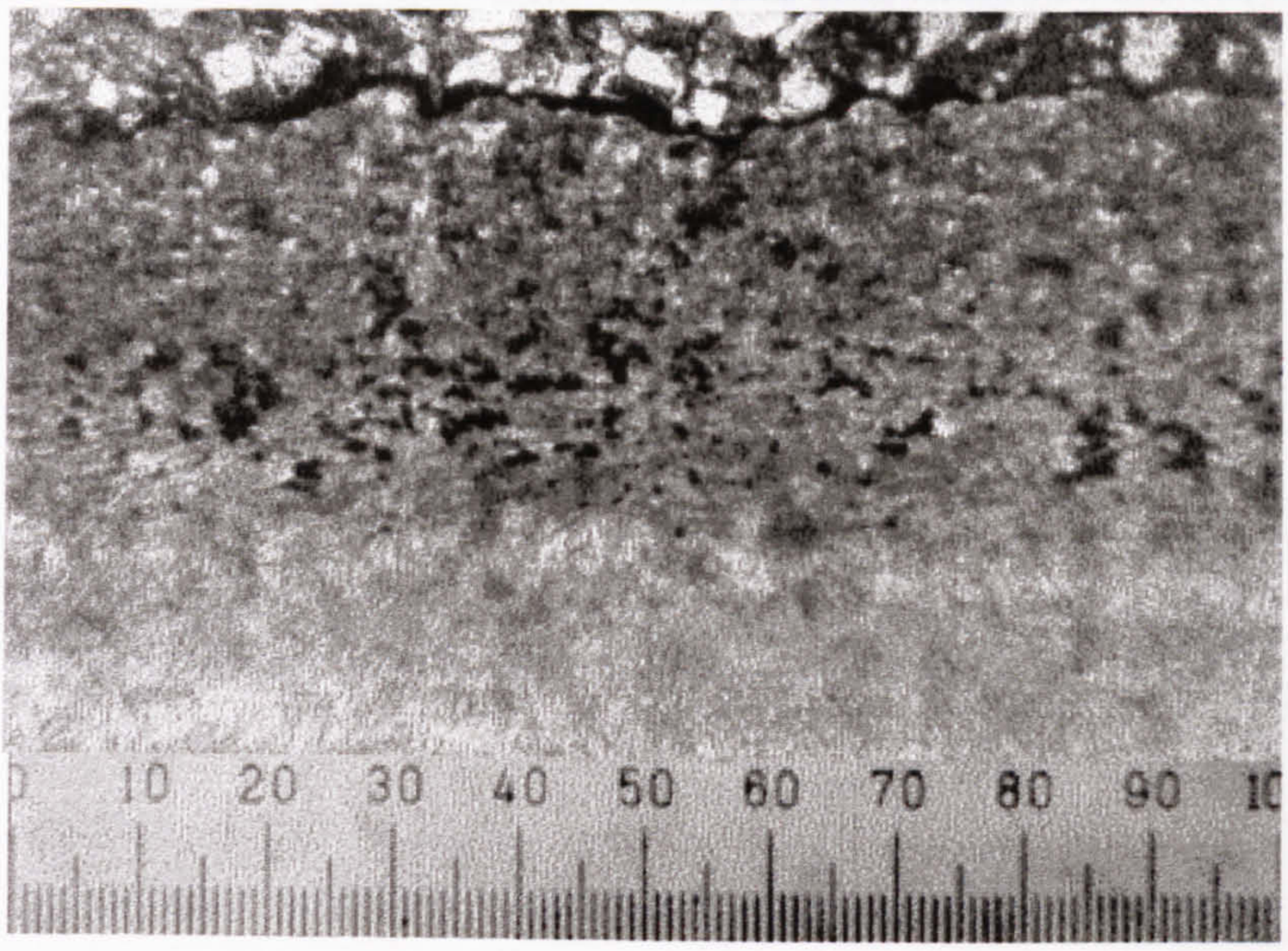


Figure 12.2.3 Taper Section of a BS S156 Disc Run at -0.14 Slide-Roll Ratio (7.8×10^6 cycles at 2.5 GPa)

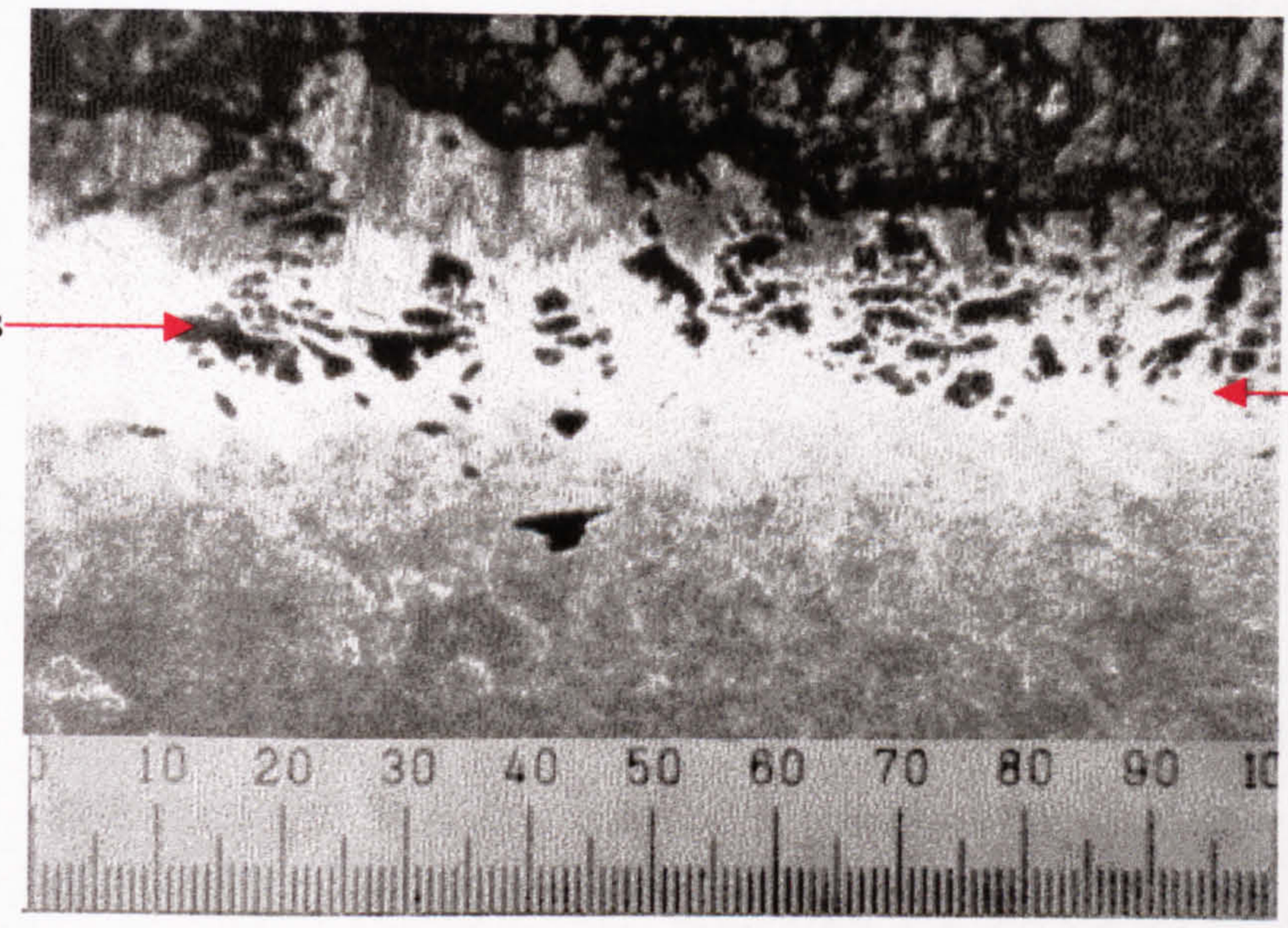


Figure 12.2.4 Taper Section of an AISI M50NiL Duplex Barrel Run at -0.14 Slide-Roll Ratio (18.1×10^6 cycles at 2.5 GPa)

12.3 S-N and Weibull Analysis for the Disc Fatigue Tests

The fatigue lives for the chamfered disc tests are shown in Figure 12.3.1. They show that the AISI M50NiL Duplex (gas nitrided) had a greatly improved life when compared to the M50NiL and BS S156 discs. The plasma nitrided duplex specimens did not perform as well. The crowned specimen fatigue results are also shown although these were done at higher Hertzian contact stress levels.

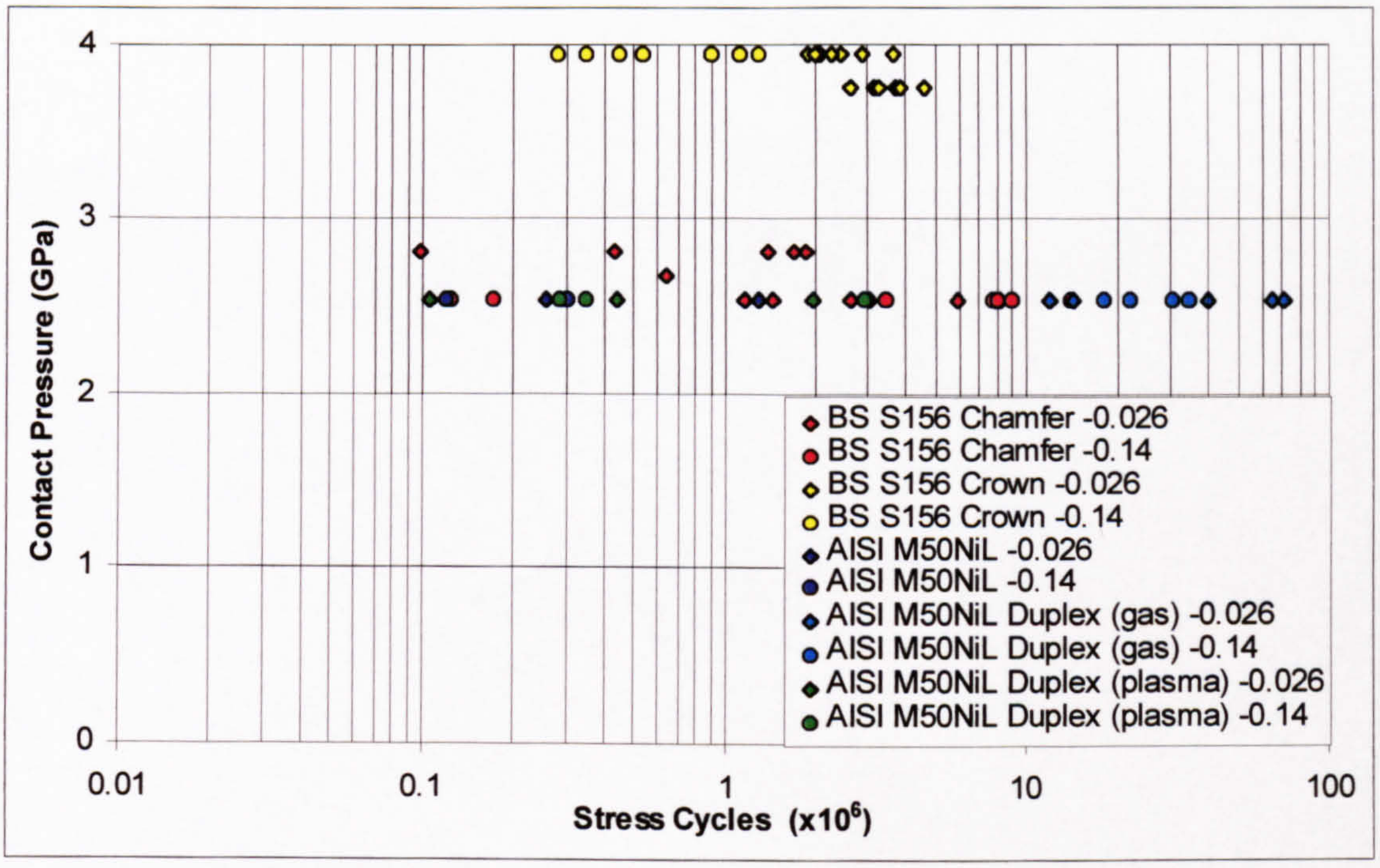


Figure 12.3.1 The BS S156, AISI M50NiL, and M50NiL Duplex Chamfered Barrel Fatigue Lives for Slide-Roll Ratios of -0.026 and -0.14

The fatigue results were plotted on a Weibull chart (Figure 12.3.2), only tests carried out at similar contact stresses should be compared on this chart.

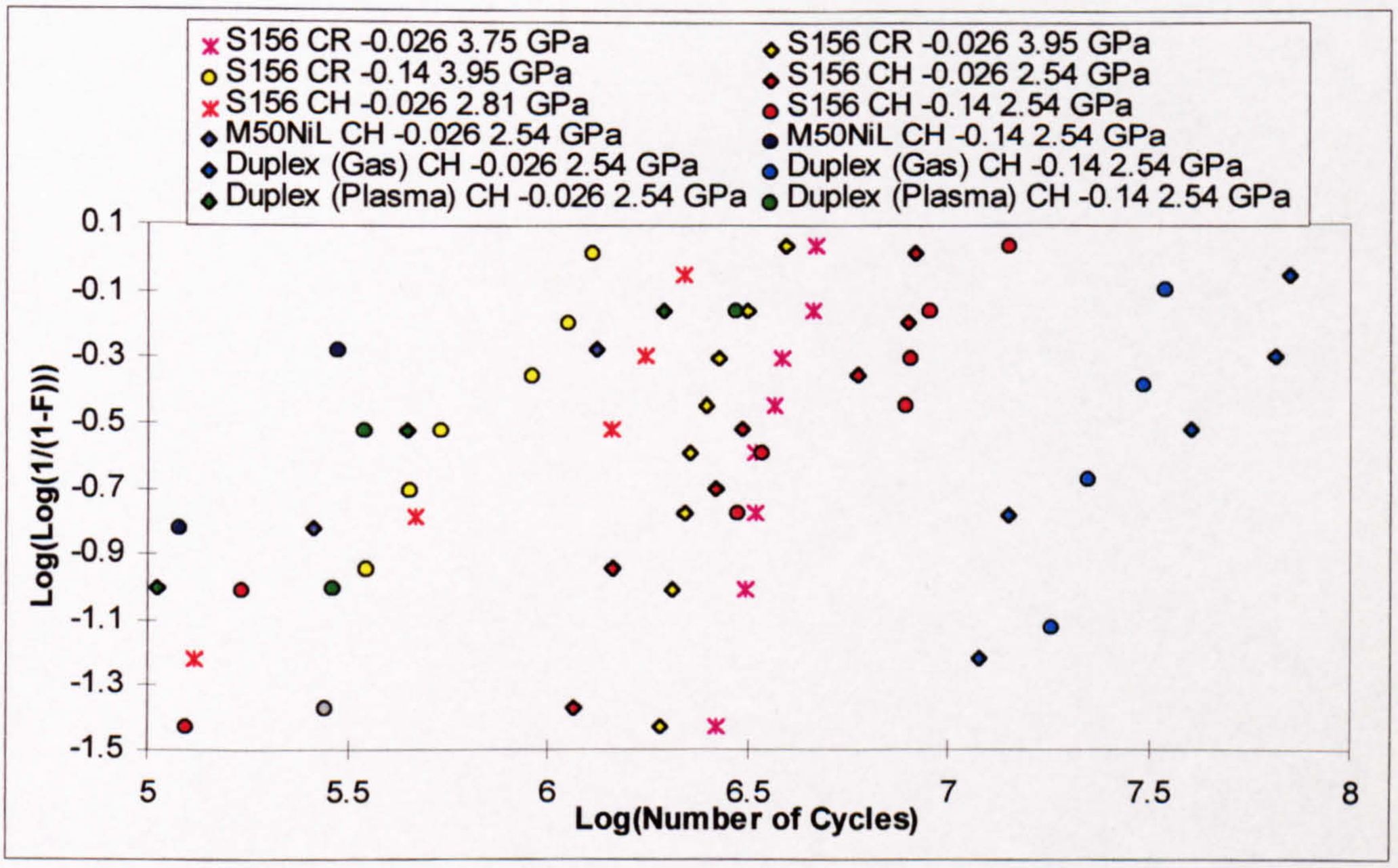


Figure 12.3.2 Weibull Plots of the Disc Fatigue Lives

L_{50} lives were obtained for these tests and plotted on an S-N chart (Figure 12.3.3) to allow comparison of the different test specimen lives'.

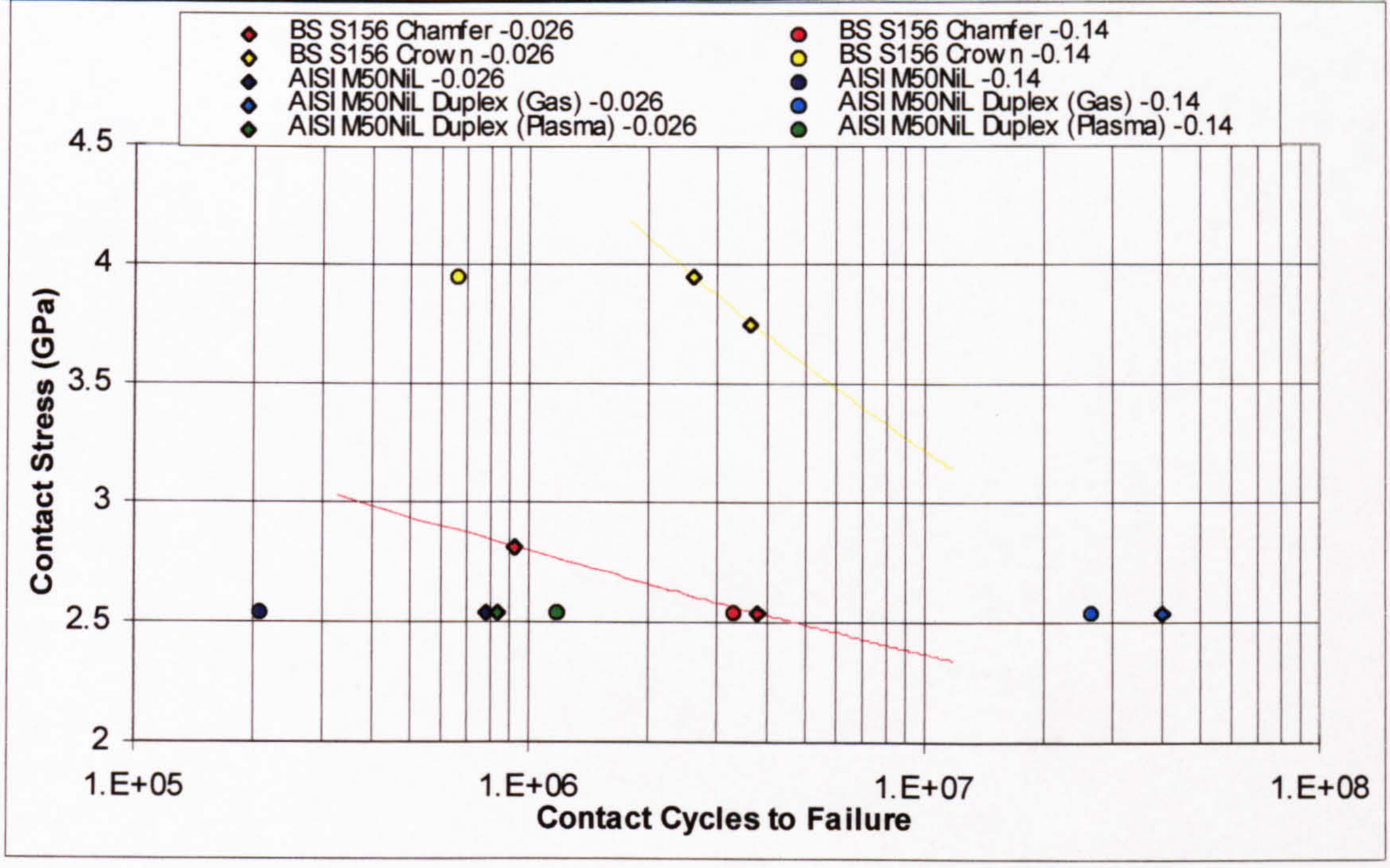


Figure 12.3.3 The L_{50} Lives for the Disc Contact Fatigue Tests

The chamfered and crowned disc tests are compared in Figure 12.3.4. These tests were only done with specimens manufactured from BS S156. There appeared to be a significant difference between the -0.026 and -0.14 slide-roll ratios for the crowned disc tests but not for the chamfered ones. The higher slide-roll ratio giving a reduced rolling contact fatigue life in the crowned specimens.

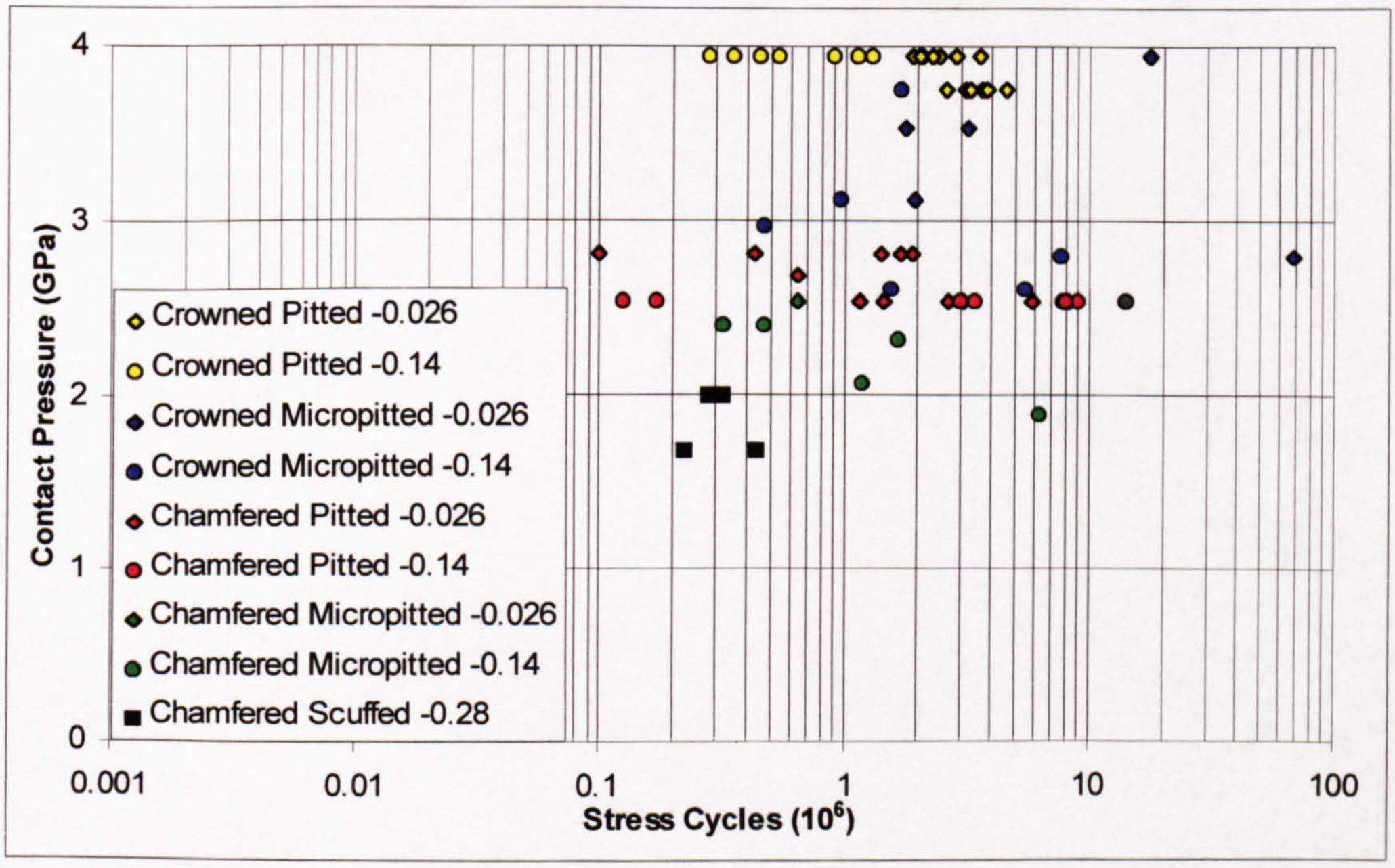


Figure 12.3.4 The Chamfered and Crowned BS S156 Disc Fatigue Tests

12.4 Conclusions from the Disc Fatigue Tests

- Scuffing occurred in the BS S156 chamfered barrels run at the high slide roll-ratio (-0.28).

- At lower slide-roll ratios (-0.14 and -0.026) pitting and micropitting occurred in the chamfered specimens. Pitting always took place on the track edge.

- Many chamfered specimens failed by pitting but also suffered from micropitting. The specimens that micropitted appeared to have longer lives than specimens that only pitted, as observed by Olver (1995).

- The crowned BS S156 specimens run at -0.14 and -0.026 slide-roll ratio also exhibited pitting and micropitting failures. The track width was much narrower than the chamfered barrel because of the crown, and there was no edge contact. The crowned discs could run at higher nominal contact stresses than the chamfered specimens for equivalent lives.

- There appeared to be a significant difference between the -0.026 and -0.14 slide-roll ratios for the crowned disc tests, but not for the chamfered ones. The higher slide-roll ratio giving a reduced rolling contact fatigue life in the crowned specimens.

- The crowned specimens all suffered micropitting, as this progressed the radius of curvature of the specimen and the track width were increased. There was a tendency for the longer life specimens to show a lower tendency to fail by pitting. If the contact stress was too low, the contact pattern would broaden due to excessive wear by micropitting. This made the contact more conforming and reduced the risk of pitting.

- The AISI M50NiL and BS S156 specimens exhibited similar failures, with pitting occurring on the chamfered barrel edges. The damage, however, was more extensive in the M50NiL specimens. Several of the AISI M50NiL rings also had some small damage on the edge of the track.

- The 32CDV13 specimens gave very poor rolling contact fatigue results. The 32CDV13 barrels were nitrided and then finish ground to remove part of the 'white' layer. The ring specimens were not finish ground. The barrel appeared heavily micropitted and the rings were even more severely damaged, with large shallow pits destroying the run surface.

- The AISI M50NiL Duplex specimens were produced by two methods, plasma and gas nitriding. These behaved differently in rolling contact fatigue, with the plasma duplex showing no significant improvement over the AISI M50NiL specimens and the gas duplex specimens performing considerably better.

- The gas nitrided AISI M50NiL duplex specimens exhibited a different failure mode to the BS S156 and AISI M50NiL specimens. They failed by pitting after extended lives with micropitting also having taken place. The failure did not occur at the edge, as is characteristic of the specimens, but in the track, with what appeared to be a subsurface initiation.

- The AISI M50NiL duplex (gas nitrided) rings suffered some micropitting too, and in a few cases developed some extensive, but very shallow pits.

Summary Part 2 - Analytical & Experimental Research

The gear and disc test rigs used by the author and the monitoring systems, as well as, the test specimens design and the test procedure were described in Chapter 7.

An analysis of the stresses on both gear and disc specimens, to determine any differences that might arise between them, was carried-out in Chapter 8.

The crowned barrel had a theoretically elliptical contact area and the chamfered barrel a line contact. The chamfered barrels have a stress concentration at the edge of the track.

The gear specimens have an elliptical contact area. A computer model was developed to find the load sharing characteristics and effects of extended contact in spur gears. It showed that non-tip-relieved gears could suffer extended contact, due to the elastic deflection of the gear teeth, which may damage the root. The contact pressure was shown to increase, and the contact width expand at points were extended tooth pair contact occurred.

The gear surface produced higher surface contact pressure and subsurface shear stress distributions than both the crowned and chamfered barrels (due to the roughness). The stressed volume was also smaller for the disc specimens when compared to the gears, particularly the crowned barrels. As a result of these factors, the disc tests could have longer fatigue lives than the gears, for equivalent Hertzian contact stresses. The residual stress distributions showed that duplex treatment by nitriding AISI M50NiL improved the residual compressive stresses near the surface. This too could be beneficial to fatigue life.

The thermal analysis, described in Chapter 9, showed that the bulk temperatures of the discs increased with increasing slide-roll ratio. The bulk and flash temperatures of the discs, and particularly the actual barrel specimen temperature, at a slide-roll ratio of -0.28 were much higher than those of the gears. Using the gear contact model extremely high flash temperatures were predicted at the extremities of the gear tooth meshing cycle, where extended contact was occurring. This combined with the high contact stresses at these points, could be a scuffing risk.

The analysis of the lubricant in Chapter 10 showed that it formed a relatively solid boundary film at high temperatures. The calculated lambda ratio was lower for the gear than the discs, but they were all low. Whether this would have any effect on fatigue life is debatable. The slide-roll ratio of -0.28 in the disc rig appeared to offer the closest match to the lowest point of single tooth contact in the gear, where the slide-roll ratio was -0.26.

The gear test results showed that the tip relieved gears could be run at higher loads than the non-relieved gears without scuffing. Scuffing occurred in the non-relieved gears if they were loaded too quickly or too much (a limit of around 2.3 GPa was found). The tip-relieved gears could run at contact stresses of up to 3 GPa without scuffing problems. The non-tip-relieved gear teeth suffered from localised damage caused by the tip of the gear tooth interfering with the root of the mating tooth, i.e. extended contact. The contact width also tended to expand at the tip and root of the tooth unlike the contact pattern in the tip-relieved gears, which had no hard marking in the gear root and was more rounded. If the non-relieved gears were loaded gently and kept at low loads the contact pattern would broaden due to excessive wear on the tooth flank. This made the gear contact more conforming and enabled the load to be increased considerably. It was found that this excessive wear was caused by micropitting.

Pitting failures were obtained in the tip-relieved gears, most pits occurring on the driving gear even though 1:1 ratio gears were used. The pits were located close to the theoretical lowest point of single tooth contact, so the idea that the disc tests should be considered relative to this position on the gear tooth seems reasonable. The running contact stresses quoted for the gears were calculated at this point.

The AISI M50NiL Duplex (plasma nitrided) gears had a greatly improved rolling contact fatigue resistance when compared to the AISI M50NiL and BS S156 gears. The AISI M50NiL gears failed in a similar fashion to the BS S156 material, exhibiting both pitting and micropitting, mainly in the dedendum, but had a shorter average life. The Duplex specimens did not fail by pitting within ten million cycles, but suffered some micropitting in the dedendum.

In the axial fatigue tests, regardless of alloy composition, the highest endurance stress was obtained with a compressive mean stress and the lowest endurance stress with the tensile mean stress. Raising the test temperature reduced the fatigue properties,

regardless of alloy composition. When the axial fatigue tests were compared, the AISI M50NiL Duplex specimens performed better than both the AISI M50NiL and the BS S156 ones.

The disc test results showed that scuffing occurred in BS S156 chamfered barrels run at the high slide roll-ratio (-0.28). At lower slide-roll ratios (-0.14 and -0.026) pitting and micropitting occurred in the chamfered specimens. Pitting always took place on the track edge. Many chamfered specimens failed by pitting but also suffered from micropitting. The specimens that micropitted appeared to have longer lives than specimens that only pitted, as observed by Olver (1995).

The crowned BS S156 specimens run at -0.14 and -0.026 slide-roll ratio also exhibited pitting and micropitting failures. The track width was much narrower than the chamfered barrel because of the crown and there was no edge contact. The crowned discs could run at higher nominal contact stresses than the chamfered specimens for equivalent lives.

There appeared to be a significant difference between the -0.026 and -0.14 slide-roll ratios for the crowned disc tests but not for the chamfered ones. The higher slide-roll ratio gave a reduced rolling contact fatigue life in the crowned specimens. The crowned specimens all suffered micropitting and as this progressed the radius of curvature of the specimen and the track width were increased. There was a tendency for the longer life specimens to show a lower tendency to fail by pitting. If the contact stress was too low, the contact pattern would broaden due to excessive wear by micropitting.

The AISI M50NiL and BS S156 disc specimens exhibited similar failures, with pitting occurring on the chamfered barrel edges. The damage, however, was more extensive in the M50NiL specimens. Several of the AISI M50NiL rings also had some small damage on the edge of the track. The 32CDV13 specimens gave very poor rolling contact fatigue results. The barrels appeared heavily micropitted and the rings were even more severely damaged, with large shallow pits destroying the run surface. The AISI M50NiL Duplex specimens were produced by two methods, plasma and gas nitriding. These behaved differently in rolling contact fatigue, with the plasma duplex showing no significant improvement over the AISI M50NiL specimens, and the gas duplex specimens performing considerably better. The gas nitrided AISI M50NiL duplex specimens exhibited a different failure mode to the BS S156 and AISI M50NiL specimens. They failed by pitting after extended lives with micropitting also having taken place. The

failure did not occur at the edge as is characteristic of the specimens, but in the track, with what appeared to be a subsurface initiation. The AISI M50NiL duplex (gas nitrided) rings suffered some micropitting too, and in a few cases developed some extensive, but very shallow pits.

The study was concentrating on rolling contact fatigue, in the form of pitting, but other failure modes such as severe wear, caused by micropitting, and scuffing have also taken place. These failure modes have, however, been identified on both gear and barrel specimens and this is an encouraging sign for the correlation of the two test methods.

Part 3 - Discussion

Chapter 13 Gear, Disc and Axial Fatigue Test Discussion

The discussion of the gear and axial fatigue tests described in Chapter 11 and the disc tests described in Chapter 12 is given here. The correlation of the gear and disc tests will be discussed in Chapter 14.

13.1 The Gear Rolling Contact Fatigue Tests

This discussion is relevant to the gear rolling contact fatigue tests carried out on both tip-relieved and non-tip-relieved gears, the results of which were described in Chapter 11.

13.1.1 The Non-Relieved Gear Tests

The computer model developed to analyse the spur gears, discussed in Chapter 8, showed that the non-tip-relieved gears could give rise to extended contact, due to the elastic deflection of the gear teeth. This may damage the root because of the high contact stresses (~7.5 GPa, Figure 8.2.16), flash temperatures (~500 °C, Figure 9.2.6), sliding speeds (~6 m s^{-1}, Figure 10.3.4), and the reversal of entrainment predicted in this area. The prediction of damage in these regions appeared to correlate with the experimental work carried out on the non-tip-relieved gears. The contact width was also predicted to expand at points where extended tooth pair contact occurred. In practice the contact pattern did assume this shape in the non-tip-relieved gears. Extended contact and the higher loads in the high sliding areas of the gear would also help explain the lower scuffing load in these gears when compared to the tip-relieved gears.

For all the non-relieved gear tests that were loaded gently and kept at low loads, the contact pattern broadened due to wear by micropitting on the tooth flank. This made the gear contact more conforming (lower contact stresses) and enabled the load to be increased considerably. These gears would probably not pit at these loads (~2 GPa) because of the micropitting wear. Similar findings have been shown with fatigue tests on rollers, especially when sliding was present, by Nakajima (1981) on normalised steel

rollers and by Nakajima and Morodomi (1986) on surface hardened rollers. Rounds (1962) found an optimum wear rate for maximum life. Further increasing or decreasing the wear rate from the optimum value, decreased fatigue life markedly. This may be caused by the reduced possibility for a unit volume to accumulate enough cycles to fail by fatigue before it is worn away.

Despite the surface being cracked by the micropitting, this did not propagate into pits. This was probably due to the damaging stress range being localised close to the surface, due to the roughness, and not penetrating deep enough into the gear to propagate large enough cracks for pitting. The micropitting wear was probably greater for these gears for a given torque, when compared to the tip-relieved gears, because of the more severe contact conditions in the non-relieved areas of tooth contact.

13.1.2 The Tip-Relieved Gear Tests

The tip-relieved gears had no hard marking in the gear root and the contact pattern was more rounded. This was due to the tip-relief, which removed load from the gear teeth in these high sliding areas, and appeared to reduce the risk of scuffing. The theoretical contact width, using Hertz theory, was 4.8 mm for a maximum contact stress of 2.64 GPa. The width measured for a gear run for about 1 million load cycles at 2.6 GPa was 6mm (Figure 11.1.8).

Most pits occurred on the driving gear even though 1:1 ratio gears were used, and therefore both gears experienced the same number of cycles. Overall, in the tip-relieved gear tests, the driving gears had about eight times as many pits as the driven gears. Where, when failure was detected, there was always at least one pit on the driving gear. One possible reason for this may be the influence of friction in the contact on the contact stresses. In a theoretical study of the efficiency of involute spur gears, the contact stress for meshing, identical, involute spur gears was shown by Martin (1981) to be slightly higher in the path of approach than in the path of recess. This would give the driving gear a greater contact stress in the dedendum than the addendum and vice-versa for the driven gear (though from a static analysis alone, it should be the same). This is important as the magnitude of the stress has a strong influence on fatigue life. This effect, combined with the fact that pitting is promoted in the dedendum of gears rather than the addendum (probably due to the contact motion and traction forces being in opposite directions),

will probably promote pitting of the driver gear dedendum over the driven gear dedendum.

13.2 The Disc Fatigue Tests

This discussion is relevant to the disc rolling contact fatigue tests carried out on both crowned and chamfered barrels, the results of which were described in Chapter 12.

13.2.1 The Crowned Disc Tests

The track width was much narrower in these specimens than the chamfered barrels because of the crown. The crowned barrel had a theoretically elliptical contact area with no edge contact. This was probably the reason why the crowned discs could be run at higher nominal contact stresses than the chamfered specimens for equivalent lives.

There appeared to be a significant difference between the -0.026 and -0.14 slide-roll ratios for the crowned disc tests. The higher slide-roll ratio gave a reduced rolling contact fatigue life in the crowned specimens. This observation, of sliding causing a reduction in fatigue life of the disc having the lower surface speed, has been reported by Dawson (1963), Diaconescu et al. (1974), Macpherson (1975), Graham (1979), and Nakajima (1990), amongst others. Nakajima (1981) also reported a reduction in life with slide roll ratio and observed that smooth surfaces showed a lower reduction in life with sliding than rough ones. This has been discussed in more detail in Section 3.2.4.4, but the increased number of asperity interactions per load cycle (increasing the rate of plastic deformation of the asperities) is a probable explanation. This is combined with the crack opening and pressurisation effects promoted by sliding.

The crowned specimens all suffered micropitting and, as this progressed, the radius of curvature of the specimen and the track width increased. There was a tendency for the longer life specimens to show a lower tendency to fail by pitting. This could be due to the reason discussed earlier of wear preventing the growth of big enough cracks for pitting, but could also be due to the broadening of the contact and reduction of the crowning radius making the contact more conforming and hence reducing the contact stresses.

13.2.2 The Chamfered Disc Tests

Of the three slide-roll ratios tested, -0.28 in the disc rig appeared to offer the closest match to the lowest point of single tooth contact in the gears, where the slide-roll ratio was -0.26. However, the disc tests at this slide-roll ratio scuffed. The analysis presented in Chapter 9, showed that, unlike the gears, the disc tests had bulk temperatures that depended on the slide-roll ratio chosen, increasing with slide-roll ratio. At a Hertzian contact stress of 2.6 GPa, the gear bulk temperature was 102 °C and the barrel temperature, at -0.28 slide-roll ratio, was measured at 188 °C, but the bulk temperature incorporating the ring temperature was 128 °C. The contact temperatures, including flash temperature effects, were calculated at 265 °C for the gear and 309 °C for the -0.28 slide-roll ratio discs. This may explain why the -0.28 slide-roll ratio disc specimens scuffed.

It was shown in a stress analysis of the chamfered specimen, Chapter 8, that it had a line contact with a stress concentration at the track edge. It was for this reason that pitting always took place on the track edge in the tests.

The difference that was observed between the -0.026 and -0.14 slide-roll ratios for the crowned specimens was not seen in the chamfered barrels. The increased number of asperity interactions per load cycle should be experienced by both the crowned and chamfered specimens. However, the edge stressing effect in the chamfered barrels may have caused plastic deformation on a scale which outweighed the effects of the increased asperity interaction rate with slide-roll ratio, therefore, giving no significant difference between the two slide-roll ratios.

13.3 The Axial Fatigue Tests

In the axial fatigue tests regardless of alloy composition, the highest endurance stress was obtained with a compressive mean stress and the lowest endurance stress with the tensile mean stress. The type and proportion of each failure was found to depend on the applied mean stress, there being more core-originated failures in the compressive stress regime and vice-versa. While the reason for these changes in behaviour are not fully understood, it is believed to be due to the inter-relationship between the characteristics of the micro-inclusions present, the residual stress distribution and notch profile (Davies 1996).

Raising the test temperature reduced the fatigue lives regardless of alloy composition. This could have been due to: the relaxation of the shot peened residual stresses; influence of free water present in the oil on initiation and propagation; or the influence of temperature on dislocation movement. Tests performed on non-shot peened specimens were also affected by temperature, so residual stress relaxation can be ruled out. Oil chemical activity was unlikely to affect the subsurface initiated failures, so the suggestion that temperature influenced dislocation movement would appear the most likely.

13.4 The Materials Tested

In the last twenty years a range of new materials and processes have become available to gears and rolling bearings. Many are being researched and adopted by the aerospace industry because of the critical nature of this area and the requirement for smaller, lighter, more reliable, and higher temperature operating components. The main uncertainty is the impact of these new materials on durability, and in particular on rolling contact fatigue, a facet of their performance which has been little studied. Some of these materials and treatments have been investigated by the author, under conditions of high stress. A brief discussion of the results obtained on the materials tested, and presented in Chapters 11 and 12, now follows.

13.4.1 BS S156

This standard carburised steel was used as a reference material with which to compare the relative performance of other steels and with which to investigate the effects of tip-relief in gears and of crowned and chamfered disc specimens. The gear and disc specimens in this material had similar failures. BS S156 was tempered at 140 °C and softens rapidly at higher temperatures; it was probably for this reason that it scuffed with the high temperatures present in the disc tests at the high slide-roll ratio.

13.4.2 32CDV13

The 32CDV13 specimens gave very poor rolling contact fatigue results. After a small number of cycles, the barrels appeared heavily micropitted and the rings were even more severely damaged, with large shallow pits destroying the run surface. The reason for this was most probably the damaging effect of the brittle white layer, that was only partially removed from the barrels and not removed from the rings (visible as a greyish layer on the surface of the specimen, or a white layer in a microscope section, Figure 7.5.9). The

rings appeared more damaged than the barrels, probably because they had no white layer removed. These results confirm observations by Bell (1973), Braza (1992), and Hutchings (1992) on the negative effect of the white layer on rolling contact fatigue. This damaging effect could also have been aggravated by the high values of surface roughness measured on these specimens, particularly the ring specimens (0.8 μm R_a), when compared to the other discs.

13.4.3 AISI M50NiL

For both the gear and the disc tests the AISI M50NiL failed in a similar fashion to the BS S156 material, exhibiting both pitting and micropitting, but had a shorter average life. The damage was also more extensive in the M50NiL specimens. The gears had more pits in the dedendum and several of the AISI M50NiL rings also had some minor damage on the edge of the track.

These results do not agree with spur gear endurance tests and rolling element surface fatigue tests conducted by Townsend and Bamberger (1991) on VIM-VAR M50NiL and VAR and VIM-VAR AISI 9310 gear material. AISI 9310 is a similar, but not identical, steel to BS S156. Townsend and Bamberger found that VIM-VAR M50NiL gears had surface fatigue lives that were 4.5 to 11.5 times that for VIM-VAR and VAR AISI 9310 gears, respectively. The surface fatigue life of the VIM-VAR M50NiL rolling contact fatigue bars was 13.2 and 21.6 times that for the VIM-VAR and VAR AISI 9310, respectively. The gears reportedly failed by subsurface pitting fatigue, despite the proper heat treatment and high cleanliness of the steels. The gears were run at 1.7 GPa and an inlet temperature of 47 °C and outlet temperature of 78 °C.

There are several possible reasons for the discrepancies between the authors results and those obtained by Townsend and Bamberger (1991). AISI 9310 may not perform as well as BS S156 in rolling contact fatigue; Townsend and Bamberger may have had insufficiently clean steels, as indicated by the subsurface failures; or the AISI M50NiL used by the present author may not have been prepared to have an optimum performance, resulting in material defects.

The last suggestion is probably the most likely explanation for the observed results. The AISI M50NiL microstructure, discussed in Section 7.5, appeared to contain high levels of retained austenite (Figure 7.5.5). High levels of retained austenite have been shown to have a deleterious effect on rolling contact fatigue life by Bradis and Schmidt (1983) and

Frankel et al. (1960) and on mechanical properties by Castleman et al. (1952), amongst others. In rolling contact fatigue tests on high-speed tool steel bearings, Scott and Blackwell (1968) found that higher austenite levels gave a mean life of less than one third of that of balls of lower austenite levels.

Frankel et al. (1960) suggested that stresses generated during operation could activate a transformation of the austenite to martensite, causing a volume change due to change in the lattice structure. This may change the shape of a component and create a local residual stress field which could help initiation of fatigue cracks and lead to a reduction in life. This hypothesis was endorsed by Scott (1968).

This would explain the poor rolling contact fatigue performance of the AISI M50NiL specimens, despite them having higher hardness values in the carburised case than the BS S156 specimens (Figure 7.5.1).

13.4.4 AISI M50NiL Duplex

In both the gear (plasma nitrided) and disc (gas nitrided) tests the AISI M50NiL Duplex specimens had a greatly improved rolling contact fatigue resistance when compared to the AISI M50NiL and BS S156 gears. This was probably due to the increased surface hardness and compressive residual stresses near the surface of the components, created by the nitriding process, coupled with the deeper hardness and compressive stress profile created by the carburising process. There could also have been the added benefit of the nitriding heat treatment reducing the high levels of retained austenite in the AISI M50NiL specimens.

The white layer in these duplex specimens was shallow, so it probably did not play a significant role in the fatigue performance of these specimens (about 10 μm in the discs). It also appeared to be more strongly bonded to the underlying material and less cracked than the white layer in the nitrided 32CDV13 specimens.

In the gears the duplex specimens did not fail by pitting within ten million cycles, but suffered some micropitting in the dedendum. The AISI M50NiL Duplex disc specimens were produced by two methods, plasma and gas nitriding. These behaved differently in rolling contact fatigue, with the plasma duplex showing no significant improvement over the AISI M50NiL specimens and the gas duplex specimens performing much better. The reason for the plasma specimens not performing at the level of the gas nitrided specimens

was the inferior hardness depth imparted on them by the plasma nitriding process (Figure 7.5.1). As mentioned in Chapters 3 and 5, hardness has a very important effect on rolling contact fatigue performance.

The hardness imparted by the plasma nitriding Duplex process, therefore, appeared to be sufficient to improve the M50NiL gear contact fatigue lives but not the disc lives. This was probably due to the shallow, high-hardness duplex layer being able to protect the gears from the stresses induced by the roughness, but being unable to protect the discs from the deeper effect of the edge stress concentration. In the gas nitrided Duplex barrels, the nitriding treatment went to greater depths and therefore helped protect against this stress concentration.

The gas nitrided AISI M50NiL Duplex disc specimens exhibited a different failure mode to the BS S156 and AISI M50NiL specimens. Despite the edge stress concentration caused by the chamfer of the specimen, fatigue spalls in duplex hardened AISI M50NiL formed in the centre of the track with origins below the surface. This may indicate that the process has the potential to suppress pitting arising from gear misalignment or of lead errors, as these tend to cause stress concentrations on the surface of a component.

The axial fatigue tests also indicated that AISI M50NiL Duplex performed better than both the AISI M50NiL and the BS S156 ones. This could have been partially due to the high compressive residual stress distribution created by the nitriding process near the surface of the specimens.

These results, therefore, confirm the improved rolling contact fatigue results obtained on nitrided M50 and M50NiL tested against softer counterfaces by Pearson and Dezzani (1993). Of course, the present work featured much higher sliding speeds, identical counterface materials, and gear, as well as disc, tests.

13.5 The Possible Effects on Gearbox Size and Weight

It is clear that a substantial increase in rolling fatigue performance (of the order of 10 % in contact pressure) results from the introduction of the additional nitriding process. As there are also improvements in bending strength (~ 6 % at $1x10^7$ cycles, inferred from the axial fatigue test results), a significant reduction in the weight of geared transmissions is likely to be possible. An important consideration is the corresponding improvement in rolling bearings which may result from similar technology, as bearing loads are increased

when gears are downsized. In weight-sensitive applications such as helicopters, the ability to incorporate integral raceways in the gear design is also a consideration. Integral bearing raceways in an AISI M50NiL gear could also be duplex hardened and hence full advantage could be taken of the improved rolling fatigue life.

13.6 Conclusions

- The non-tip-relieved gear teeth suffered from localised damage probably caused by the tip of the gear tooth interfering with the root of the mating tooth, i.e. extended contact. This was predicted by a computer model that showed high contact stresses, flash temperatures, sliding speeds, and the reversal of entrainment predicted in this area were possible.

- There appeared to be a significant difference between the -0.026 and -0.14 slide-roll ratios for the crowned disc tests. The higher slide-roll ratio giving a reduced rolling contact fatigue life. This was probably due to the increased asperity interaction per contact cycle. This difference was not seen in the chamfered barrels, where the edge stressing effect in the chamfered barrels may have caused plastic deformation on a scale which outweighed the effects of the increased asperity interaction rate with slide-roll ratio.

- For both the gear and the disc tests the AISI M50NiL failed in a similar fashion to the BS S156 material, exhibiting both pitting and micropitting, but had a shorter average life. The AISI M50NiL microstructure appeared to have high levels of retained austenite, which may have had a deleterious effect on the rolling contact fatigue life.

- In both the gear and the gas nitrided disc tests the AISI M50NiL Duplex specimens had a greatly improved rolling contact fatigue resistance when compared to the AISI M50NiL and BS S156 specimens. This was probably due to the increased surface hardness and compressive residual stresses near the surface of the components created by the nitriding process, coupled with the deeper hardness and compressive residual stresses created by the carburising process.

- The hardness imparted by the plasma nitriding Duplex process appeared to be sufficient to improve the M50NiL gear contact fatigue lives but not the disc lives. This was probably due to the shallow, high-hardness duplex layer being able to protect the

gears from the stresses induced by the roughness, but being unable to protect the discs from the deeper effect of the edge stress concentration.

- In the disc tests, despite the edge stress concentration, fatigue spalls in the gas nitrided duplex hardened AISI M50NiL (which had a deeper hardening effect than the plasma nitriding) formed in the centre of the track with origins below the surface. This may indicate that the process has the potential to suppress pitting arising from gear misalignment or lead errors.

- The axial fatigue tests also indicated that AISI M50NiL Duplex performed better than both the AISI M50NiL and the BS S156 specimens. This could have been partially due to the high compressive residual stress distribution created by the nitriding process near the surface of the specimens.

- This substantial increase in rolling fatigue performance resulting from the introduction of an additional nitriding process coupled with the improved bending strength could give a significant reduction in the weight of geared transmissions. The ability to incorporate integral raceways in the gear design is also a consideration.

Chapter 14 Comparison and Correlation of Gear and Disc Failures

In the past gear materials have been studied mainly on disc and gear rigs. Discs are often used because of the reduced cost and ease of manufacture of the specimens. As discussed in Chapters 3 and 6, the correlation between the two types of test is rendered difficult by the large number of variables thought to influence rolling contact fatigue and the difficulty in quantifying and controlling them. The correlation has been investigated, amongst others, by Benedict (1968) for scuffing and Flamand et al. (1981) for rolling contact fatigue. Gear and disc rolling contact fatigue tests carried out by the author were described in Chapters 11 and 12 and discussed in Chapter 13. The relationship between these gear and disc tests is investigated here.

14.1 Comparison of Gear and Disc Failures

The non-tip-relieved gear teeth exhibited different failure modes to the tip-relieved gears, with scuffing and micropitting being more probable. They could be compared, perhaps, to the -0.28 slide-roll ratio disc specimens, where high loads and bulk temperatures were combined with high slide-roll ratios.

The tip-relieved gears had no hard marking in the gear root and the contact pattern was more rounded. These gears failed in the centre of the track (in the lead direction) as did the crowned discs, both specimens having elliptical contacts. This was due to the Hertzian stresses being highest at this point. The track width was narrower in the crowned specimens than the gears because of its smaller lead radius.

On the other hand, the chamfered specimens failed at the edge of a line contact across the track. This stress concentration and the difficulty in analysing it, made it difficult to quantify the actual running stresses the chamfered specimen experienced during the test. In addition there is plastic deformation and wear of the edge with progressive running cycles, which will continuously alter the geometry at this point. Therefore, a theoretical comparison of the chamfered disc and tip-relieved gear tests is difficult.

Despite this edge effect, the same material ranking was obtained for the chamfered disc and tip-relieved gear tests. For both the gear and the disc tests the AISI M50NiL failed

in a similar fashion to the BS S156 material, exhibiting both pitting and micropitting. The gear and the gas nitrided disc tests also showed that the AISI M50NiL Duplex material had a greatly improved rolling contact fatigue resistance when compared to AISI M50NiL and BS S156.

14.2 Gear - Disc Correlation Factor

The use of disc testers to study pitting instead of gears has been mentioned. The motion of sliding and rolling and the contact stresses at a given instant in the gear tooth meshing cycle can be reproduced by two circular discs. Most gear design standards assume that gear tooth meshing can be entirely reproduced by the contact of 'equivalent discs' and that rolling contact fatigue cannot occur below a certain value of contact pressure: the 'endurance limit'. However, disc tests have been found to give unrealistically high endurance limits and a 'gear-disc correlation factor' must be introduced to account for this (BSI 1986) (see Figure 1.1.1). However, what effects this factor takes into account is unclear. The parameter ρ_{rel} in Figure 1.1.1 is the radius of relative curvature, m_n is the gear module, and σ_B is the ultimate tensile strength of the material. When applied to the gears used in this investigation, ρ_{rel} is 8.46 mm at the lowest point of single tooth contact and m_n is 5.08 mm. This gives a value of 1 for the disc-gear correlation factor for contact stress, Z_{G2}, meaning that no difference should be observed for the gear and disc tests. This was not the case, as will be shown next.

The results of the gear and disc rolling contact fatigue tests are plotted together for the BS S156 material in Figure 14.2.1. This shows the gear and chamfered disc tests were run at similar nominal contact stresses for similar lives, whereas the crowned discs were run at a higher stress levels for equivalent lives.

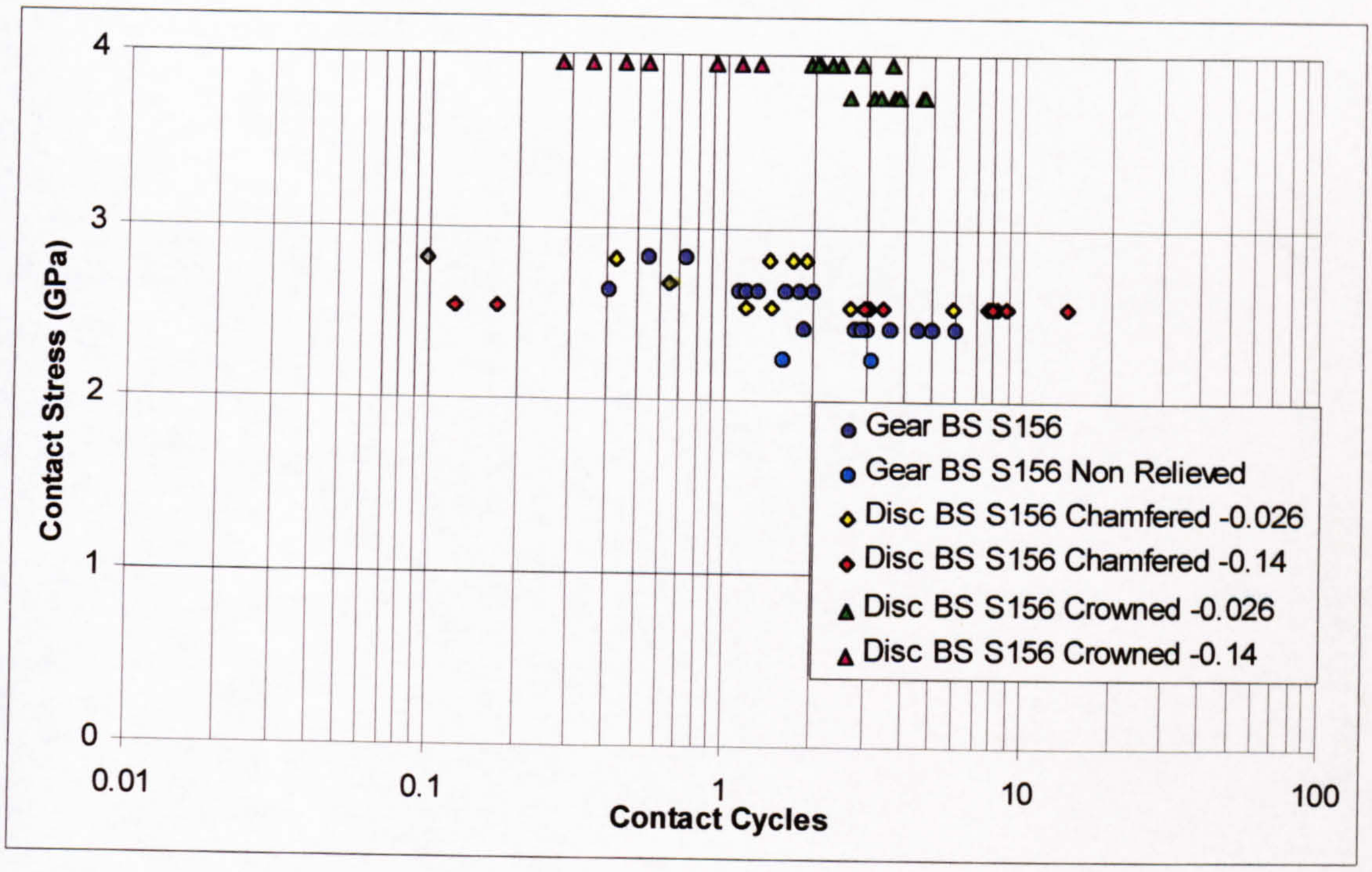


Figure 14.2.1 Rolling Contact Fatigue Lives of the Gear and Disc Experiments

These fatigue lives were plotted on Weibull charts and L_{50} lives were obtained for each specimen run at a particular stress. These L_{50} lives were plotted on an S-N chart (Figure 14.2.2) to allow comparison of the different test specimen lives.

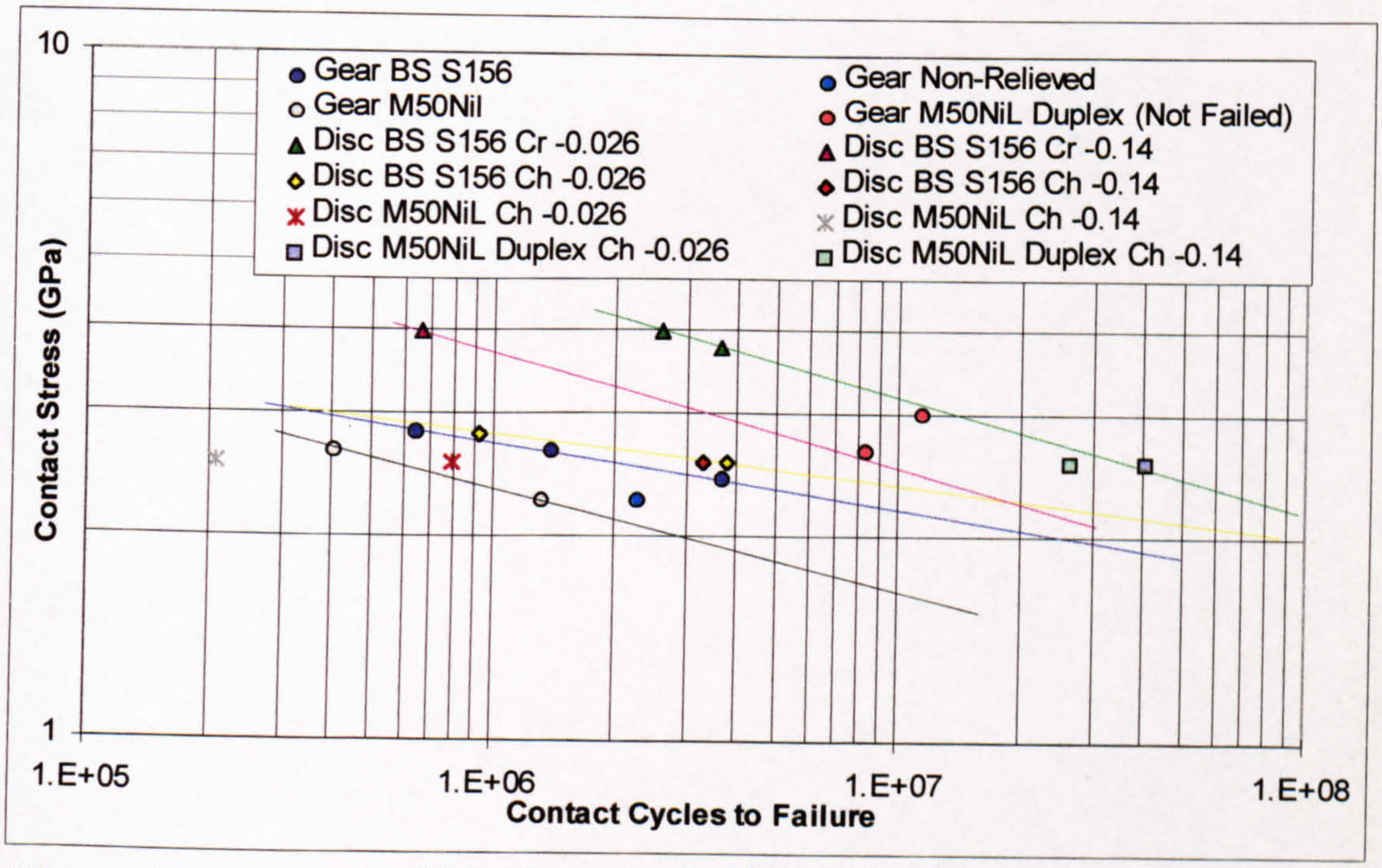


Figure 14.2.2 S-N Plot with L_{50} Lives for the Various Specimens

These results were used to compare the different tests at similar stress levels by extrapolating the crowned disc test results (Table 14.2.1).

Table 14.2.1 Comparative Fatigue Lives for the BS S156 Tests

Contact Stress	2.4 GPa	2.8 GPa
Specimen	Disc/Gear life	Disc/Gear life
Chamfered -0.026	2.1	1.3
Crowned -0.026	16.9	34
Crowned -0.14	4.3	8.6

If we compare the lives of the chamfered specimens run at the -0.026 slide-roll ratio to the tip relieved gears they are only about 1.8 times longer. However, this relatively close correlation is probably fortuitous, because of the barrel having an edge stress concentration which raises the stress above the nominal value plotted in Figure 14.2.2. The tip-relieved gear fatigue life should be compared to the crowned specimens, and these appear to have similar lives but at far higher stresses. The crowned tests could not, however, be tested at the lower stresses as micropitting would result in a change in geometry and stresses. This did not happen in the gears to such a degree, probably due to the much greater crowning radius in the lead direction. Extrapolating the curve obtained for the crowned specimens at -0.026 slide-roll ratio, values of 34 and 16.9 times the life of the gears at 2.8 and 2.4 GPa are obtained. If we compare the lives of the crowned specimens at 3.95 GPa, the -0.14 slide-roll ratio gave lives of 0.25 times those at -0.026. By using the same curve gradient for the -0.14 as was obtained for the -0.026 tests, and extrapolating the -0.14 slide-roll ratio result, lives of 8.6 and 4.3 that of the gears were obtained for contact stresses of 2.8 and 2.4 GPa respectively. It would therefore appear that the -0.14 slide-roll ratio gave a closer correlation with the gear tests than the -0.026 slide-roll ratio.

At the lowest point of single gear tooth contact the slide-roll ratio was -0.26, so tests on the discs at -0.28 might be expected to give the closest match in fatigue results. However, as mentioned in the results, scuffing of the chamfered disc surface during loading was encountered at this ratio. This was possibly due to the higher temperature of the discs, at this slide-roll ratio, when compared to the gears (around 150 °C to 102 °C from Table 9.3.1).

The slide-roll ratio therefore appears to be the most important factor in determining the correlation between the two types of test. Overall, the results indicated that the fatigue life of the discs may have been slightly higher than the gears. There are numerous

possible reasons for the discrepancies between gear and disc tests as mentioned in Chapter 6:

- The varying, rather than constant, slide-roll ratio present in gears
- Differences in the bulk metal temperatures of the test pieces as well as the film thickness
- Stress concentrations arising from the geometry and misalignment
- Roughness effects
- Extended contact in non-tip-relieved gears
- Dynamic loads
- Hunting and integral ratios may give different lives
- The size factor
- Debris effects

These will be discussed with particular attention given to their relevance to the tests described earlier.

14.2.1 The Influence of Slide-Roll Ratio

The disc tests have the ability to simulate only one point in the gear tooth meshing cycle in terms of slide-roll ratio. This is important because sliding has a considerable effect on rolling contact fatigue, as discussed in Chapter 3 and shown by the crowned disc test results, and can also affect other failure modes such as scuffing. In a gear tooth the sliding speeds are greater at the tip and root, but the load there is usually less, so a combination of the load and sliding speed will determine where failure will occur on the tooth if no other effect, such as debris indentation, prevails. The entrainment speed is that which determines the thickness of an elastohydrodynamic lubricant film in the contact, this will help separate the surfaces and improve rolling contact fatigue performance. To obtain the best correlation perhaps the disc would have to simulate the conditions where failure occurs on the gear. However, other failure modes may come into play as shown by the -0.28 slide-roll ratio discs scuffing.

14.2.2 Temperature and Film Thickness Differences

The discs were not thermally equivalent to the gears, giving the two types of specimen different bulk and flash temperatures. This is important because the minimum EHD film thickness in the contact zone, which will determine the amount of asperity contact, is

controlled by viscosity at the inlet to the contact, which is controlled by bulk temperature of the contacting bodies. The bulk temperatures of the discs tests depended on the slide-roll ratio they were run at, increasing with increasing slide roll ratio, as shown in Chapter 9. The bulk temperatures of the discs at a slide-roll ratio of -0.28 was much higher than that of the gears.

The EHD film thickness, using Dowson-Hamrock's minimum film thickness equation, and the lambda ratio were calculated for the gear and disc specimens (Chapter 10). From these results it would appear that the severity of asperity interaction on the gear tooth surfaces will be greater than that on the disc specimens. However, the lambda values were all low, indicating considerable surface contact, so there may not be any significant difference in these results.

14.2.3 Stress Concentrations arising from the geometry

As mentioned earlier, the barrel specimens failed on the edge (except for the AISI M50NiL Duplex specimens). This showed clearly that the disc experienced a local increase in stress at the edge of its track and this had an important effect on rolling contact fatigue. The non-tip relieved gears also had a stress concentration effect, discussed further in Section 14.2.5. The crowned disc and tip-relieved specimens did not have this problem because of the crowning radius in the lead direction.

14.2.4 Roughness Effects

The roughness will affect the stresses the component experiences. The gears had an axial surface finish and the discs a circumferential surface roughness lay. Therefore, the representative roughness profiles used for the roughness analysis, were in the profile direction for the gears and in the lead direction for the discs. The gear surface produced higher surface contact pressure and subsurface shear stress distributions than both the crowned and chamfered barrels. This may have contributed to the shorter lives of the gear fatigue specimens.

The circumferential surface lay in the crowned specimens may have been an added reason to that of high temperature, for them scuffing at the high slide-roll ratio (Snidle & Evans 1995).

14.2.7 Stressed Volume

When comparing fatigue test results, the size factor should be considered for specimens of different shape or size. This parameter accounts for larger component having a greater probability of containing a crack of a certain critical length for fatigue crack initiation.

In Section 8.4, it was shown that the stressed volume is smaller for the disc specimens when compared to the gears, particularly the crowned barrels. This could have been another reason for the disc tests having longer fatigue lives than the gears, for equivalent Hertzian contact stresses. From Table 8.4.3, the life of a crowned barrel specimen could be around 2 times that of a gear and that of a chamfered barrel 1.4 times that of a gear, at a contact stress of 2.6 GPa, all other factors being the same.

14.2.6 Extended Contact

The presence of extended contact in the non-tip-relieved gear teeth, due to their elastic deflection, produced premature contact of the gear tooth tip corner in the mating gear tooth root and delayed exit of the root of the gear tooth and the tip of the mating tooth. High local pressures are present at these points and are damaging to the life of the specimens.

Profile relief overcame this problem by compensating for the deflection of the gear teeth under load. This relief was considered effective up to torques of 350 N m (3 GPa contact stress). There is also the added effect that it removes part of the load on the teeth in the high sliding portions, thus reducing the risk of scuffing.

14.2.7 Dynamic Loads

A theoretical analysis of a simplified model of the gear rig (Chapter 8) showed that it would not be operating near resonant frequencies and that the slave gears were isolated from the test gears. A simple dynamic load analysis to find K_v gave a value of 1.05, indicating that dynamic loads were not thought to contribute excessively to the gear loading.

14.2.8 Other Factors

An effect, discussed in Section 6.3.2, in which a difference in fatigue resistance has been observed between hunting and integral ratios, the latter giving an extended fatigue life. The gear tests were of 1:1 ratio and thus should experience the benefits of improved

fatigue life. The disc tests at -0.14 slide-roll ratio had a ratio of 3:1. This effect, however, would not explain the extended lives of the disc specimens when compared to the gears.

Finally, rolling contact fatigue can be seriously affected by the presence of debris in the lubricant. Debris passing through the contact of disc and gear specimens is likely to produce different effects due to the difference in motion and geometry. The size of the debris in these experiments was controlled by 3μm filtration.

14.3 Conclusions

- The non-tip-relieved gear teeth exhibited different failure modes to the tip-relieved gears. They could be compared, perhaps, to the -0.28 slide-roll ratio disc specimens, where high loads and bulk temperatures were combined with high slide-roll ratios.

- The fatigue lives derived from the tip-relieved gear tests correlated well with the chamfered disc tests, however, this was thought to be fortuitous, due to the different stressing of the specimens. The chamfered barrel having a stress concentration at the edge of the track.

- Despite this edge effect, the same material ranking was obtained for the chamfered disc and tip-relieved gear tests. For both the gear and the disc tests the AISI M50NiL failed in a similar fashion to the BS S156 material, exhibiting both pitting and micropitting. The gear and the gas nitrided disc tests also showed that the AISI M50NiL Duplex material had a greatly improved rolling contact fatigue resistance when compared to AISI M50NiL and BS S156.

- The fatigue lives of the crowned disc tests gave longer lives than the gears for equivalent stresses. As the slide-roll ratio was increased towards that of the highest point of single tooth contact (-0.26) the correlation improved. At a slide-roll ratio of -0.28 on the disc specimens, where the correlation of pitting life might have been expected to be the best, scuffing of the disc occurred, possibly due to the higher temperatures and the circumferential roughness lay.

- The slide-roll ratio therefore appears to be the most important factor in determining the correlation between gear and disc tests. The other reasons thought to be important for differences in gear and disc fatigue life were: roughness effects (higher surface and subsurface stress distributions in the gears); the stressed volume (greater in the gears);

stress concentrations (affecting the chamfered barrel results); and thermal differences (capable of causing scuffing instead of pitting).

- The study was concentrating on rolling contact fatigue, in the form of pitting, but other failure modes such as severe wear, caused by micropitting, and scuffing have also taken place. These failure modes have, however, been identified on both gear and barrel specimens and this is an encouraging sign for the correlation of the two test methods.

Chapter 15 Conclusions

In this chapter a brief summary of the research presented in this thesis is given along with some of the main conclusions drawn from other chapters. Then some proposals for possible future research will be made.

15.1 Summary of Thesis

This thesis has reported an investigation of the rolling contact fatigue behaviour of several steels and treatments under conditions of high load, using both gear and disc specimens. Four materials have been tested: a standard carburised steel (BS S156); two temper resistant steels, one carburised (AISI M50NiL) and one nitrided (32CDV13); and a duplex hardened (carburised then nitrided) steel (AISI M50NiL Duplex).

In the first part of the thesis a review of the literature and main aspects relevant to the work presented here was given. This included topics such as the study of surfaces in contact, rolling contact fatigue, gear materials and failure modes, and test methods used to evaluate rolling contact fatigue. An idea of the complexity of rolling contact fatigue research was given. The statistical nature of the process and the length of the tests can be a problem, but the major difficulty is the large number of variables affecting it. Materials, surface finish, lubrication, load, temperature, geometry and sliding, are amongst the more important ones. It is difficult to incorporate all of these in an investigation and, even if just one is investigated, results from one set of tests may not correlate with similar investigations.

In the second part, the analysis and experimental work carried out by the author was reported. The analysis considered the test rigs, the specimens, stress analysis and, thermal and lubrication aspects. The results from the experimental research included lubricant tests, gear temperature measurements, and the gear and disc fatigue tests on the various materials.

In part three a discussion of the results obtained and their significance was given. Aspects such as material differences, gear-disc correlation and possible effects on gearbox sizing were considered.

15.2 Conclusions

The main conclusions that can be drawn from the work presented in this thesis are:

- The non-tip-relieved spur gears, used in the fatigue tests, suffered from localised damage on the teeth at the extremities of the meshing cycle, probably caused by the tip of the gear tooth interfering with the root of the mating tooth, i.e. extended contact. This was predicted by a computer model that showed that high contact stresses, flash temperatures, sliding speeds, and the reversal of entrainment were possible in this area.

- The tip-relieved spur gears, used in the fatigue tests, had no hard marking in the gear root and the contact pattern was more rounded. This was due to the tip-relief, which removed load from the gear teeth in these high sliding areas. This helped reduce the risk of scuffing in these gears and possibly reduced the amount of micropitting wear.

- It was shown in a stress analysis of the chamfered disc specimen, Chapter 8, that it had a line contact with a stress concentration at the track edge. This was the reason for the chamfered disc fatigue tests always pitting on the edge of the track.

- The crowned discs could run at higher nominal contact stresses than the chamfered specimens for equivalent lives. The probable reason for this was the crowned specimen having an elliptical contact area, with no edge stress concentration.

- In the disc fatigue tests, there appeared to be a significant difference between the -0.026 and -0.14 slide-roll ratios for the crowned specimens, the higher slide-roll ratio giving a reduced rolling contact fatigue life. This could have been due to the increased asperity interaction per contact cycle causing more surface plastic deformation. This difference was not seen for the chamfered specimens, where the plastic deformation caused by the edge stressing may have outweighed this effect.

- In both gear and disc tests, micropitting appeared to increase the pitting lives over specimens that only pitted. This was thought to be due to wear preventing the growth of big enough cracks for pitting, or the reduced possibility for a unit volume to accumulate enough cycles to fail by fatigue before it was worn away. It could also be due to the broadening of the contact and reduction of the crowning radius lowering the contact stresses.

- The disc tests had bulk and flash temperatures that depended on the slide-roll ratio chosen, increasing with slide-roll ratio. The bulk and flash temperatures of the discs at a slide-roll ratio of -0.28 were higher than those of the gears. These high temperatures coupled with the circumferential surface lay may explain why the -0.28 slide-roll ratio disc specimens scuffed.

- The fatigue lives derived from the tip-relieved gear tests correlated well with the chamfered disc tests, however, this was thought to be fortuitous, due to the different stressing of the specimens.

- The fatigue lives of the crowned disc tests gave longer lives than the gears for equivalent stresses. As the slide-roll ratio of the disc tests was increased towards that of the highest point of single tooth contact on the gears (-0.26) the correlation improved. At a slide-roll ratio of -0.28 on the disc specimens, where the correlation of pitting life might have been expected to be the best, scuffing of the disc occurred.

- The slide-roll ratio appeared to be the most important factor in determining the correlation between gear and disc tests. The other reasons thought to be important for differences in gear and disc fatigue life were: roughness effects (higher surface and subsurface stress distributions in the gears); the stressed volume (greater in the gears); stress concentrations (affecting the chamfered barrel results); and thermal differences (capable of causing scuffing instead of pitting).

- The study was concentrating on rolling contact fatigue, in the form of pitting, but other failure modes such as severe wear, caused by micropitting, and scuffing have also taken place. These failure modes have, however, been identified on both gear and barrel specimens and this is an encouraging sign for the correlation of the two test methods..

- Despite the edge effect in the chamfered discs, the same material ranking was obtained for the chamfered disc and tip-relieved gear tests. For both the gear and the disc tests the AISI M50NiL failed in a similar fashion to the BS S156 material, exhibiting both pitting and micropitting, but had shorter fatigue lives. The high levels of retained austenite in the AISI M50NiL specimens may have had a deleterious effect on the rolling contact fatigue life. The 32CDV13 specimens had poor rolling contact fatigue lives because of the damaging effect of the white layer, aggravated by the high surface roughness.

- The gear and gas nitrided disc tests showed that the AISI M50NiL Duplex material had a greatly improved rolling contact fatigue resistance when compared to AISI M50NiL and BS S156. This was probably due to the increased surface hardness and compressive residual stresses near the surface of the components created by the nitriding process, combined with the deeper hardness and compressive residual stresses created by the carburising process.

- The hardness imparted by the plasma nitriding Duplex process appeared to be sufficient to improve the M50NiL gear contact fatigue lives but not the disc lives. This was probably due to the shallow, high-hardness duplex layer being able to protect the gears from the stresses induced by the roughness, but being unable to protect the discs from the deeper effect of the edge stress concentration.

- In the disc tests, despite the edge stress concentration, fatigue spalls in the gas nitrided duplex hardened AISI M50NiL (which had a deeper hardening effect than the plasma nitriding) formed in the centre of the track with origins below the surface. This may indicate that the process has the potential to suppress pitting arising from gear misalignment or lead errors.

- Axial fatigue tests also indicated that AISI M50NiL Duplex performed better than both the AISI M50NiL and the BS S156 specimens. This could have been partially due to the high compressive residual stress distribution created by the nitriding process near the surface of the specimens.

- This substantial increase in rolling fatigue performance, resulting from the introduction of an additional nitriding process, coupled with the improved bending strength could give a significant reduction in the weight of geared transmissions.

15.3 Proposals for Future Research

A few suggestions for future research are made here.

15.3.1 Suggestions for Experimental Research

- The AISI M50NiL specimens did not perform as well as other researchers have found (Townsend & Bamberger 1991). Further testing and characterisation of this material should be carried out.

- Due to the poor rolling contact fatigue performance of the 32CDV13 disc specimens and the contrasting results obtained by other workers on the effects of the white layer, it would be useful to investigate more thoroughly the effects of the white layer in nitrided surfaces.

- The high temperature behaviour of some of these temper resistant gear steels could be investigated further with gear oil loss tests, for example.

- The stressed volume was thought to have an effect on fatigue life, it would be interesting to investigate this effect with crowned specimens of different radius.

- The duplex treatment (nitriding a previously carburised surface) should be investigated further due to the excellent rolling contact fatigue obtained. It would be interesting to run some rolling contact fatigue tests on plasma nitrided M50NiL crowned barrel specimens, to see whether these offered improvements in life over M50NiL specimens which were not observed in the chamfered barrels. In non-aircraft applications, the VIM-VAR steels researched here will probably be regarded as too expensive because of the complex production processes involved. Perhaps a more conventional steel should be sought that might yet provide the benefits of duplex hardening to commercial gear manufacturers.

15.2.2 Suggestions for Theoretical Research

- The chamfered specimen should be modelled more accurately to understand the interactions of the edge contact stresses, roughness, and sliding.

- The gear contact model developed to investigate the non-tip-relieved gears should be improved to allow the analysis of various gear geometries, including tip-relief and pitch errors.

- A model to assess fatigue performance including roughness, hardness and residual stress distributions, sliding, and stressed volume effects should be attempted with the aid of fatigue test results. This would help determine the ideal material properties for a particular application before proceeding to expensive and time consuming tests.

REFERENCES

AGMA Information Sheet 115.01, 1959, *Basic Gear Geometry*, AGMA.

AGMA Information Sheet 217.01, 1965, *Gear Scoring Design for Aerospace Spur and Helical Power Gears*, AGMA.

AGMA Recommended Procedure 246.01A, 1971, *Recommended Procedure for Carburized Aerospace Gearing*, AGMA.

AGMA Information Sheet 110.04, 1980, *Nomenclature of Gear Tooth Failure Modes*, AGMA. (Revised in 1995: AGMA 1010-E95).

AGMA Standard 2000-A88, 1988, *Gear Classification and Inspection Handbook, Tolerances and Measuring Methods for Unassembled Spur and Helical Gears*, AGMA.

AGMA Standard 2001-C95, 1995, *Fundamental Rating Factors and Calculation Methods for Involute Spur and Helical Gear Teeth*, AGMA.

Alban, L.E., 1985, *Systematic Analysis of Gear Failures*, American Society for Metals.

Allwood, J., Stubbs, R.E. & Bryant, G.F., 1997, An Efficient Treatment of Binary Nonlinearities Applied to Elastic Contact Problems without Friction. *J. of Engineering Mathematics*, pp. 1-19.

Anghel, V.A., 1998, A Study of Engine Fuel Efficiency and Oiliness Additives, *PhD Thesis*, Imperial College, University of London.

Archard, J.F., 1957, Elastic Deformation and the Laws of Friction, *Proceedings of the Royal Society of London*, Vol. A243, pp. 190-205.

ASTM, 1983, Petroleum Products and Lubricants - 1947, *Annual Book of ASTM Standards: Petroleum Products, Lubricants, and Fossil Fuels*, Vol. 05.02, D1661-D2896, ASTM.

Averbach, B.L., Bingzhe L., Pearson, P.K., Fairchild, R.E. & Bamberger, E.N., 1985, Fatigue Crack Propagation in Carburised High Alloy Bearing Steels, *Metallurgical Transactions*, Vol. 16A, pp. 1253-1265.

Baber, B.B., Anderson, E.L. & Ku, P.M., 1968, Effects of Lubricants, Metals, Temperature and Atmospheric Environments on Gear Load-Carrying Capacity, *Trans. ASME J. of Lubrication Technology*, Vol. 90, pp. 117-124.

Bailey, D.M., 1989, Fatigue in Helicopter Transmissions: Evaluation of the Fatigue Performance of Gear Finishing Techniques, *Mechanical Research Report, Westland Helicopters Limited*, MRR20142.

Bailey, D.M. & Sayles, R.S., 1991, Effect of Roughness and Sliding Friction on Contact Stresses, *Trans. ASME J. of Tribology*, Vol. 113, pp. 729-738.

Bamberger, E.N. & Kroeger, D.J., 1984, Rolling Element Fatigue Life of Carburised Modified M50 Bearing Steel, *NASA*, CR-168295.

Barnet, D.W. & Yildirim, N., 1994, Loaded Transmission Error Prediction using Computer Model, and its Verification, *BGA Symposium*, Newcastle.

Barragan de Ling FdM., Evans_H.P. & Snidle R.W., 1989, Micro-Elastohydrodynamic Lubrication of Circumferentially Finished Rollers. The Influence of Temperature and Roughness, *Trans. ASME J. of Tribology*, Vol.111, No.4, pp.730-736

Bartz, W.J. & Kruger, V., 1973, Pitting Fatigue of Gears- Some Ideas on Appearance, Mechanism and Lubricant Influence, *Tribology (London)*, Vol. 6, No.5, pp. 191-195.

Barus, C., 1893, Isothermals, Isopietics and Isometrics in relation to Viscosity, Am. J. of Science 3rd Series, Vol. 45, pp. 87-96.

Bell, T., 1973, *Survey of the Heat Treatment of Engineering Components*, London, The Iron and Steel Institute.

Bell, T., 1993, Engineering the Surface to Combat Wear, pp. 27-37, in '*Proceedings of the 19th Leeds-Lyon Symposium on Tribology: Thin Films in Tribology*', Leeds 1992, Dowson, D. et al. Ed., Elsevier,

Benedict, G.H. & Kelley, B.W., 1961, Instantaneous Coefficients of Gear Tooth Friction, *Trans. of the ASLE*, Vol. 4, pp. 59-70.

Benedict, G.H., 1968, Correlation of Disk Machines and Gear Tests, *J. of the ASLE: Lubrication Engineering*, Vol. 24, pp. 591-596.

Berthe, D., Michau, B., Flamand, L. & Godet, M., 1978, Effect of Roughness Ratio and Hertz Pressure on Micro-pits and Spalls in Concentrated Contacts: Theory and Experiments, pp. 233-238, *in 'Proceedings of the 4th Leeds-Lyon Symposium on Tribology: Surface Roughness Effects in Lubrication'*, Lyon 1977, Dowson, D. et al. Ed., MEP Ltd.

Berthe, D., Flamand, L., Foucher, D. & Godet, M., 1980, Micropitting in Hertzian Contacts, *Trans. ASME J. of Lubrication Technology*, Vol. 102, pp. 478-89.

Bhachu, R.S., 1980, The Influence of Debris on Rolling Fatigue Life, *PhD Thesis*, Imperial College, University of London.

Bhargava, V., Hahn, G.T. & Rubin, C.A., 1985, An Elastic-Plastic Finite Element Model of Rolling Contact. Part 1 Analysis of a Single Contact, *Trans. ASME J. of Applied Mechanics*, Vol. 52, pp. 67-74.

Blok, H., 1937, Theoretical Study of Temperature Rise at Surfaces of Actual Contact Under Oiliness Lubricating Conditions, *Proceedings of the General Discussion on Lubrication IMechE*, Vol. 32, pp. 222-235.

Blok, H., 1958, Lubrication as a Gear Design Factor, *Proceedings of the IMechE Conference on Gearing*, London, pp. 144-158.

Blok, H., 1970, Recent Developments in Gear Tribology, *Proceedings of the IMechE*, Vol. 184, Pt. 30, pp. 21-29.

Borsoff, V.N., 1959, On the Mechanism of Gear Lubrication, *Trans. ASME J. of Basic Engineering*, Vol. 81, No.1, pp. 79-93.

Bowen, C.W., 1978, The Practical Significance of Designing to Gear Pitting Life Criteria, *Trans. ASME J. Mechanical Design*, Vol. 100, No.1, pp. 46-53.

Bower, A.F., 1988, The Influence of Crack Face Friction and Trapped Fluid on Surface Initiated Rolling Contact Fatigue Cracks, *Trans. ASME J. of Tribology*, Vol. 110, pp.704-711.

Bradis, H. & Schmidt, W., 1983, Case Hardened Steels: Microstructural and Residual Stress Effects, *Conference Proceeding American Institute of Mechanical Engineers*, Atlanta, March, pp. 189.

Braza, J.F., 1992, Rolling Contact Fatigue and Sliding Wear Performance of Ferritic Nitrocarburized M-50 Steel, *Tribology Transactions*, Vol. 35, No.1, pp. 89-97.

British Gear Association (BGA) (Various Authors), 1992, *Gear Technology Teaching Pack*, British Gear Association.

British Gear Association (BGA) Design Guide, 1994, *Profile and Lead Correction*, BGA.

British Standard 1134, 1961, *Centre Line Average Height Method for the Assessment of Surface Texture*, London, British Standards Institution.

British Standards Institution (BSI), 1970, BS 436 Spur and Helical Gears. Part 2 *Basic Rack Form, Modules and Accuracy (1 to 50 Metric Module.* Superseded by BS 436 Part 4, 1996, BSI.

British Standards Institution (BSI), 1986, BS 436 Spur and Helical Gears. Part 3: *Method for Calculation of Contact and Root Bending Stress Limitations for Metallic Involute Gears*, BSI.

Bull, S.J., Evans, J.T., & Shaw, B.A., 1998, The Effect of the White Layer on Micro-Pitting and Surface Contact Fatigue Failure of Nitrided Gears, to be published in the *Proceedings of the IMechE J. of Engineering Tribology.*

Burd, W.E., 1984, Properties and Evaluation of Carpenter Pyrowear Alloy 53 for Extended Gear Life, *AGMA*, Paper 84FTM10.

Cameron, A., 1954, Surface Failure in Gears, *J. Institute of Petroleum*, Vol. 40, pp.191-202.

Cameron, A., Lewis, J.C. & MacPherson, P.B., 1971, Hydrostatic Disc Machine Preliminary Details, *Proceedings of the IMechE,* Vol. 6, No.3, pp. 317-322

Campbell, W.E., 1969, *Boundary Lubrication*, pp. 87-117, in *'Boundary Lubrication - An Appraisal of World Literature'*, New York, ASME.

Carlslaw, H.S. & Jaeger, J.C., 1959, *Conduction of Heat in Solids*, Oxford University Press.

Carnahan, B., Luther, H.A. & Wilkes, J. O., 1969, *Applied Numerical Methods*, John Wiley & Sons.

Carter, T.L., Zaretsky, E.V. & Anderson, W.J., 1960, Effect of Hardness and Other Mechanical Properties on Rolling Contact Fatigue Life of Four High-Temperature Bearing Steels, *NASA Technical Note*, D-270.

Castleman, L.S., Averbach, B.L. & Cohen, M., 1952, Effect of Retained Austenite Upon Mechanical Properties, *Trans. ASM*, Vol. 44, pp. 240-257.

Chaize, J.C. & Berthier, J.M., 1996, New Technologies, a Factor of Competitiveness for Today's Helicopters, a Must for Tomorrow's, *22nd European Rotorcraft Forum & 13th European Helicopter Association Symposium*, Paper 23.

Chang, L., Webster, M.N., and Jackson, A., 1993, On the Pressure Rippling and Roughness Deformation in Elastohydrodynamic Lubrication of Rough Surfaces, *Trans. AMSE J. of Tribology*, Vol. 115, No. 3, pp. 439-444.

Chang, L, 1995, Deterministic Modelling and Numerical Simulation of Lubrication between Rough Surfaces – A Review of Recent Developments, *Wear*, Vol. 184, pp. 155-160.

Chiu, Y.P., Tallian, T.E., McCool, J.J. & Martin, J.A., 1969, A Mathematical Model of Spalling Fatigue Failure in Rolling Contact, *Trans. ASLE*, Vol. 12, pp. 106-116

Chiu, Y.P., Tallian, T.E. & McCool, J.J., 1971, An Engineering Model of Spalling Fatigue Failure in Rolling Contact: 1. The subsurface Model, *Wear*, Vol. 17., pp. 433-446.

Chow, L.S.H. & Cheng, H.S., 1976, The Effect of Surface Roughness on the Average Film Thickness Between Lubricated Rollers, *Trans. ASME J. Lubrication Technology*, Vol. 98, pp. 117-124.

Clayton D.B. & Sachs, K., 1977, Reduction of 'White Layer' on the Surface of Nitrided Components, *Mechanik Miesiecznik Naukowotechniczny*, Vol. 50, No. 7, pp. 360.

Cole, S.J. & Sayles, R.S., 1992, A Numerical Method for the Contact of Layered Elastic Eodies with Real Rough Surfaces, *Trans. ASME J. of Tribology*, Vol. 114, pp. 334-340.

Coy, J.J., Townsend, D.P. & Zaretsky, E.V., 1975, Dynamic Capacity and Surface Fatigue Life for Spur and Helical Gears, *ASME*, Paper 75-Lub-19.

Crook, A.W., 1961, The Lubrication of Rollers II. Film Thickness with Relation to Viscosity and Speed, *Philosophical Trans. of the Royal Society London*, Series A, Vol. 254, No. 1040, pp. 223-236.

Cummings, H.N, Stulen, F.B., Schulte, W.C., 1957, Tentative Fatigue Strength Reduction Factors for Silicate-Type Inclusions in High Strength Steels, Trans. ASM, Vol. 49, pp.482-505.

Davies, D.P, 1986, Gear Materials in Helicopter Transmissions, Materials for Defence, *Institute of Materials: Metals and Materials*, June, Vol. 2, No.6, pp.342-348.

Davies, D.P. & Gittos, B.C., 1989, Gear Steels for Future Helicopter Transmissions, *Proceedings of the IMechE*, Vol. 203, pp.113-121.

Davies, D.P., 1991, Duplex Hardening: an Advanced Surface Treatment Technique Combining Nitriding and Carburising, *Heat Treatment of Metals*, Vol. 18, No.4, pp. 97-104.

Davies, 1996, Fatigue Behaviour of Gas-Carburised, Temper-Resistant, Low-Alloy Steels, *Westland Helicopters Ltd.*, Ref: LR 96,279.

Dawson, P.H., 1962, Effect of Metallic Contact on the Pitting of Lubricated Rolling Surfaces, *J. Mechanical Engineering Science*, Vol. 4, No. 1, pp. 16-21.

Dawson, P.H., 1963, The Effect of Metallic Contact and Sliding on the Shape of the S-N Curve for Pitting Fatigue, *Proceedings of the IMechE Symposium on Fatigue in Rolling Contact*, London, Paper 4, pp. 41-45.

Dezzani, M.M. & Pearson, P.K., 1995, Hybrid Ceramic Bearings for Difficult Applications, *Transactions ASME*, Paper No. 95-GT-391, Presented at the International Gas Turbine and Aeroengine Congress & Exposition, Houston Texas, June.

Diaconescu, E., Kerrison, G. & Cameron, A., 1974, Effect of Sliding on Surface Fatigue, *Nature*, Vol. 248, No. 5450, pp. 669-670.

Diaconescu, E, 1975, Pitting Under Traction in Heavily Loaded Point Contacts, *PhD Thesis*, Imperial College, University of London.

DIN 3990 (Parts. 1-5), 1987, *Calculation of Load Capacity of Cylindrical Gears*, in German, DIN.

DiRusso, R., 1986, Advances and Applications of Pyrowear 53 in Helicopter Transmission Systems, *Presented at the Rotary Wing Propulsion System Specialist Meeting*, Williamsburg, Virginia, pp. 8:1-8.

Dowson, D. & Higginson, G.R., 1977, *Elastohydrodynamic Lubrication - The Fundamentals of Roller and Gear Lubrication*, (First Edition 1966) , London, Pergamon Press.

Drago, R., 1974, Heavy-lift helicopter Brings up Drive Ideas: Advanced Gear Materials, *Power Transmission Design*, Vol. 16, No. 3, pp. 49-53.

Drago, R.J., 1988, *Fundamentals of Gear Design*, Stoneham, Butterworths.

DTI (Department of Trade and Industry), 1985, *Wear Resistant Surfaces in Engineering (A Guide to their Production, Properties and Selection)* , London, HMSO.

Dyson, A., Evans, H.P. & Snidle, R.W., 1989, Wildhaber-Novikov Circular Arc Gears : Some Properties of Relevance to their Design, *Proceedings of the Royal Society of London*, Vol. A425, pp. 341-363.

Flamand, L., Berthe, D., 1978, A Brief Discussion of Different Forms of Wear Observed in Hertzian Contacts at Low Slide/Roll Ratios, pp. 239-242, in *'Proceedings of the 4th Leeds-Lyon Symposium on Tribology: Surface Roughness Effects in Lubrication'*, Lyon 1977, Dowson, D. et al. Ed., MEP Ltd.

Flamand, L., Berthe, D. & Godet, M., 1981, Simulation of Hertzian Contacts Found in Spur Gears with a High Performance Disk Machine, *Trans. ASME J. of Mechanical Design*, Vol. 103, pp.204-209.

Foroughi, R. & Spikes, H.A., 1988, The Application of Fracture Mechanics to Rolling Contact Fatigue, *Tribology Section, Department of Mechanical Engineering, Imperial College*, Report No. TS 008/88.

Frankel, H.E., Bennett, J.A. & Pennington, W.A., 1960, Fatigue Properties of High Strength Steels, *Trans. ASM*, Vol. 52, pp. 257-276.

Fujita, K. & Yoshida, A., 1981, Effects of Case Depth and Relative Radius of Curvature on Surface Durability of Case-Hardened Chromium Molybdenum Steel Roller, *Trans. ASME J. of Mechanical Design*, Vol. 103, pp. 474-481.

Galvin, G.D. & Naylor, H., 1964-5, Effect of Lubricants on the Fatigue of Steel and Other Metals, *Proceedings of the IMechE*, Vol. 179, Pt.1 No.27, pp. 857-871.

Graham, R., 1979, Pitting of Hard Steel Rolling-Sliding Elastohydrodynamically Lubricated Line Contacts, *PhD Thesis*, Imperial College, University of London.

Greenwood, J.A. & Williamson, J.B.P., 1966, Contact of Nominally Flat Surfaces, *Proceedings of the Royal Society of London*, Vol. A295, pp. 300-319.

Grubin, A.N. & Vinogradova, I.E., 1949, *Central Scientific Research Institute for Technology and Mechanical Engineering*, Moscow (D.S.I.R. Translation No. 337), Book No. 30.

Grunberg, L. & Scott, D., 1958, The Acceleration of Pitting Failure by Water in the Lubricant, *J. Institute of Petroleum*, Vol. 44, No. 419, pp. 406-10.

Grunberg, L. & Scott, D., 1960, The Effect of Additives on the Water-Induced Pitting of Ball Bearings, *J. Institute of Petroleum*, Vol. 46, No. 440, pp. 259-266.

Gupta, P.K. & Walowit, J.A., 1974, Contact Stresses between an Elastic Cylinder and a Layered Elastic Solid, *Trans. ASME J. Lubrication Technology*, Vol. 96, No.2, pp. 250-257.

Hamer, J.C., Hutchinson, J.M., Olver, A.V., Sayles, R.S. & Ioannides, E., 1991, Fatigue Life Modelling of Gear Contacts, *BGA Annual Congress*, Sheffield, BGA.

Hamlin, M.R., 1978, The Operation of Helicopter Gearboxes Under Loss-of-Lubricant Conditions, *Westland Helicopters Limited.*

Hampshire, J.M., 1986, Bearing Materials Advances, *Presented at the IMechE Seminar 'Pushing Back The Frontiers Of Failure', 18th Dec*, IMechE.

Hamrock, B.J. & Dowson, D., 1977, Isothermal Elastohydrodynamic Lubrication of Point Contacts. Part III-Fully Flooded Results, *Trans. ASME J. Lubrication Technology*, Vol. 99, No.2, pp. 264-275.

Hamrock, B.J. & Dowson, D., 1981, *Ball Bearing Lubrication*, Chichester, Wiley.

Hetenyi, M., 1950, *Handbook of Experimental Stress Analysis*, New York, John Wiley & Sons.

Hearle , A.D. & Johnson, K.L., 1985, Mode II Stress Intensity Factors for a Crack Parallel to the Surface of an Elastic Half-Space Subjected to a Moving Point Load, *J. of the Mechanics and Physics of Solids*, Vol. 33, No. 1, 61-81.

Hirst, W. & Hollander A.E., 1974, Surface Finish and Damage in Sliding Contact, *Proceedings Royal Society London*, Vol. A337, pp. 379-394.

Hobbs, R.A. & Mullet, G.W., 1968-69, Effects of some Hydraulic Fluid Lubricants on the Fatigue Lives of Rolling Bearings, *Proceedings of the IMechE*, Vol.183, Pt. 3P, pp.21-27.

Hooke, C.J., 1994, The Minimum Film Thickness in Lubricated Line Contacts During a Reversal of Entrainment- General Solution and Development of a Design Chart. *Proceedings of the IMechE J. of Engineering Tribology*, Vol. 208, pp. 53-64.

Howes, M.A.H., Bhattacharyya, S., Bock, F.C. & Parikh, N.M., 1976, Chemical Effects of Lubrication in Contact Fatigue. Part 1: The Test Programme, Data and Metallurgical Observations, *Trans. ASME J. Lubrication Technology*, Vol. 98, pp. 286-98.

Hua, D.Y., Wang, S.H. & Zhang, H.H., 1987, Effect of Surface Roughness and its Orientation on EHL, pp. 261-265, *in 'Proceedings of the 13th Leeds-Lyon Symposium on Tribology: Fluid Film Lubrication'*, Leeds 1986, Dowson, D et al. Ed., Elsevier.

Hutchings, I.M., 1992, *Tribology: Friction and Wear of Engineering Materials*, London, Edward Arnold.

Ichimaru, K., Nakajima, A. & Hirano, F., 1980, Effect of Asperity Interaction on Pitting in Rollers and Gears, *Trans. ASME J. of Mechanical Design*, Vol. 103, pp. 482-491.

Ioannides, E. & Harris, T.A., 1985, A New Fatigue Life Model for Rolling Bearings, *Trans. ASME J. Tribology*, Vol. 107, pp. 367-378.

IOP (Institute of Petroleum) Test Method No. 239, 1981a, Extreme Pressure Properties. Friction and Wear Tests for Lubricants: Four Ball Machine, *IP test methods*, 239/79.

IOP (Institute of Petroleum) Test Method No. 300, 1981b, Rolling Contact Fatigue Tests for Fluids in a Modified Four-Ball Machine, *IP test methods*, 300/379.

IOP (Institute of Petroleum),1992, Standard Methods for Analysis Testing of Petroleum and Related Products, *Institute of Petroleum*, London.

Ishibashi, A. & Tanaka, S., 1981, Effects of Hunting Gear Ratio Upon Surface Durability of Gear Teeth, *Trans. ASME J. of Mechanical Design*, Vol. 103, pp.227-235.

Jacobsen, B., 1983, Pitting and Micropitting in Rolling Contacts, pp.347-350, *in 'Proceedings of the 9th Leeds-Lyon Symposium on Tribology: Tribology of Reciprocating Engines'*, Leeds 1982, Dowson, D. et al. Ed., Butterworths.

Jatczak, C.F., 1978, Speciality Carburising Steels for Elevated Temperature Service, *Metal Progress*, Vol. 113, No.4 , pp.70-78.

Johnson, K.L., 1985, *Contact Mechanics*, Cambridge University Press.

Johnson, K.L., 1988, The Strength of Surfaces in Rolling Contact, *Third Annual BP IMechE Tribology Lecture*, London.

Johnson, K.L. & Shercliff, H.R., 1992, Shakedown of 2-Dimensional Asperities in Sliding Contact, *International J. of Mechanical Sciences*, Vol. 34, No.5, pp. 375-394.

Johnson, K.L., 1994, Contact Failure in Transmission Components, *A One Day Seminar On Recent Advances in Drive Line Technology, 3 November, London*, IMechE.

Johnson, L.G., 1964, *The Statistical Treatment of Fatigue Experiments*, Amsterdam, Elsevier.

Johnston, G.J., Wayte, R. & Spikes, H.A., 1991,The Measurement and Study of Very Thin Lubricated Films in Concentrated Contact, *STLE Trans.*, Vol. 34, pp 187-194.

Kalner, V.D., Nikonov, N.F. & Yurasoz, S.A., 1973, Modern Carburising and Carbonitriding Techniques, *Metal Science and Heat Treatment*, Vol. 15, pp. 752.

Kaneta, M. & Murakami, Y., 1987, Effects of Oil Hydraulic Pressure on Surface Crack Growth in Rolling/Sliding Contact, *Tribology International*, Vol. 20, No. 4, pp. 210-217.

Kapoor, A. & Johnson, K.L., 1993, Steady State Topography of Surfaces in Repeated Boundary Lubricated Sliding, pp. 81-90, *in 'Proceedings of the 19th Leeds-Lyon Symposium on Tribology: Thin Films in Tribology'*, Leeds, 1992, Dowson et al. Ed., Elsevier.

Keer, L.M., Bryant, M.D. & Haritos, G.K., 1982, Subsurface and Surface Cracking Due to Hertzian Contact, *Trans. ASME J. Lubrication Technology*, Vol. 104, pp. 347-351.

Keer, L.M. & Bryant, M.D., 1983, A Pitting Model for Rolling Contact Fatigue, *Trans. ASME J. Lubrication Technology*, Vol. 105, pp. 198-205.

Kelly, D.A. & Barnes, C.G., 1994, Effects of Speed on Scuffing in Mixed Lubrication, *Proceedings of the IMechE*, Vol. 208, pp.269-279.

Kelly, B.W. & Lemanski, A.J., 1967-68, Lubrication of Involute Gearing, *Proceedings of the IMechE Conference on Lubrication and Wear: Fundamentals and Application to Design*, Vol. 182, Pt. 3A, pp. 173.

Kerrison, G., 1975, Fatigue of Rolling Point Contacts and the Effect of Traction, *PhD Thesis*, Imperial College, University of London.

Kim, T, and Olver, A V, 1997, Fatigue and Brittle Fracture Analysis of Surface Engineered Materials in Rolling Contact, pp. 37-48, *in 'Proceedings of the 23rd Leeds - Lyon Symposium on Tribology: Elastohydrodynamics'*, Leeds, 1996, Dowson, D. et al. Ed., Elsevier.

Kirk, D., Nelms, P.R. & Arnold, B., 1966, Residual Stresses and Fatigue Life of Case Carburised Gears, *Acta Metallurgica*, Vol. 74, pp. 255.

Kotorii, H., 1992, Tooth Surface Fatigue of AISI 9310 Steel Spur Gears, *Proceedings of the ASME International Power Transmission and Gearing Conference*, Vol. 43, No. 2, pp. 741-748.

Krauss, G., 1989, *Steels: Heat Treatment and Processing Principles*, Ohio, ASM International.

Lin, M.R., Fine, M.E. & Mura, T., 1986, Fatigue Crack Initiation on Slip Bands: Theory and Experiment, *Acta Metallurgica*, Vol. 34, No. 4, pp. 619-628.

Littmann, W.E. & Widner, R.L., 1966, Propagation of Contact Fatigue from Surface and Subsurface Origins, *Trans. ASME J. of Basic Engineering*, Vol. 88, pp. 624-635.

Lockwood, F.E., Cristodoulou, L. & Langan, T.J., 1986, Anti-Fatigue Additives, Vol. 2, Paper 11.6, in *'Proceedings of the 5th International Colloquium: Additives for Lubricants and Operational Fluids'*, Technische Akademie Esslingen, Ed. Bartz, W.J.

Loewenthal, S.H. & Moyer, D.W., 1979, Filtration Effects on Ball Bearing Life and Condition in a Contaminated Lubricant, *Trans. ASME J. Lubrication Technology*, Vol. 101, pp.171-176.

Lundberg, L. & Palmgren, A., 1947, Dynamic Capacity of Roller Bearings, *Acta Polytechnica, Mechanical Eng. Series* , Vol. 1, No. 3.

Mack, J.C. & Binder, S., 1980, Experience with Advanced High Performance Gear Steels, *ASME*, Paper 80-C2/DET-77.

Macpherson, P.B., 1975, Investigation into the Influence of Traction and Sliding on Rolling Fatigue in Lubricated Contacts, *Westland Helicopters Ltd.*, Research Papers 495 & 510.

Mansion, H.D., 1952, Some Factors Affecting Gear Scuffing, *Proceedings of the Gear Lubrication Symposium J. Institute Petroleum*, Vol. 38, pp. 633-645.

Martin, J.A., Borgese, S.F. & Eberhardt, A.D., 1966, Microstructural Alterations of Rolling-Bearing Steels Undergoing Cyclic Stressing, *Trans. ASME J. Basic Engineering*, Vol. 88, pp. 555-67.

Martin, J.A. & Eberhardt, A.D., 1967, The Identification of Potential Failure Nuclei in Rolling Contact Fatigue, *Trans. ASME J. Basic Engineering*, Vol. 89, No.4, pp. 932-942.

Martin, K.F., 1978, A Review of Friction Predictions in Gear Teeth, *Wear*, Vol. 49, pp.201-238.

Martin, K.F., 1981, The Efficiency of Involute Spur Gears, *Trans. ASME J. of Mechanical Design*, Vol. 103, pp.160-169.

Mattson, R.L. & Roberts, J.G., 1959, in *Internal Stresses and Fatigue of Metals*, Eds. Rassweiler, G.M. & Brube, W.L., London, Elsevier Press.

McKelvey, R.E. & Moyer, C.A., 1963, The Relation Between Critical Maximum Compressive Stress and Fatigue Life Under Rolling Contact, *Proceedings of the IMechE Conference on Fatigue in Rolling Contact*, pp. 1-10.

Merritt, H.E., 1935, Worm Gear Performance, *Proceedings of the IMechE*, Vol. 129, pp. 127-194.

Morimoto, T. & Tamamura, K., 1992, Burnishing Process using a Rotating Ball-Tool-Effect of Material on the Burnishing Process, *Wear*, Vol. 147, pp. 185-193.

Morrison, T.W., Tallian, T.E., Walp, H.O. & Baile, G.H., 1963, The Effect of Trace Element Content and Multiple Vacuum Remelting on the Fatigue Life of Ball Bearings Made From AISI 52100, *Proc. IMechE Symp. on Fatigue in Rolling Contact*, pp. 86-94.

Murakami, Y., Kaneta, M. & Yatsuzuka, H., 1985, Analysis of Surface Crack Propagation in Lubricated Rolling Contact, ASLE Trans., Vol. 28, pp. 60-68.

Murch, L.E. & Wilson, W.R.D., 1975, A Thermal Elastohydrodynamic Inlet Zone Analysis, *Trans. ASME J. Lubrication Technology*, Vol. 97, No. 2, pp.212-216.

Nakajima, A., 1981, Effect of Asperity Interaction Frequency on Surface Durability, *Proceedings of the International Symposium on Gearing and Power Transmissions*, Tokyo, Vol. 1, Paper B-26, pp. 401-406.

Nakajima, A., Ichimaru, K., Hirano, F., Nishimura, M., 1983, Effects of Combination of Rolling Direction and Sliding Direction on Pitting of Rollers, *J. JSLE (International Edition)*, Vol. 4, pp. 93-98.

Nakajima, A. & Morodomi, H., 1986, Effect of Asperity Interacting Frequency on Rolling Contact Fatigue, *Bulletin of JSME*, Vol. 29, No. 256, pp.3560-3565

Nakajima, A., 1990, Effects of Surface Roughness and Oil Viscosity on Rolling Contact Fatigue of Case-Hardened Steel Rollers, *Proceedings of the Japan International Tribology Conference*, Nagoya, pp. 773-778.

Nakajima, A. & Mawatari, T., 1993, Effects of Surface Roughness and Running-in Upon Rolling Contact Fatigue, *Proceedings of the 6th of the International Congress on Tribology*, Budapest, Vol. 5, pp. 290-295.

Neale, M.J., 1995, *The Tribology Handbook*, 2nd Edition (1st Edition 1973) , Oxford, Butterworth-Heinemann Ltd.

Nicolson, D.M., 1996, Scuffing At High Speed and Temperature, *PhD Thesis*, Imperial College, University of London.

Olver, A.V., 1984, Micropitting and Asperity Deformation, pp. 319-324, in *'Proceedings of the 10th Leeds-Lyon Symposium on Tribology: Developments in Numerical and Experimental Methods Applied to Tribology'*, Lyon 1983, Dowson, D. et al. Ed., Butterworths.

Olver A.V., Spikes, H.A. & Macpherson P.B., 1986, Wear In Rolling Contact, *Wear*, Vol. 112, pp. 121-144.

Olver, A.V., 1989, Fatigue in Helicopter Transmissions: Rolling Fatigue Studies, *Westland Helicopters Ltd.*, Research Paper No. 758.

Olver, A.V., 1992, Private Communication, Tribology Section, Imperial College, London.

Olver, A.V., Cole, S.J. & Sayles, R.S., 1993, Contact Stresses in Nitrided Steels, pp. 71-80, *in 'Proceedinggs of the 19th Leeds-Lyon Symposium on Tribology: Thin films in Tribology'*, Leeds 1992, Dowson, D. Ed., Elsevier.

Olver, A.V., 1994, Thermal Matching of Tribological Systems, pp. 453-463, *in 'Proceedings of the 20th Leeds-Lyon Symposium on Tribology: Dissipative Processes in Tribology'*, Lyon, 1993, Dowson, D. et al. Ed., Elsevier.

Olver, A.V., 1995, Micropitting of Gear Teeth: Design Solutions, *Paper Presented at Aerotech '95*, NEC Birmingham October 1995, published IMechE.

Olver, A V, Nicolson, D M, and Barnett, D W, 1995, Tooth Tip Lubrication in Spur Gears, *Proceedings of the BGA Annual Congress*, Sheffield, British Gear Association.

Olver, A.V., 1998, Private Communication, Tribology Section, Imperial College, London.

Olver, A.V. & Spikes, H.A., 1998, Prediction of Traction in Elastohydrodynamic Lubrication, to be published in the *Proc. of the IMechE J. of Engineering Tribology.*

Ostvik, R. & Christenson, H., 1968-69, Changes in Surface Topography with Running-In, *Proceedings of the IMechE*, Vol. 183, Part 3P, pp. 59-67.

Paliwal, M.C. & Snidle, R.W., 1987, Running-in and Scuffing Failure of Marine Gears, *Department of Mechanical Engineering & Energy Studies, University College Cardiff*, Final Report on Contract No. D/ER1/9/4/2072/045 - RAE(C).

Paris, P. & Erdogan, F., 1963, A Critical Analysis of Crack Propagation Laws, *Trans. ASME J. Basic Engineering*, Vol. 85, No. 4, pp. 528-534.

Parker, R.J. & Zaretsky, E.V., 1972, Rolling Element Fatigue Lives of Through-Hardened Bearing Materials, *Trans. ASME J. Lubrication Technology*, Vol. 94, pp. 164-173

Parker, R.J., Zaretsky, E.V. & Bambarger, E.N., 1974, Evaluation of Load-Life Relation with Bearings at 500 °F, *Trans ASME J. Lubrication Technology*, Vol. 96, No. 3, pp. 391.

Parsons, S.A.J., 1970, *Metrology and Gauging*, 2nd Edition (1st Edition 1957), MacDonald & Evans Ltd.

Patir, N. & Cheng, H.S., 1979, Effect of Surface Roughness Orientation on the Central Film Thickness in EHD Contacts, pp. 15-21, in *'Proceedings of the 5th Leeds-Lyon Symposium on Tribology: Elastohydrodynamics and Related Topics'*, Leeds, 1978, Dowson, D. et al. Ed., MEP Ltd.

Pearson, P.K. & Becker M.E., 1989, M50NiL: A Bearing Material that Prevents Radial Cracking and Fracture Failures, *Presented at the Institution of Mechanical Engineers, Aerospace Industries Division, Aerospace Bearing Technology Seminar*, May 17, Solihull.

Pearson, P.K. & Dezzani, M.M., 1993, Rolling Contact Behaviour of Nitrided Surfaces, *Proceedings of the IMechE Conference on Advanced Materials and Processes for Aerospace Transmission Systems*, Solihull.

Pearson, P.K., 1995, Rolling Contact Behaviour Of High Hardness Surfaces, *Presented at the ASC Metal 2nd International Bearing Steel Symposium, June.*

Polk, C.J., Murphy, W.R. & Rowe, C.N., 1975, Determining Fatigue Crack Propagation Rates in Lubricating Environments through the Application of a Fracture Mechanics Technique, *Trans. of the ASLE*, Vol. 18, No. 4, pp. 290-298.

Polk, C.J. & Rowe, C.N., 1976, Crack Growth Rate: Its Measurement and a Controlling Factor in Rolling Contact Fatigue, *Trans. of the ASLE*, Vol. 19, pp.23-32.

Poon, C.Y. & Sayles, R.S., 1992, The Classification of Rough Surface Contacts in Relation to Tribology, *J. Physics D: Applied Physics*, Vol. 25, No. 1A, pp. A249-256.

Reynolds, O., 1886, On the Theory of Lubrication and its Application to Mr. Beauchamp Tower's Experiments, Including an Experimental determination of the Viscosity of Olive Oil, Phil. Trans., Vol. 177, pp. 157-234.

Riopelle, J.A., 1975, Short Cycle Atmosphere Nitriding, *Trans. American Foundrymen's Society Proc. 79th Annual Meeting*, St. Louis, Vol. 83, pp. 185192.

Rounds, F.G., 1962, Effects of Base Oil Viscosity and Type on Bearing Ball Fatigue, *Trans. of the ASLE*, Vol. 5, pp. 172-82.

Rowe, G.W., Kaliszer, H., Trmal,G. & Cotter, A., 1975, Running-in of Plain Bearing, *Wear*, Vol. 34, pp. 1-14.

Saulnier, J.D., 1989, Development of High Temperature Gearing for Helicopter Transmissions, *Proceedings of the ASM Conference: Carburizing- Processing and Performance*, Colorado, July, pp.211-219.

Sayles, R.S., 1982, The Profile as a Random Process, *in 'Rough Surfaces'*, Edited by Thomas, T.R., 1982, London, Longman.

Sayles, R.S. & Macpherson, P.B., 1982, Influence of Wear Debris on Rolling Contact Fatigue, *ASTM Special Publication*, No. 771, pp. 225.

Sayles, R.S. & Ioannides, E., 1988, Debris Damage in Rolling Bearings and Its Effects on Fatigue Life, *Trans. ASME J. of Tribology*, Vol. 110, pp. 26-31.

Sayles, R.S., 1994, Roughness and Debris in Machine Element Contacts: Some Current and Future Engineering Implications, *9th B.P. IMechE Tribology Lecture*, 3 November, London.

Schatzberg, P. & Felsen, I.M., 1968, Effects of Water and Oxygen During Rolling Contact Lubrication, *Wear*, Vol. 12, pp. 331-342.

Schlicht, H. & Zwirlein, O., 1980, Varying Heat Treatment Parameters to Optimize Material and Rolling Contact Fatigue Strength, *Trans. ASME J. Heat Treating*, Vol.1, No. 3, pp.73-80.

Schmidt, M.L., 1990, Pre-oxidation Prior to Gas Carburizing: Theory and its Effect on Pyrowear 53 Alloy, Carburizing: Processing and Performance, *Trans. ASME J. of Heat Treating*, Vol. 8, No.1, pp. 5-19.

Scott, D., 1964, The Effect of Material Properties, Lubricants and Environment on Rolling Contact Fatigue Life, *Proceedings of the IMechE Symposium Fatigue in Rolling Contact*, pp. 103-115.

Scott, D., 1967, Hard Materials for Tribological Applications, *Ministry of Technology National Engineering Laboratory*, Report No. 313.

Scott, D., 1968, Ball Bearing Steels - Factors Influencing Rolling Contact Fatigue Resistance, *Ministry of Technology National Engineering Laboratory*, Report No. 360.

Scott, D. & Blackwell, J., 1968, Steel Refining as an Aid to Rolling Bearing Life, *Presented at the IMechE 6th Lubrication and Wear Convention.*

Scott, D., 1977, Lubricant Effects on Rolling Contact Fatigue, pp. 3-15, in *'Rolling Contact Fatigue - The Performance Testing of Lubricants'*, Eds. Tourret, R. & Wright, E.P. , London, Institute of Petroleum.

Seabrook, J.B., & Dudley, D.W., 1963, Results of a Fifteen Year Program of Flexural Fatigue Testing of Gear Teeth, *ASME Publication*, Paper 63-WA-199.

Sharma, V.K., Walter, G.H. & Breen, D.H., 1977, An Analytical Approach for Establishing Case Depth Requirements in Carburized Gears, *ASME Publication*, Paper No. 77-DET-152, *Presented at the ASME Design Engineering Conference*, Chicago.

Sheppard, S., Barber, J.R. & Comninou, M., 1987, Subsurface Cracks Under Conditions of Slip, Stick and Separation Caused by a Moving Compressive Load, *Trans. ASME J. Applied Mechanics*, Vol. 54, pp. 393-402.

Shotter, B.A., 1958, Experiments with a Disc Machine to Determine the Possible Influence of Surface Finish on Gear Tooth Performance, *Proceedings of the IMechE International Conference on Gearing*, London, pp.120-125.

Shotter, B.A., 1981, Micro-pitting, its Characteristics and Implications, *Proceedings of the Institute of Petroleum Conference on Performance and Testing of Gear Oils and Transmission Fluids*, pp. 53-65.

Small, P.J. & Gittos, B.C., 1987, Investigation to Determine the Fatigue Properties of Case Hardened S156 in a Hot Oil Environment, *Westland Helicopters Limited*, LR 87, 093.

Smeeth, M. & Spikes, H.A., 1996, The Influence of Slide Roll Ratio on the Film Thickness of an EHD Contact Operating Within the Mixed Lubrication Regime, pp. 695-704, in '*Proceedings of the 22nd Leeds-Lyon Symposium on Tribology: The Third Body Concept*', Lyon 1995, Dowson, D. et al. Ed., Elsevier.

Smeeth, M., 1998, Private Communication, Tribology Section, Imperial College, London.

Smith, J.O. & Liu, C.K., 1953 , Stresses Due to Tangential and Normal Loads on an Elastic Solid with Application to Some Contact Stress Problems, *Trans. ASME J. of Applied Mechanics*, Vol. 20, pp. 157-166.

Snidle, R.W. & Evans, H.P., 1995, Elastohydrodynamic Lubrication of Real Surfaces, pp. 219-227, in '*Proceedings of the 21st Leeds-Lyon Symposium on Tribology: Lubricants and Lubrication*', Leeds 1994, Dowson, D. et al. Ed., Elsevier.

Spikes, H.A. & Macpherson, P.B., 1980, Water Content of Helicopter Gear Oils, *ASME Publication*, Paper 80-C2/DET-12.

Spikes, H.A., 1993, Boundary Lubrication and Boundary Films, pp. 331-346, in '*Proceedings of the 19th Leeds-Lyon Symposium on Tribology: Thin Films in Tribology*', Leeds 1992, Dowson, D. et al. Ed., Elsevier.

Spikes, H.A, 1997, Advances in the Study of Thin Lubricant Films, pp.355-369, in '*New Directions in Tribology*', Hutchings, I.M. Ed., London, MEP Ltd.

Stribeck, R., 1902, Die Wesentlichen Eigenschaften der Gleit und Rollenlager (The Essential Conditions of Sliding and Roller Bearings), Zeitschr. Ver. Deutsher Ing., Vol. 46, No. 38, pp. 1341-8; No. 39, pp. 1463-70.

Tallian, T.E., 1962, Weibull Distribution of Rolling Contact Fatigue Life and Deviations Therefrom, *Trans. of the ASLE*, Vol. 5, pp. 183-196.

Tallian, T.E., Chiu, Y.P., Huttenlocher, D.F., Kamenshine, J.A., Sibley, L.B. & Sindlinger, N.E., 1964, Lubricant films in Rolling Contact of Rough Surfaces, *Trans. of the ASLE*, Vol. 7, No. 2, pp. 109-126.

Tallian, T.E., McCool, J.I. & Sibley, L.B., 1965-66, Partial Elastohydrodynamic Lubrication in Rolling Contact, *Proceedings of the IMechE*, Vol. 180, 3B , Paper 14, pp. 169-184.

Tallian, T.E., 1967-68, Rolling Contact Failure Control Through Lubrication, *Proceedings of the IMechE Conference on Lubrication and Wear: Fundamentals and Application to Design*, Vol. 182, Pt. 3A, pp. 205-236.

Tallian, T.E. & McCool J.J., 1971, An Engineering Model of Spalling Fatigue Failure in Rolling Contact, II. The Surface Model, *Wear*, Vol. 17, pp. 447-461.

Tallian, T.E., 1971, An Engineering Model of Spalling Fatigue Failure in Rolling Contact, III. Engineering Discussion and Illustrative Examples, *Wear*, Vol. 17, pp. 463-480.

Tallian, T.E., 1976a, Prediction of Rolling Contact Fatigue Life in Contaminated Lubricant. Part 1 - Mathematical Model, *Trans. ASME J. of Lubrication Technology*, Vol. 98, No. 2, pp. 251-257.

Tallian, T.E., 1976b, Prediction of Rolling Contact Fatigue Life in Contaminated Lubricant. Part 2 - Experimental, *Trans. ASME J. of Lubrication Technology*, Vol. 98, No.3, pp. 384-392.

Tallian, T.E., 1982, A Unified Model for Rolling Contact Fatigue, *Trans. ASME J. of Lubrication Technology*, Vol. 104, pp. 336-346.

Tallian, T.E, 1992, *Failure Atlas for Hertz Contact Machine Elements*, New York, ASME Press.

Thomas, G.G., 1974, *Engineering Metrology*, London, Butterworths.

Thomas, T.R., 1982, Stylus Instruments, in '*Rough Surfaces*', edited by Thomas, T.R., London, Longman.

Thorne, N.R. & Gittos, B.C., 1985, The Effect of Excessive Stoving Temperature and Duration on the Fatigue Properties of Case Hardened BS S156, *Westland Helicopters Limited*, LR 85, 008.

Timoshenko & Goodier, 1970, *Theory of Elasticity*, 3rd Edition (1st Edition 1951), NewYork, McGraw-Hill.

Townsend, D.P., Coy, J.J. & Zaretsky, E.V., 1978, Experimental and Analytical Load-Life Relation for AISI 9310 Steel Spur Gears, *Trans. ASME J. of Mechanical Design*, Vol. 100, pp. 54-60.

Townsend, D.P. & Zaretsky, E.V., 1981, Endurance and Failure Characteristics of Modified Vaco X-2, CBS 600 And AISI 9310 Spur Gears, *Trans. ASME J. of Mechanical Design*, Vol. 103, pp. 506-515.

Townsend, D.P., 1983, Status of Understanding for Gear Materials, *NASA Conference: Tribology in the 80's*, Cleveland OHIO, NASA, Vol. 2, pp. 795-809.

Townsend, D.P., & Bamberger, E.N., 1991, Surface Fatigue Life of M50NiL and AISI 9310 Gears and Rolling-Contact Bars, *J. of Propulsion*, Vol. 7, No. 4, pp.642-649.

Tuplin, W.A., 1962, *Involute Gear Geometry*, London, Chatto & Windus.

US National Materials Advisory Board (NRC), 1979, Materials for Helicopter gears, *US Department of Commerce National Technical Information Service*, PB80-153463.

Vanes, S.E., 1995, Review Of Process And Materials Developments For Aerospace Rolling Bearings, *Proceedings of the IMechE Conference 'AeroTech'*, Paper C505/10/123.

Vogel, H., 1922, Die Bedeutung der Temperaturabängigkeit der Viscositat für die Beurteilung von Ölen (The Significance of Dependence of Viscosity on Temperature for Judging Oils), Zeit. Für Agenwandte Chemie, Vol. 35, No. 82, pp. 561-563.

Way, S., 1935, Pitting due to Rolling Contact, *Trans. ASME J. of Applied Mechanics*, Vol. 2, No. 1, pp. 49-58.

Webster, M.N. & Norbart, C.C.J., 1995, An Experimental Investigation of Micropitting Using a Roller Disk Machine, *Tribology Transactions*, Vol. 38, No. 4, pp. 883-895.

Webster, M.N. & R.S. Sayles, 1986, A Numerical Model for the Elastic, Frictionless Contact of Real Rough Surfaces, *Trans. ASME J. of Tribology*, Vol. 108, No. 3, pp. 314-320.

Weck, M., Kruse, A. & Gohritz, A., 1978, Determination of Surface Fatigue of Gear Material by Roller Tests, *Trans. ASME J. of Mechanical Design*, Vol. 100, pp. 433-439.

Wedeven, L.D., Evans, D. & Cameron, A., 1971, Optical Analysis of Ball Bearing Starvation, *Trans. ASME J. of Lubrication Technology*, Vol. 93, No. 3, pp.349.

Weibull, 1951, A Statistical Distribution Function of Wide Applicability, *Trans. ASME J. of Applied Mechanics*, Vol. 18, pp. 293-297.

West, M.A. & Sayles, R.S., 1988, A 3-Dimensional Method of Studying 3-Body Contact Geometry and Stress on Real Rough Surfaces, pp. 195-200, in *'Proceedings of the 14th Leeds-Lyon Symposium on Tribology: Interface Dynamics'*, Lyon 1987, Dowson, D. et al. Ed., Elsevier

Whitehouse, D.J. & Archard, J.F., 1970, The Properties of Random Surfaces of Significance in their Contact, *Proceedings of the Royal Society of London*, Vol. A316, pp. 97-121.

Whitehouse, D.J., 1994, *Handbook of Surface Metrology*, Bristol & Philadelphia, IOP Publishing Ltd.

Winter, H. & Weiss, T., 1981, Some Factors Influencing the Pitting, Micro-Pitting (Frosted Areas) and Slow Speed Wear of Surface Hardened Gears, *J. of Mechanical Design*, Vol. 103, pp. 499-505.

Yoshida, A., Fujita, K., Kanehara, T., Kominami, K. & Ota, K., 1985, Study on the Effect of Tooth Fatigue on Dynamic Performance of Gear Pair, *Bulletin of the JSME*, Vol. 28, No. 236, pp.322-328.

Yoshimura, H., Rubin, C.A. & Hahn, G.T., 1984, Cyclic Crack Growth Under Repeated Rolling Contact, *Proceedings of the 11th Canadian Fracture Conference on Time-Dependent Fracture, June 1984*, Ottawa Ont., pp. 271-280, Martinus Nijhoff Publ, Dordrecht, Neth. and Boston, MA.

Yoshioko, T. & Fujiwara, T., 1988, Measurement of Propagation Initiation and Propagation Time of Rolling Contact Fatigue Cracks by Observation of Acoustic Emission and Vibration, pp. 29-40, in '*Proceedings of the 14th Leeds-Lyon Symposium on Tribology: Interface Dynamics*', Lyon 1987, Dowson, D. et al. Ed., Elsevier.

Appendix

Appendix A Material Specification

BS S156

Table A1 BS S156 Material Specification

The composition of the alloy (percentages by weight):

Element	Actual
Carbon	0.165
Manganese	0.31
Silicon	0.30
Phosphorus	0.007
Sulphur	0.002
Chromium	1.18
Nickel	4.16
Molybdenum	0.22
Copper	--
Vanadium	--
Tungsten	--
Iron	Balance
Cast No.	G37413
Material Supplier	Special Melted Products

AISI M50NiL

Table A2 M50NiL Material Specification

The composition of the alloy (percentages by weight):

Element	Min	Max	Actual
Carbon	0.11	0.15	0.15
Manganese	0.15	0.35	0.30
Silicon	0.10	0.25	0.23
Phosphorus	--	0.015	0.006
Sulphur	--	0.008	0.002
Chromium	4.00	4.25	4.09
Nickel	3.20	3.60	3.50
Molybdenum	4.00	4.50	4.29
Copper	--	0.10	--
Vanadium	1.13	1.33	1.21
Material Supplier	Latrobe		

32CDV13

Table A3 32CDV13 Material Specification

The composition of the alloy (percentages by weight):

Element	Actual
Carbon	0.34
Manganese	0.52
Silicon	0.32
Phosphorus	0.009
Sulphur	0.002
Chromium	2.87
Nickel	0.12
Molybdenum	0.87
Copper	--
Vanadium	0.31
Tungsten	--
Iron	Balance
Cast No.	HX 2914/1
Material Supplier	Aubert and Duval

Material Properties

Table A4 BS S156, AISI M50NiL, and AISI M50NiL Duplex Material Properties

Property	BS S156	AISI M50NiL	32CDV13
0.2 % Proof Stress (MPa)	1085	1154.6	1001.3
Material Strength (MPa)	1420	1424.7	1195.2
Young's Modulus (GPa)	207	197.9	2310
Area (mm^2)	49.84	49.64	50.01
% Elongation	14.4	15.0	17.5
% Reduction of Area	62	66	66
Impact (ft lbs)	56	9.6	

Appendix B Material Heat Treatment Specification

Table B1 Material Heat Treatment for BS S156 and 32CDV13

Operation	BS S156	32CDV13
Method of Manufacture	Electric furnace air melt followed by vacuum arc consumable electrode remelting.	Vacuum induction melting followed by vacuum arc consumable electrode remelting.
Normalise	At 930°C for 3 hours. Air cool.	At 680°C for 1.5 hours, raise temperature to 975°C and soak for 3 hours. Air cool.
Anneal	At 650°C for 6 hours. Furnace Cool.	At 750°C for 3 hours. Furnace Cool.
Machine	To final dimensions, except gear teeth which must be 0.2 mm ±0.05 mm oversize. Do not machine keyway.	To final dimensions, except gear teeth which must be 0.2 mm ±0.05 mm oversize. Do not machine keyway.
Carburise	Carburise at 925°C for 12 hours, to achieve a surface carbon content of 0.8% C ± 0.05% C and a minimum case depth of 1.5 mm, prior to machining. Vestibule cool to room temperature under protective atmosphere.	--
Anneal	At 650°C for 2 hours, under protective atmosphere	--
Harden	At 810°C for 1 hour, under protective atmosphere.	At 670°C for 1 hour, raise temp to 950°C and soak for 1 hour under protective atmosphere.
Quench	Oil	Oil
Deep Freeze	At -70°C for 2 hours. Ensure that the operation is carried out within 5 hours of quenching	--
Temper	At 140°C for 4 hours. Ensure the operation is carried out within 5 hours of refrigeration.	At 625°C for 3 hours. Air cool.
For 32CDV13 Only		
Nitride	Ensure the involute gears are stacked to achieve an unrestricted gas flow around the gear teeth. Nitride according to Aubert and Duval standard operating procedure for deep case nitriding, to achieve a nitrided case depth of 0.7 mm min. And a surface hardness of 800 kgf mm^{-2} min.	
White Layer	Remove white layer by vacu-blasting with 180/220 alumina grit.	

Table B2 Material Heat Treatment for AISI M50NiL and AISI M50NiL Duplex

Operation	AISI M50NiL	AISI M50NiL Duplex
Method of Manufacture	Vacuum induction melting followed by vacuum arc consumable electrode remelting.	Vacuum induction melting followed by vacuum arc consumable electrode remelting.
Normalise	At 930°C for 3 hours. Air cool.	At 930°C for 3 hours. Air cool.
Anneal	At 650°C for 6 hours. Furnace Cool.	At 650°C for 6 hours. Furnace Cool.
Machine	To final dimensions, except gear teeth which must be 0.2 mm ±0.05 mm oversize. Do not machine keyway.	To final dimensions, except gear teeth which must be 0.2 mm ±0.05 mm oversize. Do not machine keyway.
Preoxidise	--	At 950°C for 30 min. in air. Air cool to room temp. Do not remove scale.
Carburise	Carburise at 925°C for 12 hours, to achieve a surface carbon content of 0.8% C ± 0.05% C and a minimum case depth of 1.5 mm, prior to machining. Vestibule cool to room temperature under protective atmosphere.	Carburise at 925°C for 12, to achieve a surface carbon content of 0.8% C ± 0.05% C and a minimum case depth of 1.5 mm, prior to machining. Vestibule cool to room temperature under protective atmosphere.
Anneal	At 650°C for 4 hours, under protective atmosphere	At 650°C for 4 hours, under protective atmosphere
Harden	At 1050°C for 1 hour, under vacuum	At 1050°C for 1 hour, under vacuum
Quench	Argon Gas	Argon Gas
Deep Freeze	At -70°C for 2 hours. Ensure that the operation is carried out within 5 hours of quenching	At -70°C for 2 hours. Ensure that the operation is carried out within 5 hours of quenching
Temper	At 550°C for 4 hours under protective atmosphere. Ensure the operation is carried out within 5 hours of refrigeration	At 550°C for 4 hours under protective atmosphere. Ensure the operation is carried out within 5 hours of refrigeration
For AISI M50NiL Duplex Only		
Gas Nitride	Ensure the involute gears are stacked to achieve an unrestricted gas flow around the gear teeth. Nitride for 24 hours at a temperature of 520°C and with an ammonia dissociation rate of 35%, to achieve a case depth of 0.15 mm.	

Appendix C Spur Gear Design Specification

Table C1 Involute Spur Gear Data

FEATURE	DIMENSION (mm)
Normal module	5.08 (5 D.P.)
Number of teeth	17
Basic rack flank angle	20°
Addendum modification coefficient (Correction factor)	0.25
Mating gear	Same
Centre distance with mating gear (nominal)	88.900
Backlash with mating gear Min. Max.	0.175 0.272
Reference circle diameter (pitch circle diameter. Generated)	86.360
Base circle diameter	81.152
Outside diameter	99.190 99.063
Root diameter	76.584 76.330
Facewidth	10
Diameter SAP	82.673
Diameter EAP	99.06
Length of roll	20.510
Pitch variation (error) : Accumulated pitch Variation AGMA 10	0.0114 0.0343
Size over two teeth (base tangent value)	24.580 24.534
Size over rollers (dia. 8.778 mm)	100.025 99.929
Material Specification :	WHMS471, AISI M50NiL, AISI M50NiL Duplex, 32CDV13
Tooth surface finish	Ground 0.4μm Ra
Full fillet radius	2.172 Max.
Contact Ratio	1.368
Max. Hertzian Contact Stress (Torque 350 Nm)	1.95 GPa
Maximum bending Stress (Torque of 350 Nm)	426 MPa
Maximum Contact Stress when Crowning Radius of 260 mm on each gear is introduced (Torque of 350 Nm)	3.0 GPa

Appendix D Spur Gear Design Drawing

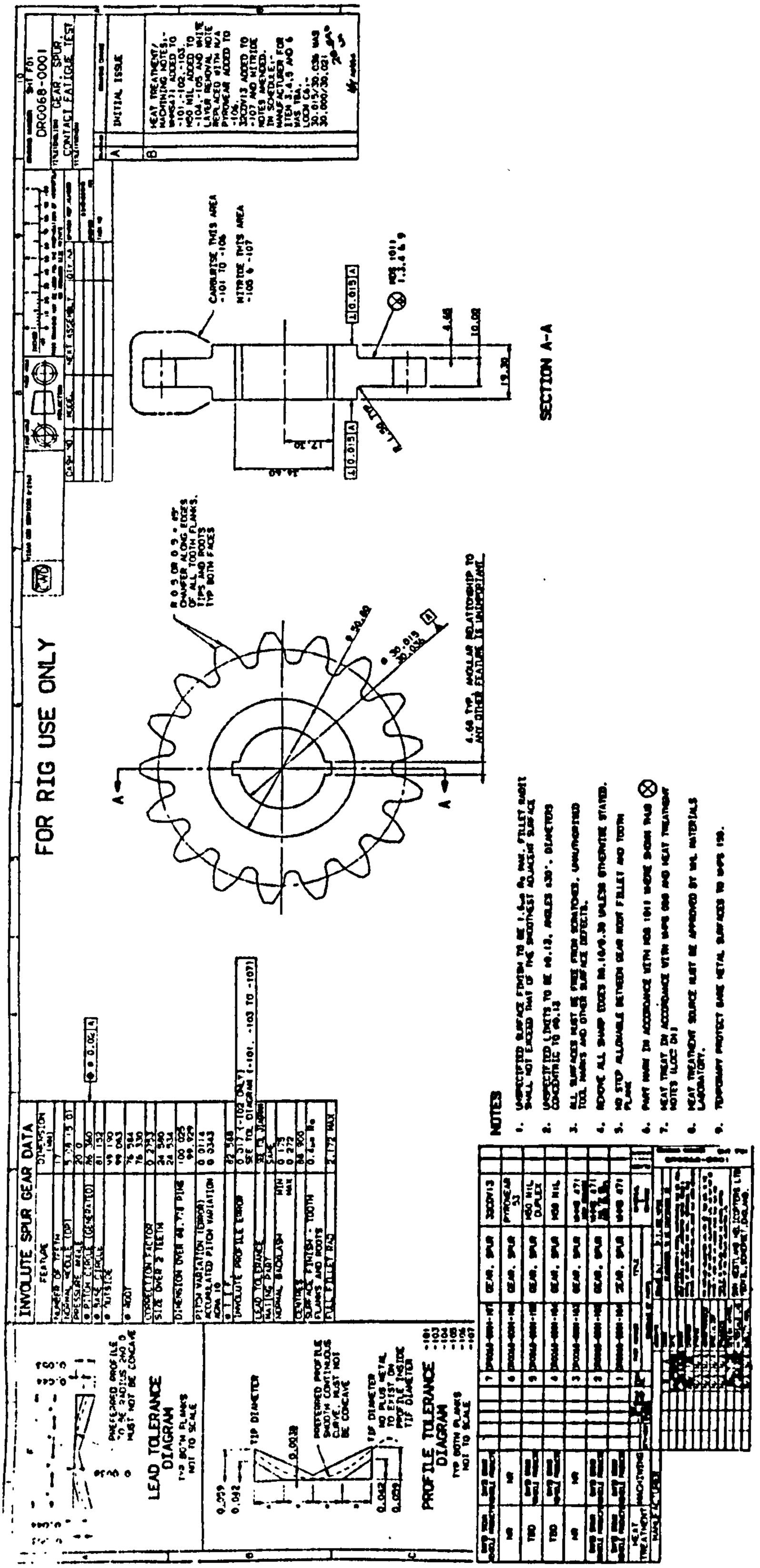


Figure D1 Spur Gear Design Drawing

Appendix E Barrel and Ring Design Drawings

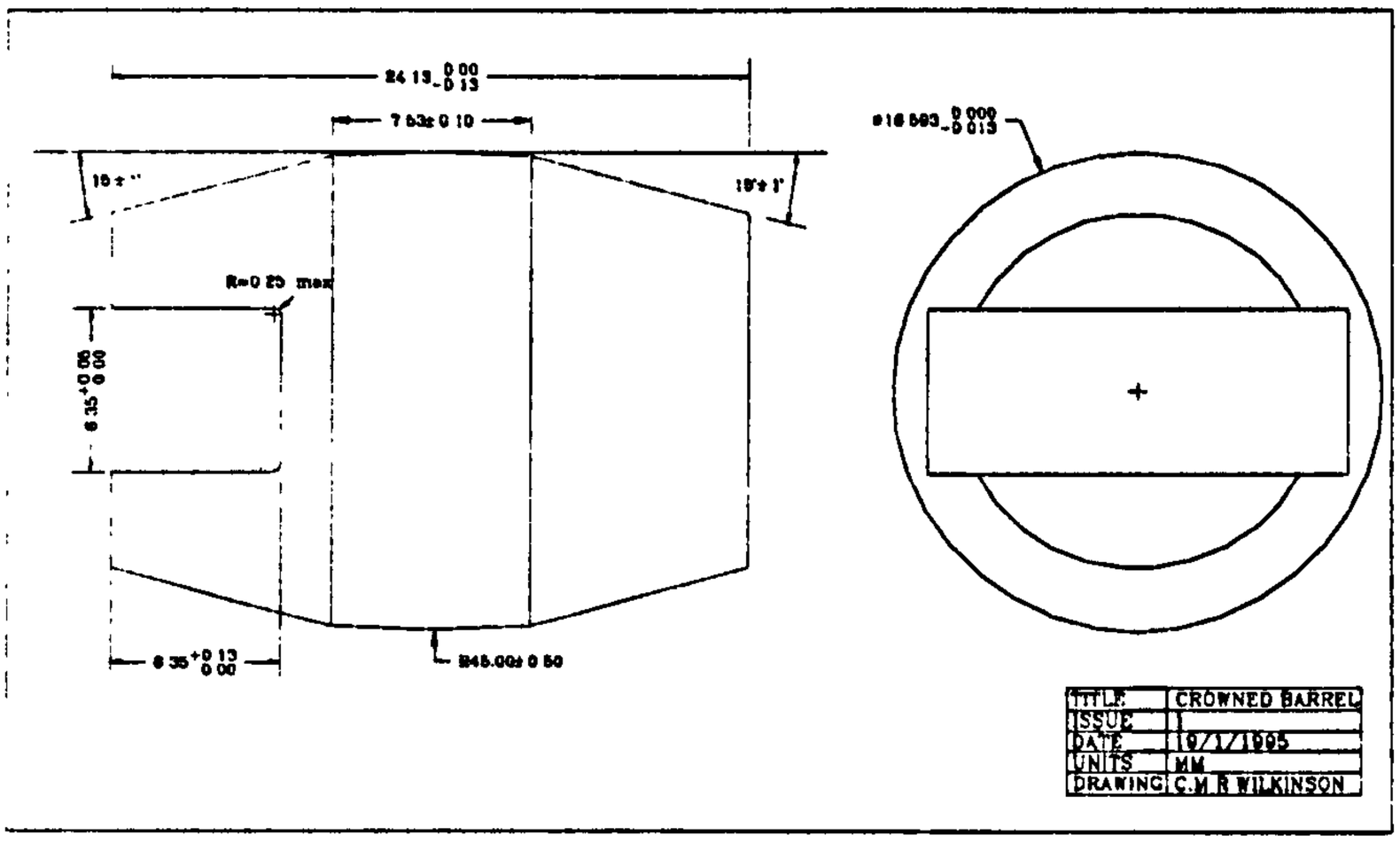


Figure E1 Crowned Barrel Design Drawing

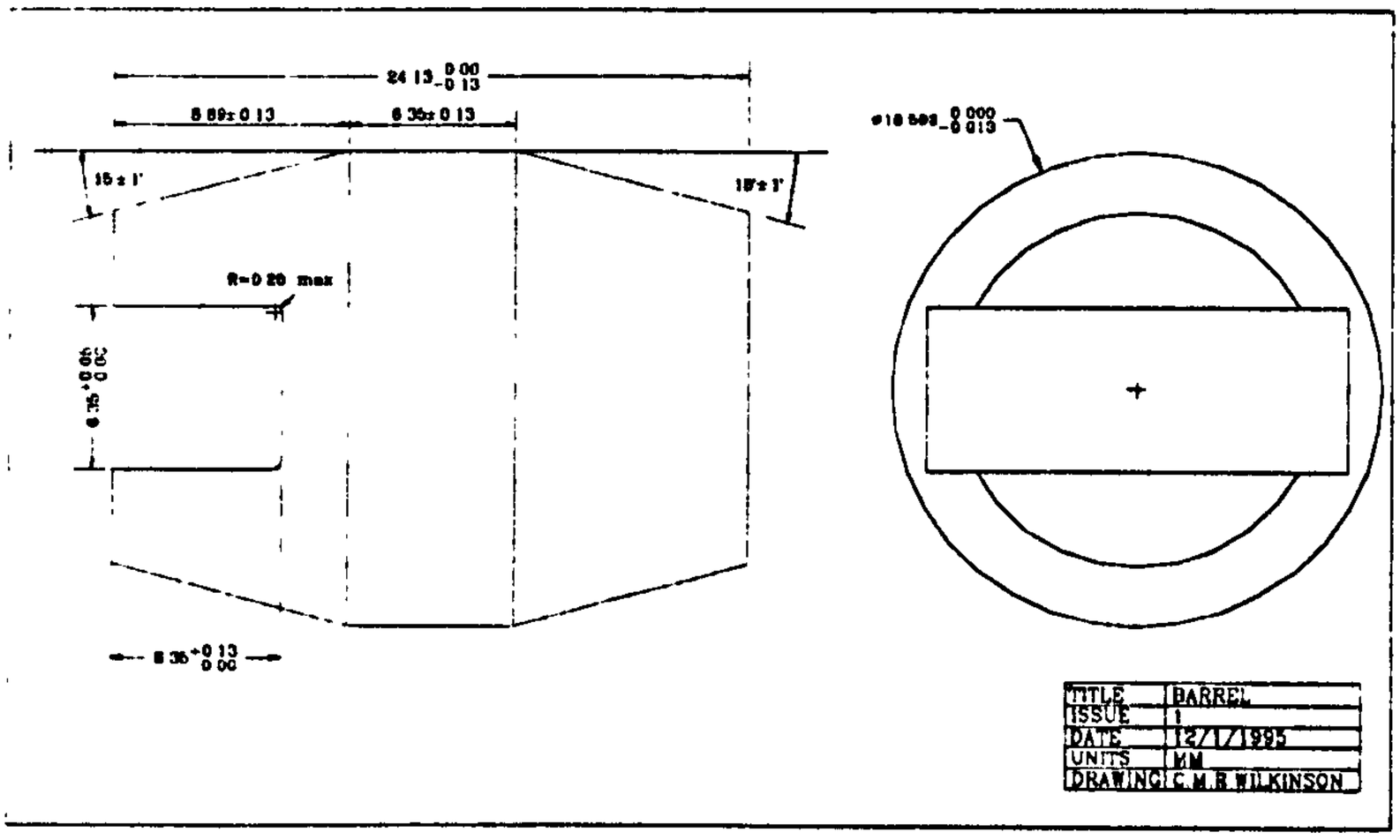


Figure E2 Chamfered Barrel Design Drawing

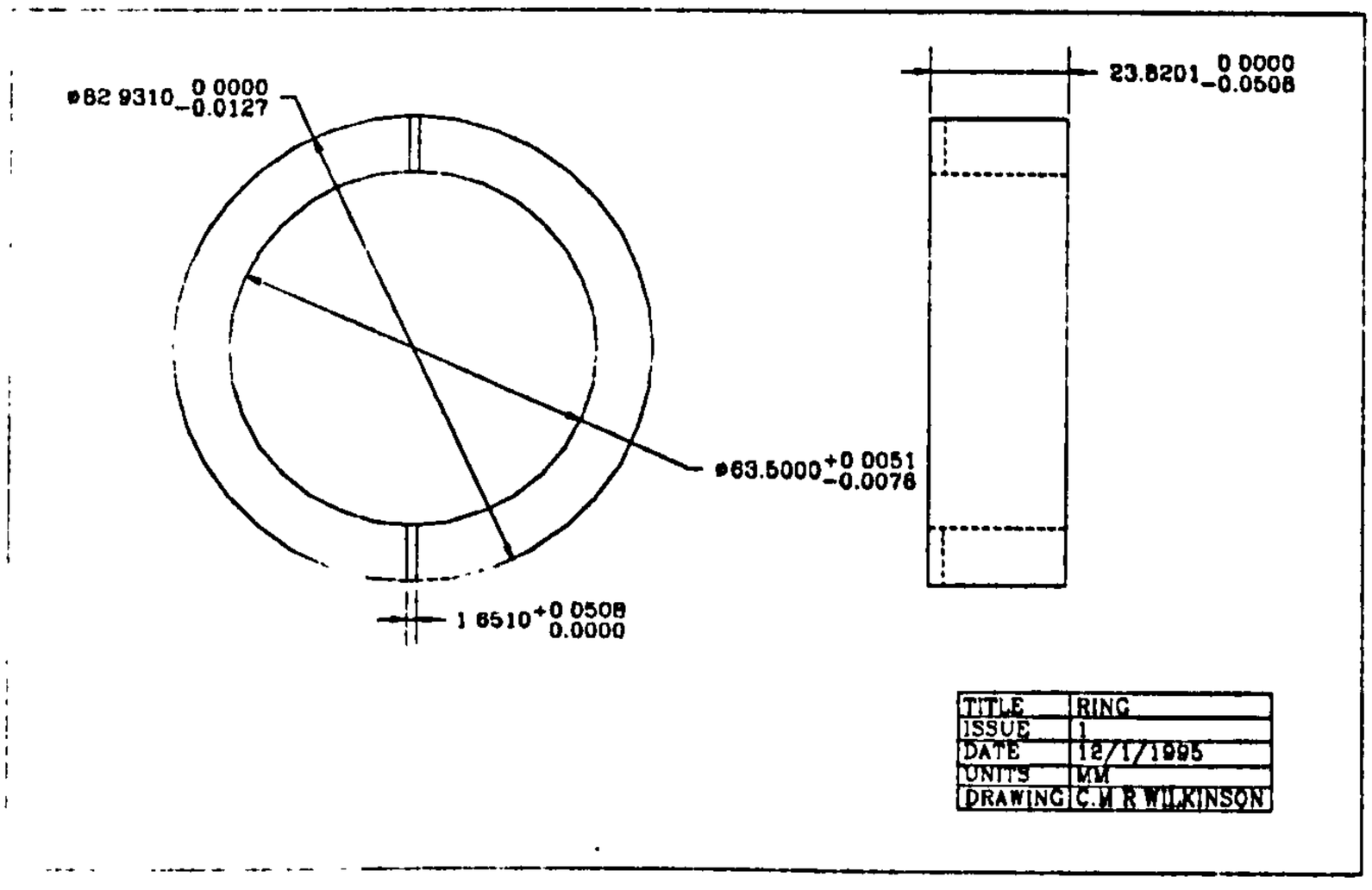


Figure E3 Ring Design Drawing

Appendix F Lubricant Specification

Chemical Composition:

Pentaerythritol Ester of Heptanoic Caprylic and Capric Acids

Trimethylolpropane Ester of Heptanoic Caprylic and Capric Acids

Tri(isopropylphenyl) Phosphate

Triphenyl Phosphate

Triphenyl Phosphorothionate

Appearance: Clear and bright straw coloured fluid with blue bloom

Table F1 Lubricant Specification (Castrol AN157)

Property	Sample A	Sample B
Specific Gravity, 15/15 °C	0.9867	0.9854
Kinematic Viscosity, cS		
at 100 °C	8.96	9.00
at 40 °C	52.24	52.65
at -32 °C	12667	10593
% Change after 72 hrs at -32 °C	1.93	-
Viscosity Index	-	152
Low Temperature Viscosity at -29 °C. cP at 30 rpm	-	4130
Pour Point, °C	-	-56
Flash Point (Closed) °C (IP 34)	-	227
Specific Heat Capacity		
ASTM D 3947 at 50 °C	-	1.78
J/g °C at 100 °C	-	1.77
Ryder Gear Test, 100 °C		
Relative Rating, % Herco Lube A	204.7	
Average Reference Oil Rating lb/in	2007	
Load Carrying Capacity FZG, Failure Load Stage	13/13+	
AN157 successfully completed all of schedules 1 and 2. In schedule 3 it gave a normal gear failure, i.e. every third tooth scuffed at a load of 1342 m		
	Author's Measurements	
Density at 40 °C, kg m^{-3}	968	
Density at 76 °C, kg m^{-3}	942.5	
Kinematic Viscosity, Cs at 40 °C	53	
Kinematic Viscosity, Cs at 100 °C	15.93	
Load Carrying Capacity FZG, Failure Load Stage	11/12	

Appendix G Dynamic Load Analysis

G1 The Dynamic Factor

The dynamic factor, K_v, calculation is only valid for gears running well below torsional resonance, defined by the mesh stiffness and the inertia of the mating gears. If the pinion and wheel are solid, method C from DIN 3990 (DIN 1987) can be used.

For gears running below resonance, that is where:

$$v \cdot z_1 \sqrt{\left(\frac{u^2}{1+u^2}\right)} < 1000 \text{ ms}^{-1}$$

Teeth on pinion, $z_1 = 17$

Gear ratio, $u = 1$

Peripheral velocity, $v = d.w/19098 = 11.3 \text{ m s}^{-1}$

The value was 135.89 m s^{-1} which meant it was below resonance

The dynamic factor can be calculated by the following equation:

$$K_v = 1 + \left(K_1 \cdot \frac{b}{F_{tD}} + K_2\right) \cdot \frac{z_1 v}{100} \cdot \sqrt{\frac{u^2}{1+u^2}}$$

Facewidth, $b = 10$ mm

Torque, $T = 219.6$ N m

Reference diameter, $d = m_n . z_1 = 86.36$ mm

Design tangential load, $F_{tD} = 2000.T/d = 5085.7$ N

K_1 and K_2 are taken from Tables G1 and G2 (from BGA (1992) for the appropriate gear quality to BS 436 Part 2 (BSI 1970)).

The test gear had pitch error and accumulated pitch error tolerance to grade 10 by AGMA standards (AGMA 1988). This translates to grade 5-6 gear accuracy to BS 436 Pt. 2 (BSI 1970).

The value of, $K_1 = 7.5+14.9/2 = 11.2$

Table G1 Values of Effective Pitch Error Used to Calculate K_1 (μm)

	Gear Accuracy Grade to BS 436 Pt.2 1970									
	3	4	5	6	7	8	9	10	11	12
f_{pt}	3	6	12	25	45	70	100	150	201	282
$f_{pb} = f_{pt}\cos\alpha_t$	2.8	5.6	11.3	23.5	42	66	94	140	189	266
y_α	0	0.5	1.5	4	7	15	25	40	55	75
$f_{pe\ eff} = f_{pb} - y_\alpha$	2.8	5.1	9.8	19.5	35	51	69	100	134	191

Table G2 Factors K_1 and K_2 for the Dynamic Factor

	K_1 Gear Accuracy Grade to BS 436 PT.2 1970										K_2 For all accuracy grades
	3	4	5	6	7	8	9	10	11	12	
ISO Spur Gears	2.1	3.9	7.5	14.9	26.8	39.1	52.8	76.6	102.6	146.3	0.0193
Helical Gears	1.9	3.5	6.7	13.3	23.9	34.8	47.0	68.2	91.4	130.3	0.0057

The dynamic factor for the test gears was, $K_v = 1.06$

The real contact stress, σ_H, is related to the nominal contact stress , σ_{HO}, by the equation

$$\sigma_H = \sigma_{HO}\sqrt{K_v \cdot K_{HB} \cdot K_{H\alpha}}$$

K_{HB} = The face load distribution factor for contact stress (accounts for unequal load distribution across facewidth due to lead errors and misalignment).

$K_{H\alpha}$ = The transverse load distribution factor (to allow for the effect of pitch and profile errors on load sharing between teeth in mesh).

Neglecting the two parameters K_{HB} and $K_{H\alpha}$, the real contact stress will have fluctuations of up to 2.8 % times greater than the nominal contact stress.

G2 Determination of Natural Frequencies in the Gear System

An analysis was carried out to determine the natural frequencies of the gear rig and make sure that these were far from the operating frequencies of the rig, in order to avoid any excessive dynamic effects.

The natural frequencies were calculated by two methods: translational and rotational methods (Figure G1), to check they gave the same results. The gear rig was treated as a

system consisting of two masses, representing the gears, connected by three springs, the two lateral ones representing the shafts and the central one representing the meshing gear stiffness.

Table G3 Notation for the Natural Frequency Analysis

k_{eff}	Total effective stiffness of the shaft
k_t	Torsional stiffness
k_l	Linear stiffness
k	Stiffness
r_b	Base circle radius
r_f	Reference circle radius
a	Linear acceleration
θ	Angular acceleration
F	Tangential force
I	Moment of inertia
J	Moment of inertia
m	Mass
M	Effective moment
T	Torque
x	Displacement

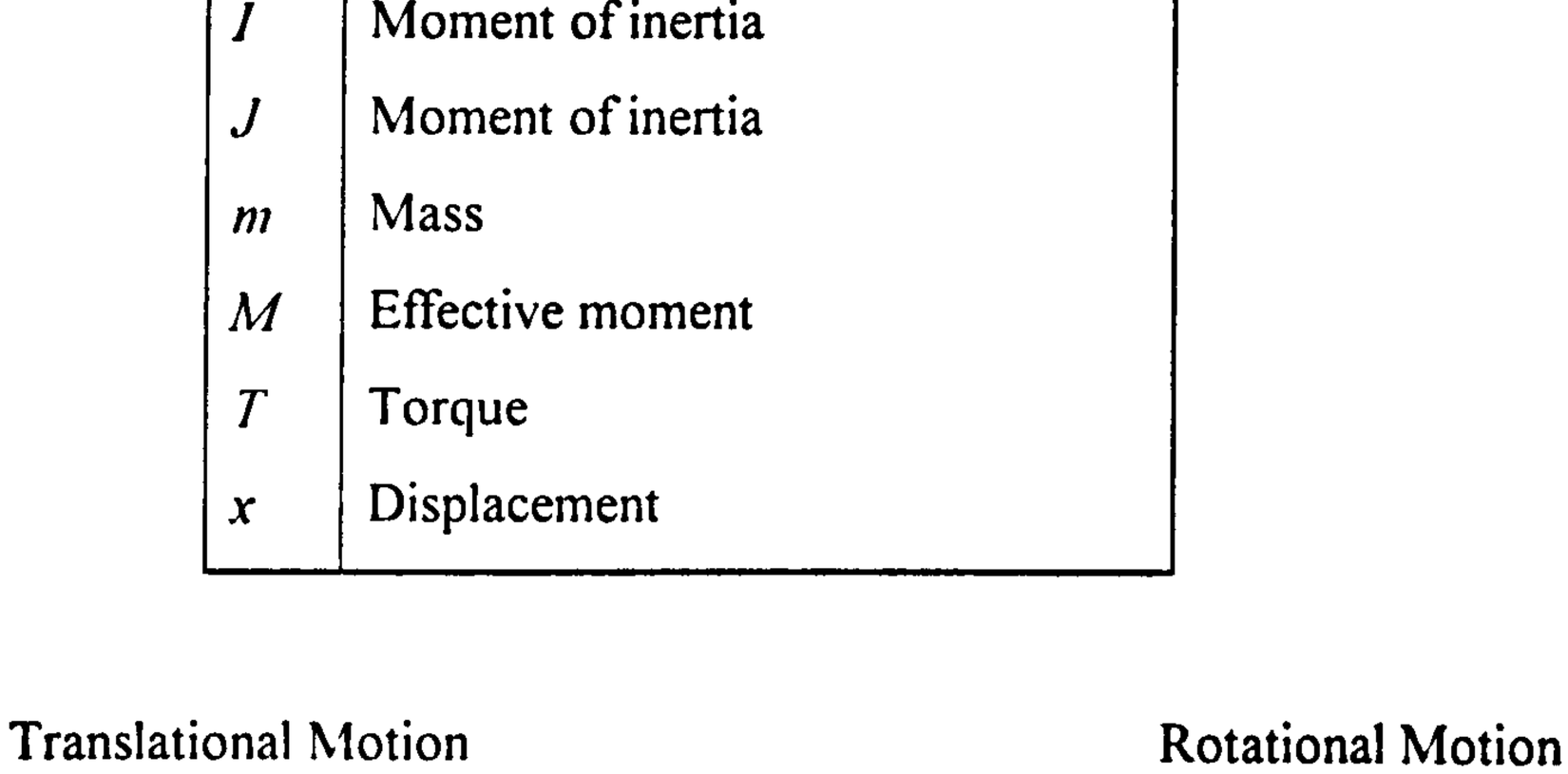


Figure G1 The Two Systems Used to Model the Natural Frequencies of the Gear System

Rotational Motion Method

Equations of motion

$$\text{for } J_1 \Rightarrow \; -k_2(\theta_1-\theta_2)-k_1\theta_1 = J_1\ddot{\theta}_1$$

$$\text{for } J_2 \Rightarrow \; -k_2(\theta_2-\theta_1)-k_3\theta_2 = J_2\ddot{\theta}_2$$

let

$$\theta = A\cos(\omega t+\phi)$$

$$\ddot{\theta} = A(-\omega^2)\cos(\omega t+\phi)$$

$$\theta = B\cos(\omega t+\phi)$$

$$\ddot{\theta} = B(-\omega^2)\cos(\omega t+\phi)$$

A, B and ϕ are arbitrary constants

$$J_A \Rightarrow (k_1+k_2-J_1\omega^2)A - k_2B = 0$$

$$J_B \Rightarrow (k_2+k_3-J_2\omega^2)B - k_2A = 0$$

For non - trivial solution

$$\begin{bmatrix} k_1+k_2-J_1\omega^2 & -k_2 \\ -k_2 & k_2+k_3-J_2\omega^2 \end{bmatrix} = 0$$

Finally

$$J_1J_2\omega^4 + \left((k_1+k_2)J_2+(k_2+k_3)J_1\right)\omega^2 + k_1k_2+k_2k_3+k_1k_3 = 0$$

Determination of the Relevant Mode Shapes

From the translational motion equations

$$\frac{A_A}{A_B} = \frac{-k_C}{-k_C-k_A-m_A\omega_1} = \frac{1}{\alpha_1}$$

$$\frac{A_A}{A_B} = \frac{-k_C}{-k_C-k_B-m_B\omega_2} = \frac{1}{\alpha_2}$$

From the rotational motion equations

$$\frac{A_1}{B_1} = \frac{k_2}{k_1 + k_2 - J_1\omega_1^2} = \frac{1}{\alpha_1}$$

$$\frac{A_2}{B_2} = \frac{k_2}{k_1 + k_2 - J_1\omega_2^2} = \frac{1}{\alpha_2}$$

The gear rig shafts had varying cross-sections as shown in Figure 7.1.5. The total effective shaft stiffness was found by calculating the stiffness of the individual sections and combining them.

Shaft k_{eff}= 13.6720x10^3 N m rad^{-1}

Test gears linear stiffness, k_c = 1.55x10^8 N m^{-1}

The relationship between linear stiffness and torsional stiffness is given by

$$k_t = \frac{T}{\theta} \text{ N m / rad}$$

$$k_l = \frac{F}{x} \text{ N / m}$$

$$\text{Therefore } k_t = k_l r_b^2$$

The tooth mesh excitation frequencies for the test gears and slave gears were 708 Hz and 1417 Hz respectively. The shaft frequency was 42 Hz.

Table G4 Calculated Values of Mass, Stiffness, and Moments of Inertia

m_a	1.779	kg
m_b	1.779	kg
k_a	8304119	N/m
k_b	8304119	N/m
k_c	1.55E+08	N/m
J_1	0.002929	m^2
J_2	0.002929	m^2

Table G5 Natural Frequencies of the Gear System

Assumption	f_1 Hz	f_2 Hz
Flexible	2115	242
Rigid	2129	344

It was uncertain how the hydraulic loading system, described in Chapter 7, behaved (whether this was perfectly rigid, allowing no motion at the end of the shafts, or was totally flexible, or something in between). Two approaches were taken to model the system, a flexible loading assumption with the stiffness k_B being taken as zero, and offering no stiffness, and a rigid loading assumption where the stiffness of the shaft was considered. The values of mass, m, moments of inertia, J, and stiffness values, k, are shown in Table G4. These were approximated from measurements on the rig. The results of the two assumptions can be seen in Table G5.

For the first assumption of a loading system with great flexibility the resonant frequencies obtained were $f_1 = 2115$ Hz and $f_2 = 242$ Hz

The mode shape for the first frequency would give the shafts a vibratory motion in opposite directions to each other imposed on the normal motion of the shafts. The second frequency would give a vibratory motion in the same direction imposed on the normal motion of the shafts.

For the second assumption of a rigid loading system the resonant frequencies obtained were $f_1 = 2129$ Hz and $f_2 = 344$ Hz. The first frequency would give the shafts a vibratory motion in opposite directions and the second frequency would give a vibratory motion in the same direction.

Both assumptions gave resonant frequencies which were far from the test and slave gear meshing frequencies and the shaft frequency. This indicated that resonance induced by tooth mesh excitation or by shaft imbalance should not be a problem and that the test gears were effectively isolated from the slave gears.

Appendix H Calculation of Gear Tooth Gaps for Pre-engagement

This analysis is based on work carried out by Barnett and Yildirim (1994). Considering involute spur gear teeth, we look at the first point of contact of a rigid tooth pair (on the path of contact) as seen in Figure H1.

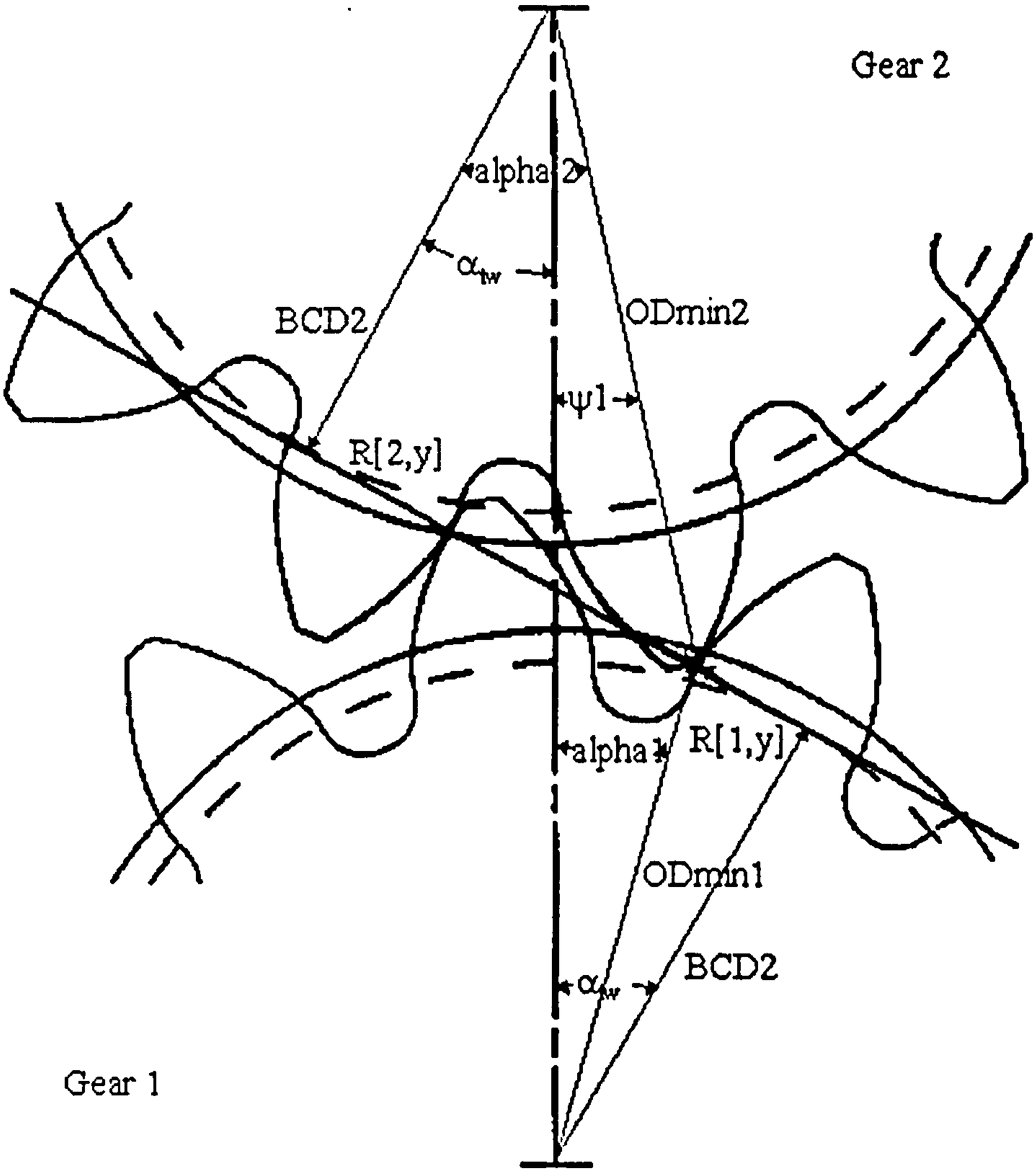


Figure H1 Gear Teeth Meshing at the First Point of Tooth Contact (on the Path of Contact)

At this first point of tooth contact N = y

$$R[1,y] = BCD1 \times \frac{\tan(\alpha_{tw})}{2} - AP$$

$$R[2,y] = BCD2 \times \frac{\tan(\alpha_{tw})}{2} + PB$$

Where AP and PB are lengths shown in Figure H2.

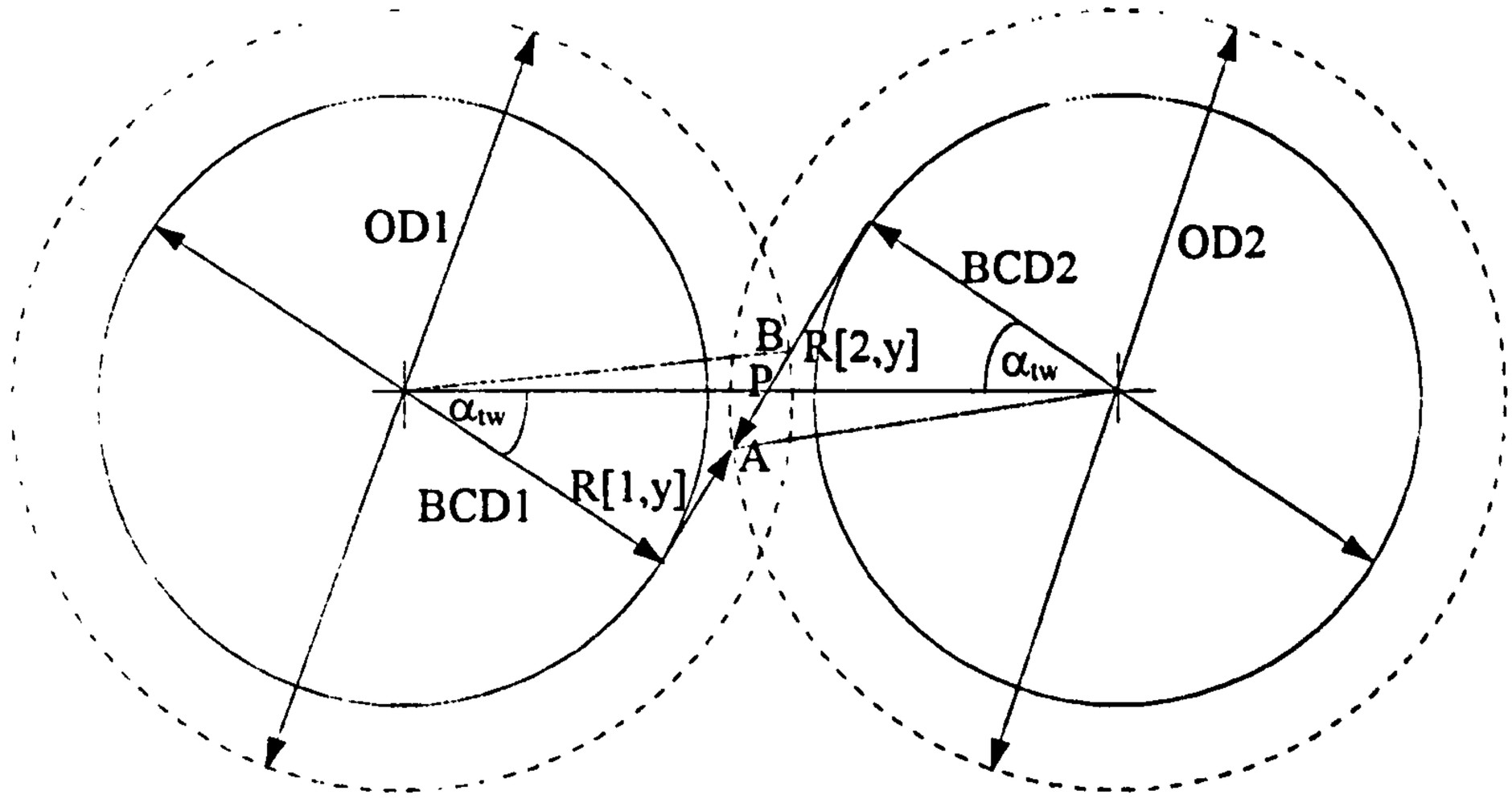


Figure H2 Gear Tooth Meshing Simulated by the Crossed Belt Analogy

$$AP = \sqrt{\left(\frac{OD2}{2}\right)^2 - \left(\frac{BCD2}{2}\right)^2} - \frac{BCD2}{2} \times \tan(\alpha_{tw})$$

$$PB = \sqrt{\left(\frac{OD1}{2}\right)^2 - \left(\frac{BCD1}{2}\right)^2} - \frac{BCD1}{2} \times \tan(\alpha_{tw})$$

The roll angle at engagement, $RAe = \frac{R[1,y]}{\left(\frac{BCD1}{2}\right)}$

$$OD\min 1 = 2 \times \sqrt{R[1,y]^2 + \left(\frac{BCD1}{2}\right)^2}$$

$$OD\min 2 = 2 \times \sqrt{R[2,y]^2 + \left(\frac{BCD2}{2}\right)^2}$$

$$alpha1 = \cos^{-1}\left(\frac{BCD1}{OD\min 1}\right)$$

$$alpha2 = \cos^{-1}\left(\frac{BCD2}{OD\min 2}\right)$$

$$\psi 1 = alpha2 - \alpha_{tw}$$

If we now consider points before the tooth pair comes into contact. We chose a step in roll angle, then

$$\theta = \text{Roll Angle Step (RAs)} \times \text{Gear ratio}$$

If there are y steps before contact we start at y steps from theoretical contact, and

$$\psi 1 = alpha2 - a_{tw} + y \times \theta$$
$$RA = RAe - y \times RAs$$

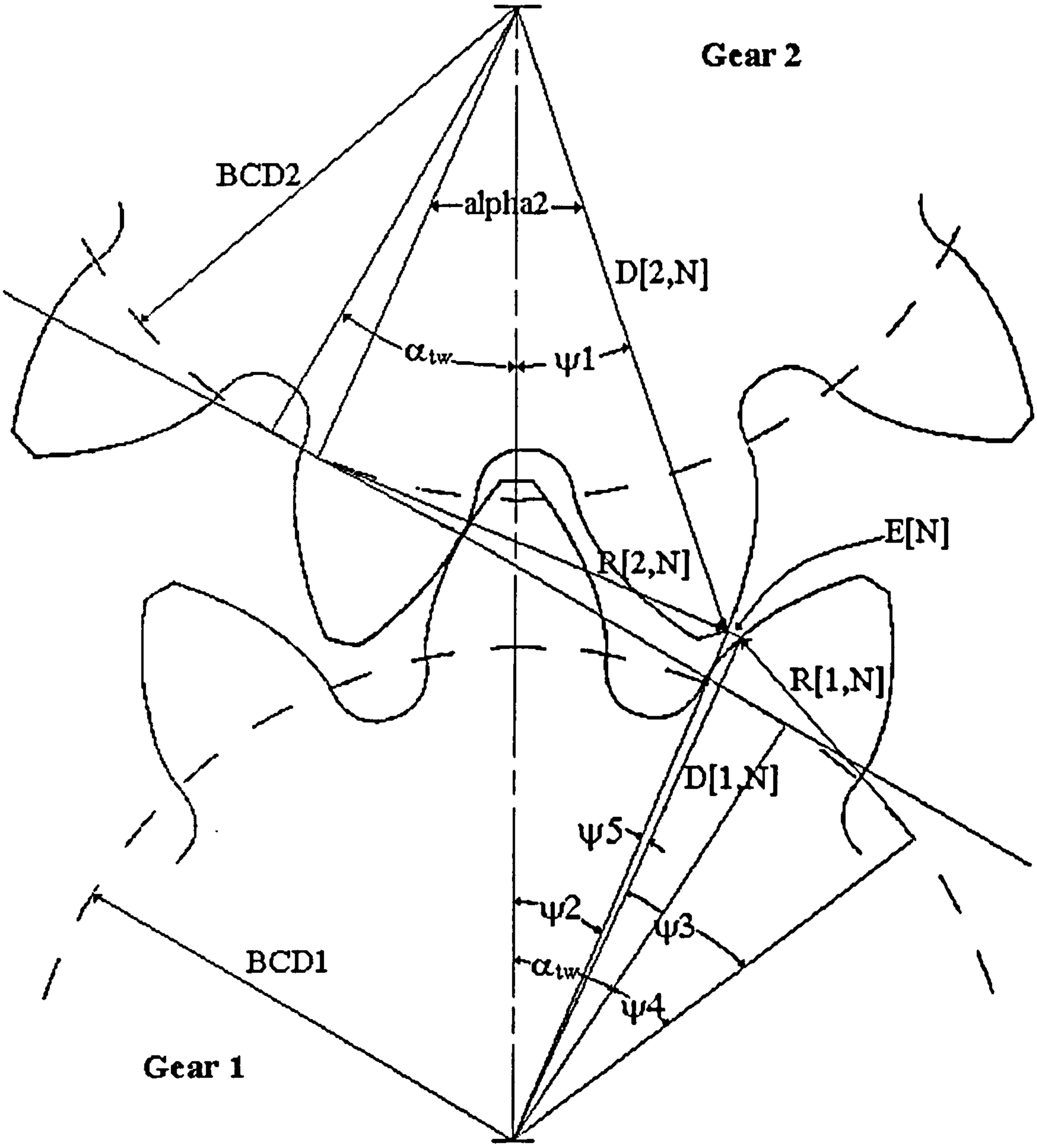


Figure H3 Gear Geometry for Pre-engagement Analysis

We then increase the roll angle by the roll angle step and evaluate the size of the gap until the gears come into contact

$$\psi 1 = \psi 1 - \theta$$
$$RA = RA + RAs$$

Then from geometry (as seen in Figure H4)

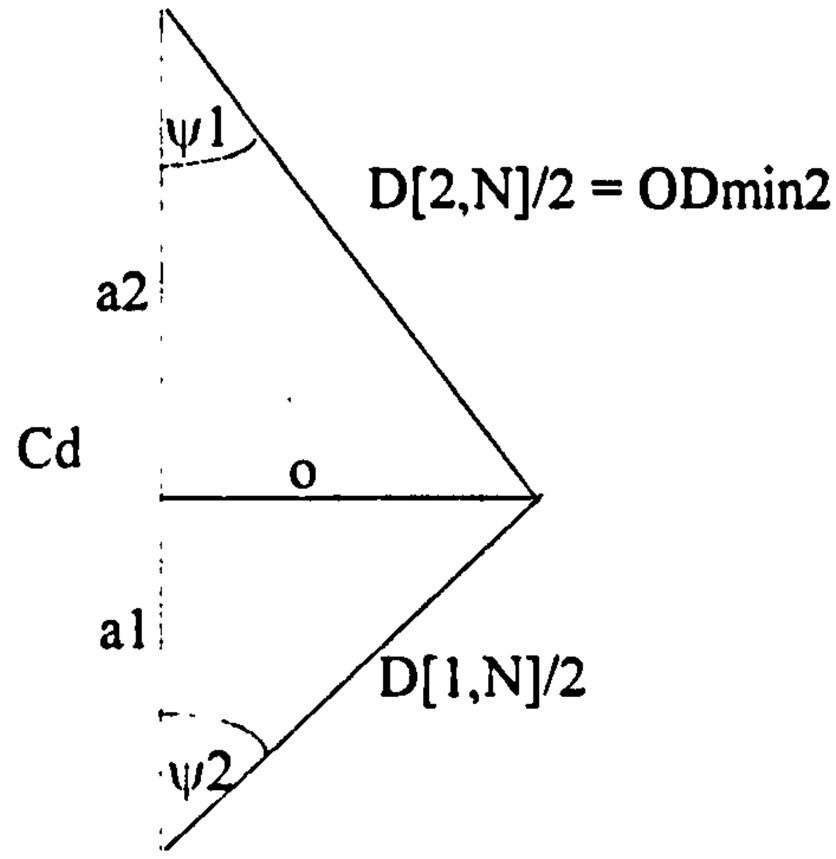


Figure H4 Specific Geometry

$$D[1,N] = \sqrt{o^2 + a1^2}$$
$$o = \left(\frac{OD\min 2}{2}\right) \times \sin \psi 1$$
$$Cd = a1 + a2$$
$$a2 = \left(\frac{OD\min 2}{2}\right) \times \cos(\psi 1)$$
$$a1 = Cd - \left(\frac{OD\min 2}{2}\right) \times \cos(\psi 1)$$
$$D[1,N] = \sqrt{\left[\left(\frac{OD\min 2}{2}\right)^2 \sin^2(\psi 1) + \left(Cd - \left(\frac{OD\min 2}{2}\right)\cos(\psi 1)\right)^2\right]}$$
$$= \sqrt{\left[\left(\frac{OD\min 2}{2}\right)^2 + Cd^2 - Cd \times OD\min 2 \times \cos(\psi 1)\right]}$$
$$D[2,N] = OD\min 2$$

$$\psi 2 = \sin^{-1}\left(\frac{o}{D[1,N]}\right)$$

$$\psi 2 = \sin^{-1}\left(\frac{\sin\psi 1 \times OD\min 2}{D[1,N]}\right)$$

$$\psi 3 = \cos^{-1}\left(\frac{BCD1}{D[1,N]}\right)$$

$$R[1,N] = 0.5 \times \sqrt{\left[D[1,N]^2 - BCD1^2\right]}$$

$$R[2,N] = 0.5 \times \sqrt{\left[D[2,N]^2 - BCD2^2\right]}$$

The final angles used to evaluate the tooth gap shown in Figure H5 below are calculated next.

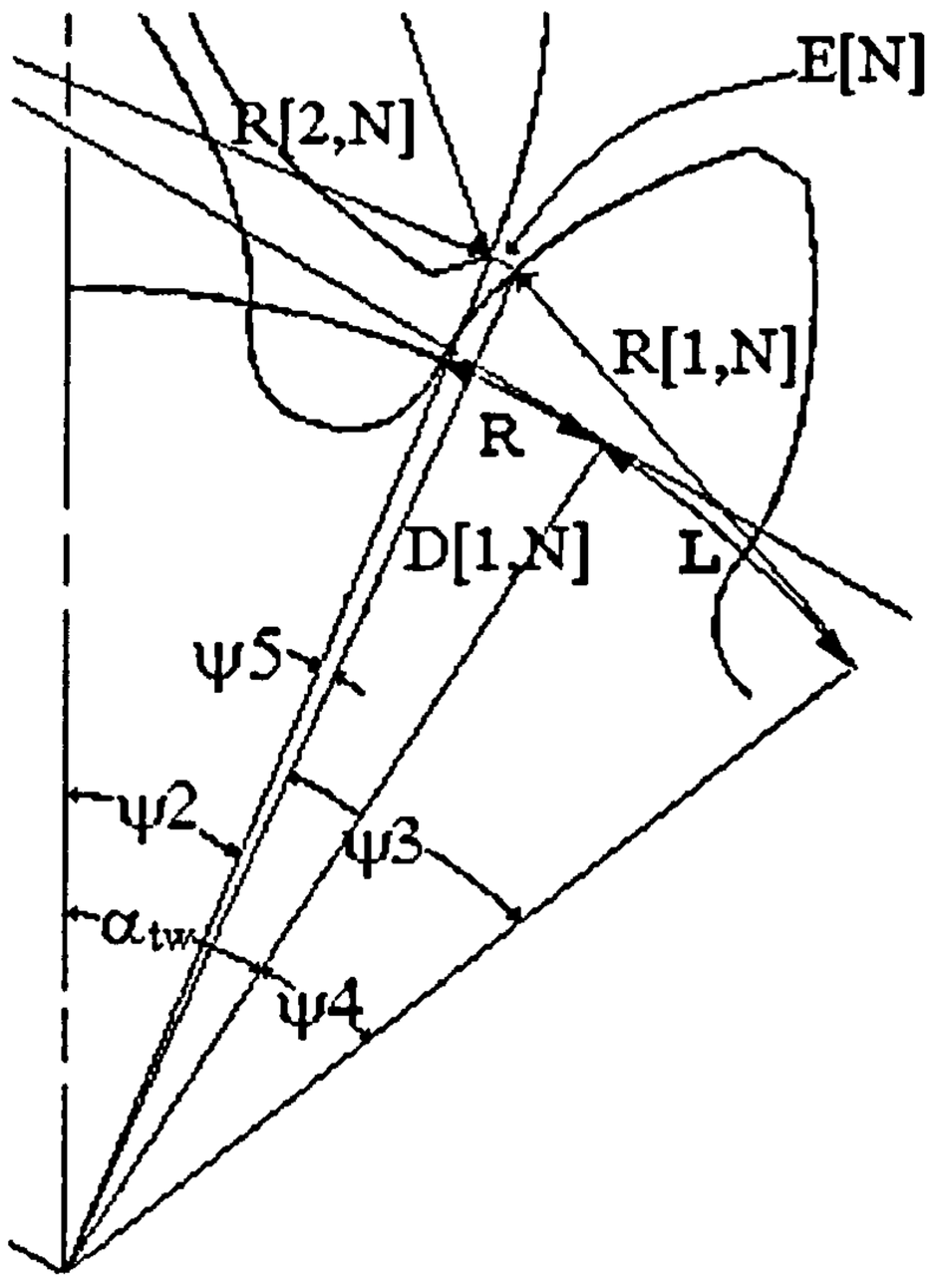


Figure H5 Detailed Diagram for the Gear Teeth Pre-engagement Analysis

$$\psi 4 = \frac{L}{\left(\frac{BCD1}{2}\right)}$$

$$= \frac{(R[1,N] - R)}{\left(\frac{BCD1}{2}\right)}$$

$$R = \frac{RA \times BCD1}{2}$$

$$\psi 4 = \frac{2 \times R[1,N]}{BCD1} - RA$$

$$\psi 5 = \alpha_{in} - \psi 2 - (\psi 3 - \psi 4)$$

The gap between the teeth, $E[N] = \psi 5 \times \frac{D[1,N]}{2}$

APPENDIX I Pre-Engagement Computing Program

I1 Program Listing

Global Variables

```
Global N, J As Integer
Global Const z = 1800, Y = 60
Global A(z), Angle(z), B(z), Dx1(z), Dx2(z), E1(z), E2(z) As Double
Global hc(z), ho(z), LS(z), Po(z), Tfm(z) As Double
Global Ey1, Ey2, Poiss1, Poiss2, Fw, T, Fbn, w1, GR As Double
Global Const pi = 3.14159265358979
Global R(2, z), D(2, z), Vr1(z), Vr2(z), Vs(z), Ve(z) As Double
```

'Notation

```
'Aen= Pressure angle at highest point of single tooth pair contact
'Afen= Angle for application of load at highest point of single tooth pair contact
'alpha= Involute pressure angle (Rack flank angle)
'alphatw= Operating pressure angle
'alphay1= Angle between the BCD1 and the diameter to the pinion tooth point being considered
'alphay2= Angle between the BCD2 and the diameter to the wheel tooth point being considered
'alpha1= Angle associated with tooth gap calculations
'alpha2= Angle associated with tooth gap calculations
'alphan1= Pressure angle at point of load on pinion
'alphan2= Pressure angle at point of load on wheel
'Angle(z)= Roll angle at point z
'AP= Length from SAP radius to pitch point
'BCD1= Base circle diameter of pinion
'BCD2= Base circle diameter of the wheel
'Cd= Centre distance
'Corr= Total correction advised on gears
'C1= Length to pinion SAP
'C2= Length to lowest point of single tooth pair contact
'C3= Length to operating pitch point
'C4= Length to highest point of single tooth pair contact
'C5= Length to pinion EAP
'C6= Length of line tangent to the base circles
'Dd= Tool diameter
'Den= Diameter to highest point of single tooth pair contact
'Dfix= Diameter at highest point of single tooth contact (pinion & wheel)
'Di2= Diameter to point of contact to the second tooth pair
'Dref1= Reference diameter of the pinion
'Dref2= Reference diameter of the wheel
'Dsec1= The diameter to the point of contact of the pinion in the second tooth pair
'Dsec2= The diameter to the point of contact of the wheel in the second tooth pair
'Dx1(z)= Deflection of first tooth pair
'Dx2(z)= deflection of second tooth pair
'D(2, z)= Array containing the diameters associated with a specific radius of curvature
'E(z)= Array containing the tooth separations
```

'Ey1= Young's Modulus of pinion
'Ey2= Young's Modulus of wheel
'Fbn= Actual normal load
'frac= Division of the path of contact
'Fw= Gear Facewidth
'G= Parameter for calculating the critical tooth dimensions
'galpha= Length of the line of contact
'Gamma= Angle between diameter at max height of single tooth contact and vertical
'GR= Gear Ratio
'Ge= Angle used for calculating the critical tooth dimensions
'H= Parameter for calculating the critical tooth dimensions
'Hfp= Tool Addendum
'Hf1= Bending arm for pinion at highest point of single
'Hf2= Bending arm for wheel at highest point of single
'Hf11= Bending arm for pinion at a point along the tooth in gear tooth pair 1
'Hf12= Bending arm for pinion at a point along the tooth in gear tooth pair 2
'Hf21= Bending arm for wheel at a point along the tooth in gear tooth pair 1
'Hf22= Bending arm for wheel at a point along the tooth in gear tooth pair 2
'k11= Total stiffness of pinion in gear tooth pair 1
'k12= Total stiffness of pinion in gear tooth pair 2
'k21= Total stiffness of wheel in gear tooth pair 1
'k22= Total stiffness of wheel in gear tooth pair 2
'kb11= Bending stiffness of pinion in gear tooth pair 1
'kb12= Bending stiffness of pinion in gear tooth pair 2
'kb21= Bending stiffness of wheel in gear tooth pair 1
'kb22= Bending stiffness of wheel in gear tooth pair 2
'ks11= Shear stiffness of pinion in gear tooth pair 1
'ks12= Shear stiffness of pinion in gear tooth pair 2
'ks21= Shear stiffness of wheel in gear tooth pair 1
'ks22= Shear stiffness of wheel in gear tooth pair 2
'ktot1(z)= Total stiffness of gear tooth pair 1
'ktot2(z)= Total stiffness of gear tooth pair 2
'LS(z)=Load sharing at point z
'Mn= Module
'N= Counter
'O= Parameter for calculating the critical tooth dimensions
'ODmin1= Diameter to point of SAP or EAP
'ODmin2= Diameter to end of EAP or SAP
'Onew= Parameter for calculating the critical tooth dimensions
'PB= Length from pitch point to EAP radius
'Poiss1= Poisson ratio of the pinion
'Poiss2= Poisson ratio of the wheel
'Ptb= Base pitch
'R12= Crowning radius on pinion
'R22= Crowning radius on wheel
'RA= Divisions of Roll angle near entrance to contact
'Rad=Reduced radius of curvature
'Ri2= Radius to point of contact to the second tooth pair
'Rofp= Root fillet radius of the basic rack of the gearing
'Rsec1= The radius of the point of contact of the pinion in the second tooth pair
'Rsec2= The radius of the point of contact of the wheel in the second tooth pair

```
'R(2, z)= Array containing the radii of curvature of the pinion and wheel teeth
'Sfn1= Thickness of pinion tooth at critical section
'Sfn2= Thickness of wheel tooth at critical section
'Spr= Residual undercut left by the protuberance
'Stref1= Reference tooth thickness of the pinion
'Stref2= Reference tooth thickness of the wheel
'Sty1= Pinion tooth thickness for a given diameter
'Sty2= Wheel tooth thickness for a given diameter
'T= Torque
'TCR= Contact ratio
'Theta= Angle (takes into account gear ratio) for gap calculation of wheel
'Theta1= Roll angle associated with C1
'Theta2= Roll angle associated with C2
'Theta3= Roll angle associated with C3
'Theta4= Roll angle associated with C4
'Theta5= Roll angle associated with C5
'Theta6= Roll angle associated with C6
'Toh1= Angle between diameter at point of contact for pinion and vertical
'Toh2= Angle between diameter at point of contact for pinion and vertical
'Vr1= Rolling velocity of pinion at point of contact
'Vr2= Rolling velocity of wheel at point of contact
'Vs= Sliding velocity at point of contact
'Ve= Rolling velocity of pinion at point of contact
'w1= Rotational velocity
'X1= Addendum modification coefficient on pinion
'X2= Addendum modification coefficient on wheel
'Psi1,Psi2,Psi3= Angles used in calculating the tooth separation
'y= Number of steps to contact
'y1= Height to max height of single tooth contact from BCD of pinion
'y11= Height to point of contact from BCD of pinion
'y2= Height to max height of single tooth contact from BCD of wheel
'y22= Height to point of contact from BCD of wheel
'z= Number of steps across the tooth contact
'Z1= Pinion tooth number
'Z2= Wheel tooth number
'++++++++++++++++++++++++++++++++++++++++++++++++++++++++++++++++++++++++++++++++
```

Form1

```
Dim alpha, Cd, Corr, RA, Mn  As Double
Dim x1, x2, Z1, Z2 As Double
Dim Loadfile, savefile As String * 40

'For the user to use a standard method for calculating the correction coefficients
'A standard addendum modification coefficient is calculated

    'Total correction for the two meshing gears
    Corr = (Cd - ((Z1 * Mn + Z2 * Mn) / 2)) / Mn
    'Correction on the pinion
    x1 = 1 / 3 - 1 / (3 * GR) + Corr / (1 + GR)
    'Correction on the wheel
    x2 = Corr - x1
```

```
Private Sub progrun() ' For Calculation of Tooth Gaps, Stiffness, Speeds, and Load Sharing
Dim Aen, Afen, alphatw, alphay1, alphay2 As Double
Dim alpha1, alpha2, alphan1, alphan2  As Double
Dim BCD1, BCD2, C1, C2, C3, C4, C5, C6 As Double
Dim Dd, Den, Dfix, Dref1, Dref2, Dsec1, Dsec2 As Double
Dim fracRA, G, Ge, Gamma, galpha As Double
Dim H, Hfp, Hf1, Hf2, Hf11, Hf22, Hf12, Hf21 As Double
Dim k11, k12, k21, k22, kb11, kb12, kb21, kb22 As Double
Dim ks11, ks12, ks21, ks22 As Double
Dim O, Onew, ODmin1, ODmin2 As Double
Dim Ptb, Psi1, Psi2, Psi3, Psi5 As Double
Dim Rofp, Rsec1, Rsec2 As Double
Dim Sfn1, Sfn2, Spr, Sref1, Sty1, Sref2, Sty2 As Double
Dim Theta, Theta1, Theta2, Theta3, Theta4, Theta5, Theta6 As Double
Dim TCR, Toh1, Toh2 As Double
Dim y1, y11, y2, y22  As Double
ReDim ktot1(z), ktot2(z) As Double

'Basic Gear Geometry Calculations

'Base Circle diameter of pinion and wheel
BCD1 = Z1 * Mn * Cos(alpha)
BCD2 = Z2 * Mn * Cos(alpha)

'Base pitch of gears
Ptb = pi * Mn * Cos(alpha)

'Outer diameter of pinion and wheel
OD1 = Z1 * Mn + 2 * Mn * (1 + x1)
OD2 = Z2 * Mn + 2 * Mn * (1 + x2)

'The reference diameter of the pinion and wheel
Dref1 = Z1 * Mn
Dref2 = Z2 * Mn

'The reference tooth thickness of the pinion and the wheel
Sref1 = Mn * ((pi / 2) + 2 * x1 * Tan(alpha))
Sref2 = Mn * ((pi / 2) + 2 * x2 * Tan(alpha))

'Operating pressure angle
alphatw = Arccos((BCD1 + BCD2) / (2 * Cd))
'*****************************************************************************

'Various lengths along the path of contact and their respective roll angles

'Length of line tangent to base circles
C6 = Cd * Sin(alphatw)

'Length to pinion end of active profile (EAP)
C5 = 0.5 * Sqr(OD1 ^ 2 - BCD1 ^ 2)
```

```
'Length to pinion start of active profile (SAP)
C1 = (C6 - 0.5 * Sqr(OD2 ^ 2 - BCD2 ^ 2))

'Length to highest point of single tooth pair contact
C4 = C1 + Ptb

'Length to operating pitch point
C3 = C6 / (GR + 1)

'Length to lowest point of single tooth contact
C2 = C5 - Ptb

'Roll angle to pinion start of active profile (SAP)
Theta1 = 2 * C1 / BCD1

'Roll angle to lowest point of single tooth contact
Theta2 = 2 * C2 / BCD1

'Roll angle to operating pitch point
Theta3 = 2 * C3 / BCD1

'Roll angle to highest point of single tooth pair contact
Theta4 = 2 * C4 / BCD1

'Roll angle to pinion end of active profile (EAP)
Theta5 = 2 * C5 / BCD1

'Roll angle of line tangent to base circles
Theta6 = 2 * C6 / BCD1
'*************************************************************************

'More gear geometry calculations

'Length of path of contact
galpha = C5 - C1

'Transverse contact ratio
TCR = galpha / Ptb

'Radii of the pinion and wheel teeth at the first point of contact if perfectly rigid
R(1, Y) = C1
R(2, Y) = C6 - C1

'Radii of the pinion and wheel teeth at the last point of contact if perfectly rigid
R(1, z - Y) = C5
R(2, z - Y) = C6 - C5

'The length of each division along the path of contact
fracRA = (Theta5 - Theta1) / (z - 2 * Y)
'*************************************************************************
```

```
'The dimensions of the basic rack
'For tools without protuberance Spr=0
Spr = 0

'Radius of rack etc. (see Figure 14 p. 16 sec. 9 Gear design course handbook)
Rofp = 0.39 * Mn
Hfp = 1.25 * Mn
'**********************************************************************

'BS procedures from gear design course handbook for tooth thickness and height
calcultions used for stiffness
'For the pinion tooth the critical dimensions for bending are calculated here

'Procedure on p. 17 sec. 9 Gear design course handbook
G = Rofp / Mn - Hfp / Mn + x1
Dd = pi * Mn / 4 - Hfp * Tan(alpha) + Spr / Cos(alpha) - (1 - Sin(alpha)) * (Rofp /
     Cos(alpha))
H = (2 / Z1) * (pi / 2 - Dd / Mn) - pi / 3

Onew = pi / 6
Do
   O = Onew
   Onew = 2 * G * Tan(O) / Z1 - H
   If Abs(O - Onew) < 0.0001 Then
      Exit Do
   End If
Loop

Den = 2 * Sqr((Sqr((OD1 / 2) ^ 2 - (BCD1 / 2) ^ 2) - (pi * Dref1 * Cos(alpha) / Z1) *
      (TCR - 1)) ^ 2 + (BCD1 / 2) ^ 2)
Aen = Arccos(BCD1 / Den)
Ge = (pi / 2 + 2 * x1 * Tan(alpha)) / Z1 + Tan(alpha) - alpha - Tan(Aen) + Aen
Afen = Aen - Ge

'Tooth thickness of the pinion at the critical section
Sfn1 = Mn * Z1 * Sin(pi / 3 - O) + Mn * Sqr(3) * (G / Cos(O) - Rofp / Mn)

'Bending arm for the pinion at the highest point of single tooth contact (probably) ?
Hf1 = (Mn / 2) * ((Cos(Ge) - Sin(Ge) * Tan(Afen)) * Den / Mn - Z1 * Cos(pi / 3 - O) -
      G / Cos(O) + Rofp / Mn)

'Diameter,load angle and tooth thickness at highest point of single tooth contact for the
pinion

'Diameter at highest point of single tooth contact
Dfix = 2 * Sqr(C4 ^ 2 + (BCD1 / 2) ^ 2)

'Angle between BCD and diameter
alphay = Arccos(BCD1 / Dfix)
```

```
'Tooth thickness arc at point of contact
Sty = Dfix * ((Stref1 / Dref1) + Tan(alpha) - Tan(alphay) + alphay - alpha)

'Half angle
Gamma = Sty / Dfix

'Height above BCD of point of highest single tooth contact
y1 = (Dfix / 2) * Cos(Gamma) - BCD1 / 2 - Tan(alphay - Gamma) * Sin(Gamma) * Dfix
     / 2
'-----------------------------------------------------------------------------

'For the wheel tooth the critical dimensions for bending are calculated here
G = Rofp / Mn - Hfp / Mn + x2
Dd = pi * Mn / 4 - Hfp * Tan(alpha) + Spr / Cos(alpha) - (1 - Sin(alpha)) * (Rofp /
     Cos(alpha))
H = (2 / Z2) * (pi / 2 - Dd / Mn) - pi / 3

Onew = pi / 6
Do
   O = Onew
   Onew = 2 * G * Tan(O) / Z2 - H
   If Abs(O - Onew) < 0.0001 Then
      Exit Do
   End If
Loop

Den = 2 * Sqr((Sqr((OD2 / 2) ^ 2 - (BCD2 / 2) ^ 2) - (pi * Dref2 * Cos(alpha) / Z2) *
      (TCR - 1)) ^ 2 + (BCD2 / 2) ^ 2)
Aen = Arccos(BCD2 / Den)
Ge = (pi / 2 + 2 * x2 * Tan(alpha)) / Z2 + Tan(alpha) - alpha - Tan(Aen) + Aen
Afen = Aen - Ge

'Tooth thickness of the wheel at the critical section
Sfn2 = Mn * Z2 * Sin(pi / 3 - O) + Mn * Sqr(3) * (G / Cos(O) - Rofp / Mn)

'Bending arm for the wheel at the highest point of single tooth contact (probably) ?
Hf2 = (Mn / 2) * ((Cos(Ge) - Sin(Ge) * Tan(Afen)) * Den / Mn - Z2 * Cos(pi / 3 - O) -
      G / Cos(O) + Rofp / Mn)

'Diameter,load angle and tooth thickness at highest point of single tooth contact for the
wheel

'Diameter at highest point of single tooth contact
Dfix = 2 * Sqr((C6 - C2) ^ 2 + (BCD2 / 2) ^ 2)

'Angle between BCD and diameter
alphay = Arccos(BCD2 / Dfix)

'Tooth thickness
Sty = Dfix * ((Stref2 / Dref2) + Tan(alpha) - Tan(alphay) + alphay - alpha)
```

```
'Half angle
Gamma = Sty / Dfix

'Height above BCD of point of highest single tooth contact
y2 = (Dfix / 2) * Cos(Gamma) - BCD2 / 2 - Tan(alphay - Gamma) * Sin(Gamma) * Dfix
     / 2
'*************************************************************************

'Calculation of the gap and roll angle for the gear tooth pair 1
'For this section see appendix of report on pre-engagement to understand equations

For N = 0 To z Step 1

'For points before they come into contact
If N < Y Then
   ODmin1 = 2 * ((BCD1 / 2) ^ 2 + C1 ^ 2) ^ 0.5
   ODmin2 = 2 * ((BCD2 / 2) ^ 2 + (C6 - C1) ^ 2) ^ 0.5
   alpha1 = Arccos(BCD1 / ODmin1)
   alpha2 = Arccos(BCD2 / ODmin2)

   Psi1 = alpha2 - alphatw + (Y - N) * RA * GR

   'Diameter to point on pinion and wheel
   D(1, N) = 2 * ((ODmin2 / 2) ^ 2 + Cd ^ 2 - ODmin2 * Cd * Cos(Psi1)) ^ 0.5
   D(2, N) = ODmin2

   'Radius to point on pinion and wheel
   R(1, N) = 0.5 * (D(1, N) ^ 2 - BCD1 ^ 2) ^ 0.5
   R(2, N) = 0.5 * (D(2, N) ^ 2 - BCD2 ^ 2) ^ 0.5
   Psi2 = Arcsine(Sin(Psi1) * ODmin2 / D(1, N))
   Psi3 = Arccos(BCD1 / D(1, N))

   'Roll angle
   Angle(N) = Theta1 - RA * (Y - N)
   Psi5 = (alphatw - Psi2 - Psi3 + ((2 * R(1, N) / BCD1) - Angle(N)))

   'Tooth gap for tooth pair 1 before coming into contact
   E1(N) = (D(1, N) / 2) * Psi5

   'Calculation of velocities at contact
   Vr1(N) = (2 * pi * w1 / 60) * D(1, N) / 2
   Vr2(N) = (2 * pi * w1 / (60 * GR)) * D(2, N) / 2

   'Entrainment velocity
   Ve(N) = -0.5 * Sqr((Vr1(N) * Sin(Psi2) + Vr2(N) * Sin(Psi1)) ^ 2 + (Vr1(N) *
           Cos(Psi2) - Vr2(N) * Cos(Psi1)) ^ 2)

   'Sliding velocity
   Vs(N) = 2 * Ve(N)
```

```
'For point just after they leave contact
   Elself N > z - Y Then
      ODmin1 = 2 * ((BCD1 / 2) ^ 2 + C5 ^ 2) ^ 0.5
      ODmin2 = 2 * ((BCD2 / 2) ^ 2 + (C6 - C5) ^ 2) ^ 0.5
      alpha1 = Arccos(BCD1 / ODmin1)
      alpha2 = Arccos(BCD2 / ODmin2)

      Psi1 = alpha1 - alphatw + (N + Y - z) * RA

      'Diameter to point on wheel and wheel
      D(1, N) = ODmin1
      D(2, N) = 2 * ((ODmin1 / 2) ^ 2 + Cd ^ 2 - ODmin1 * Cd * Cos(Psi1)) ^ 0.5

      'Radius to point on pinion and wheel
      R(1, N) = 0.5 * (D(1, N) ^ 2 - BCD1 ^ 2) ^ 0.5
      R(2, N) = 0.5 * (D(2, N) ^ 2 - BCD2 ^ 2) ^ 0.5
      Psi2 = Arcsine(Sin(Psi1) * ODmin1 / D(2, N))
      Psi3 = Arccos(BCD2 / D(2, N))

      'Roll angle
      Angle(N) = Theta5 + RA * (N - z + Y)
      Psi5 = (alphatw - Psi2 - Psi3 + ((2 * R(2, N) / BCD2) - ((2 * (C6 - C5) / BCD2) -
             RA * (N + Y - z))))

      'Tooth gap for tooth pair 1 just after leaving contact
      E1(N) = (D(2, N) / 2) * Psi5

      'Calculation of velocities at contact
      Vr1(N) = (2 * pi * w1 / 60) * D(1, N) / 2
      Vr2(N) = (2 * pi * w1 / (60 * GR)) * D(2, N) / 2

      'Entrainment velocity
      Ve(N) = -0.5 * Sqr((Vr1(N) * Sin(Psi2) + Vr2(N) * Sin(Psi1)) ^ 2 + (Vr1(N) *
              Cos(Psi2) - Vr2(N) * Cos(Psi1)) ^ 2)

      'Sliding velocity
      Vs(N) = -2 * Ve(N)

   Else
      'When tooth pair 1 are in contact
      'Roll angle
      Angle(N) = Theta1 + (N - Y) * fracRA

      'Radius to point on pinion and wheel
      R(1, N) = Angle(N) * BCD1 / 2
      R(2, N) = C6 - R(1, N)

      'Diameter to point on pinion and wheel
      D(1, N) = 2 * (R(1, N) ^ 2 + (BCD1 / 2) ^ 2) ^ 0.5
      D(2, N) = 2 * (R(2, N) ^ 2 + (BCD2 / 2) ^ 2) ^ 0.5
```

```
'Tooth gap for first tooth pair
E1(N) = 0

'Calculation of velocities at contact
Vr1(N) = (2 * pi * w1 / 60) * R(1, N)
Vr2(N) = (2 * pi * w1 / (60 * GR)) * R(2, N)

'Sliding velocity
Vs(N) = (Vr1(N) - Vr2(N))

'Entrainment velocity
Ve(N) = 0.5 * (Vr1(N) + Vr2(N))
  End If
'*****************************************************************************

'Calculation of stiffness of first gear tooth pair

'Angle between bcd and D(1,N)
alphay1 = Arccos(BCD1 / D(1, N))
alphay2 = Arccos(BCD2 / D(2, N))

'Arc length of the pinion and wheel at the various points of contact of gear tooth pair 1
Sty1 = D(1, N) * ((Stref1 / Dref1) + Tan(alpha) - Tan(alphay1) + alphay1 - alpha)
Sty2 = D(2, N) * ((Stref2 / Dref2) + Tan(alpha) - Tan(alphay2) + alphay2 - alpha)

'Half angles for the various arc lengths
Toh1 = Sty1 / D(1, N)
Toh2 = Sty2 / D(2, N)

'Heights of bending arm for gear tooth pair 1
'Height of point on pinion and wheel above BCD
y11 = (D(1, N) / 2) * Cos(Toh1) - BCD1 / 2 - Tan(alphay1 - Toh1) * Sin(Toh1) *
      D(1, N) / 2
y21 = (D(2, N) / 2) * Cos(Toh2) - BCD2 / 2 - Tan(alphay2 - Toh2) * Sin(Toh2) *
      D(2, N) / 2

'Bending arm height for stiffness calcs in pinion and wheel
Hf11 = (y11 - y1) + Hf1
Hf21 = (y21 - y2) + Hf2

'Pressure angle at point of load of pinion and wheel
alphan1 = alphay1 - Toh1
alphan2 = alphay2 - Toh2

'The first tooth pair stiffness
'Bending stiffness pinion and wheel
kb11 = 1 / ((Cos(alphan1) / (Ey1 * Fw)) * ((12 * Cos(alphan1) * Hf11 ^ 2 / Sfn1 ^ 3)
       * (Hf11 + Sfn1 / 2)))
kb21 = 1 / ((Cos(alphan2) / (Ey2 * Fw)) * ((12 * Cos(alphan2) * Hf21 ^ 2 / Sfn2 ^ 3)
       * (Hf21 + Sfn2 / 2)))
```

```
'Shear stiffness pinion and wheel
ks11 = 1 / ((Cos(alphan1) / (Ey1 * Fw)) * (3 * Cos(alphan1) ^ 2 + Sin(alphan1) ^ 2) *
       (1 + Hf11 / Sfn1))
ks21 = 1 / ((Cos(alphan2) / (Ey2 * Fw)) * (3 * Cos(alphan2) ^ 2 + Sin(alphan2) ^ 2) *
       (1 + Hf21 / Sfn2))

'Total stiffness of the pinion
k11 = (kb11 + ks11)

'Total stiffness of the wheel
k21 = (kb21 + ks21)

   'Total stiffness of the tooth pair 1
   ktot1(N) = (1 / k11 + 1 / k21) ^ -1
Next N
'*****************************************************************************

'For calculating tooth gaps and stiffness of the second tooth pair

For N = 0 To z Step 1
   'Second tooth pair leaving contact
   If N <= z / 2 Then

      'If the second pair are in contact the gap is zero otherwise it is calculated
      If R(1, N) + Ptb <= C5 Then

      'Radius of the pinion and wheel
      Rsec1 = R(1, N) + Ptb
      Rsec2 = C6 - Rsec1

      'Diameter of the pinion and wheel
      Dsec1 = 2 * (Rsec1 ^ 2 + (BCD1 / 2) ^ 2) ^ 0.5
      Dsec2 = 2 * (Rsec2 ^ 2 + (BCD2 / 2) ^ 2) ^ 0.5

      'Tooth gap for second tooth pair
      E2(N) = 0

Else
      'Second tooth pair are leaving contact
      ODmin1 = 2 * ((BCD1 / 2) ^ 2 + C5 ^ 2) ^ 0.5
      ODmin2 = 2 * ((BCD2 / 2) ^ 2 + (C6 - C5) ^ 2) ^ 0.5
      alpha1 = Arccos(BCD1 / ODmin1)
      alpha2 = Arccos(BCD2 / ODmin2)

      Psi1 = alpha1 - alphatw + (Angle(N) + 2 * Ptb / BCD1 - Theta5)

      'Diameter of the pinion and wheel at the point of contact
      Dsec1 = ODmin1
      Dsec2 = 2 * ((ODmin1 / 2) ^ 2 + Cd ^ 2 - ODmin1 * Cd * Cos(Psi1)) ^ 0.5
      'To account for points very far from contact
      If BCD2 <= Dsec2 Then
```

```
'Radius of wheel at point of contact
Rsec2 = 0.5 * (Dsec2 ^ 2 - BCD2 ^ 2) ^ 0.5
Psi2 = Arcsine(Sin(Psi1) * ODmin1 / Dsec2)
Psi3 = Arccos(BCD2 / Dsec2)

'RAc2=Theta5
'Angle2(N)= Angle(N)+2*Ptb/BCD1
'AnglePastContact=Angle2(N)-RAc
'AnglePastContact=Angle(N)+2*Ptb/BCD1-Theta5

Psi5 = (alphatw - Psi2 - Psi3 + ((2 * Rsec2 / BCD2) - ((2 * (C6 - C5) / BCD2)
        - (Angle(N) + 2 * Ptb / BCD1 - Theta5))))

        'Tooth gap for the second tooth pair
        E2(N) = (Dsec2 / 2) * Psi5

        'If far away from contact an arbitrary value is assigned
      Else
        E2(N) = 10
      End If
   End If
Else
   'Second tooth pair entering contact

   'If the second pair are in contact the gap is zero otherwise it is calculated
   If R(1, N) - Ptb >= C1 Then

      'Radius of pinion and wheel teeth at point of contact
      Rsec1 = R(1, N) - Ptb
      Rsec2 = C6 - Rsec1

      'Diameter of pinion and wheel at point of contact
      Dsec1 = 2 * (Rsec1 ^ 2 + (BCD1 / 2) ^ 2) ^ 0.5
      Dsec2 = 2 * (Rsec2 ^ 2 + (BCD2 / 2) ^ 2) ^ 0.5

      'Tooth gap for second tooth pair
      E2(N) = 0

Else
   'Second tooth pair are entering contact
   ODmin1 = 2 * ((BCD1 / 2) ^ 2 + C1 ^ 2) ^ 0.5
   ODmin2 = 2 * ((BCD2 / 2) ^ 2 + (C6 - C1) ^ 2) ^ 0.5
   alpha1 = Arccos(BCD1 / ODmin1)
   alpha2 = Arccos(BCD2 / ODmin2)

   Psi1 = alpha2 - alphatw + (Theta1 - (Angle(N) - 2 * Ptb / BCD1)) * GR

   'Diameter of the pinion and wheel teeth at the point of contact
   Dsec1 = 2 * ((ODmin2 / 2) ^ 2 + Cd ^ 2 - ODmin2 * Cd * Cos(Psi1)) ^ 0.5
   Dsec2 = ODmin2
```

```
'To account for points very far from contact
If BCD1 <= Dsec1 Then

    'Radius of wheel at point of contact
    Rsec1 = 0.5 * (Dsec1 ^ 2 - BCD1 ^ 2) ^ 0.5
    Psi2 = Arcsine(Sin(Psi1) * ODmin2 / Dsec1)
    Psi3 = Arccos(BCD1 / Dsec1)

    'RAc2=Theta1
    'Angle2(N) = Angle(N)-2*Ptb/BCD1
    'AngleBeforeContact=RAc-Angle2(N)
    'AngleBeforeContact=Theta1-(Angle(N)-2*Ptb/BCD1)
        Psi5 = (alphatw - Psi2 - Psi3 + ((2 * Rsec1 / BCD1) - (Angle(N) - 2 * Ptb /
               BCD1)))

        'Tooth gap for second tooth pair
        E2(N) = (Dsec1 / 2) * Psi5

    'If far away from contact an arbitrary value is assigned
    Else: E2(N) = 10
    End If
  End If
End If
'*****************************************************************************
'Stiffness calculations for the second tooth pair

'This accounts for points very far from contact
If Dsec1 > BCD1 And Dsec2 > BCD2 Then

    'Angle between bcd and Dsec
    alphay1 = Arccos(BCD1 / Dsec1)
    alphay2 = Arccos(BCD2 / Dsec2)

    'Arc length for the pinion and wheel at the various points of contact of gear tooth
    pair 2
    Sty1 = Dsec1 * ((Stref1 / Dref1) + Tan(alpha) - Tan(alphay1) + alphay1 - alpha)
    Sty2 = Dsec2 * ((Stref2 / Dref2) + Tan(alpha) - Tan(alphay2) + alphay2 - alpha)

    'Half angles for the various arc lengths
    Toh1 = Sty1 / Dsec1
    Toh2 = Sty2 / Dsec2

    'Heights of bending arm for gear tooth pair 2
    'Height of point on pinion and on wheel above BCD
    y12 = (Dsec1 / 2) * Cos(Toh1) - BCD1 / 2 - Tan(alphay1 - Toh1) * Sin(Toh1) *
          Dsec1 / 2
    y22 = (Dsec2 / 2) * Cos(Toh2) - BCD2 / 2 - Tan(alphay2 - Toh2) * Sin(Toh2) *
          Dsec2 / 2
```

```
'Bending arm height for stiffness calcs in pinion and wheel
Hf12 = (y12 - y1) + Hf1
Hf22 = (y22 - y2) + Hf2

'Pressure angle at point of load of pinion and wheel
alphan1 = alphay1 - Toh1 / 2
alphan2 = alphay2 - Toh2 / 2

'The second tooth pair stiffness

'Bending stiffness pinion and wheel
kb12 = 1 / ((Cos(alphan1) / (Ey1 * Fw)) * ((12 * Cos(alphan1) * Hf12 ^ 2 / Sfn1 ^
       3) * (Hf12 + Sfn1 / 2)))
kb22 = 1 / ((Cos(alphan2) / (Ey2 * Fw)) * ((12 * Cos(alphan2) * Hf22 ^ 2 / Sfn2 ^
       3) * (Hf22 + Sfn2 / 2)))

'Shear stiffness pinion and wheel
ks12 = 1 / ((Cos(alphan1) / (Ey1 * Fw)) * (3 * Cos(alphan1) ^ 2 + Sin(alphan1) ^
       2) * (1 + Hf12 / Sfn1))
ks22 = 1 / ((Cos(alphan2) / (Ey2 * Fw)) * (3 * Cos(alphan2) ^ 2 + Sin(alphan2) ^
       2) * (1 + Hf22 / Sfn2))

'Total stiffness of the pinion
k12 = (kb12 + ks12)

'Total stiffness of the wheel
k22 = (kb22 + ks22)

'Total stiffness of the tooth pair 2
ktot2(N) = (1 / k12 + 1 / k22) ^ -1

'An arbitrary high value for points very far from contact
Else
   ktot2(N) = 1E+30
End If
Next N
'*****************************************************************************

'Deflection and load sharing calculations for the meshing gear

'Normal load
Fbn = T / (BCD1 / 2)

'This accounts for a negative gap meaning the teeth are in contact
For N = 0 To z Step 1
   If E1(N) >= 0 Then
      E1(N) = E1(N)
   Else
      E1(N) = 0
   End If
```

```
If E2(N) >= 0 Then
   E2(N) = E2(N)
Else
   E2(N) = 0
End If

'If the first tooth pair are in contact
If E1(N) = 0 Then

   'The deflection of the first tooth pair
   Dx1(N) = Fbn / ktot1(N)

'If the deflection is less than the second tooth pair gap then the load is all on the first
tooth pair
If Dx1(N) < Abs(E2(N)) Then

   'The deflection of the first tooth pair is as calculated above
   Dx1(N) = Dx1(N)

   'Load sharing
   LS(N) = 1

'If the deflection is more than the second tooth pair gap then the load is shared
 between the two tooth pairs
Else

   'The deflection of the first tooth pair is recalculated to take into account both
   gears in contact
   Dx1(N) = (Fbn + ktot2(N) * Abs(E2(N))) / (ktot1(N) + ktot2(N))

   'Load sharing
   LS(N) = ktot1(N) * Dx1(N) / (ktot1(N) * Dx1(N) + ktot2(N) * (Dx1(N) -
           Abs(E2(N))))
End If

'The second tooth pair are in contact
Else
   E2(N) = 0

   'The deflection of the second tooth pair
   Dx2(N) = Fbn / ktot2(N)

'If the deflection is less than the first tooth pair gap then the load is all on the second
tooth pair
If Dx2(N) < Abs(E1(N)) Then

   'The deflection of the second tooth pair is as calculated above
   Dx2(N) = Dx2(N)

   'Load sharing
   LS(N) = 0
```

```
    Else

        'The deflection of the second tooth pair is recalculated to take into account both
        gears in contact
        Dx2(N) = (Fbn + ktot1(N) * Abs(E1(N))) / (ktot1(N) + ktot2(N))

        'Load sharing
        LS(N) = (ktot1(N) * (Dx2(N) - Abs(E1(N)))) / (ktot2(N) * Dx2(N) + ktot1(N) *
                (Dx2(N) - Abs(E1(N))))

    End If
End If
Next N
'++++++++++++++++++++++++++++++++++++++++++++++++++++++++++++++++++++++++++++++++++++++
```

Form3

```
Private Sub conrun() ' Calculation of the Contact Stresses on the Tooth Surface
Dim A1, A1new, B1, B1new, D As Double
Dim Em, Ered, Km, Lambda, Lambdai, m As Double
Dim P1, P1new, Q1, Q1new, Rad, V As Double

'The reduced Young's modulus
Ered = ((1 - Poiss1 ^ 2) / Ey1 + (1 - Poiss2 ^ 2) / Ey2) ^ -1

'This gives the points before rigid contact the radius at the corner of one tooth
For N = 0 To z Step 1
    If N < Y Then
        R(1, N) = TipRad
    ElseIf N > z - Y Then
        R(2, N) = TipRad
    Else
        R(1, N) = R(1, N)
        R(2, N) = R(2, N)
    End If
Next N
'*****************************************************************************

'If the user choses a crowning radius the contact will be elliptical

'For a line contact
If option1(1) = True Then

'For table of results
J = 1

For N = 0 To z Step 1
    'Reduced Radius of contact
    Rad = (1 / R(1, N) + 1 / R(2, N)) ^ -1

    'Major and minor semi-contact widths
    A(N) = Fw
```

```
        B(N) = 2 * ((Fbn * LS(N) / Fw) * Rad / (pi * Ered)) ^ 0.5

        'Maximum  Hertzian contact pressure
        Po(N) = ((Fbn * LS(N) / Fw) * Ered / (pi * Rad)) ^ 0.5
        'D = (2 * (Fbn / Fw) / pi) * ((1 - Poiss1) ^ 2 * Log(4 * R(1, N) / A(N) - .5) / Ey1 +
              (1 - Poiss2) ^ 2 * Log(4 * R(2, N) / A(N) - .5) / Ey1)
    Next N
'-------------------------------------------------------------------------------

Else
    'The contact is elliptical

    'For table of results
    J = 2

    'The elliptical integrals have to be solved by iteration
    For N = 0 To z Step 1

        'Method detailed in Wildhaber-Novikov gear paper
        Lambda = (0.5 * ((R(1, N) + R(2, N)) / (R(1, N) * R(2, N))) ^ -1) / (0.5 * ((R12 +
                 R22) / (R12 * R22)) ^ -1)
        m = Lambda ^ (4 / 3)

        Do
            P1 = 1
            Q1 = Sqr(m)
            A1 = 1
            B1 = m
            Do
                B1new = (Q1 * A1 + P1 * B1) / (Q1 + P1)
                A1new = 0.5 * (B1 + A1)
                Q1new = Sqr(Q1 * P1)
                P1new = 0.5 * (Q1 + P1)
                B1 = B1new
                A1 = A1new
                Q1 = Q1new
                P1 = P1new
            Loop Until Abs(P1 - Q1) < 0.000000001

            Lambdai = (1 - A1) / ((A1 / m) - 1)
            m = m + ((2 * m * (1 - m) * (Lambda - Lambdai)) / (Lambdai ^ 2 + 2 * (1 - m) *
                Lambdai - m))

        Loop Until Abs(Lambda - Lambdai) < 0.000000001

        k = Sqr(m)
        Km = pi / (2 * P1)
        Em = (pi * A1) / (2 * P1)
        V = ((3 * LS(N) * Fbn * (((1 / R(1, N) + 1 / R(2, N)) ^ -1 * (1 / R12 + 1 / R22) ^ -
            1) ^ 0.5)) / (4 * Ered)) ^ (2 / 3) * (4 / (pi * (1 - m) ^ 2)) ^ (2 / 3) * (((1 / k) ^ 2
            * Em - Km) * (Km - Em)) ^ (1 / 3) * k
```

```
If V = 0 Then
   B(N) = 0
   A(N) = 0
   Po(N) = 0
Else

   'Minor and major elliptical contact half-widths
   B(N) = Sqr(V * k)
   A(N) = V / B(N)

   'Maximum Hertzian contact pressure
   Po(N) = (3 * LS(N) * Fbn) / (2 * pi * V)
         D = (3 * Fbn * Km) / (2 * pi * A1 * Ered)
      End If
   Next N
End If
'++++++++++++++++++++++++++++++++++++++++++++++++++++++++++++++++++++++++++++++++++++++++++++++++++++++++++++++++++++++++
```

Form4

```
Dim alpha, eta, R12, R22, TipRad As Double

Private Sub filmrun() 'Calculation of the Film Thickness in the Gear Contact
Dim Ered, Rx, Ry, ke As Double

'Reduced Young's modulus
Ered = ((1 - Poiss1 ^ 2) / Ey1 + (1 - Poiss2 ^ 2) / Ey2) ^ -1

'This gives the points before rigid contact the radius at the corner of one tooth
For N = 0 To z Step 1
   If N < Y Then
      R(1, N) = TipRad
   ElseIf N > z - Y Then
      R(2, N) = TipRad
   Else
      R(1, N) = R(1, N)
      R(2, N) = R(2, N)
   End If
Next N
'*****************************************************************************************

For N = 0 To z Step 1
   GRAPH1.ThisPoint = N + 1
   GRAPH1.XPosData = (180 / pi) * Angle(N)

   Rx = (1 / R(1, N) + 1 / R(2, N)) ^ -1
   Ry = (1 / R12 + 1 / R22) ^ -1
'-----------------------------------------------------------------------------------------

   'If the user choses a crowning radius
   If Frame5.Visible = True Then
```

```
'If the user wants to use Dowson-Hamrock (any contact central film)
If option5(0).Value = True Then

    'To account for not in contact situations
    If LS(N) > 0 Then

    'Dowson-Hamrock (central film thickness)
    ke = 1.03 * (Ry / Rx) ^ 0.64
    hc(N) = 2.69 * Rx * (Abs(Ve(N)) * eta / (Ered * Rx)) ^ 0.67 * (alpha * Ered) ^
            0.53 * ((Fbn * LS(N)) / (Ered * Rx ^ 2)) ^ -0.067 * (1 - 0.61 * Exp(-
            0.73 * ke))
    GRAPH1.GraphTitle = "Central Film Thickness (Dowson-Hamrock)"
    GRAPH1.LeftTitle = "Film Thickness, hc (m)"
    GRAPH1.GraphData = hc(N)
    'for results table
    J = 1
    Else
    End If
'-------------------------------------------------------------------------------

'If the user wants to use Dowson-Hamrock (any contact Min. film)
Else

    'To account for not in contact situations
    If LS(N) > 0 Then

    'Dowson-Hamrock (Minimum film thickness)
    ke = 1.03 * (Ry / Rx) ^ 0.64
    ho(N) = 3.63 * Rx * (Abs(Ve(N)) * eta / (Ered * Rx)) ^ 0.68 * (alpha * Ered)
            ^ 0.49 * ((Fbn * LS(N)) / (Ered * Rx ^ 2)) ^ -0.073 * (1 - Exp(-0.68
            * ke))
    GRAPH1.GraphTitle = "Minimum Film Thickness (Dowson-Hamrock)"
    GRAPH1.LeftTitle = "Film Thickness, ho (m)"
    GRAPH1.GraphData = ho(N)
    J = 2
  Else
  End If
End If
'-------------------------------------------------------------------------------

'If there is no crowning
Else

'If the user wants to evaluate the minimum film thickness
If option2(0).Value = True Then

    'If the user wants to use Dowson-Higginson (Line-min. film)
    If option3(0).Value = True Then

    'To account for not in contact situations
    If LS(N) > 0 Then
```

```
            'Dowson-Higginson (Minimum film thickness)
            ho(N) = 2.65 * Rx * (Abs(Ve(N)) * eta / (Ered * Rx)) ^ 0.7 * (alpha *
                    Ered) ^ 0.54 * ((Fbn * LS(N)) / (Ered * Rx * Fw)) ^ -0.13
            GRAPH1.GraphTitle = "Minimum Film Thickness (Dowson-Higginson)"
            GRAPH1.LeftTitle = "Film Thickness, ho (m)"
            GRAPH1.GraphData = ho(N)
            J = 3
         Else
         End If
'-------------------------------------------------------------------------

      'If the user wants to use Dowson-Hamrock (Line-min. film)
      Else

         'To account for not in contact situations
         If LS(N) > 0 Then

            'Dowson-Hamrock (Minimum film thickness)
            ho(N) = 3.63 * Rx * (Abs(Ve(N)) * eta / (Ered * Rx)) ^ 0.68 * (alpha *
                    Ered) ^ 0.49 * ((Fbn * LS(N)) / (Ered * Rx ^ 2)) ^ -0.073
            GRAPH1.GraphTitle = "Minimum Film Thickness (Dowson-Hamrock)"
            GRAPH1.LeftTitle = "Film Thickness, ho (m)"
            GRAPH1.GraphData = ho(N)
            J = 4
         Else
         End If
      End If
'-------------------------------------------------------------------------

      'If the user wants to evaluate the central film thickness
      Else

         'If the user wants to use Grubin (Line-central film)
         If option4(0).Value = True Then

            'To account for not in contact situations
            If LS(N) > 0 Then

            'Grubin (Central film thickness)
            hc(N) = 1.95 * Rx * (Abs(Ve(N)) * eta / (Ered * Rx)) ^ (8 / 11) * (alpha *
                    Ered) ^ (8 / 11) * ((Fbn * LS(N)) / (Ered * Rx * Fw)) ^ -(1 / 11)
            GRAPH1.GraphTitle = "Central Film Thickness (Grubin)"
            GRAPH1.LeftTitle = "Film Thickness, hc (m)"
            GRAPH1.GraphData = hc(N)
            J = 5
            Else
            End If
'-------------------------------------------------------------------------
```

```
'If the user wants to use Dowson-Hamrock (any contact central film)
Else

   'To account for not in contact situations
   If LS(N) > 0 Then

      'Dowson-Hamrock (Central film thickness)
      hc(N) = 2.69 * Rx * (Abs(Ve(N)) * eta / (Ered * Rx)) ^ 0.67 * (alpha *
              Ered) ^ 0.53 * ((Fbn * LS(N)) / (Ered * Rx ^ 2)) ^ -0.067
      GRAPH1.GraphTitle = "Central Film Thickness (Dowson-Hamrock)"
      GRAPH1.LeftTitle = "Film Thickness, hc (m)"
      GRAPH1.GraphData = hc(N)
                  J = 6
               Else
               End If
            End If
         End If
      End If
Next N
'++++++++++++++++++++++++++++++++++++++++++++++++++++++++++++++++++++++++++++++++
```

Form10

```
Dim beta, K1, K2, Roe1, Roe2, Sigma1, Sigma2 As Double
Dim miu, Xsi1, Xsi2, Tfm1, Tfm2 As Double
Dim A11, A21, A22, A3, Ered, Rad, TipRad As Double

'These values will be assigned to the parameters below once run is selected

'Thermal Conductivity pinion,K1
'Density pinion, Roe1
'Specific heat pinion, Sigma1
'Thermal Conductivity wheel, K2
'Density wheel, Roe2
'Specific heat wheel, Sigma2
'Friction Coefficient, miu
'Tip Radius of gear, TipRad
```

Private Sub flashrun() 'Calculation of the Gear Tooth Flash Temperatures

```
ReDim U1(z), U2(z) As Double

'Contact stresses and contact dimensions

'The reduced Young's modulus
Ered = ((1 - Poiss1 ^ 2) / Ey1 + (1 - Poiss2 ^ 2) / Ey2) ^ -1

'This gives the points before rigid contact the radius at the corner of one tooth
For N = 0 To z Step 1
   If N < Y Then
      R(1, N) = TipRad
   ElseIf N > z - Y Then
      R(2, N) = TipRad
```

```
    Else
        R(1, N) = R(1, N)
        R(2, N) = R(2, N)
    End If
Next N

'Line contact pressures
For N = 0 To z Step 1

    'Reduced Radius of contact
    Rad = (1 / R(1, N) + 1 / R(2, N)) ^ -1

    'Major and minor semi-contact widths
    A(N) = Fw
    B(N) = 2 * ((Fbn * LS(N) / Fw) * Rad / (pi * Ered)) ^ 0.5
Next N

'*************************************************************************

'Flash temperature calculation

For N = 0 To z Step 1
    If N < Y Then
        U1(N) = Abs(Vs(N))
        U2(N) = 0
    ElseIf N > z - Y Then
        U1(N) = 0
        U2(N) = Abs(Vs(N))
    Else
        U1(N) = Vr1(N)
        U2(N) = Vr2(N)
    End If
Next N

Xsi1 = K1 / (Roe1 * Sigma1)
Xsi2 = K2 / (Roe2 * Sigma2)

For N = 0 To z Step 1

If LS(N) > 0 Then
    Beta1 = U1(N) * B(N) / (2 * Xsi1)
    Beta2 = U2(N) * B(N) / (2 * Xsi2)

'Contact points on gear1 and gear2 are fast
If Beta1 > 5 And Beta2 > 5 Then

    Tfm(N) = 1.11 * LS(N) * Fbn * miu * Abs(Vs(N)) / (Sqr(2 * B(N)) * Fw *
             (Sqr(U1(N) * Roe1 * Sigma1 * K1) + Sqr(U2(N) * Roe2 * Sigma2 *
              K2)))
```

```
'Contact point on gear1 is fast and gear2 is slow
ElseIf Beta1 > 5 And Beta2 < 0.1 Then
   If Beta2 = 0 Then
      A3 = 2.303 * Log10(Fw / B(N))
      Tfm(N) = 1.5958 * (Fbn * LS(N) / (2 * B(N) * Fw)) * miu * Abs(Vs(N)) /
               (1.6713 * K2 / (A3 + 2 * B(N) / (3 * Fw) + 0.5) + K1 / Sqr(Xsi1 *
               B(N) / U1(N)))
   Else
      A22 = -2.303 * Beta2 * Log10(2 * Beta2) + 1.616 * Beta2
      Tfm(N) = 1.5958 * (Fbn * LS(N) / (2 * B(N) * Fw)) * miu * Abs(Vs(N)) /
               (0.8357 * K2 * U2(N) / (Xsi2 * A22) + K1 / Sqr(Xsi1 * B(N) /
               U1(N)))
   End If
'Contact point on gear1 is slow and gear2 is fast
ElseIf Beta1 < 0.1 And Beta2 > 5 Then
   If Beta1 = 0 Then
      A3 = 2.303 * Log10(Fw / B(N))
      Tfm(N) = (Fbn * LS(N) * miu / (pi * Fw * K1)) * Abs(Vs(N)) * (A3 + 1) / (1 +
               0.5983 * B(N) * K2 * (A3 + 2 * B(N) / (3 * Fw) + 0.5) / (K1 *
               Sqr(Xsi2 * B(N) / U2(N))))
   Else
      A11 = -2.303 * Beta1 * Log10(Beta1) + 1.116 * Beta1
      A21 = -2.303 * Beta1 * Log10(2 * Beta1) + 1.616 * Beta1
      Tfm(N) = (Fbn * LS(N) * miu / (2 * B(N) * Fw)) * Abs(Vs(N)) / (0.7854 * K1 *
               U1(N) / (Xsi1 * A11) + A21 * K2 / (1.064 * A11 * Sqr(Xsi2 * B(N) /
               U2(N))))
   End If

'Contact points on gear1 and gear2 are slow
ElseIf Beta1 < 0.1 And Beta2 < 0.1 Then
   If Beta1 = 0 Then
      A22 = -2.303 * Beta2 * Log10(2 * Beta2) + 1.616 * Beta2
      A3 = 2.303 * Log10(Fw / B(N))
      Tfm(N) = 0.3183 * (Fbn * LS(N) * miu / (K1 * Fw)) * Abs(Vs(N)) * (A3 + 1) /
               (1 + 1.5708 * (A3 + 2 * B(N) / (3 * Fw) + 0.5) * K2 * U2(N) / (Xsi2 *
               A22))

   ElseIf Beta2 = 0 Then
      A11 = -2.303 * Beta1 * Log10(Beta1) + 1.116 * Beta1
      A21 = -2.303 * Beta1 * Log10(2 * Beta1) + 1.616 * Beta1
      A3 = 2.303 * Log10(Fw / B(N))
      Tfm(N) = (Fbn * LS(N) * miu / (2 * B(N) * Fw)) * Abs(Vs(N)) / (0.7854 * K1 *
               U1(N) / (Xsi1 * A11) + 1.5708 * A21 * K2 * (A3 + 2 * B(N) / (3 *
               Fw) + 0.5) / (A11 * B(N)))
   Else
      A11 = -2.303 * Beta1 * Log10(Beta1) + 1.116 * Beta1
      A21 = -2.303 * Beta1 * Log10(2 * Beta1) + 1.616 * Beta1
      A22 = -2.303 * Beta2 * Log10(2 * Beta2) + 1.616 * Beta2
      Tfm(N) = (Fbn * LS(N) * miu / (2 * B(N) * Fw)) * Abs(Vs(N)) * A11 / (0.7854
               * K1 * U1(N) / Xsi1 + 0.7854 * A21 * K2 * U2(N) / (A22 * Xsi2))
End If
```

```
'Contact point on gear1 is fast and gear2 is intermediate
ElseIf Beta1 > 5 And Beta2 > 0.1 And Beta2 < 5 Then

    'fast-fast
    Tfm1 = 1.11 * LS(N) * Fbn * miu * Abs(Vs(N)) / (Sqr(2 * B(N)) * Fw *
           (Sqr(U1(N) * Roe1 * Sigma1 * K1) + Sqr(U2(N) * Roe2 * Sigma2 * K2)))

    'fast-static
    A3 = 2.303 * Log10(Fw / B(N))
    Tfm2 = 1.5958 * (Fbn * LS(N) / (2 * B(N) * Fw)) * miu * Abs(Vs(N)) / (1.6713 *
           K2 / (A3 + 2 * B(N) / (3 * Fw) + 0.5) + K1 / Sqr(Xsi1 * B(N) / U1(N)))
    Tfm(N) = (Tfm1 ^ -2 + Tfm2 ^ -2) ^ -0.5

'Contact point on gear1 is slow and gear2 is intermediate
ElseIf Beta1 < 0.1 And Beta2 > 0.1 And Beta2 < 5 Then

    If Beta1 = 0 Then
        'static-fast
        A3 = 2.303 * Log10(Fw / B(N))
        Tfm1 = (Fbn * LS(N) * miu / (pi * Fw * K1)) * Abs(Vs(N)) * (A3 + 1) / (1 +
               0.5983 * B(N) * K2 * (A3 + 2 * B(N) / (3 * Fw) + 0.5) / (K1 *
               Sqr(Xsi2 * B(N) / U2(N))))

        'static-static
        Tfm2 = Fbn * LS(N) * miu * (A3 + 1) / ((Fw * pi * K1) * (1 + K2 / K1))
        Tfm(N) = (Tfm1 ^ -2 + Tfm2 ^ -2) ^ -0.5

    Else
        'slow-fast
        A11 = -2.303 * Beta1 * Log10(Beta1) + 1.116 * Beta1
        A21 = -2.303 * Beta1 * Log10(2 * Beta1) + 1.616 * Beta1
        Tfm1 = (Fbn * LS(N) * miu / (2 * B(N) * Fw)) * Abs(Vs(N)) / (0.7854 * K1 *
               U1(N) / (Xsi1 * A11) + A21 * K2 / (1.064 * A11 * Sqr(Xsi2 * B(N) /
               U2(N))))

        'slow-static
        A3 = 2.303 * Log10(Fw / B(N))
        Tfm2 = (Fbn * LS(N) * miu / (2 * B(N) * Fw)) * Abs(Vs(N)) / (0.7854 * K1 *
               U1(N) / (Xsi1 * A11) + 1.5708 * A21 * K2 * (A3 + 2 * B(N) / (3 * Fw)
               + 0.5) / (A11 * B(N)))

        Tfm(N) = (Tfm1 ^ -2 + Tfm2 ^ -2) ^ -0.5
    End If

'Contact point on gear1 is intermediate and gear2 is fast
ElseIf Beta1 > 0.1 And Beta1 < 5 And Beta2 > 5 Then
    'fast-fast
    Tfm1 = 1.11 * LS(N) * Fbn * miu * Abs(Vs(N)) / (Sqr(2 * B(N)) * Fw *
           (Sqr(U1(N) * Roe1 * Sigma1 * K1) + Sqr(U2(N) * Roe2 * Sigma2 * K2)))
```

```
        'static-fast
        A3 = 2.303 * Log10(Fw / B(N))
        Tfm(N) = (Fbn * LS(N) * miu / (pi * Fw * K1)) * Abs(Vs(N)) * (A3 + 1) / (1 +
                  0.5983 * B(N) * K2 * (A3 + 2 * B(N) / (3 * Fw) + 0.5) / (K1 *
                  Sqr(Xsi2 * B(N) / U2(N))))

        Tfm(N) = (Tfm1 ^ -2 + Tfm2 ^ -2) ^ -0.5

    'Contact point on gear1 is intermediate and gear2 is slow
    ElseIf Beta1 > 0.1 And Beta1 < 5 And Beta2 < 0.1 Then

        If Beta2 = 0 Then
            'static-static
            A3 = 2.303 * Log10(Fw / B(N))
            Tfm1 = Fbn * LS(N) * miu * (A3 + 1) / ((Fw * pi * K1) * (1 + K2 / K1))

            'fast-static
            Tfm2 = 1.5958 * (Fbn * LS(N) / (2 * B(N) * Fw)) * miu * Abs(Vs(N)) / (1.6713
                  * K2 / (A3 + 2 * B(N) / (3 * Fw) + 0.5) + K1 / Sqr(Xsi1 * B(N) /
                  U1(N)))

            Tfm(N) = (Tfm1 ^ -2 + Tfm2 ^ -2) ^ -0.5
        Else
            'static-slow
            A22 = -2.303 * Beta2 * Log10(2 * Beta2) + 1.616 * Beta2
            A3 = 2.303 * Log10(Fw / B(N))
            Tfm1 = 0.3183 * (Fbn * LS(N) * miu / (K1 * Fw)) * Abs(Vs(N)) * (A3 + 1) / (1
                  + 1.5708 * (A3 + 2 * B(N) / (3 * Fw) + 0.5) * K2 * U2(N) / (Xsi2 *
                  A22))

            'fast-slow
            A22 = -2.303 * Beta2 * Log10(2 * Beta2) + 1.616 * Beta2
            Tfm2 = 1.5958 * (Fbn * LS(N) / (2 * B(N) * Fw)) * miu * Abs(Vs(N)) / (0.8357
                  * K2 * U2(N) / (Xsi2 * A22) + K1 / Sqr(Xsi1 * B(N) / U1(N)))

            Tfm(N) = (Tfm1 ^ -2 + Tfm2 ^ -2) ^ -0.5
        End If

    'Contact points on gear1 and gear2 are intermediate
    ElseIf Beta1 < 5 And Beta1 > 0.1 And Beta2 < 5 And Beta2 > 0.1 Then
        'static-static
        'fast-static
        'static-fast

        Tfm(N) = 1
    End If
Else: Tfm(N) = 0
End If
Next N
'++++++
```

I2 Program Outputs

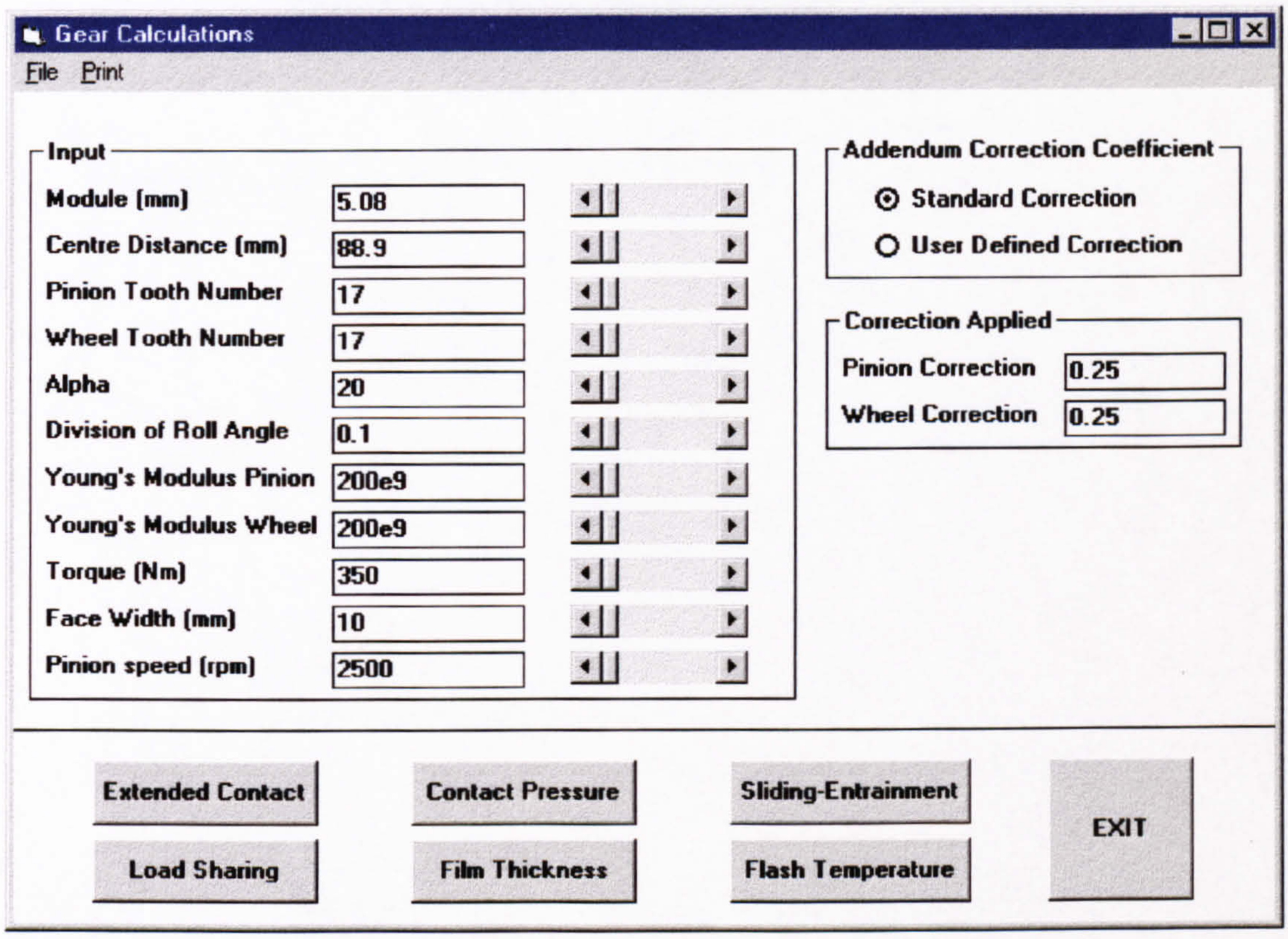


Figure I1 Input Page to the Program

Extended Contact Results

Print Close

Step	Roll Angle (°)	Gap 1 (mm)	Gap 2 (mm)	Deflect.1 (mm)	Deflect.2 (mm)	Load Sharing
43	9.447	0.0603645	0.0000000	0.0000000	0.0121023	0.0000000
44	9.547	0.0533704	0.0000000	0.0000000	0.0120167	0.0000000
45	9.647	0.0468192	0.0000000	0.0000000	0.0119311	0.0000000
46	9.747	0.0407083	0.0000000	0.0000000	0.0118453	0.0000000
47	9.847	0.0350352	0.0000000	0.0000000	0.0117596	0.0000000
48	9.947	0.0297972	0.0000000	0.0000000	0.0116739	0.0000000
49	10.047	0.0249919	0.0000000	0.0000000	0.0115882	0.0000000
50	10.147	0.0206168	0.0000000	0.0000000	0.0115027	0.0000000
51	10.247	0.0166694	0.0000000	0.0000000	0.0114173	0.0000000
52	10.347	0.0131473	0.0000000	0.0000000	0.0113321	0.0000000
53	10.447	0.0100480	0.0000000	0.0000000	0.0107132	0.0474726
54	10.547	0.0073693	0.0000000	0.0000000	0.0094790	0.1508205
55	10.647	0.0051087	0.0000000	0.0000000	0.0084376	0.2383692
56	10.747	0.0032640	0.0000000	0.0000000	0.0075864	0.3099949
57	10.847	0.0018329	0.0000000	0.0000000	0.0069225	0.3655745
58	10.947	0.0008133	0.0000000	0.0000000	0.0064434	0.4049850
59	11.047	0.0002030	0.0000000	0.0000000	0.0061462	0.4281047
60	11.147	0.0000000	0.0000000	0.0060283	0.0000000	0.4348127
61	11.164	0.0000000	0.0000000	0.0060288	0.0000000	0.4350469
62	11.181	0.0000000	0.0000000	0.0060293	0.0000000	0.4352814
63	11.199	0.0000000	0.0000000	0.0060299	0.0000000	0.4355162
64	11.216	0.0000000	0.0000000	0.0060304	0.0000000	0.4357513
65	11.233	0.0000000	0.0000000	0.0060309	0.0000000	0.4359866
66	11.250	0.0000000	0.0000000	0.0060314	0.0000000	0.4362222
67	11.268	0.0000000	0.0000000	0.0060320	0.0000000	0.4364581
68	11.285	0.0000000	0.0000000	0.0060325	0.0000000	0.4366942

Figure I2 Program Output Showing the Calculated Tooth Gaps, Deflections, and Load Sharing for Non-Relieved Gear Teeth

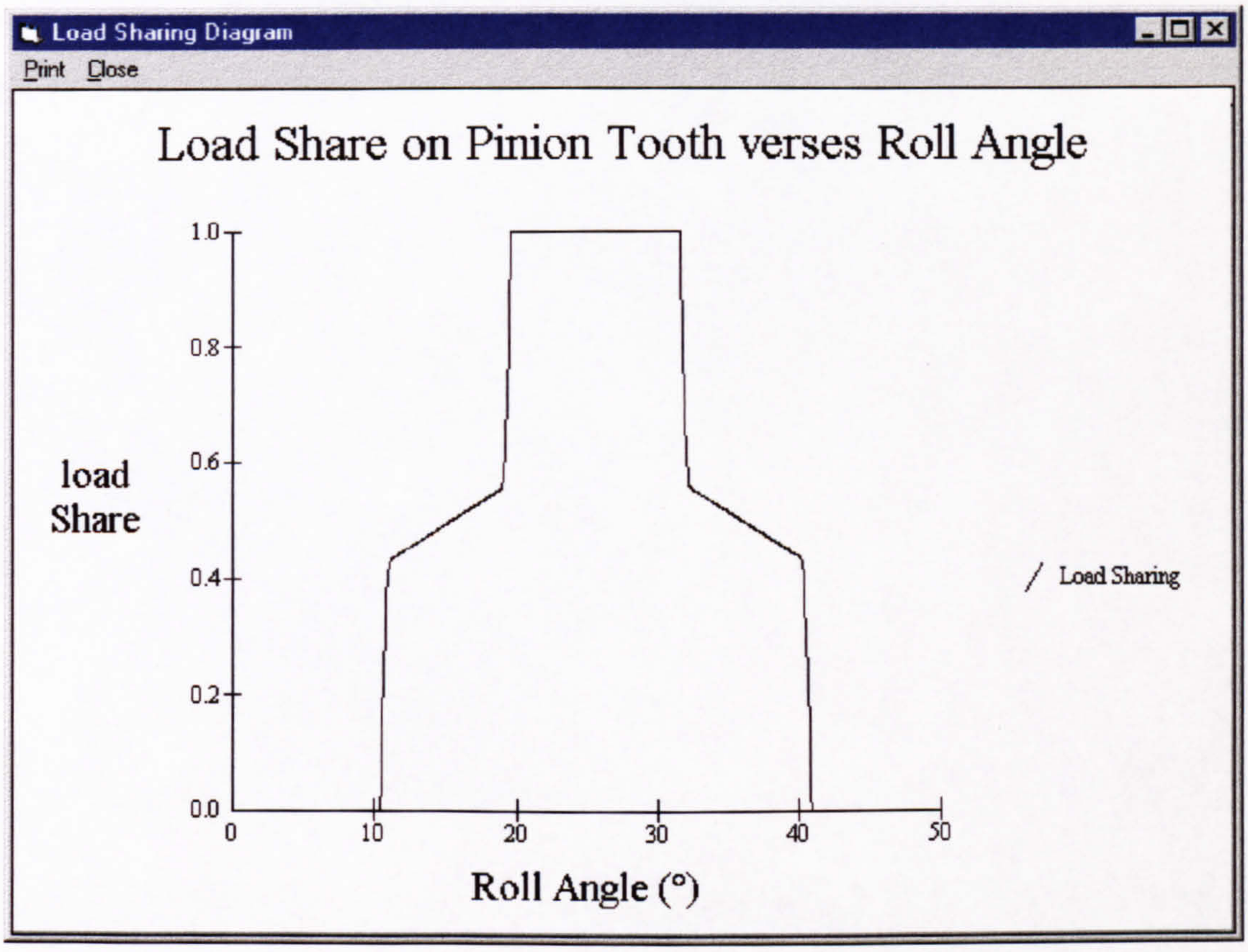


Figure I3 Program Output Showing the Load Sharing Diagram

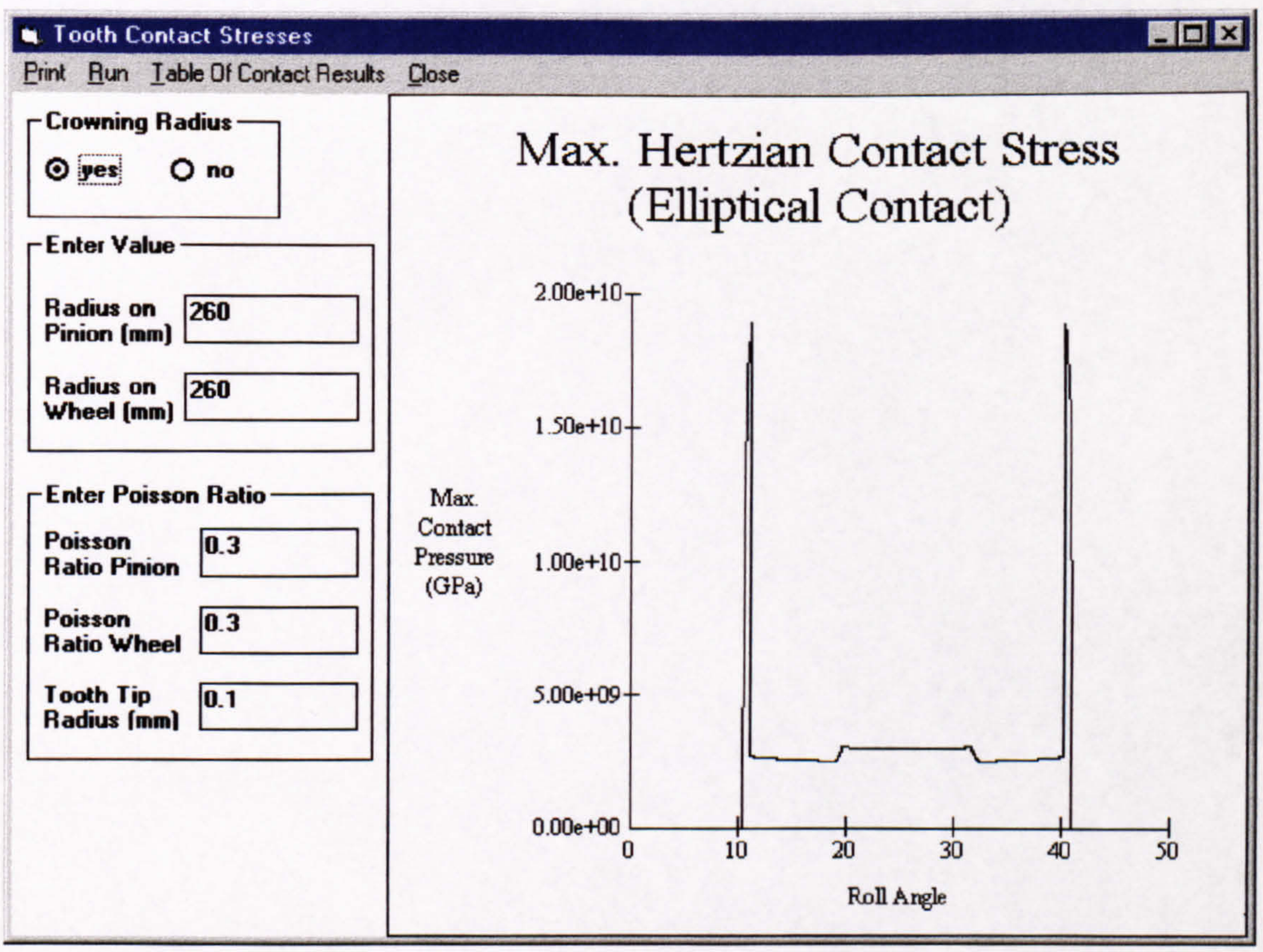


Figure I4 The Contact Stresses on a Crowned Non-Tip-Relieved Gear Tooth Suffering Extended Contact at the Extremities of the Mesh Cycle

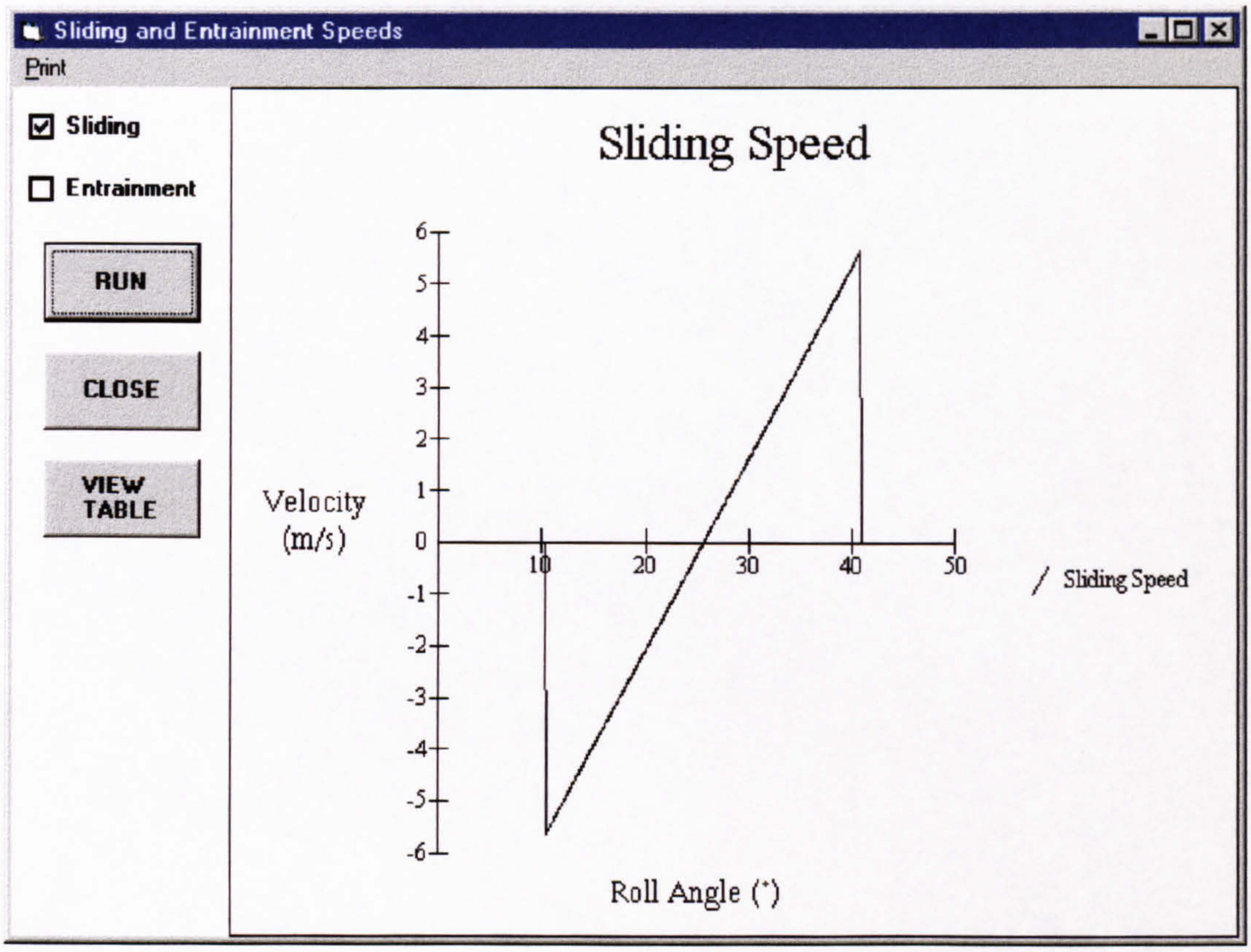


Figure I5 The Sliding Speed Along the Non-Relieved Gear Tooth Meshing Cycle Showing the Effects of Extended Contact

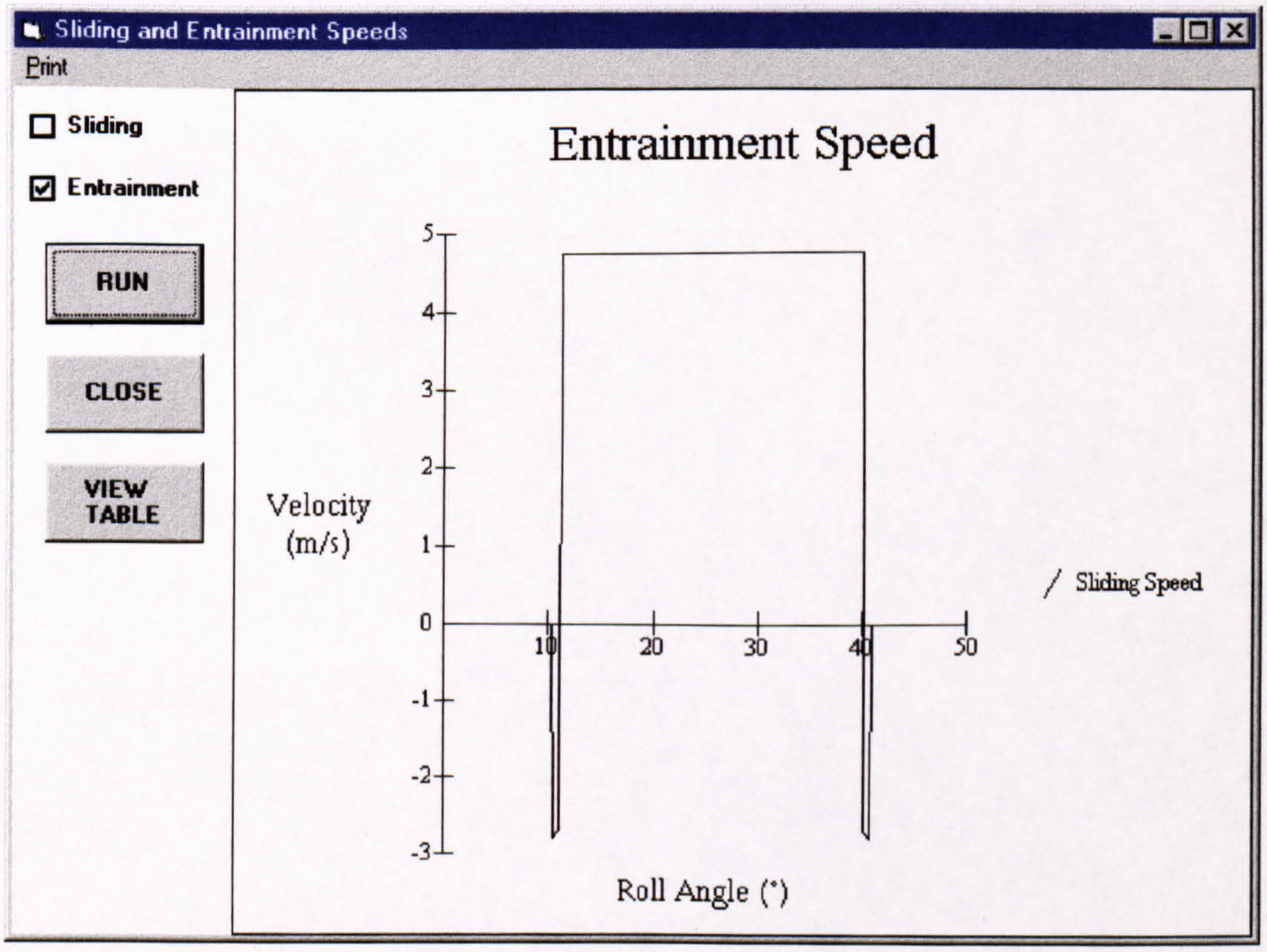


Figure I6 The Entrainment Speed Along the Non-Relieved Gear Tooth Meshing Cycle Showing the Effects of Extended Contact

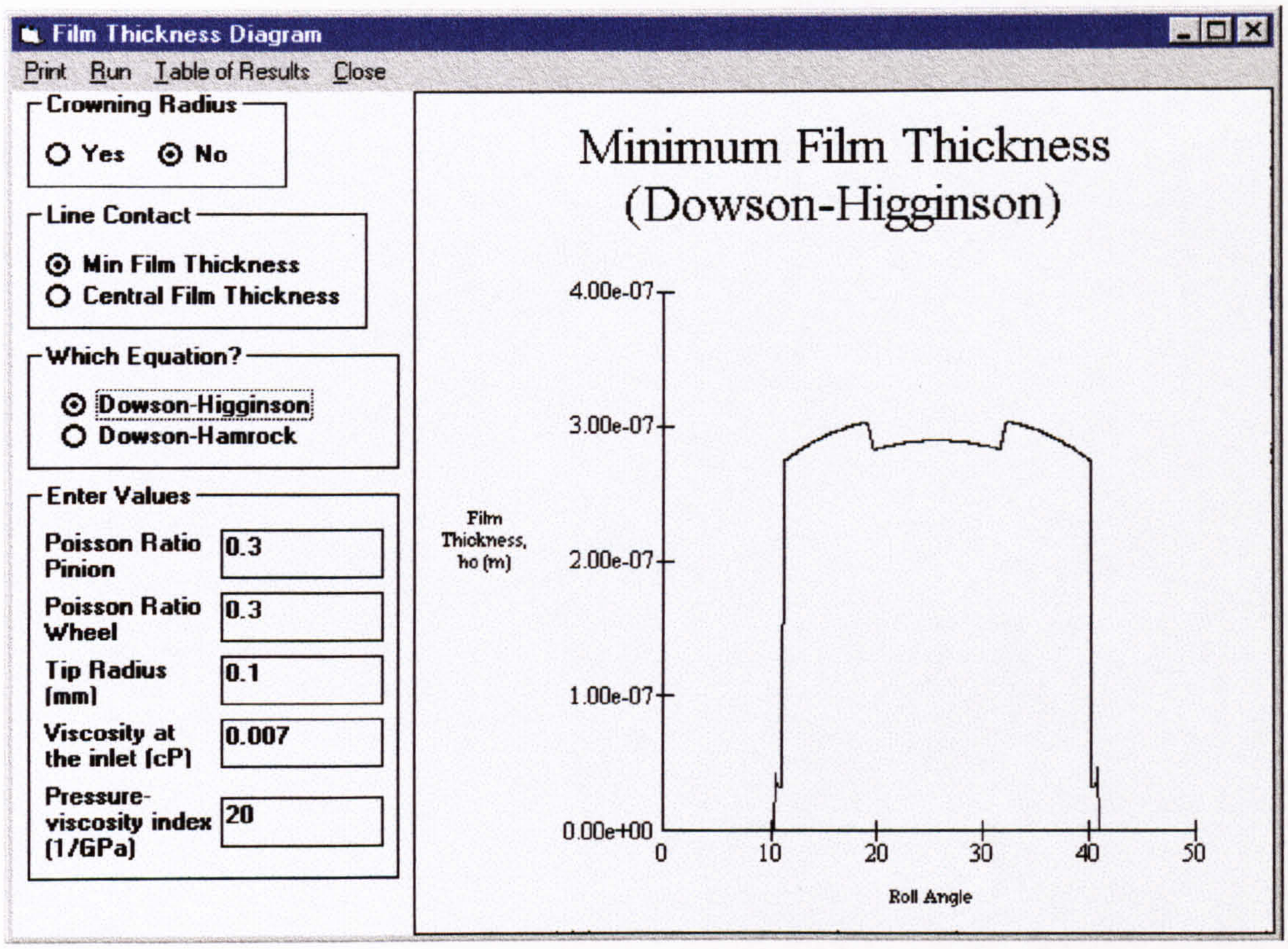


Figure I7 The Minimum Film Thickness for a Non-Tip-Relieved Gear Tooth Contact Suffering Extended Contact at the Extremities of the Mesh Cycle

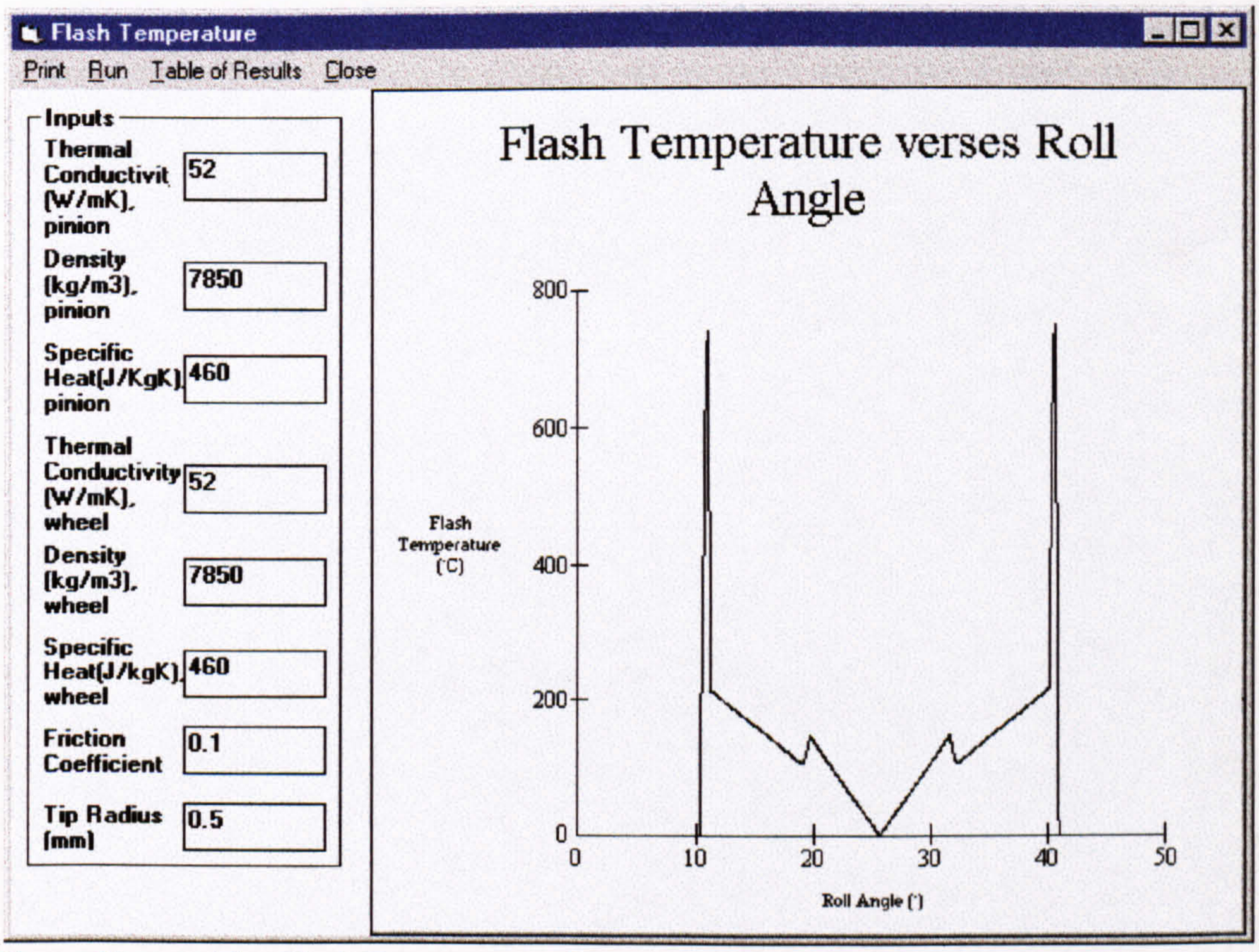


Figure I8 The Flash Temperature Generated Along The Non-Relieved Gear Tooth with Extended Contact at the Extremities of the Meshing Cycle ($\mu = 0.1$)

Appendix J Monitoring System Software Program

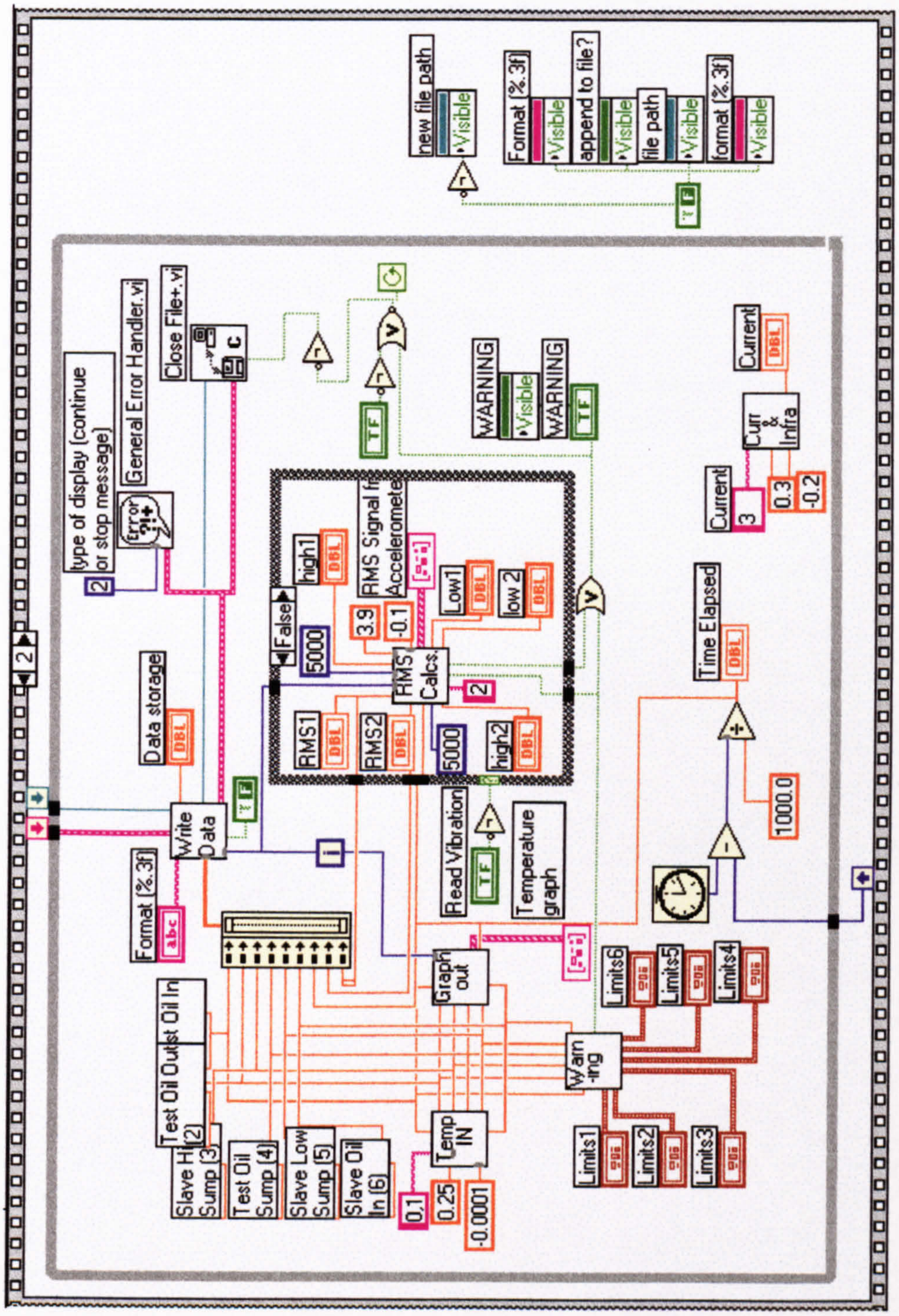


Figure J1 Gear Rig Control Program Block Diagram

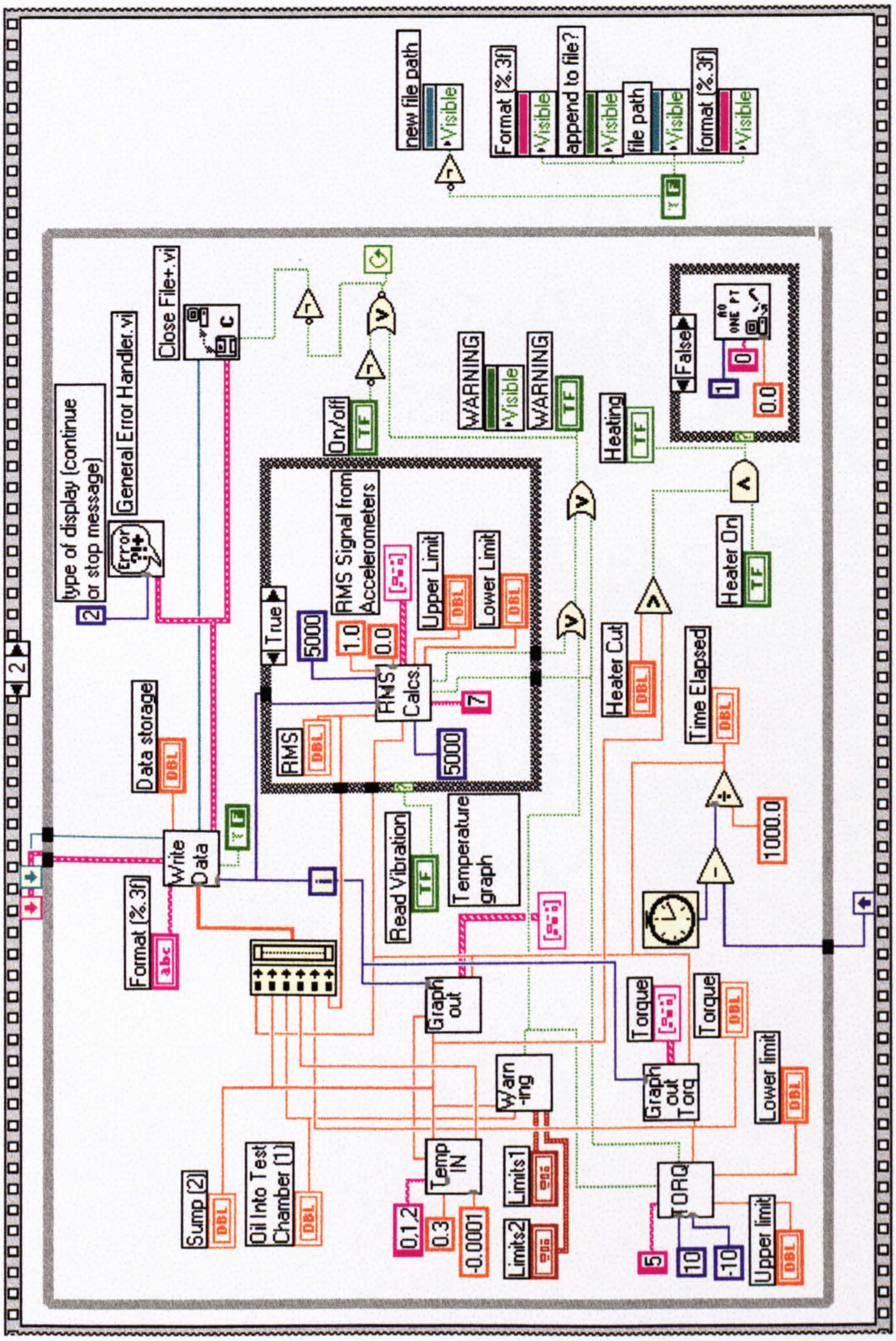


Figure J2 Disc Rig Control Program Block Diagram

Appendix K Spur Gear Design and Geometry Nomenclature

K1 Gear Terminology

The definition of several important terms in gear geometry are given here:

- **Addendum**: the portion of the tooth above the pitch circle
- **Base Circle**: the circle from which involute tooth profiles are generated and is tangent to the line of action.
- **Base Pitch**: the pitch measured on the base circle.
- **Centre Distance**: the shortest distance between two gear axes. For parallel axes, it is the distance between the two gear centres.
- **Dedendum**: the portion of the tooth below the pitch circle.
- **Diametral Pitch**: a term used for imperial designs and is a scale factor based on the number of teeth and the diameter of the gear. It is the tooth number divided by the reference diameter.
- **Fillet Curve**: is the curve which is the prolongation of the flank down to the root. It is of complex form, and depends upon the form of the cutting or finishing tools.
- **Gear Ratio**: the ratio of the number of teeth in two engaging gears. It is also the ratio of the gear speeds and gear diameters (pitch and base, not tip and root).
- **Pitch Point**: is on the line of centres and divides the centre distance in the same proportions as the gear ratio.
- **Pitch Circle**: the circle for two engaging gears passing through the pitch point.
- **Line Of Action**: passes through the pitch point and is normal to the tooth profile. It is the line along which the tooth pressure acts. With an involute tooth profile this is also the path of the point of contact.
- **Module**: a metric scale factor for gears, it is the reference diameter of the gear divided by the number of teeth.
- **Pressure Angle**: is the angle between the line of action and the pitch line. It is the nominal pressure angle of design and refers to the basic rack which is used to generate the gear.
- **Tip Radius**: a radius replacing an otherwise sharp cornered tip in a gear.

K2 Gear Design Calculations

The shape of any standard gear can be determined by the basic rack (Figure K1), which is defined by standard proportions. To obtain a particular size gear these proportions have to be multiplied by the module (in millimetres); only specific values being permitted by the standards.

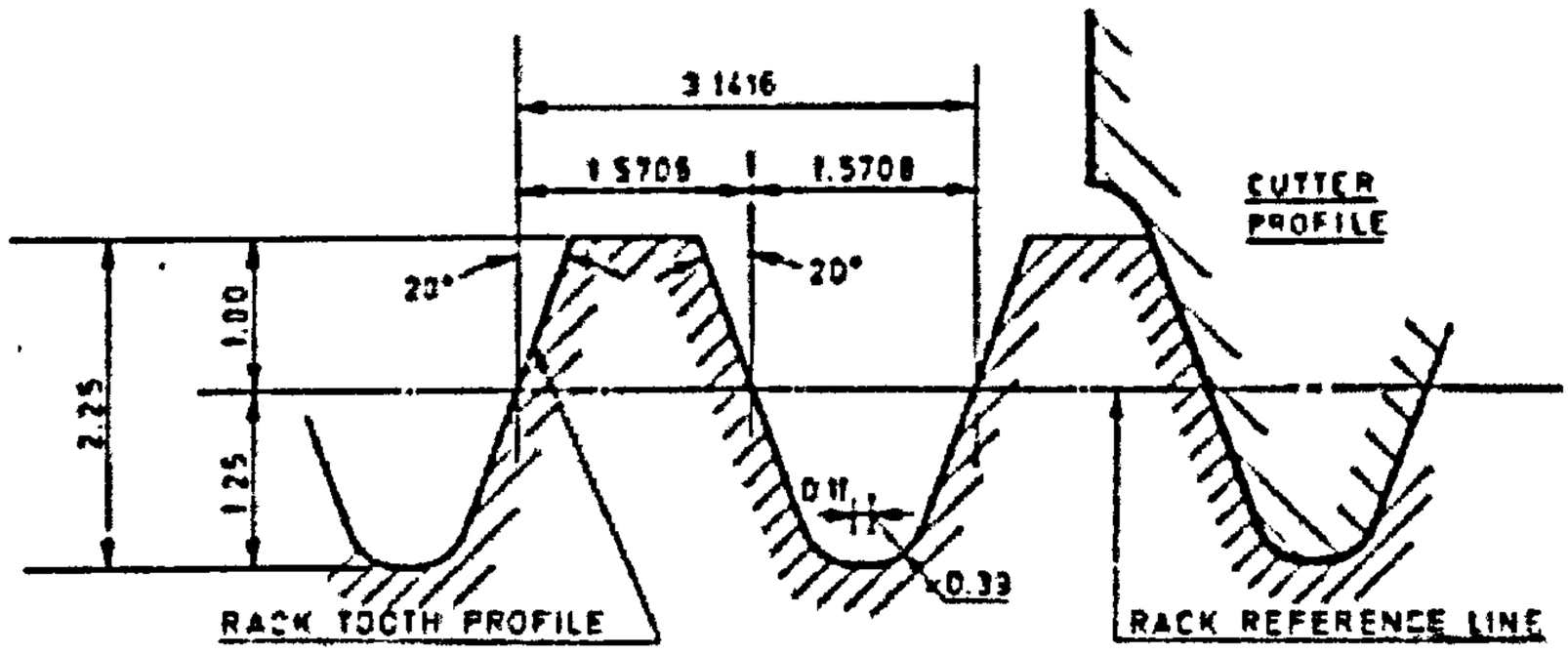


Figure K1 Rack Form Covering the Range of Modules 1-50 (from BS 436 Part 2 (BSI 1970))

The gear test rig had a fixed centre distance between the driving shafts and the existing slave gears were thirty-five tooth spur gears. This restricted the options for test gear design; the two test gears had to be 1:1 ratio spur gears. With this in mind, the variables were tooth number and module, the addendum modification coefficient, thence, being determined by the fixed centre distance. The addendum modification coefficient is a non-dimensional number indicating the radial distance the gear cutter reference line and gear reference diameter are apart. It helps determine the shape of the gear teeth, and must be within practical limits to avoid undercutting the teeth or giving them too narrow a crest width. This correction factor, however, had to be a reasonable value, lying within an advised range, that suggested by BSI (1970), for example.

A tooth number of seventeen was chosen, more teeth would have presented a risk of bending fatigue due to the finer pitch and less teeth would have posed the problem of tooth undercutting, again being detrimental to bending fatigue resistance. This meant a module of 5.08 mm, or 5 diametral pitch, was appropriate. This gave an addendum modification coefficient of 0.25 for each gear.

Centre distance, $a = 88.9$ mm

Tooth Number, z_1 and $z_2 = 17$

Module, m_n = 5.08 mm

Pressure Angle, α_n = 20 °

Base Pitch, $p_{tb} = \pi M_n . \cos(\alpha_n)$ = 15.00 mm

Pitch Circle Diameter, $PCD = \pi M_n$ = 86.36 mm

Base Circle Diameter, $D_B = z M_n$ = 81.15 mm

Dedendum standard, Ded_s = 1.157 x M_n to 1.35 x M_n = 5.88 to 6.86 mm

Outside Diameter Standard, $D_{os} = PCD + 2 \times Add_s$ = 96.52 mm

Gear Centres Standard = $(PCD_1 / 2) + (PCD_2 / 2)$ = 86.36 mm

Correction on Centres, *Corr* = Actual Centres - Standard Centres = 2.54 mm

Outside Diameter Corrected, $D_o = D_{os} + Corr$ = 99.06 mm

Correction, $\Sigma x = Corr / (2M_n)$ = 0.5

Path of Contact, $g_\alpha = 2 \times \left[\sqrt{\left(\frac{D_o}{2}\right)^2 - \left(\frac{D_B}{2}\right)^2} - \frac{D_B}{2} \tan \alpha_{tw} \right]$ = 20.51 mm

Contact Ratio = g_α / p_{tb} = 1.37

The combined gear tooth correction, Σx, had to lie within the safe range for the gear tooth number chosen, as shown in Figure K2. The individual correction factors, x, for the two gears were chosen to lie within the safe operation region shown in Figure K3.

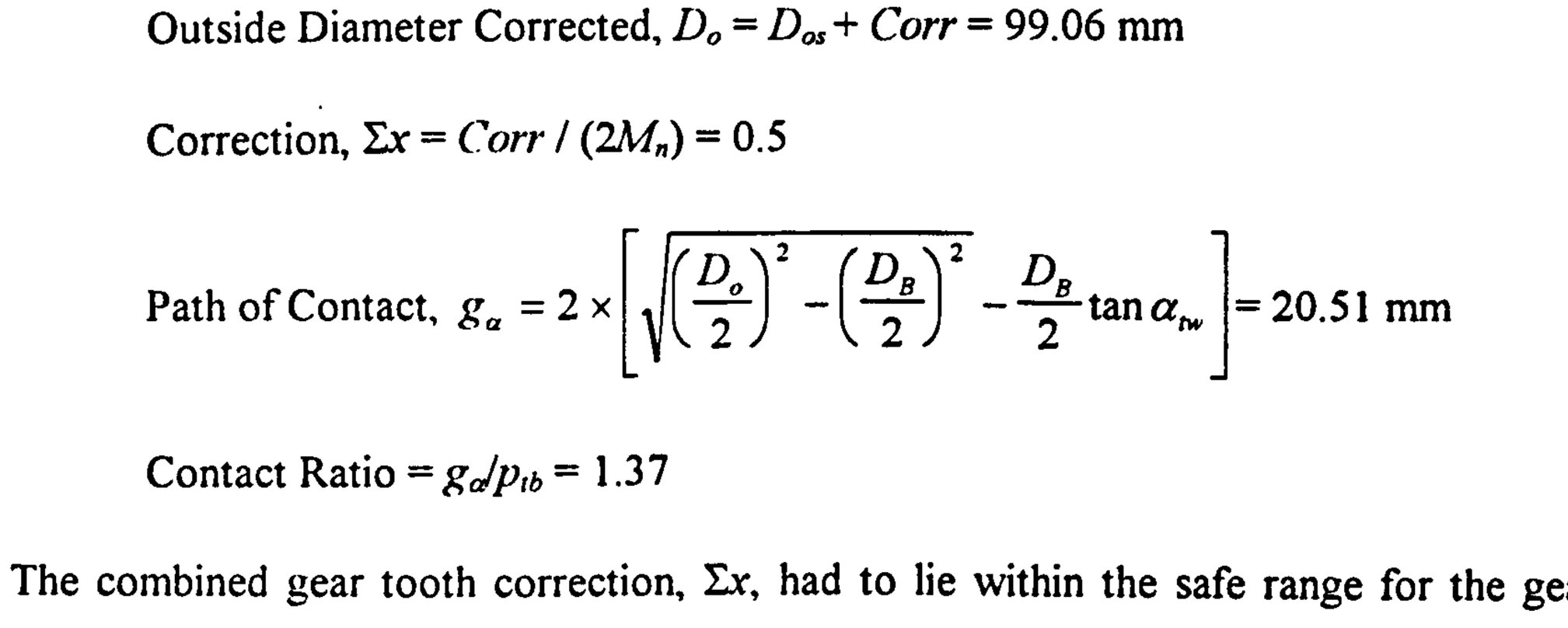


Figure K2 Limiting Values of the Sum of the Addendum Modification Coefficients Σx for a Gear Pair from BGA (1992) Chart Modified from BSI (1970)

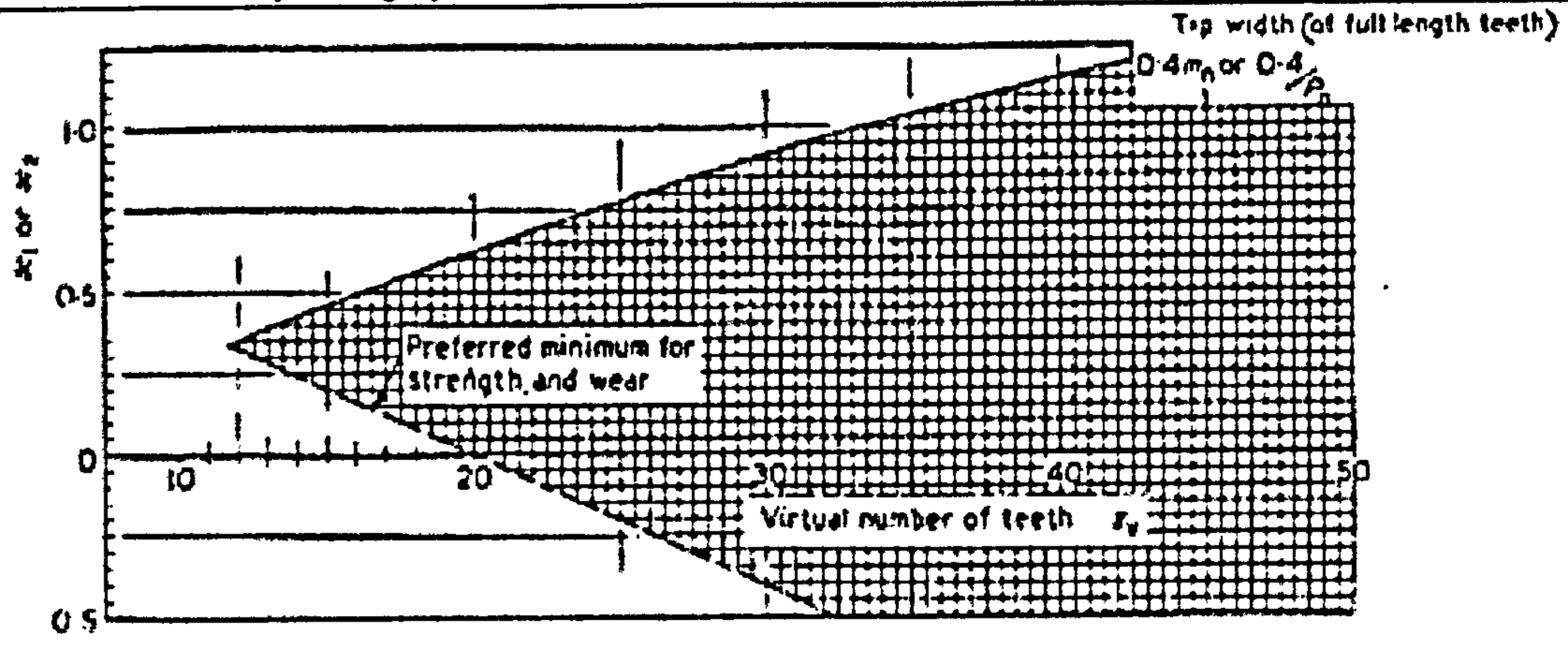


Figure K3 Limiting Values of Addendum Modification Coefficient, x, for a Single Gear from BGA (1992) Chart Modified from BSI (1970)

Having determined the basic gear geometry, the lead and profile corrections had to be defined.

K3 Profile Correction

Two different gear geometries were used to study the effect of tooth pre-engagement: one with tip relief and one without. The gears without tip relief would give rise to tooth pre-engagement, whereas, the tip relieved ones would not. The tip relief was designed with the aid of a survey on current practices compiled by the BGA (1994).

The correction applied depends on what is used as the design load. This was chosen to be the maximum load, since it was thought that the load would be fairly constant during the test. Long correction was thought preferable.

The design procedure adopted was to apply an additional amount of relief equal to the maximum adjacent pitch error. The adjacent pitch error tolerances from the AGMA standards for a specified gear accuracy were used (AGMA 1988).

For a maximum applied torque of 350 Nm.

The maximum stiffness of one pair of teeth in the normal plane = 15.4673 N/.mm.μm

The tooth pair deflection at the maximum calculated load = 55.768 μm

Pitch variation allowable to AGMA 10 (AGMA 1988) $\pm V_{pa}$ = 11.45 μm

Profile tolerance, V_{pt} = 16.70 μm

Then apply additional amount of tip relief equal to maximum adjacent pitch error

Tooth pair relief = 55.768 + 2 x 11.45 = 78.67 μm

The suggested profile tolerance diagram for one tooth is shown in Figure K4. The actual profile diagram, adopted for the gear manufacturing reasons, is shown in Appendix D and a profile is given in Figure 7.4.9.

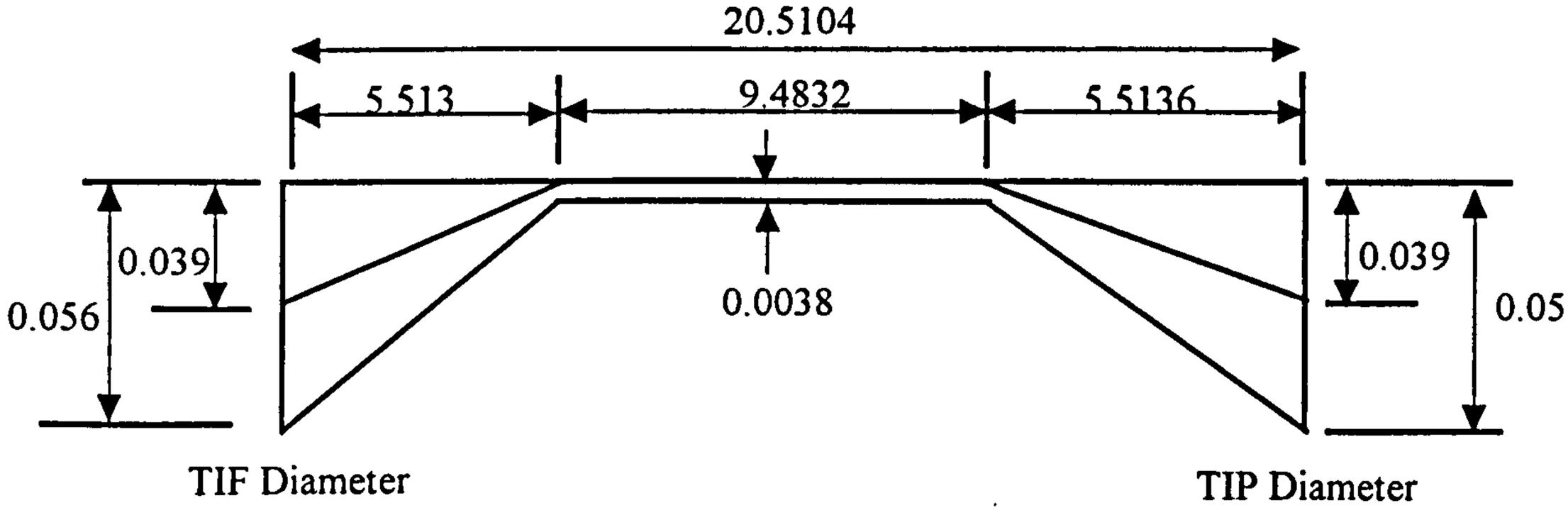


Figure K4 The Profile Tolerance Diagram for the Test Gears (mm)

In order to maintain a high contact stress, but a low bending stress on the gear teeth, a crowning radius was applied to the gear teeth. It was important that the contact width along the tooth face was less than the facewidth itself. The crowning applied can be seen in Appendix D and a lead profile for a test gear is shown in Figure 7.4.5.

The case depth of the carburised and nitrided test specimens was evaluated using AGMA 246.01A (1971) and AGMA 2001-C95 (1995). The hardness profiles can be seen in Figure 7.5.1.

BIBL LONDON UNIV.